

## CONTRIBUTING EDITOR

ABDULLAH A. AL-BADR

GUNAWAN INDRAYANTO

## FOUNDING EDITOR

KLAUS FLOREY

Academic Press is an imprint of Elsevier  
525 B Street, Suite 1900, San Diego, CA 92101-4495, USA  
225 Wyman Street, Waltham, MA 02451, USA  
32 Jamestown Road, London NW1 7BY, UK

First edition 2011

Copyright © 2011 Elsevier Inc. All rights reserved.

No part of this publication may be reproduced, stored in a retrieval system or transmitted in any form or by any means electronic, mechanical, photocopying, recording or otherwise without the prior written permission of the publisher

Permissions may be sought directly from Elsevier's Science & Technology Rights Department in Oxford, UK: phone (+44) (0) 1865 843830; fax (+44) (0) 1865 853333; email: [permissions@elsevier.com](mailto:permissions@elsevier.com). Alternatively you can submit your request online by visiting the Elsevier web site at <http://www.elsevier.com/locate/permissions>, and selecting, *Obtaining permission to use Elsevier material*

#### Notice

No responsibility is assumed by the publisher for any injury and/or damage to persons or property as a matter of products liability, negligence or otherwise, or from any use or operation of any methods, products, instructions or ideas contained in the material herein. Because of rapid advances in the medical sciences, in particular, independent verification of diagnoses and drug dosages should be made

ISBN: 978-0-12-387667-6

ISSN: 1871-5125 (Series)

For information on all Academic Press publications visit our website at <a href="http://elsevierdirect.com">elsevierdirect.com</a>
---

Printed and Bound in United States of America

11 12 13 14 10 9 8 7 6 5 4 3 2 1

Working together to grow  
libraries in developing countries

[www.elsevier.com](http://www.elsevier.com) | [www.bookaid.org](http://www.bookaid.org) | [www.sabre.org](http://www.sabre.org)

ELSEVIER

BOOK AID  
International

Sabre Foundation

## PREFACE TO VOLUME 36

The comprehensive profiling of drug substances and pharmaceutical excipients as to their physical and analytical characteristics remains essential to all phases of pharmaceutical development, and such profiles are of immeasurable importance to workers in the field. Consequently, the compilation and publication of comprehensive summaries of physical and chemical data, analytical methods, routes of compound preparation, degradation pathways, uses and applications, etc., have always been and will continue to be a vital function to both academia and industry.

As the science of pharmaceuticals grows and matures, the need for information similarly expands along new fronts, and this growth causes an equivalent growth in the repository sources where investigators find the information they need. The content of the *Profiles* series continues to respond and expand to meet this need, and so chapters are published that fall into one or more of the following main categories:

1. Comprehensive profiles of a drug substance or excipient
2. Physical characterization of a drug substance or excipient
3. Analytical methods for a drug substance or excipient
4. Detailed discussions of the clinical uses, pharmacology, pharmacokinetics, safety, or toxicity of a drug substance or excipient
5. Reviews of methodology useful for the characterization of drug substances or excipients
6. Annual reviews of areas of importance to pharmaceutical scientists

The current volume contains profiles on Buclizine, Chitin, Ezetimibe, Gemfloxacin, Glimepiride, Lornoxicam, Magnesium Silicate, and Tadalafil. The volume also contains a chapter reviewing the direct crystallization of enantiomers and dissociable diastereomers and a review of the literature published during 2009 that pertains to cocrystal systems having pharmaceutical interest.

As always, I welcome communications from anyone in the pharmaceutical community who might want to provide an opinion or a contribution.

Harry G. Brittain

Editor, Profiles of Drug Substances,  
Excipients, and Related Methodology

hbrittain@centerpharmphysics.com

# CHAPTER 1

## Buclizine

**Gamal A.E. Mostafa** and **Abdullah A. Al-Badr**

---

<b>Contents</b>	1. Description	2
	1.1. Nomenclature	2
	1.1.1. Systematical chemical names	2
	1.1.2. Nonproprietary names	2
	1.1.3. Proprietary names	2
	1.2. Formulae	2
	1.2.1. Empirical formula, molecular weight, and CAS number	3
	1.2.2. Structural formula	3
	1.3. Elemental analysis	3
	1.4. Appearance	3
	2. Uses and Application	3
	3. Methods of Preparation	4
	4. Physical Characteristics	6
	4.1. Solubility	6
	4.2. Melting range	6
	4.3. X-ray powder diffraction pattern	6
	4.4. Spectral properties	7
	4.4.1. UV/VIS spectroscopy	7
	4.4.2. Infrared spectrum	7
	4.4.3. Nuclear magnetic resonance spectrometry	7
	4.5. Mass spectrometry	11

Department of Pharmaceutical Chemistry, College of Pharmacy, King Saud University, Riyadh, Kingdom of Saudi Arabia



5. Methods of Analysis	12
5.1. Compendial methods	12
5.1.1. British pharmacopoeia methods [11]	12
5.2. Spectrophotometric methods	16
5.3. Potentiometric methods	18
5.4. Chromatographic methods	20
5.4.1. Thin layer chromatography	20
5.4.2. Gas chromatography	28
5.4.3. High-performance liquid chromatography	28
6. Stability	32
Acknowledgment	32
References	32

## 1. DESCRIPTION

### 1.1. Nomenclature

#### 1.1.1. Systematical chemical names

1-[(4-chlorophenyl)phenylmethyl]-4-[(4-*tert*-butylphenyl)methyl]piperazine;

1-(*p*-*tert*-butylbenzyl)-4-(*p*-chloro- $\alpha$ -phenylbenzyl)piperazine;

1-(*p*-chlorobenzhydryl)-4-(*p*-*tert*-butylbenzyl)diethylenediamine;

1-(*p*-*tert*-butylbenzyl)-4-(*p*-chlorodiphenylmethyl)piperazine;

(*RS*)-1-(4-*tert*-butylbenzyl)-4-(4-chlorobenzhydryl)piperazine dihydrochloride;

Piperazine, 1[(4-chlorophenyl)phenylmethyl]-4-[[4-(1,1-dimethylethyl)phenyl]methyl];

1-(*p*-chlorobenzhydryl)-4-(4-*tert*-butylbenzyl)-hexahydropyrazine;

1-[(4-chlorophenyl)phenylmethyl]-4-[(4-*tert*-butylphenyl)-methyl]piperazine [1–6].

#### 1.1.2. Nonproprietary names

Buclizine; Histabutyline; Histabutizine; NSC-25141; UCB 4445

#### 1.1.3. Proprietary names

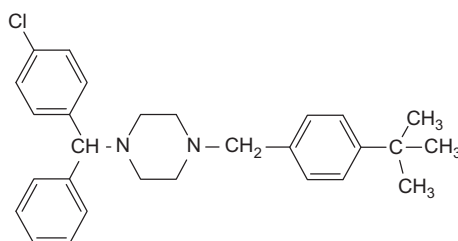
Aphilan, Bucladin-S, Buclifen, Buclina, Longifene, Posdel, Postadoxine, Postafen Postafeno, Softran, Vibazine [1–6].

## 1.2. Formulae

### 1.2.1. Empirical formula, molecular weight, and CAS number

Buclizine	$C_{28}H_{33}ClN_2$	433.0	82-95-1
Buclizine·2HCl	$C_{28}H_{35}Cl_3N_2$	506.0	129-74-8

### 1.2.2. Structural formula



## 1.3. Elemental analysis

- Buclizine: C 77.66%, H 7.68%, Cl 8.19%, N 6.47% [1].
- Buclizine HCl: C 66.47%, H 6.97%, Cl 21.02%, N 5.54% [1].

## 1.4. Appearance

A white or slightly yellowish, crystalline powder, odorless and tasteless [5,6].

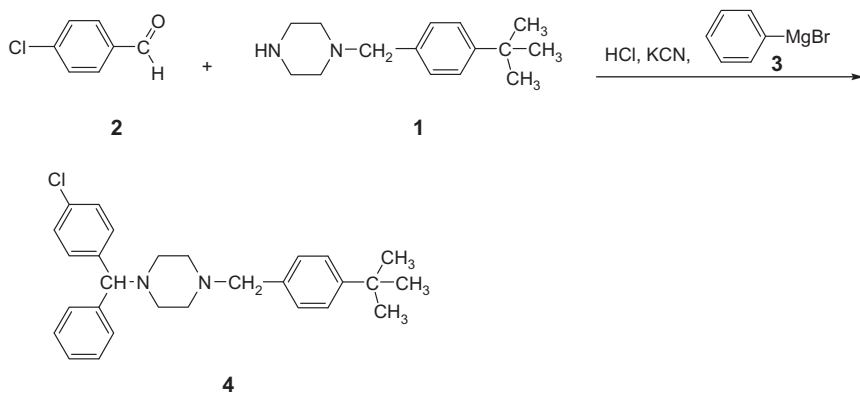
## 2. USES AND APPLICATION

Buclizine hydrochloride, a piperazine derivative, is a sedating antihistamine with antimuscarinic and moderate sedative action. The drug is used mainly for its antiemetic action, particularly in the prevention of motion sickness, and in the treatment of migraine in combination with analgesics. In some countries, it is given in the management of allergic conditions and in the pruritic skin disorders. Buclizine has also been used in the treatment of vertigo associated with disorders of vestibular system, although its value in these conditions remains to be established [2–6].

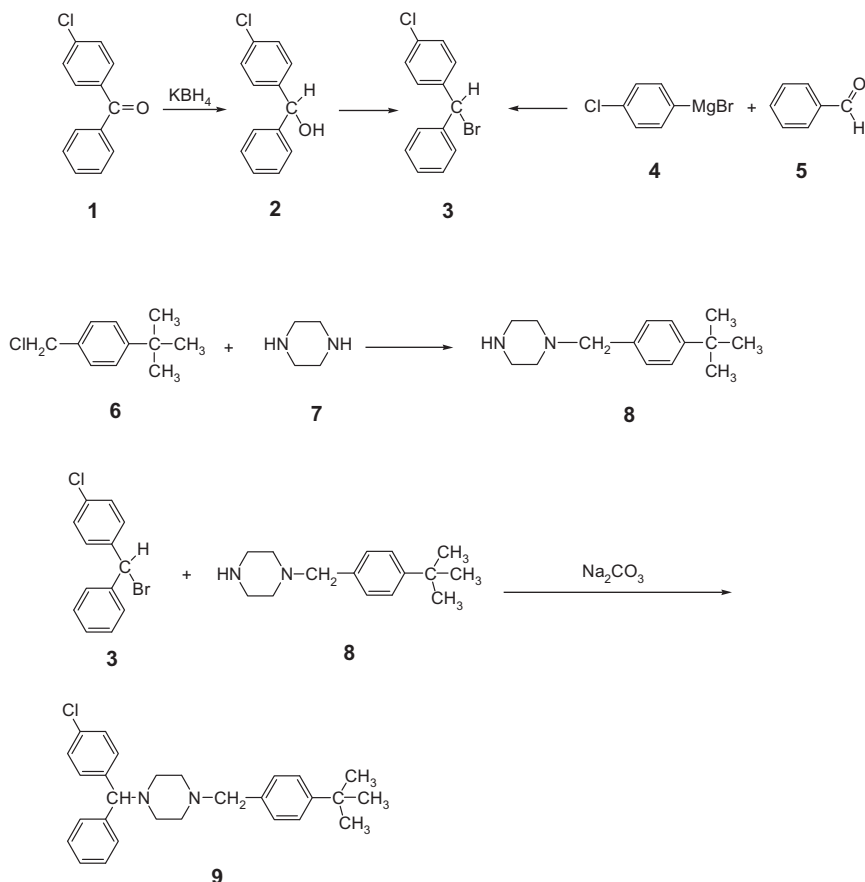
To prevent motion sickness, the drug is given at least 30 min before travelling in a dose of 50 mg by mouth which may be repeated, if necessary, after 4–6 h. The usual dose to alleviate nausea is 50 mg given up to three times daily. In the treatment of migraine, the drug is given in usual doses of 12.5 mg at the start of an attack or when one is known to be imminent. In pruritic skin disorders, the usual dose of buclizine hydrochloride is 25–50 mg daily [2–5]. The drug has an antihistaminic [2], antimycobactrium [3], anticonvulsant [4], and motion sickness prevention activities [5].

### 3. METHODS OF PREPARATION

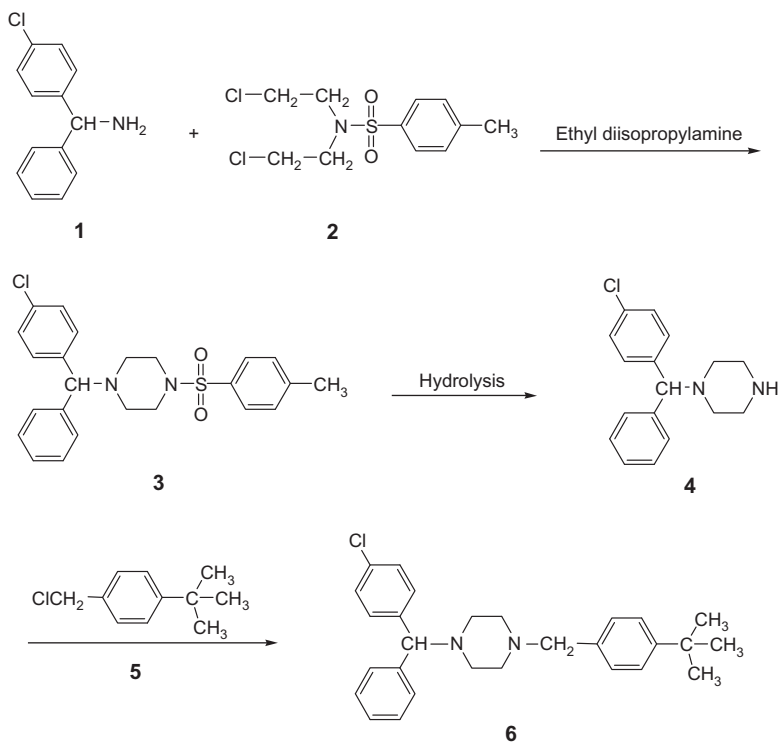
Morren and Strubbe [7] prepared buclizine by mixing hydrochloric acid with 0.5 mol of 1-(*p*-*tert*-butylbenzyl)-piperazine **1**, adding 0.5 mol *p*-chlorobenzaldehyde **2**, and adding dropwise aqueous 0.55 M potassium cyanide, then heating on a water bath for 2 h, yields an addition product which is separated in toluene and dried before reaction with phenylmagnesium bromide **3** to give buclizine **4**.



Lui *et al.* [8] prepared buclizine by reducing *p*-chlorophenyl phenyl ketone **1** with potassium borohydride to *p*-chlorobenzhydriol **2**, which was converted into *p*-chlorobenzhydriol bromide **3**. The latter compound **3** was prepared by reaction of *p*-chlorophenylmagnesium bromide **4** with benzaldehyde **5**. *p*-*tert*-Butylbenzyl chloride **6** was condensed directly with piperazine **7** to give *p*-*tert*-butylbenzylpiperazine **8**. Treatment of *p*-chlorobenzhydriol bromide **3** with *p*-*tert*-butylbenzylpiperazine **8** in the presence of anhydrous sodium carbonate gave buclizine **9** hydrochloride.



Cossement *et al.* [9] synthesized the enantiomers of 1-(*p*-chlorobenzhydryl)-4-(*p*-methylphenyl)sulfonyl piperazine **3** and used it as an intermediate for the preparation of buclizine **6** and other histamines. The enantiomers of (+)- and (–)-1-(*p*-chlorobenzhydryl)-4-(*p*-toluene sulfonyl)piperazine **3** were prepared and converted by hydrolysis to the enantiomers of (+)- or (–)- *p*-chlorobenzhydryl piperazine **4**. Compound **3** was prepared by refluxing *p*-chlorobenzhydrylamine **1** with *N*-bis-2-chloroethyl-*p*-toluene sulfonamide **2** with ethyl diisopropylamine. Reaction of *p*-*tert*-butylbenzyl chloride **5** with *p*-chlorobenzhydryl piperazine **4** gives buclizine **6**.



## 4. PHYSICAL CHARACTERISTICS

### 4.1. Solubility

Practically insoluble in water; sparingly soluble in chloroform and in propane-1, 2-diol; very slightly soluble in ethanol (96%) [5].

### 4.2. Melting range

230–240 °C.

### 4.3. X-ray powder diffraction pattern

X-ray powder diffraction pattern (Fig. 1.1) has been obtained on D 8-Advanced Bruker AXE Germany, diffractometer equipped with scintillation detector using copper Ka ( $=1.5406 \text{ \AA}$ ) radiation with scanning range between  $2\theta$  and  $50\theta$  at scanning speed of  $2^\circ \text{ min}^{-1}$ . A full data summary is compiled in Table 1.1.

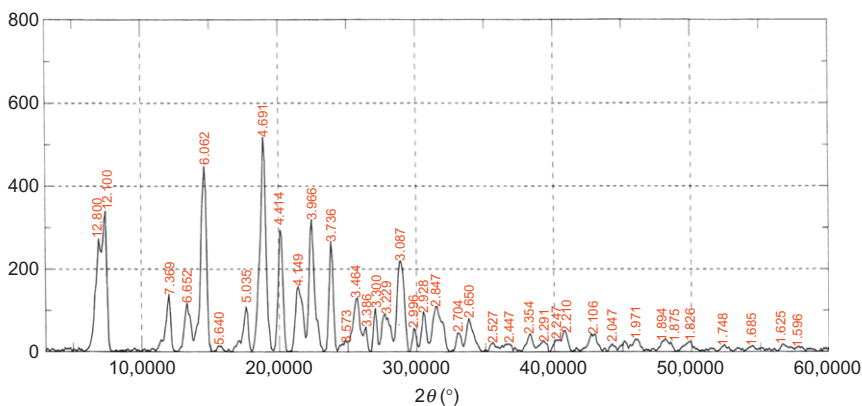


**FIGURE 1.1** X-ray powder diffraction pattern of buclizine hydrochloride.

## 4.4. Spectral properties

### 4.4.1. UV/VIS spectroscopy

The ultraviolet absorption spectrum of buclizine in methanol was scanned from 200 to 400 nm, using UV/VIS spectrometer (Shimadzu Ultraviolet-visible spectrophotometer 1601 PC) and is shown in Fig. 1.2. The compound exhibited two maxima at 230 and 209 nm. Clarke [10] reported the following: methanol 255, 260 nm.

### 4.4.2. Infrared spectrum

The infrared absorption spectrum of buclizine (Fig. 1.3) was obtained in KBr pellet using a Perkin-Elmer infrared spectrophotometer. The principle peaks were observed at 3051, 2961, 1093, 1604, 1312, and 1071  $\text{cm}^{-1}$ . Assignments for the major infrared absorption band are provided in Table 1.2. Clarke [10] reported principal peaks at 1002, 1131, 754, 800, 1075, and 694  $\text{cm}^{-1}$ .

### 4.4.3. Nuclear magnetic resonance spectrometry

$^1\text{H}$  and  $^{13}\text{C}$  NMR spectra of buclizine were recorded with a Varian Gemini 200 spectrometer (200 MHz). Chemical shifts were expressed in parts per million with respect to the tetramethylsilane (TMS) signal for  $^1\text{H}$  and  $^{13}\text{C}$  NMR.

**4.4.3.1.  $^1\text{H}$  NMR spectrum** The one-dimensional proton  $^1\text{H}$  NMR spectrum of buclizine base dissolved in  $\text{CDCl}_3$  is shown in Figs. 1.4 and 1.5. The corresponding spectral assignments  $^1\text{H}$  NMR for buclizine are provided in Table 1.3.

**TABLE 1.1** Data deduced from X-ray powder diffraction pattern of buclizine

Peak no.	Diffraction angel ( $2\theta$ )	Flex width	$d$ -value	Intensity	$I/I_0$
1	6.9	0.353	12.8002	273	53
2	7.300	0.353	12.0996	321	62
3	12.0	0.353	7.3691	139	27
4	13.3	0.706	6.6516	118	23
5	14.6	0.471	6.0621	447	87
6	15.7	0.471	5.6398	13	3
7	17.6	0.353	5.0350	108	21
8	18.9	0.353	4.6915	518	100
9	20.1	0.471	4.4140	295	57
10	21.4	0.706	4.1487	159	31
11	22.4	0.471	3.9657	320	62
12	23.8	0.353	3.7355	267	52
13	24.9	0.353	3.5729	23	5
14	25.7	0.471	3.4635	131	26
15	26.3	0.353	3.3858	60	12
16	27.0	0.353	0.353	105	21
17	27.6	0.471	0.471	86	17
18	28.9	0.706	0.706	216	42
19	29.8	0.353	0.353	57	12
20	30.5	0.353	0.353	97	19
21	31.4	0.588	2.8466	109	22
22	33.1	0.471	2.7041	45	9
23	33.8	0.35	2.6497	81	16
24	35.5	0.471	2.5266	22	5
25	36.7	0.471	2.4467	19	4
26	38.2	0.471	2.3540	42	9
27	39.3	0.588	2.2906	24	5
28	40.1	0.588	2.2468	28	6
29	40.8	0.353	2.2098	51	10
30	42.9	0.588	2.1064	41	8
31	44.2	0.471	2.0474	18	4
32	46.0	0.588	1.9714	28	6
33	48.0	0.588	1.8938	26	5
34	48.5	0.353	1.8754	23	5
35	49.9	0.471	1.8261	25	5
36	52.3	0.353	1.7478	14	3
37	54.4	0.588	1.6852	13	3
38	56.6	0.471	1.6248	18	4
39	57.7	0.588	1.5964	10	3
40	60.6	0.353	1.5267	11	3
41	62.5	0.471	1.4848	11	3
42	65.0	0.353	1.4336	11	3

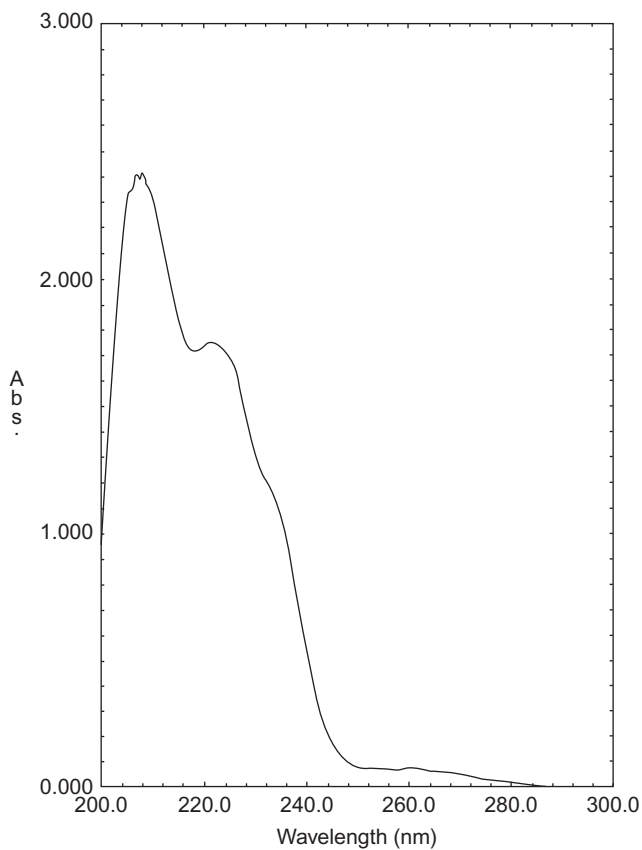


FIGURE 1.2 Ultraviolet spectrum of buclizine hydrochloride.

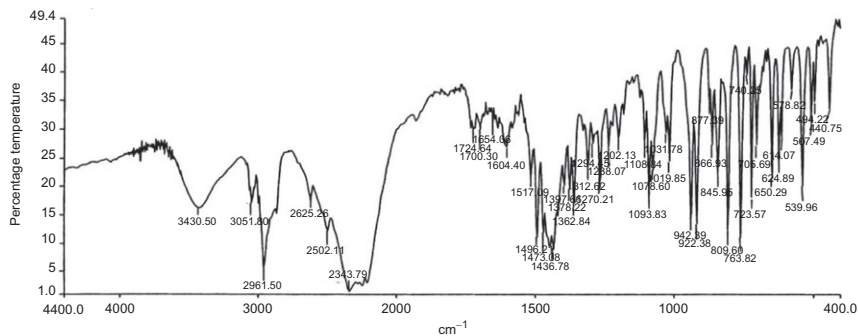
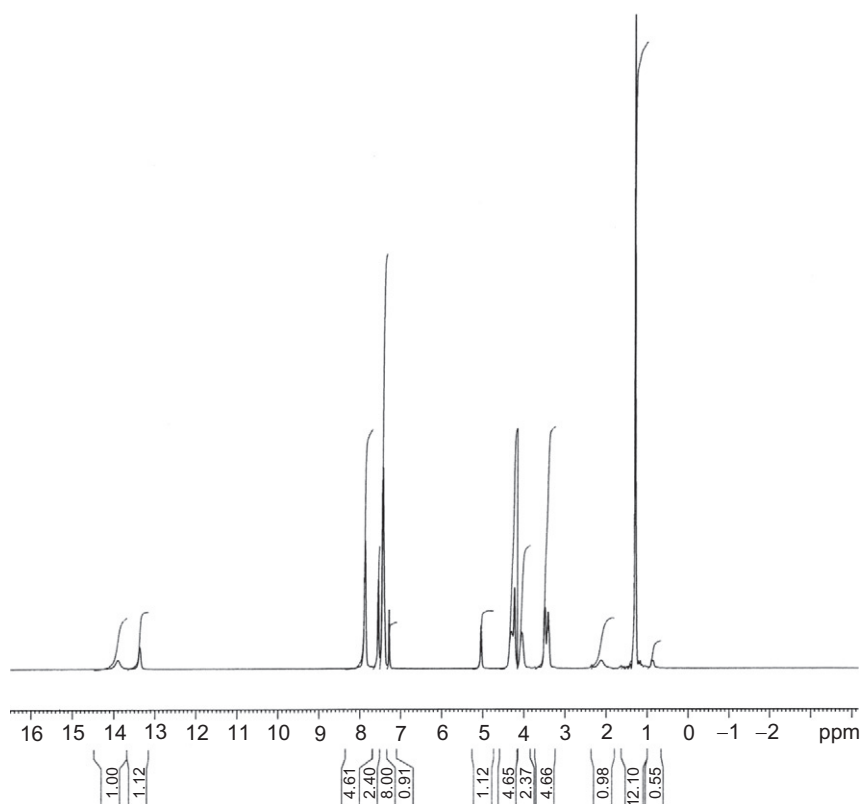


FIGURE 1.3 The IR spectrum of buclizine hydrochloride.

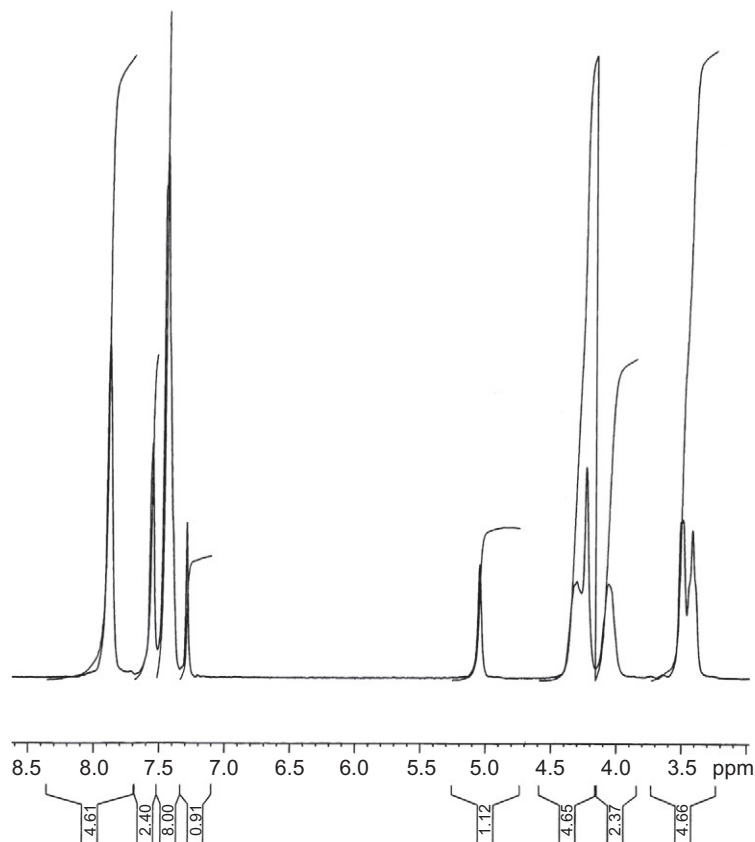


**TABLE 1.2** Vibrational assignments for buclizine infrared absorption bands

Frequency (cm <sup>-1</sup> )	Assignment
3051	Aromatic CH
2961	Aliphatic CH
1093	C–C
1604	C=C
1312	C–N
1111	C–Cl

**FIGURE 1.4** <sup>1</sup>H NMR spectrum of buclizine in CDCl<sub>3</sub>.

**4.4.3.2. <sup>13</sup>C NMR spectrum** The one-dimensional <sup>13</sup>C NMR spectrum of buclizine dissolved in CDCl<sub>3</sub>, which was recorded at 24 °C and internally referenced to TMS. The <sup>13</sup>C NMR assignments are presented in

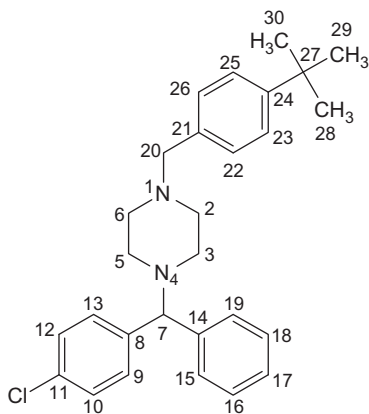


**FIGURE 1.5** Expanded  $^1\text{H}$  NMR spectrum of buclizine in  $\text{CDCl}_3$ .

[Figs. 1.6–1.8](#). The assignments for the observed resonance bands associated with the various carbons are listed in [Table 1.4](#). [Figures 1.9–1.15](#) show the HSQC, HMBC, DEPT 90 and DEPT 135 NMR spectra, respectively.

#### 4.5. Mass spectrometry

Mass spectra of buclizine, carried out with electron impact method, were registered using Varian 320-GC/MS spectrometer. [Figure 1.16](#) shows the detailed mass fragmentation pattern and [Table 1.5](#) shows the mass fragmentation pattern of the drug substance. Clarke [10] reported the presence of the following principle peaks at  $m/z = 231, 147, 285, 232, 201, 132, 165$ , and 166.

**TABLE 1.3** Assignment of the resonance bands in the  $^1\text{H}$  NMR spectrum of buclizine

Chemical shift (ppm, relative to TMS)	Number of protons	Multiplicity	Assignment (proton at carbon atom)
1.17, 1.21, 1.30	9	3s	28, 29, 30
2.12–2.47	8	m	2, 3, 5, 6
3.64	2	d	20
7.20–8.06	13	m	9, 10, 12, 13, 15, 16, 17, 18, 19, 22, 23, 25, 26

s, singlet; d, doublet; m, multiplet.

## 5. METHODS OF ANALYSIS

### 5.1. Compendial methods

#### 5.1.1. British pharmacopoeia methods [11]

Bucizine hydrochloride is (RS)-1-(4-*tert*-butylbenzyl)-4-(4-chlorobenzhydryl)piperazine dihydrochloride. It contains not less than 99% and not more than 100.5% of  $\text{C}_{28}\text{H}_{33}\text{ClN}_2 \cdot 2\text{HCl}$ , calculated with reference to the dried substance. It is a histamine H-receptor antagonist and antiemetic.

**5.1.1.1. Characteristics** A white or slightly yellowish, crystalline powder. Practically insoluble in water, sparingly soluble in *chloroform* and in *propan-1,2-diol*, very slightly soluble in *ethanol* (96%).

#### 5.1.1.2. Identification

**Test A:** The infrared absorption spectrum, Appendix IIA, is concordant with the reference spectrum of buclizine hydrochloride (RS O32).

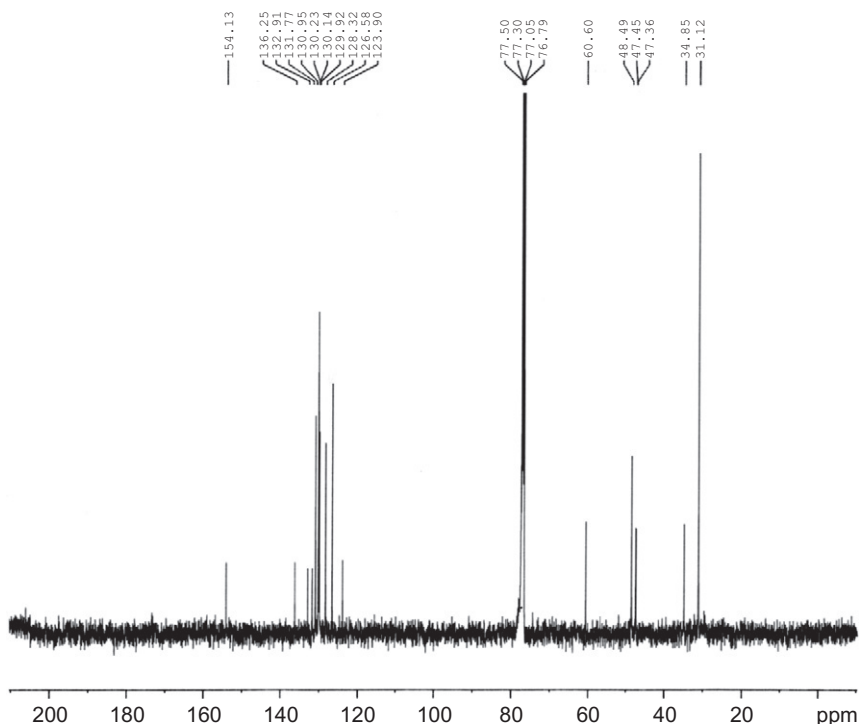


**FIGURE 1.6**  $^{13}\text{C}$  NMR spectrum of buclizine in  $\text{CDCl}_3$ .

*Test B:* A 0.25% (w/v) solution in *ethanol* (50%) yields solution A characteristic of *chlorides*, Appendix VI.

### 5.1.1.3. Tests

- *Related substances*

Carry out the method for *liquid chromatography*, Appendix IIID, using four solutions in the initial mobile phase containing (1) 0.001% (w/v) of buclizine hydrochloride; (2) 0.50% (w/v) of buclizine hydrochloride; (3) 0.001% (w/v) of 1,4-bis(4-chlorobenzhydryl)piperazine BPCRS; and (4) 0.50% (w/v) of buclizine hydrochloride impurity standard BPCRS.

The chromatographic procedure may be carried out using a stainless steel column (20 cm  $\times$  4 cm) packed with *octadecylsilyl silica gel* for *chromatography* (10  $\mu\text{m}$ ) (Nucleosil,  $\text{C}_{18}$  is suitable). Use as the initial mobile phase 0.01 M *sodium heptane sulfonate* in a mixture of 55 volumes of *water* and 45 volumes of *acetonitrile* and as the final mobile phase 0.01 M *sodium*

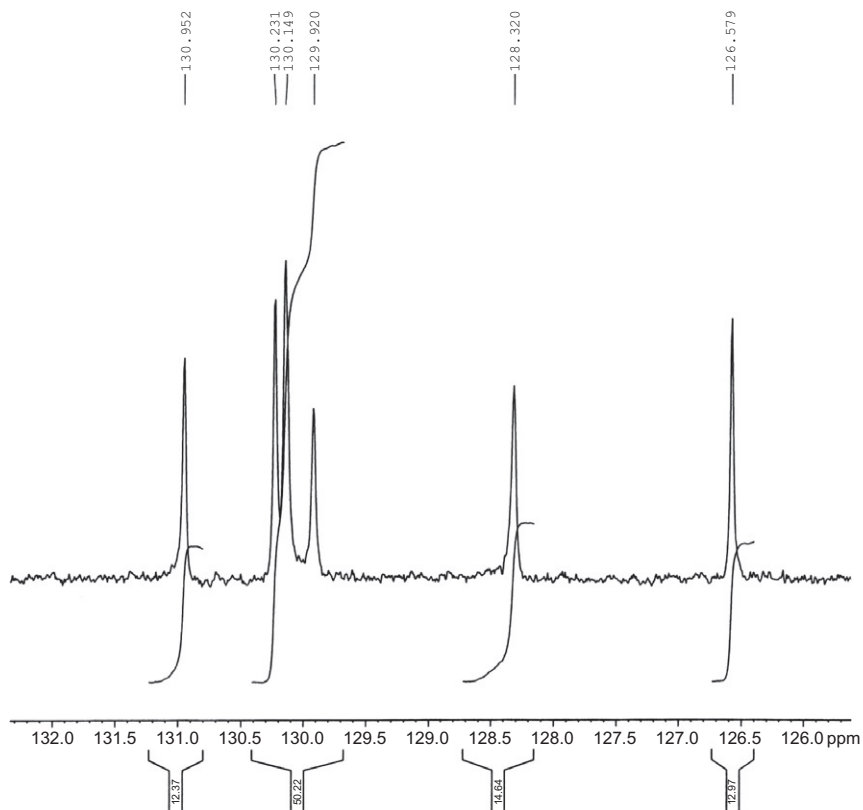


**FIGURE 1.7** Expanded  $^{13}\text{C}$  NMR spectrum of buclizine in  $\text{CDCl}_3$ .

heptanesulfonate in a mixture of 20 volumes of *water* and 80 volumes of *acetonitrile*. Before use, adjust the pH of both the initial and final mobile phases to 4 with 1 M *orthophosphoric acid*. Carry out a linear gradient elution with a flow rate of 2 ml/min for 30 min and maintain the final mobile phase for 10 min with the same flow rate. Use a detection wavelength of 230 nm.

The test is not valid unless the chromatogram obtained with solution (4) closely resembles the chromatogram supplied with buclizine hydrochloride impurity standard BPCRS.

In the chromatogram obtained with solution (2) the area of any peak corresponding to 1,4-bis-(4-chlorobenzylhydrazide)piperazine is not greater than the area of the peak obtained in the chromatogram with solution (3) and the area of any other *secondary* is not greater than the area of the peak in the chromatogram obtained with solution (1).

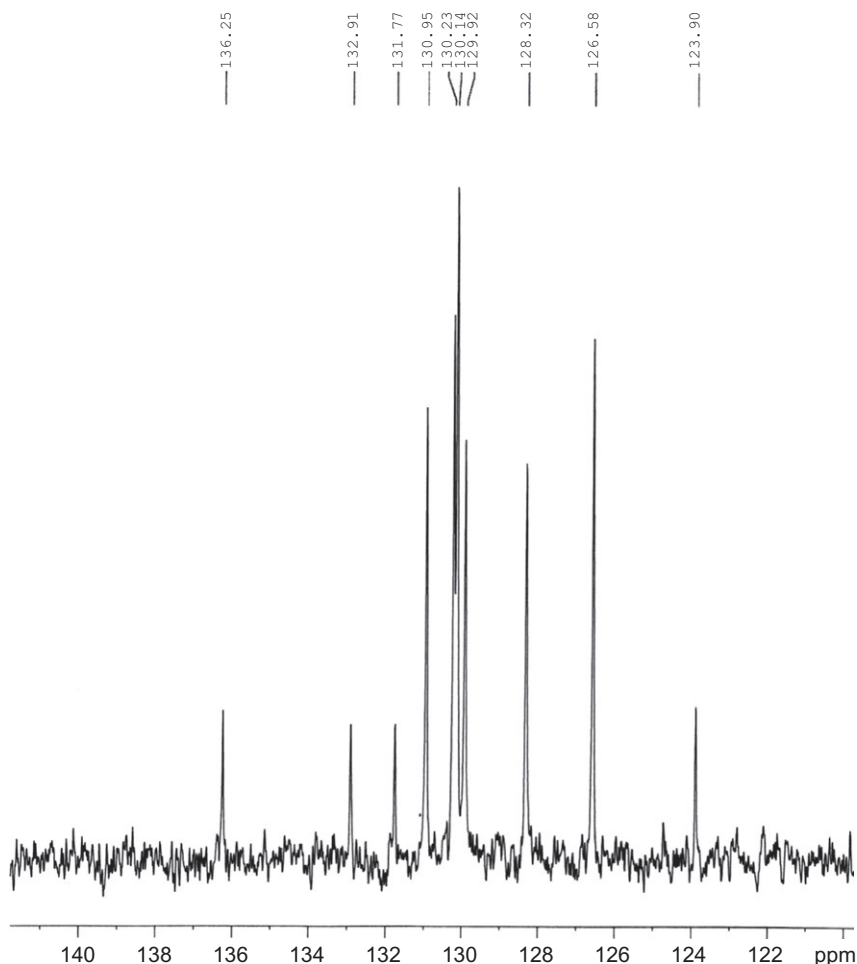


**FIGURE 1.8** Expanded  $^{13}\text{C}$  NMR spectrum of buclizine in  $\text{CDCl}_3$ .

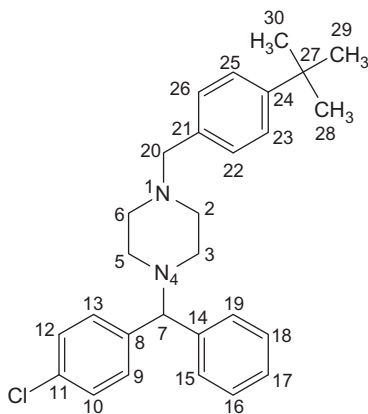
- *Loss on drying*

When dried to constant weight at 100–105 °C, loses not more than 1% of its weight. Use 1 g.

- *Sulfate ash*

Not more than 0.1, Appendix IXA.

**5.1.1.4. Assay** Carry out Method 1 for *nonaqueous titration*, Appendix VIIIA, using 0.4 g and determining the end-point potentiometrically. Each milliliter of 0.1 M *perchloric acid VS* is equivalent to 25.3 mg of  $\text{C}_{28}\text{H}_{33}\text{ClN}_2 \cdot 2\text{HCl}$ .

**TABLE 1.4** Assignment for the resonance bands in the  $^{13}\text{C}$  NMR spectrum of buclizine

Chemical shift (ppm)	Carbon number
31.0	28, 29, 30
34.85	27
47.36	3,5
47.45	2,6
48.49	20
60.6	7
123.90	23, 25
126.58	17
129.92	22, 26
128.32	15, 19
130.14	16,18
130.23	9, 13, 10, 12
130.95	11
131.77	21
132.91	8
136.25	14
154.13	24

#### 5.1.1.5. Impurities

- A. 1,4-bis-(4-chlorobenzyl)piperazine.  
 B. 4-chlorobenzylol, 1-(4-chlorobenzyl)piperazine, 4-chlorobenzophenone.

## 5.2. Spectrophotometric methods

Pregmollato and Pissalto [12] presented methods for the determination of buclizine dihydrochloride by titration with perchloric acid, using a crystal violet indicator; by thin-layer chromatography with subsequent

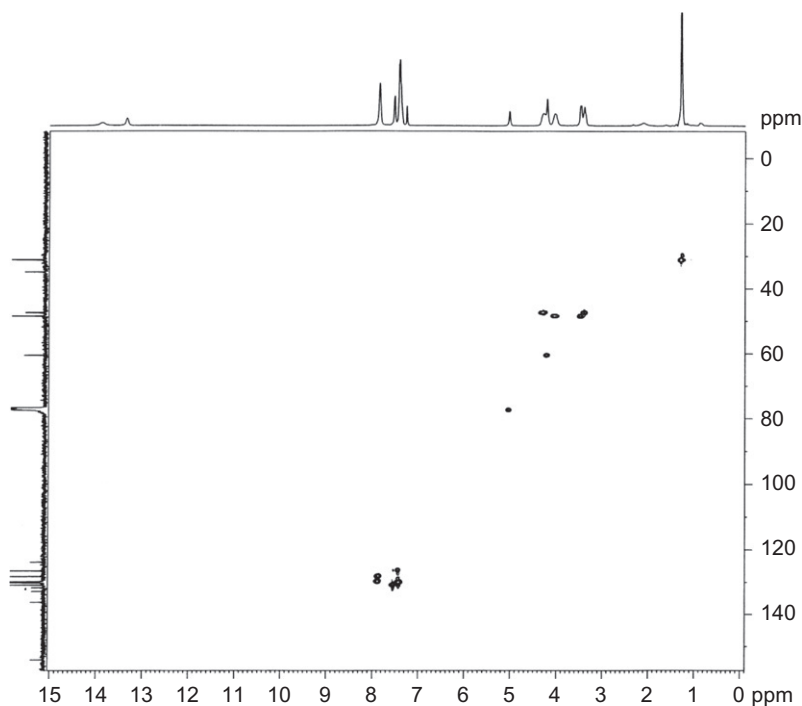


**FIGURE 1.9** The HSQC NMR spectrum of buclizine in  $\text{CDCl}_3$ .

spectrophotometric determination at 239 nm (in chloroform) or 274 nm (in benzene); and by infrared spectrophotometric determination of buclizine dihydrochloride formulations. Spectral absorption data for the drugs are also given.

Annappurna *et al.* [13] established simple, accurate, and reproducible UV spectrophotometric methods for the assay of buclizine based on the formation of precipitation, charge transfer, and redox products. Precipitation/charge transfer complex formation of the buclizine with  $\text{I}_2$ /*p*-nitro methyl amino phenol sulfate-sulfanilic acid by method A, the precipitation/complex formation with ammonium molybdate/potassium thiocyanate by method B and precipitation/redox reaction of buclizine with phosphomolybdic acid/ $\text{Co}^{2+}$ /EDTA by method C were proposed. Determination of buclizine in bulk form and in pharmaceutical formulations was also incorporated.

El-Walily *et al.* [14] described a simple and sensitive spectrophotometric method for the determination of buclizine in bulk and tablets was based on the formation of charge-transfer complex between buclizine as n-donor and iodine as  $\sigma$ -acceptor measurement of the absorbance at 295 and 355 nm. A Job's plot indicated a 1:1 complex between the drug and iodine,



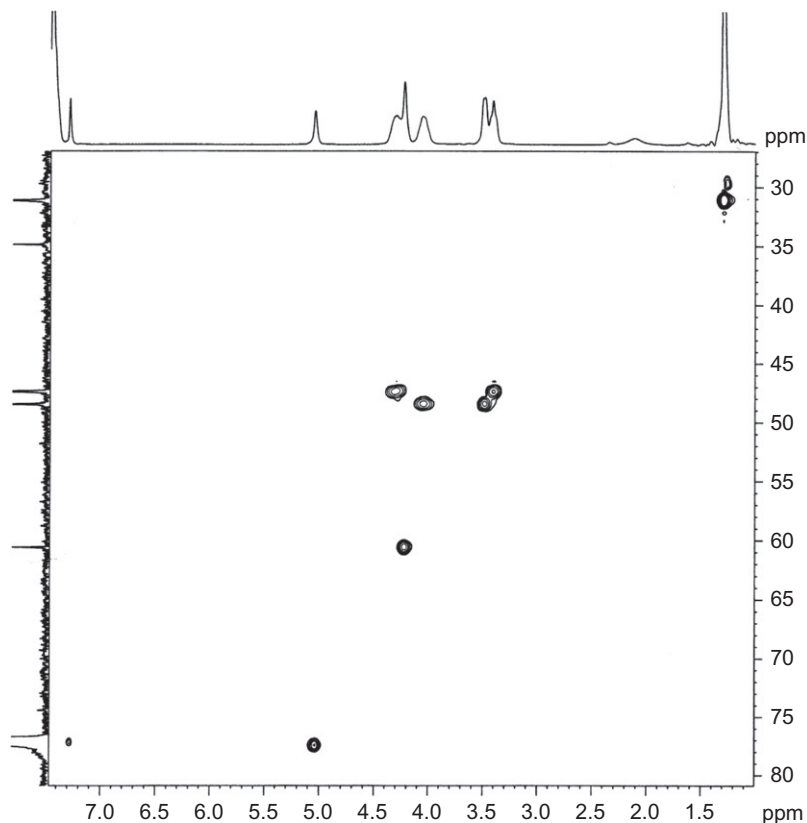


**FIGURE 1.10** The expanded HSQC NMR spectrum of buclizine in  $\text{CDCl}_3$ .

and Beer's law was obeyed in the concentration range of 4–30  $\mu\text{g/ml}$ . To validate the method, the results obtained were compared statistically with a newly developed UV-derivative spectrophotometric method. The charge-transfer method was favored due to its higher sensitivity.

### 5.3. Potentiometric methods

Zakkari *et al.* [15] described a potentiometric nonaqueous titration of buclizine and other halides of nitrogen bases using bismuth oxyacetate and perchloric acid or trifluoromethylsulfonic acid. Samples of buclizine and the other bases were dissolved in anhydrous acetic acid with heating if necessary and treated with a 2% solution of bismuth oxyacetate in anhydrous acetic acid. The mixture was stirred until any precipitation formed re-dissolved, then titrated potentiometrically with

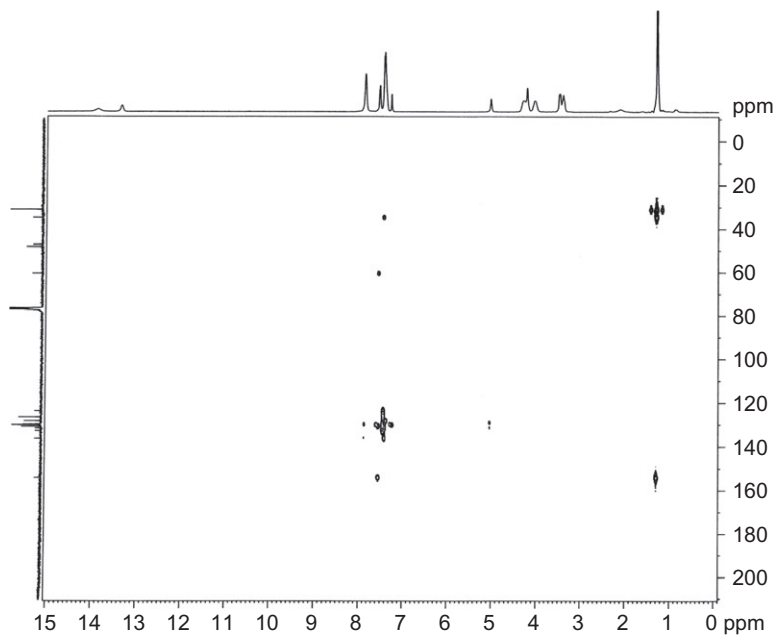


**FIGURE 1.11** The HMBC NMR spectrum of buclizine in  $\text{CDCl}_3$ .

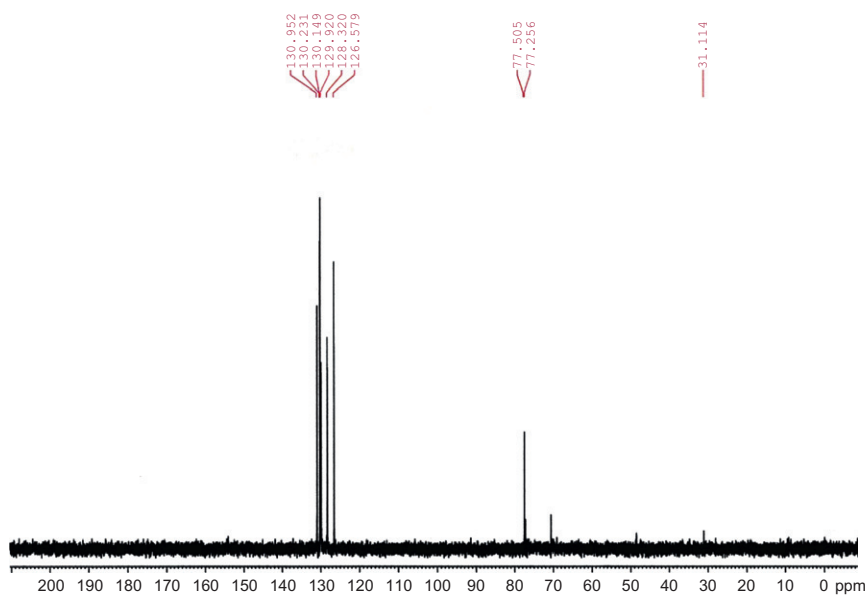


**FIGURE 1.12** DEPT 90 NMR of buclizine in  $\text{CDCl}_3$ .

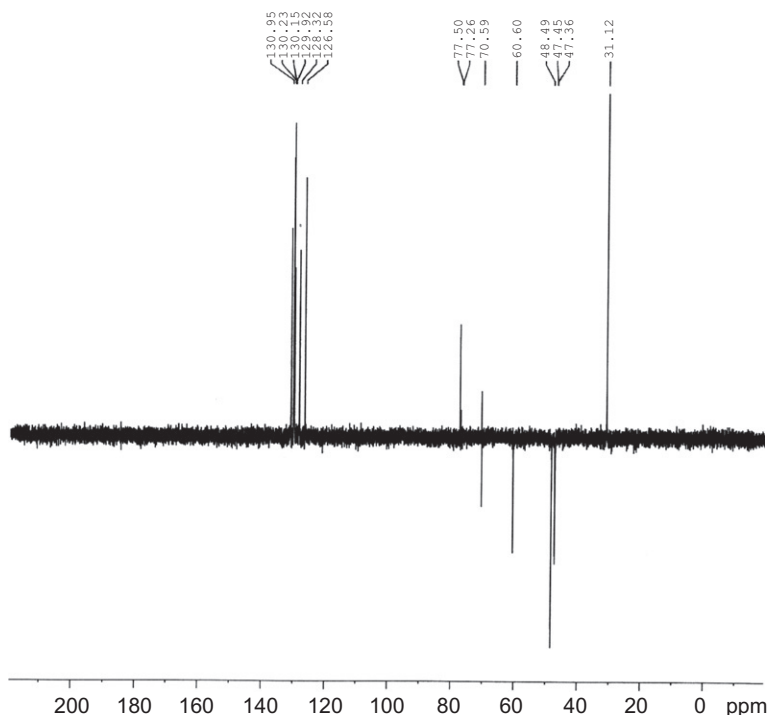


**FIGURE 1.13** The DEPT 135  $^{13}\text{C}$  NMR of buclizine in  $\text{CDCl}_3$ .

0.1 N-trifluoromethyl sulfonic acid. The end-point was detected with use of glass Ag/AgCl combination electrode. Results compared well with those obtained using perchloric acid as titrant. The coefficient of variation were  $\leq 0.42\%$  and recoveries were  $>99\%$ .

## 5.4. Chromatographic methods

### 5.4.1. Thin layer chromatography

Tang [16] described an improved method for thin layer chromatographic identification of compound buclizine. Compound buclizine contains mainly buclizine hydrochloride, bromhexine hydrochloride, and promethazine hydrochloride. A 20 ml portion of sample solution was made alkaline with 0.05 M sodium hydroxide (2.5 ml) and extracted with chloroform (5 ml). Standard solution of buclizine hydrochloride, bromhexine, hydrochloride, and promethazine together or separately were similarly prepared. The chloroform solution were spotted on to Silica gel G plates (previously treated with 0.5% sodium hydroxymethylcellulose solution and activated at  $100^\circ\text{C}$  for 1 h) with chloroform:methanol:

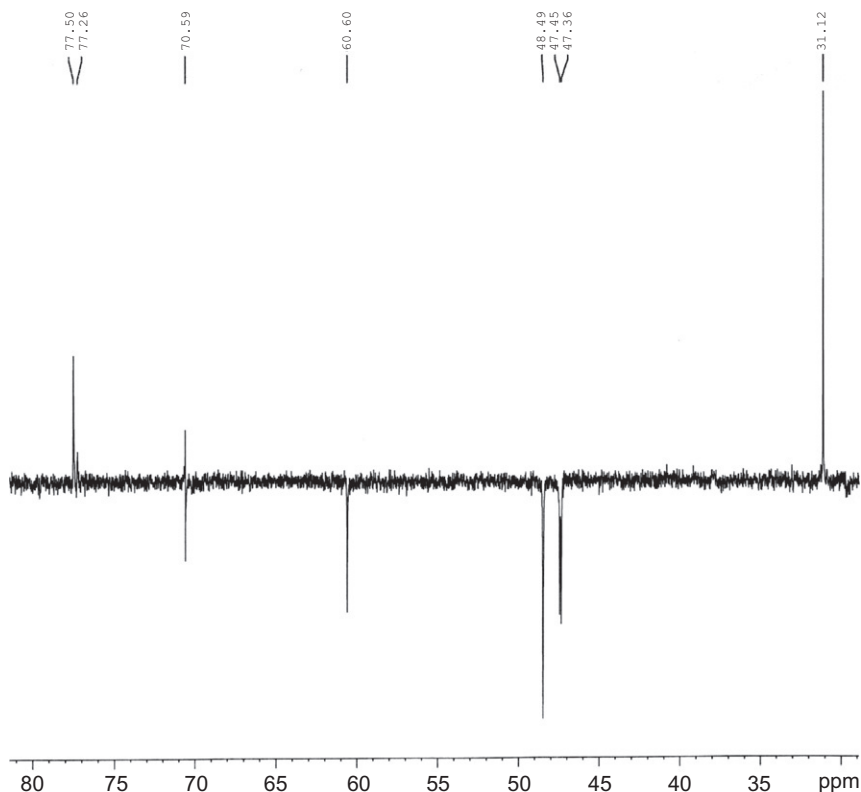


**FIGURE 1.14** The expanded DEPT  $^{13}\text{C}$  NMR of buclizine in  $\text{CDCl}_3$ .

dimethylformamide (20:2:1) as mobile phase. Visualization was performed in iodine vapor. Results were satisfactory. The method is simple and has good reproducibility.

Clarke [10] reported the following thin layer chromatography systems.

*Plates:* Silica gel G, 250  $\mu\text{m}$  thick, dipped in or sprayed with 0.1 M potassium hydroxide in methanol, and dried.

*Mobile phase:* Methanol:strong ammonia solution (100:1.5).

*Reference compounds:* Atropine  $R_f$  18, Codeine  $R_f$  33, Chlorprothexaine  $R_f$  56, Diazepam  $R_f$  75.

$R_f = 75$  [17,18].

*Plates:* Silica gel G, 250  $\mu\text{m}$  thick, dipped in or sprayed with 0.1 M potassium hydroxide in methanol, and dried.

*Mobile phase:* Cyclohexane:toluene:diethylamine (75:15:10).

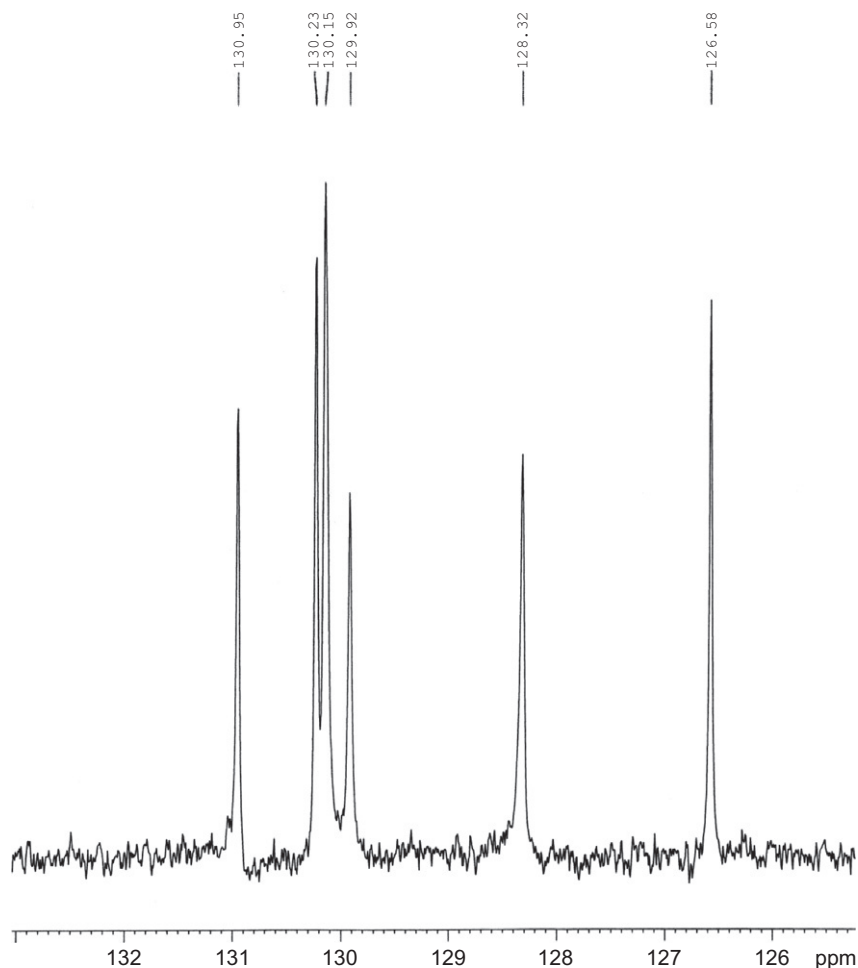


**FIGURE 1.15** The expanded DEPT 135  $^{13}\text{C}$  NMR of buclizine in  $\text{CDCl}_3$ .

*Reference compounds:* Codeine  $R_f$  06, Desipramine  $R_f$  20, Prazepam  $R_f$  36, and Trimipramine  $R_f$  62.

$R_f = 61$  [17,18].

*Plates:* Silica gel G, 250  $\mu\text{m}$  thick, dipped in or sprayed with 0.1 M potassium hydroxide in methanol, and dried.

*Mobile phase:* Chloroform: methanol (90:10).

*Reference compounds:* Desipramine  $R_f$  11, Physostigmine  $R_f$  36, Trimipramine  $R_f$  54, and Lidocaine  $R_f$  71.

$R_f = 83$  [18,19].

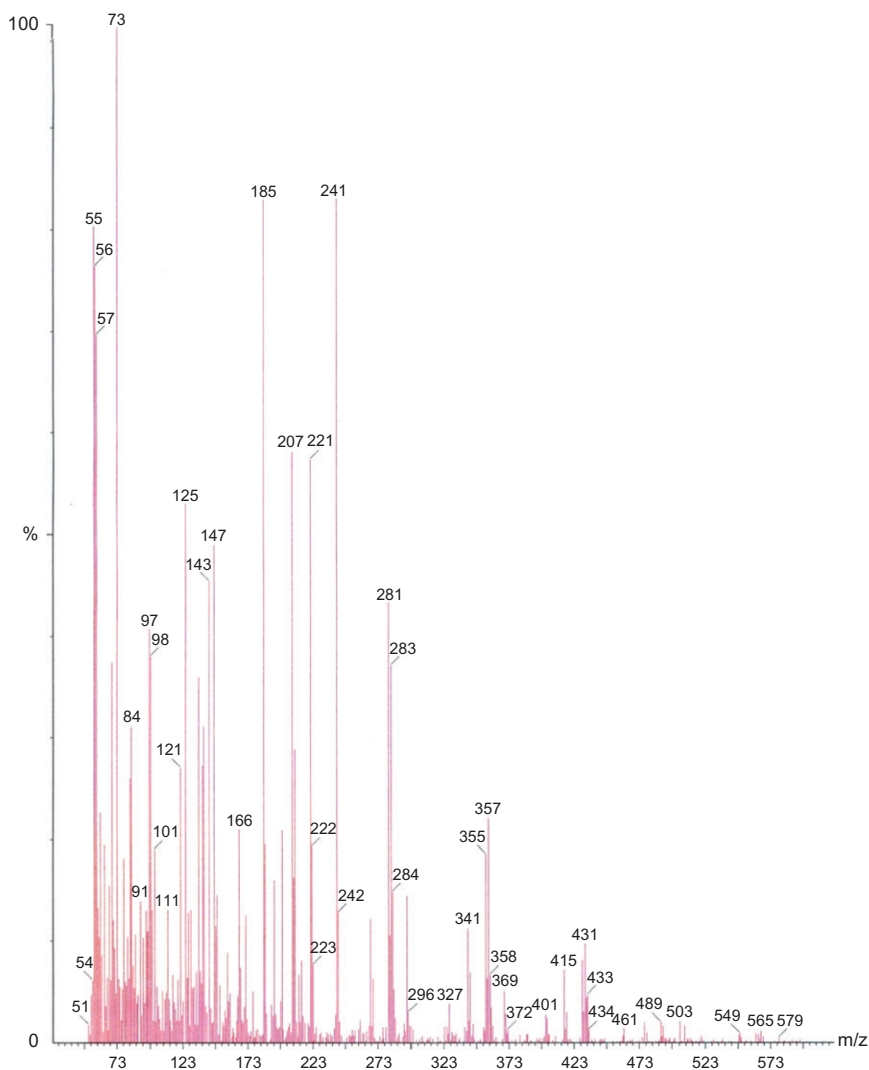


**FIGURE 1.16** Mass spectrum of buclizine hydrochloride.

*Plates:* Silica gel G, 25  $\mu\text{m}$  thick, dipped in or sprayed with 0.1 M potassium hydroxide in methanol, and dried.

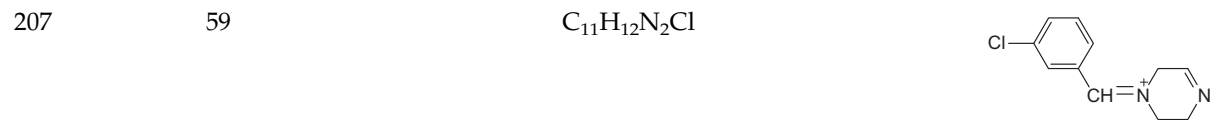
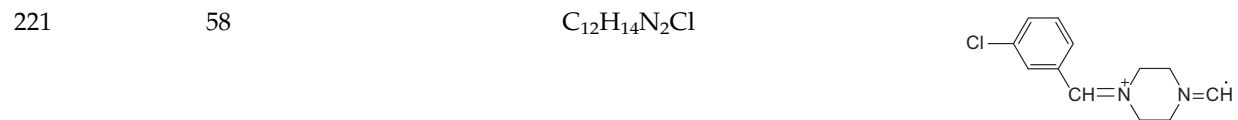
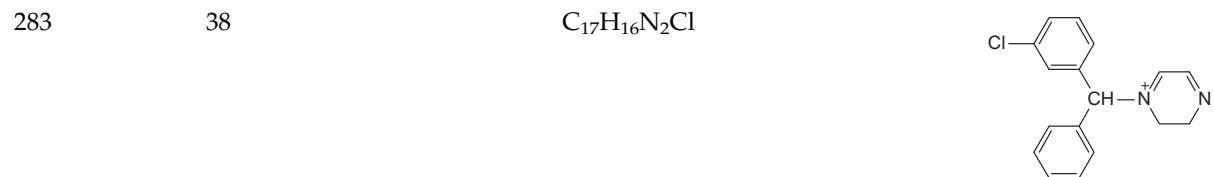
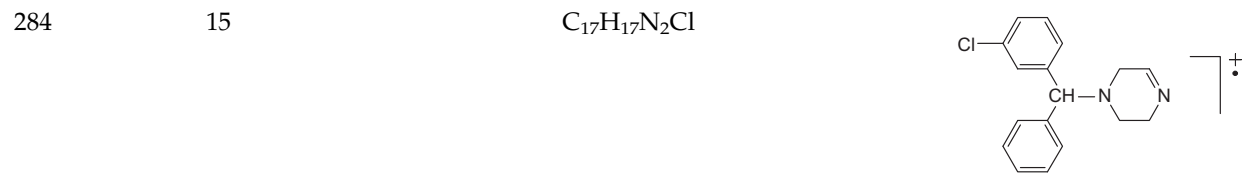
*Mobile phase:* Acetone.

*Reference compounds:* Amitriptyline  $R_f$  15, Procaine  $R_f$  30, Papaverine  $R_f$  47, and Cinnarizine  $R_f$  65.

$R_f = 72$  (acidified iodoplatinated solution: positive) [17,18].

**TABLE 1.5** Mass spectral fragmentation pattern of buclizine

<i>m/z</i>	Relative intensity (%)	Fragment	
		Formula	Structure
433	5	$C_{28}H_{33}N_2Cl$	
355	18	$C_{22}H_{28}N_2Cl$	
341	13	$C_{21}H_{26}N_2Cl$	
285	5	$C_{17}H_{18}N_2Cl$	

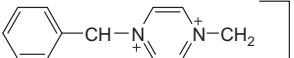
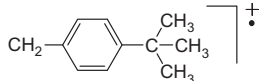
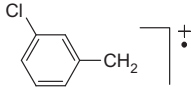
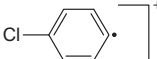
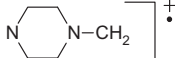



---

(continued)

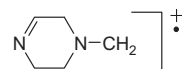


**TABLE 1.5** (continued)

<i>m/z</i>	Relative intensity (%)	Fragment	
		Formula	Structure
185	85	C <sub>12</sub> H <sub>13</sub> N <sub>2</sub>	
147	49	C <sub>11</sub> H <sub>15</sub>	
125	55	C <sub>7</sub> H <sub>6</sub> Cl	
111	15	C <sub>6</sub> H <sub>4</sub> Cl	
98	38	C <sub>5</sub> H <sub>10</sub> N <sub>2</sub>	

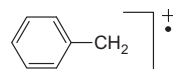
97

40

 $C_5H_9N_2$ 

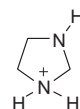
91

14

 $C_7H_7$ 

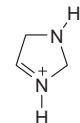
73

100

 $C_3H_9N_2$ 

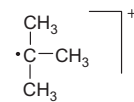
71

38

 $C_3H_7N_2$ 

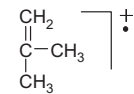
57

72

 $C_4H_9$ 

56

76

 $C_4H_8$ 

### 5.4.2. Gas chromatography

Clarke [10] reported the following gas chromatographic systems:

*Packed column:* 3% SE-30 or OV-1 on 80–100 mesh Chromosorb G HP (acid washed and dimethyldichlorosilane treated) 2 m × 2 mm i.d. glass column: it is essential that the support be fully deactivated.

*Column temperature:* Normally between 100 and 300 °C; for isothermal conditions, an approximate guide to temperature is to use the RI ÷ 10.

*Carrier gas:* Nitrogen at 45 ml/min.

*Capillary column:* 10–15 m × 0.32 or 0.53 mm i.d., 100% dimethyl-PSX (X-I) with a 1.5–3 µm film thickness.

*Carrier gas:* Helium.

*Temperature program:* 4 min at 135 °C, 13 °C min<sup>-1</sup> to 200 °C, 6 °C min<sup>-1</sup> to 312 °C, 6 min final hold.

RI = 3360 [19].

*Capillary column:* 20–30 m × 0.2 or 0.25 mm i.d., 5% phenyl-95%-dimethyl-PSX (X-5) with a 0.5–1 µm film thickness.

*Carrier gas:* Helium, constant flow 1 ml/min.

*Temperature program:* 0.7 min at 90 °C, 35 °C min<sup>-1</sup> to 240 °C, 8 °C min<sup>-1</sup> to 290 °C, 25 °C min<sup>-1</sup> to 325 °C, 6 min final hold.

*Reference compounds:* *n*-Alkanes with an even number of carbon atoms or a reference drug mix that contains amphetamine (1125), ephedrine (1365), benocaine (1545), methyl phenidate (1725), diphenylhydramine (1870), tripeleminamine (1976), methaqualone (2135), trimetoprim (2215), codeine (2375), nordazepam (2490), prazepam (2648), papaverine (2825), haloperidol (2930), and strychnine (3116).

RI = 3461 [10].

### 5.4.3. High-performance liquid chromatography

Gaillard and Pepin [20] screened and identified buclizine and other drugs in human hair by high-performance liquid chromatography-photodiode-array ultraviolet detection and gas chromatography-mass spectrometry after solid-phase extraction. Powdered hair (75 mg) is incubated for 12 h at 56 °C in 2 ml of distilled water (acidic compounds) or 0.1 M hydrochloric acid (neutral and basic compounds). A twin solid-phase extraction on C<sub>18</sub> cartridge is used for sample clean-up procedure. Acidic drugs are fixed at pH 2 and eluted with 1% ammoniacal methanol while natural and basic drugs are retained on the column at pH 8.5 and eluted with methanol containing 0.5% acetic acid. The internal standard for acidic extraction was bupivacaine and for basic extraction was prazepam. The separation of the drugs was performed using both the liquid and the gas chromatography, whereas identification was achieved using photodiode array and

mass spectrometric detection, respectively. The liquid chromatography system gives an elution of the drugs following a multi step gradient from a symmetry C<sub>8</sub> 5 µm column (25 cm × 4.6 mm) at 30 °C with acetonitrile–phosphate buffer (pH 3.8). Identification is achieved using the reference data (retention times and spectra) of buclizine and many other pharmaceuticals, toxicants and drugs of abuse.

Wheals [21] described an isocratic multicolumn high-performance liquid chromatography for qualitative analysis and characterization of buclizine and several basic drugs using an aqueous methanol solvent. A variety of high-performance liquid chromatography packing materials were prepared and their chromatographic properties compared for separating buclizine and several basic drugs using a single solvent system.

Massart and Detaevernier [22] selected the preferred systems for the high-performance liquid chromatography of buclizine and other basic drugs and applied them to the separation of the antihistamine drugs. Two preferred systems (combination of a stationary phase and a mobile phase) for the high-performance liquid chromatography analysis of buclizine and the other basic drugs are selected. The same nitrile stationary phases are combined with a polar and a non polar eluent. The preferred systems were applied to the separation of the drugs with excellent results.

Jane *et al.* [23] used high-performance liquid chromatographic method for the analysis of buclizine and numerous basic drugs on silica columns using nonaqueous ionic eluents. Low wavelength ultraviolet and fluorescence detection were used, and fluorescence was optimized by a post-column pH change or derivatization of primary aliphatic amines with *o*-phthlaldehyde. Retention and relative response data, UV, 254 nm and electrochemical, +1.2 V, have been generated for buclizine and the other basic compounds using a 125 mm Spherisorb S5W silica column and methanolic ammonium perchlorate (10 mM, pH 6.7) as eluent. This system was used isocratically in qualitative analyses and also for quantitative work, when either the wavelength or the applied potential is adjusted to optimize the response.

Wahbi *et al.* [24] used a high-performance liquid chromatographic method for the determination of buclizine dihydrochloride in the presence of acid-induced degradation products. The kinetic of the drug degradation at different temperatures was studied. The assay was carried out using a 300 × 3.9 mm (i.d.) stainless steel column; packed with Waters Bondapak C<sub>18</sub> (10 µm) at ambient temperature, a mobile phase consisting of acetonitrile–water (85:15) containing 0.5% triethanolamine at pH 6.6; filtered through 0.45-µm membrane filter; and degassed by vacuum, a flow rate of 2 ml/min and detection at 260 nm. Laboratory-made tablets containing buclizine dehydrochloride, 50 mg and nicotinic acid, 25 mg per tablet were analyzed by the method and the mean percentage recovery was found to be 100 ± 0.17 (*n* = 6).

Aryne *et al.* [25] developed an isocratic reversed-phase high-performance liquid chromatographic method with UV detection at 230 nm for the determination of buclizine hydrochloride in human serum and dosage formulation. Methylparaben was used as an internal standard. Good chromatographic separation between buclizine and internal standard peaks was achieved by using a stainless steel analytical column Nucleosil, C<sub>18</sub> (10  $\mu$ m, 25 cm  $\times$  0.46 cm). The system was operated at room temperature using a mobile phase consisting of acetonitrile–water (1:1) (pH 2.6) with phosphoric acid 85% at a flow rate of 2 ml/min. The calibration curve for buclizine hydrochloride in human serum was linear over the tested concentration range of 10, 3, 1.5, 0.5, 0.15, 0.05, and 0.025  $\mu$ g/ml with a correlation coefficient of 0.9999. The intra- and inter-run precision and accuracy results were 98.07–100.34. The method was validated for selectivity, linearity, accuracy, and precision. The method was found to be suitable for the quality control of buclizine hydrochloride in bulk drug as well as in human serum.

Aryne *et al.* [26] presented rapid liquid chromatographic procedures for quality control of pharmaceuticals and human serum containing antihistamines, meclizine, and buclizine alone or in combination with pyridoxine using acetonitrile:water (80:20) as a mobile phase (pH adjusted to 2.6), methylparaben as internal standard deviation and UV detection was made at 230 nm. The results obtained showed a good agreement with the declared content. The method had good linearity in the range of 0.03–10  $\mu$ g/ml for pyridoxine and (0.025–10  $\mu$ g/ml) for meclizine and buclizine serum concentration with a correlation coefficient of 0.9999.

Dhakane and Ubale [27] developed and validated an isocratic reversed-phase stability indicating high-performance liquid chromatographic assay method for the quantitative determination of buclizine hydrochloride in the bulk drugs and the degradation products generated from forced decomposition. The method uses a Grace Alpha C<sub>18</sub> (250 mm  $\times$  4.6 mm) (5  $\mu$ m) column and the mobile phase containing the mixture of triethylamine–phosphoric acid buffer (pH 3) by orthophosphoric acid–acetonitrile (20:80). The detection was carried out at wavelength 230 nm. The method was validated with respect to linearity, accuracy, precision, system suitability, selectivity, robustness, and the forced degradation studies prove the stability indicating ability of the method.

Siddiqui *et al.* [28] developed and validated an analytical spectral calibration method to quantify buclizine hydrochloride, which is a piperazine derivative and used a single active principle in pharmaceutical forms were done. The quantification of buclizine hydrochloride was performed in the wavelength range of 218–226 nm at  $N = 6$ . The linear regression equation has been constructed using relationship between concentration and absorbance at 218, 220, 222, 224, and 226 nm.

The method was applied directly and easily to the analysis of the pharmaceutical tablet preparations. Mean percent relative standard deviation was found to be 0.6231% (Longifene<sup>®</sup> tablet 25 mg). The method was completely validated and proven to be rugged. This validated UV spectrophotometric method is potentially useful for a routine laboratory analysis because of its simplicity, rapidity, sensitivity, precision, and accuracy.

Arayne *et al.* [29] developed and validated a reversed-phase high-performance liquid chromatographic method for the estimation of buclizine hydrochloride and other H<sub>1</sub>-receptor antagonists in the presence of gliquidone. A good chromatographic separation between these drugs was achieved using a mobile phase containing methanol–water (80:20) at pH 3.5 with a flow rate of 1 ml/min; and detection was performed at 230 nm with a UV detector. Validation of the method was performed in terms of linearity, accuracy, precision, and limit of detection and quantification. The linearity of the calibration curve of buclizine hydrochloride was 0.325–50 µg/ml ( $r = 0.9967$ ). There was no significant difference between the amount of drug spiked in serum and the amount recovered, and serum did not interfere in the simultaneous estimation. The method is suitable for the simultaneous analysis of the active ingredients in tablet dosage forms and human serum.

Arun *et al.* [30] developed and validated a rapid high-performance liquid chromatographic method for the estimation of buclizine hydrochloride in tablet dosage form. The stationary phase used was precoated silica gel 60 F<sub>254</sub>. The mobile phase used was a mixture of methanol:chloroform:ammonia (8:1:1). The detection of spots was carried out at 234 nm. The method was validated in terms of linearity, accuracy, precision, and specificity. The calibration curve was linear between 100 and 700 ng/spot. The limit of detection and the limit of quantification were 20 and 100 ng/spot, respectively. The method can be used to determine the drug content of tablet dosage formulation.

Clarke [10] reported the following HPLC systems:

*Column:* Silica Spherisorb S5W (125 × 4.9 mm, 5 µm).

*Mobile phase:* Solution containing 1.175 g (0.01 M) of ammonium perchlorate in 1 l methanol; adjust to pH 6.7 by the addition of 1 ml 0.1 M sodium hydroxide in methanol.

*K values* 0.7 [23].

*Column:* C<sub>18</sub> symmetry (250 × 4.6 mm, 5 µm).

*Column temperature:* 40 °C.

*Mobile phase:* (A:B) Sulfuric acid (0.5 ml of 2.5 M) in water (500 ml); sulfuric acid (0.5 ml of 2.5 M) in acetonitrile (500 ml).

*Elution program:* (98:2) for 3 min to (2.88) over 23 min, hold for 10 min back to initial conditions over 2 min with equilibration of 8 min before next injection.

*Detection:* UV diode-array.

*Standards:* Nitro-*n*-alkanes (C<sub>1</sub> to C<sub>16</sub>) 10 µl in 10 ml acetonitrile.

RI = 454 [31].

## 6. STABILITY

Buclicine should be stored in highly closed containers at temperatures less than 40 °C, preferably between 15 and 30 °C [32].

## ACKNOWLEDGMENT

The authors wish to thank Mr. Tanvir A. Butt, Pharmaceutical Chemistry Department, College of Pharmacy, King Saud University for his secretarial assistance in preparing this profile.

## REFERENCES

- [1] The Merck Index, An Encyclopedia of Chemicals, Drugs, and Biologicals, 14th ed., Merck & Co., INC, Whitehouse Station, NJ, USA, 2006, p. 240.
- [2] S.Y. P'an, J.F. Gardocki, J.C. Reilly, J. Am. Pharm. Assoc. 43 (1954) 653–656.
- [3] W. Meindl, Arch. Pharm. 321 (1988) 473–476.
- [4] V.C. Saxena, S.K. Bapat, B.N. Dhawan, Jpn. J. Pharmacol. 19 (1969) 477–784.
- [5] Martindale, The Extra Pharmacopeia, 31st ed., Royal Pharmaceuticals Society of Great Britain, 1996, 435–436.
- [6] A.R. Gennaro (Ed.), Remington's: The Science and Practice of Pharmacy, 18th ed., Mack Publishing Co., Pennsylvania, USA, 1995, p. 1019.
- [7] H.G. Morren, H. Strubbe, J. Pharm. Belg. 10 (1955) 239–245.
- [8] C.M. Lui, I.C. Yu, L.Y. Li, Yaoxue Xuebao 11 (1964) 317–320.
- [9] E. Cossement, G. Bodson, J. Gobert, Eur. Pat. (1994) EP 617028 A1 19940928.
- [10] A.C. Moffat, M.D. Osselton, B. Widdop, Clark's Analysis of Drugs and Poisons, Vol. 2, 3rd ed., The Pharmaceutical Press, 2004, Royal Pharmaceutical Society of Great Britain, p. 954.
- [11] British Pharmacopoeia, Vol. 1, The Stationary Office, London, 2005, p. 290.
- [12] W. Pregnotatto, N.L. Pissatto, Rev. Inst. Adolfo Lutz 34 (1974) 69–77.
- [13] V. Annapurna, G. Jyothi, V. Nagalakshmi, B.B.V. Sailaja, J. Indian Chem. Soc. 86 (2009) 358–363.
- [14] A.M. El Walily, A. El Gindy, A.A.M. Wahbi, Spectrosc. Lett. 29 (1996) 217–230.
- [15] N.A. Zakhari, S.M. Ahmed, K.A. Kovar, Pharmeuropa 3 (1991) 269–273.
- [16] S. Tang, Yaoxue Tongbao 22 (1987) 292–293.
- [17] A.H. Stead, R. Gill, T. Wright, J.B. Gibbs, A.C. Moffat, Analyst 107 (1982) 1106–1168.
- [18] R.A. de Zeeuw, J.P. Franke, F. Degel, G. Machbert, H. Schutz, J. Wijsbeek (Eds.), Thin layer chromatographic Rf values of Toxicologically Relevant Substances on Standardized Systems, 2nd ed., VCH, Weinheim, 1992, Report XVII of the DFG Commission for Clinical-Toxicological Analysis.
- [19] R.A. de Zeeuw (Ed.), Gas Chromatographic Retention Indices of Toxicologically Relevant Substances on Packed or Capillary Columns with Dimethylsilicone Stationary Phases, 3rd ed., The International Association of Forensic Toxicologists and Deutsche,

- Forschungsgemeinschaft, Weinheim, 2002 Report XVIII of the DFG Commission for Clinical-Toxicological Analysis.
- [20] Y. Gaillard, G. Pepin, J. Chromatogr. 762 (1997) 251–267.
  - [21] B.B. Wheals, J. Chromatogr. 187 (1980) 65–85.
  - [22] D.L. Massart, M.R. Detaevernier, J. Chromatogr. Sci. 18 (1980) 139–143.
  - [23] I. Jane, A. McKinnon, R.J. Flanagan, J. Chromatogr. 323 (1985) 191–225.
  - [24] A.A.M. Wahbi, A.F. El-Walily, A. El-Gindy, J. Pharm. Pharmacol. 50 (Supplement) (1998) 119–124.
  - [25] M.S. Arayne, N. Sultana, F.A. Siddiqui, Pak. J. Pharm. Sci. 19 (2006) 326–329.
  - [26] M.S. Arayne, N. Sultana, F.A. Siddiqui, Chromatographia 67 (2008) 941–945.
  - [27] V.D. Dhakane, M.H. Ubale, Anal. Chem. 8 (2009) 602–607.
  - [28] F.A. Siddiqui, A.Z. Mirza, M.H. Zuberi, F. Qureshi, Med. Chem. Res. (2010), <http://www.springerlink.com/content/9281287gv71733x7>doi:10.1007/s00044-009-9286-5.
  - [29] M.S. Arayne, N. Sultana, A.Z. Mirza, F.A. Siddiqui, J. Chromatogr. Sci. 48 (2010) 382–385.
  - [30] B.E. Arun, A. Suganthi, A. Fathimunnisa, T.K. Ravi, College of Pharmacy, Sri Ramakrishna Institute of Paramedical Science, Coimbatore-44, Tamil Nadu. Online. Unpublished work. [http://www.camag.com/downloads/free/cbs/CBS104\\_yellow\\_pages.pdf](http://www.camag.com/downloads/free/cbs/CBS104_yellow_pages.pdf).
  - [31] R.K. Waters, R.A. Waters and A.C. Moffat, Unpublished Information, through Clarke [10].
  - [32] Drugdex Drug Evaluation, Micromedex Healthcare Series, (2010) Vol.146, expires 12/2010.



# CHAPTER 2

## Chitin

**Nidal H. Daraghmeh,<sup>\*,†</sup> Babur Z. Chowdhry,<sup>†</sup>  
Stephen A. Leharne,<sup>†</sup> Mahmoud M. Al Omari,<sup>\*</sup> and  
Adnan A. Badwan<sup>\*</sup>**

---

<b>Contents</b>		
1. Description		37
1.1. Nomenclature		37
1.1.1. Systematic chemical names		37
1.1.2. Nonproprietary names		37
1.2. Formulae		37
1.2.1. Empirical formula		37
1.2.2. Molecular weight		38
1.2.3. CAS number		38
1.2.4. Structural formula		38
1.3. Elemental analysis [2]		38
1.4. Appearance		38
2. Preparation of Chitin and Its Derivatives		38
2.1. Preparation of chitin		38
2.2. Preparation of chitin derivatives		39
2.2.1. Chitosan		39
2.2.2. Hydrolysis products of chitin (oligomers) [12]		39
2.2.3. Other derivatives [13–15]		39
3. Physical Characteristics		46
3.1. Solubility characteristics [2,16,17]		46
3.2. Morphology		46
3.3. Polymorphism		47
3.3.1. Chitin polymorphs and their sources [19,20]		47
3.3.2. Molecular modeling [18]		49
3.3.3. X-ray powder diffractometry		50

\* The Jordanian Pharmaceutical Manufacturing Company, Naor, Jordan

† School of Science, University of Greenwich, Chatham Maritime, Kent, United Kingdom

3.4. Thermal methods of analysis	52
3.4.1. Differential scanning calorimetry	52
3.4.2. Thermogravimetric analysis	54
3.5. Spectroscopy	55
3.5.1. Ultraviolet/visible spectrophotometry [18]	55
3.5.2. Fourier-transform infrared spectroscopy [20,21]	55
3.5.3. Raman spectroscopy	57
3.5.4. Proton nuclear magnetic resonance spectroscopy [25]	60
3.5.5. Carbon NMR spectroscopy	61
3.5.6. Mass spectroscopy [26]	63
4. Methods of Analysis	63
4.1. Identification [27]	63
4.2. Solution appearance	64
4.3. Chitin swelling and hydrophilicity [28]	65
4.4. Specific optical rotation [29]	65
4.5. Molecular weight determination [30]	66
4.6. Electrical properties	68
4.7. Determination of degree of <i>N</i> -acetylation [31,32]	69
4.7.1. Fourier-transform infrared spectroscopy [33,34]	69
4.7.2. Proton NMR spectroscopy [35]	70
4.7.3. Carbon and Nitrogen NMR spectroscopy [36]	73
4.7.4. X-ray powder diffraction analysis [37]	74
4.7.5. Elemental analysis [38–40]	77
4.7.6. Ultraviolet/visible spectrophotometry [41]	77
4.7.7. Differential scanning calorimetry [42]	78
4.7.8. Mass spectroscopy [35]	78
4.7.9. Hydrolysis [43]	81
4.7.10. Pyrolysis [44]	81
4.8. Determination of degree of depolymerization (hydrolysis)	81
4.8.1. Mass spectroscopy [19]	81
4.8.2. Proton nuclear magnetic resonance [45]	81
4.9. Chromatographic methods of analysis	84
4.9.1. Analysis of chitin impurities using HPLC [46]	84
5. Uses and Applications	84
5.1. Chitin: The solid dosage form excipient	85
5.1.1. Selection of chitin as an excipient	85
5.2. Other applications [17]	94
5.2.1. Production of chitin sheets	94
5.2.2. Chitin fibers	94
5.2.3. As an analgesic	96

5.2.4. Antimicrobial activity	96
5.2.5. Antitumor effect (immuno-enhancing function) [12]	96
5.2.6. Wound healing acceleration	96
5.2.7. In agriculture [56]	97
5.2.8. In cosmetics [57]	97
5.2.9. In the food industry	97
5.2.10. In chromatography [6]	98
5.2.11. Chitin and chitosan [4]	98
6. Stability	98
7. Biodegradability and Toxicology [17,59,61]	98
References	101

## 1. DESCRIPTION

### 1.1. Nomenclature

“Chitin” and “chiton” (a marine animal) both derive from the same Greek word meaning “tunic,” referring to the protective shell.

#### 1.1.1. Systematic chemical names

$\beta$ -(1,4)-2-Acetamido-2-deoxy-D-glucopyranose  
 Poly-N-acetyl-D-glucosamine [poly (D-GlcNAc)]  
 $\beta$ -(1,4)-Poly-N-acetyl-D-glucosamine  
 Poly- $\beta$ -(1,4)-N-acetyl-glucosamine  
 Poly-(acetyl amino glucose)  
 $\beta$ -(1,4)-2-Acetamido-2-deoxy-D-glucose  
 2-Acetamido-2-deoxy-D-glucose  
 $\beta$ -(1,4)-2-Amino-2-deoxy-D-glucose  
 Poly-(N-acetyl-1,4- $\beta$ -D-glucopyranosamine)  
 Fully acetylated chitosan

#### 1.1.2. Nonproprietary names

Chitin, poly-acetyl glucosamine; shell protein; poly-acetylglucosaminyl-transferase; shell; ming keratinocytes; chitosan; shell protein,  $\beta$ -farming; chitina.

### 1.2. Formulae

#### 1.2.1. Empirical formula

$[C_8H_{13}NO_5]_n$

### 1.2.2. Molecular weight

[203.19] $n$

Chitin has an average molecular weight ranging from 1.0 to 2.5 million Da. The variation in the molecular weight is a function of the extent of *N*-acetylation [1].

### 1.2.3. CAS number

1398-61-4

### 1.2.4. Structural formula

A schematic of the chemical structure of the monomeric unit of chitin is shown in Fig. 2.1.

## 1.3. Elemental analysis [2]

The calculated elemental composition of fully acetylated chitin is shown in Table 2.1.

## 1.4. Appearance

Chitin is a white, hard, inelastic, nitrogenous polysaccharide found in the outer skeletons of crabs, and lobsters and in the internal structures of other invertebrates [3].

## 2. PREPARATION OF CHITIN AND ITS DERIVATIVES

### 2.1. Preparation of chitin

The crude chitin is isolated from the outer skeletons of crustaceans, molluscs or invertebrate animals, insects, and certain fungi. Commercially, crab and shrimp shells are the major sources of chitin. Crustacean shells not only consist of 30–40% protein, 30–50% calcium carbonate, and

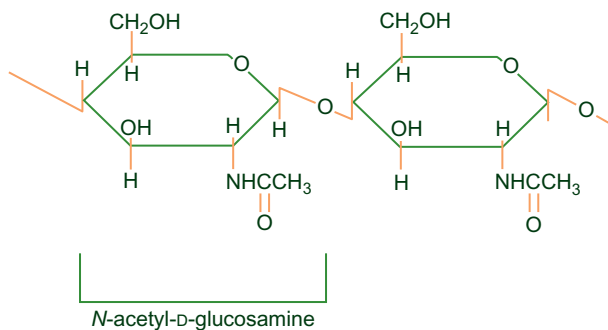


**FIGURE 2.1** Chemical structure of chitin showing its monomer: *N*-acetyl-D-glucosamine.

**TABLE 2.1** Elemental analysis of chitin

Element	Composition (%)
Carbon	47.29
Hydrogen	6.45
Nitrogen	6.89
Oxygen	39.37

20–30% chitin but also contain pigments of a lipidic nature such as carotenoids. These components have to be quantitatively removed to obtain pure chitin necessary for biological applications [4]. Several published methods for the extraction of chitin from crustacean shells in addition to enzymatic preparation are summarized in Table 2.2.

## 2.2. Preparation of chitin derivatives

### 2.2.1. Chitosan

The most important derivative of chitin is chitosan obtained by partial deacetylation of chitin in the solid state under alkaline conditions or by enzymatic hydrolysis in the presence of a chitin deacetylase. The ratio of 2-acetamido-2-deoxy-D-glucopyranose to 2-amino-2-deoxy-D-glucopyranose moieties determines the identity of the product, that is, chitin or chitosan [9]. The published methods used for the production of chitosan from chitin are summarized in Table 2.3.

### 2.2.2. Hydrolysis products of chitin (oligomers) [12]

Chitin is hydrolyzed to form smaller oligosaccharides by different methods including acetolysis using acetic anhydride/H<sub>2</sub>SO<sub>4</sub>, hydrolysis with HCl/sonolysis under ultrasound irradiation, or fluorohydrolysis using anhydrous HF (Fig. 2.4).

Enzymatic hydrolysis is a useful method for the preparation of monomers from chitin and chitosan because the yield of monomers is greater by enzymatic hydrolysis than by acid hydrolysis. The enzyme chitin deacetylase hydrolyzes the acetamido group in the *N*-acetylglucosamine units of chitin and chitosan, thus generating glucosamine units and acetic acid (Fig. 2.5).

### 2.2.3. Other derivatives [13–15]

Carboxymethyl-chitin (CM-chitin), as a water-soluble anionic polymer, is the second most studied derivative of chitin after chitosan. The carboxymethylation of chitin is undertaken in a similar manner to that of

**TABLE 2.2** Methods for the preparation of chitin

Method	Procedure
Method 1 [5–7]	Crude chitin is washed with water, dried at room temperature, and cut into small pieces, then treated with acid (HCl, HNO <sub>3</sub> , H <sub>2</sub> SO <sub>4</sub> , CH <sub>3</sub> COOH, or HCOOH) (demineralization), followed by alkali using NaOH at 105–110 °C (deproteinization). The decoloration is performed by refluxing in ethanol or by using oxidizing or bleaching agents (e.g., KMnO <sub>4</sub> , NaOCl, and H <sub>2</sub> SO <sub>4</sub> )
Method 2 [5–7]	Crude chitin is washed with water, dried at room temperature, and cut into small pieces, then soaked for 3 days in 10% NaOH solution (freshly prepared and degassed every day at room temperature). The obtained solid is then treated with 95% ethanol to clean the pigment products. The white protein free-residue is then suspended in 37% HCl at 20 °C for 4 h. The solid is filtered and washed with water, ethanol, and ether
Method 3 [5,6,8]	The shells are partially digested with an organic acid, followed by 2 N HCl for 5 h at room temperature. The decalcified shells are shaken for 18 h with 90% formic acid at room temperature and then filtered. The solid is washed with water and treated for 2.5 h with 10% NaOH solution on a steam bath. The suspension is then filtered, washed with water, ethanol, and ether
Method 4 [7,8]	Decalcification with EDTA at pH 10 at room temperature for 2 or 3 weeks. Large cuticle fragments of the crab <i>Cancer parugus</i> are reacted slowly (2 or 3 weeks) with EDTA at pH 9.0. The solid is then further treated with EDTA at pH 3, extracted with ethanol for pigment removal and with ether for the removal of lipids. The protein is removed with formic acid (98–100%) followed by treatment with hot alkali
Method 5 [6,7]	Decalcification with EDTA at pH 10 at room temperature, followed by digestion with a proteolytic enzyme such as tuna proteinase at pH 8.6 and 37.5 °C, or papain at pH 5.5–6.0 and 37.5 °C, or a bacterial proteinase at pH 7.0 and 60 °C for over 60 h. The remaining protein (5%) is removed by treatment with sodium dodecylbenzenesulfonate or dimethylformamide

- Method 6 [6,7] Decalcification is carried out by a simple treatment with 1.4 N HCl at room temperature in a plastic or wooden container. After completion of the decalcification treatment, proteins are removed using papain, pepsin or trypsin. This method is simple and suitable for the mass production of chitin with little deacetylation
- Method 7 [6] The shell wastes are treated with hot 1% Na<sub>2</sub>CO<sub>3</sub> solution followed by dilute HCl (1–5%) at room temperature, and then 0.4% Na<sub>2</sub>CO<sub>3</sub> solution
- Method 8 [6] Hydrolysis of protein present in the shell followed by digestion of CaCO<sub>3</sub>. The shells are treated with hot 5% NaOH solution, followed by cold NaOCl solution and then with warm 5% HCl solution
- Method 9 [6] Trehalose is hydrolyzed with the enzyme trehalase, followed by phosphorylation with ATP/enzyme hexokinase to form glucose-6-phosphate, which is transformed to fructose-6-phosphate in the presence of the enzyme glucose phosphate isomerase. Amination occurs in the presence of glutamine aminotransferase and the amino acid glutamine to form  $\alpha$ -D-glucosamine-6-phosphate. Acetylation by acetyl-CoA in the presence of the enzyme glucosamine-6-phosphate-*N*-acetyl transferase causes the formation of *N*-acetylglucosamine-6-phosphate. The latter rearranges via the enzyme phosphoacetylglucosamine mutase to form *N*-acetylglucosamine-1-phosphate, which is converted to uridine diphosphate-*N*-acetyl glucosamine (UDP-*N*-acetylglucosamine) via the enzyme uridine diphosphate-*N*-acetylglucosamine pyrophosphorylase and UTP. The final product, chitin, is produced via the enzyme chitin synthetase by the loss of UDP (Fig. 2.2)
-

**TABLE 2.3** Methods of deacetylation of chitin to form chitosan

Method	Procedure
Method 1 (aqueous sodium hydroxide) [10]	40% NaOH solution is added to chitin and refluxed under nitrogen at 115 °C for 6 h. The cooled mixture is then filtered and washed with water until the washings are neutral to phenolphthalein. The crude chitosan is purified as follows. It is dispersed in 10% acetic acid and then centrifuged for 24 h, to obtain a clear supernatant liquid. The latter is treated drop-wise with 40% NaOH solution and the white flocculent precipitate formed at pH 7. The precipitate is then recovered by centrifugation, washed repeatedly with water, ethanol, and ether, and the solid collected and air dried (Fig. 2.3)
Method 2 [6,7]	Fusion with solid KOH at very high temperature in a nickel crucible under nitrogen atmosphere. The melt is poured carefully into ethanol and the precipitate washed with water to neutrality
Method 3 [6,7]	Heating in 40% NaOH solution at 115 °C for 6 h under nitrogen. After cooling, the mixture is filtered and washed with water until neutral. This method does not include a purification step
Method 4 [6,7]	Kneading with NaOH and liquid paraffin in a 1:1:10 ratio, and stirred for 2 h at 120 °C. The mixture is poured into cold water, filtered, and thoroughly washed with water
Method 5 [6,7]	Steam heating with a solution containing 50% KOH, 25% EtOH (96%), and 25% monoethylene glycol. The temperature of the system is 120 °C. The obtained chitosan is filtered, washed with water until neutral, and then dried at moderate temperatures
Method 6 [6]	Recovery of shell proteins, sodium acetate, and calcium carbonate in addition to chitosan as commercial pure products. The extraction procedure includes different reaction and crystallization steps
Method 7 [11]	The fungal order <i>mucorales</i> contains chitosan as a cell wall component. <i>Absidia coerulea</i> a member of this class is readily cultured on nutrients (e.g., glucose or molasses) and the cell wall material recovered by simple chemical procedures



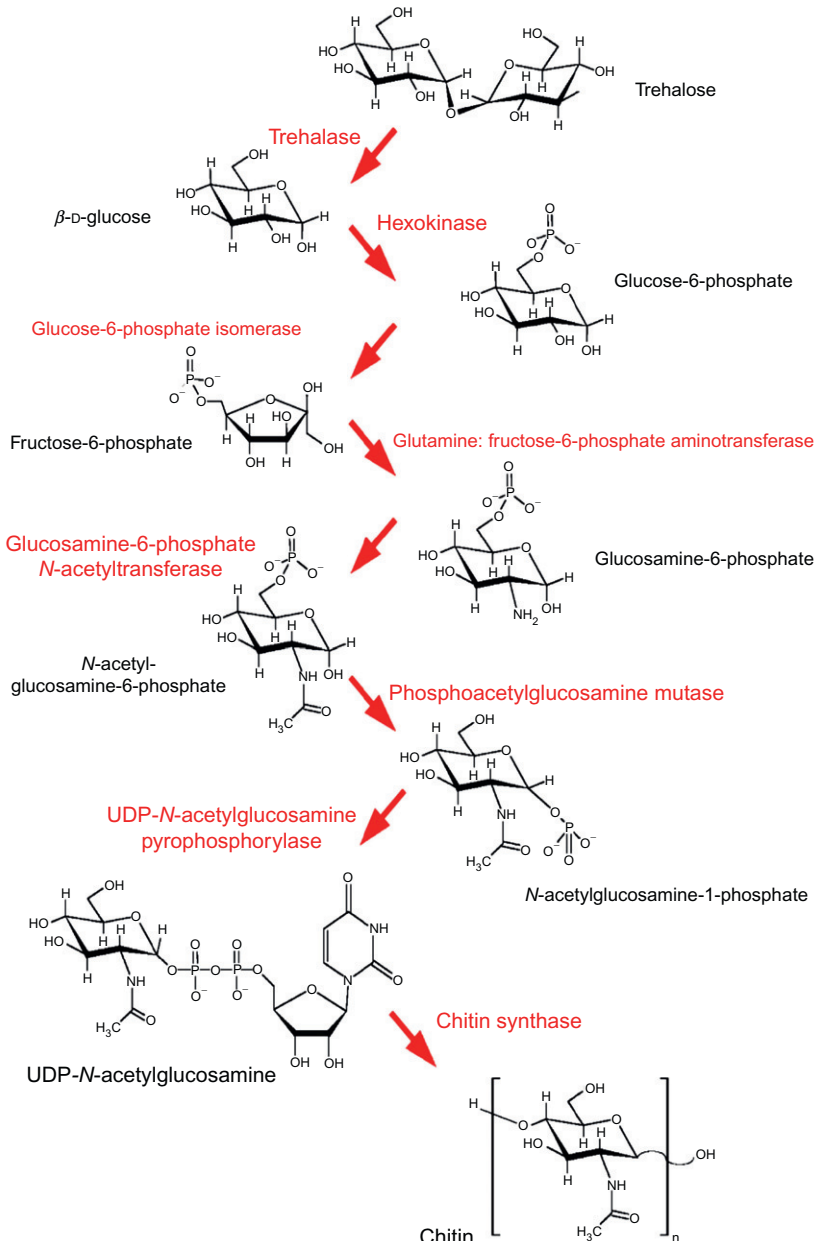


**FIGURE 2.2** Biosynthesis of chitin.

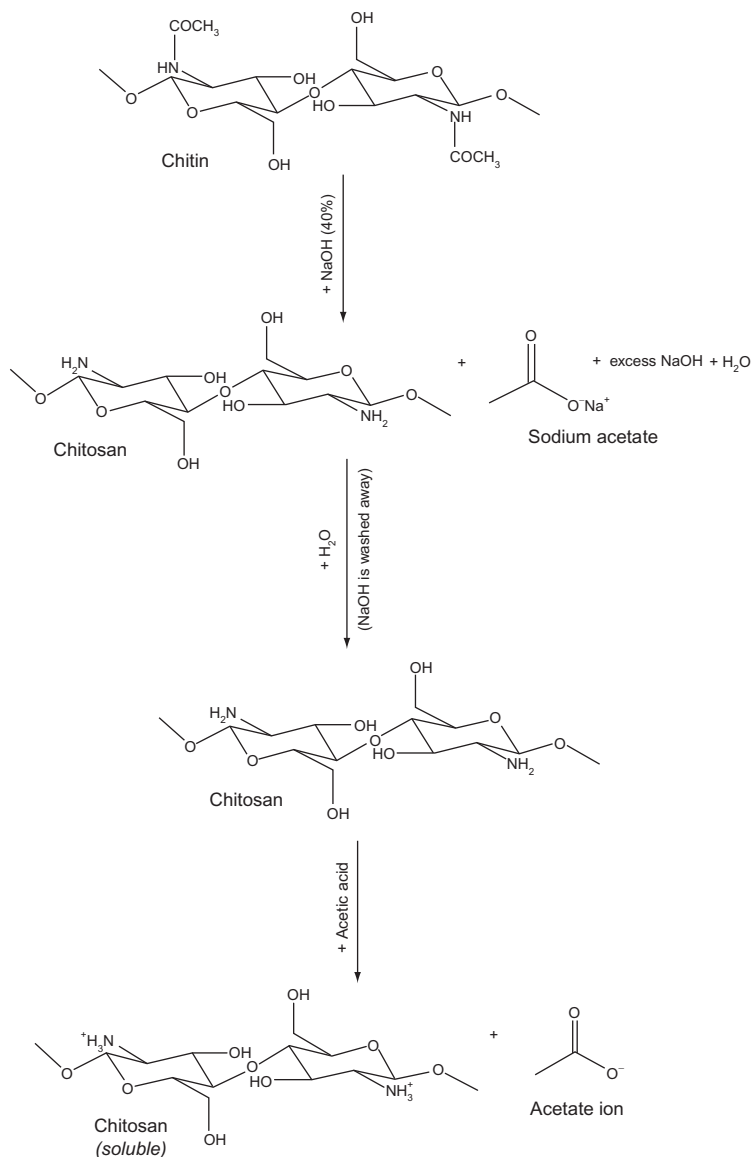


**FIGURE 2.3** Scheme for the deacetylation of chitin.

cellulose. Chitin is treated with monochloroacetic acid in the presence of concentrated NaOH. The same cellulose derivatization procedure can be used to prepare hydroxypropyl-chitin, which is a water-soluble derivative used for artificial lachrymal drops.

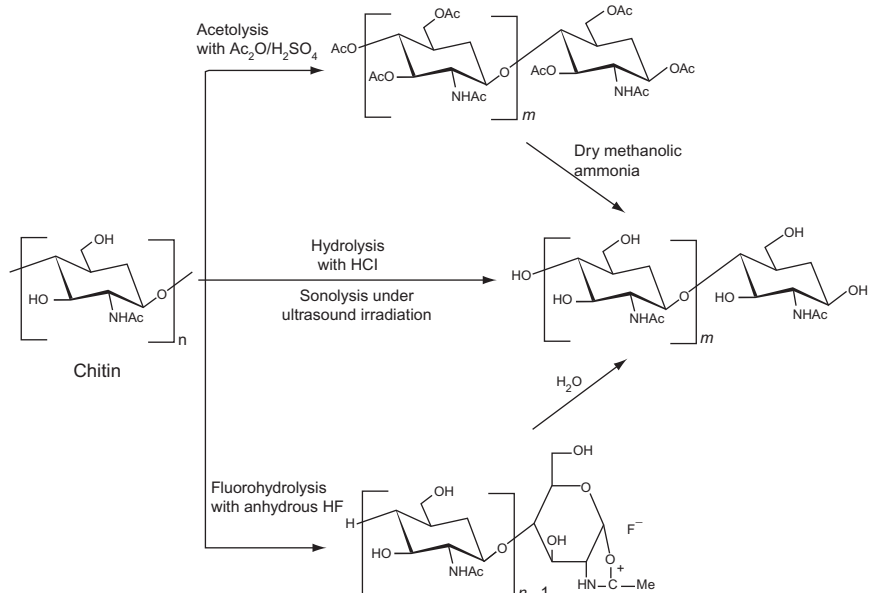


**FIGURE 2.4** Mechanisms for the acid hydrolysis of chitin.

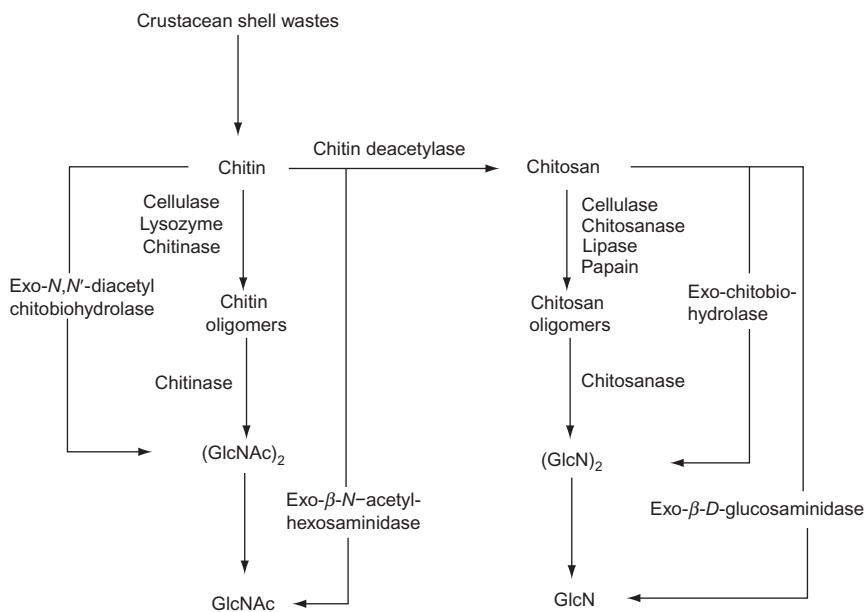


**FIGURE 2.5** Enzymatic hydrolysis of chitin and chitosan into their monomers.

Fluorinated chitin, *N*- and *O*-sulfated chitin, (diethylamino) ethylchitin, phosphoryl chitin, mercaptochitin, and chitin carbamates have also been reported and described in the literature. Similar chemical modifications (e.g. etherification and esterification), as for cellulose, can be performed for chitin. Chitin can be used in blends with natural or synthetic polymers; it can be cross-linked by the reagents used for cellulose (e.g., epichlorohydrin and glutaraldehyde) or grafted in the presence of ceric salt or after selective modification. Another chitin derivative dibutylchitin (DBCH) is prepared from krill chitin by esterification with butyric anhydride in the presence of perchloric acid. DBCH can be used in fiber spinning. DBCH fibers have been manufactured from a polymer solution in ethyl alcohol by extrusion.

### 3. PHYSICAL CHARACTERISTICS

#### 3.1. Solubility characteristics [2,16,17]

The solubility of magnesium silicate in different media is shown in Table 2.4. The dissolution mechanism of  $\alpha$ -chitin in *N,N*-dimethylacetamide (DMAc)/5% LiCl can be attributed to the formation of a weak complex between  $\text{Li}^+$  ions and the carbonyl oxygens of the DMAc, which solvates the polyelectrolyte formed between the  $\text{Cl}^-$  ions and labile proton groups (OH and  $\text{NHCOCH}_3$ ) of the chitin chain, disrupting the extensive intra- and intermolecular hydrogen bonds of the crystalline sheet structure of  $\alpha$ -chitin.

Table 2.5 shows the effect of different solvent mixtures containing methanol, ethanol, and anhydrous and hydrate forms of calcium and magnesium salts.

Comparing the solubility behavior of  $\alpha$ - and  $\beta$ -chitins (although the later exists in a crystalline-hydrated structure, which is much looser than that of the  $\alpha$ -chitin),  $\beta$ -chitin shows lower solubility due to the penetration of water between the chains of the lattice. Based upon chitin molecule-solvent conformation and solubility mechanisms,  $\beta$ -chitin starts gelling at a lower concentration than  $\alpha$ -chitin. Table 2.6 illustrates the solubility of chitin and structurally related compounds in a saturated  $\text{CaCl}_2 \cdot 2\text{H}_2\text{O}$ -methanol solvent system.

#### 3.2. Morphology

The morphology was determined using a Quanta-200 3D scanning electron microscope (SEM) operated at an accelerating voltage of 1200 V. The sample (0.5 mg) was mounted onto a  $5 \times 5$  mm silicon wafer affixed via graphite tape to an aluminum stub. The powder was then sputter-coated for 105 s at a beam current of  $20 \text{ mA/dm}^2$  with a 100-Å layer of gold/palladium alloy.

**TABLE 2.4** Solubility, at room temperature, of  $\alpha$ -chitin in different solvents and solvent mixtures

Solvent/solvent mixture	Solubility
Water	i
Dilute acids	i
Dilute and concentrated alkalies	i
Alcohol	i
Organic solvents	i
Concentrated HCl, H <sub>2</sub> SO <sub>4</sub> or H <sub>3</sub> PO <sub>4</sub> , anhydrous HCOOH	s (with depolymerization)
<i>N,N</i> -Dimethylacetamide (DMAc)/5% LiCl	s
Dinitrogen tetroxide/ <i>N,N</i> -dimethylformamide (DMF)	s
Fluoroisopropanol/hexafluoroacetone	s
<i>N,N</i> -Dimethylacetamide/ <i>N</i> -methyl-2-pyrrolidone/ LiCl	s
<i>N</i> -Methyl-2-pyrrolidone/5% LiCl	s

i and s represent insoluble and soluble, respectively.

**TABLE 2.5** Solubility of  $\alpha$ -chitin in various calcium and magnesium salt–alcohol solutions

Solvent system	Solubility <sup>a</sup>
Saturated anhydrous CaCl <sub>2</sub> –methanol	p.s.
Saturated CaCl <sub>2</sub> ·2H <sub>2</sub> O–methanol	s
Saturated CaCl <sub>2</sub> ·2H <sub>2</sub> O–ethanol	p.s.
Saturated MgCl <sub>2</sub> ·6H <sub>2</sub> O–methanol	i
100% (w/v) Ca(NO <sub>3</sub> ) <sub>2</sub> ·4H <sub>2</sub> O–methanol	i
100% (w/v) Mg(NO <sub>3</sub> ) <sub>2</sub> ·6H <sub>2</sub> O–methanol	i
200% (w/v) Ca(SCN) <sub>2</sub> ·4H <sub>2</sub> O–methanol	p.s.

s, p.s., and i represent soluble, partially soluble, and insoluble, respectively.

<sup>a</sup> 0.5 g chitin was stirred in 50 mL of each solution at room temperature.

The SEM images in Fig. 2.6 show the highly porous structure of  $\alpha$ -chitin in addition to the high particulate surface area [18].

### 3.3. Polymorphism

#### 3.3.1. Chitin polymorphs and their sources [19,20]

Chitin is isolated from the exoskeletons of crustaceans (e.g., crabs, lobsters, crayfish, shrimp, krill, barnacles), molluscs or invertebrate animals (e.g., squid, octopus, cuttlefish, nautilus, chitons, clams, oysters, scallops,

geoducks, mussels, fossils, snails), insects (e.g. ants, scorpions, cockroaches, beetles, spiders, brachiopods), and certain fungi. Commercially, crab and shrimp shells are the major sources of  $\alpha$ -chitin, whereas squid is the source of  $\beta$ -chitin. There are three polymorphic forms of chitin:  $\alpha$ ,  $\beta$ , and  $\gamma$ . They differ in the arrangement of chains in the crystalline phase. The most abundant and stable form is  $\alpha$ -chitin, which displays orthorhombic crystals. The crystallographic parameters of  $\alpha$ - and  $\beta$ -chitins are shown in Table 2.7. The neighboring sheets in  $\alpha$ - and  $\beta$ -chitin are

**TABLE 2.6** Solubility of  $\alpha$ - and  $\beta$ -chitins and structurally related compounds in a saturated  $\text{CaCl}_2 \cdot 2\text{H}_2\text{O}$ –methanol solvent system

Material	Solution (g/100 mL)	Solubility
$\alpha$ -Chitin	2.00	s
$\beta$ -Chitin	1.25	t
Chitosan	5.00	i
Bacterial cellulose	0.15	g
O-Acetylated chitin	1.25	t
Nylon-6	5.00	s

s, t, g, and i represent soluble, turbid or gelation, gelation, and insoluble, respectively,

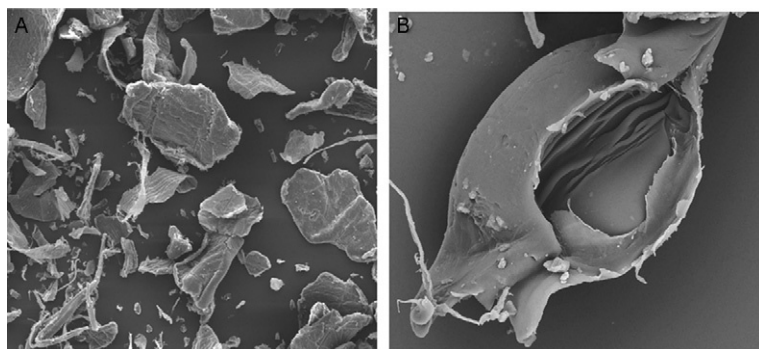


**FIGURE 2.6** SEM images of  $\alpha$ -chitin with magnifications of (A)  $\times 160$  and (B)  $\times 1600$ .

**TABLE 2.7** Crystallographic parameters of  $\alpha$ - and  $\beta$ -chitins

Compound	<i>a</i> (nm)	<i>b</i> (nm)	<i>c</i> (nm)	$\gamma$ (°)	Space group
$\alpha$ -Chitin	0.474	1.886	1.032	90.0	$P2_12_12_1$
$\beta$ -Chitin	0.485	0.926	1.038	97.5	$P2_1$

connected by hydrogen bonds via C=O and N–H groups. In addition, each chain has intramolecular hydrogen bonds between the neighboring sugar rings (C=O and OH groups on C-6 and a second hydrogen bond between the OH– group on C-3 and the ring oxygen) (Fig. 2.7). The differences among chitin polymorphs are due to the arrangement of the chains in the crystalline regions.  $\alpha$ -Chitin has a structure of antiparallel chains,  $\beta$ -chitin has intra-sheet hydrogen bonding resulting in parallel chains, and  $\gamma$ -chitin, being a combination of  $\alpha$ - and  $\beta$ -chitin, has both parallel and antiparallel structures. Because of these differences, each chitin polymorph differs in specific properties. The poor solubility of chitin is a result of the close packing of chains and its strong inter- and intramolecular bonds between the hydroxyl and acetamide groups. However,  $\beta$ -chitin lacks these interchain hydrogen bonds; therefore, it swells readily in water, and it is more prone to *N*-deacetylation than  $\alpha$ -chitin.

### 3.3.2. Molecular modeling [18]

Molecular modeling was performed by employing a molecular mechanics (MM<sup>+</sup>) (dipole moment) force field using HyperChem6 software. The chitin polymer was built using *N*-acetylated glucosamine monomer as

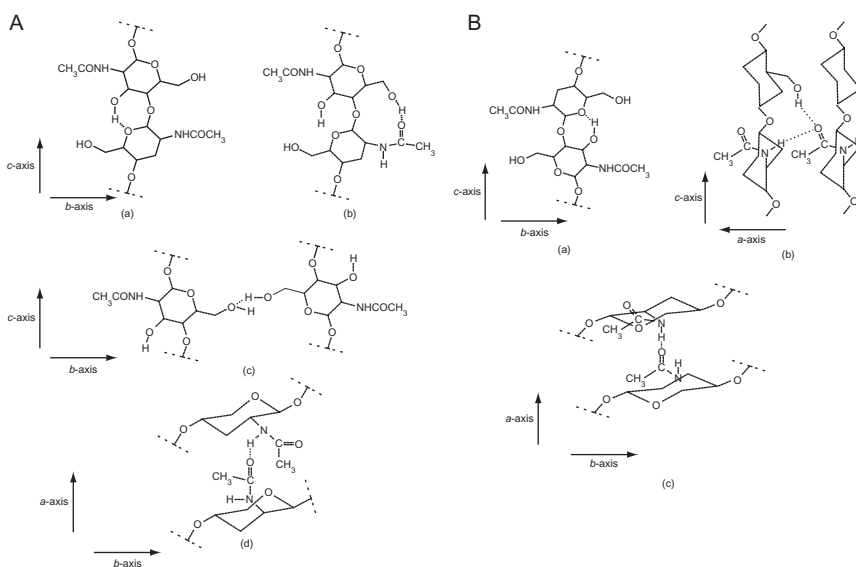


**FIGURE 2.7** Modes of hydrogen bonding in (A)  $\alpha$ -chitin: (a) intrachain C(3') OH...OC(5) bond, (b) intrachain C(6')OH...O=C(7<sub>3</sub>) bond, (c) interchain C(6')O...HOC(6<sub>2</sub>) bond, and (d) interchain C(2<sub>1</sub>)NH...O=C(7<sub>3</sub>); (B)  $\beta$ -chitin: (a) intrachain C(3')OH...OC(5) bond, (b) interchain C(2<sub>1</sub>)NH...O=C(7<sub>3</sub>) bond, and C(6')OH...O=C(7<sub>3</sub>) bond (ac plane projection); (c) interchain C(2<sub>1</sub>)NH...O=C(7<sub>3</sub>) bond (ab plane projection).

the repeating unit. The molar mass of the resulting chitin is 10 kDa; for modeling purposes, two chitin polymers of the same molar mass were used. One chitin polymer was kept fixed (static), while the other was left to move manually to fix chitin in different orientations. In each orientation, the system was optimized using MM<sup>+</sup> calculations; the binding energy was calculated in order to find the optimum structure between the two chitins. The orientation of the two chitin chains is such that inter- and intra-hydrogen bonds exist between the same chitin molecule and between the two chitin molecules. The presence of intramolecular H-bonds between primary hydroxyl groups and nitrogen atoms and between carbonyl groups and N-H groups was noted. Also the presence of intermolecular H-bonds between the two sheets was observed (Fig. 2.8).

### 3.3.3. X-ray powder diffractometry

The X-ray powder diffractometry (XRPD) patterns of  $\alpha$ -chitin and chitosan of different molecular weights were obtained using a Bruker AXS D8 Advance X-ray diffractometer with Cu K $\alpha_1$  radiation at  $\lambda = 1.54184$  Å. About 20 mg of the sample was spread on a sample stage, and the relative intensity was recorded in the scattering range ( $2\theta$ ) of 5–55°. Figure 2.9A shows the XRPD patterns of  $\alpha$ -chitin and chitosans of different molecular weights (100,000, 28,000, 13,000, 2800, and 1300 Da). The XRPD pattern of  $\alpha$ -chitin exhibits well-resolved and intense peaks, while a broad diffuse scattering and less intense peaks are observed for chitosan indicating that

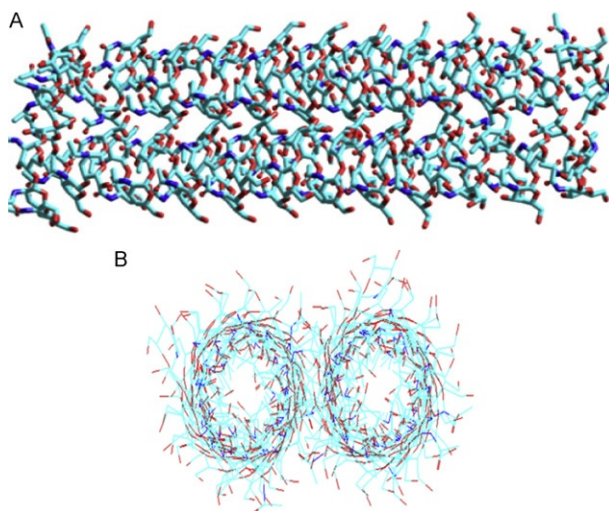


**FIGURE 2.8** Molecular modeling of two sheets of chitin: (A) side and (B) front views.



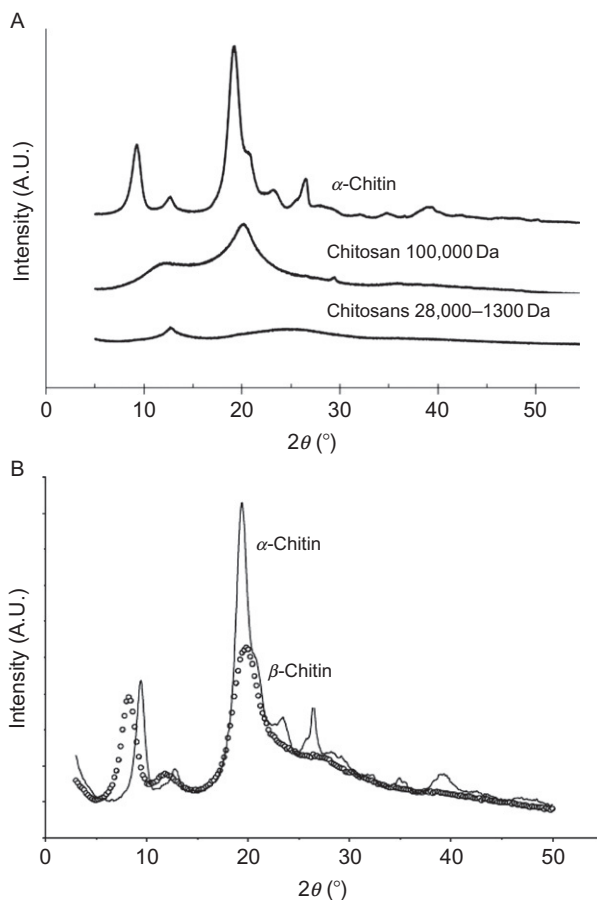


**FIGURE 2.9** The XRPD patterns of (A)  $\alpha$ -chitin and chitosan of different molecular weights and (B) of  $\alpha$ - and  $\beta$ -chitins.

$\alpha$ -chitin is more crystalline than chitosan. Chitosans having molecular weights in the range of 1300–28,000 Da have the same XRPD pattern in comparison with that of chitosan 100,000 Da [18].

The XRPD patterns of  $\alpha$ - and  $\beta$ -chitins are shown in Fig. 2.9B. The XRPD pattern of  $\beta$ -chitin exhibits a broad diffuse scattering and less intense peaks compared with the profile for  $\alpha$ -chitin. The clear difference in the spectra of the two polymorphs is due to differences in the crystallographic arrangements of these two polymorphs [21].

Figure 2.10 shows the XRPD patterns of  $\alpha$ -chitin (A) obtained from different sources and the corresponding hydrolysis product, chitosan (B). All  $\alpha$ -chitin samples show strong reflections at  $2\theta$  around  $10^\circ$  and  $20^\circ$  and minor reflections at higher  $2\theta$  values, for example, at  $26.4^\circ$  and higher.

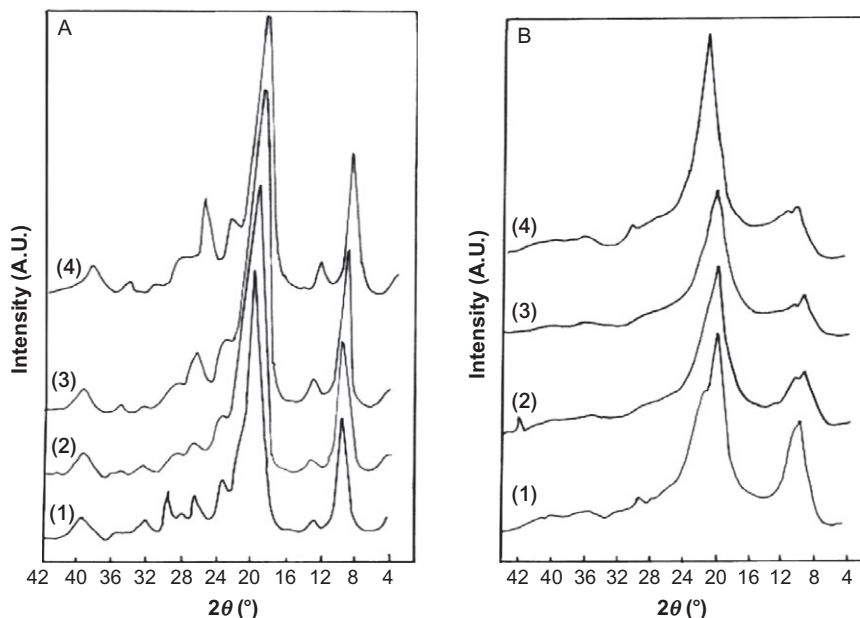


**FIGURE 2.10** XRPD patterns for (A)  $\alpha$ -chitin from different sources: (1) brown shrimp shells, (2) pink shrimp shells, (3) crabs shells, and (4) crayfish shells; (B) the corresponding chitosan.

Generally, the sharpness of the bands is higher in the chitin samples than in their chitosan analogs due to the decrease in crystallinity. Figure 2.11 shows the XRPD patterns of  $\beta$ -chitin and the corresponding hydrolysis product chitosan. The band at around  $2\theta$  of  $10^\circ$  decreases after deacetylation and is accompanied by a significant decrease in crystallinity [22].

### 3.4. Thermal methods of analysis

#### 3.4.1. Differential scanning calorimetry

The thermal behavior of  $\alpha$ -chitin was examined by differential scanning calorimetry (DSC) using a DSC-25 Mettler instrument. Samples (each 5 mg) were hermetically sealed in aluminum pans and scanned over a temperature range of 0–350 °C at a scan rate of 5 °C/min. The instrument was calibrated using indium, and the calorimetric data were analyzed using STAR software (version 9).

Figure 2.12 shows the DSC thermogram of  $\alpha$ -chitin. The melting transition is accompanied by compound decomposition above 300 °C [18].

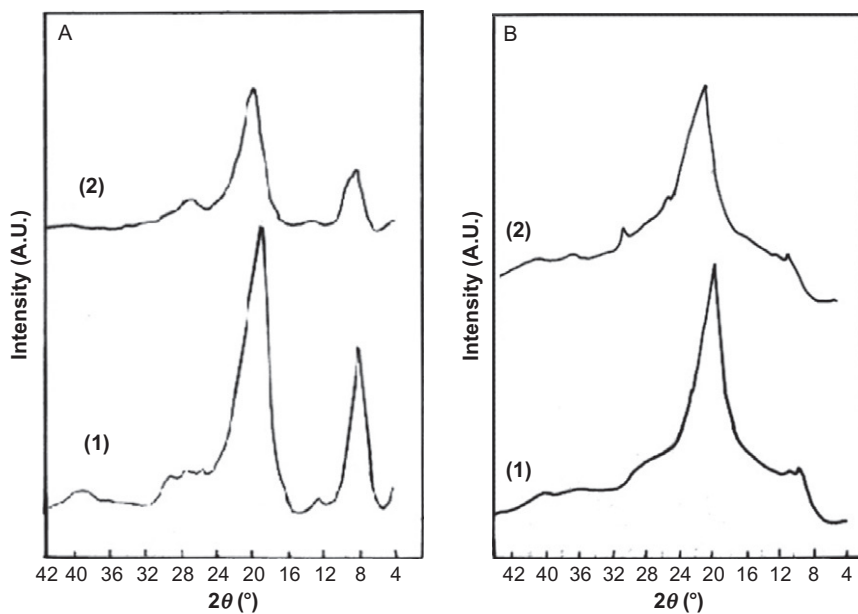


**FIGURE 2.11** XRPD patterns for (A)  $\beta$ -chitin from different sources (1) cuttlefish pens and (2) squid pens, and (B) the corresponding chitosan.

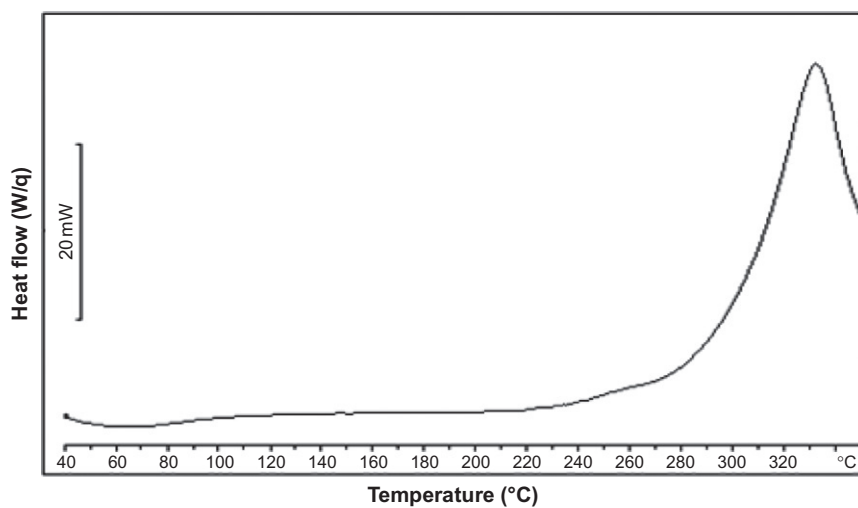


**FIGURE 2.12** The DSC thermogram of  $\alpha$ -chitin.

### 3.4.2. Thermogravimetric analysis

The thermogravimetric analysis (TGA) of  $\alpha$ -chitin was conducted using a TGA 2950 instrument. The sample was heated from ambient to 600 °C at a scan rate of 5 °C/min, using a sample mass of 3 mg. Figure 2.13A shows two weight loss steps, the first of about 6.2% (w/w) was due to water loss, and the other step starts at about 300 °C of 81.5% (w/w) corresponds to  $\alpha$ -chitin decomposition [18].

The TGA thermograms of  $\alpha$ -chitin obtained from different sources are shown in Fig. 2.13B. The thermal degradation of chitin occurs between 300 and 460 °C. The TGA thermograms for all samples showed a single major degradation step and the differences between chitin of different origins are relatively small (chitin from krill shows the highest thermal stability) [23].

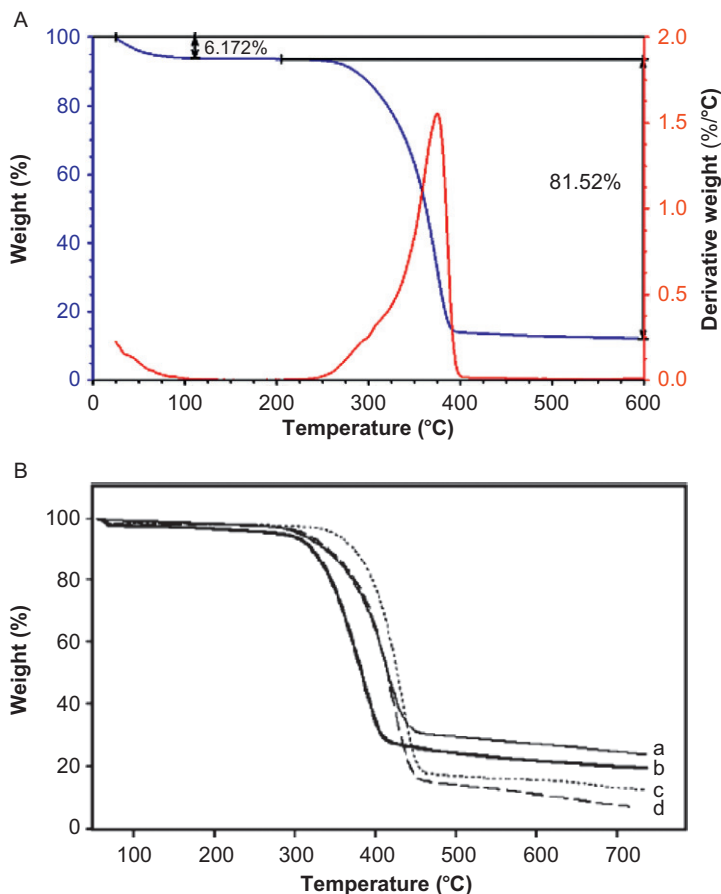


**FIGURE 2.13** The TGA thermograms of  $\alpha$ -chitin from (A) shrimp and (B) different sources: (a) crab, (b) squid, (c) krill, and (d) shrimp.

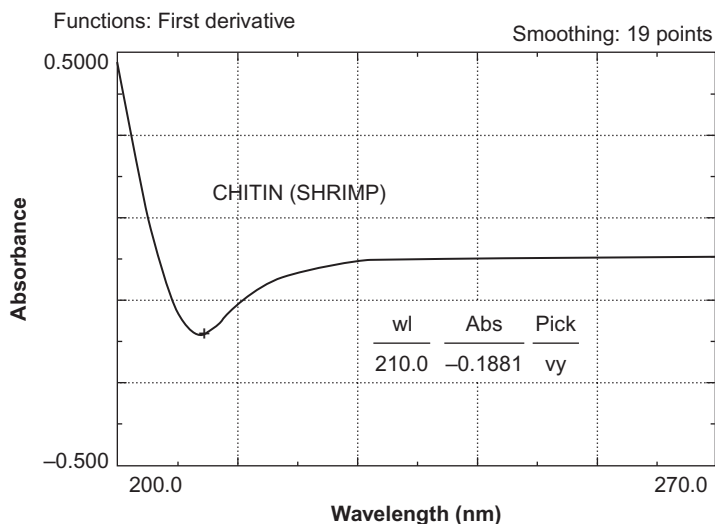


**FIGURE 2.14** The first derivative UV/Vis absorption spectrum of  $\alpha$ -chitin (100 mg/100 mL) dissolved in saturated solution of calcium chloride dihydrate in methanol.

### 3.5. Spectroscopy

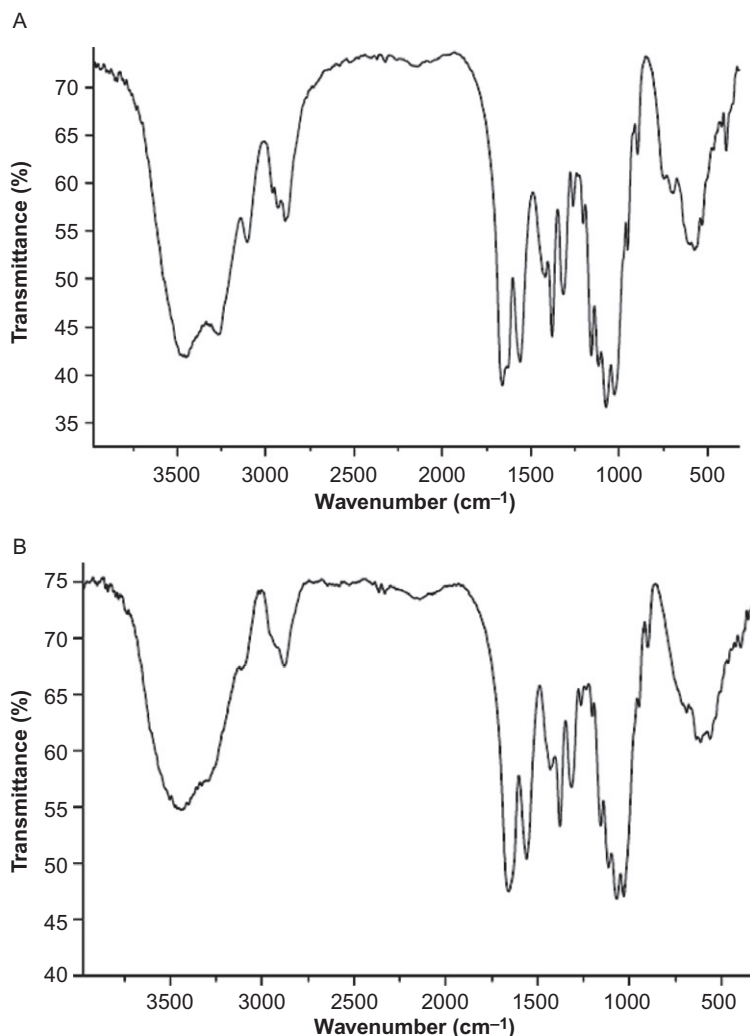
#### 3.5.1. Ultraviolet/visible spectrophotometry [18]

Figure 2.14 shows the first-derivative ultraviolet/visible (UV/Vis) scan of  $\alpha$ -chitin in a saturated solution of calcium chloride dihydrate in methanol. The minimum absorbance is observed at 210 nm. No absorbance maximum is observed in the investigated region.

#### 3.5.2. Fourier-transform infrared spectroscopy [20,21]

The Fourier-transform infrared (FT-IR) spectra of  $\alpha$ - and  $\beta$ -chitin are shown in Fig. 2.15. For  $\alpha$ -chitin, the amide I band is split at about 1650 and 1620  $\text{cm}^{-1}$  (Fig. 2.15A), whereas it is a single sharp band at about 1657  $\text{cm}^{-1}$  for  $\beta$ -chitin (Fig. 2.15B). The amide II band appears at about 1555 and 1559  $\text{cm}^{-1}$  for  $\alpha$ - and  $\beta$ -chitin, respectively. Both polymorphs show strong absorption bands in the 3100–3285  $\text{cm}^{-1}$  region which corresponds to the N–H group. The bands in the 2840–2960  $\text{cm}^{-1}$  region are due to CH, CH<sub>2</sub>, and CH<sub>3</sub> in both chitin polymorphs. The FT-IR vibrational modes of  $\alpha$ - and  $\beta$ -chitins are summarized in Table 2.8.

For comparison purposes, between  $\alpha$ -chitin and its deacetylated derivative chitosan, FT-IR spectra were obtained for  $\alpha$ -chitin and chitosan of different molecular weights. It is clear that the split bands at about 1650 and 1620  $\text{cm}^{-1}$  in the  $\alpha$ -chitin spectra (corresponding to amide I) appear as one band in the spectra of chitosans of molecular weights 1300–28,000 Da (Fig. 2.16). Also the band corresponding to NH in the range of



**FIGURE 2.15** FT-IR absorption spectrum of (A)  $\alpha$ - and (B)  $\beta$ -chitin.

$3100\text{--}3285\text{ cm}^{-1}$  disappears in the spectra of chitosan, which may indicate that the free  $\text{NH}_2$  group in chitosan becomes available to form H-bonds and subsequently broadens. Chitosans having molecular weights in the range of  $1300\text{--}2800\text{ Da}$  have the same FT-IR spectra in comparison with spectra of chitosan  $100,000\text{ Da}$ . The FT-IR spectra of chitosan  $100,000\text{ Da}$  showed little similarity to that of  $\alpha$ -chitin. This may indicate incomplete deacetylation of chitin in the case of high molecular weight chitosan ( $100,000\text{ Da}$ ) [18].

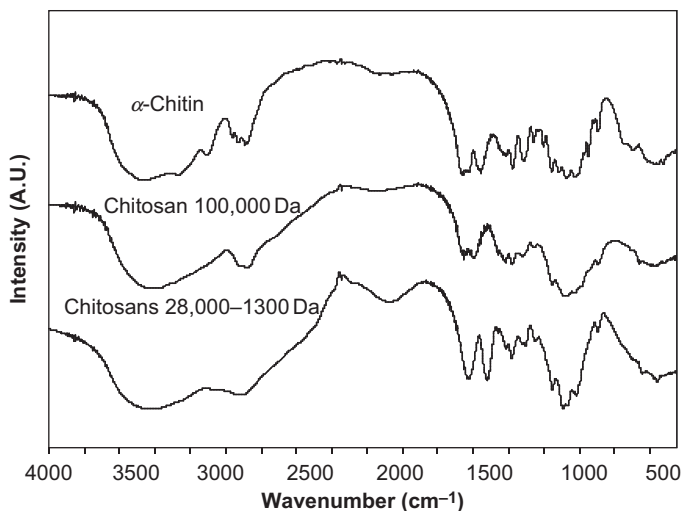
**TABLE 2.8** FT-IR vibrational modes of  $\alpha$ - and  $\beta$ -chitin

Vibration modes	Wave number ( $\text{cm}^{-1}$ )	
	$\alpha$ -Chitin	$\beta$ -Chitin
OH out-of-plane bending	685	690
NH out-plane bending	730	–
Ring stretching	890	899
CH <sub>3</sub> wagging along chain	975	–
CO stretching	1020	–
CO stretching	1025	1030
CO stretching	1065	–
CO stretching	1070	1069
Asymmetric in-phase ring stretching mode	1110	1114
Asymmetric bridge oxygen stretching	1155	1156
Amid III band and CH <sub>2</sub> wagging	1310	1314
CH bending and symmetric CH <sub>3</sub> deformation	1378	1377
CH <sub>2</sub> bending and CH <sub>3</sub> deformation	1420	1421
CH <sub>2</sub> bending and CH <sub>3</sub> deformation	1430	1430
Amide II band	1555	1559
Amide I band	1619	–
Amide I band	1652	1657
CH <sub>2</sub> symmetric stretching	2840	–
CH stretching	2878	2877
CH stretching	2890	–
Symmetric CH <sub>3</sub> stretching and asymmetric CH <sub>2</sub> stretching	2929	2931
CH <sub>3</sub> stretching	2962	2960
NH stretching	3106	3106
NH stretching	3264	3284
OH stretching	3447	–
OH stretching	3480	–

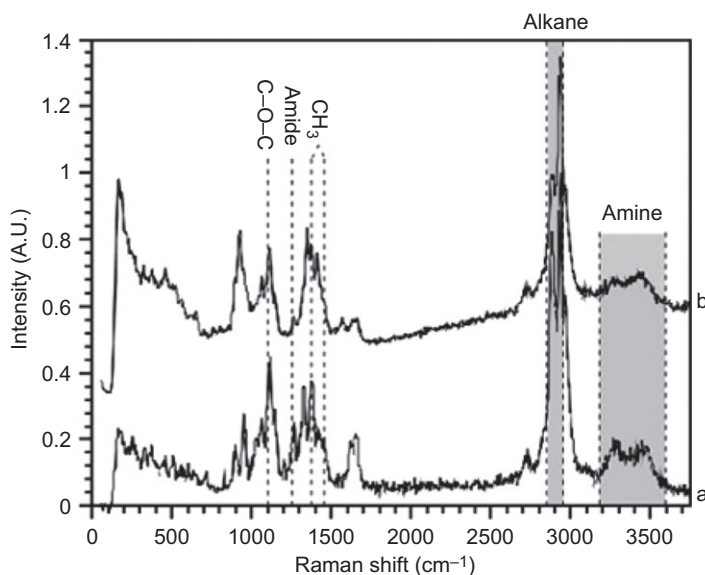
### 3.5.3. Raman spectroscopy

Figure 2.17 shows the Raman spectra of crab chitin (A) and spindles extracted from *Cratena peregrina* (B) as performed using a confocal Raman microscope (WITec GmbH, Ulm, Germany) equipped with a NdYag laser at a excitation wavelength of 532 nm [24].

The Raman spectra of spindles are almost identical with the spectrum of crab chitin. The close resemblance of the spectral profile between 1000



**FIGURE 2.16** FT-IR spectra of  $\alpha$ -chitin for chitosans of different molecular weights. The spectra of chitosans of molecular weights in the range of 1300–28,000 Da are represented by one spectrum for simplification.



**FIGURE 2.17** The Raman spectra of (a) the reference crab chitin and (b) the spindles of *Cratena peregrina*.



and  $1600\text{ cm}^{-1}$  suggests a comparable degree of *N*-acetylation for both samples. The characteristic Raman bands are listed in Table 2.9.

Raman spectra (Fig. 2.18) were obtained for both commercially available  $\alpha$ -chitin and after different acid treatments (demineralization) using a Lab-Ram Raman spectrometer. Raman measurements largely consisted of acquiring multiple spectral windows in the range of  $50\text{--}4000\text{ cm}^{-1}$  (Stokes shifts). The demineralization procedures for chitin are shown in Table 2.10 [18].

The Raman data in Fig. 2.18 show that the demineralized samples exhibit a similar spectral profile, both to each other and the commercial sample of chitin; however, the band intensities of the commercial sample are almost twice those of the chemically treated samples. The decrease in

**TABLE 2.9** Characteristic Raman bands

Group	Characteristic frequency ( $\text{cm}^{-1}$ )
Methyl: $\text{CH}_3$	1460 (bending) 1375 (deformation)
Alkane: C–C, C–H (methylene)	2850–2960
Alcohol: C–OH	3200–3600
Ether: C–O–C	1100
Amine: $\text{NH}_2$ (primary)	3359–3400 and 3200–3270
NH (secondary)	3100–3350
Monosubstituted amide: $\text{NH–C=O–CH}_3$	1260

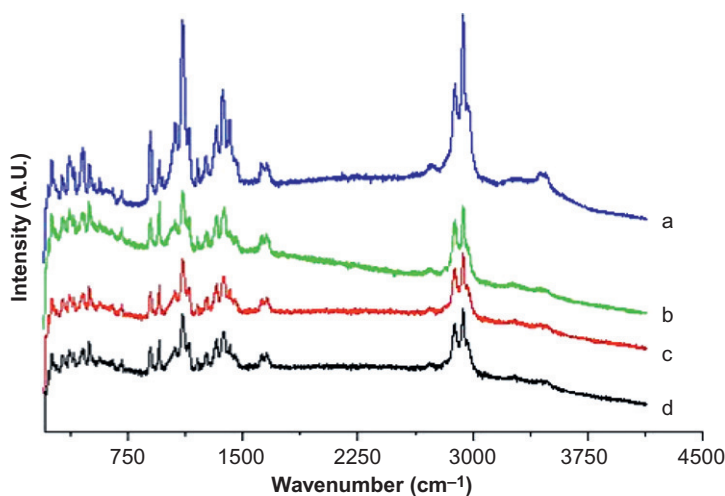


**FIGURE 2.18** The Raman spectra of (a)  $\alpha$ -chitin and (b, c, and d) demineralized samples using different acid solutions (see Table 2.9).

the peak intensities is most probable due to the loss of some crystallinity during the purification process. The significant decrease in the amine peaks at 3359–3400 and 3270–3200  $\text{cm}^{-1}$  may indicate the removal of acid soluble amine-containing contaminants.

### 3.5.4. Proton nuclear magnetic resonance spectroscopy [25]

The proton nuclear magnetic resonance ( $^1\text{H}$  NMR) spectrum of chitin was obtained in concentrated and deuterated hydrochloric acid (DCl) (Fig. 2.19). Chitin can be rapidly dissolved in concentrated acid after wetting in dilute acid. The assignment of the resonances and their chemical shifts (ppm) is given in Table 2.11. The  $^1\text{H}$  NMR spectrum shows the

**TABLE 2.10** Demineralization procedures used for different samples of  $\alpha$ -chitin

Demineralization solution	Sample			
	a	b	c	d
0.1 N nitric acid/2 h at 20 °C	Commercially available chitin			✓
1.2 N hydrochloric acid/2 h at 20 °C			✓	
1.0 N sulfuric acid/2 h at 20 °C			✓	
1.0 N sodium hydroxide solution/2 h at 20 °C		✓	✓	✓
Washing filtered chitin with distilled water to pH 6–8 and drying at 60 °C		✓	✓	✓

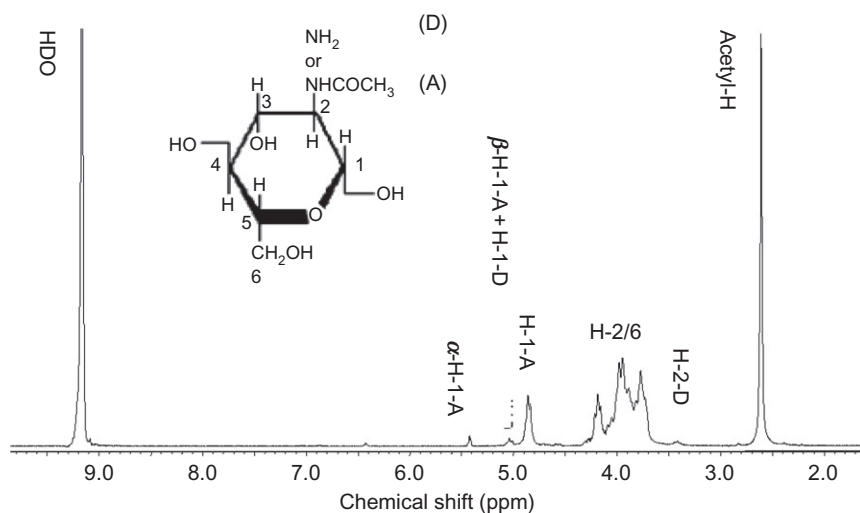


**FIGURE 2.19** The  $^1\text{H}$  NMR spectrum (400 MHz) of chitin in concentrated DCl at 25 °C obtained after 30 min of dissolution.

**TABLE 2.11**  $^1\text{H}$  NMR chemical shifts (relative to TSP at 0.00 ppm) of proton resonances for chitin in concentrated DCl at 25 °C

	H-1	H-1 (reducing end)		H-2	H-2 (reducing end)		H-2/6	Acetyl-H
GlcNAc (A)	4.91	5.43	5.05	3.44	3.57	3.32	3.5–4.4	2.62
GlcN (D)	5.07	5.65	5.21				3.5–4.4	

characteristic resonances in the anomeric region of the acetylated  $\alpha$ - and the  $\beta$ -anomer at about 5.43 and 5.05 ppm, respectively. H-1 of internal deacetylated units resonates at 5.07 ppm, overlapping with the  $\beta$ -anomeric proton, while H-1 of internal acetylated units resonates at about 4.91 ppm. H-2 of internal deacetylated units resonates at 3.44 ppm. Acetyl protons are found at about 2.62 ppm, while the remaining ring protons appear between 3.6 and 4.4 ppm. The  $\alpha$ - and  $\beta$ -anomer reducing end resonances from a deacetylated unit, which would be expected to appear at 5.65 and 5.21 ppm, are completely absent in the spectrum because there is no significant deacetylation in the sample (less than 2% after 24 h) and due to the specificity of the acid hydrolysis of the glycosidic bonds. The resonance from the protons of acetic acid appears at 2.24 ppm, meaning that any deacetylation of the chitin after its dissolution in concentrated DCl can easily be observed and quantified. The  $^1\text{H}$  NMR spectra of chitin in concentrated DCl can also be used to give an indication of the purity of the chitin sample as methyl-proton resonances from protein present in the sample would appear between 1.0 and 1.5 ppm.

### 3.5.5. Carbon NMR spectroscopy

The carbon NMR ( $^{13}\text{C}$  NMR) spectra for  $\alpha$ -chitin and chitosan of different molecular weights in the solid state were obtained using a Jeol Eclipse, 300 MHz FT-NMR spectrometer, incorporating a SH30T6/HS solid-state probe (Fig. 2.20). Samples were referenced with respect to a solid-state spectrum of 4,4-dimethyl-4-silapentane-1-sulphonic acid (DSS). The  $^{13}\text{C}$  NMR spectra were acquired using a standard  $^1\text{H}$  decoupled pulse sequence, with a relaxation delay of 1 s, the number of spectral accumulations was 10,240 scans, and the pulse width was 12.5  $\mu\text{s}$  [18]. In the spectra of chitosans, the gradual disappearance of the signals of the carbonyl and methyl groups of chitin by decreasing the molecular weight of chitosan is observed. This indicates that the depolymerization of chitin to form high molecular weight chitosan does not result in complete deacetylation, while further depolymerization to form low molecular weight chitosans leads to complete disappearance of these two signals. The well-resolved  $^{13}\text{C}$  NMR spectra of  $\alpha$ - and  $\beta$ -chitins are shown in Fig. 2.21. Each spectrum

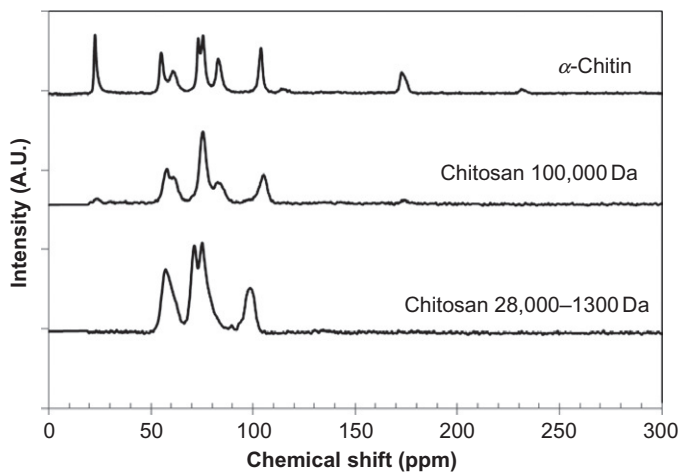


**FIGURE 2.20**  $^{13}\text{C}$  NMR spectra of  $\alpha$ -chitin and different molecular weight chitosan.

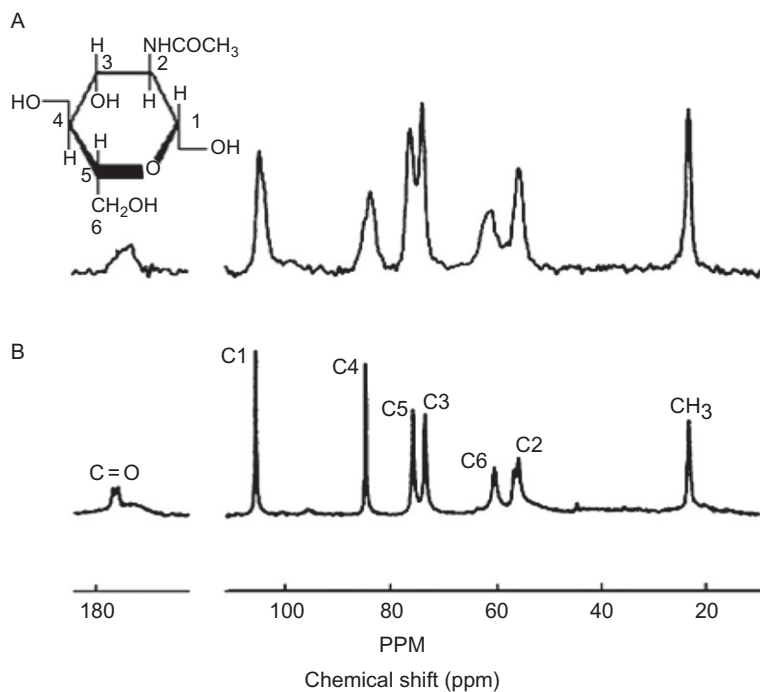


**FIGURE 2.21**  $^{13}\text{C}$  NMR solid-state spectra of (a)  $\alpha$ -chitin from deproteinized lobster tendon, (b)  $\beta$ -chitin from dried deproteinized tube of *Tevnia jerichonana*.

consists of six single-line signals and two doublets at C-2 and C=O, but these doublets are in fact singlets that are split by the effect of the  $^{14}\text{N}$  quadruple coupling. The splitting disappears if the spectra are acquired at higher field strength and becomes broader at lower field strength. In accounting for this phenomenon, there are therefore only eight signals for the eight carbon atoms of  $\alpha$ - and  $\beta$ -chitin. The corresponding chemical shifts are given in Table 2.12 [20].

The *N*-acetyl-D-glucosamine moiety in both chitins can be considered as the magnetic independent residue in full agreement with the crystal structure of  $\alpha$ - and  $\beta$ -chitin where this residue is also the crystallographic independent unit. Table 2.12 shows the similarity in  $\alpha$ - and  $\beta$ -chitin NMR signals which means that solid-state  $^{13}\text{C}$  NMR is not the appropriate technique to differentiate them.

### 3.5.6. Mass spectroscopy [26]

The mass spectrum (MS) of chitin was recorded using a VG Micro-mass 7070 F gas chromatography mass spectrometer unit. The electron paramagnetic resonance (EPR) spectra were recorded using a Varian EPR spectrometer. The MS recorded at a temperature of 300 °C is shown in Fig. 2.22. This temperature was used to obtain a more stable and rich fragmentation pattern. Table 2.13 presents the list of fragments that can be attributed to the ions detected in the recorded mass spectra (MS).

## 4. METHODS OF ANALYSIS

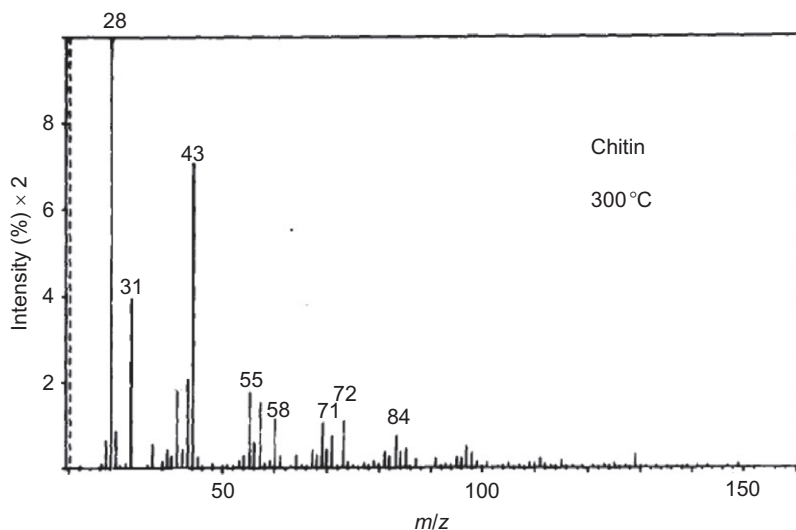
### 4.1. Identification [27]

$\alpha$ -Chitin may be identified on the basis of its characteristic infrared absorption spectrum using the KBr disc method as discussed previously in Section 3.5.2 (Fig. 2.23).

**TABLE 2.12** Assignments of the chemical shifts in the  $^{13}\text{C}$  NMR spectrum of chitin

Assigned carbon atom	Anhydrous $\beta$ -chitin from diatom spines (ppm)	$\alpha$ -Chitin from lobster tendon (ppm)
C <sub>1</sub>	105.4	104.6
C <sub>2</sub> <sup>a</sup>	55.3, 73.1	55.6
C <sub>3</sub>	73.1	73.7
C <sub>4</sub>	84.5	—
C <sub>5</sub>	75.5	83.6
C <sub>6</sub>	59.9	61.1
C=O <sup>a</sup>	175.6, 176.4	173
CH <sub>3</sub>	22.8	23.1

<sup>a</sup> The splitting for C<sub>2</sub> and C=O is due to the  $^{14}\text{N}$  quadruple coupling.

**FIGURE 2.22** Typical chitin MS (pH 4).**TABLE 2.13** Mass fragmentation pattern of chitin

Peak ( <i>m/z</i> )	Fragment
28	$>C=O$
31	$-CH_2OH$
43	$-COCH_3$
55	$-CHCHNH_2C$ 
58	$-NHCOCH_3$ 
71	$-CHNHCOCH_3$ 
72	$-COHHCNH_2CH$ 
84	$-CHNHCOCH_3CH$ 

## 4.2. Solution appearance

Chitin (1%, w/v) in saturated calcium chloride dehydrate-methanol produces a clear viscous solution.

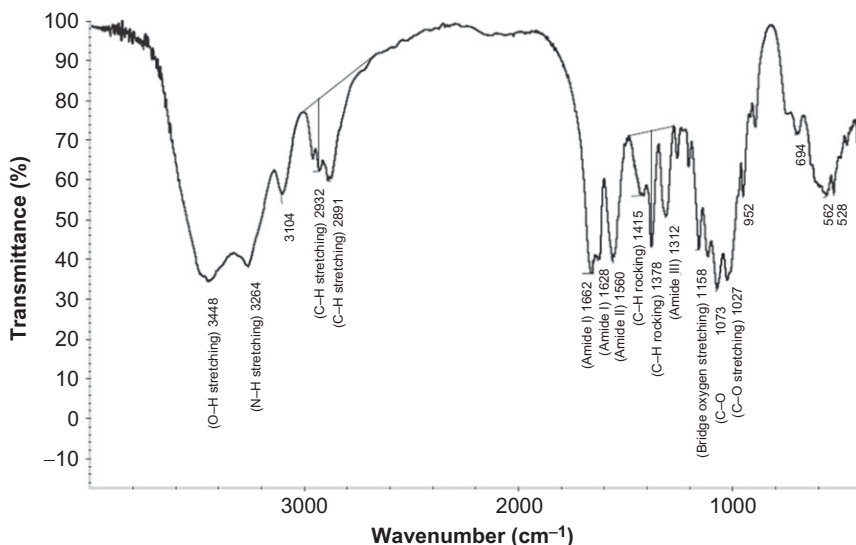


**FIGURE 2.23** Typical FT-IR spectra for  $\alpha$ -chitin.

#### 4.3. Chitin swelling and hydrophilicity [28]

Repeated freezing and thawing of chitin in alkali solution cause it to swell and dissolve because the chitin structure becomes friable during these physical changes. Water molecules are retained on the inner surface of chitin molecules. XRPD, FT-IR, and DSC were employed to investigate the structural changes for chitin treated by alkali-freezing. The formation, recrystallization, and growth of ice crystals could significantly reduce the intra- and intermolecular hydrogen bonds in chitin, destroy the highly rigid molecular structure, and reduce the crystallinity. The structural damage during slow freezing is more apparent than that during rapid freezing. The intensity of the five clear diffraction peaks in the XRPD spectra was obviously decreased in intensity by increasing the duration of the alkali-freezing treatment (Fig. 2.24).

#### 4.4. Specific optical rotation [29]

The presence of chitin in its natural levorotary conformation is believed to be of considerable importance for the use of chitin in acceleration of wound healing and other physiological activities. During the preparation and isolation of chitin (which involve using strong acid, alkali, or heat treatments), denaturation with consequent shifts in optical rotation to the dextrorotary (+) form occurs. When chitin is dissolved in a solution, it undergoes shift in optical rotation upon solution storage from dextrorotary to the natural levorotary structure (Table 2.14).

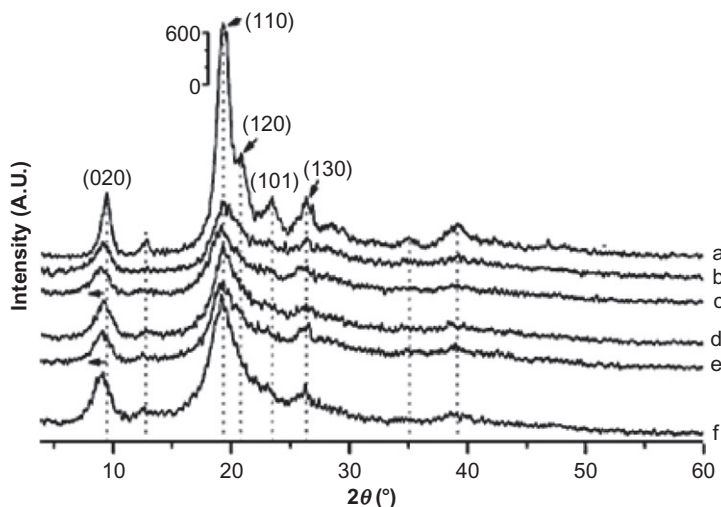


**FIGURE 2.24** XRPD profiles of (a) crude chitin and (b, c, d, e, and f) regenerated chitin samples frozen at  $-18^{\circ}\text{C}$  in alkaline solution for 1, 2, 3, 4, and 5 days, respectively.

**TABLE 2.14** Optical activity of chitin obtained from different sources

Chitin source	Optical activity of chitin ( $^{\circ}$ )	
	Initial $[\alpha]_{\text{D}}^{25}$	$[\alpha]_{\text{D}}^{25}$ after 2 weeks
Horseshoe crab	$-56$	$-56$
Blue crab	$+33$	$-52$
Red crab	$+23$	$-22$
Pink shrimp	$+75$	$-54$
Brown shrimp	$-36$	$-36$

#### 4.5. Molecular weight determination [30]

Size exclusion chromatography (SEC), which is also known as gel permeation chromatography (GPC) or gel filtration chromatography (GFC), using either viscometric, differential index, or multi-angle light scattering detectors can be used to study the different molecular weights (MW) and the distribution in solution of chitin and its derivatives. Determination of the molecular weight ( $M$ ) of chitin is related to the intrinsic viscosity  $[\eta]$  by the Mark–Houwink–Sakurada equation:

$$[\eta] = KM^a$$



where  $K$  and the exponent constant  $a$  values both depend on the polymer solvent system and the temperature. Using the GPC technique, the average molecular weight values for chitin polymer and molecular weight distribution (MWD) were obtained. The solution characteristic parameters (including the weight-average molecular weight ( $M_w$ ), number-average molecular weight ( $M_n$ ), and molecular weight polydispersity ratio ( $M_w/M_n$ )] were calculated and determined. Using a viscometer detector in GPC analysis, additional parameters to help define solution behavior such as weight-average intrinsic viscosity ( $[\eta]_w$ ), weight-average radius of gyration ( $R_{gw}$ ), and Mark–Houwink constants ( $a$  and  $\log K$ ) were determined as shown in Table 2.15. Chitin shows multiple peaks over the molecular range as shown in Fig. 2.25. The higher MW components were less resolved than the two distinct lower MW components. The value for the Mark–Houwink constant  $a$  obtained in this evaluation using 0.5% LiCl in DMAc was 0.6 (Table 2.15) (0.69 and 0.71 are reported

**TABLE 2.15** Calculated parameters for chitin in DMAc–LiCl solution

$M_w$ supplied	$M_w$	$M_n$	$M_w/M_n$	$[\eta]_w$ (dL/g)	$R_{gw}$ (nm)	Mark–Houwink		$\lambda$
	calculated	calculated				$a$	$\log K$	
Not available	$5.4 \times 10^6$	$1.8 \times 10^4$	360.6	0.16	12.5	0.6	−4.0	0.82

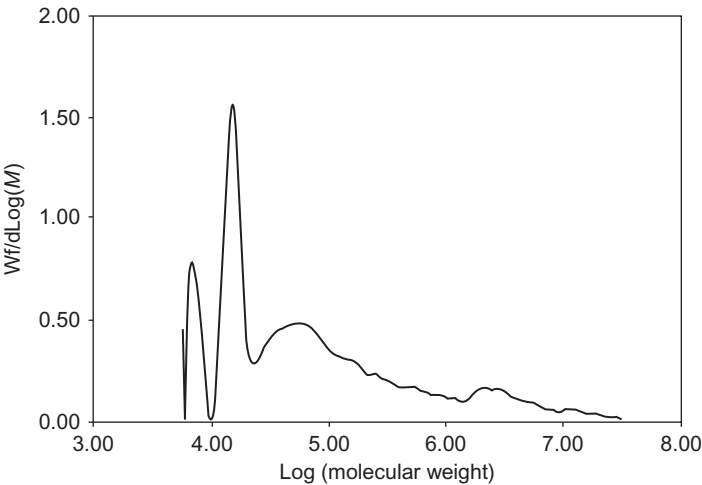


**FIGURE 2.25** Molecular weight distribution of chitin.

values for chitin in DMAc/5% LiCl). To reiterate, the lower concentration of LiCl facilitates GPC analysis because the lower viscosity of the mobile phase allows higher flow rates leading to faster time for complete elution.

#### 4.6. Electrical properties

$\alpha$ -Chitin has been reported to have electrical properties referred to as piezoelectricity, associated with anisotropic crystals, when subjected to pressure. The piezoelectricity properties depend on the mechanical and dielectric properties of chitin. The low dielectric values that have been reported may be due to the many microvoids that exist in the polymer. The dielectric constant increases with an increase in the adsorbed water content [6].

The dielectric constant ( $\epsilon'$ ) of chitin and chitin treated with acid, base, and hypochlorite was measured in the 0.1 kHz to 3 MHz frequency range (Fig. 2.26). It was noted that  $\epsilon'$  is decreased by increasing the applied frequency. This is due to the dielectric dispersion as a result of the lag of the molecules behind the alternation of the electric field which was observed when the frequency is less than 10 kHz. The  $\epsilon'$  value of chitin hypochlorite is higher than that of acid and base treated chitin up to 10 kHz. This can be attributed to strengthening of the intermolecular interaction by hydrogen bonding. The rigidity of the structure formed by intermolecular hydrogen bonding will decrease the mobility of molecules and thus result in an increase in  $\epsilon'$  values [3].

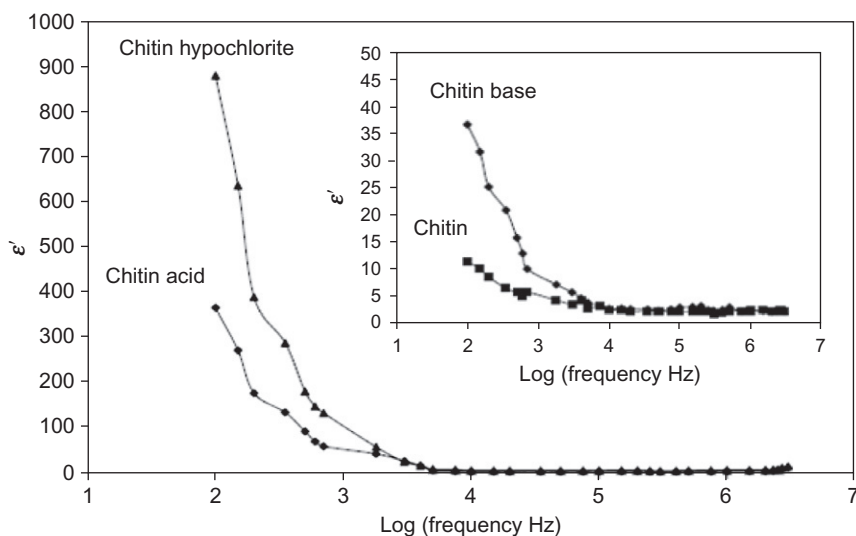


**FIGURE 2.26** Variation of the real part of the dielectric constant ( $\epsilon'$ ) with log frequency for chitin acid, base and hypochlorite at  $T = -30^\circ\text{C}$ .

#### 4.7. Determination of degree of *N*-acetylation [31,32]

The degree of *N*-acetylation (DA) is the ratio of 2-acetamido-2-deoxy-*D*-glucopyranose to 2-amino-2-deoxy-*D*-glycopyranose units. The DA may be obtained directly by determining the concentration of acetyl groups (GlcNAc), or indirectly by determining the amine group (GlcN) concentration. Methods used in the determination of DA for chitin can be classified as destructive and nondestructive. Nondestructive methods have the advantage of avoiding manipulation of the polymer. The consequences of destructive methods such as hydrolysis, pyrolysis or derivatization are not always well known/understood. A single technique cannot be adopted to analyze the full range of DA for chitin/chitosan. Due to the limited solubility of chitin,  $^{13}\text{C}$  CP/MAS NMR, DSC, and IR spectroscopy can be used for the analysis of chitin in the solid state. Generally, all techniques used in the determination of DA of chitin/chitosan show advantages and difficulties.

##### 4.7.1. Fourier-transform infrared spectroscopy [33,34]

The FT-IR spectrum of  $\alpha$ -chitin shows two absorption bands at approximately  $1625$  and  $1655\text{ cm}^{-1}$ , characteristic of hydrogen-bonded amide groups. The DA of chitin can be determined by the ratios of different IR absorption bands (Fig. 2.27), as these bands disappear upon deacetylation of chitin.

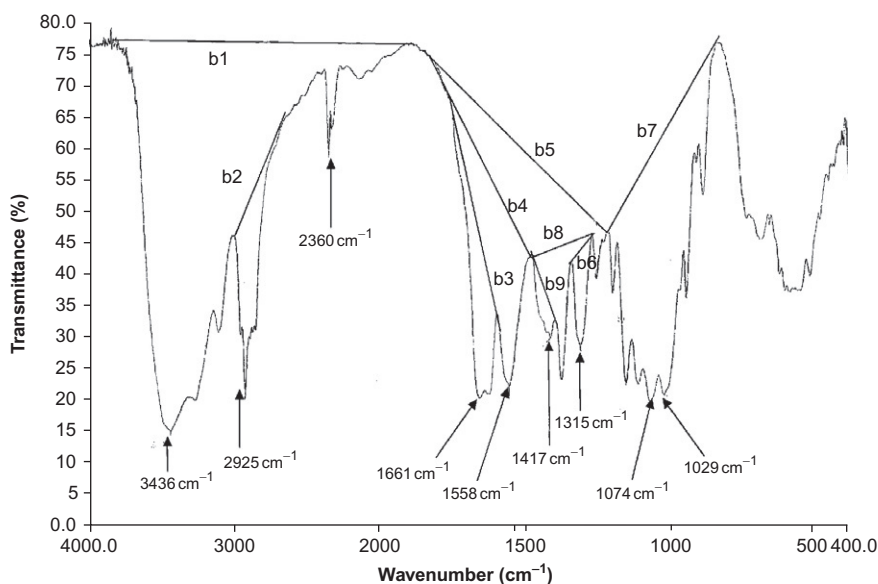


**FIGURE 2.27** FT-IR spectrum of chitin together with different baselines.

Several IR band absorption ratios have been used (Table 2.16) to determine the DA. Each band ratio is generally applicable for a limited range of the DA. Good initial data for quantitative analysis are obtained if a good baseline is selected and the spectrum is highly resolved. Crystalline  $\alpha$ -chitin displays more highly resolved spectra than those of amorphous  $\beta$ -chitin. The IR method has some disadvantages including the complicated statistical procedures for the evaluation of various absorption ratios; interference from the sample (minerals, proteins, water content, and pigments), and the long time required for calculating the DA. IR spectroscopy is generally used for qualitative analysis, and it is rarely used alone for quantitative analysis of the DA. In order to use IR spectroscopy quantitatively, appropriate probe and references bands must be selected, and a good baseline must be drawn for crystalline chitin/chitosan samples. IR was employed for quantitative analysis via statistical evaluation of several absorption ratios; a multivariate regression method; or determination of an absorption ratio and construction of a calibration curve (absorption ratio versus DA), where the DA of reference samples is obtained by IR or a reference method such as  $^1\text{H}$  NMR spectroscopy.

#### 4.7.2. Proton NMR spectroscopy [35]

The determination of the average DA of partially *N*-acetylated chitooligomers was preferentially carried out using proton NMR ( $^1\text{H}$  NMR) spectroscopy. The proton assignment of the diverse signals was deduced from  $^1\text{H}$  NMR data of GlcN and GlcNAc homo-oligomers. Compared with the  $^1\text{H}$  NMR spectrum of the GlcN oligomer mixture, spectra of *N*-acetylated chitooligomers differ essentially by the presence of characteristic signals of the GlcNAc units by (1) two singlets at  $\delta = 2.06/2.08$  ppm assigned to the *N*-acetyl protons and (2) a broad signal at 5.20 ppm corresponding to H-1 protons of the reducing end R anomer residues (Fig. 2.28). Consequently, the average DA of the different acetylated samples could be determined by considering both signal areas of H-2 protons of GlcN units ( $A_{\text{GlcN H-2}}$ ) and acetyl protons of GlcNAc units ( $A_{\text{CH}_3}$ ) according to the equation:

$$\text{DA}(\%) = \frac{1/3A_{\text{CH}_3}}{1/3A_{\text{CH}_3} + A_{\text{GlcNH-2}}} \times 100$$

The average DA values determined by this method are close to the expected values calculated from the molar ratio GlcNAc versus GlcN units used for the *N*-acetylation reaction (Table 2.17).

**TABLE 2.16** The different chitin/chitosan reported IR absorption band ratios, their corresponding degree of *N*-acetylation ranges: advantages and disadvantages

IR absorption band ratio	DA	Advantages	Disadvantages
$A_{1655}/A_{2870}$	0–20		Broadening and shoulder effects are observed in the region of the probe band; low resolution for small values of the DA
$A_{1655}/A_{3450}$	15–80	Suitable for crystalline and well-dried samples	Possible errors arising from the humidity or OH groups of polysaccharides; low resolution for small values of the DA
$A_{1630}/A_{3450}$	0–60		Possible errors arising from the humidity or OH groups of polysaccharides; possible error for high values of the DA
$(A_{1655} + A_{1630})/A_{3450}$	0–100	No broadening and shoulder problem; and suitable for crystalline and well-dried samples	Possible errors for high values of the DA
$A_{1560}/A_{2870}$	0–60		Many bands appear in the region of the reference band; broadening and shoulder effects are observed in the region of the probe band; low resolution for small values of the DA; OH bending band of water molecule appears in the region of the probe band
$A_{1655}/A_{1070}$	0–60		Many bands appear in the region of the reference band and possible error for high values of the DA
$(A_{1655} + A_{1630})/A_{1070}$	0–100	No broadening and shoulder problem, suitable for the effect of acetylation/deacetylation process on the DA	Many bands appear in the region of the reference band; broadening and shoulder effects are observed in the probe band region; and low resolution for small values of the DA
$A_{1655}/A_{1030}$	0–60		

(continued)

**TABLE 2.16** *(continued)*

IR absorption band ratio	DA	Advantages	Disadvantages
$(A_{1655} + A_{1630})/A_{1030}$	0–100	No broadening and shoulder problem	Many bands appear in the region of the reference band
$A_{1560}/A_{1070}$	0–100		
$A_{1560}/A_{1030}$	0–100		
$A_{1560}/A_{897}$	0–100		Possible error for high values of the DA
$A_{1560}/A_{1160}$	0–100		Possible error for high values of the DA
$A_{7669}/A_{7474}$	0–60	Reliable results for small values of the DA	
$A_{6039}/A_{5342}$	8–22	Applicable for small values of the DA	

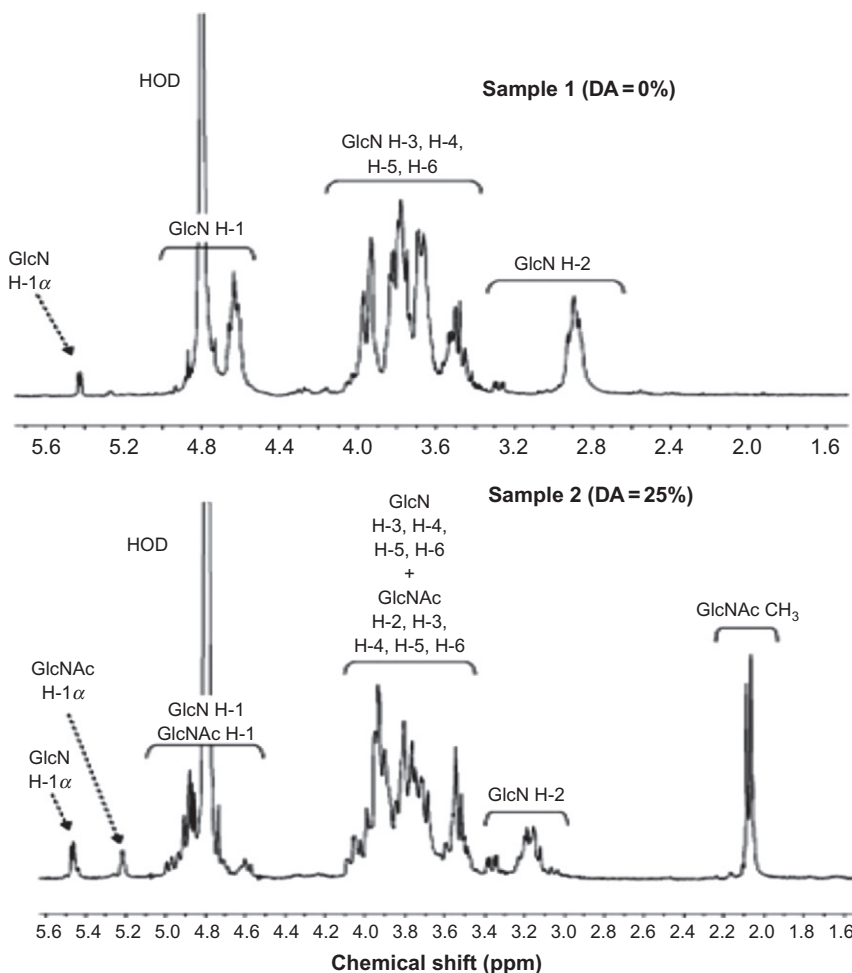


**FIGURE 2.28**  $^1\text{H}$  NMR spectra (300 MHz, in  $\text{D}_2\text{O}$ ) of fully deacetylated (DA) 0%, sample 1 and partially *N*-acetylated (DA) 25%, sample 2 chitooligomers. HOD, GlcN H-1 $\alpha$ , and GlcNAc H-1 $\alpha$  are the peaks of the HOD from  $\text{H}_2\text{O}$  exchange with  $\text{D}_2\text{O}$ , the anomeric proton of the deacetylated monomer and the *N*-acetyl proton, respectively.

#### 4.7.3. Carbon and Nitrogen NMR spectroscopy [36]

The carbon ( $^{13}\text{C}$  NMR) and nitrogen nuclear magnetic resonance ( $^{15}\text{N}$  NMR) spectra have been used for the determination of DA in solid chitin. Determination of the chemical composition of chitin using  $^{15}\text{N}$  NMR is considerably less sensitive than  $^{13}\text{C}$  NMR especially in the detection of acetylation levels lower than 10% which is not applicable due to the lower

**TABLE 2.17** Average degree of *N*-acetylation (DA) for the series of chitooligomers

Expected <sup>a</sup>	DA (%)	
	By <sup>1</sup> H NMR <sup>b</sup>	By mass spectroscopy <sup>c</sup>
25	24 ± 1	29 ± 2
40	41 ± 1	43 ± 2
60	60 ± 1	61 ± 2
80	78 ± 1	77 ± 2
90	90 ± 1	88 ± 2

<sup>a</sup> Calculated from the proportion GlcNAc versus GlcN residues used (mol/mol).

<sup>b</sup> Determined by <sup>1</sup>H NMR spectroscopy.

<sup>c</sup> Determined by MALDI-TOF mass spectroscopy.

abundance of this isotope and line-broadening effects. The <sup>13</sup>C and <sup>15</sup>N NMR spectra for the whole range of acetyl content from 0 to 100% are illustrated in Fig. 2.29A and B, respectively. <sup>15</sup>N NMR spectroscopy is a particularly powerful method for calculating the acetyl content in complex associations of chitin and other polysaccharides.

The carbon atom of carbonyl or methyl group has been used to calculate the DA from the integration of methyl carbon divided by the summation integrals of carbon atoms of the D-glucopyranosyl ring [C1–C6 atoms (*d* = 50–105 ppm)] as follows:

$$\text{DA}(\%) = I_{\text{N-CH}_3} / \left[ \frac{(I_{\text{C1}} + I_{\text{C2}} + I_{\text{C3}} + I_{\text{C4}} + I_{\text{C5}} + I_{\text{C6}})}{6} \right] \times 100$$

$$= I_{\text{N-CH}_3} / (1/6 \Sigma I_{\text{main chain carbons}}) \times 100$$

The <sup>15</sup>N NMR spectrum only shows two well-separated peaks corresponding to acetamide (NH–CO–CH<sub>3</sub>) and amine (NH<sub>2</sub>) groups (Fig. 2.29B). These two major peaks have been recognized in the spectra of chitin/chitosan, and the DA was calculated according to:

$$\text{DA} = \frac{I_{\text{N-acetyl group C1}}}{(I_{\text{N-acetyl group}} + I_{\text{amine group}})}$$

#### 4.7.4. X-ray powder diffraction analysis [37]

Figure 2.30A shows the X-ray powder diffraction (XRPD) patterns of chitin and chitosan with different degree of deacetylation (DD). Five crystalline index (CrI) reflections 020, 110, 120, 101, and 130 from the lower



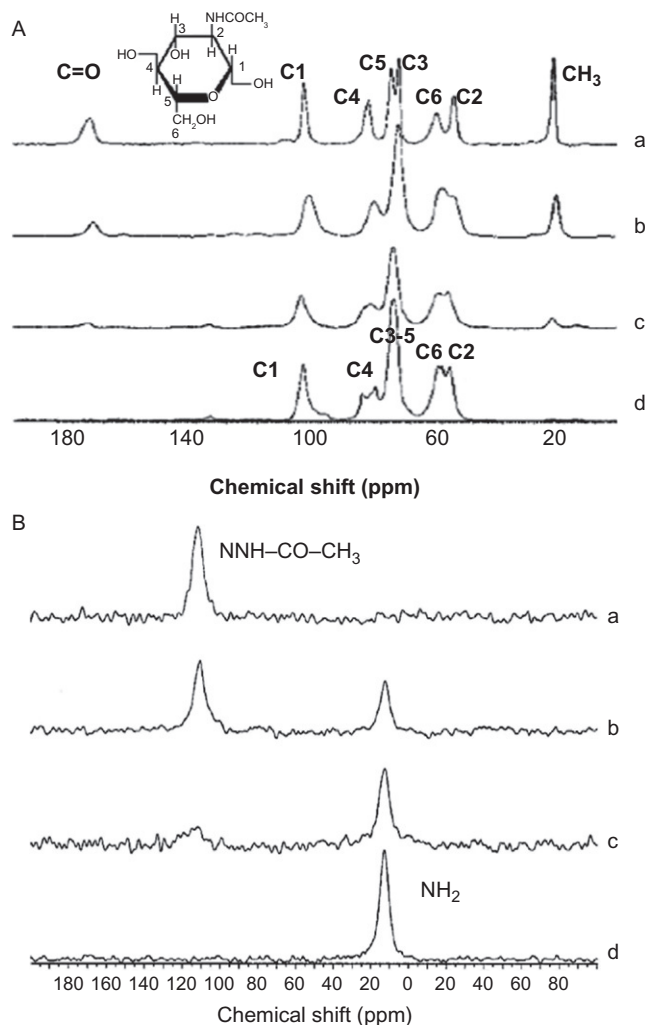


**FIGURE 2.29** (A)  $^{13}\text{C}$  NMR and (B)  $^{15}\text{N}$  NMR spectra of chitin/chitosan with different degree of *N*-acetylation (DA): (a) DA = 1.0, (b) DA = 0.58, (c) DA = 0.21, and (d) DA = 0.0.

angle for chitin were indexed, where  $\text{CrI}\%$  expressed as  $\text{CrI}_{020} = (I_{020} - I_{\text{am}})100/I_{020}$ ; another equation using  $I_{110}$  was expressed as  $\text{CrI}_{110} = (I_{110} - I_{\text{am}})100/I_{110}$ . It is noted that the maximum peak intensity at 020 reflection decreased linearly with an increase in DD as shown in Fig. 2.30B and moved to a higher angle, and the second maximum peak of

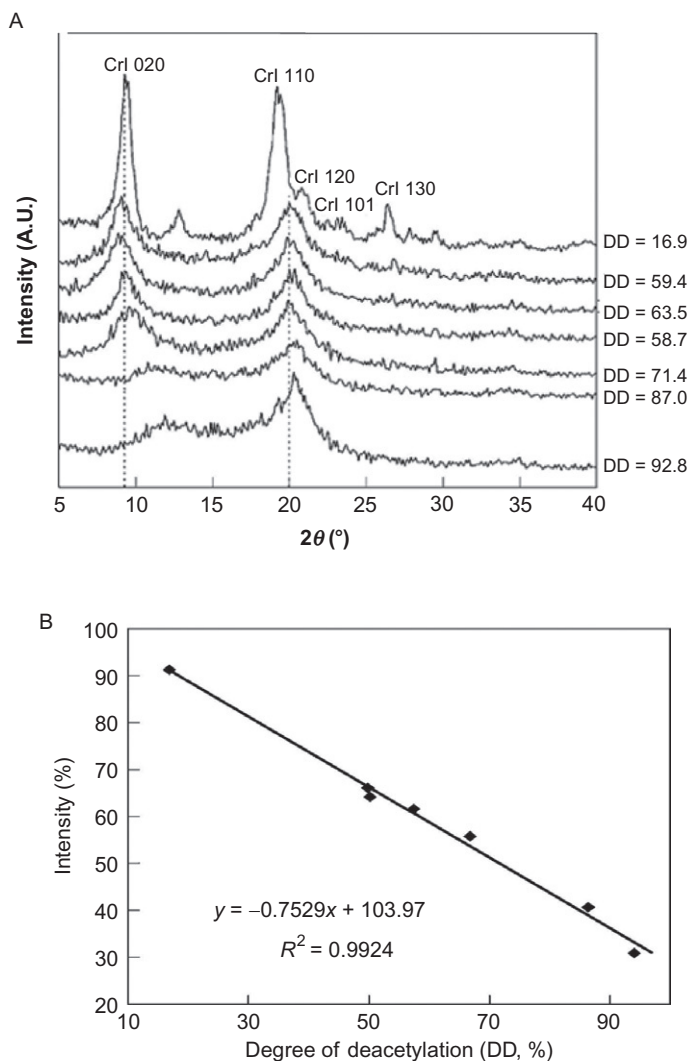


**FIGURE 2.30** (A) Comparison of XRPD patterns of chitin and chitosan with different DD, (B) crystalline index ( $\text{CrI}_{020}$ ) as a function of DD.

intensity at 110 reflection also decreased with the increase of DD and this linear relationship between  $\text{CrI}_{020}$  and DD suggested a possibility for XRPD to determine the DD content of macromolecular chitin and chitosan. The XRPD parameters of chitin and its deacetylated chitosan with different degree of *N*-acetylation are shown in [Table 2.18](#).

**TABLE 2.18** XRPD parameters for chitin/chitosan at different degrees of deacetylation (DD)

DD	$2\theta$ (°)	$d$ -Spacing (Å°)	Relative intensity (%)
16.9	9.39, 19.22, 20.73, 23.41, 26.39	9.41, 4.61, 4.28, 3.79, 3.37	100, 94.2, 38.1, 21.9, 28.7
59.4	9.06, 20.00, 23.78, 26.85	9.76, 4.43, 3.74, 3.33	100, 92.8, 37.4, 35.1
63.5	8.98, 19.87, 26.67	9.84, 4.46, 3.34	100, 96.4, 31.3
58.7	9.08, 19.91, 26.52	9.73, 4.45, 3.36	96.9, 100, 29.8
71.4	9.58, 20.14	9.22, 4.40	95.6, 100
87.0	10.65, 20.20	8.29, 4.39	58.9, 100
92.8	11.91, 20.35	7.42, 4.36	59.9, 100

#### 4.7.5. Elemental analysis [38–40]

Ideally, pure chitin with a DA of 1.0 ( $C_8NO_6H_{13}$ ) has a nitrogen content of 6.89%, while chitosan with a DA of 0.0 ( $C_6NO_4H_{11}$ ) has 8.69%. Accordingly, it is possible to determine the DA from data on the nitrogen content. However, because of the problems caused by the presence of moisture, which is difficult to eliminate, and the possible presence of inorganic materials, the use of the nitrogen/carbon (N/C) ratio is preferred. The chitin sample should be pure and free of protein (the absence of protein is indicated by no absorbance at 280 nm), since the N/C ratio of proteins is considerably different from those of chitin and chitosan. The DA of chitin can be determined using the following equation:

$$DA(\%) = \left[ \frac{\left( \frac{C}{N} - 5.14 \right)}{1.72} \right] \times 100$$

where C/N is the ratio (w/w) of carbon to nitrogen.

#### 4.7.6. Ultraviolet/visible spectrophotometry [41]

Chitin and chitosan can be assayed by first-derivative UV/Vis method using phosphoric acid (85%) as solvent. The chitin and chitosan solution is heated to 60 °C for 40 min to enhance solubilization and then incubated in diluted solutions at 60 °C for 2 h, and the first-derivative absorption is measured at 203 nm (Fig. 2.31). The developed method was reported to be useful for the determination of DA in the whole range (20–90%). Similar wavelength selection was made in a previous study where a wavelength of 202 nm was used, when acetic acid was used as a solvent.

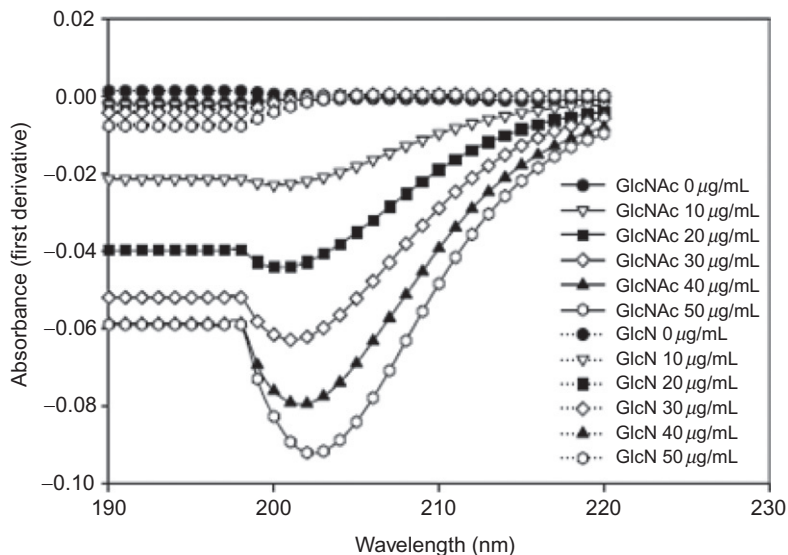


**FIGURE 2.31** First-derivative UV spectra of acetyl-glucosamine (GlcNAc) and glucosamine (GlcN) standards at concentrations ranging from 0 to 50  $\mu\text{g/mL}$ .

#### 4.7.7. Differential scanning calorimetry [42]

This method is based on the exothermic degradation peak observed for chitin and chitosan, which changes in temperature, area, and intensity depending on the DA. Under optimized conditions (heating rate, sample mass, and gas flow), a linear relationship between peak area and height with the DA could be achieved with linear correlation coefficients of  $-0.998$  and  $-0.999$ , respectively. Figure 2.32 shows the DSC curves for alkaline treated  $\alpha$ -chitin sample at  $100^\circ\text{C}$  for different time intervals to obtain different DAs. The exothermic peaks at  $295$  and  $400^\circ\text{C}$  were attributed to amine (GlcN) and acetyl (GlcNAc) groups, respectively. The peak area and height ascribed to the amine (GlcN) group increased and the acetyl (GlcNAc) residues decreased while the thermochemical alkaline deacetylation proceeds. The values and temperatures for peak area and height of the exothermic event relating to the decomposition of the amine (GlcN) group in addition to the temperature intervals used to integrate the peak areas are presented in Table 2.19.

#### 4.7.8. Mass spectroscopy [35]

The MS of a series of chito oligomers samples with different DA values from 25% to 90% obtained using this technique are shown in Fig. 2.33. The characterization of this series of samples with different DA values by

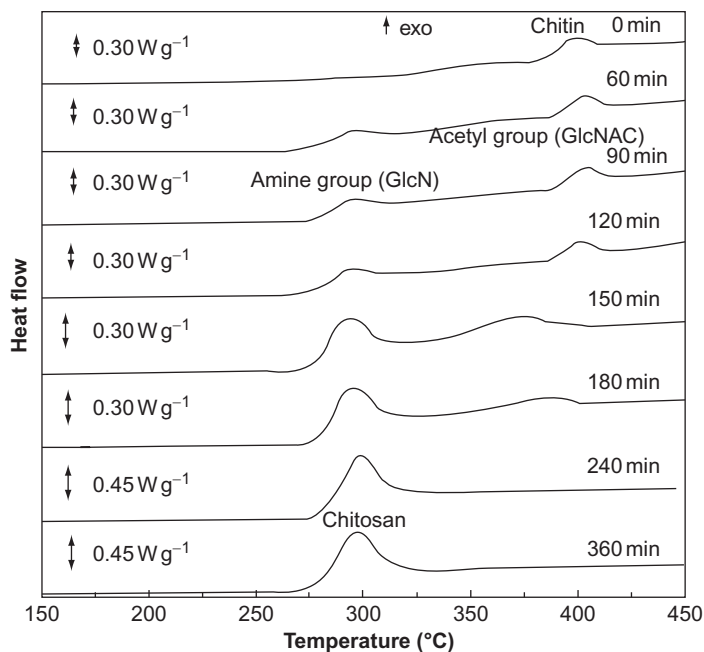


**FIGURE 2.32** The DSC thermograms under nitrogen atmosphere (50 mL/min), sample mass 3 mg at 5 °C/min for chitin/chitosan samples obtained at different reaction times of thermochemical heterogeneous deacetylation.

**TABLE 2.19** The DSC peak areas, peak heights, and the temperatures used in these determinations regarding the amine (GlcN) residues decomposition for chitin/chitosan samples with different degree of acetylation (DA)

DA (%) <sup>a</sup>	Interval temperature (°C)	Peak temperature (°C)	Peak area (J g <sup>-1</sup> )	Peak height (W g <sup>-1</sup> )
74.3	268–312	296	20.74	0.237
73.0	267–315	295	24.31	0.258
69.7	266–317	297	27.14	0.293
51.5	265–319	294	85.76	0.511
43.7	265–323	297	114.7	0.593
19.6	264–325	299	199.5	0.896
15.9	263–328	298	204.4	0.945

<sup>a</sup> Mean values from different techniques (<sup>1</sup>H NMR, <sup>13</sup>C NMR, and IR spectra).

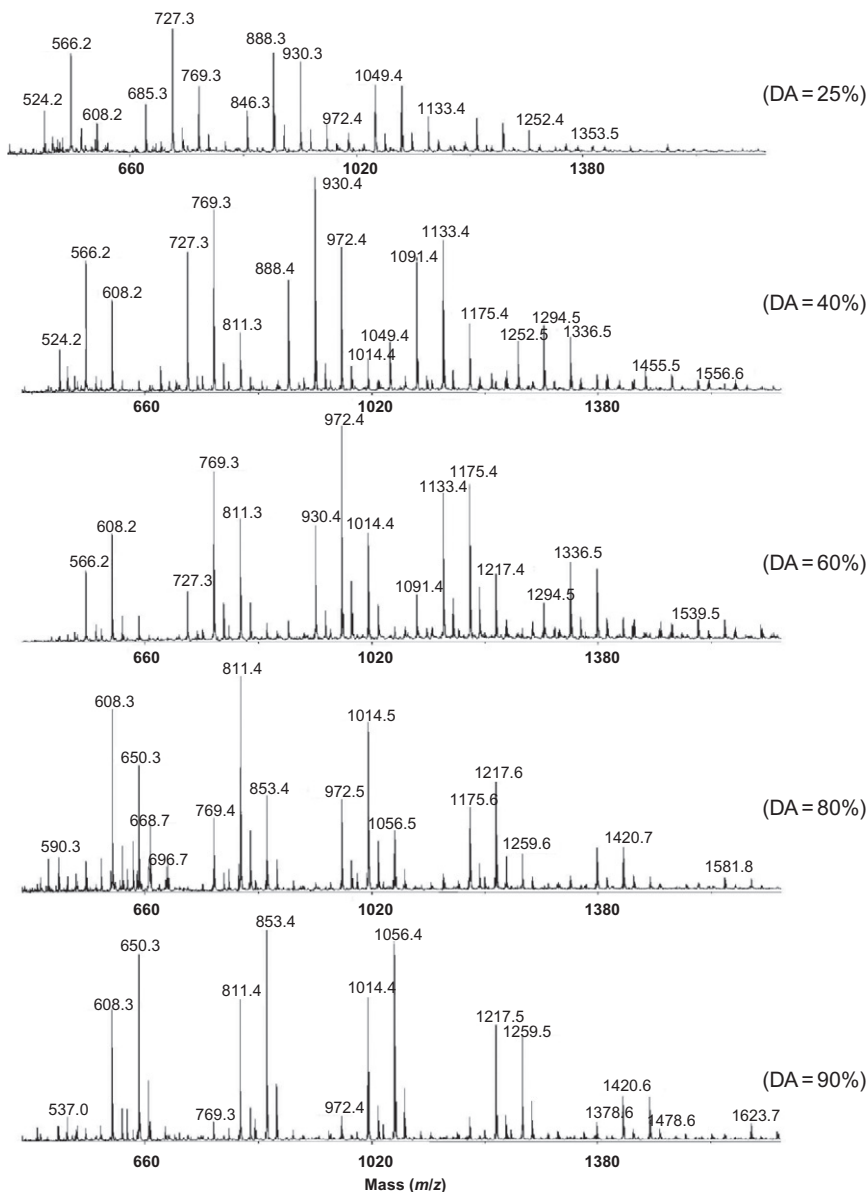


**FIGURE 2.33** Mass spectra of chitoooligosaccharides with different degrees of acetylation (DA).

$^1\text{H}$  NMR and MS allows the determination of their average DA and identifies the main oligomer structures constituting each mixture.

The % DA is calculated using the following equation:

$$\text{DA}(\%) = \left[ \frac{\sum_i \left( \text{DA}^{\text{th}}(\%) \right)_i \times (\text{ion intensity})_i}{\sum_i (\text{ion intensity})_i} \right]$$

where  $\text{DA}^{\text{th}}$  is the theoretical DA value directly deduced from the  $\text{D}_x\text{A}_y$  structure (D, for GlcN, and A, for GlcNAc) of the corresponding oligomer determined by MS. Compared to DA values determined by  $^1\text{H}$  NMR, the average DA values calculated by MS were found to be very similar for most of the samples (Table 2.17).

#### 4.7.9. Hydrolysis [43]

The DA of chitin can be determined by different hydrolytic techniques including chitin hydrolysis followed by determination of acetic acid or amino sugars produced. These methods have no requirement for the sample to be soluble.

#### 4.7.10. Pyrolysis [44]

This method can also be used in the determination of the DA of chitin based on reactive pyrolysis gas chromatography in the presence of oxalic acid aqueous solution. The DA could be determined from chromatography of the characteristic products of thermal decomposition of chitin in the absence of oxygen.

### 4.8. Determination of degree of depolymerization (hydrolysis)

#### 4.8.1. Mass spectroscopy [19]

This method is based on measuring the content of glucosamine monomers, after degradation with 6 N HCl, by liquid chromatographic–mass spectroscopic (LC–MS) techniques. The MS of the acid hydrolyzed chitin are shown in Fig. 2.34.

#### 4.8.2. Proton nuclear magnetic resonance [45]

The degree of deacetylation (DD) of chitin/chitosan samples was successfully determined using  $^1\text{H}$  NMR spectroscopy. Chitin/chitosan samples were dissolved in a mixture of 25% DCl in  $\text{D}_2\text{O}$  and chitosan samples in a mixture of 0.25% DCl in  $\text{D}_2\text{O}$ . The concentration of chitosan in the solution was about 0.5% (w/v). The  $^1\text{H}$  NMR spectra were recorded using a Varian Mercury 400 MHz spectrometer (Fig. 2.35). Table 2.20 shows the chemical shifts of chitin/chitosan protons in  $\text{D}_2\text{O}$ /DCl at 70 °C. The DD values were calculated using integrals of the peak of proton H1 of

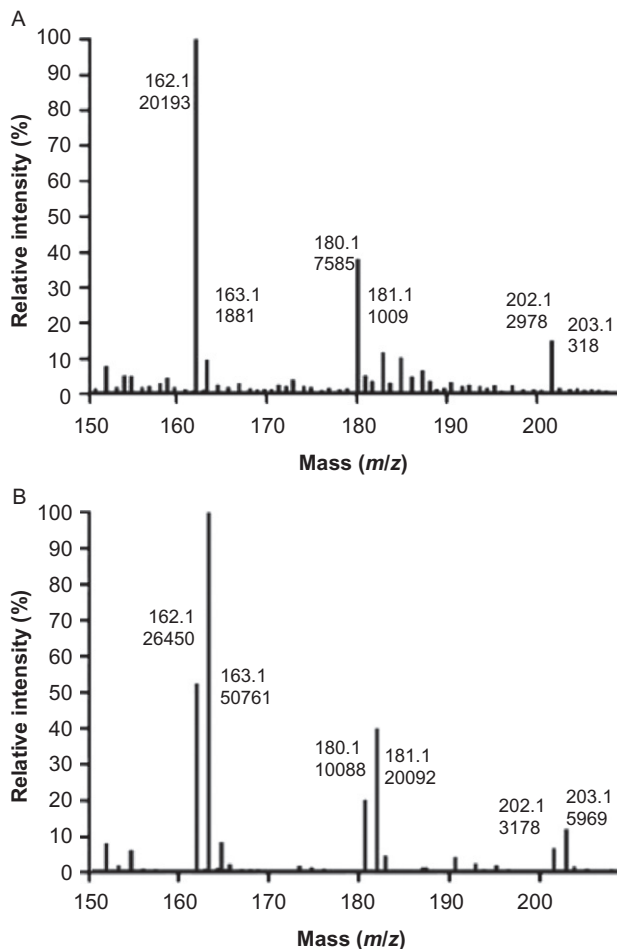


**FIGURE 2.34** MS spectra of acid hydrolyzed chitin from *P. chrysogenum* grown on (A) minimal medium, (B) medium with the addition of  $(^{15}\text{NH}_4)_2\text{SO}_4$  (rich medium—Blakeslee's formula).

deacetylated monomer (H1-D) and of the peak of the three protons of the acetyl group (H-Ac):

$$\text{DD}(\%) = \left( \frac{\text{H1-D}}{\text{H1-D} + \frac{\text{H-Ac}}{3}} \right) \times 100$$

For comparison, the DD values were also calculated using the signal from protons (H2-6) of both monomers and the peak of the acetyl group (H-Ac):



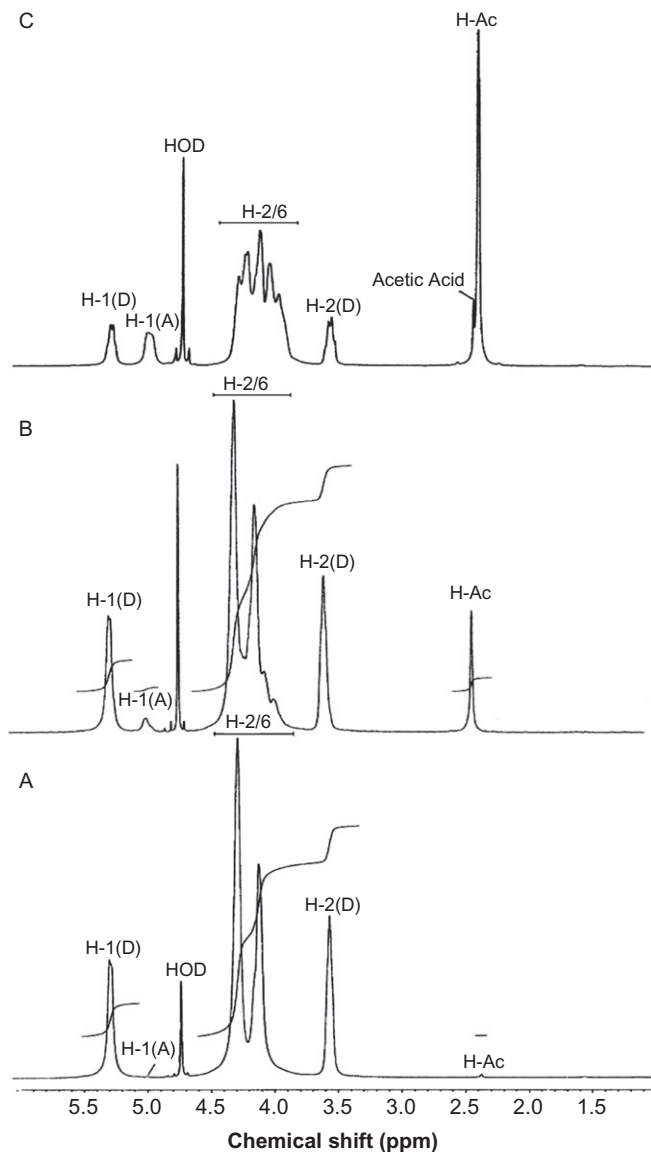


**FIGURE 2.35** The 400-MHz  $^1\text{H}$  NMR spectra at 70 °C for (A) chitosan with DD  $\cong 100\%$ , (B) chitosan with DD  $\cong 87\%$ , (C) chitosan with DD  $\cong 48\%$  (the peak at 2.41 ppm originates from acetic acid). The small peak at 2.36 ppm originates from the acetyl protons of chitosan. The RMS for the signal to noise ratio for this peak is about 3.1.

**TABLE 2.20**  $^1\text{H}$  NMR chemical shifts of chitin/chitosan in  $\text{D}_2\text{O}/\text{DCl}$  at  $70^\circ\text{C}$ 

	Protons				
	H-1(D)	H-1(A)	H-2/6	H-2(D)	Acetyl protons
Chemical shift (ppm)	5.21	4.92	3.9–4.2	3.52	2.36

$$\text{DD}(\%) = \left( 1 - \left( \frac{\frac{1}{3}\text{H-Ac}}{\frac{1}{6}\text{H-2/6}} \right) \right) \times 100$$

When the H-Ac peak is not well resolved due to the presence of contaminants (such as acetic acid in the sample) and also for samples with DD lower than 90%, the DD can be calculated by using the peaks of protons H1 of both deacetylated and acetylated monomer (H1-D and H1-A):

$$\text{DD}(\%) = \left( \frac{\text{H1-D}}{\text{H1-D} + \text{H1-A}} \right) \times 100$$

This equation is not suitable for high DD values because the H1-A signal does not appear in the NMR spectrum.

## 4.9. Chromatographic methods of analysis

### 4.9.1. Analysis of chitin impurities using HPLC [46]

A simple, rapid, selective, and specific HPLC method was developed to quantitate glucosamine, and its application for estimating the purity of chitin was investigated. The chromatographic separation was achieved using a reversed-phase C-8 column, pre-column derivatization with 9-fluorenylmethoxycarbonyl chloride (Fmoc-Cl) and ultraviolet detection ( $\lambda = 254$  nm). The mobile phase consisted of  $\text{CH}_3\text{CN}$  and  $\text{H}_2\text{O}$ . The optimum conditions of acid hydrolysis of chitin (concentration of HCl, temperature, and heating time) were obtained by performing the orthogonal array design (OAD) procedure, and the released glucosamine was determined by the aforementioned HPLC method. The accuracy of the method was checked by the standard addition technique. The method was found to be specific with good linearity, accuracy, precision, and well suited for quantitation of glucosamine and determination of the purity of chitin in biological materials and food products.

## 5. USES AND APPLICATIONS

Because chitin is a nontoxic material biodegradable material [13,47], it is attractive for use in a wide variety of applications.

## 5.1. Chitin: The solid dosage form excipient

### 5.1.1. Selection of chitin as an excipient

Lack of the amine group " $\text{NH}_2$ " makes chitin almost chemically inactive. In addition, the availability of chitin as the second most abundant material after cellulose allows its use as an excipient in processing solid drug dosage forms. This facilitates its use with other common excipients, namely microcrystalline cellulose (MCC), lactose, starch, and calcium hydrogen phosphate. Consequently, this monograph will focus on chitin applications as a solid dosage form excipient.

**5.1.1.1. Chitin as a tablet/capsule disintegrant [48]** Chitin is well known as a disintegrant in pharmaceutical solid dosage formulations in tablets to facilitate their breakup or disintegration after oral administration. Chitin, as a disintegrant, can be used at the 2–20% (w/w) level.

**5.1.1.2. Chitin as a tablet diluent and disintegrant [49]** A study was undertaken of directly compressed tablet matrices containing chitin or chitosan in addition to lactose, MCC, or starch formulation. Using lactose/chitin, lactose/chitosan, and lactose/MCC, tablet hardness increases with the addition of chitin, chitosan, and MCC as shown in Fig. 2.36A. Comparing the hardness of starch/MCC tablets with that of starch/chitin, there was no statistical difference at 10% and 30% (w/w) addition. The hardness of the tablets containing chitin, chitosan, and MCC is increased by increasing the compression force (Fig. 2.36B). This study also shows that the hardness of chitin tablets is greater than that of chitosan due to the structural rigidity of chitin, attributed to the acetylamino groups. Results suggest that chitin and chitosan can be used as direct compression diluents. Rapid disintegration time was obtained for tablets produced from lactose/chitin, lactose/chitosan, lactose/MCC, potato starch/chitosan, and potato starch/MCC below a certain concentration level of excipient (chitin, chitosan, and MCC) as shown in Fig. 2.36C.

**5.1.1.3. Directly compressed tablets containing chitin or chitosan in addition to mannitol** Mannitol is not a compressible material. The addition of chitin, chitosan, and MCC improves the compressibility of mannitol. The measured hardness for the tablets composed of mannitol/chitin, mannitol/chitosan, and mannitol/MCC increased with increase in the concentration of chitin, chitosan, or MCC (Fig. 2.37). Chitin, chitosan, and MCC should be added at a level  $>20\%$  (w/w) to improve the compressibility of mannitol tablets. The relationship between the disintegration time of tablets and the concentration of chitin chitosan or MCC excipients added to mannitol was investigated. Results showed that all tablets

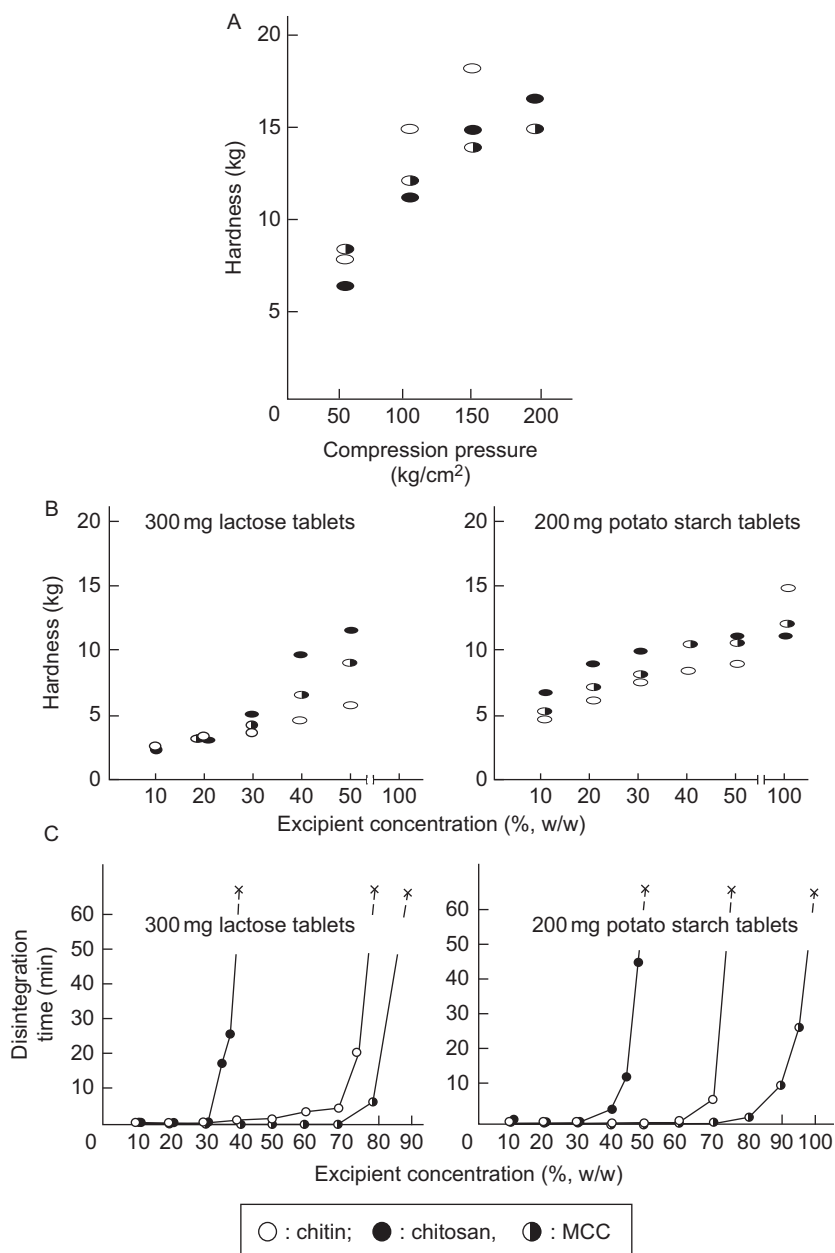


**FIGURE 2.36** (A) Relationship between tablet hardness and applied compression pressure. (B) Relationship between the tablet hardness and concentration of used excipient. (C) Relationship between tablet disintegration time and concentration of excipient (x, disintegration was not completed within 60 min).

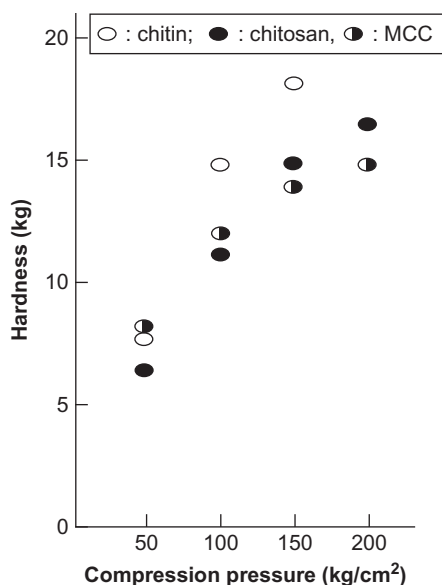


**FIGURE 2.37** The relationship between the tablet hardness and excipient concentration.

obtained disintegrate within 1 min except for those containing 80% (w/w) chitosan [50].

The compactibility of chitin and chitosan was evaluated by investigating the relationship between applied compression pressure and obtained tablet crushing strength (Fig. 2.38). Chitin and chitosan exhibited almost identical compression pressure-crushing strength profiles, being clearly more compressible than dibasic calcium phosphate (DBCP) and pregelatinized starch (PGS). MCC showed the highest tablet crushing strength values (highest slope of the curve) [51].

Table 2.21 shows the compression and friction properties (tensile strength, net work, compactibility, and  $R$ -value) of the chitin and chitosan in comparison with the commercial available reference excipients at an applied compression pressure of 94 MPa. The tensile strength and compactibility values for MCC were the highest among the others, while chitin and chitosan presented similar results of these parameters, and DBCP the lowest values. The excipients exhibited the same order with the present parameters as was found with the compression profiles. MCC, chitin, and chitosan presented the highest  $R$  values. The magnitude of this effect conformed to the following descending rank order: MCC, chitosan, chitin, PGS, and DBCP. Chitin and chitosan were found to be potential co-excipients for direct compression applications.

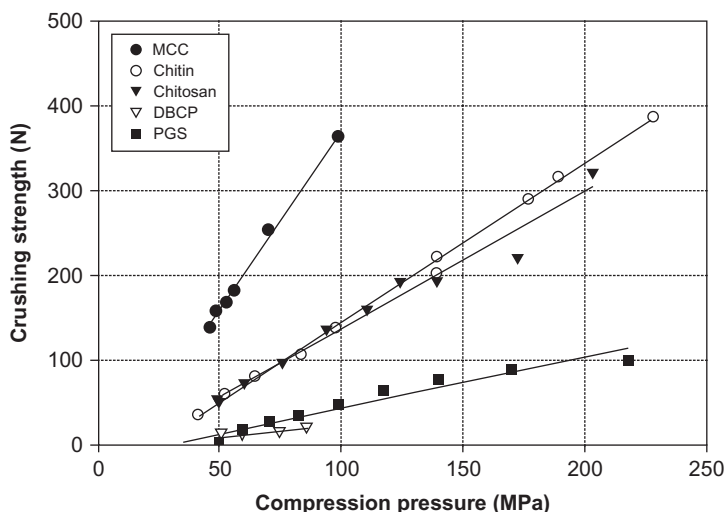


**FIGURE 2.38** Effect of compression pressure on the crushing strength of chitin, chitosan and direct-compressed reference tablets.

**TABLE 2.21** Compression and compaction properties of chitin, chitosan and direct compression reference excipients

Material	Tensile strength (MPa)	R-value <sup>a</sup>	$W_{\text{net}}$ (J)	Compactibility <sup>b</sup> (MPa/J)
Chitin	64.91	0.919	4.31	15.06
Chitosan	60.19	0.921	3.74	16.10
MCC "Avicel PH 102 <sup>®</sup> "	146.87	0.920	5.45	26.93
DBCP "Emcopress <sup>®</sup> "	8.96	0.679	2.62	3.41
PGS "Starch 1500"	18.16	0.726	3.18	5.72

<sup>a</sup> R-value is the lubrication coefficient.

<sup>b</sup> Compactibility is calculated from the ratio between tensile strength and net work " $W_{\text{net}}$ ".

#### 5.1.1.4. Coprocessed tablet excipient composed of chitin and silicon dioxide [52]

Chitin is a water-insoluble hydrophilic polymer that can absorb water and function as a disintegrant. Due to the unacceptable flow and compression properties of chitin, coprecipitation with silicon dioxide was used to provide a new excipient with excellent flow, compaction and disintegration properties when compared to the individual components or commercially available direct compression fillers and disintegrants. The optimal composition of the coprocessed excipient contains a silicon concentration of about 50% (w/w).

**5.1.1.5. Chitin metal silicates coprecipitates [53]** Coprecipitation of a metal silicate on chitin particles offers industrial potential for use as a single filler which has binding as well as super-disintegration properties and can be used in directly compressed tablets or in wet granulation methodologies. The coprecipitation process causes physical adsorption of the metal silicates onto chitin particles (Fig. 2.39) without any chemical interaction which has been proved by IR and XRPD analysis.

The good disintegration properties of the highly nonhygroscopic product are most likely to be related to capillary action (Fig. 2.40). Disintegration and binding properties were found to be independent of particle size and applied compression force (Fig. 2.41). The mechanical strength of the tablets produced, powder compressibility, and plasticity were all found to be dependent on the identity of the metal silicate (Fig. 2.42). Pharmaceutical applications including tablet formulations containing different active pharmaceutical ingredients indicated the good binding and disintegration abilities of chitin-metal silicates with poorly compressible and/or nonpolar drugs. The addition of magnesium stearate as a lubricant did not result in significant variation in disintegration, dissolution, and crushing strength of compacts prepared from chitin-Mg silicate. Such variation was clearly observed when a comparison was made with Avicel<sup>®</sup> 200 [54].

**5.1.1.6. Multifunctional excipient composed of  $\alpha$ -chitin and crystalline mannitol [55]** The coprocessing of  $\alpha$ -chitin with crystalline mannitol was investigated and found to significantly improve the performance and functionality of the obtained excipient when compared to individual components.  $\alpha$ -Chitin forms nonhygroscopic (Fig. 2.43), highly compactable, disintegrable compacts when coprocessed with crystalline mannitol.

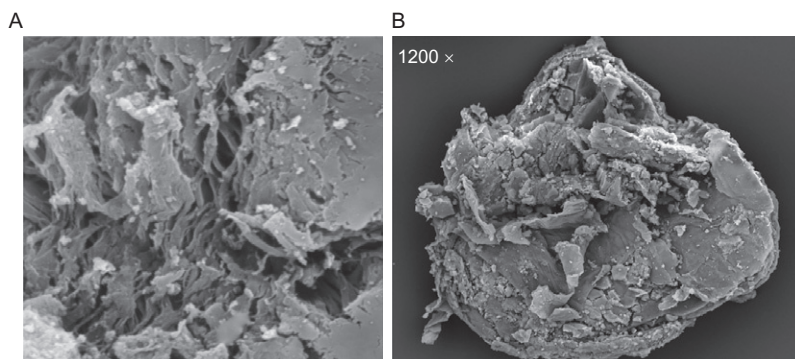


**FIGURE 2.39** SEM images of chitin-magnesium silicate coprecipitate particle (A)  $\times 24,000$  and (B)  $\times 1200$ .

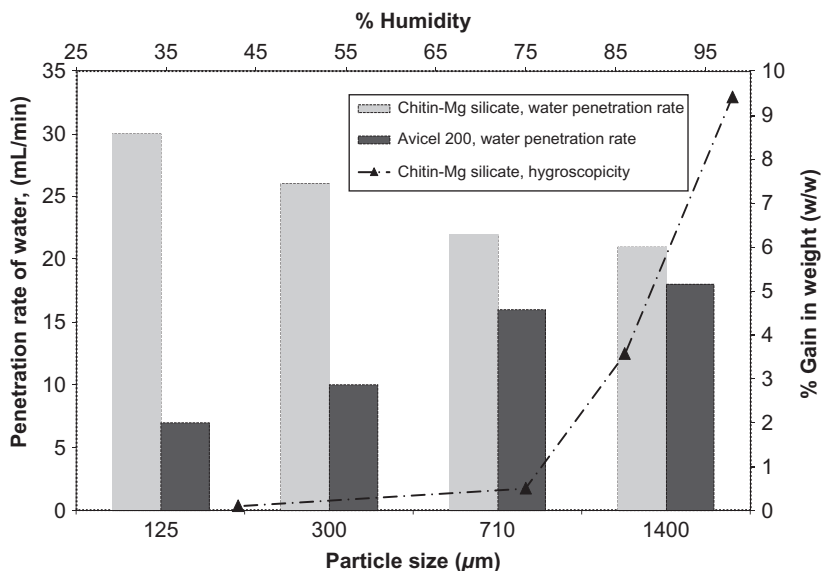


**FIGURE 2.40** Water penetration rate of chitin-Mg silicate and Avicel<sup>®</sup> 200 as a function of particle size (primary axis). Hygroscopicity measurements of chitin-Mg silicate coprecipitate under different humidity conditions, performed using standard salt solutions stored inside desiccators at room temperature for 1 week (secondary axis).

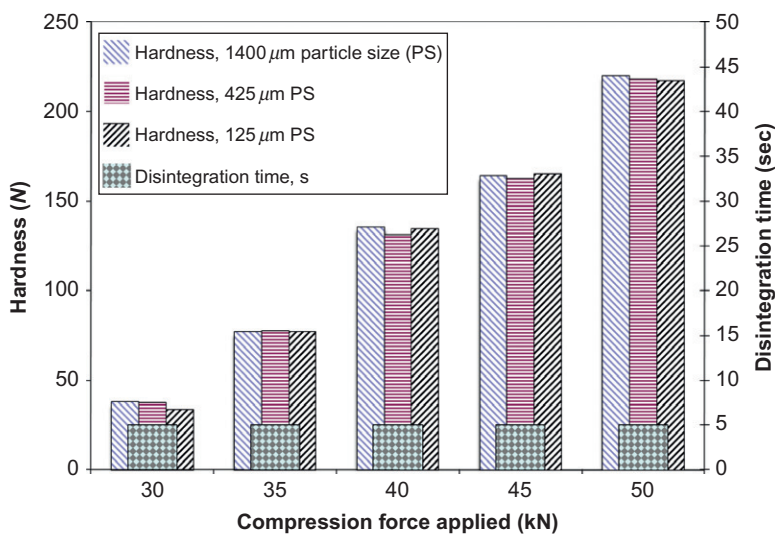


**FIGURE 2.41** Hardness and disintegration time as a function of compression force for different particle size of chitin-Mg silicate coprecipitate. Tablets were 12 mm in diameter and 400 mg in weight.



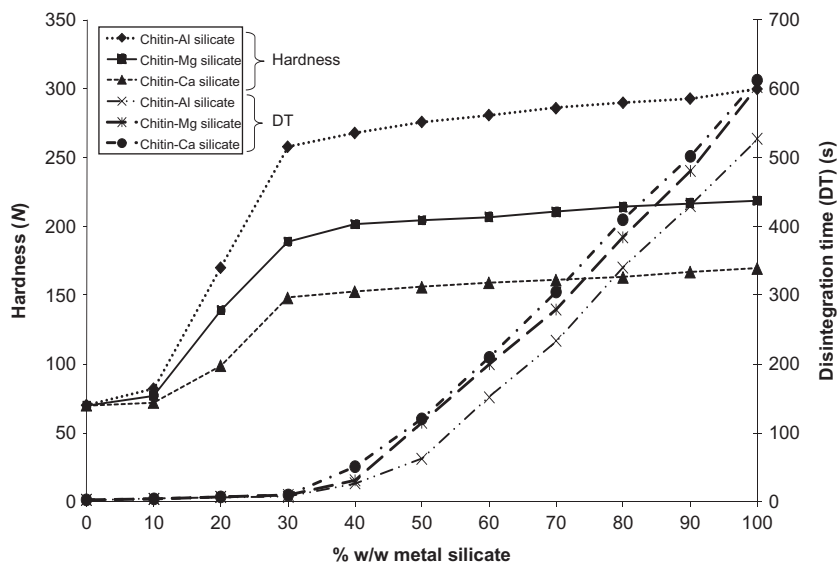


**FIGURE 2.42** Hardness and disintegration time as a function of chitin-metal (Al, Mg, and Ca) silicate content. Tablets were 12 mm in diameter and 400 mg in weight.

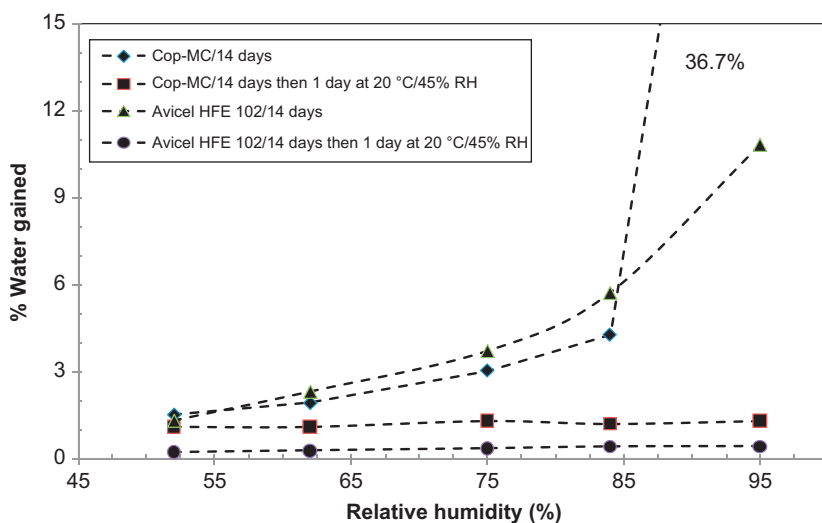


**FIGURE 2.43** The water gained by coprocessed chitin-mannitol excipient and Avicel HFE 102 kept in an open container at different humidity conditions at 20 °C.

The mechanical strength of the tablets and lubricant sensitivity were found to be dependent upon the mannitol content and the processing

technique used in the preparation of the coprocessed excipient. Optimal physicochemical properties of the excipient, from a manufacturing perspective, were obtained using a coprocessed mannitol–chitin (2:8 w/w) mixture prepared by wet granulation (Cop-MC) (Figs. 2.44 and 2.45).

Disintegration time, crushing strength, and friability of tablets, produced from Cop-MC using magnesium stearate as a lubricant, were found to be independent of the particle size of the prepared granules (Fig. 2.46).

This offers a potential use of this coprocessed additive as a single tablet excipient displaying super-disintegrating properties. The functionality of the Cop-MC excipient is not affected by the tablet preparation procedure whether it is direct mixing or dry/wet granulation. Utilization of Cop-MC, as an excipient, in tablet formulations containing active pharmaceutical ingredients, offers excellent chemical stability, binding, and disintegration properties.

#### 5.1.1.7. Oral disintegration tablet (ODT) excipient composed of crystalline mannitol and $\alpha$ -chitin [18]

A novel coprocessed excipient composed of crystalline mannitol and  $\alpha$ -chitin (Cop-CM) was investigated. The coprocessed excipient offers a unique multifunctional base for oral dissolving formulations. The driving force behind the fast dissolving behavior of the coprocessed mannitol and chitin mixture is obtained from the fast aqueous solubility of mannitol and the super-disintegration capabilities of the chitin. Disintegration time, wetting time, water absorption, crushing force, and friability of tablets, produced from Cop-CM using sodium stearyl fumarate as a lubricant, were not significantly altered by the change in the particle size of the prepared granules (Fig. 2.47). The good compaction and compression properties shown by Cop-CM were found to be dependent upon the quantity of added chitin in addition to the processing technique used in the preparation of the coprocessed excipient. FT-IR, DSC, and XRPD studies were used to prove the

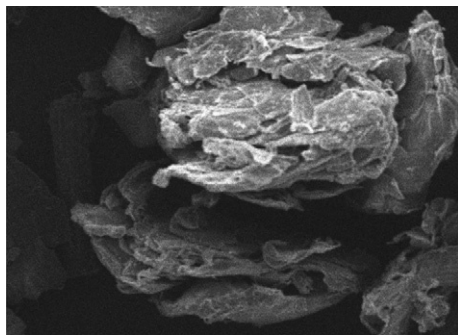


**FIGURE 2.44** SEM images of the coprocessed mannitol–chitin excipient.

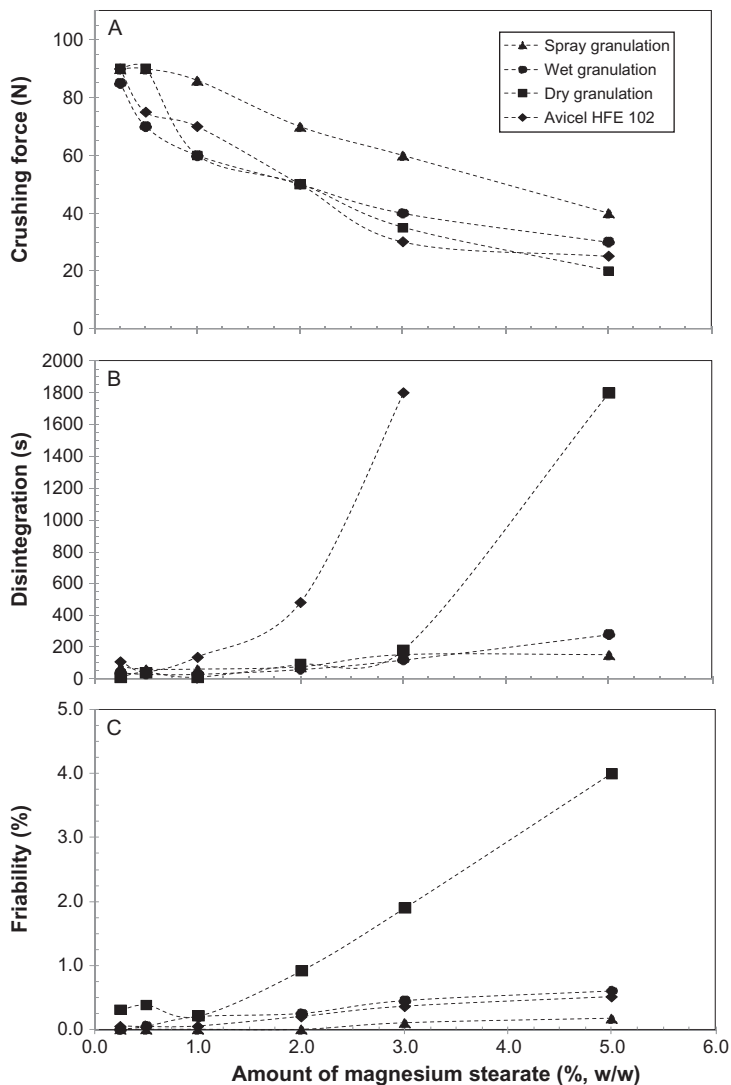


**FIGURE 2.45** Plots of the physical properties (crushing strength, disintegration time, and friability) of the coprocessed chitin-mannitol mixtures prepared by different granulation techniques versus the amount of magnesium stearate added.

absence of any chemical interaction between the mannitol and chitin in the Cop-CM mixture. These excellent binding and fast disintegration properties of Cop-CM can be successfully used in the formulation of fast disintegrating/dissolving tablets in addition to the conventional immediate release formulation as a multifunctional excipient.

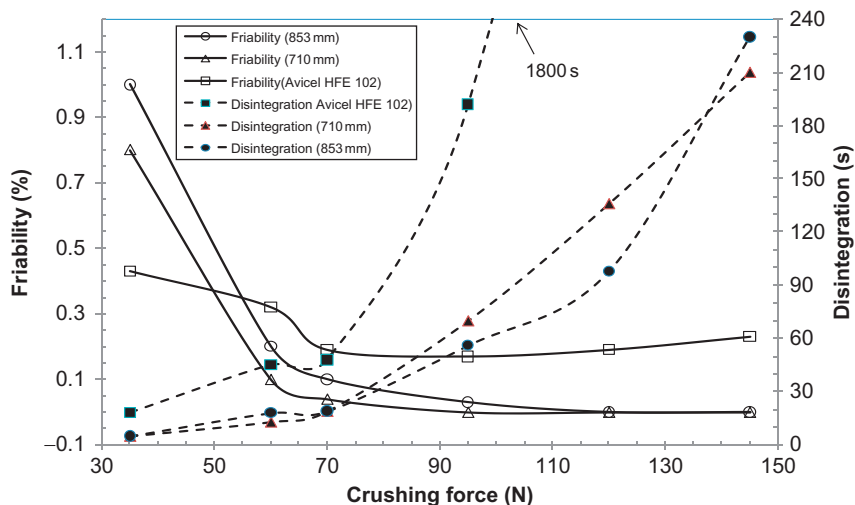


**FIGURE 2.46** Effect of the particle size of the coprocessed excipient of chitin–mannitol on tablet crushing strength, disintegration time, and friability prepared from this excipient. The tablets were 9 mm in diameter and 180 mg in weight. All samples were lubricated with 0.5% (w/w) magnesium stearate.

## 5.2. Other applications [17]

### 5.2.1. Production of chitin sheets

Chitin sheets are excellent for use in biomedical devices due to their biodegradability and lack of toxicity. These sheets can be prepared by simple procedures. A solution of  $\alpha$ -chitin, in saturated calcium chloride dihydrate–methanol solvent system, is dropped into excess of distilled water with gentle mixing to desolubilize the  $\alpha$ -chitin; the obtained chitin hydrogel is decanted several times with distilled water and filtered.  $\alpha$ -Chitin sheets are obtained after the evaporation of water.

Due to the loose crystalline structure of  $\beta$ -chitin, it can be highly swollen in water by vigorous mixing using a suitable blender and forms a hydrogel. A suspension will be formed by the addition of excess water to the  $\beta$ -chitin hydrogel which is then filtered to form the  $\beta$ -chitin sheets.

### 5.2.2. Chitin fibers

One of the major uses of chitin fibers is as sutures for surgery. Another important use is the production of paper by applying deproteinized ground chitin particles from a homogenized suspension to a continuous paper making machine.

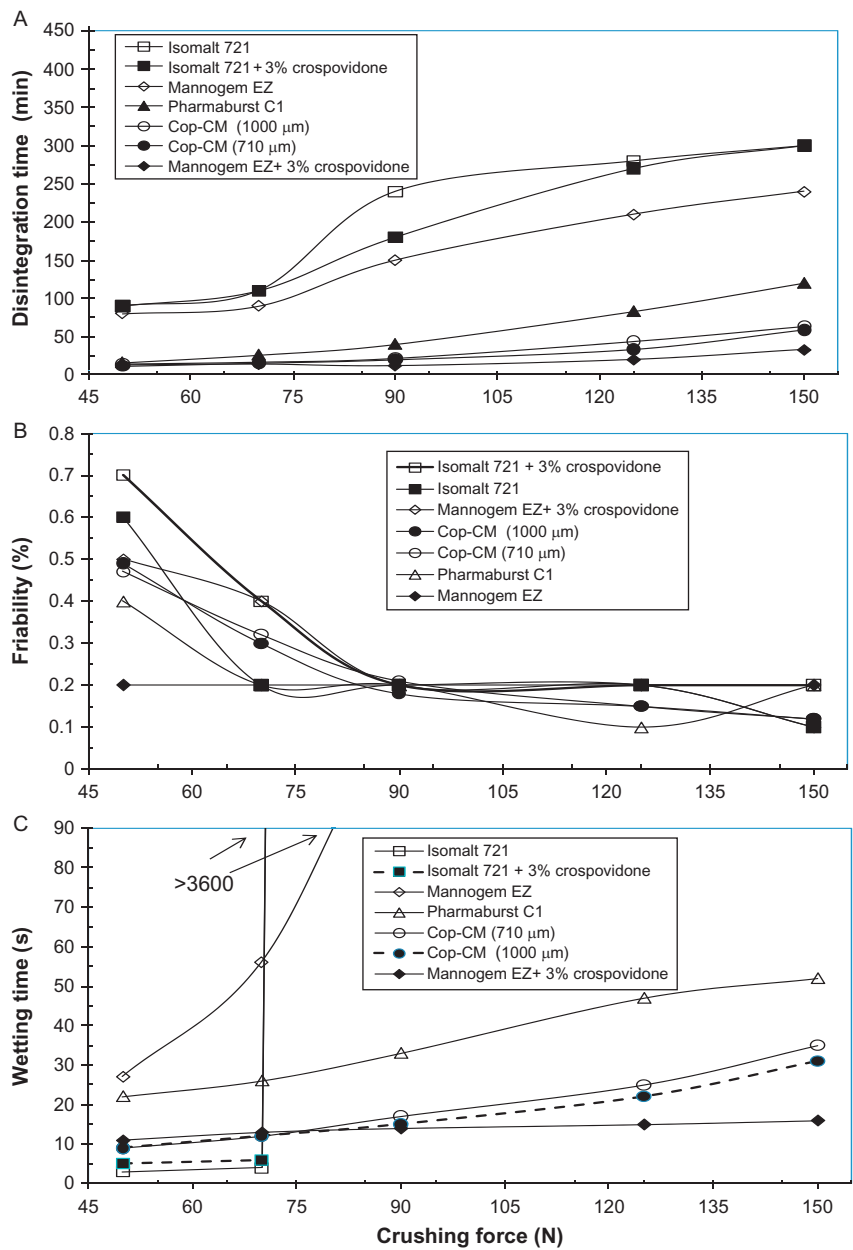


**FIGURE 2.47** Physical properties of the coprocessed mannitol–chitin excipient compared with commercially available ODT excipients.

### 5.2.3. As an analgesic

It is reported that chitin causes significant pain relief in the majority of cases treated with chitin over open wounds (including burns, skin abrasion, skin ulcer, skin graft areas). Studies undertaken on animals showed that animals treated with chitin and chitosan have no or less feeling of pain.

### 5.2.4. Antimicrobial activity

Studies on chitin and chitosan have already revealed inhibition of growth of several fungi and microbacteria, especially phyto-pathogens. Chitosan has a higher antifungal activity than chitin because the positively charged amino groups on chitosan inhibit the growth of fungi or microbacteria by forming polyelectrolyte complexes with negatively charged carboxyl anion groups present in their cell walls.

### 5.2.5. Antitumor effect (immuno-enhancing function) [12]

Chitin and chitosan oligomers were shown to act as antitumor agents via inhibition of the growth of tumor cells by immuno-enhancing effects. Chitin oligomers from (GlcNAc)<sub>4</sub> to (GlcNAc)<sub>7</sub> also display strong attracting responses to peritoneal exudate cells in BALB/c mice, whereas chitosan oligomers from (GlcN)<sub>2</sub> to (GlcN)<sub>6</sub> did not show this effect. Regarding the antitumor effect of chitin and chitosan oligomers with hexamers, (GlcNAc)<sub>6</sub> and (GlcN)<sub>6</sub>, respectively, it was found that the growth-inhibitory effect of both oligomers against allogeneic and syngeneic mouse systems, including sarcoma 180 and MM46 solid tumors, respectively, was pronounced.

### 5.2.6. Wound healing acceleration

The wound healing process passes three overlapped phases including [I]: inflammation, [II]: granulation tissue formation, and [III]: remodeling. The inflammation phase is divided into early and late parts that denote polymorphonuclear cell-rich and mononuclear cell-rich infiltrates, respectively. Collagen accumulation starts shortly after the onset of granulation tissue formation and continues throughout the remodeling phase. The wound healing will be delayed if inflammation continues in the wound due to the delay in the granulation tissue formation. Accordingly, to accelerate the wound healing cycle, each phase must be completed in the proper time. Although the effects on various aspects of biological activity produced by chitin varied, the action of chitin and chitosan was basically similar. [Figure 2.48](#) explains the wound healing process presented by chitosan and based on the biological activities.

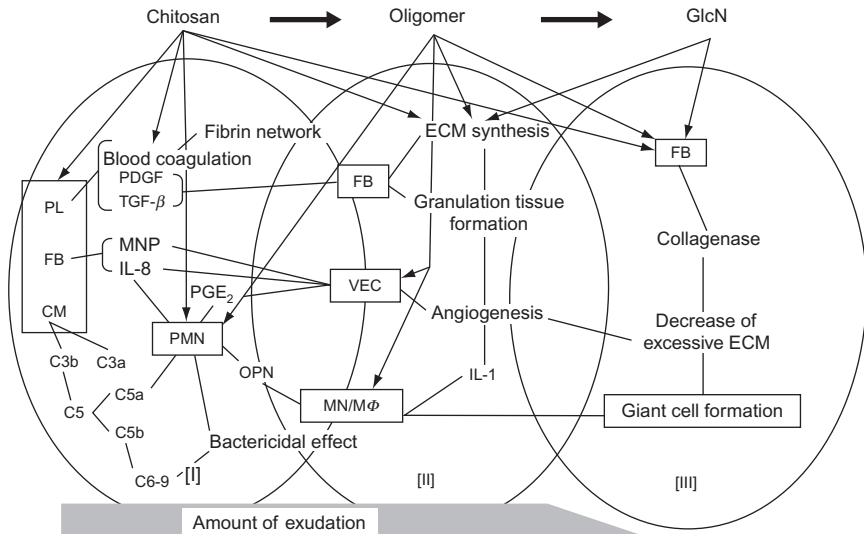


**FIGURE 2.48** Overview of promotion of wound healing by chitosan. Oligomer, chitosan oligosaccharide; GlcN, D-glucosamine; PL, platelet; FB, fibroblast; CM, complement; PDGF, platelet-derived growth factor; TGF-β, transforming growth factor β; MMP, matrix metalloproteinase; IL-8, interleukin-8; PGE<sub>2</sub>, prostaglandin E<sub>2</sub>; OPN, osteopontin; VEC, vascular endothelial cell; MN/Mφ, monocyte/macrophage; ECM, extracellular matrix; IL-1, interleukin-1. [I], inflammation phase; [II], granulation tissue formation phase; and [III], remodeling phase.

### 5.2.7. In agriculture [56]

Chitin showed growth accelerating and enhancing effects on crop production. Chitin also has antifungal properties that can be used to protect seeds from soil fungi by coating the seeds with chitin. Chitin can be used as an anti-nematode agent in soil.

### 5.2.8. In cosmetics [57]

Since chitin and chitosan are nontoxic and nonallergenic, they can be applied on the human body. They have been used in the production of emulsifiers, antistatic agents and emollients to extend the cosmetic product shelf life (e.g., shampoos and hair styling products).

### 5.2.9. In the food industry

Microcrystalline chitin has been used as a thickening/gelling agent in the binding, stabilizing, and texturing of food [58]. Chitin is widely used to immobilize enzymes and whole cells; enzyme immobilization has applications in the food industry, such as clarification of fruit juices and

processing of milk when  $\alpha$ - and  $\beta$ -amylases or invertase is grafted on chitin [20].

#### 5.2.10. In chromatography [6]

Chitin has been used as the stationary phase to separate mixtures of phenols, amino acids, nucleic acid derivatives, and inorganic ions by thin layer chromatography. Also chitin has been used to prepare affinity chromatography columns to isolate lectins and determine their structure.

#### 5.2.11. Chitin and chitosan [4]

Chitosan, the main derivative of chitin, has many applications in different fields. Some of these applications are summarized in Table 2.22 and compared with those of chitin.

## 6. STABILITY

Chitin is a stable compound, incompatible with oxidizing agents [59]. In the solid state under alkaline condition (e.g., NaOH, KOH, heat at about 120 °C) or by enzymatic hydrolysis in the presence of a chitin deacetylase, it hydrolyses to form the deacetylated degradation product chitosan [6,7,10,11]. It was found that the presence of urea in basic media and at low temperature (−20 °C) had little effect on chitin structure and that urea is of benefit to the stability of chitin solution [38].

In acidic condition including acetolysis with acetic anhydride/H<sub>2</sub>SO<sub>4</sub>, hydrolysis with HCl/sonolyses under ultrasound irradiation, and fluorohydrolysis with anhydrous HF or by the enzyme chitin deacetylase, it forms smaller oligosaccharides [12].

The effect of hydrogen peroxide on the stability of chitin by microwave radiation was investigated, it was suspended in water, and 30% hydrogen peroxide was added in quantities to achieve H<sub>2</sub>O<sub>2</sub> concentrations of 1%, 5%, 9%, and then subjected to 600 W microwave radiation for 10–30 min. The results indicated that chitin degradation with hydrogen peroxide in a microwave field caused significant changes in the molecular weight and the chemical structure of the polymer in a short period (up to 30 min). The limiting viscosity numbers of the degradation products were from 15% to 83% lower than those of the initial chitin [60].

## 7. BIODEGRADABILITY AND TOXICOLOGY [17,59,61]

Chitin is a biodegradable material and undergoes biodegradation by enzymes such as lysozyme and chitinase. *In vivo* studies showed that lysozyme plays an important role in the degradation of chitin to produce



**TABLE 2.22** Comparison of the application of chitosan versus chitin

Application	Use recommendations
Wound healing	<ul style="list-style-type: none"> <li>– High degree of deacetylation (DD) chitosan preferred over chitin</li> <li>– Low molecular weight samples (oligomers)</li> </ul>
Drug delivery systems	<ul style="list-style-type: none"> <li>– High DD</li> <li>– High molecular weight</li> </ul>
Gene Delivery	<ul style="list-style-type: none"> <li>– <math>DD \leq 80</math></li> <li>– Low Mw (around 10 kDa)</li> </ul>
Scaffolds (tissue engineering)	<ul style="list-style-type: none"> <li>– DD around 85 (good proliferation and structure)</li> <li>– High Mw (prolonged biodegradation)</li> </ul>
Cell immobilization	Chitosan is preferred over chitin (high DD)
Enzyme immobilization	<ul style="list-style-type: none"> <li>– Depends on the enzyme, immobilization method and reaction media</li> <li>– Low ash content</li> <li>– <math>\beta</math>-Chitin preferred over <math>\alpha</math>-chitin in organic reaction media</li> </ul>
Adsorption	<ul style="list-style-type: none"> <li>– Chitin for neutral or positively charged proteins</li> <li>– Chitosan for negatively charged proteins. High DD</li> </ul>
Covalent	<ul style="list-style-type: none"> <li>– Chitosan for multipoint immobilization. High DD</li> <li>– Chitin or chitosan with low DD for single point immobilization</li> </ul>
Encapsulation	<ul style="list-style-type: none"> <li>– Chitosan–TPP high Mw, high DD better retention</li> <li>– Chitosan–alginate PECs Medium molecular weight better stability</li> </ul>

*(continued)*

**TABLE 2.22** *(continued)*

Application	Use recommendations
Dietary ingredient	<ul style="list-style-type: none"> <li>– High DD; high Mw (viscosity)</li> <li>– Fine particle</li> </ul>
Food preservative	<ul style="list-style-type: none"> <li>– High DD</li> <li>– Medium–low Mw (5–80 kDa)</li> </ul>
Emulsifying agent	<ul style="list-style-type: none"> <li>– Low DD for emulsion stability</li> <li>– High viscosity</li> </ul>
Waste water treatment	<ul style="list-style-type: none"> <li>– Depends on pollutant and water conditions (pH, ionic strength)</li> <li>– In general, chitosan preferred over chitin</li> <li>– High DD, low crystallinity</li> </ul>
Molecular imprinting	<ul style="list-style-type: none"> <li>– Not yet tested</li> <li>– High DD is expected to improve cross-linking</li> <li>– In general, low molecular weight chitosan is used</li> </ul>
Metal reduction	<ul style="list-style-type: none"> <li>– Metal reduction depends on chitosan characteristics (not yet fully tested)</li> <li>– High DD and low molecular weight seems to stabilize the nanoparticles</li> </ul>
	Clear relationship between morphology and molecular weight <ul style="list-style-type: none"> <li>– Low Mw chitosan 2D chains</li> <li>– Medium molecular weight chitosan: single nanoparticles</li> <li>– High molecular weight chitosan: nanoplates</li> </ul>

the mostly soluble oligomers like *N*-acetylglucosamine upon hydrolysis. Chitin is not believed to present a significant health risk. Also no risk on humans is expected when products containing chitin are used according to label directions. Chitin is closely structurally related to the active ingredient chitosan (poly-D-glucosamine), which shows no toxicity in mammals, and is approved by the FDA as a food additive. The LD<sub>50</sub> for the intravenous administration of chitin is 50 mg/kg in rats.

## REFERENCES

- [1] C.K.S. Pillai, W. Paul, C.P. Sharma, *Prog. Polym. Sci.* 34 (2009) 641–678.
- [2] S. Budavari (Ed.), *The Merck Index*, 13th ed., Merck and Co., New Jersey, 2001.
- [3] R. Seoudi, A.M.A. Nada, *Carbohydr. Polym.* 68 (2007) 728–733.
- [4] I. Aranaz, M. Mengibar, R. Harris, I. Paños, B. Miralles, N. Acosta, et al., *Curr. Chem. Biol.* 3 (2009) 203–230.
- [5] J.N. Bemiller (Ed.), *Methods in Carbohydrate Chemistry*, Academic Press, New York, 1965.
- [6] R.A.A. Muzzarelli, *Chitin*, Pergamon Press, New York, 1976.
- [7] R.A.A. Muzzarelli, *Natural Chelating Polymers: Alginic Acid, Chitin and Chitosan*, Pergamon Press, Oxford, 1973.
- [8] G.F. Warner, *The Biology of Crabs*, Paul Elek Scientific Ltd., London, 1977.
- [9] A. Baxter, M. Dillon, K.D.A. Taylor, G.A.F. Roberts, *Int. J. Biol. Macromol.* 14 (1992) 166–169.
- [10] D. Horton, D.R. Lineback, *Methods Carbohydr. Chem.* 5 (1995) 405–411.
- [11] W.J. McGahren, G.A. Perkinson, J.A. Growich, R.A. Leese, G.A. Ellestad, *Process Biochem.* 19 (1984) 88–90.
- [12] Y.-J. Jeona, F. Shahidia, S.-K. Kim, *Food Rev. Int.* 16 (2000) 159–176.
- [13] C.K.S. Pillai, W. Paul, C.P. Sharma, *Prog. Polym. Sci.* 34 (2009) 641–678.
- [14] R. Jayakumar, N. Nwe, S. Tokura, H. Tamura, *Int. J. Biol. Macromol.* 40 (2007) 175–181.
- [15] S. Santhosh, P.T. Mathew, *J. Appl. Polym. Sci.* 107 (2008) 280–285.
- [16] R.C. Capozza, US Patent 3,989,535, issued November 2, 1976.
- [17] T. Uragami, S. Tokura, *Material Science of Chitin and Chitosan*, Springer, Germany and Kodansha, Japan, 2006.
- [18] The Jordanian Pharmaceutical Manufacturing (JPM) Co., Personal communication.
- [19] J. Kumirska, M. Czerwicka, Z. Kaczyński, A. Bychowska, K. Brzozowski, J. Thöming, et al., *Mar. Drugs* 8 (2010) 1567–1636.
- [20] M. Rinaudo, *Prog. Polym. Sci.* 31 (2006) 603–632.
- [21] R.L. Lavall, O.B.G. Assis, S.P. Campana-Filho, *Bioresour. Technol.* 98 (2007) 2465–2472.
- [22] E.S. Abdou, K.S.A. Nagy, M.Z. Elsabee, *Bioresour. Technol.* 99 (2008) 1359–1367.
- [23] D. Stawski, S. Rabiej, L. Herczynska, Z. Draczynski, *J. Therm. Anal. Calorim.* 93 (2008) 489–494.
- [24] R. Martin, S. Hild, P. Walther, K. Ploss, W. Boland, K.-H. Tomaschko, *Biol. Bull* 213 (2007) 307–315.
- [25] A. Einbu, *Characterisation of Chitin and a Study of its Acid-Catalysed Hydrolysis*, Ph.D. thesis, Norwegian University of Science and Technology (NTNU), January, 2007.
- [26] M. Tsezos, *Biotechnol. Bioeng.* 25 (1983) 2025–2040.
- [27] T.G. Liu, B. Li, W. Huang, B. Lv, J. Chen, J.X. Zhang, et al., *Carbohydr. Polym.* 77 (2009) 110–117.

- [28] T. Liua, B. Li, X. Zheng, S. Liang, X. Song, B. Zhu, *et al.*, *Carbohydr. Polym.* 82 (2010) 753–760.
- [29] P.R. Austin, US Patent 4,165,433, issued August 21, 1979,.
- [30] A.M. Striegel, J.D. Timpa, *Carbohydr. Res.* 267 (1995) 271–290.
- [31] M.L. Duarte, M.C. Ferreira, M.R. Marvao, J. Rocha, *Int. J. Biol. Macromol.* 31 (2002) 1–8.
- [32] M.N.V.R. Kumar, *React. Funct. Polym.* 46 (2000) 1–27.
- [33] J. Brugnerotto, J. Lizardi, F.M. Goycoolea, W. Arguelles-Monal, J. Desbrieres, M. Rinaudo, *Polymer* 42 (2001) 3569–3580.
- [34] M.R. Kasaai, *Carbohydr. Polym.* 71 (2008) 497–508.
- [35] S. Trombotto, C. Ladavière, F. Delolme, A. Domard, *Biomacromolecules* 9 (2008) 1731–1738.
- [36] M.R. Kasaai, *Carbohydr. Polym.* 79 (2010) 801–810.
- [37] Y. Zhang, C. Xue, Y. Xue, R. Gao, X. Zhang, *Carbohydr. Res.* 340 (2005) 1914–1917.
- [38] X. Hu, Y. Du, Y. Tang, Q. Wang, T. Feng, J. Yang, *et al.*, *Carbohydr. Polym.* 70 (2007) 451–458.
- [39] A. Pelletier, I. Lemire, J. Sygusch, E. Chornet, R.P. Overend, *Biotechnol. Bioeng.* 36 (1990) 310–315.
- [40] E. Layne, *Methods Enzymol.* 3 (1957) 447–455.
- [41] T. Wu, S. Zivanovic, *Carbohydr. Polym.* 73 (2008) 248–253.
- [42] L.S. Guinesi, E.T.G. Cavaleiro, *Thermochim. Acta* 444 (2006) 128–133.
- [43] C.-H. Ng, S. Hein, S. Chandkrachang, W.F. Stevens, J. Biomed. Mater. Res. B Appl. Biomater. 76B (2006) 155–160.
- [44] H. Sato, S. Mizutani, S. Tsuge, H. Ohtani, K. Aoi, A. Takasu, *et al.*, *Anal. Chem.* 70 (1998) 7–12.
- [45] M. Lavertu, Z. Xia, A.N. Serreqi, M. Berrada, A. Rodrigues, D. Wang, *et al.*, *J. Pharm. Biomed. Anal.* 32 (2003) 1149–1158.
- [46] X. Zhu, J. Cai, J. Yang, Q. Su, *Carbohydr. Res.* 340 (2005) 1732–1738.
- [47] P.K. Dutta, J. Dutta, V.S. Tripathi, *J. Sci. Ind. Res.* 63 (2004) 20–31.
- [48] F.N. Bruscato, A.G. Danti, US Patent 4,086,335, issued April 25, 1978.
- [49] Y. Sawayanagi, N. Nambu, T. Nagai, *Chem. Pharm. Bull.* 30 (1982) 2935–2940.
- [50] Y. Sawayanagi, N. Nambu, T. Nagai, *Chem. Pharm. Bull.* 30 (1982) 4216–4218.
- [51] V.G. Mir, J. Heinamaki, O. Antikainen, O.B. Revoredo, A.I. Colarte, O.M. Nieto, *et al.*, *Eur. J. Pharm. Biopharm.* 69 (2008) 964–968.
- [52] A. Badwan, M. Al-Remawi, I.S. Rashid, EP patent 1 852 110, issued November 7, 2007.
- [53] I. Rashid, N. Daraghmeh, M. Al-Remawi, S.A. Leharne, B.Z. Chowdhry, A. Badwan, *J. Pharm. Sci.* 98 (2009) 4429–4974.
- [54] I. Rashid, N. Daraghmeh, M. Al-Remawi, S.A. Leharne, B.Z. Chowdhry, A. Badwan, *Powder Technol.* 203 (2010) 609–619.
- [55] N. Daraghmeh, I. Rashid, M.M.H. Al Omari, S.A. Leharne, B.Z. Chowdhry, A. Badwan, *AAPS PharmSciTech.* 11 (2010) 1558–1571.
- [56] K.V.H. Prashanth, R.N. Tharanathan, *Trends Food Sci. Technol.* 18 (2007) 117–131.
- [57] G.C. Gleckler, J.C. Goebel, US Patent 4,035,267, issued July 12, in: 1977.
- [58] H.J. Dunn, M.P. Farr, US Patent 4,034,121, issued July 5, 1977.
- [59] Safety data for chitin. <http://msds.chem.ox.ac.uk/CH/chitin.html> (September 20, 2010).
- [60] A. Wojtasz-Pajak, J. Szumilewicz, Polish Chitin Soc. (2007) Monograph XII, 13–24.
- [61] Chitin; Poly-N-acetyl-D-glucosamine (128991) Fact Sheet. [http://www.epa.gov/opppbd1/biopesticides/ingredients/factsheets/factsheet\\_128991.htm](http://www.epa.gov/opppbd1/biopesticides/ingredients/factsheets/factsheet_128991.htm) (September 20, 2010).

# CHAPTER 3

## Ezetimibe

**Maria L.A.D. Lestari,<sup>\*</sup> Febry Ardiana,<sup>†</sup> and  
Gunawan Indrayanto<sup>\*</sup>**

---

<b>Contents</b>		
	1. Introduction	104
	1.1. Chemical names	104
	1.2. Molecular formula and molecular weight	104
	1.3. Solubility characteristics, partition coefficient, and $pK_a$ value	104
	1.4. Melting point and optical rotation	105
	1.5. Crystal form and polymorphism	105
	1.6. Known impurities	106
	2. Thermal Methods of Analysis	108
	3. Spectrophotometric Methods of Analysis	108
	3.1. Vibrational spectrophotometric	108
	3.2. Nuclear magnetic resonance	109
	3.3. UV spectrophotometry	110
	4. Chromatographic Methods of Analysis	113
	4.1. Thin layer chromatography	113
	4.2. Liquid chromatography	121
	4.3. Micellar electrokinetic capillary chromatography	122
	5. Degradation of Ezetimibe	127
	6. Determination of Ezetimibe in Biological Sample	134
	6.1. Liquid chromatography	145
	6.2. Gas chromatography	146
	References	147

<sup>\*</sup> Faculty of Pharmacy, Airlangga University, Dharmawangsa Dalam, Surabaya, Indonesia

<sup>†</sup> Research and Development (R&D) Bernofarm Pharmaceutical Company, Buduran-Sidoarjo, Indonesia

## 1. INTRODUCTION

Ezetimibe is a drug substance which belongs to the new class of lipid altering drugs. The drug substance inhibits intestinal absorption of biliary and dietary cholesterol and is classified as a low-density lipoprotein cholesterol (LDL-C) lowering drug substance. Ezetimibe is given orally once daily, either alone or in combination with other lipid lowering drugs such as statins and fenofibrates [1–3].

### 1.1. Chemical names

1-(4-Fluorophenyl)-3(R)-[3-(4-fluorophenyl)-3(S)-hydroxypropyl]-4-(S)-(4-hydroxyphenyl)-2-azetidinone [3,4] or (3R,4S)-1-(*p*-fluorophenyl)-3-[(3S)-3-(*p*-fluorophenyl)-3-hydroxypropyl]-4-(*p*-hydroxyphenyl)-2-azetidinone [1]

The systematic CAS name of ezetimibe is (3R,4S)-1-(4-fluorophenyl)-3-[(3S)-3-(4-fluorophenyl)-3-hydroxypropyl]-4-(4-hydroxyphenyl)-2-azetidinone [5].

### 1.2. Molecular formula and molecular weight

The molecular formula of ezetimibe is  $C_{24}H_{21}F_2NO_3$ , and its molecular weight is 409.4 [3]. The molecular structure of ezetimibe is as described in Fig. 3.1.

### 1.3. Solubility characteristics, partition coefficient, and $pK_a$ value

Ezetimibe is freely to very soluble in ethanol, methanol and acetone, but it is practically insoluble in water. The solubility of both ezetimibe anhydrous and ezetimibe hydrate is detailed in Table 3.1.

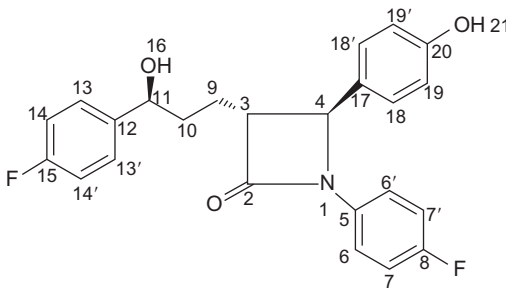


**FIGURE 3.1** Molecular structure of ezetimibe.

**TABLE 3.1** Solubility of ezetimibe anhydrate and ezetimibe monohydrate [3]

Solvent	Solubility (mg/mL) at ambient temperature (about 23 °C)	
	Ezetimibe anhydrate	Ezetimibe monohydrate
Water	0.012	0.008
0.1 N hydrochloric acid	0.011	0.024
<i>n</i> -Hexane	<0.001	<0.001
Acetonitrile	68.6	77.8
Ethanol	168	169
1:1 ethanol:0.1 N HCl	1.7	1.8
0.05 M phosphate buffer (pH 4.5), with 1% sodium lauryl sulfate	0.16	0.16

In the *n*-octanol/0.1 N HCl system, ezetimibe is characterized by a log(octanol/water) partition coefficient of 4.52, while in *n*-octanol/pH 7 buffer pH 7, it has  $\log K_{o/w} = 4.51$ .

The  $pK_a$  of ezetimibe is 9.75, determined by potentiometric titration [3,6].

#### 1.4. Melting point and optical rotation

Ezetimibe was reported to exhibit a melting point in the range of 163–166 °C, with the onset of melting taking place at 163 °C. The compound is reported to be stable at ambient temperature [3,5,6], and the hydrate form was reported to lose water at 25–70 °C [3]. The optical rotation of ezetimibe was found as  $[\alpha]_D^{22} = 33.9^\circ$  ( $c = 3$  in methanol) [5].

#### 1.5. Crystal form and polymorphism

There are two crystal forms of ezetimibe, an anhydrate and a monohydrate [3]. Ezetimibe anhydrate is hygroscopic and will therefore absorb water from the atmosphere, converting to the monohydrate form. In an earlier publication, Ravikumar *et al.* [7] reported the structural analysis of ezetimibe monohydrate, including the use of X-ray diffraction to obtain the structure of a single crystal. The chemical formula of ezetimibe monohydrate developed was  $C_{24}H_{21}F_2NO_3 \cdot H_2O$ , and the molecular weight was calculated as 427.43. In the Ravikumar report, the crystal of ezetimibe monohydrate used in the X-ray diffraction study was prepared by dissolving ezetimibe in a 90:10 mixture of methanol/water, and then allowing

the solution to evaporate slowly. X-ray diffraction was conducted using Mo K $\alpha$  radiation, over an angle range of 2.3° 2 $\theta$ –21.9° 2 $\theta$ .

A few patents encompass polymorphs of ezetimibe [6,8–11]. The scope of the claims encompasses at least two different forms of ezetimibe, which can be identified from characterization data such as X-ray diffraction and IR data. The polymorphs can be anhydrous, monohydrated, or amorphous. It should also be noted that different preparation process may be used to produce different polymorphs of ezetimibe. It is also known that the various crystal forms can be interconverted. In a patent reported by Aronhime *et al.* [6], ezetimibe Form-A was found to be more stable relative to Form-B. The amorphous form can be generated by heating Form-A at temperatures higher than 60 °C. Most likely, the amorphous form will be obtained when ezetimibe is prepared by dissolving in alcohol, ketone, or ester solvent or combination of those solvents.

In a patent reported for ezetimibe Form-S, it was disclosed that ezetimibe hydrated Form-H was converted to ezetimibe anhydrous Form-A when heated at about 40 °C. The ezetimibe Form-S itself was produced by isolating the hydrated Form-H or anhydrous Form-A from *tert*-butanol [11].

In a recent publication, Brüning *et al.* [12] developed ezetimibe anhydrate from the monohydrate form by drying at 393 K for 1 day in an oven. This anhydrate form was then characterized using X-ray diffraction with  $\lambda = 1.5406$  Å and Cu K $\alpha$  as the radiation source. Scanning was done at 2 $\theta = 3$ –69.99°. It was found that the anhydrate structure analyzed in this research is quite similar to the monohydrate structure, with the exception that due to fewer donor and acceptor atoms, a different conformation of the propyl group and a different hydrogen-bond pattern occurred.

A summary of the characterization data associated with the X-ray diffraction of each crystal form of ezetimibe is provided in Table 3.2.

## 1.6. Known impurities

Structural elucidation studies have revealed the existence of two impurities of ezetimibe, which have been termed impurity-I and impurity-II. These impurities formed as a result of the debenzoylation process used to form ezetimibe. Where during the synthesis process, benzyl ezetimibe undergoes a debenzoylation reaction to yield ezetimibe. Accompanying this reaction, the ezetimibe  $\beta$ -lactam ring is able to open, thus yielding impurity-I.

Only the structure of impurity-I has been successfully confirmed with nuclear magnetic resonance (NMR) and infrared (IR) spectroscopic analysis and has been shown to be 2-(4-hydroxybenzyl)-N-5-bis-(4-fluorophenyl)-5-hydroxypentanamide, as detailed in Fig. 3.2.

In the high-performance liquid chromatography (HPLC) method of analysis, it was found that impurity-I, impurity-II, and ezetimibe are characterized by retention times of 8.4, 18.9, and 10.2 min, respectively.



**TABLE 3.2** X-ray powder diffraction data for the crystal forms of ezetimibe

Polymorphic identity	X-ray diffraction peaks (degrees $2\theta$ )	Additional data	Reference
H1	8.3; 13.7; 13.9; 16.5; 18.7; 19.1; 20.2; 22.5; 23.1; 23.7; 23.9; 25.7; 28.1; 29.8	n/a	[9]
H2	16.4; 18.6; 19.0; 19.4; 20.2; 22.4; 22.9; 23.6; 23.9; 25.6; 27.9; 29.7		
Form-I	Radiation source : Copper-Kr 7.9 $\pm$ 0.1; 13.8 $\pm$ 0.1; 15.8 $\pm$ 0.1; 22.9 $\pm$ 0.1; 23.4 $\pm$ 0.1; 24.5 $\pm$ 0.1; 26.5 $\pm$ 0.1	DSC data : Form-I: endotherm at 163 °C	[10]
Form-II	8.2 $\pm$ 0.1; 13.6 $\pm$ 0.1; 16.4 $\pm$ 0.1; 20.2 $\pm$ 0.1; 29.7 $\pm$ 0.1	Form-II: endotherm at 164 °C	
Form-A	Radiation source : Cu K $_{\alpha 1}$ 16.4 $\pm$ 0.2; 20.2 $\pm$ 0.2; 22.5 $\pm$ 0.2; 24.0 $\pm$ 0.2; 25.6 $\pm$ 0.2	Water content: Form-A:	[6]
Form-B	18.7 $\pm$ 0.2; 19.5 $\pm$ 0.2; 23.0 $\pm$ 0.2; 23.5 $\pm$ 0.2; 24.6 $\pm$ 0.2 Radiation source: n/a	TGA : 0.1% by weight KF: 0.2% by weight Form-B: TGA: 4–28% KF: 3–23% by weight	
Single crystal	14.16, 15.11, 16.44; 17.22, 19.11, 20.09, 21.33, 22.04, 22.89, 23.42, 25.11 Radiation source: n/a	n/a	[13]
Form-S	7.3, 15.3, 16.7, 18.7, 21.8, 24.0 Additional peaks: 6.2, 20.1, 25.3 Radiation source: n/a	Water content KF: 0–2%	[11]

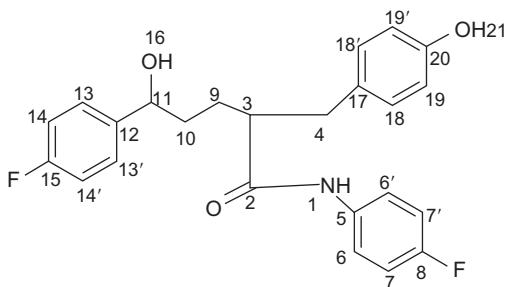


**FIGURE 3.2** Impurity-I of ezetimibe.

Typical percentages of impurity-I in bulk drug substance range from 0.1% to 0.5%, and the typical ranges for impurity-II are 0.04–0.12% [14].

## 2. THERMAL METHODS OF ANALYSIS

The thermal analysis methods reported for the characterization of ezetimibe were conducted using thermogravimetric analysis (TGA), differential thermal analysis (DTA), and differential scanning calorimetry (DSC). As detailed in Table 3.2, the TGA and DSC characterization of polymorphs of ezetimibe was reported in a patent publication.

Kane *et al.* [13] presented the DSC analysis for crystalline ezetimibe, where the sample (contained in aluminum pans) was heated from 30 to 300 °C at a scan rate of 10 °C/min under a nitrogen flow of 40 mL/min. The endothermic melting of ezetimibe was observed at 184 °C.

In a more recent publication, Brüning *et al.* [12] reported the combination of DTA–TG assay for ezetimibe monohydrate. Samples of ezetimibe monohydrate was placed in a corundum crucible and heated from room temperature to 273 °C (under a nitrogen atmosphere) at a heating rate of 3 °C/min. It was observed that the monohydrate underwent dehydration continuously between 38 and 80 °C.

## 3. SPECTROPHOTOMETRIC METHODS OF ANALYSIS

### 3.1. Vibrational spectrophotometric

Several IR and FTIR methods have been reported for the characterization of ezetimibe, including characterization of its alkaline degradation product as well as impurity analyses [10,13–16].

For the analysis of polymorphs of ezetimibe, it was found that the Form-I gave strong signal at 3270 cm<sup>−1</sup>, while the Form-II has strong

signals at  $3272\text{ cm}^{-1}$  as well as at  $3438\text{ cm}^{-1}$  [10]. FTIR analysis for ezetimibe derived from a synthesis process showed that the strong characteristic absorption bands of ezetimibe were observed at energies of 3270, 2918, 1862, 1718.4, and  $1510\text{ cm}^{-1}$  [16].

In the structure elucidation of the degradant of ezetimibe, it was found that alkaline hydrolysis causes the opening of azetidinone, the four-membered ring of ezetimibe structure. Therefore, comparison between intact and degraded ezetimibe revealed that the intact drug showed a  $\text{C}=\text{O}$  band at about  $1728\text{ cm}^{-1}$ . This band was not observed in the IR spectrum of the two degradation products. In addition, the primary amine band at  $3462\text{ cm}^{-1}$  was observed in the spectrum of one of the degradation products. The suggested structure of the alkaline degradant product is detailed in Fig. 3.3. In addition, structural elucidation for impurity-I of ezetimibe exhibited strong peak at  $1650\text{ cm}^{-1}$  for  $\text{C}=\text{O}$  stretching [14]. Results for the IR and FTIR analysis of ezetimibe are detailed in Table 3.3.

### 3.2. Nuclear magnetic resonance

An NMR method had been utilized as part of a patent claim by Štimac *et al.* [11], in a publication dealing with the synthesis of ezetimibe. Here,  $^1\text{H}$  and  $^{13}\text{C}$  NMR assignments were applied to characterize ezetimibe anhydrate in Form-S. In the  $^{13}\text{C}$  NMR assay, the methyl group of hexamethylbenzene ( $\delta = 17.3\text{ ppm}$ ) was used as the external reference, and the compound resonance bands were observed over 28.4–170.2 ppm.

Sasikala *et al.* [16] used  $^1\text{H}$  NMR, MS, and FTIR to characterize ezetimibe as synthesized from oxazolidinone. Moreover,  $^1\text{H}$  and  $^{13}\text{C}$  NMR assays were used to determine impurity-I in samples of ezetimibe. According to the results obtained,  $^1\text{H}$  NMR spectral data of impurity-I have additional NMR bands at 2.74 and 9.82 ppm. The signal at 9.82 ppm was not observed on ezetimibe and was assigned to the  $-\text{NH}$  group. Further analysis confirmed that impurity-I has an extra  $-\text{CH}_2$  group at 38.61 ppm when compared to ezetimibe. To confirm the difference between impurity-I and ezetimibe, a  $^1\text{H}$ – $^1\text{H}$  correlation study and a  $^1\text{H}$ – $^{13}\text{C}$  experimental study were conducted. Results revealed that the

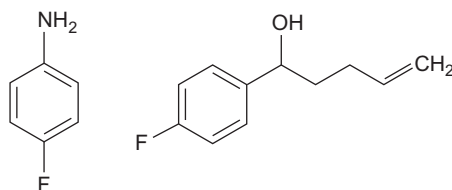


**FIGURE 3.3** Proposed structure for alkaline degradant of ezetimibe.

**TABLE 3.3** IR and FTIR result of ezetimibe (cited from Ref. [13])

Frequency (cm <sup>-1</sup> )	Assignment
3259.81	Broad, intermolecular hydrogen bonded, O–H stretch
2958.9	Aromatic C–H stretch
1884.52	C=O stretch of lactone ring
1716.7	C=O stretch
1602.9	C–C stretch
1402.3	C–N stretch
1440.87	C–N stretch
1359.86	In plane O–H bend
1269.2	C–F stretch
1220.98	C–F stretch
1166.97	C–F stretch
1068.6	C–O stretch of secondary alcohol
1105.25	C–O stretch of secondary alcohol
941.29	Ring vibration of alkyl cyclobutanes
827.49	Ring vibration due to <i>para</i> -disubstituted benzene

C<sub>4</sub> in the former structure of ezetimibe changes to –CH<sub>2</sub> and becomes linked to two protons found at 2.74 and 2.48 ppm, while the signals at 5.22 and 9.16 ppm showed no correlation with any carbon atom and confirmed as exchangeable protons [14].

Results for <sup>1</sup>H and <sup>13</sup>C NMR chemical shift of ezetimibe and its impurity-I are detailed in Table 3.4.

### 3.3. UV spectrophotometry

There are few spectrophotometric methods published to determine ezetimibe in pharmaceutical dosage forms. The first one was established by Mishra *et al.* [17] by applying colorimetric assay of phenol group. This method was developed based on the reaction between Folin-Ciocalteu's (FC) phenol reagent and phenol group of ezetimibe, which results in a blue chromogen that was then observed at 760 nm.

A similar colorimetric principle was adopted by Lakshmi *et al.* [18]. Here, the principle used was oxidation of the phenolic group which was followed by complex formation that can be examined at visible wavelengths. In this method, two different approaches were examined. The first one was complexation with phenanthroline in the presence of ferric chloride which resulting pink colored chromogen observed at 510 nm. The second method was utilization of excess ferric ion which was added to the ezetimibe solution. The excess then oxidized ezetimibe, resulting in

**TABLE 3.4** NMR data of ezetimibe and impurity-I (modified from Ref. [14])

Ezetimibe			Impurity-I		
Position	<sup>1</sup> H in ppm (multiplicity, H–H coupling constant, <i>J</i> (Hz))	<sup>13</sup> C in ppm ( <sup>13</sup> C– <sup>19</sup> F coupling constant, <i>J</i> (Hz))	Position	<sup>1</sup> H in ppm (multiplicity, H–H coupling constant, <i>J</i> (Hz))	<sup>13</sup> C in ppm ( <sup>13</sup> C– <sup>19</sup> F coupling constant, <i>J</i> (Hz))
1 (N)	–	–	1 (NH)	9.82 (s)	–
2 (C=O)	–	167.8	2 (=O)	–	173.9
3 (C–H)	3.06 (m)	59.8	3 (C–H)	2.48 (m)	49.3
4 (C–H)	4.80 (d, 2.3)	60	4 (C)	2.48 (m)	38.1
5 (C)	–	142.6 (2.9)		2.74 (m)	
6,6' (C–H)	7.09 (m)	118.7(8.1)	5 (C)	–	135.9 (2.2)
7,7' (C–H)	7.09 (m)	116.4 (22.7)	6,6' (C–H)	7.52 (m)	121.4 (7.3)
8 (C)	–	158.4 (240.0)	7,7' (C–H)	7.07 (m)	115.6 (22.0)
9 (CH <sub>2</sub> )	1.67 (m)	24.9	8 (C–F)	–	158.4 (239.3)
10 (CH <sub>2</sub> )	1.87 (m)	36.8	9 (CH <sub>2</sub> )	1.43 (m)	29
11 (C–H)	4.47 (m)	71.5	10 (CH <sub>2</sub> )	1.65 (m)	37.6
12 (C)	–	134.4 (2.6)	11 (C–H)	4.45 (m)	72.1
13,13' (C–H)	7.28 (m)	127.9 (7.3)	12 (C)	–	142.8 (2.9)
14,14' (C–H)	7.09 (m)	115.1 (20.5)	13,13' (C–H)	7.25 (m)	128.0 (7.3)
15 (C–F)	–	161.5 (241.5)	14,14' (C–H)	7.07 (m)	115.1 (21.2)
16 (OH)	5.29 (d, 4.6)	–	15 (C–F)	–	161.5 (241.5)
17 (C)	–	128.3	16 (OH)	5.22 (d, 4.6)	–
18,18' (C–H)	7.09 (d, 8.5)	128	17 (C)	–	130.4
19,19' (C–H)	6.74 (d, 8.5)	116.1	18,18' (C–H)	6.95 (d, 8.5)	130.2
20 (C)	–	157.8	19,19' (C–H)	6.62 (d, 8.5)	115.4
21 (OH)	9.55 (s)	–	20 (C)	–	156
			21 (OH)	9.16 (s)	–

the reduction of Fe(III) into Fe(II). This Fe(II) form was then reacted with potassium ferricyanide, forming ferrous ferricyanide which was examined at 740 nm. Although these colorimetric methods can be considered as being simple, it should be noted that for this reaction, a few considerations have to be taken. First, the concentration of the reagent should be optimized, as well as the time needed for color development and the stability of the color absorbance. In addition, for the FC method, the alkalinity of the reagent used should be optimized as well. It was found that in the FC reaction method, 1 mL of 1 N FC in 2 mL of 1 N NaOH was successful in completing the reaction [17].

Another spectrophotometric method used the derivative method. Rajput and Raj [19] developed a first-order derivative zero-crossing method to analyze ezetimibe in combination with simvastatin. This method was further applied to determine ezetimibe in combination with lovastatin. The first derivation method also applied to determine ezetimibe in combination with rosuvastatin [20]. Besides the first-derivative method, second- and third-derivative methods were also reported for determining ezetimibe as a single compound in its dosage form [21]. However, the third-derivative method yielded the lowest limits of detection and quantitation relative to other methods used in this research. The maximum wavelength also remained constant regardless of the derivative method applied.

Other spectrophotometric techniques have also been proposed to determine ezetimibe in combination with other drugs. The *Q*-absorption ratio method and the dual wavelength method were applied to determine ezetimibe in combination with rosuvastatin [20]. For the *Q*-absorption method, the underlying principle is that the absorbances observed at any two wavelengths have a constant ratio and do not depend on either concentration or pathlength [22]. Ezetimibe was observed at two different wavelengths, one being the isoabsorptive point and the other its maximum wavelength. Calculation of ezetimibe was based on a mathematical equation which involving absorbances and absorptivity of both ezetimibe and rosuvastatin at the two wavelengths used. Further, in the dual wavelength method, selection of the wavelengths is based on the principle that at the same wavelength, the interfering component shows same absorbance as for the substance of interest. The wavelengths of this interfering component were then used to observe the substance of interest. The difference of absorbance between these wavelengths is then plotted against the concentration to establish the calibration curve. From the *Q*-absorption method and the dual wavelength method, validation results showed that there was no significant difference observed for percentage of recovery. Although the LOD and LOQ were not reported, both have linearity in the range of 1–25 µg/mL.

Unlike the previously described methods, Sonawane *et al.* [23] utilized a simultaneous equation method to determine ezetimibe in combination with atorvastatin calcium. In this method, absorption bands of either ezetimibe or atorvastatin calcium were observed at two different wavelengths belonging to each substance. The absorbance of ezetimibe was observed at the wavelength of ezetimibe itself and at the wavelength of atorvastatin calcium, while the absorbance of atorvastatin was determined in a similar manner. The concentration of each substance was then calculated using the absorbance and absorption coefficient of both substances.

In more recent development, chemometric or multivariate calibration techniques have been applied into spectrophotometric methods. As reported by Palabiyik and Onur [24], principal component regression and partial least square were used to determine ezetimibe in combination with simvastatin. This method offers advantages such as no chemical pretreatment prior to analysis as well as no need to observe graphical spectra and calculations as with the derivative method. In addition, the instrumentation used is also simpler.

The simplest UV-spectrophotometric method was developed by Rajesh and Reddy [25] to determine ezetimibe as a single compound. This method was based only on an absorbance measurement of ezetimibe at one wavelength. Similarly, Jain *et al.* [26] also employed a simple method to determine ezetimibe in combination with simvastatin. In this method, ezetimibe was observed at a wavelength where simvastatin did not give interference. While no LOD and LOQ values were reported, the linearity of the method was over the range of 5–20 µg/mL.

A summary of spectrophotometric methods for the determination of ezetimibe is detailed in Table 3.5.

## 4. CHROMATOGRAPHIC METHODS OF ANALYSIS

### 4.1. Thin layer chromatography

Several high-performance thin layer chromatography (HPTLC) methods and one thin layer chromatography (TLC) method have been reported to determine ezetimibe, either as a single component or in combination with another drug [15,28–33]. Those methods are detailed in Table 3.6. Most of the methods use methanol as a solvent since ezetimibe is very soluble in methanol. It should also be noted that the chambers are saturated prior to the plate development since it was found that saturation could confirm reproducible migration of the analyte as well as its resolution, enabling well-defined bands to be obtained [29–31]. In addition, saturated chambers could reduce the  $R_f$  value, therefore, reducing consumption of the

**TABLE 3.5** Summary of UV-spectrophotometric method used to analyze ezetimibe

Analyte(s)	Method used	Solvent	Measurement wavelength (nm)	Limit of detection (LOD), limit of quantitation (LOQ), and % Recovery (Rec)	Reference
Ezetimibe Atorvastatin	Simultaneous equation method	MeOH	232.5	LOD: n/a LOQ: n/a Rec: 99.52–100.69	[23]
Ezetimibe	Reduction reaction with Folin-Ciocalteu's (FC) reagent	Standard solution: Dissolved and diluted with 1 N NaOH, added with 1 N FC reagent and 1 N NaOH, made up to volume with water Sample : Dissolved in MeOH, made up to volume with water, then reacted as for standard solution	760	LOD: n/a LOQ: n/a Rec: 100 ± 0.04	[17]
Ezetimibe Simvastatin	First-order derivative zero crossing	MeOH	265.2	LOD: 0.39 mg/mL LOQ: 1.10 mg/mL Rec: 99.63–101.9	[19]



Ezetimibe	UV, first derivative, second derivative, and third derivative	MeOH	UV: 233 First derivative: 259.5 Second derivative: 269 Third derivative: 248	UV LOD: 0.36 mg/mL LOQ: 1.09 mg/mL Rec: 98.45–100.85 First derivative LOD: 0.23 µg/mL LOQ: 0.69 µg/mL Rec: 98.07–99.83 Second derivative LOD: 0.21 µg/mL LOQ: 0.63 µg/mL Rec: 100.13–100.70 Third derivative LOD: 0.15 µg/mL LOQ: 0.46 µg/mL Rec: 100.49–101.46	[21]
Ezetimibe Simvastatin	Chemometric with principal component regression (PCR) and partial least square (PLS-1)	MeOH	Wavelength range 240–300 with intervals DI = 1 nm	LOD: n/a LOQ: n/a Rec: PCR: 102.50 PLS-1: 103.10	[24]
Ezetimibe Lovastatin	First-order derivative zero crossing	MeOH	265.2	LOD: 0.39 µg/mL LOQ: 1.30 µg/mL Rec: 99.90–100.38	[27]

---

(continued)

**TABLE 3.5** (continued)

Analyte(s)	Method used	Solvent	Measurement wavelength (nm)	Limit of detection (LOD), limit of quantitation (LOQ), and % Recovery (Rec)	Reference
Ezetimibe	UV	MeOH	234	LOD: 0.1 µg/mL LOQ: 0.25 µg/mL Rec: 98.21–109.7	[25]
Ezetimibe, simvastatin	UV	MeOH:phosphate buffer, pH 7.4 = 7:3	258.5	LOD: n/a LOQ: n/a Rec: 99.19–99.93	[26]
Ezetimibe	Colorimetric based on redox/complex formation	Standard stock : Dissolved in 0.1 N NaOH then diluted with water Method A: 0.5–3 mL standard stock added with 1.5 mL Fe(III) and 2.0 mL <i>o</i> -phen, then made to 10 mL with water, heated for 30 min. This mixture then added with 2.0 mL <i>o</i> -phosphoric acid and made to	Method A: 510 Method B: 740	Method A LOD: 2.0 µg/mL LOQ: n/a Rec: 99.25–100.02 Method B LOD: 5.5 µg/mL LOQ: n/a Rec: 98.91–100.02	[18]

		<p>volume with water</p> <p>Method B:</p> <p>0.5–2.5 mL standard stock added with 1 mL of <math>3.32 \times 10^{-3}</math> M ferric chloride solution, shaken for 5 min then added with 0.5 mL of <math>3.02 \times 10^{-3}</math> M potassium ferricyanide solution. After 5 min reacted, added with 1 mL HCl made up to 10 mL volume with water</p>			
<p>Ezetimibe</p> <p>Rosuvastatin</p>	<ol style="list-style-type: none"> <li>1. Q-absorption method</li> <li>2. Dual wavelength method</li> <li>3. First-order derivatization technique</li> </ol>	<p>MeOH</p>	<p>Method 1:</p> <p>232.4 and 237</p> <p>Method 3:</p> <p>223.4</p>	<p>Method 1</p> <p>LOD: n/a</p> <p>LOQ: n/a</p> <p>Rec: 99</p> <p>Method 2:</p> <p>LOD: n/a</p> <p>LOQ: n/a</p> <p>Rec: 98.9–99.1</p> <p>Method 3</p> <p>LOD: n/a</p> <p>LOQ: n/a</p> <p>Rec: 99.3–99.6</p>	<p>[20]</p>

---

**TABLE 3.6** Summary of TLC/HPTLC methods for analysis of ezetimibe in bulk and pharmaceutical dosage forms

Analyte(s)	Stationary phase	Mobile phase (v/v)	Solvent	Wavelength (nm)	TLC preparation	Sample	Limit of detection (LOD), limit of quantitation (LOQ), and recovery (Rec)	Reference
Atorvastatin Ca Ezetimibe	Precoated silica gel 60 F254	Chloroform:benzene: MeOH:acetic acid = 6.0:3.0:1.0:0.1	MeOH	250	<ul style="list-style-type: none"> <li>– Prewashing plate with MeOH and dried in an oven at 50 for 5 min</li> <li>– Heated at 105 °C for 20 min for activation</li> </ul>	Drug powder and tablets	LOD: 20 ng/spot LOQ: 70 ng/spot Rec: 99.87–101.23%	<a href="#">[28]</a>
Ezetimibe Simvastatin	Precoated silica gel 60 F254	Ethyl acetate: chloroform = 80:20	n/a	220	n/a	Drug powder and tablets	LOD: n/a LOQ: n/a Rec: 99.73–99.59%	<a href="#">[19]</a>
Ezetimibe Simvastatin	Silica gel 60 F254 HPTLC plate	<i>n</i> -Hexane: acetone = 6:4	MeOH	234	<ul style="list-style-type: none"> <li>– Prewashing plate with MeOH and dried in an oven at 105–110 °C for 15 min</li> <li>– Saturating chamber with mobile phase for 20 min</li> </ul>	Drug powder and dry emulsion powder in capsule	LOD: 25 ng/spot LOQ: 150 ng/spot Rec: 95.02–96.44%	<a href="#">[31]</a>

Ezetimibe	Silica gel 60 F254	Toluene:ethyl acetate = 7:3	MeOH	254	<ul style="list-style-type: none"> <li>– Prewashing plate with MeOH and dried in an oven at 110 °C for 5 min</li> <li>– Saturating chamber with mobile phase for 30 min</li> </ul>	Pure drug	LOD: 50 ng/spot LOQ: 100 ng/spot Rec: 98.2–103.2%	[32]
Ezetimibe	Silica gel 60 F254	Isopropanol:ammonia 33% = 9:1	MeOH	250	<ul style="list-style-type: none"> <li>– Saturating chamber with mobile phase for 1 h</li> </ul>	Drug powder and tablets	LOD: n/a LOQ: n/a Rec: 98.96–99.46%	[15]
Atorvastatin Ca Ezetimibe	Silica gel 60 F254	Toluene:MeOH = 8:2	MeOH	240	<ul style="list-style-type: none"> <li>– Prewashing plate with MeOH and dried in an oven at 105 °C for 20 min</li> <li>– Saturating chamber with mobile phase for 20min</li> </ul>	Drug powder and tablets	LOD: n/a LOQ: n/a Rec: 99.01 ± 0.15%	[30]

---

(continued)

**TABLE 3.6** (continued)

Analyte(s)	Stationary phase	Mobile phase (v/v)	Solvent	Wavelength (nm)	TLC preparation	Sample	Limit of detection (LOD), limit of quantitation (LOQ), and recovery (Rec)	Reference
Ezetimibe Simvastatin	Aluminum-backed silica gel 60 F254	Toluene:2-propanol = 8:2	MeOH	240	<ul style="list-style-type: none"><li>– Prewashing plate with MeOH</li><li>– Heated at 105 °C for 20 min for activation</li><li>– Saturating chamber with mobile phase for 20min</li></ul>	Drug powder and tablets	LOD: n/a LOQ: n/a Rec: 98.99 ± 0.38%	<a href="#">[29]</a>

mobile phase. Further, prewashing the plates with methanol is generally intended to reduce the contaminant level contained in the plates (particularly for silica plates) resulting from the manufacturing process [34].

For the purpose of analyzing ezetimibe in combination with simvastatin, three HPTLC methods have been developed. The first method was developed by Shivshankar *et al.* [33] and yielded higher  $R_f$  values for either ezetimibe or simvastatin. In the method developed by Dhaneshwar *et al.* [30], a combination of toluene and isopropanol was shown to produce shorter  $R_f$  times for ezetimibe and simvastatin, leading to methods of shorter duration and lower mobile phase consumption. The recent method developed by Dixit *et al.* [31] used combination of acetone and *n*-hexane as the mobile phase and resulted in shorter  $R_f$  values when compared to the other two methods for assessing ezetimibe in combination with simvastatin. This method has also been validated to distinguish the degradation products of ezetimibe. Further, during the determination of ezetimibe in combination with atorvastatin, shorter  $R_f$  values were obtained as well as better peak shape when a combination of toluene and methanol was used as the mobile phase [30].

## 4.2. Liquid chromatography

Most of the analytical methods for assessing ezetimibe, in bulk as well as in pharmaceutical dosage forms, are based on HPLC methodology. These methods enable analysis of ezetimibe, either as a single compound or in combination with another drug. In the method developed by Jain *et al.* [26], a mobile phase of methanol and water was applied first to analyze ezetimibe in combination with simvastatin, resulting greater peak asymmetry. Acetonitrile was then introduced to the system, and the combination of methanol, acetonitrile, and water produced better peak shapes. This is due to the ability of acetonitrile to reduce the tailing factor, as well as the reduce viscosity of the mobile phase, therefore decreasing the backpressure, resulting in longer lifetime of the column.

In another method, Pandey and Rathanand [35] used a combination of acetonitrile and water to analyze ezetimibe as a single compound. In contrast, Sistla *et al.* [36] reported that combination of water and acetonitrile produced peak tailing and poor resolution of ezetimibe with amoxicillin trihydrate as the internal standard. To overcome this, an ion pair reagent was added to the system, successfully reducing the peak tailing and increasing resolution between ezetimibe and amoxicillin trihydrate.

In most of the methods reported, the mobile phase contained organic solvents such as acetonitrile and methanol with buffers of various pH values. This resulted in improved peak shapes, reduced tailing, and good separation for analysis of ezetimibe in combination with other compounds. It should also be noted that the percentage of acetonitrile in

mobile phase has a strong effect on the retention time, translating to the duration of analysis as well as the efficiency of the analysis itself. Ashfaq *et al.* [37] revealed that increasing the proportion of acetonitrile up to 80% will reduce the retention time of both ezetimibe and simvastatin and provide better resolution. However, greater peak tailing was also occurred. When the proportion of acetonitrile was reduced to 60%, the retention time for both substances increased and the same tailing factor was produced. Therefore, the optimum composition chosen was 70% acetonitrile and 30% buffer. Similar findings were also observed in the micellar electrokinetic capillary chromatography (MECC) method detailed in Section 4.3 [38].

Another consideration when conducting analysis with HPLC is the type of stationary phase used. In most of the published methods, either C<sub>8</sub> or C<sub>18</sub> columns were utilized. However, as detailed in Table 3.7, some of the analytical studies considered use of Phenomenex column, reporting high retention, high resolving capacity, better reproducibility, low back pressure, and low tailing factors [35,42]. In their report, Hefnawy *et al.* [43] promoted the benefit of using monolithic silica columns over conventional packed columns. Smaller particle sizes present in the monolithic silica columns provide higher porosity, and, therefore, the mass transfer of the mobile phase is greater than that in conventional silica packed columns. As a result, the separation process is faster with lower back-pressure, and the analytical process can be shortened [55].

### 4.3. Micellar electrokinetic capillary chromatography

Two MEKC methods have been reported for the analysis of ezetimibe and simvastatin in pharmaceutical dosage forms. This method offers several advantages over conventional HPLC technology, such as highly efficient with fast separation processes, smaller sample sizes, low reagent consumption, and durable columns [38]. The underlying principle of this method is based on the differential migration between the ionic micelles used and the bulk running buffer under electrophoresis condition, as well as interaction between the analyte and the micelle. The micelle acts as the stationary phase with the surrounding aqueous solution (i.e., buffer) acts as the mobile phase [56].

In both MEKC methods reported, the mobile phase consisted of borate buffer containing surfactant and acetonitrile. It was found that mobile phase prepared at pH 9.75 gave better resolution compared to other conditions, and increasing pH also increased the migration time of ezetimibe. An analyte concentration of 25 mM was chosen due to its lower current, and the sharp peaks observed [41]. In addition, for the analysis of ezetimibe in combination with another drug such as simvastatin, increasing the borate concentration increased both resolution and migration times.



**TABLE 3.7** Summary of HPLC methods for analysis of ezetimibe in bulk and pharmaceutical dosage forms

Analyte(s)	Samples	Internal standard	Column	Mobile phase	Column temperature (°C)	Detection (nm)	Solvent	Limit of detection (LOD), limit of quantitation (LOQ), and recovery (Rec)	Reference
Ezetimibe	Tablets	n/a	Chromasil C8 (250 × 4.6 mm)	ACN:0.02 M potassium dihydrogen orthophosphate buffer solution = 72:28	Ambient	232	Mobile phase	LOD: 0.0413 µg/mL LOQ: 0.1253 µg/mL Rec: 99.66 ± 0.606%	[39]
Ezetimibe–simvastatin	Tablets	n/a	Merck C18 column (250 × 4.6 mm; 5 µm)	0.1 M ammonium acetate buffer, pH 5.0:ACN = 30:70	n/a	240	Mobile phase	LOD: n/a LOQ: 0.19 µg/mL Rec: 99.12–100.3%	[37]
Atorvastatin Ca Ezetimibe	Tablets	n/a	Hypersil® phenyl-2 column (250 × 4.6 mm; 5 µm)	0.1 M ammonium acetate (pH 6.5): ACN = 28:72	35	242	Standard stock solution: MeOH Working standard solution: mobile phase Sample: MeOH dilution by mobile phase	LOD: n/a LOQ: n/a Rec: 98.25–101.75%	[40]
Ezetimibe	Tablets	Nimesulide	Phenomenex Luna C18 (250 × 4.6 mm; 5 µm)	Phosphate buffer 0.03 M, pH 4.5: ACN = 35:65	45	234	Acetonitrile	LOD: 0.05 µg/mL LOQ: 0.5 µg/mL Rec: 99.95–101.04%	[41]
Ezetimibe	Tablets	n/a	Phenomenex Luna C18 (150 × 4.6 mm; 5 µm)	Phosphoric acid 0.1%:ACN = 50:50	n/a	232	Standard:water: ACN:MeOH = 40:50:10	LOD: n/a LOQ: n/a Rec: 100.8–102.7%	[42]
	Tablets	Ranitidine			n/a	240	ACN		[43]

(continued)

**TABLE 3.7** (continued)

Analyte(s)	Samples	Internal standard	Column	Mobile phase	Column temperature (°C)	Detection (nm)	Solvent	Limit of detection (LOD), limit of quantitation (LOQ), and recovery (Rec)	Reference
Ezetimibe–simvastatin			Chromolith column RP 18-e (100 × 4.6 mm)	ACN:ammonium acetate 50 mM, pH 5.0 = 65:35				LOD: 13.2 ± 0.4029 ng/mL LOQ: 39.5 ± 1.446 ng/mL Rec: 98.99–100.4%	
Ezetimibe–simvastatin	Tablets	n/a	Luna C18 column (250 × 4.6 mm)	MeOH:water:ACN = 75:18.75:6.25	(25 ± 0.5)	231	70% MeOH	LOD: n/a LOQ: n/a Rec: 99.36–99.46%	[26]
Ezetimibe–simvastatin	Tablets	n/a	C18 Supelcosil column (250 × 4.6 mm; 5 µm)	0.01 M ammonium acetate buffer: ACN = 35:65	n/a	240	Mobile phase	LOD: 0.1 µg/mL LOQ: 0.3 µg/mL Rec: 99.4–100.8%	[44]
Ezetimibe	Tablets	n/a	Phenomenex Luna C18 (250 × 4.6 mm; 5 µm)	ACN:0.02 M phosphate buffer: MeOH = 70:20:10	n/a	235	MeOH	LOD: 1 µg/mL LOQ: 3.2 µg/mL Rec: 99.6–101%	[45]
Ezetimibe	Capsules	n/a	Phenomenex Luna C18 (250 × 4.6 mm; 5 µm)	Water:ACN = 60:40	25	225	Water: ACN = 50:50	LOD: 1.41 µg/mL LOQ: 4.30 µg/mL	[35]
Ezetimibe	Tablets	n/a	Phenomenex Luna C18 (250 × 4.6 mm; 5 µm)	Acetonitrile:water: glacial acetic acid = 50:50:0.1	n/a	235	Mobile phase	LOD : n/a LOQ : n/a Rec: 99.05–99.93%	[15]
Ezetimibe–simvastatin	Tablets	n/a	LiCrospher 100 C18 (250 × 4.6 mm; 5 µm)	ACN:water: MeOH = 60:25:15	Ambient	238	n/a	LOD: n/a LOQ: n/a Rec: 100.43%	[46]
Ezetimibe	Tablets	Amoxycillin trihydrate	Kromasil 100 C18 (250 × 4.6 mm; 5 µm)	Water (0.05% 1-heptane sulfonic acid, pH 6.8):CN = 30:70	Ambient	234	Mobile phase	LOD: n/a LOQ: n/a Rec: 100.43%	[36]

Atorvastatin Ezetimibe	Tablets	n/a	Inertsil ODS-3V column (250 × 4.6 mm; 5 µm)	0.01 M ammonium acetate buffer (pH 3.0):ACN = 50:50	Ambient (25 ± 2)	254	Mobile phase	LOD: 1.48 µg/mL LOQ: 4.98 µg/mL Rec: 99.21–99.87%	[47]
Atorvastatin Ezetimibe	Tablets	Ibuprofen	Phenomenex Luna C18 (250 × 4.6 mm; 5µ m)	Ammonium acetate buffer, pH 5.0: ACN: triethylamine = 50:50:0.2	Ambient	240	MeOH	LOD: n/a LOQ: n/a Rec: 98.8–100.32%	[23]
Simvastatin Ezetimibe	Tablets	n/a	Phenomenex C18 column (250 × 4.6 mm; 5 µm)	1 M ammonium acetate buffer: ACN = 55:45	(25 ± 0.5)	230	ACN and buffer solution	LOD: n/a LOQ: n/a Rec: 100.06–100.16%	[48]
Ezetimibe	Bulk drug (degradation study)	n/a	Merck C8 column (250 × 4.0 mm; 5 µm) Inertsil C8 (250 × 4.6 mm; 5 µm)	0.02 M ammonium acetate, pH 7 (adjusted with ammonium hydroxide):ACN gradient:30–100% ACN in 80 min and brought back to initial in the next 10 min	n/a	250	n/a	LOD: n/a LOQ: n/a Rec: 97.78–103.85%	[49]
Ezetimibe	Tablets	Etoricoxib	Phenomenex Synergi fusion C18 (150 × 4.6 mm; 4 µm)	0.02 M phosphate buffer, pH 7:ACN: MeOH = 40:55:5	40	232	Stock solution/ stock sample solution in ACN, then diluted with ACN: water = 80:20	LOD: n/a LOQ: n/a Rec: 99.46–103.33%	[50]

(continued)

**TABLE 3.7** (continued)

Analyte(s)	Samples	Internal standard	Column	Mobile phase	Column temperature (°C)	Detection (nm)	Solvent	Limit of detection (LOD), limit of quantitation (LOQ), and recovery (Rec)	Reference
Ezetimibe	Tablets	Etoricoxib	Phenomenex Luna C18 column (50 × .0 mm; 3 µm)	ACN:water = 85:15	n/a	ESI in positive mode, MRM mode Ezetimibe: 392 → 161 Internal standard: 359.3 → 280	Stock solution/stock sample solution in ACN, then diluted with ACN: water = 80:20	LOD: n/a LOQ: n/a Rec: 100.83–103.91%	[50]
Ezetimibe–simvastatin	Tablets	n/a	ODS hypersil column (250 × 4.6 mm; 5 µm)	ACN:phosphate buffer 0.01 M, pH 4.5 = 65:35	n/a	232	MeOH	LOD: 20 ng/mL LOQ: 100 ng/mL Rec: 97.91–107.18%	[51]
Ezetimibe Fenofibrate	Bulk synthetic mixture	n/a	Kromasil (25 cm × 4.6 mm; 5 µm)	ACN:0.05 M ammonium acetate buffer = 85:15	n/a	253	n/a	LOD: n/a LOQ: n/a Rec: 99–101%	[52]
Ezetimibe Simvastatin	Tablet	n/a	Phenomenex Synergi fusion (150 mm × 4.6 mm)	Phosphate buffer 0.03 M, pH 4.5: ACN = 35:65	45	234	Dissolved in ACN then diluted with mobile phase	LOD: 0.05 µg/mL LOQ: 0.18 µg/mL Rec: 99.79–101.13%	[53]
Ezetimibe Simvastatin	Tablet	n/a	Phenomenex C18 (250 × 4.6 mm; 5 µm)	ACN:buffer (0.1%, v/v orthophosphoric acid, pH 3) = 75:25	Ambient	238	Dissolved in MeOH then diluted with mobile phase	LOD: 0.34 µg/mL LOQ: 1.10 µg/mL Rec: 99.86%	[54]

The concentration of 25 mM was shown to increase resolution as well as migration times. Acetonitrile was added as an organic modifier due to its capability to change the zeta potential as well as the buffer viscosity, which resulted in changes in the electroosmotic flow (EOF). Therefore, the distribution of solutes between the buffer and the micelle was strongly affected by the involvement of acetonitrile. This was then shown to improve the poor resolution between ezetimibe and simvastatin [57].

In an MEKC method, the choice of surfactant to form the micellar stationary phase is also important. In both published methods, sodium dodecyl sulfate (SDS) was utilized to form the micelle, in which this compound was added to the buffer composition at levels above its critical micelle concentration. It should also be noted that at SDS concentrations lower than 20 mM, the observed peak shapes deteriorated, and that increasing the concentration of SDS increased migration times. Moreover, increasing the applied voltage enables increment of EOF and shortened analysis time as well as resulting in higher efficiency. However, higher currents accompany the use of higher voltages, resulting in heating inside the capillary, and, therefore, the voltage used was limited to 30 kV. The temperature at which the procedure is run also affects the efficiency of the separation and analysis, since it changes EOF, electrophoretic mobilities, injection volume, and the peak shape [41,57]. The conditions of both MEKC methods are detailed in Table 3.8.

## 5. DEGRADATION OF EZETIMIBE

During the course of several validation studies, stress or degradation studies of ezetimibe were conducted concurrently. In general, three different degradation conditions were applied: acidic (effect of HCl), alkaline (effect of NaOH), and oxidative (effect of H<sub>2</sub>O<sub>2</sub>). However, some other methods also included degradation studies using heat, light, and wet as well as dry conditions. Details for the conditions of degradation applied, and the results obtained, are summarized in Table 3.9.

In the first study developed by Sistla *et al.* [36], only alkaline condition gave significant decrease in recovery, accompanied by a peak observed after the main ezetimibe peak, which was attributed to a degradation product of ezetimibe. Similarly, Dixit *et al.* [31] found that using lower concentrations of HCl and keeping the solution at room temperature did not have any degradation effect on ezetimibe. Other workers reported that alkaline conditions caused major degradation of ezetimibe. Of all the reported degradation studies of ezetimibe, the lowest concentration of NaOH used was 0.01 M [49], and here, the degradation process was complete in 4 h. The maximum concentration of NaOH used was 1 M [15,36]. Further, the proposed structure for the alkaline degradant of

**TABLE 3.8** Summary of MEKC method for analysis of ezetimibe in pharmaceutical dosage form

Analyte(s)	Electrophoretic procedure	Electrolyte	Capillary	Separation condition	Standard and sample preparation	Limit of detection (LOD), limit of quantitation (LOQ), and recovery (Rec)	Reference
Ezetimibe	Preparation conditioning: Rinsing with 1 M NaOH (10 min), water (10 min), and running electrolyte (15 min) Capillary conditioning: 1 M NaOH (2 min), water (1 min), and running buffer (5 min)	25 mM borate buffer and 25 mM SDS, pH 9.75: ACN = 90:10	Fused-silica capillary (50 $\mu$ m i.d., length 40 cm)	$T = 35\text{ }^{\circ}\text{C}$ Voltage: 30 kV Injection: pressure mode 50 mbar for 5 s Detection: 232 nm	Dissolved and diluted in ACN	LOD: 0.41 $\mu$ g/mL LOQ: 2 $\mu$ g/mL Rec: 99.95–101.04%	[57]
Ezetimibe Simvastatin	Before the first use of capillary: Flushing with 1.0 M NaOH (30 min) then water (20 min) Preparation conditioning: 0.1 M NaOH (15 min), water (10 min), and running buffer (10 min) Capillary conditioning: 0.1 M NaOH (2 min), water (2 min), and running buffer (4 min)	25 mM borate buffer and 25 mM SDS, pH 9:ACN = 90:10	Fused-silica capillary (50 $\mu$ m i.d., length 56 cm)	$T = 30\text{ }^{\circ}\text{C}$ Voltage: 30 kV Injection: pressure mode 50 mbar for 3 s	Standard: ACN Sample: Dissolved in ACN, diluted with running buffer	LOD: 1.0 $\mu$ g/mL LOQ: 2.0 $\mu$ g/mL Rec: 102.96 $\pm$ 1.06%	[41]

**TABLE 3.9** Degradation study of ezetimibe

Analyte(s)	Method	Treatment	Result	Reference
Ezetimibe	TLC	<ul style="list-style-type: none"> <li>– 200 mg ezetimibe dissolved in 200 mL of methanol + 1 M NaOH, refluxed for 1 h</li> <li>– Neutralized with methanol + 1 M hydrochloric acid, filtered and the filtrate was evaporated to about 10 mL</li> <li>– The filtrate was spotted on silica gel TLC glass plates (0.5 mm thickness) in the form of bands, developed in mobile phase</li> <li>– Each developed bands scratched from silica gel TLC plate</li> <li>– Extracted with methanol, filtered, evaporated until obtaining two degradation products</li> </ul>	<p>Ezetimibe <math>R_f</math>: <math>0.81 \pm 0.16</math></p> <p>Degradation product 1, <math>R_f</math>: 0</p> <p>Degradation product 2, <math>R_f</math>: <math>0.29 \pm 0.15</math></p>	[15]
Ezetimibe	HPLC	<ul style="list-style-type: none"> <li>– 0.5 mg/mL ezetimibe in 30% ACN and subjected to:               <ol style="list-style-type: none"> <li>1. Acid: 0.1 M and 0.1 M HCl, each heated at 80 °C for 8 h</li> <li>2. Alkaline:                   <ol style="list-style-type: none"> <li>a. 0.1 M NaOH at 80 °C for 8 h</li> <li>b. 0.01 M NaOH at 40 °C for 4 h</li> </ol> </li> <li>3. 3% H<sub>2</sub>O<sub>2</sub> and 20% H<sub>2</sub>O<sub>2</sub> at room temperature, stored for 24 h</li> <li>4. Neutral: in water at 80 °C for 8 h</li> </ol> </li> </ul>	<ol style="list-style-type: none"> <li>1. Acid: gradually degraded, Relative Retention Time (RRT) 0.48–1.14</li> <li>2. Alkaline: degraded so fast, major degradation has RRT 1.14, minor degradation has RRT 0.48 and 1.88</li> <li>3. H<sub>2</sub>O<sub>2</sub>: stable</li> <li>4. Neutral: complete degradation in 1 h with RRT 1.14</li> <li>5. Photodegradation: stable</li> </ol>	[50]

*(continued)*

**TABLE 3.9** (continued)

Analyte(s)	Method	Treatment	Result	Reference
		5. Photodegradation: a. Water, exposed to sunlight during day time for 2 days b. 1 M HCl, exposed to sunlight during day time for 2 days 6. Dry heat: a. Heated at 50 °C for 45 days b. Heated at 60 °C for 7 days	6. Dry heat: stable	
Ezetimibe	TLC	– 100 mg dissolved in 100 mL methanol and subjected to: 1. Acid: 0.1 M HCl and 1 M HCl at 80 °C for 8 h 2. Alkaline: 0.1 M NaOH and 1 M NaOH at 80 °C for 8 h 3. 3% H <sub>2</sub> O <sub>2</sub> for 6 h and 30% H <sub>2</sub> O <sub>2</sub> for 24 h and then heated in a boiling water bath for 10 min 4. Dry heat: oven 50 °C for 30 days 5. Wet heat: 50 °C, 75% Relative Humidity (RH) 6. Photo: sunlight (60,000–70,000 lux) for 2 days	1. Acid: degradation product Rf 0.22 2. Alkaline: degradation product Rf 1 0.21, Rf 2 0.55 3. H <sub>2</sub> O <sub>2</sub> : ezetimibe stable in H <sub>2</sub> O <sub>2</sub> 3% and 30% 4. Dry and wet heat: ezetimibe stable 5. Photo: minor degradation Rf 0.40, 0.52, 0.60 and 0.70	[32]
	HPTLC			[31]



Simvastatin,  
ezetimibe

- 50 mg dissolved in 50 mL methanol and subjected to:
    - 1. Acid: 0.1 M HCl, kept at room temperature for 2 h
    - 2. pH 6.8 phosphate buffer, kept at room temperature for 2 h
    - 3. 10% H<sub>2</sub>O<sub>2</sub>, heated under reflux 2 h at room temperature, heated in boiling water
    - 4. Dry heat: drug powder in oven at 60 °C for 2 h
    - 5. Wet heat: 1 mg/mL heated under reflux for 2 h on water bath
- 1. Acid: ezetimibe remain stable
  - 2. pH 6.8 phosphate buffer: two peaks with R<sub>f</sub> 0.3 and 0.44
  - 3. H<sub>2</sub>O<sub>2</sub>: ezetimibe stable
  - 4. Ezetimibe stable
  - 5. Ezetimibe stable

Ezetimibe

HPLC

- 50 mg ezetimibe subjected to:
    - 1. Acid: heated under reflux with 1 M HCl at 80 °C for 1 h and the mixture was neutralized
    - 2. Alkaline: 0.1 M NaOH at room temp for 90 min and the mixture was neutralized
    - 3. 3% H<sub>2</sub>O<sub>2</sub> under reflux at 80 °C for 1 h
    - 4. Thermal: exposed at 70 °C for 72 h
- 1. Acid: major degradation up to 74%
  - 2. Alkaline: rapidly degraded by 24%
  - 3. H<sub>2</sub>O<sub>2</sub>: degraded 9%
  - 4. Thermal: stable
  - 5. Photolytic: minor degradation (4%)

[38]

---

(continued)

**TABLE 3.9** (continued)

Analyte(s)	Method	Treatment	Result	Reference
		5. Photolytic: exposed to sunlight for 72 h		
Ezetimibe, simvastatin	HPLC	<ul style="list-style-type: none"> <li>– Stock solution contains 5.0 mg ezetimibe and simvastatin in 5.0 mL acetonitrile subjected to:               <ol style="list-style-type: none"> <li>1. Acid: 0.1 M HCl for 2 h at room temperature</li> <li>2. Base : 0.1 M NaOH for 2 hours at room temperature</li> <li>3. 3% H<sub>2</sub>O<sub>2</sub> for 6 h at room temperature and 30% H<sub>2</sub>O<sub>2</sub> for 24 h at room temperature, heated in boiling water bath for 10 min</li> <li>4. Dry heat: oven at 70 °C for 2 h</li> </ol> </li> </ul>	<ol style="list-style-type: none"> <li>1. Acid: ezetimibe stable</li> <li>2. Base: ezetimibe completely degraded</li> <li>3. H<sub>2</sub>O<sub>2</sub>: ezetimibe stable</li> <li>4. Dry heat: ezetimibe stable</li> </ol>	[42]
Ezetimibe	HPLC	<ul style="list-style-type: none"> <li>– 5 mg ezetimibe subjected to:               <ol style="list-style-type: none"> <li>1. Acid: 1 mL 1 N HCl, placed in water bath at 60 °C for 1 h</li> <li>2. Alkaline: 1 mL 1 N NaOH, placed in water bath at 60 °C for 1 h</li> <li>3. Reductive: 1 mL Zn + 1 N HCl</li> </ol> </li> </ul>	<ol style="list-style-type: none"> <li>1. Acid: ezetimibe not fully degraded</li> <li>2. Alkaline: ezetimibe become unstable</li> <li>3. Reduction: ezetimibe not fully degraded</li> <li>4. Oxidation: ezetimibe not fully degraded</li> <li>5. Photolytic: ezetimibe not fully degraded</li> </ol>	[58]

		4. Oxidative: 1 mL 5% H <sub>2</sub> O <sub>2</sub> 5. Photolytic: UV light at 254 nm for 8 h	
Ezetimibe	HPLC	– 50 mg ezetimibe subjected 1. Acid: 1 M HCl at 60 °C for 1 h 2. Alkaline: 1 M NaOH 60 °C for 1 h 3. Oxidizing: 3% and 20% H <sub>2</sub> O <sub>2</sub> at room temperature 4. Thermal: 70 °C for 72 h 5. Photolytic: UV light 254 nm for 8 h	[57]
Simvastatin Ezetimibe	HPLC	– Solutions of drugs in methanol containing 1000 µg/mL were mixed with: 1. 0.1 N HCl to obtain the concentration of drug 5 µg/mL, kept at room temperature 2. pH 7.4 phosphate buffer to obtain the concentration of drug 5 µg/mL, kept at room temperature 3. 10% H <sub>2</sub> O <sub>2</sub> to obtain the concentration of drug 5 µg/mL, heated at 60 °C for 30 min	[58]

1. Acid: ezetimibe forming major degradation and minor degradation
2. Alkaline: ezetimibe rapidly decreased, major degradation increased
3. Oxidizing: ezetimibe stable
4. Thermal: ezetimibe stable
5. Photolytic: minor degradation

1. Acid: ezetimibe remain stable
2. Phosphate buffer: ezetimibe degradation peak was detected following the peak of ezetimibe and separated from ezetimibe peak
3. H<sub>2</sub>O<sub>2</sub>: ezetimibe remain stable

ezetimibe was proposed from structure elucidation using IR spectra as detailed in Fig. 3.3.

In a study using phosphate buffer pH 6.8 at room temperature, ezetimibe was completely degraded after 2 h. Phosphate buffer was chosen to slow the degradation process in alkaline condition, proving that alkaline conditions have a major degradation effect on ezetimibe [31]. Interestingly, Doshi *et al.* [42] found that the degradation of ezetimibe was higher in acidic condition relative to alkaline condition, but the procedure to induce the degradation was different than other methods published (i.e., ezetimibe was acidified and then heated under reflux). Exposure of ezetimibe to oxidizing conditions, or to exposure to low humidity and heat, did not lead to instability of ezetimibe. In addition, other studies showed that minor degradation took place when ezetimibe exposed to either ultraviolet light (254 nm) or sunlight [32,35,36,42].

## 6. DETERMINATION OF EZETIMIBE IN BIOLOGICAL SAMPLE

Ezetimibe is given orally to inhibit cholesterol absorption. Following oral administration, this substance is rapidly metabolized in the intestine by glucuronidation of the 4-hydroxyphenyl group, forming a glucuronide metabolite (known as SCH 60663). This metabolite is the predominant metabolite in plasma and urine, and appears to act as the more potent inhibitor of cholesterol absorption [4,59]. In addition, hydrolysis of ezetimibe glucuronide in the intestine together with unabsorbed ezetimibe then forms unconjugated ezetimibe.

Besides the major glucuronide metabolite, oxidation of the benzylic hydroxyl group of ezetimibe results in a ketone of ezetimibe as the minor metabolite known as SCH 57871. Another minor metabolite is the 4-hydroxyphenyl glucuronide, which is the conjugate of SCH 57871 (ketone–glucuronide) [4].

In another study, Ghosal *et al.* [60] determined that *in vitro* incubation of human liver microsomes supplemented with UDP glucuronic acid and ezetimibe also formed ezetimibe glucuronide as the major metabolite. Moreover, in an *in vitro* study in human jejunum microsomes, ezetimibe was found to convert into two glucuronide compounds. One of these was a phenolic glucuronide metabolite (the major metabolite known), and the other was a benzylic glucuronide of ezetimibe.

Liquid chromatographic methods for determining ezetimibe and its metabolites are summarized in Table 3.10 and described in subsequent sections. The chemical structure of metabolites of ezetimibe is illustrated in Fig. 3.4.

**TABLE 3.10** Summary of HPLC analysis for the determination of ezetimibe in biological sample

Analyte(s)	HPLC conditions	Sample	Preparation of standard, sample extraction, and clean up	Limit of detection (LOD), Limit of quantitation (LOQ), and extraction efficiency (rec)	Reference
Ezetimibe (SCH 58235) <sup>13</sup> C <sub>6</sub> SCH 58235 (i.s.)	Column: Zorbax SB-C18 (7.5 cm × 4.6 mm; 3.5 μm particle size) Mobile phase: MeOH:0.025 ammonium acetate = 80:20 Detector: LC-MS in positive ion mode Ezetimibe: 392.0 → 133.4 i.s.: 398.4 → 139.4	Human plasma	Standard: n/a Sample: Extraction method: LLE Extracting solvent: chlorobutane Unchanged ezetimibe: 1 mL sample added with 100 μL i.s. and 1.0 mL water then extracted with extracting solvent. Total ezetimibe: 200 μL sample added with 100 μL i.s., 500 μL sodium acetate, 0.5 M, pH 5.0, and 50 μL β-glucuronidase. Sample was vortexed and incubated at 50 °C for 60 min, then added with sodium borate, 0.1 M, and then extracted with extracting solvent.	Unchanged ezetimibe LOD: n/a LOQ: 20 pg/mL Rec: n/a Total ezetimibe LOD: n/a LOQ: 0.25 ng/mL Rec: n/a	[58]

(continued)

**TABLE 3.10** (continued)

Analyte(s)	HPLC conditions	Sample	Preparation of standard, sample extraction, and clean up	Limit of detection (LOD), Limit of quantitation (LOQ), and extraction efficiency (rec)	Reference
Ezetimibe (SCH 60663)	Column: Spherisorb ODS2 (10 × 0.46 cm; 10 μm)	Human plasma	After being extracted, sample was centrifuged and the organic layer was drawn and evaporated.	LOD: n/a	[59]
SCH 58053 (i.s.)	Mobile phase: MeOH:0.025 M ammonium acetate = 90:10		Residue was dissolved in MeOH, reevaporated and reconstituted in MeOH:water = 80:20	LOQ:	
	Detector: LC–MS with positive ion mode		Standard: n/a	Unconjugated ezetimibe:	
	Ezetimibe: $m/z$ 392.3 → 133.1		Sample:	1.00 ng/mL	
	i.s.: $m/z$ 434.2 → 216.1		Extraction method: LLE	Total ezetimibe:	
			Extracting solvent: 1-chlorobutane	5.02 ng/mL	
			Unconjugated ezetimibe: 200 μL sample + 100 μL i.s.		
			+ 1.0 mL water, vortexed and extracted with 8.0 mL extracting solvent		
			Total ezetimibe: 200 μL sample + 100 μL i.s.		
			+ 500 μL sodium acetate 0.5 M, pH 5.0, then added with 50 μL β-glucuronidase and incubated at 50 °C for 60 min.		

			<p>Sample was then added with 500 <math>\mu</math>L sodium borate 1.0 M and extracted with 8.0 mL extracting solvent</p> <p>After extracted with extracting solvent, both samples for unconjugated or total ezetimibe were then centrifuged at 20 °C. The organic layer was drawn, evaporated in evaporator then the residue dissolved with 500 <math>\mu</math>L MeOH, evaporated again, and reconstituted with 50 <math>\mu</math>L MeOH</p>		
Metabolite profiling for ezetimibe	<p>Column: Inertsil C8 (150 <math>\times</math> 4.6 mm; 5 <math>\mu</math>m)</p> <p>Mobile phase: A: 20 mM ammonium acetate pH 7 (adjusted with 1% aqueous ammonium hydroxide)</p> <p>B: ACN</p> <p>Gradient: 0–0.1 min: 70% A, 30% B 0.1–44.9 min: exponentially increased to 100% B</p> <p>Detector:</p>	<p>Human plasma</p> <p>Urine</p> <p>Feces</p> <p>(all sample containing radioactive tracer)</p>	<p>Human plasma</p> <p>Extraction method: SPE with tC18 cartridges (Waters)</p> <p>SPE column conditioning: 20 mL 0.1% TFA in MeOH, followed with 40 mL MeOH, and then with 40 mL water</p> <p>Sample extraction: 8 mL sample eluted through SPE column and eluted with 40 mL of 0.1% TFA in MeOH. Eluant was then evaporated in room</p>	<p>LOD: n/a</p> <p>LOQ: n/a</p> <p>Rec: n/a</p>	[59]

(continued)

**TABLE 3.10** (continued)

Analyte(s)	HPLC conditions	Sample	Preparation of standard, sample extraction, and clean up	Limit of detection (LOD), Limit of quantitation (LOQ), and extraction efficiency (rec)	Reference
	LC-MS and LC-MS/MS equipped with radioactivity detector. Other details n/a		<p>temperature, dissolved in minimum amount of MeOH, reevaporated under N<sub>2</sub> at 23 °C, then dissolved in 100 µL DMSO and injected</p> <p>Urine: As for human plasma</p> <p>Feces: Extraction method: LLE using Extrelut 3</p> <p>Extracting solvent: Isopropanol:ethyl acetate:dichloromethane = 20:60:20</p> <p>2 g sample was homogenized then eluted through Extrelut 3 using the extracting solvent. The solvent containing the analyzed substance was then evaporated and dissolved with MeOH, reevaporated under N<sub>2</sub> at 23 °C. Final residue reconstituted in 150–200 µL DMSO and centrifuged. Supernatant was then injected</p>		



Radiolabeled ezetimibe ( $^{14}\text{C}$ -SCH 58235 )	Column: C8 Inertsil (150 × 4.6 mm; 5 $\mu\text{m}$ ) Mobile phase: A = 20 mM ammonium acetate adjusted to pH 7 with 1% aqueous ammonium hydroxide B = ACN Gradient: 0–0.1 min: 30% B, then rapidly increased to 100% B, hold for 5 min then reequilibrated at 30%B Detector: LC/MS/radiometric UV—245 nm	Human liver microsome incubated with ezetimibe Human jejunum microsome incubated with ezetimibe	Standard: n/a Sample: HPLC UV detection: After incubation treatment, sample was vortexed and centrifuged. Supernatant was withdrawn and injected LC–MS detection: Extraction method: SPE using tC18 Sep-Pak Cartridge Column washed: MeOH followed with water Sample extraction: Sample placed in SPE then washed with water then eluted with MeOH	LOD: n/a LOQ: n/a Rec: n/a	[60]
Phenolic glucuronide (SCH 60663) Benzylic glucuronide of ezetimibe (SCH 488128)					
Ezetimibe glucuronide 4-Hydroxychalcone (i.s.)	Column: XTerra <sup>®</sup> MS C18 (2.1 × 100 mm; 3.5 $\mu\text{m}$ ) Mobile phase: ACN:water = 60:40 Detector: LC/MS/MS with MRM mode Ezetimibe: $m/z = 408 \rightarrow 271$ i.s.: $m/z = 223 \rightarrow 117$	Human serum, urine, feces	Standard: n/a Sample: Extraction method: LLE Extracting solvent: methyl <i>tert</i> -butyl ether Free ezetimibe: 0.5 mL sample + 0.5 mL deionized water + 25 $\mu\text{L}$ i.s., then extracted with 4 mL extracting solvent	LOD: n/a LOQ: Serum: 0.05 ng/mL Urine: 1.0 ng/mL Feces: 10 ng/mL Rec: Serum: 91.3–114% Urine: 97.7–102% Feces: 83.6–92.2%	[64,65]

(continued)

**TABLE 3.10** (continued)

Analyte(s)	HPLC conditions	Sample	Preparation of standard, sample extraction, and clean up	Limit of detection (LOD), Limit of quantitation (LOQ), and extraction efficiency (rec)	Reference
Ezetimibe Etoricoxib (i.s.)	Column: Phenomenex Luna C18 column (50 × 3.0 mm; 3 μm) Mobile phase:	Human plasma	<p>Total ezetimibe 0.5 mL sample + 450 μL deionized water + 50 μL β-glucuronidase then incubated at 50°C for 60 min. After incubation, 25 μL i.s. was added, then sample extracted as for free ezetimibe</p> <p>For free and total ezetimibe, after being extracted, sample was then centrifuged. The organic layer was drawn and evaporated at 50°C under gentle air stream. Residue was then reconstituted with ACN: water = 60:40. Volume of reconstitution was 100 μL for serum and 200 μL for urine or feces</p> <p>Standard: ACN Sample: Extraction method: LLE Extracting solvent: <i>tert</i>-butyl</p>	<p>Free ezetimibe LOD: 0.1 ng/mL LOQ: 0.25 ng/mL Rec: 65.35–97.07%</p>	[50]

ACN:water = 85:15

Detector:

ESI in positive mode, MRM mode

Ezetimibe: 392 → 161

i.s.: 359.3 → 280

methyl ether

Free ezetimibe:

500 µL sample + 50 µL i.s. then  
extracted with 4 mL extracting  
solvent

Total ezetimibe:

200 µL sample + 20 µL i.s. + 500  
µL sodium acetate buffer 0.5 M  
pH 5.0 + 50 µL β-glucuronidase,  
then incubated at 50 °C for 60  
min, and extracted with 3 mL  
extracting solvent

After being extracted, sample was  
centrifuged. Supernatant was  
drawn and evaporated under  
nitrogen whilst immersed in  
water bath at 40 °C. Residue  
was then dissolved in ACN:  
water = 80:20 with volume 500  
and 200 µL for free and total  
ezetimibe, respectively

Total ezetimibe

LOD: 0.1 ng/mL

LOQ: 1 ng/mL

Rec: 62.13–64.85%

Ezetimibe  
Ezetimibe  
glucuronide

Column: C18 symmetry shield  
column (4.6 × 250 mm; 5 µm,  
Waters)

Rat bile

Standard: MeOH

LOD: n/a

LOQ: n/a

[61]

(continued)

**TABLE 3.10** (continued)

Analyte(s)	HPLC conditions	Sample	Preparation of standard, sample extraction, and clean up	Limit of detection (LOD), Limit of quantitation (LOQ), and extraction efficiency (rec)	Reference
Ezetimibe ketone Theophylline (i.s.)	Mobile phase: A = 0.05 M formic acid, pH 3.0 B = water:ACN = 10:90 C = water:MeOH = 10:90 Gradient mode: Time      A (%)   B (%)   C (%) (min)    0       100  2       90      0 10 9       50      20 30 12      50      25 25 30      50      20 25 28–35        10       85      5 36–40        100      0       0		Sample: Extraction method: LLE Extracting solvent: 25% perchloric acid in ACN Bile was collected, added with 100 µL buffer ammonium acetate 0.1 M, pH 4.5 then stored at (–) 20 °C . Prior to extraction, 500 µL sample added with 10 µL i.s. then extracted with extracting solvent. Aliquot of the organic layer was injected and analyzed	Rec: Ezetimibe: 70–85% Ezetimibe glucuronide: 70–85% Ezetimibe ketone: 50%	
Detector: UV 250 nm LC–MS/MS: CID negative ion mode Ezetimibe: $m/z$ 408 Ezetimibe glucuronide: $m/z$ 584 Ezetimibe ketone: $m/z$ 406					

Ezetimibe <sup>13</sup> C6-ezetimibe (i.s.)	Column: Capcell Pak C18 MG column (50 × 2 mm i.d.; 5 µm) Mobile phase: A: ACN B: 5 mM ammonium acetate Gradient mode: 0–0.1 min: 70–0% B 0.1–1.5 min: 0% B 1.5–1.6 min: 0–70% B 1.6–5 min: 70% B Detector: LC/MS/MS with negative ESI, MRM Ezetimibe: $m/z = 408.5 \rightarrow 270.8$ i.s.: $m/z = 414.5 \rightarrow 276.8$	Human plasma	Standard: n/a Sample: Extraction method: LLE Extracting solvent: <i>tert</i> -butyl methyl ether Free ezetimibe: 200 µL sample + 10 µL i.s. then extracted with 1.0 mL extracting solvent  Total ezetimibe: 100 µL sample + 10 µL i.s. + 250 µL sodium acetate buffer 0.5 M pH 5.0 + 50 µL β-glucuronidase. Sample was then vortexed and incubated at 50 °C for 60 min, then added with 250 µL sodium borate 0.1 M and extracted with 2.0 mL extracting solvent For both free and total ezetimibe, after extraction, sample was then centrifuged. Supernatant was drawn and evaporated at 40 °C under nitrogen stream. Residue was reconstituted with 100 µL MeOH	Free ezetimibe: LOD: n/a LOQ: n/a Rec: 78.6%  Total ezetimibe: LOD: n/a LOQ: n/a Rec: n/a	[63]
--	--	-----------------	--	---	------

(continued)

**TABLE 3.10** (continued)

Analyte(s)	HPLC conditions	Sample	Preparation of standard, sample extraction, and clean up	Limit of detection (LOD), Limit of quantitation (LOQ), and extraction efficiency (rec)	Reference
Ezetimibe Zidovudine (i.s.)	Column: Inertsil C18 (4.6 × 50 mm; 3.0 μm) Mobile phase: 25.0 mM ammonium acetate:ACN = 10:90 Detector: LC–MS/MS monitored in MRM mode Ezetimibe: $m/z = 408.3 \rightarrow 271.2$ i.s: $m/z$ = not available	Human plasma	Standard: n/a Sample: Extraction method: LLE Extracting solvent: <i>tert</i> -butyl methyl ether	LOD: n/a LOQ: 0.0915 ng/mL Rec: 84%	<a href="#">[62]</a>

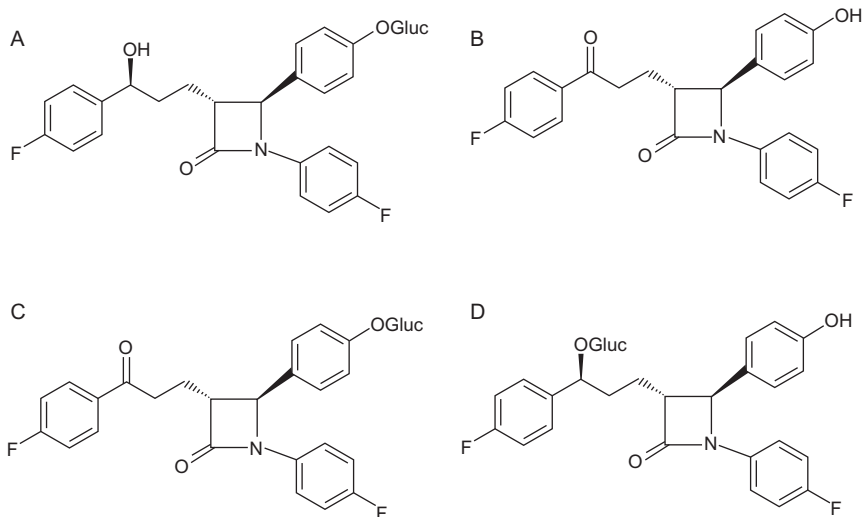


**FIGURE 3.4** Metabolites of ezetimibe: (A) ezetimibe glucuronide/phenolic glucuronide of ezetimibe (SCH 60663); (B) ketone ezetimibe (SCH 57871); (C) ketone glucuronide of ezetimibe; and (D) benzylic glucuronide of ezetimibe (SCH 488128).

## 6.1. Liquid chromatography

The first liquid chromatography method introduced to determine ezetimibe and its metabolites was developed by Ezzet *et al.* [58], and the method was used to model the pharmacokinetics of ezetimibe in humans. The liquid chromatography–mass spectrometry (LC–MS) method was used to determine unchanged ezetimibe and total ezetimibe (unchanged ezetimibe together with ezetimibe glucuronide) in human plasma samples.

Following this publication, Patrick *et al.* [59] reported a quantitative method using the combination of LC–MS/MS and radioactivity for the determination of ezetimibe in biological samples as well as the metabolite profiling of ezetimibe by. Similarly, Ghosal *et al.* [60] also applied the combination of LC–MS/MS and radioactivity to analyze ezetimibe and its metabolites. However, there were no details reported for validation of the analysis of both LC–MS/MS and radioactivity methods.

More recent publications [50,61–65] reported the development and validation of LC methods for the analysis of ezetimibe and its metabolites in biological samples. Most of the extraction methods used liquid extraction with *tert*-butyl methyl ether as the extracting solvent, since this solvent gave higher efficiency of recovery of ezetimibe as compared to other organic solvents [50]. In this analysis method, attention was given to the sample stability before and during analysis, and it was reported that

on average, samples were stable when stored in the autosampler for 24 h at either 4 or 15 °C [63–65]. Further, for the freeze–thaw cycle, samples can be stable for at least two freeze–thaw cycles (Oswald) and also three freeze–thaw cycles [50,63]. Oswald *et al.* reported that biological samples containing ezetimibe were stable for 6 h at room temperature [64]. Li *et al.* [63] found that biological samples containing ezetimibe were stable at room temperature for as long as 16 h. This latter finding is particularly important since the analysis of total ezetimibe (i.e., free ezetimibe and conjugated ezetimibe), samples have to be incubated with the  $\beta$ -glucuronidase enzyme at 50 °C for 60 min [58,63].

## 6.2. Gas chromatography

Uçaktürk *et al.* [66] reported a gas chromatography (GC) method (with prior molecular derivatization) for the determination of ezetimibe in human plasma samples. The derivatization process was required due to the unstable character of ezetimibe, and the fact that ezetimibe does not have volatility at high temperature. Silylation was selected for the derivatization, since this method is widely used for GC–MS analysis. In this process, one or more active hydrogen atoms from the organic molecule are replaced by a trialkyl-substituted silyl group. In this method, *N*-methyl-*N*-trimethylsilyl-trifluoroacetamide (MSTFA) was chosen as the silylating agent, as this compound is known to be the most volatile trimethylsilyl (TMS) donor available [67]. In this derivatization reaction, MSTFA reacts with labile hydroxyl group of ezetimibe, and the hydroxyl groups are then converted into TMS–ether derivatives under trimethylsilylation derivatization conditions.

The effect of two different catalysts in the derivatization process was also investigated to improve the reactivity of MSTFA as well as the efficiency of the silylation process. The first catalyst used was imidazole, and the other was a mixture of  $\beta$ -mercaptoethanol/ammonium iodide. The effect of temperature was also investigated to optimize the conversion. Results showed that both catalysts produced derivatives in high yield, with the optimum temperature being 80 °C when the reaction was run for 60 min. Since the degree of reproducibility using MSTFA/ $\beta$ -mercaptoethanol/ $\text{NH}_4\text{I}$  was higher, this catalyst was chosen for the derivatization of ezetimibe.

The analysis was conducted on HP-5ms (5% phenyl methylpolysiloxane, 30 m  $\times$  0.25 mm i.d. with 0.25 mm film thickness) stationary phase, with helium being used as the carrier gas. The column temperature was initially set as 200 °C, then increased to 250 °C at a rate of 50 °C/min, and then increased gradually to 280 °C at a rate of 30 °C/min. This temperature was maintained for 8 min, raised to 300 °C at a rate of 20 °C/min, and then held at 300 °C for 4 min. Throughout this temperature programming,



the total run time was 15 min. Detection was performed under SIM mode with  $m/z = 326$ , and methyltestosterone was used as an international standard. After method validation, limit of detection and limit of quantitation values were reported as 10 and 15 ng/mL, respectively. For the detection of ezetimibe in human plasma samples, the percent recovery ranged from 70.87% to 85.06%.

## REFERENCES

- [1] Martindale: The Complete Drug Reference, 35 ed., The Pharmaceutical Press, London, 2007.
- [2] H. Bays, *Expert Opin. Invest. Drugs* 11 (2002) 1587–1604.
- [3] G.P. Merck Frosst-Schering Pharma, Product Monograph Ezetrol. <http://www.merck-frosst.ca/mfcl/en/corporate/products/ezetrol.html>, 2009 (4 July 2010).
- [4] C. Simard, J. Turgeon, *Can. J. Clin. Pharmacol.* 10 (2003) 13A–20A.
- [5] M.J. O'Neil, *The Merck Index*, 13th ed., Merck & Co, Inc., New Jersey, 2001.
- [6] R.J. Aronhime, N.T. Koltai, G.-H. Samburski, G. Lerman, M.B. Izsak, US Patent 2006/0160785, 2006.
- [7] K. Ravikumar, B. Sridhar, *Acta Crystallogr. E* 61 (2005) 2907–2909.
- [8] J.A. Doney, A.W. Brzezczko, C.S. Shores, US Patent 2008/0085315 A1, in: 2008.
- [9] B.P. Reddy, K.R. Reddy, R.R. Reddy, D.M. Reddy, K.S.C. Reddy, Patent WO 2005/009955 A1, 2005.
- [10] V. Sundaram, S.T. Rajan, V.P. Ramayya, S.V. Vardhan, B. Subrahmanyam, C.V. A. Sasikala, US Patent No. US 2005/0171080 A1, 2005.
- [11] A. Štimac, B. Mohar, M. Stephan, M. Bevc, R. Zupet, A. Gartner, Patent WO 2008/089984 A2, 2008.
- [12] J. Brüning, E. Alig, M.U. Schmidt, *Acta Crystallogr. C* 66 (2010) 341–344.
- [13] R.N. Kane, B.S. Kuchekar, S.R. Naik, S.B. Bumrela, *Int. J. Chem. Anal. Sci.* 1 (2010) 22–27.
- [14] B. Raman, B.A. Sharma, R. Butala, P.D. Ghugare, A. Kumar, *J. Pharm. Biomed. Anal.* 52 (2010) 73–78.
- [15] S.M. El-Moghazy, M.A.E.-A. Mohamed, M.F. Mohamed, N.F. Youssef, *J. Chin. Chem. Soc.* 56 (2009) 360–367.
- [16] C.H.V.A. Sasikala, P.R. Padi, V. Sunkara, P. Ramayya, P.K. Dubey, V.B.R. Uppala, C. Praveen, *Org. Process. Res. Dev.* 13 (2009) 907–910.
- [17] P. Mishra, A. Gupta, K. Shah, *J. Indian Chem. Soc.* 84 (2007) 945–947.
- [18] P.B.S. Lakshmi, D. Ramchandran, C. Rambabu, *E-J. Chem.* 7 (2010) 101–104.
- [19] S.J. Rajput, H.A. Raj, *Indian J. Pharm. Sci.* 69 (2007) 759–762.
- [20] A.K. Gajjar, V.D. Shah, *Int. J. Pharm. Pharm. Sci.* 2 (2010) 131–138.
- [21] M. Sharma, D.V. Mhaske, M. Mahadik, S.S. Kadam, S.R. Dhaneshwar, *Indian J. Pharm. Sci.* 70 (2008) 258–260.
- [22] M. Pernarowski, A.M. Knevel, J.E. Christian, *J. Pharm. Sci.* 50 (1961) 943–945.
- [23] S.S. Sonawane, A.A. Shirkhedkar, R.A. Fursule, S.J. Surana, *Eur. J. Anal. Chem.* 1 (2006) 31–41.
- [24] I.M. Palabiyik, F. Onur, *Quim. Nova* 31 (2008) 1121–1124.
- [25] T. Rajesh, P.D. Reddy, *J. Pharm. Res.* 2 (2009) 815–818.
- [26] N. Jain, R. Jain, H. Swami, S. Pandey, D.K. Jain, *Int. J. Pharm. Pharm. Sci.* 1 (2009) 170–175.
- [27] S.J. Rajput, H.A. Raj, *Int. J. PharmTech. Res.* 1 (2009) 894–899.
- [28] B.G. Chaudhari, N.M. Patel, P.B. Shah, K.P. Modi, *Indian J. Pharm. Sci.* 68 (2006) 790–793.

- [29] S. Dhaneshwar, P. Deshpande, M. Patil, G. Vadnerkar, S. Dhaneshwar, *Acta Chromatogr.* 20 (2008) 71–79.
- [30] S. Dhaneshwar, S. Dhaneshwar, P. Deshpande, M. Patil, *Acta Chromatogr.* 19 (2007) 141–148.
- [31] R.P. Dixit, C.R. Barhate, M.S. Nagarsenker, *Chromatographia* 67 (2008) 101–107.
- [32] M.V. Mahadik, R.S. Dhaneshwar, *Asian J. Pharm. Sci.* 2 (2007) 182–190.
- [33] K. Shivshankar, N. Sreekanth, N. Harikrishnan, *Asian J. Chem.* 19 (2007) 3627–3632.
- [34] B. Fried, J. Sherma, *Thin-Layer Chromatography*, fourth ed., Marcel Dekker, Inc., New York, 1999.
- [35] S. Pandey, M. Rathanand, *Int. J. Pharm. Sci. Rev. Res.* 1 (2010) 53–57.
- [36] R. Sistla, V.S. Tata, Y.V. Kashyap, D. Chandrasekar, P.V. Diwan, *J. Pharm. Biomed. Anal.* 39 (2005) 517–522.
- [37] M. Ashfaq, I.U. Khan, S.S. Qutab, S.N. Razzaq, *J. Chil. Chem. Soc.* 52 (2007) 1220–1223.
- [38] N. Özalpin, E. Uçaktürk, *Chromatographia* 66 (2007) S87–S91.
- [39] S.K. Akmar, L. Kothapalli, A. Thomas, S. Jangam, A.D. Deshpande, *Indian J. Pharm. Sci.* 69 (2007) 695–697.
- [40] S.S. Qutab, S.N. Razzaq, I.U. Khan, M. Ahfaq, Z.A. Shuja, *J. Food Drug Anal.* 15 (2007) 139–144.
- [41] S.L. Dalmora, P.R. Oliveira, T. Barth, V. Todeschini, *Anal. Sci.* 24 (2008) 499–503.
- [42] A.S. Doshi, P.K. Kachhadia, H.S. Joshi, *Chromatographia* 67 (2007) 137–142.
- [43] M. Hefnawy, M. Al-Omar, S. Julkhuf, *J. Pharm. Biomed. Anal.* 50 (2009) 527–534.
- [44] D.A. Kumar, D.P. Sujana, V. Vijayasree, J.V.L.N.S. Rao, E.-J. Chem. 6 (2009) 541–544.
- [45] P. Nagaraju, K. Krishnachaitanya, D. Chandrababu, *Int. J. Pharm. Pharm. Sci.* 2 (2010) 33–37.
- [46] B. Chaudhari, N. Patel, P. Shah, *J. AOAC Int.* 90 (2007) 1242–1249.
- [47] U. Seshachalam, C.B. Kothapally, *J. Liq. Chromatogr. Relat. Technol.* 31 (2008) 714–721.
- [48] B.S. Rathinaraj, S.V. Kumar, S. Sudharshini, B. Thirupathy, Gurusharan, *Int. J. Pharm. BioSci.* 1 (2010) 1–7.
- [49] S. Singh, B. Singh, R. Bahuguna, L. Wadhwa, R. Saxena, *J. Pharm. Biomed. Anal.* 41 (2006) 1037–1040.
- [50] P.R. Oliveira, L.B. Junior, M. Fronza, L.S. Bernardi, S.M.K. Masiero, S.L. Dalmora, *Chromatographia* 63 (2006) 315–320.
- [51] R. Dixit, C. Barhate, S. Padhye, C. Viswanathan, M. Nagarsenker, *Indian J. Pharm. Sci.* 72 (2010) 204–210.
- [52] H. Pawar, L. Kothapalli, A. Thomas, R. Nanda, S. Mare, *Res. J. Pharm. Technol.* 1 (2008) 25–28.
- [53] P.R. Oliveira, T. Barth, V. Todeschini, S.L. Dalmora, *J. AOAC Int.* 90 (2007) 1566–1572.
- [54] P. Nagaraju, Z.V. Vardana, *J. Glob. Pharm. Technol.* 2 (2010) 113–117.
- [55] T. Ikegami, N. Tanaka, *Curr. Opin. Chem. Biol.* 8 (2004) 527–533.
- [56] S. Terabe, *Annu. Rev. Anal. Chem.* 2 (2009) 99–120.
- [57] C. Yardimci, N. Özalpin, *J. Chromatogr. Sci.* 48 (2010) 95–99.
- [58] F. Ezzet, G. Krishna, D.B. Wexler, P. Statkevich, T. Kosoglou, V.K. Batra, *Clin. Ther.* 23 (2001) 871–885.
- [59] J.E. Patrick, T. Kosoglou, K.L. Stauber, K.B. Alton, S.E. Maxwell, Y. Zhu, P. Statkevich, R. Iannucci, S. Chowdhury, M. Affrime, M.N. Cayen, *Drug Metab. Dispos.* 30 (2002) 430–437.
- [60] A. Ghosal, N. Hapangama, Y. Yuan, J. Achanfu-Yeboah, R. Iannucci, S. Chowdhury, K. Alton, J.E. Patrick, S. Zbaida, *Drug Metab. Dispos.* 32 (2004) 314–320.
- [61] S.J. Basha, S.A. Naveed, N.K. Tiwari, D. Shashikumar, S. Muzeeb, T.R. Kumar, N.V. Kumar, N.P. Rao, N. Srinivas, R. Mullangi, N.R. Srinivas, *J. Chromatogr. B Anal. Technol. Biomed. Life Sci.* 853 (2007) 88–96.
- [62] C. Kandasamy, R. Palarapu, S. Savale, V. Sam, A. Arvind, AAPS Annual Meeting and Exposition. Atlanta, Georgia, USA, 2008.

- [63] S. Li, G. Liu, J. Jia, X. Li, C. Yu, J. Pharm. Biomed. Anal. 40 (2006) 987–992.
- [64] S. Oswald, T. Giessmann, D. Luetjohann, D. Wegner, D. Roszkopf, W. Weitschies, W. Siegmund, Clin. Pharmacol. Ther. 80 (2006) 477–485.
- [65] S. Oswald, E. Scheuch, I. Cascorbi, W. Siegmund, J. Chromatogr. B 830 (2006) 143–150.
- [66] E. Uçaktürk, N. Özaltın, B. Kaya, J. Sep. Sci. 32 (2009) 1868–1874.
- [67] R.E. Kirk, D.F. Othmer (Eds.), Silylating Agents, fifth ed., In: Encyclopedia of Chemical Technology, vol. 22, John Wiley & Sons, Inc., New Jersey, 2006.

# CHAPTER 4

## Gemifloxacin

**Badraddin M.H. Al-Hadiya\*** and  
**Ashraf M.M. Mahmoud<sup>†</sup>**

---

<b>Contents</b>		
	1. Introduction	152
	2. Description [6]	152
	2.1. Nomenclature	152
	2.1.1. CAS name	152
	2.1.2. IUPAC name	152
	2.1.3. Proprietary names	153
	2.1.4. Nonproprietary names	153
	2.2. Formulae	153
	2.2.1. Empirical	153
	2.2.2. Structural	153
	2.2.3. CAS Registry Number	153
	2.3. Molecular weight	153
	2.4. Elemental composition for gemifloxacin	153
	2.5. Appearance, color, and odor	154
	3. Physical Characteristics	154
	3.1. Melting behavior	154
	3.2. Solubility	154
	3.3. Hydrophobicity	154
	4. Synthesis [2]	154
	5. Mechanism of Action and Uses	154
	6. Spectroscopy	156
	6.1. UV–VIS spectroscopy	156
	6.2. Fluorescence spectroscopy	156
	6.3. IR spectroscopy	157
	6.4. <sup>1</sup> H NMR spectroscopy	159
	6.5. Mass spectrometry	159

\* Department of Clinical Pharmacy, College of Pharmacy, King Saud University, Riyadh, Kingdom of Saudi Arabia

<sup>†</sup> Pharmaceutical Chemistry, College of Pharmacy, King Saud University, Riyadh, Kingdom of Saudi Arabia

7. Methods of Analysis	159
7.1. UV-analysis	159
7.2. Colorimetric analysis	159
7.3. Fluorimetric analysis	163
7.4. HPLC analysis	163
7.5. Capillary electrophoresis	164
8. Clinical Pharmacokinetics and Toxicity	164
8.1. Pharmacokinetics	164
8.1.1. Absorption and bioavailability	165
8.1.2. Distribution	165
8.1.3. Metabolism	165
8.1.4. Excretion	166
8.2. Toxicity and side effects	166
8.3. Overdosage and contraindications	167
8.4. Drug interactions	167
Acknowledgment	167
References	168

## 1. INTRODUCTION

Gemifloxacin is a fourth generation synthetic broad-spectrum fluorinated quinolone antibacterial agent for oral administration ([http://en.wikipedia.org/wiki/Gemifloxacin\\_mesylate](http://en.wikipedia.org/wiki/Gemifloxacin_mesylate)). It is discovered by Hong *et al.* [1] since 1997, and is present in two forms; either as free gemifloxacin base or as gemifloxacin mesylate salt. Gemifloxacin has a broad-spectrum activity against both Gram-negative and Gram-positive microorganisms [2–5]. The new oxime-pyrrolidine derivative moiety of gemifloxacin is the responsible moiety for its new unique activity as compared to the reported fluoroquinolones.

## 2. DESCRIPTION [6]

### 2.1. Nomenclature

#### 2.1.1. CAS name

7-[3-(Aminomethyl)-4-(methoxyimino)-1-pyrrolidinyl]-1-cyclopropyl-6-fluoro-1,4-dihydro-4-oxo-1,8-naphthyridine-3-carboxylic acid

#### 2.1.2. IUPAC name

7-[(4Z)-3-(Aminomethyl)-4-methoxyimino-pyrrolidin-1-yl]-1-cyclopropyl-6-fluoro-4-oxo-1,8-naphthyridine-3-carboxylic acid

### 2.1.3. Proprietary names

Factive® (tablets were formulated by Oscient Pharmaceuticals, USA)

### 2.1.4. Nonproprietary names

Gemifloxacin

LB20304

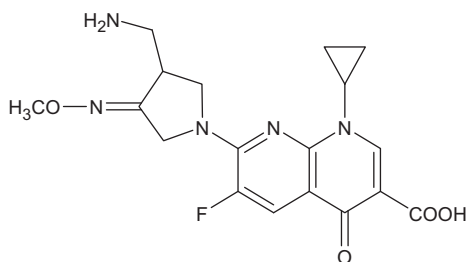
SB-265805

## 2.2. Formulae

### 2.2.1. Empirical

Gemifloxacin	$C_{18}H_{20}FN_5O_4$
Gemifloxacin mesylate	$C_{18}H_{20}FN_5O_4 \cdot CH_4O_3S$

### 2.2.2. Structural



### 2.2.3. CAS Registry Number

175463-14-6 is the CAS Registry Number of gemifloxacin

## 2.3. Molecular weight

Gemifloxacin has molecular weight of 389.38, whereas gemifloxacin mesylate has molecular weight of 485.49.

## 2.4. Elemental composition for gemifloxacin

C: 55.52%

H: 5.18%

F: 4.88%

N: 17.99%

O: 16.44%

## 2.5. Appearance, color, and odor

Gemifloxacin is off-white, amorphous solid from chloroform–ethanol. It has only a slight characteristic odor. However, the mesylate salt is a white to light brown solid.

## 3. PHYSICAL CHARACTERISTICS

### 3.1. Melting behavior

The melting point range of gemifloxacin mesylate is 235–237 °C.

### 3.2. Solubility

Gemifloxacin mesylate is freely soluble in water at neutral, pH 7.0. Its water solubility has been reported (<http://www.rxlist.com/factive-drug.htm>) as 350 mg/ml at 25 °C. It is soluble in methanol, 0.1 N hydrochloric acid and 0.1 N sodium hydroxide solutions.

### 3.3. Hydrophobicity

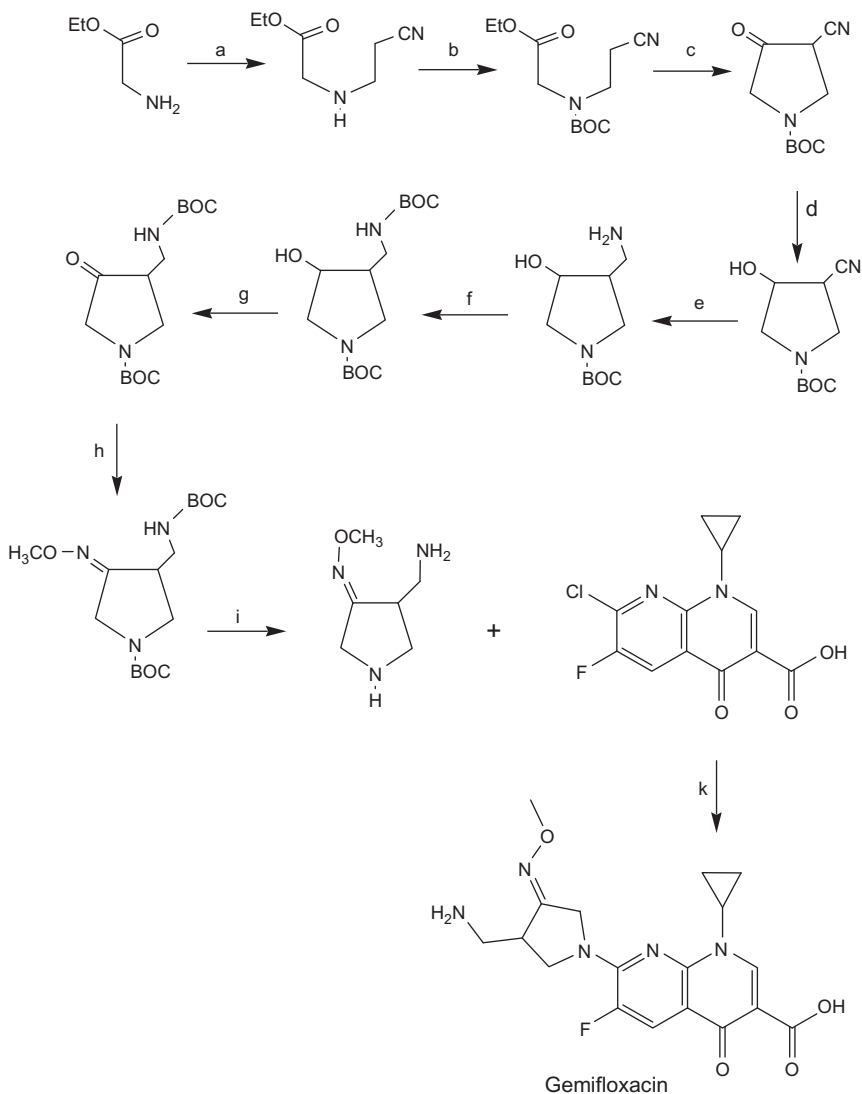
The Experimental Log P/Hydrophobicity of gemifloxacin mesylate is 2.3.

## 4. SYNTHESIS [2]

The design and synthesis of the new oxime-functionalized pyrrolidine derivative of gemifloxacin, which bear an alkyloxime substituent in the 4-position and an aminomethyl substituent in the 3-position of the pyrrolidine ring, was first described in [Scheme 4.1](#) starting from step (a) to step (i) in the scheme. Then, the new pyrrolidine derivative moiety was coupled with a certain quinoline carboxylic acid derivative (7-chloro (or fluoro)-1-cyclopropyl-6-fluoro-1,4-dihydro-4-oxo-1,8-naphthyridine-3-carboxylic acid) to form the new fluoroquinolone drug, gemifloxacin as described in [Scheme 4.1](#).

## 5. MECHANISM OF ACTION AND USES

Gemifloxacin is a third generation, oral broad-spectrum, fluorinated quinolone antibacterial agent. It acts by inhibiting DNA synthesis through the inhibition of both DNA gyrase and topoisomerase IV (TOPO IV), which are essential for cellular replication and bacterial growth [7]. It is



**SCHEME 4.1** Synthetic pathway for synthesis of gemifloxacin. (a)  $\text{CH}=\text{CH}-\text{CN}$ , NaOH, 60 °C; (b) (t-BOC)<sub>2</sub>O, CHCl<sub>3</sub>; (c) NaOEt, EtOH, reflux; (d) NaBH<sub>4</sub>, EtOH, 0 °C; (e) LiAlH<sub>4</sub>, THF, -5 °C; (f) (t-BOC)<sub>2</sub>O (dioxane-water), NaHCO<sub>3</sub>, pH 8.5; (g) (SO<sub>3</sub>-pyridine), DMSO, Et<sub>3</sub>N, 5 °C; (h) MeO-NH<sub>2</sub>·HCl, NaHCO<sub>3</sub>, EtOH-THF, 40 °C; (i) CH<sub>3</sub>-CO-Cl, MeOH, 0 °C; (k) 1,8-diazabicyclo[5.4.0]undec-7-ene (DBU) at 0 °C, stirring 30 min at 25 °C, CH<sub>3</sub>CN.



well known that *Streptococcus pneumoniae* has been showed mutations in both DNA gyrase and TOPO IV (double mutants), and they are resistant to most fluoroquinolones [8]. Thus, gemifloxacin is considered the only fluoroquinolone which has the ability to inhibit both enzyme systems (dual targeting of both DNA Gyrase and TOPO IV) at therapeutically relevant drug levels in *S. pneumoniae* [7–9]. Further, it has a minimum inhibitory concentration values that are still in the susceptible range for some of these double mutants. The main advantage of gemifloxacin over the older agents of fluoroquinolones is retaining the excellent activity against Gram-negative bacilli and improving Gram-positive activity (including *S. pneumoniae* and *Staphylococcus aureus*) [9,10]. Therefore, gemifloxacin was approved by the Food and Drug Administration (FDA) in April 2003 for treatment of acute bacterial exacerbation of chronic bronchitis, mild-to-moderate pneumonia, and multidrug resistant *S. pneumoniae* as well as community-acquired pneumonia [9,11,12].

## 6. SPECTROSCOPY

### 6.1. UV–VIS spectroscopy

The ultraviolet absorption spectra of gemifloxacin mesylate were recorded on A Shimadzu UV-1601 PC double beam spectrophotometer with matched 1-cm quartz cells in water, methanol, 0.1 N hydrochloric acid, and 0.1 N sodium hydroxide solutions. Figure 4.1 shows the recorded absorption spectra of these solutions. The recorded spectra were essentially identical and exhibiting two peak maxima for each spectrum at 266 and 340, 272 and 342, 272 and 344, and 262 and 342 nm for the solutions in water, methanol, 0.1 N hydrochloric acid and 0.1 N sodium hydroxide, respectively. The molar absorptivity of gemifloxacin mesylate was found to be moderately affected by the solvent used. The calculated molar absorptivity in water, methanol, 0.1 N hydrochloric acid, and 0.1 N sodium hydroxide solutions at the two maxima was tabulated in Table 4.1. However, the position of the maxima, as compared to water, was slightly red shifted for methanol and 0.1 N hydrochloric acid solutions and slightly blue shifted for 0.1 N sodium hydroxide solution.

### 6.2. Fluorescence spectroscopy

Gemifloxacin mesylate was found to be very strongly fluorescent when dissolved in water and moderately fluorescent in 0.1 N hydrochloric acid and 0.1 N sodium hydroxide (the fluorescence intensity of gemifloxacin mesylate in 0.1 N HCl was about twofolds more than that of 0.1 N NaOH).

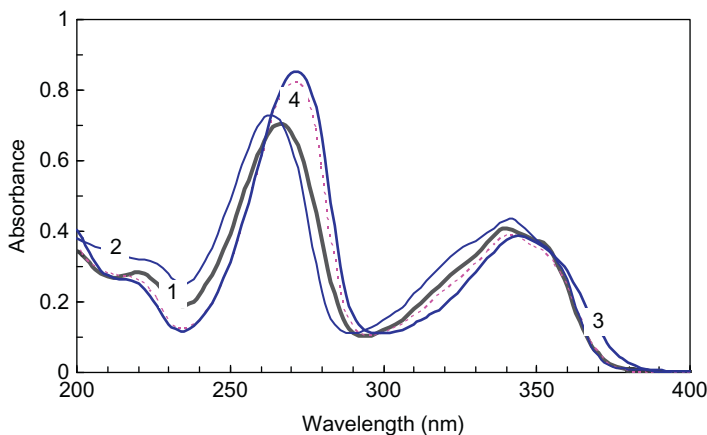


**FIGURE 4.1** The ultraviolet absorption spectra of 10 ppm gemifloxacin mesylate in water (1), 0.1 N sodium hydroxide (2), 0.1 N hydrochloric acid (3), and methanol (4) solutions.

**TABLE 4.1** The calculated molar absorptivity of gemifloxacin in different solvents

Molar absorptivity ( $\epsilon$ )	Water	Methanol	0.1 N HCl	0.1 N NaOH
( $\epsilon$ ) at 266–272 nm	36,902	40,975	43,230	38,356
( $\epsilon$ ) at 340–344 nm	19,219	19,545	19,409	23,078

Spectrofluorimeter, Kontron SFM 25 equipped with a 150-W xenon high-pressure lamp was used for recording the fluorescence spectrum of gemifloxacin mesylate in water. As shown in Fig. 4.2, the fluorescence spectrum exhibited two excitation maxima at 266 and 342 nm and one emission maximum at 391 nm. The fluorescence intensity obtained at  $\lambda_{\text{ex}}$  266 nm was found to be more (5–25% depending on the solvent used) than that obtained at  $\lambda_{\text{ex}}$  342 nm. Moreover, the position of the emission maximum was red shifted in 0.1 N HCl solution (405 nm) and blue shifted in 0.1 N NaOH solution (390 nm).

### 6.3. IR spectroscopy

The infrared absorption spectrum of gemifloxacin mesylate was recorded on FT-IR model Spectrum BX spectrophotometer (Perkin-Elmer, USA) using a KBr disc (~2 mg of gemifloxacin mesylate was dispersed in 200 mg KBr). The obtained infrared spectrum is shown in Fig. 4.3, and the assignments of the characteristic bands are tabulated in Table 4.2.

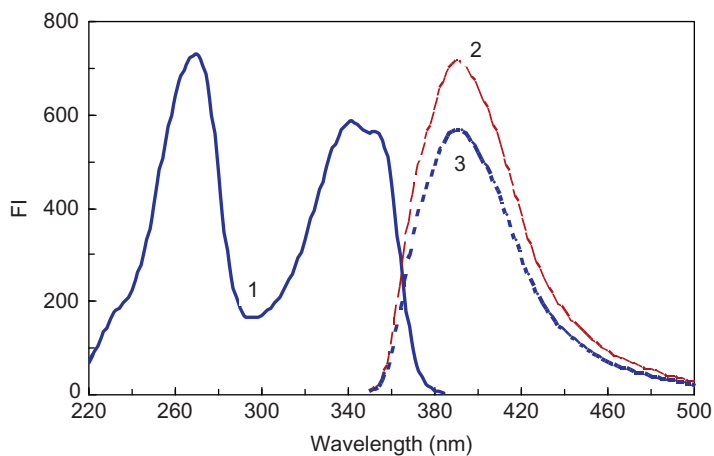


**FIGURE 4.2** The excitation (1) and emission spectra (2, 3) of aqueous solution of gemifloxacin mesylate (2 ppm). The emission spectra (2) and (3) were obtained at excitation wavelength of 266 and 342 nm, respectively.

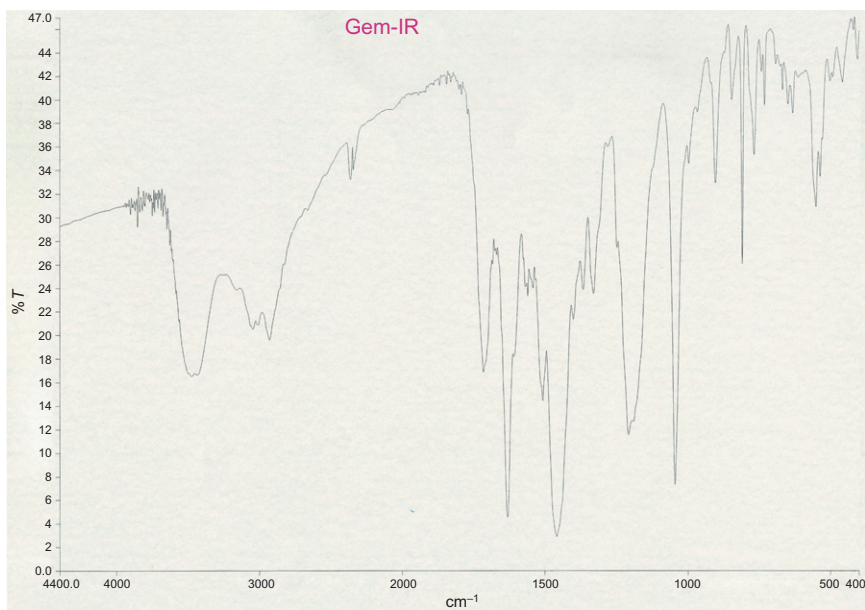


**FIGURE 4.3** Infrared absorption spectrum of gemifloxacin mesylate using KBr disc.

**TABLE 4.2** Assignments of the characteristic infrared absorption bands of gemifloxacin mesylate

Energy (cm <sup>-1</sup> )	Band assignment
3474	–NH <sub>2</sub> stretching mode and –OH hydrogen bonded
2930	–CH stretching mode
2343, 2364	
1718	Carboxylic –CO stretching mode
1631	–CO stretching mode
1458	C=C stretching mode
1300 and below	Fingerprint region

#### 6.4. <sup>1</sup>H NMR spectroscopy

The <sup>1</sup>H NMR absorption spectrum of gemifloxacin mesylate was recorded on a Bruker-Ultra Shield spectrometer (Bruker Co., USA) at 500 MHz in deuterated water. The obtained <sup>1</sup>H NMR spectrum is shown in Figs. 4.4 and 4.5, and the assignments of the observed bands are tabulated in Table 4.3. The four protons of the hydroxyl and amino groups are disappeared in deuterated water.

#### 6.5. Mass spectrometry

The gas chromatography-mass spectrum of gemifloxacin mesylate is presented in Fig. 4.6, and the assignments for the main observed fragments are tabulated in Table 4.4.

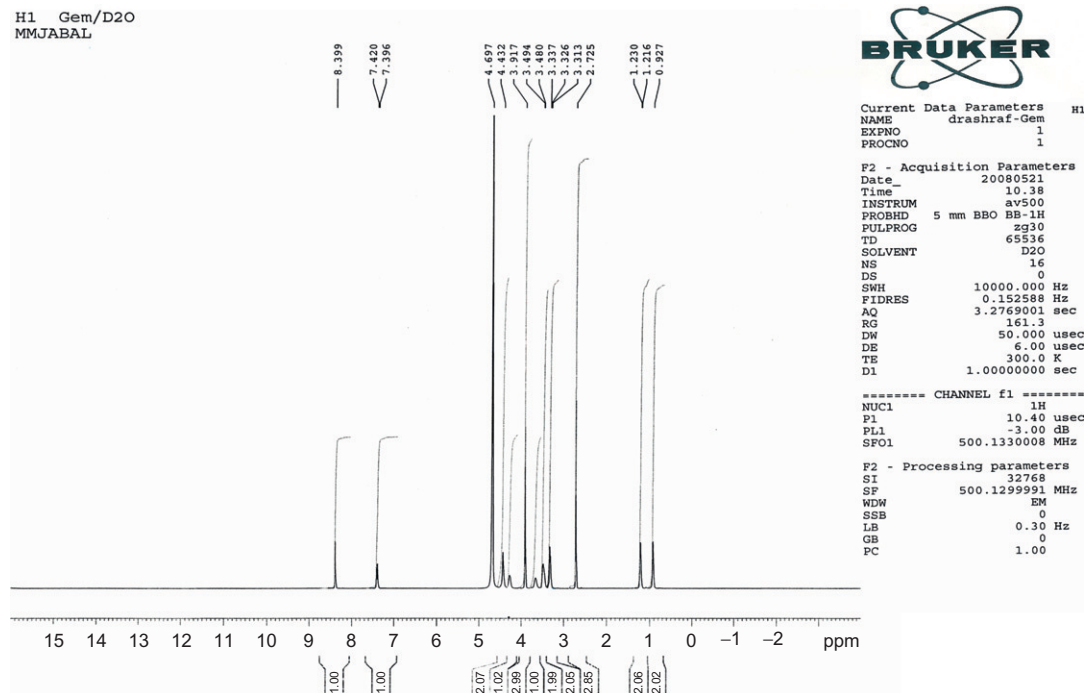
### 7. METHODS OF ANALYSIS

#### 7.1. UV-analysis

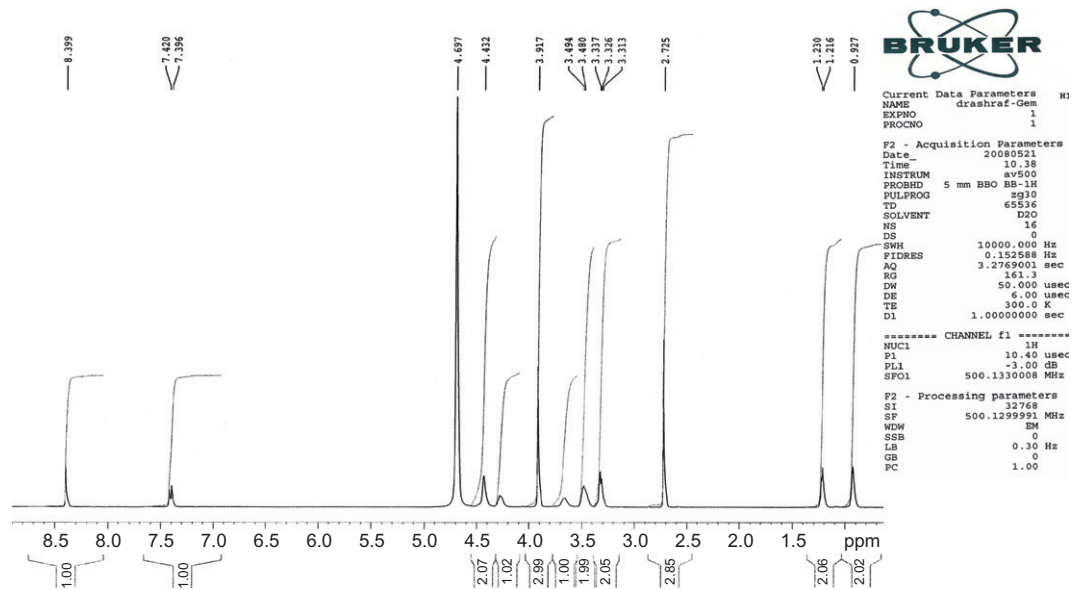
Gemifloxacin mesylate in 0.1 N sodium hydroxide solution was determined in our laboratory using UV spectrophotometry at 342 nm in bulk and its pharmaceutical preparations. Beer's law was obeyed in the concentration range 2.0–20.0 µg/ml at 342 nm, respectively.

#### 7.2. Colorimetric analysis

Gemifloxacin mesylate was oxidized with Fe (III) and determining Fe(II) produced from the oxidation process by its chelation with either 1,10-phenanthroline, 2,2'-bipyridyl, or ferricyanide at 515, 520, and 760 nm,



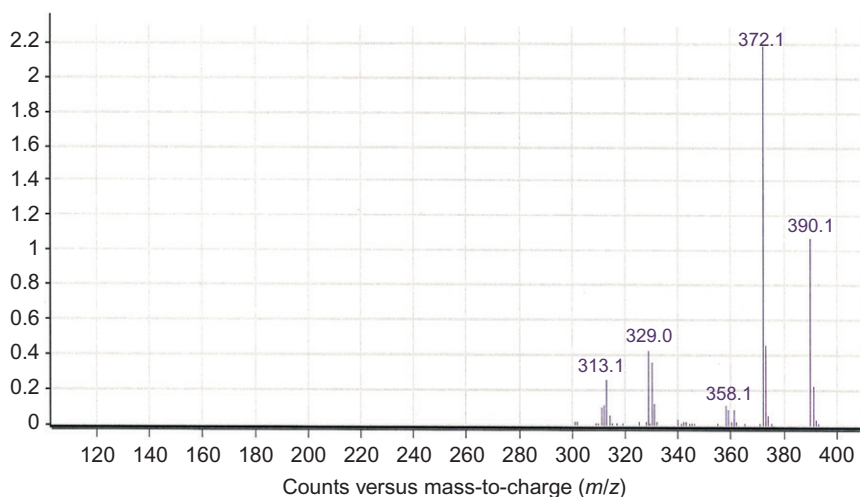
**FIGURE 4.4**  $^1\text{H}$  NMR spectrum of gemifloxacin mesylate (at 500 MHz) in deuterated water.



**FIGURE 4.5** Expanded (3.0 to 7.5 ppm)  $^1\text{H}$  NMR spectrum of gemifloxacin mesylate (at 500 MHz) in deuterated water.

**TABLE 4.3**  $^1\text{H}$  NMR spectral assignments for gemifloxacin mesylate

Chemical shift (ppm)	Multiplicity	Number of protons	Assignment
0.93	Singlet	2	Cyclopropyl-2-H
1.23	Duplet	2	Cyclopropyl-3-H
2.73	Singlet	3	Mesylate-H
3.31–3.34	Multiplet	2	3-Aminomethyl-H (–CH <sub>2</sub> )
3.48–3.49	Duplet	2	Pyrrolidinyl-2-H
3.65	Singlet	1	Cyclopropyl-1-H
3.92	Singlet	3	Methoxy-H
4.28	Multiplet	1	Pyrrolidinyl-3-H
4.43	Singlet	2	Pyrrolidinyl-5-H
7.40–7.42	Duplet	1	1,8-Naphthyridine-5-H
8.40	Singlet	1	1,8-Naphthyridine-2-H

**FIGURE 4.6** Gas chromatography-mass spectrum of gemifloxacin mesylate.

respectively [13]. Beer's law was obeyed in the concentration ranges of 3–15, 4–20, and 2–10  $\mu\text{g/ml}$ , respectively. Another method for determination of gemifloxacin mesylate was based on its interaction with ammonium heptamolybdate tetrahydrate resulting in formation of molybdenum blue of  $\lambda_{\text{max}}$  825 nm. The linear dynamic range was 6–30  $\mu\text{g/ml}$  [13].

**TABLE 4.4** Gas chromatography mass spectral data of gemifloxacin mesylate

<i>m/z</i> ratio	Relative intensity (%)	Fragment assignment
390.1	49	[M <sup>+</sup> ]
372.1	100	[M – 18] <sup>+</sup>
358.1	5.5	[M – 32] <sup>+</sup>
329	19	[M – 61] <sup>+</sup>
313.1	13.6	[M – 77] <sup>+</sup>

### 7.3. Fluorimetric analysis

The direct native fluorescence of propanolic gemifloxacin mesylate solution was used for its assay in the range of 0.05–3 µg/ml in our laboratory. Gemifloxacin mesylate was also determined depending on its ability to form ternary complex with Lanthanide, europium (III) ion in presence of Tris buffer, pH 11–12 [14]. Europium (III) ion enhanced the fluorescence in presence of 0.1 M EDTA, and quenched it in presence of 1% Tween 60. The enhancement and quenching of the fluorescence by europium (III) ion were applicable over the concentration range of 0.1–0.5 and 0.2–0.8 µg/ml of gemifloxacin mesylate, respectively.

### 7.4. HPLC analysis

High-performance liquid chromatography-tandem mass spectrometry method for the determination of gemifloxacin in human plasma was based on the protein precipitation of plasma samples with acetonitrile containing [<sup>13</sup>C<sup>2</sup>H<sub>3</sub>] gemifloxacin as an internal standard. The supernatant was injected onto a PLRP-S column without any further clean-up. The mass spectrometer was operated in positive ion mode, and the ions were detected in multiple reaction-monitoring (MRM) mode. The assay requires 50 µl of plasma and is precise and accurate within the range 10–5000 ng/ml [15].

The enantiomers of gemifloxacin mesylate were well enantioseparated on a Crownpak CR(+) chiral stationary phase (CSP). This enantioseparation was the first reported direct separation of the quinolones enantiomers on chiral crown ether coated Crownpak CR CSP [16]. Another more effective CSP derived from (+)-(18-crown-6)-2,3,11,12-tetracarboxylic acid was also used for the resolution of racemic gemifloxacin mesylate. The only difference from the previous one was the analytical time [17]. More recently, CSP recently developed by bonding (diphenyl-substituted 1,1'-binaphthyl) crown ether to silica gel was applied to the liquid chromatographic separation of gemifloxacin enantiomers [18]. The resolution of gemifloxacin and its analogs was excellent and even greater than that on the commercial



Crownpak CR(+). Chiral separation of gemifloxacin was performed in analytical counter-current chromatography using (+)-(18-crown-6)-tetracarboxylic acid as CSP. A successful separation of gemifloxacin enantiomers could be achieved using a two-phase solvent system composed of 1-butanol-ethyl-acetate-bis(2-hydroxyethyl)amino tris (hydroxymethyl)methane acetate buffer with a small amount of  $^{18}\text{C}_6\text{H}_4$  [19].

## 7.5. Capillary electrophoresis

Capillary electrophoresis for the analysis of gemifloxacin enantiomers and its analogs using (+)-18-crown-6-tetracarboxylic acid ( $^{18}\text{C}_6\text{H}_4$ ) as a chiral selector was performed on urine samples [18]. The presence of alkaline metal ions ( $\text{Na}^+$  or  $\text{K}^+$  ions) in the sample solution as well as in the run buffer is undesirable due to their strong competitive binding with the chiral selector. The method designed a channel-coupled microchip electrophoresis device to clean up alkaline metal ions from the samples matrix for the chiral analysis of gemifloxacin [20]. In the first channel, the metal ions in the sample were monitored by indirect detection using quinine as a chromophore and drained to the waste. In the second separation channel, gemifloxacin enantiomers, free of the alkaline metal ions, were successfully separated using only a small amount of the chiral selector ( $50\text{ }\mu\text{M}$   $^{18}\text{C}_6\text{H}_4$ ). Another capillary electrophoretic method used a chelating agent, ethylenediaminetetraacetic acid (EDTA), to the run buffer to greatly improve the separation efficiencies and peak shapes in the chiral analysis of gemifloxacin in a saline sample matrix [21]. Capillary electrophoretic method has been also developed for the assay of gemifloxacin in tablets. The method was performed on a  $75\text{ }\mu\text{m} \times 35\text{ cm}$  fused silica capillary using  $25\text{ mM H}_3\text{PO}_4\text{--NaOH}$  running buffer (pH 8.5) at temperature of  $25\text{ }^\circ\text{C}$  and applied voltage of  $12\text{ kV}$ . The detection wavelength was  $254\text{ nm}$  and the internal standard was Flumequine. The calibration was linear from  $5$  to  $50\text{ }\mu\text{g/ml}$  for gemifloxacin mesylate [22].

## 8. CLINICAL PHARMACOKINETICS AND TOXICITY

### 8.1. Pharmacokinetics

The pharmacokinetic properties of fluoroquinolone antibacterial agents have been well described [23]. Gemifloxacin is rapidly absorbed with a time to maximum plasma concentration ( $T_{\text{max}}$ ) of  $0.5\text{--}2\text{ h}$  in healthy subjects and displays linear pharmacokinetics over the dose range studied ( $20\text{--}800\text{ mg}$ ), with an apparent plasma terminal half-life ( $t_{1/2}$ ) after single or repeated administration of about  $8\text{ h}$ . A minimum of  $20\text{--}30\%$  of the oral dose is excreted unchanged in the urine. Following repeat oral

administration of 320 mg gemifloxacin once daily, steady-state is achieved by the third day of dosing. Plasma protein binding of gemifloxacin is low as 70% [24–28].

### 8.1.1. Absorption and bioavailability

Gemifloxacin, given as an oral tablet, was rapidly absorbed from the gastro-intestinal tract. Peak plasma concentrations of gemifloxacin were observed between 0.5 and 2 h following oral tablet administration. The absolute bioavailability of 320 mg tablet was approximately 71%. Following repeat oral doses of 320 mg to healthy subjects, the mean maximal gemifloxacin plasma concentrations ( $C_{\max}$ ) and systemic drug exposure ( $AUC_{0-24}$ ) were  $1.61 \pm 0.51 \mu\text{g/ml}$  (range 0.70–2.62  $\mu\text{g/ml}$ ) and  $9.93 \pm 3.07 \mu\text{g h/ml}$  (range 4.71–20.1  $\mu\text{g h/ml}$ ), respectively.

The pharmacokinetics of gemifloxacin was not significantly altered when a 320 mg dose was administered with a high-fat meal. Therefore, the drug may be administered without regard to meals.

### 8.1.2. Distribution

*In vitro* binding of gemifloxacin to plasma proteins in healthy subjects was approximately 60–70% and is concentration independent. After repeated oral doses, the *in vivo* plasma protein binding in healthy elderly and young subjects ranged from 55% to 73% and was unaffected by age. Renal impairment did not significantly affect the protein binding of gemifloxacin. The blood-to-plasma concentration ratio of gemifloxacin was 1.2:1. The geometric mean for  $V_{\text{dss}}/F$  is 4.18 l/kg (range, 1.66–12.12 l/kg).

Gemifloxacin was widely distributed throughout the body after oral administration. Concentrations of gemifloxacin in bronchoalveolar lavage fluid exceeded those in plasma. Gemifloxacin penetrated well into lung tissue and fluids. After five daily doses of 320 mg gemifloxacin, the found concentrations in plasma, bronchoalveolar macrophages, epithelial lining fluid, and bronchial mucosa at ~2 h were tabulated in Table 4.5.

### 8.1.3. Metabolism

Gemifloxacin was metabolized to a limited extent by the liver. The unchanged compound was the predominant drug-related component detected in plasma (~65%) up to 4 h after dosing. All formed metabolites were minor and represents <10% of the administered oral dose; the main metabolites were *N*-acetyl gemifloxacin (the *E*-isomer of gemifloxacin) and the carbamyl glucuronide of gemifloxacin. Cytochrome P450 enzymes did not play an important role in gemifloxacin metabolism, and the metabolic activity of these enzymes was not significantly inhibited by gemifloxacin.

**TABLE 4.5** Gemifloxacin concentrations in plasma and tissues (320 mg oral dosing)

Tissue	Concentration (mean $\pm$ SD)	Ratio compared with plasma (mean $\pm$ SD)
Plasma	1.40 (0.442) $\mu\text{g/ml}$	–
Bronchoalveolar macrophages	107 (77) $\mu\text{g/g}$	90.5 (106.3)
Epithelial lining fluid	2.69 (1.96) $\mu\text{g/ml}$	1.99 (1.32)
Bronchial mucosa	9.52 (5.15) $\mu\text{g/g}$	7.21 (4.03)

#### 8.1.4. Excretion

Gemifloxacin and its metabolites were excreted via dual routes of excretion. Following oral administration of gemifloxacin to healthy subjects, a mean ( $\pm$ SD) of  $61 \pm 9.5\%$  of the dose was excreted in the feces and  $36 \pm 9.3\%$  in the urine as unchanged drug and metabolites. The mean ( $\pm$ SD) renal clearance following repeat doses of 320 mg was approximately  $11.6 \pm 3.9$  l/h (range 4.6–17.6 l/h), which indicates that the active secretion is involved in the renal excretion of gemifloxacin. The mean ( $\pm$ SD) plasma elimination half-life at steady state following 320 mg to healthy subjects was  $\sim 7 \pm 2$  h (range 4–12 h).

## 8.2. Toxicity and side effects

A study on 40 healthy male and female volunteers receiving repeated dosing for 7 days with 160 or 320 mg of gemifloxacin (o.d., p.m) demonstrated that the drug has a low potential to cause mild photosensitivity [29].

The cardiac electrophysiological effect of gemifloxacin was investigated, by using conventional microelectrode recording techniques. The data obtained suggested that in the electrophysiological aspect, gemifloxacin had no significant effects at concentrations up to 30  $\mu\text{M}$  (which is 25-fold more than the free plasma concentration after a single therapeutic injection in humans) [30].

The majority of gemifloxacin adverse reactions experienced by patients in clinical trials were considered to be of mild to moderate severity, primarily due to rash (0.8% of patients), nausea (0.3%), diarrhea (0.3%), urticaria (0.2%), and vomiting (0.2%). Most of the postmarketing adverse events reported were cutaneous and most of these were rash. Some of these cutaneous adverse events were considered serious. The majority of rashes occurred in women and in patients under 40 years of age.

### 8.3. Overdosage and contraindications

Any signs or symptoms of overdosage should be treated symptomatically. No specific antidote is known. In the event of acute oral overdosage, the stomach should be emptied by inducing vomiting or by gastric lavage; the patient should be carefully observed and treated symptomatically with appropriate hydration maintained. Hemodialysis removes approximately 20–30% of an oral dose of gemifloxacin from plasma. Mortality occurred at oral gemifloxacin doses of 1600 mg/kg in rats and 320 mg/kg in mice. The minimum lethal intravenous doses in these species were 160 and 80 mg/kg, respectively. Toxic signs after administration of a single high oral dose (400 mg/kg) of gemifloxacin to rodents included ataxia, lethargy, piloerection, tremor, and clonic convulsions. The drug is contraindicated in patients with a history of hypersensitivity to gemifloxacin or any of the product components.

### 8.4. Drug interactions

Administration of repeat doses of gemifloxacin had no effect on the repeat dose pharmacokinetics of theophylline, digoxin, or an ethinylestradiol/levonorgestrol oral contraceptive product in healthy subjects. Concomitant administration of gemifloxacin and calcium carbonate, cimetidine, omeprazole, or an estrogen/progesterone oral contraceptive produced minor changes in the pharmacokinetics of gemifloxacin, which were considered to be without clinical significance. Concomitant administration of gemifloxacin with probenecid resulted in a 45% increase in systemic exposure to gemifloxacin. Gemifloxacin had no significant effect on the anticoagulant effect of warfarin in healthy subjects on stable warfarin therapy.

Quinolones form chelates with alkaline earth and transition metals. The absorption of oral gemifloxacin is significantly reduced by the concomitant administration of an antacid containing aluminum and magnesium. Magnesium- and/or aluminum-containing antacids, products containing ferrous sulfate (iron), multivitamin preparations containing zinc or other metal cations, or Videx<sup>®</sup> (didanosine) chewable/buffered tablets or the pediatric powder for oral solution should not be taken within 3 h before or 2 h after gemifloxacin mesylate tablets (Factive<sup>®</sup>).

## ACKNOWLEDGMENT

The authors are grateful to Dr. Abdullah A. Al-Badr, Professor of medicinal Chemistry, Department of Pharmaceutical Chemistry, College of Pharmacy, King Saud University, Riyadh, Kingdom of Saudi Arabia for his help and encouragement.

## REFERENCES

- [1] C.Y. Hong, Y.K. Kim, J.H. Chang, S.H. Kim, H. Choi, D.H. Nam, et al., *J. Med. Chem.* 40 (1997) 3584–3593.
- [2] M.G. Cormican, R.N. Jones, *Antimicrob. Agents Chemother.* 41 (1997) 204.
- [3] T.A. Davies, L.M. Kelly, D.B. Hoellman, L.M. Ednie, C.L. Clark, S. Bajaksouzian, et al., *Antimicrob. Agents Chemother.* 44 (2000) 633.
- [4] T.A. Davies, L.M. Kelly, G.A. Pankuch, K.L. Credito, M.R. Jacobs, P.C. Appelbaum, *Antimicrob. Agents Chemother.* 44 (2000) 304.
- [5] A.F. Hohl, R. Frei, V. Punter, A. Graevenitz, C. Knapp, J. Washington, et al., *Clin. Microbiol. Infect.* 4 (1998) 280.
- [6] The Merck Index, 13th ed., Merck Co. Inc., Whitehouse Station, NJ, USA, 2001 779.
- [7] T.P. Le, Y.Q. Xiong, *Drugs Today (Barc).* 37 (2001) 401–410.
- [8] G.G. Zhanel, S. Fontaine, H. Adam, K. Schurek, M. Mayer, A.M. Noreddin, et al., *Treat. Respir. Med.* 5 (2006) 437–465.
- [9] S.M. Bhavnani, D.R. Andes, *Pharmacotherapy* 25 (2005) 717–740.
- [10] B.K. Yoo, D.M. Triller, C.S. Yong, T.P. Lodise, *Ann. Pharmacother.* 38 (2004) 1226–1235.
- [11] J.M. Blondeau, B. Missaghi, *Expert Opin. Pharmacother.* 5 (2004) 1117–1152.
- [12] I. Morrissey, S. Clark, I. Mathias, *J. Med. Microbiol.* 49 (2000) 841–844.
- [13] M.V. Krishna, D.G. Sankar, *Pharma. Rev.* 6 (2007) 148–150.
- [14] N.F. Youssef, L.I. Bebaawy, *Bull. Fac. Pharm. (Cairo University)* 44 (2006) 215–227.
- [15] E. Doyle, S.E. Fowles, D.F. McDonnell, R. McCarthy, White SA, J. *Chromatogr. B Biomed. Sci. Appl.* 746 (2000) 191–198.
- [16] W. Lee, C.Y. Hong, *J. Chromatogr. A* 879 (2000) 113–120.
- [17] M.H. Hyun, S.C. Han, Y.J. Cho, J.S. Jin, W. Lee, *Biomed. Chromatogr.* 16 (2002) 356–360.
- [18] M.H. Hyun, S.C. Han, *J. Biochem. Biophys. Methods* 54 (2002) 235–243.
- [19] E. Kim, Y.M. Koob, D.S. Chung, *J. Chromatogr. A* 1045 (2004) 119–124.
- [20] S.I. Cho, J. Shim, M.S. Kim, Y.K. Kim, D.S. Chung, *J. Chromatogr. A* 1055 (2004) 241–245.
- [21] S.I. Cho, K.N. Lee, Y.K. Kim, J. Jang, D.S. Chung, *Electrophoresis* 23 (2002) 972–977.
- [22] A.A. Elbashir, B. Saad, A. Ali, M. Salhin, K.M.M. Al-Azzam, H.Y. Aboul-Enein, *J. Liq. Chrom. Relat. Tech.* 31 (2008) 1465–1477.
- [23] R.C. Owens Jr., P.G. Ambrose, *Med. Clin. North Am.* 84 (2000).
- [24] A. Allen, E. Bygate, M. Teillol-Foo, S.D. Oliver, M.R. Johnson, C. Ward, *J. Antimicrob. Chemother.* 44 (Suppl. A) (1999) 137.
- [25] A. Allen, E. Bygate, M. Teillol-Foo, S.D. Oliver, M.R. Johnson, C. Ward, *J. Antimicrob. Chemother.* 44 (Suppl. A) (1999) 133.
- [26] A. Allen, E. Bygate, S.D. Oliver, M.R. Johnson, C. Ward, A.J. Cheon, et al., *Antimicrob. Agents Chemother.* 44 (2000) 1604–1608.
- [27] F. Islinger, R. Bouw, M. Stahl, E. Lackner, P. Zeleny, M. Brunner, et al., *Antimicrob. Agents Chemother.* 48 (2004) 4246–4249.
- [28] T. Gee, J.M. Andrews, J.P. Ashby, G. Marshall, R. Wise, *J. Antimicrob. Chemother.* 47 (2001) 431–434.
- [29] M. Vousden, J. Ferguson, J. Richards, N. Bird, A. Allen, *Chemotherapy* 45 (1999) 512–520.
- [30] D. Seop Kim, K.S. Kim, K. Hwan Choi, H. Na, J.I. Kim, W.H. Shin, et al., *Drug Chem. Toxicol.* 29 (2005) 303–312.

# CHAPTER 5

## Glimepiride

**Maria L.A.D. Lestari** and **Gunawan Indrayanto**

---

<b>Contents</b>		
	1. Introduction	170
	1.1. Chemical name	170
	1.2. Molecular formula and molecular weight	170
	1.3. Solubility characteristics, partition coefficient and $pK_a$ value	170
	1.4. Melting point	170
	1.5. Polymorphism	171
	1.6. Known impurities	171
	1.7. Degradation products of glimepiride	172
	2. Compendial Method of Analysis	174
	2.1. Identification	174
	2.2. Impurity analysis	175
	2.3. Assay	177
	2.3.1. Bulk drug substance	177
	2.3.2. Pharmaceutical dosage form	178
	3. Method of Analysis	179
	3.1. Spectroscopic method of analysis	179
	3.1.1. Ultraviolet absorption spectroscopy	179
	3.1.2. Infrared absorption spectroscopy	181
	3.2. Chromatographic method	181
	3.2.1. Thin layer chromatography	181
	3.2.3. High performance liquid chromatography	182
	3.3. X-ray crystallography	187
	3.4. Thermal method of analysis	188
	4. Determination of Glimepiride in Biological Sample	188
	References	203

Faculty of Pharmacy, Airlangga University, Dharmawangsa Dalam, Surabaya, Indonesia

---

Profiles of Drug Substances, Excipients, and Related Methodology, Volume 36  
ISSN 1871-5125, DOI: 10.1016/B978-0-12-387667-6.00005-1

© 2011 Elsevier Inc.  
All rights reserved.

## 1. INTRODUCTION

Glimepiride is an oral antidiabetic drug which belongs to the sulfonylurea group and usually given as an oral antidiabetic therapy for patients with type 2 diabetes mellitus. Glimepiride acts to lower blood glucose by stimulating the release of insulin from pancreatic  $\beta$ -cells [1,2].

### 1.1. Chemical name

Glimepiride has several chemical names as follows:

1-[[4-[2-(3-Ethyl-4-methyl-2-oxo-3-pyrroline-1-carboxamido)-ethyl]phenyl]sulfonyl]-3-*trans*-(4-methylcyclohexyl)urea [3,4] or  
1-({*p*-[2-(3-Ethyl-4-methyl-2-oxo-3-pyrroline-1-carboxamido)-ethyl]phenyl}sulfonyl)-3-*trans*-(4-methylcyclohexyl)urea [1,5] or  
3-Ethyl-2,5-dihydro-4-methyl-N-[2-[4-[[[*trans*-4-methylcyclohexyl]-amino]carbonyl]-amino]sulfonyl]phenyl]ethyl]-2-oxo-1H-pyrrole-1-carboxamide [4,6], or  
1H-Pyrrole-1-carboxamide,3-ethyl-2,5-dihydro-4-methyl-N-[2-[4-[[[(4-methylcyclohexyl)-amino]carbonyl]amino]sulfonyl]phenyl]ethyl]-2-oxo,*trans*- [5]

Glimepiride also has another name as N-[4-[2-(3-ethyl-4-methyl-2-oxo-3-pyrroline-1-carboxamido)-ethyl]-benzenesulfonyl]-N'-4-methylcyclohexylurea [4].

### 1.2. Molecular formula and molecular weight

The molecular formula of glimepiride is  $C_{24}H_{34}N_4O_5S$  and the substance is characterized by a molecular weight of 490.6 [1,4,6]

### 1.3. Solubility characteristics, partition coefficient and $pK_a$ value

British Pharmacopoeia 2009 and European Pharmacopoeia 6.0 [3,7] specify that glimepiride is insoluble in water but it is soluble in dimethylformamide, slightly soluble in methylene chloride and very slightly soluble in methanol. Further, its log partition coefficient in octanol–water is 3.81, with log distribution coefficient in octanol–phosphate buffer pH 7.4 valued for 2.38 [8]. The  $pK_a$  value of glimepiride was found to be  $6.2 \pm 0.1$  at  $37^\circ\text{C}$  [2].

### 1.4. Melting point

Glimepiride has been reported to have melting point at  $207^\circ\text{C}$  [2,4,6].

## 1.5. Polymorphism

Glimepiride is polymorphic and known to have two forms of polymorphs, form I and form II [9,10]. The form I is more stable compared to form II, and it is useful in the treatment of diabetes mellitus [11].

## 1.6. Known impurities

British Pharmacopoeia (BP) as well as European Pharmacopoeia (EP) [3,7] specifies three impurities of glimepiride which are impurity A, impurity B, and impurity D. According to these compendia, impurity A has systematic name as 1-[[4-[2-[(3-ethyl-4-methyl-2-oxo-2,3-dihydro-1H-pyrrol-1-yl)carbonyl]amino]ethyl]phenyl]-sulfonyl]-3-(*cis*-4-methylcyclohexyl)urea, while impurity B has systematic name as 3-ethyl-4-methyl-2-oxo-*N*-[2-(4-sulphamoylphenyl)ethyl]-2,3-dihydro-1H-pyrrole-1-carboxamide. As reported by Bansal *et al.* [12], this impurity was also found as glimepiride degradation product II. Further, impurity D has systematic name as 1-[[3-[2-[(3-ethyl-4-methyl-2-oxo-2,3-dihydro-1H-pyrrol-1-yl)carbonyl]amino]ethyl]phenyl]sulfonyl]-3-(*trans*-4-methylcyclohexyl)urea. Besides those three impurities A, B, and D, the BP and EP also suggest other seven impurities, C, E, F, G, H, I, and J. These impurities are used as control of impurities in substance of pharmaceutical use. However, those seven impurities are not mandatory to be determined, unlike those three others impurity (A, B, and D). It should also be noted that according to the results reported by Bansal *et al.* [12], product III of glimepiride degradation was in correspond with impurity J, while product V of glimepiride degradation was analog to impurity C.

In contrast with the BP and EP, the USP32 NF27 [5] classifies four impurities of glimepiride, which are glimepiride related compound A or glimepiride *cis*-isomer, glimepiride related compound B or glimepiride sulfonamide, glimepiride related compound C or glimepiride-urethane, and glimepiride related compound D or glimepiride 3-isomer. In more defined manner, Khan *et al.* [13] revealed five impurities of glimepiride. Those impurities as well as systematic name for each impurity are detailed as follows:

- impurity A (glimepiride sulfonamide): [*N*-(4-[2-(3-ethyl-4-methyl-2-oxo-3-pyrroline 1-carboxamido)-ethyl]benzene sulfonamide);
- impurity B (glimepiride-*cis*-isomer): 1-[[4-[2-(3-ethyl-4-methyl-2-oxo-3-pyrroline-1-carboxamido)-ethyl]phenyl]sulfonyl]-3-*cis*-(4-methylcyclohexyl)urea;
- impurity C (glimepiride-*meta*-isomer): 1-[[3-[2-(3-ethyl-4-methyl-2-oxo-3-pyrroline-1-carboxamido)-ethyl]phenyl-sulfonyl]-3-(4-methylcyclohexyl)urea;



- impurity D (glimepiride-*ortho*-isomer): 1-[[2-[2-(3-ethyl-4-methyl-2-oxo-3-pyrroline-1-carboxamido)-ethyl]phenyl]-sulfonyl]-3-(4-methylcyclohexyl) urea;
- impurity E (glimepiride-urethane): *N*-[4-[2-(3-ethyl-4-methyl-2-oxo-3-pyrroline-1-carboxamido)-ethyl]-benzenesulfonyl]ethyl carbamate

The chemical structure of glimepiride and its impurities are detailed in Figs. 5.1 and 5.2, respectively.

### 1.7. Degradation products of glimepiride

Based on the forced degradation study of glimepiride on acidic, alkaline, neutral hydrolysis, and oxidation, Bansal and Kovaříková [12,14] have revealed five degradation products of glimepiride. In the acidic condition and alkaline condition, two and three degradation products were found, respectively. In contrast, Jones *et al.* [15] found two and four degradation products of acidic and alkaline degradation, respectively. Further, oxidizing glimepiride using H<sub>2</sub>O<sub>2</sub> either in low concentration (4%) or in high concentration (10%) was resulting in two degradation products which were in line with the degradation products obtained from acidic degradation but with higher declining concentration of glimepiride [12,14,15]. Similarly, neutral hydrolysis degradation of glimepiride using water at 85 °C for 72 h was producing degradation products as for acid hydrolysis [12]. Based on the calculation of rate constants, Kovaříková [14] found out that the degradation rate was increasing in the following manner: neutral condition < alkaline condition < acid condition < oxidative condition. The condition employed was done by dissolving glimepiride in MeOH prior to adding of 0.2 M HCl, 0.2 M NaOH, or 4% H<sub>2</sub>O<sub>2</sub> into each vial, followed by maintaining those forced degradation samples at 90 °C up to 360 min. It should also be noted that although the rate of degradation in neutral condition was the slowest, the decreasing concentration of glimepiride was considerably significant. On the contrary, Jones *et al.* [15] suggested that based on the calculation of kinetic rate, the rate of

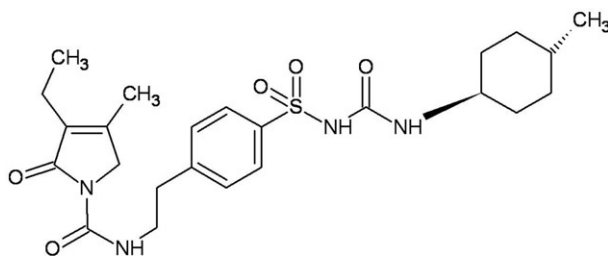


**FIGURE 5.1** Chemical structure of glimepiride.

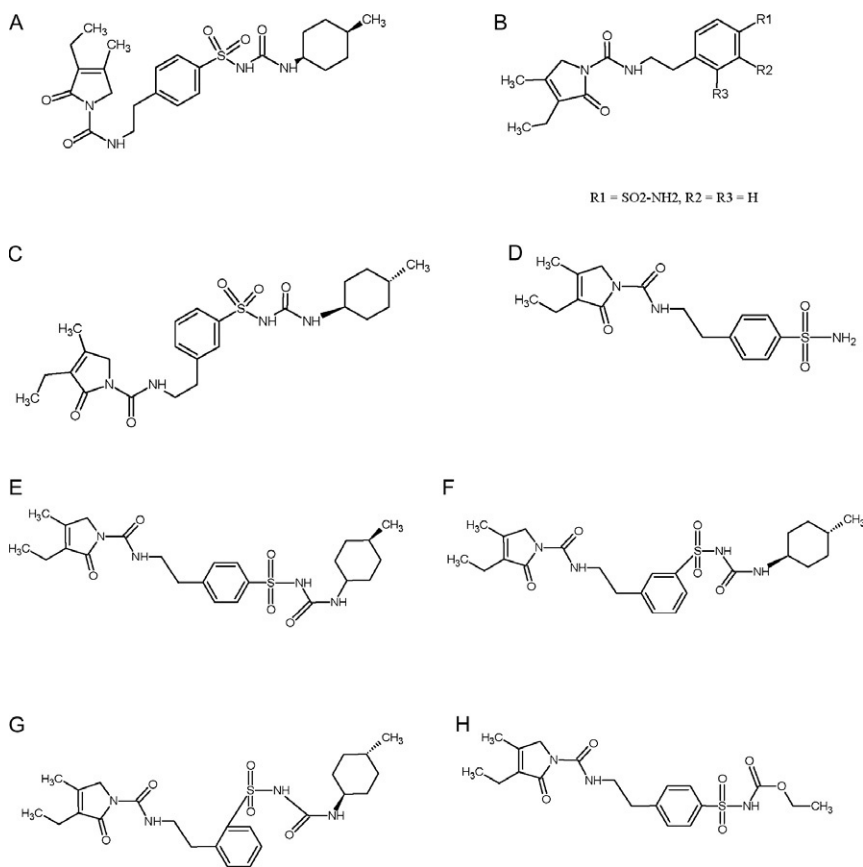


**FIGURE 5.2** Impurities of glimepiride according to BP and EP: (A) impurity A, (B) impurity B, and (C) impurity D. Impurities of glimepiride according to USP and Ref. [13]: (D) glimepiride sulfonamide, (E) glimepiride *cis*-isomer, (F) glimepiride-*meta*-isomer, (G) glimepiride-*ortho*-isomer, (H) glimepiride-urethane.

degradation was increasing in the following manner: acid < oxidative < thermal < alkaline. Maintenance condition applied was identical with Kovaříková, except that the duration of the degradation study was up to 180 min and the concentration of acid and alkaline used was 0.5 N HCl and 0.5 N NaOH, respectively.

As reported by Bansal *et al.* [12], glimepiride was stable to dry heat (50 °C for 31 days) since no decreasing of glimepiride peak area was observed. Similar result was also showing by photodegradation study. Exposure of 1.2 million lux hour fluorescent and 200 Wh/m<sup>2</sup> of UV-A

illumination at 40 °C showed no photodegradation products, indicating that glimepiride is stable to light exposure. Degradation products I–V of glimepiride were also characterized by LC–MS. Products I, III, and IV are results of alkaline hydrolysis, while products I and V are generated from acidic and neutral hydrolysis as well as oxidation. Characterization of the products disclosed that structure of product II was comparable to impurity B of BP and EP. Product III was recognized as 1-[4-(2-aminoethyl) phenyl-sulfonyl]-3-*trans*-(4-methylcyclohexyl)urea, which matched with impurity J of BP and EP. Product IV of glimepiride degradation was [[4-[2-(*N*-carbamoyl)aminoethyl]phenyl]sulfonyl]-3-*trans*-(4-methylcyclohexyl)urea. Product V was correspond to impurity C of BP and EP and recognized as methyl[4-[2-[3-ethyl-4-methyl-2-oxo-3-pyrroline-1-carbox-amido)ethyl]phenyl]sulfonyl]carbamate. It should also be noted that product I of degradation of glimepiride could not be detected, possibly due to the poor ionizability of this degradant. Moreover, maximum wavelength of UV absorption of products II–V was found at about 236 nm, which matched with maximum wavelength of glimepiride (235 nm). In contrast, product I showed  $\lambda_{\max}$  at 254 nm, suggesting that the drug cremophor was lost or altered during the conversion process of glimepiride to product I, which was not occurred on the other processes. The chemical structure of those degradation products is depicted in Fig. 5.3.

## 2. COMPENDIAL METHOD OF ANALYSIS

### 2.1. Identification

Both BP and EP [3,7] as well as USP32 NF27 [5] specify the identification method of glimepiride as bulk drug substance using infrared absorption spectrophotometry method. For the IR absorption test, BP and EP recommend that the spectra are recorded in the region of 4000–650  $\text{cm}^{-1}$  (2.5–15.4  $\mu\text{m}$ ), while USP32 NF27 recommends that the spectra are recorded in the region of 3800–650  $\text{cm}^{-1}$  (2.6–15  $\mu\text{m}$ ). The infrared absorption spectra obtained for the glimepiride drug substance sample must correspond with that of the reference standard for a successful outcome. For the sample preparation, USP32 NF27 requires that the sample is mixed intimately with potassium bromide prior to infrared spectrophotometry examination, while BP and EP do not specify a sample preparation method. Further, for the identification of glimepiride in tablets, USP32 NF27 recommends chromatographic method as for assay of glimepiride tablets. The major peak recorded in the chromatogram of sample should correspond to the major peak of the chromatogram of the standard.

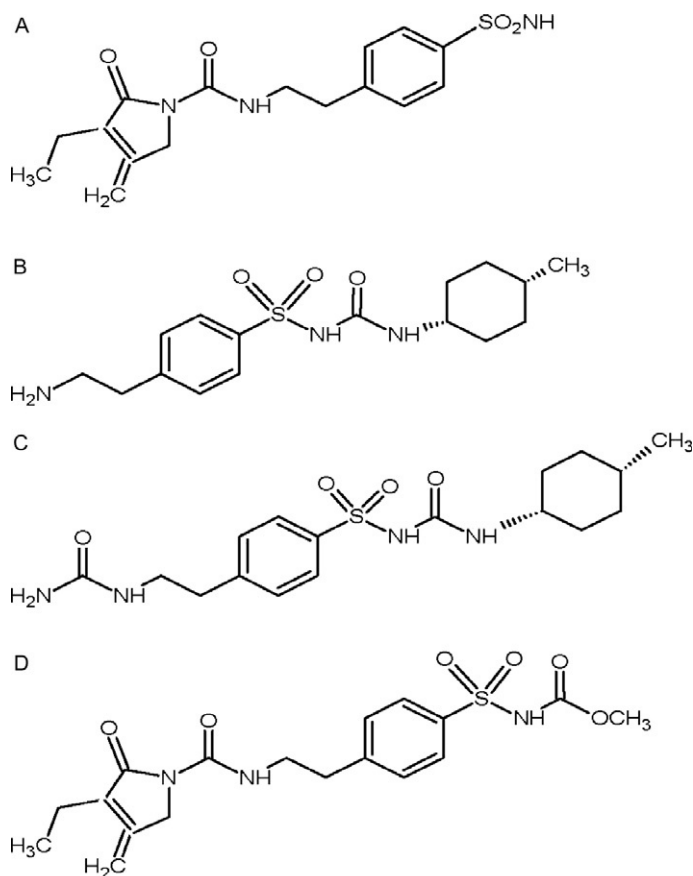


**FIGURE 5.3** Degradation products of glimepiride: (A) product II, (B) product III, (C) product IV, and (D) product V.

## 2.2. Impurity analysis

The BP and EP require liquid chromatographic method to determine impurities of glimepiride [3,7]. However, BP and EP differentiate between liquid chromatographic method used to determine impurity A and liquid chromatographic used to examine other impurities. For the determination of impurity A, test solution and reference solution should be prepared freshly and stored at a temperature not exceeding 12 °C for not more than 15 h. For the test solution, 10.0 mg of the assayed substance is dissolved first in 5 mL of methylene chloride and diluted to 20.0 mL with mobile phase. For the reference solution, 1 mg of glimepiride CRS which contains impurity A is dissolved in 1 mL methylene chloride and diluted to 4.0 mL with the mobile phase. The mobile phase comprises of anhydrous

acid:2-propanol:heptanes = 1:100:899 v/v/v, with diol silica gel for chromatography (0.15 m × 4 mm i.d.) used as the stationary phase. Analysis is done at wavelength 228 nm. Acceptance limit of impurity A is not more than 0.8%t. For analysis of other impurities, the reference used is glimepiride for system suitability which contains impurities B, C, and D. One vial of this reference is dissolved in 2.0 mL of the test solution and used as reference (a). The test solution is made by dissolving 20.0 mg of the assayed substance with solvent mixture to 100 mL of volume. This solution is further diluted with solvent mixture to make concentration of 0.2 µg/mL, and used as reference solution (b). Solvent mixture used is a mixture of water:ACN = 1:4. To analyze the impurities, end-capped octadecylsilyl silica gel column (0.25 m × 4 mm i.d.) is used as stationary phase with mobile phase consists of mixture of 0.5 g sodium dihydrogen phosphate in 500 mL which adjusted to pH 2.5 with phosphoric acid, then mixed with 500 mL of ACN. Reference solutions (a) and (b) are injected and analyzed. Acceptance limit of impurity B, D, and unspecified impurities are 0.4%, 0.2%, and 0.1%, respectively. Sum of impurities other than impurity B is not more than 0.5%.

Similar to BP and EP, USP32 NF27 [5] also differentiates the liquid chromatographic method employed to determine glimepiride related compound A with liquid chromatographic method applied to determine glimepiride related compounds B, C, and D. For glimepiride related compound A, glimepiride assayed is dissolved in methylene chloride then diluted with mobile phase. Standard of glimepiride related compound A is treated similarly. Mobile phase use consists of 100 mL isopropyl alcohol and 1 mL of glacial acetic acid which then diluted to 1 L with hexane. Chromatographic column used is a 15 cm × 3 mm column containing 5 µm packing L20 which is a column consists of dihydroxypropane groups chemically bonded to porous silica particles. Wavelength applied is 228 nm. The percentage of related compound A is calculated using formula as follows:

$$100r_{cis}/(r_{cis} + r_s)$$

in which  $r_{cis}$  and  $r_s$  are the peak areas of glimepiride *cis*-isomer and glimepiride, respectively. The percentage of glimepiride *cis*-isomer should not exceed than 0.8%.

Liquid chromatographic condition for other related substances of glimepiride is as for the assay of glimepiride, as detailed in Section 2.3. For this assay purpose, reference standard contains 0.1 mg of each impurity (glimepiride related compounds B, C, and D) is dissolved in the same solvent as for assay and used further as test solution. This test solution is then diluted with the same solvent to make *diluted test solution 1*, which contains 0.001 mg of glimepiride per milliliter. From this *diluted test*

*solution 1*, 1.0 mL of the solution is diluted with 10.0 mL solvent to make *diluted test solution 2*. The *test solution*, *diluted test solution 1* and *diluted test solution 2* are injected. Any peak area which has area less than that of the glimepiride peak obtained from *diluted test solution 2* should be disregarded. Elution process is continued up to 2.5 times of the retention time of glimepiride. Percentage calculation of each impurity of glimepiride is calculated as follows:

$$100(C_S/C_T)(r_i/r_s)$$

in which  $C_S$  is the concentration (in mg/mL) of glimepiride in *diluted test solution 1*;  $C_T$  is the concentration (in mg/mL) of glimepiride in the *test solution*;  $r_i$  is the peak response for each individual peak obtained from the *test solution*; and  $r_s$  is the glimepiride peak obtained from *diluted test solution 1*. Relative retention time and limit of each impurity of glimepiride are detailed in Table 5.1. In addition, any unspecified individual impurity found should not exceed 0.1%, and not more than 0.5% of a total impurity, excluding glimepiride related compound B, is found.

## 2.3. Assay

### 2.3.1. Bulk drug substance

BP and EP [3,7] utilize liquid chromatographic method as for the method used for test of related substances, except that the reference solution used is glimepiride CRS in solvent mixture. The percentage of glimepiride found is calculated from the areas of the peaks and the declared content of glimepiride CRS.

According to the USP32 NF27 [5], mobile phase used for liquid chromatographic method consists of 0.5 g of monobasic sodium phosphate in 500 mL water which is adjusted with phosphoric acid to a pH of 2.1–2.7, and added with 500 mL of ACN. The solvent or diluents used is a mixture of ACN:water = 4:1. For the standard, USP glimepiride RS diluted in the diluents to make final concentration of 0.2 mg/mL, while the assay is prepared by dissolving 20.0 mg glimepiride assayed with the diluents to

**TABLE 5.1** Relative retention time and limit of each impurity of glimepiride according to USP

Name	Relative retention time	Limit (%)
Glimepiride relative compound A	0.9	0.8
Glimepiride relative compound B	0.2	0.4
Glimepiride relative compound C	0.3	0.1
Glimepiride relative compound D	1.1	0.2

make 100 mL of volume. The 25 cm  $\times$  4 mm i.d. of L1 or octadecyl silane chemically bonded to porous silica is used as the stationary phase. Detection is done at 228 nm. Percentage of  $C_{24}H_{34}N_4O_5S$  in the portion of glimepiride is taken by following formula:

$$10.000(C/W)[100/(100 - L)](r_u/r_s)$$

in which  $C$  is the concentration (in mg/mL) of USP glimepiride reference standard;  $W$  is the weight (in mg) of glimepiride in the assay solution;  $L$  is the percentage of water as determined in the test for water; and  $r_u$  and  $r_s$  are the peak responses for the glimepiride obtained from the assay preparation and the standard preparation, respectively.

### 2.3.2. Pharmaceutical dosage form

BP and EP do not specify assay for the glimepiride in the dosage form [3,7]. In contrast, the USP32 NF27 [5] details assay of the glimepiride in the dosage form, dissolution of glimepiride tablet, and uniformity of dosage form. For the assay of glimepiride in the dosage form, the column, mobile phase, and observation wavelength used are as for assay of bulk drug substance. In this assay, sample solution prepared contains 0.1 mg/mL glimepiride. Tablets are placed in the volumetric flask and dissolved with water. Volume of water used is 10% of the volume of the flask. After being dissolved, ACN is added to about 70% of the volume of the flask, then swirl. The sample is then sonicated in a water bath not to exceed 20 °C for 5–10 min. The sample solution was then cooled to room temperature and filtered. Standard solution is made by dissolving USP reference standard of glimepiride in the diluent (ACN:water = 9:1) to make concentration of 0.1 mg/mL. The percentage of glimepiride in the tablet portion is calculated as follows:

$$100(C_s/C_u)(r_u/r_s)$$

in which  $C_s$  is the concentration (in mg/mL) of glimepiride in the standard;  $C_u$  is the concentration of glimepiride in the assay preparation, based on the labeled quantity per tablet and the extent of the dilution; and  $r_u$  and  $r_s$  are the peak responses for glimepiride obtained from the assay preparation and the standard preparation, respectively.

For the purpose of dissolution assay, solution drawn from the dissolution medium is diluted with diluting solution consists of MeOH and water (50:50). Standard solution of glimepiride reference standard is prepared by diluting 4.0 mL of 0.125 mg/mL of glimepiride in ACN: water = 9:1, diluted with dissolution medium to 200 mL. This solution is then diluted with the diluting solution to make final concentration 0.00075 mg/mL of glimepiride. Dissolution medium comprises phosphate buffer pH 7.8, made by dissolving 0.58 g monobasic potassium

phosphate and 8.86 g of dibasic sodium phosphate anhydrous in 1000 mL. pH is adjusted with 10% phosphoric acid or 1 N NaOH.

USP32 NF27 sets the preparation of standard, sample, mobile phase, and diluent used for uniformity of dosage form as for the assay method. For the sample solution, the solution is centrifuged, and supernatant is injected. Standard solution contains about 0.02 mg/mL for each of glimepiride reference solution, glimepiride related compound B, and glimepiride related compound C. Aliquot (5.0 mL) of this standard solution is diluted to 50 mL with the diluents. Percentage calculation of each impurity in the portion of tablets is taken by the following formula:

$$100(1/F)(r_u/r_s)$$

in which  $F$  is the relative response factor, which is equal to 1.3 for glimepiride related compound B and 1.0 for any other impurity;  $r_u$  is the peak response for each impurity obtained from the test solution; and  $r_s$  is the sum of the responses of all the peaks in the test solution. Any peak less than 0.1% is disregarded.

### 3. METHOD OF ANALYSIS

#### 3.1. Spectroscopic method of analysis

##### 3.1.1. Ultraviolet absorption spectroscopy

Second-order derivative UV spectrophotometric method was developed by Altinöz and Tekeli [16] to determine glimepiride in tablet dosage form. Standard solution of glimepiride as well as the sample was dissolved in DMF due to its complete solubility in this solvent. At zero-order derivatives, UV spectrum of glimepiride showed maximum wavelength at 268.2 and 271.8 nm. However, when applying these maximum wavelengths, low concentration of glimepiride resulting in wavelength broadening while higher concentration showing shouldered peaks. Therefore, second-order derivative was applied since this method resulting sharper and better-defined peaks. Limit of detection (LOD) and limit of quantitation (LOQ) of glimepiride obtained by this method were 0.4 and 1.00 mg/mL, respectively. Mean recovery found was 100.10%.

In contrast with previous UV spectrophotometric method, Khan *et al.* [17] reported first -derivative spectrophotometric method to determine glimepiride in pharmaceutical dosage form. In this method, formation of drug complex was carried out by reacting glimepiride in MeOH with 2,3,5-triphenyl-2H-tetrazolium chloride in NaOH 0.1 M as an alkaline media. This mixture was then heated at  $60 \pm 2$  °C for 60 min. Drug complex formed was showing maximum absorption at



413.5 nm with mean recovery acquired was 100.3%. Robustness of this method was also assessed for several parameters such as concentrations of reagent and NaOH, temperature, and heating time. Results showed that for a change of  $\pm 0.5$  mL reagent,  $\pm 5$   $\mu$ L NaOH,  $\pm 3$  °C temperature, and 28–33 min heating time were showing similar absorbance of glimepiride.

Shveta *et al.* [18] developed spectrophotometric method based on simultaneous equation method to determine glimepiride in mixture with another drug in tablets. From the overlain spectra, 268.6 and 227.6 nm were used as two analytical wavelengths to determine glimepiride in combination with pioglitazone hydrochloride. Standard and sample solution were dissolved in MeOH. Absorbance and absorptivity of each drug substance were measured, and concentration for each substance was calculated using solving simultaneous equation. Mean percentage recovery obtained was 100.55%. Further, absorbance ratio method was also investigated. This method is based on the principle that the ratio of absorbance at any two wavelengths is a constant value and has to be independent of concentration. In this method, 251 nm was used as the isosbestic point to determine glimepiride. At this wavelength, both substances were showing equal absorptivity. Percent recovery obtained with this method was found to be 99.46%. Similar to Shveta, Goyal and Singhvi [19] were reported simultaneous equation method as well as two wavelength calculation method and first-order derivative spectroscopy method to assess glimepiride in combination with rosiglitazone maleate, with NaOH 0.1 N used as solvent for standard and sample. In the simultaneous equation method, 238 and 318 nm were used to determine glimepiride in mixture with rosiglitazone maleate. The absorptivity coefficient of both drugs was found at 238 nm, with a recovery percentage of 99.4–100.03% gained for glimepiride. For the two wavelengths calculation method, 244.8 and 257.2 nm were chosen based on the principle that the absorbance difference of two points on the spectra of the mixture is proportional to the concentration of the compound of interest and no interfering components are observed. Percentage of recovery found was ranging from 100.30% to 100.72%. In addition, the first-order derivative spectroscopy method was performed at 252 nm with percent recovery obtained was 98.23–101.14%. The wavelength applied was chosen and set on the basis that, at zero-crossing point of one component, the other component should have considerable absorbance as well.

For the purpose of studying dissolution of glimepiride, spectrophotometric method was utilized to measure release of glimepiride from pharmaceutical dosage form. In these studies, phosphate buffer solution pH 5.5 was used as the dissolution media as well as the solvent. Wavelength measurement was set at 226 nm [20–23].

### 3.1.2. Infrared absorption spectroscopy

Cides *et al.* [24] reported the use of IR absorption spectroscopy to analyze glimepiride and its interaction with lactose and Mg Stearate. IR analysis was conducted in the range of 4000–400  $\text{cm}^{-1}$  in KBR pellet. From the spectra obtained, no interaction between glimepiride and those excipients occurred since there was no appearance of new bands in the IR spectra of the mixture compared to the glimepiride only. In addition, as revealed by Ammar *et al.* [20,22], from the IR spectrum observed, there were peaks present at 3369 and 3288  $\text{cm}^{-1}$  which were due to the N–H stretch for urea. As an effect of N–H bending, a major peak occurred at 1673  $\text{cm}^{-1}$ . Other peaks observed at 1345 and 1153  $\text{cm}^{-1}$  were related to the sulfonamide group, while peaks observed at 1708 and 1674  $\text{cm}^{-1}$  were correspond to the carbonyl group. Several peaks as results of C–H and =C–H bending were also observed in the frequency range of 600–1500  $\text{cm}^{-1}$ . Further, Endo *et al.* [10] reported that from the comparison between glimepiride form I and form II, it was found that the form II had lost an intramolecular hydrogen bond between N(1) and O(I) resulting in the conformation change of glimepiride form II.

## 3.2. Chromatographic method

### 3.2.1. Thin layer chromatography

A thin layer chromatography (TLC) method has been reported by Kumasa *et al.* [25] for screening and qualitative analysis of glimepiride and other sulfonyl urea drugs in the health food. In this method, a silica gel 60 precoated high performance thin layer chromatography (HPTLC) plates, with 0.25 mm thickness which contain a fluorescent indicator at 254 nm, were used. Mobile phase applied was *n*-butyl acetate containing various concentrations from 0.2% to 2.0% formic acid. Prior to the analysis, the developing chamber was saturated with the mobile phase for 1 h, followed by plate's equilibration for 30 min in the chamber. After being developed in the chamber, plates were then air dried and examined under UV irradiation at 254 nm with Dragendorff's test solution (DD), or 10% of phosphomolybdic acid methanol solution (PM), or 30% sulfuric acid methanol solution (SA). From the results obtained, it was found that mixture of *n*-butyl acetate with 0.4% formic acid was giving the best resolution of all of the sulfonyl urea drugs analyzed, including glimepiride. Further, spraying the plate with DD was producing pale-yellow red spots for glimepiride, while others two spraying solution were not resulting any spots of glimepiride.

Furthermore, two HPTLC methods for determination of glimepiride in pharmaceutical dosage form have been reported [26,27]. In the HPTLC method developed by Menon *et al.* [27], standard, sample, and internal

standard were dissolved in MeOH. Internal standard use was atorvastatin calcium. This method is used to determine glimepiride in mixture with pioglitazone HCl. Chromatography was performed on silica gel 60 F<sub>254</sub> which was prewashed with MeOH and dried at 105 °C for 2 h in the oven. Mobile phase used was a mixture of toluene–MeOH–ethyl acetate–formic acid = 7 + 2 + 1.5 + 0.001 v/v. The developing chamber was saturated with the mobile phase prior to use. Plate was scanned using densitometry at  $\lambda = 235$  nm. Mean recovery obtained for glimepiride was 102.74%.

Similar to Menon, Patel *et al.* [26] also used MeOH to prepare standard and sample solution. Mobile phase was comprised of toluene:ethyl acetate:MeOH = 50:45:5 v/v. HPTLC silica gel 60F<sub>254</sub> was used as the stationary phase, which was developed in the chamber that previously saturated for 30 min with the mobile phase. After developed in the chamber, the HPTLC plate was then dried in the air, and analysis was conducted at  $\lambda = 230$  nm. LOD and LOQ value obtained were 23.15 and 70.15 ng/spot, respectively. The automatic spotter used was filled with 100  $\mu$ L volume of standard solution. Percent accuracy attained was 98.53–99.23%.

### 3.2.3. High performance liquid chromatography

HPLC methods are the most common method reported to determine glimepiride, and this is also the preferred methods suggested by compendias. Summary of the HPLC method for analyzing glimepiride in the dosage form is detailed in Table 5.2. Since the active form of glimepiride is the *trans* form [13], HPLC methods applied should also be able to distinguish the *trans* form from the *cis* form, as reported by Song and Pathare [28,31]. Both methods were utilizing C18 column for the purpose of analysis. In the method developed by Song *et al.* [28], it was revealed that the mixture of MeOH and ACN used in combination with buffer was having significant effect on the separation process between *cis* and *trans* glimepiride. When MeOH was used solely, decreasing its percentage in the mobile phase was increasing the separation between *cis* and *trans*. However, the retention times of both isomers were significantly increased from 14 min to 3 h, resulting in longer duration of analysis. In addition, the baseline became noisy with peak broadening occurred. In contrast, the use of ACN in the mobile phase was resulting in lower resolution factor at lower than 1.0, although the retention time of both isomers was shorter with smoother baseline observed. By mixing ACN and MeOH with buffer, higher resolution of *cis* and *trans* isomers of glimepiride was achieved as well as shorter retention time and smooth baseline observed. In the method developed by Pathare *et al.* [31], setting column temperature at 30 °C was giving symmetrical peaks for both isomers. Compared to the previous method, this method is less time consuming with 10 min of total running time needed.

**TABLE 5.2** Summary of HPLC methods used to analyze glimepiride in bulk drug substance and pharmaceutical dosage form

Column	Mobile phase	Column temperature (°C)	Detection (nm)	Solvent	Limit of detection (LOD), limit of quantitation (LOQ), and recovery (Rec)	Reference
Dikmonsil C18 (250 × 4.6 mm)	MeOH:ACN:NH <sub>4</sub> Ac buffer solution 1.5 M, pH 4.5 = 1.1:1.3:1.0 v/v	n/a	228	MeOH	LOD: 0.88 µg/mL LOQ: n/a Rec: n/a	[28]
LiChroCART (250 × 4.6 mm) with Purospher (RP-18e)	ACN:Phosphate buffer 0.03 M, pH 3.5	n/a	228	MeOH	LOD: n/a LOQ: n/a Rec: 98.1–102.7%	[14]
Phenomenex® Luna C8 (250 × 4.6 mm)	Phosphate buffer, pH 7.0:ACN: THF = 73:18:9	35	228	Standard: diluent A Sample: diluent B Diluent A: ACN:THF = 65:35 Diluent B: Phosphate buffer pH 7 (6.8 g KH <sub>2</sub> PO <sub>4</sub> in 1000 mL added with 10 mL TEA)	LOD: n/a LOQ: n/a Rec: 99.13–100.47%	[13]
Agilent Zorbax XDB C18 (150 × 4.6 mm)	Aqueous buffer (10 mM disodium hydrogen phosphate and 10 mM sodium dodecyl sulfate, pH 7.5):ACN = 68:32	40	226	10 mM disodium hydrogen phosphate, pH 8: ACN = 60:40	LOD: 0.007 µg/mL LOQ: 0.022 µg/mL Rec: 98.8–99.8%	[29]

(continued)

TABLE 5.2 (continued)

Column	Mobile phase	Column temperature (°C)	Detection (nm)	Solvent	Limit of detection (LOD), limit of quantitation (LOQ), and recovery (Rec)	Reference
Superspher 100 RP 18e (125 mm × 4 mm)	650 mg sodium phosphate dehydrate in 550 g water, pH adjusted to 3.0 with H <sub>3</sub> PO <sub>4</sub> 85% and 351.5 g ACN then solution was made up to 1000 mL	35	228	4 mM phosphate buffer, pH 7.0: ACN = 20:80 Phosphate buffer was prepared as detailed in BP 1999	LOD: 0.1520 µg/mL LOQ: 0.506 µg/mL Rec: 98.80–100.75%	[30]
Waters Symmetry C18 (50 × 4.6 mm)	Water:THF = 75:25	30	228	THF	LOD: 200 ng/mL LOQ: 600 ng/mL Rec: 96.7–102.4%	[31]
Nucleosil 100-5SA (250 × 4.6 mm)	NH <sub>4</sub> H <sub>2</sub> PO <sub>4</sub> buffer, pH 3.0:ACN = 70:30	n/a	230	Standard: Standard stock was prepared in 80% ACN in water then diluted with mobile phase Sample solution Prepared in 80% ACN in water then made up to volume, filtered, and diluted with mobile phase	LOD: n/a LOQ: n/a Rec: 99.51–100.99%	[32]

Chromolith Performance RP-18e (100 × 4.6 mm)	Buffer, pH 3.0: ACN = 55:45  Buffer pH 3.0:1.182 g sodium dihydrogen phosphate in 1000 g water, adjusted to pH 3.0 with phosphoric acid 85%	30	228	Phosphate buffer 4 mM, pH 7: ACN = 20:80	LOD: n/a LOQ: n/a Rec: n/a	[33]
Inertsil ODS (25 cm × 4.6 mm)	ACN:20 mM ammonium acetate buffer = 60:40, adjusted to pH 4.5 ± 0.2	Ambient	230	Standard solution Standard stock was prepared in MeOH then diluted with mobile phase Sample solution MeOH	LOD: 0.1 µg/mL LOQ: 0.5 µg/mL Rec: 101.67– 102.5%	[34]
Spherisorb® C8 (150 × 4.6 mm) with Nucleosil® C8 (8 × 4.6 mm)	ACN:ammonium acetate 0.02 M pH 3.0 = 20:80 LC–MS for detecting the degradation products:carried out using (+)ESI and (–) ESI with ionization mode in the range of 50–3000 <i>m/z</i>	n/a	235	n/a	LOD: n/a LOQ: n/a Rec: n/a	[12]

(continued)

**TABLE 5.2** (continued)

Column	Mobile phase	Column temperature (°C)	Detection (nm)	Solvent	Limit of detection (LOD), limit of quantitation (LOQ), and recovery (Rec)	Reference
Acquity UPLC BEHC18	Mobile phase A: 20 mM ammonium formate, pH 3.0	30	UPLC–MS with ESI positive mode $m/z$ range 100–600	MeOH	LOD: n/a LOQ: n/a Rec: n/a	<a href="#">[15]</a>
	Mobile phase B: ACN					
	Gradient elution 5–95% B in 5 min					
Inertial ODS-3 (250 × 4.6 mm)	MeOH:buffer phosphate, pH 4.3 = 75:25	25	258	n/a	LOD: n/a LOQ: n/a Rec: 100.2%	<a href="#">[35]</a>
Varian C18 (256 × 4.6 mm)	ACN:2% formic acid, pH 3.5 = 80:20	n/a	228	Mobile phase	LOD: n/a LOQ: n/a Rec: 100.17–100.84%	<a href="#">[17]</a>

Additionally, for the analysis of glimepiride in combination with other drugs such as metformin, Kolte *et al.* [29] revealed that the application of sodium dodecyl sulfate in the mobile phase was resulting in good separation of metformin HCl and glimepiride.

For the purpose of analyzing glimepiride using HPLC, most of the methods are using C8 or C18 column [12,14,15,17,28–31,34,36]. In contrast, Pawar *et al.* [32] was utilizing a Nucleosil column which is notably an ion exchanger column. This selection was due to the fact that glimepiride is ionized in the acidic mobile phase applied. Smaller particle size used also gave better retention compared to the larger particle size. Further, the application of monolithic column was investigated by Deeb *et al.* [30]. Results showed that faster analysis time and better separation were achieved, compared to the conventional packed column. This is due to the fact that the time required for equilibrate or wash monolithic column was six times shorter since the higher flow rates were applied. From the column efficiency observed, monolithic column is able to operate at high flow rate with only small decrease occurred in its efficiency.

With respect to the HPLC methods applied, different liquid chromatographic method was developed by Jones *et al.* [15] to assess glimepiride and its degradation products. A Ultra Performance Liquid Chromatography (UPLC) method was utilized in conjunction with the MS detection. The use of UPLC can enhance the resolution as well as specificity of MS detection. In addition, shorter retention time is able to gained compared to HPLC [15,37]

### 3.3. X-ray crystallography

The first X-ray crystallographic method was developed by Iwata *et al.* [9] to determine the crystal structure of glimepiride form I. In this method, Cu K $\alpha$  was used as the radiation source with scanning range done from 28.20° to 28.47°,  $T = 297$  K, and  $l = 1.5418$  Å. Results obtained were also suggested the intra- and intermolecular hydrogen-bonding interactions in the crystal of glimepiride form I. Another X-ray crystallographic method has also been reported for crystal determination of glimepiride–cyclodextrin complex [38]. In this method, single crystal diffractometer is used, which also equipped with Rigaku rotating anode and graphite monochromator. Scanning mode was done at  $2\theta$  with the range of data collection from 2.75° to 50°.

Further, several X-ray powder diffraction (XRPD) methods have been reported to determine glimepiride form I in its crystalline form. In some researches conducted by Ammar *et al.* [20,22,23], source of XRPD radiation used was the Cu K $\alpha$  with scanning range 5–80° and  $2\theta$  step size. Tube voltage used was 45 kV with 9 mA current. Sharp diffraction pattern observed suggesting the crystallinity of glimepiride with the highest peak detected at 24.5°. Another research reported by Kadam *et al.* [11] has shown that at



angle of  $2\theta$  and scanning range  $6.363\text{--}40.413^\circ$ , the highest intensity of glimepiride observed was at  $21.044^\circ$ . However, in this finding, details of the XRPD condition were not reported. In addition, Ilić *et al.* [39] also reported the XRPD method of glimepiride using Cu  $K_\alpha$  as the radiation source with scanning range from  $2^\circ$  to  $40^\circ$  and  $2\theta$  scan steps. Other details were not reported. From the diffractogram shown, highest peak intensity of glimepiride was detected at about  $21\text{--}22^\circ$ . In addition, Endo *et al.* [10] reported the transformation of glimepiride form II to form I at heating temperature over  $140^\circ\text{C}$  as observed with X-ray crystallographic method.

### 3.4. Thermal method of analysis

Cides *et al.* [24] outlined the use of differential scanning calorimetry (DSC) and Thermogravimetry/derivative thermogravimetry (TG/DTG) to investigate thermal behavior and kinetic study of glimepiride. DSC analysis was done under dynamic nitrogen atmosphere (flow rate  $50\text{ mL/min}$ ) with temperature range from  $25$  to  $600^\circ\text{C}$  and  $10^\circ\text{C/min}$  of heating rate. A sharp endothermic peak at  $212^\circ\text{C}$  was shown in the DSC curve. This result was in line with the melting of glimepiride which was then followed by decomposition. The decomposition itself took place in two endothermic stages. Kinetic study of glimepiride with respect to its degradation was conducted using TGA under  $50\text{ mL/min}$  of dynamic nitrogen atmosphere and heating rate at  $10^\circ\text{C/min}$ . Temperature range was set at  $25\text{--}900^\circ\text{C}$ . For dynamic experiments, heating rates used were  $2.5$ ,  $5.0$ ,  $7.5$ ,  $10$ , and  $15^\circ\text{C/min}$ . For the isothermal method, temperature was set from  $170$  to  $210^\circ\text{C}$  with  $10^\circ\text{C}$  temperature increment. The Ozawa's method was utilized to determine the activation energy ( $E_a$ ). Results showed that  $E_a$  value obtained using dynamic method was  $157$  and  $150\text{ kJ/mol}$  in air and nitrogen, respectively, while the  $E_a$  value by isothermal method was  $123\text{ kJ/mol}$ . From the DSC curve resulted, a sharp endothermic peak was observed at  $212^\circ\text{C}$  which was in line with the melting condition followed by thermal decomposition, in which the decomposition was defined in two endothermic stages.

Similar to the TG/DTG mentioned earlier, Ammar *et al.* [22] were also employed TGA scanning of glimepiride under a dynamic  $\text{N}_2$  purging gas atmosphere at a constant rate of  $50\text{ mL/min}$  but with  $5^\circ\text{C/min}$  heating rate. From the TGA thermogram, it was observed that  $65.87\%$  of glimepiride weight was lost at  $190^\circ\text{C}$ , which was in correspond with its melting point.

## 4. DETERMINATION OF GLIMEPIRIDE IN BIOLOGICAL SAMPLE

Glimepiride is metabolized *in vivo* through oxidative biotransformation and producing two major metabolites, cyclohexyl hydroxy methyl derivative (M1) and the carboxyl derivative (M2). M1 is the active metabolite

which is further metabolized to the inactive M2 metabolite by one or several cytosolic enzymes [2,40]. The first analytical method developed to determine glimepiride and its metabolites in human serum as well as human urine was done by applying precolumn derivatization technique. In this method, either human serum or human urine was extracted using Liquid Liquid Extraction (LLE) method using diethyl ether. 2,4-dinitrofluorobenzene (DNFB) was used to trap the resulting amines, while the thermolysis process of sulfonylureas was done at 100 °C [41]. Further, most of the HPLC methods used were utilizing LC–MS–MS to detect glimepiride in biological sample, in which the ionization source can be either the electrospray ionization (ESI) or atmospheric pressure chemical ionization (APCI) [42–50]. Based on the result found by Kim *et al.* [42], in the ESI condition, glimepiride was showing a fairly high sensitivity in positive ion detector mode rather than in the negative ion detection mode. Therefore, Kim concluded that for compounds with basic sites such as glimepiride which has the amine group, the analytical condition should be performed at a low pH with positive ion detection. Although the APCI is able to reduce ion suppression which might lead to false negative results and showed high sensitivity when used with LC–MS [51,52], ESI was proven to have higher selectivity and sensitivity as shown by Salem *et al.* [53]. As revealed by Kim [42,43], the presence of ACN in the mobile phase was giving better sensitivity and resolution compared to MeOH. Moreover, ammonium acetate buffer was employed in the mobile phase composition due to its ability to improve peak symmetry and higher ion intensities achieved [42]. In contrast with another method developed by Kim *et al.* [42], the same author also found that the use of acetic acid was better in adjusting pH of the mobile phase since formic acid was decreasing the peak intensity of the glimepiride [43].

One of the non-LC–MS methods for detecting glimepiride in biological sample was developed by Rabbaa-Khabbaz *et al.* [54]. This method was successfully used to determine glimepiride in human serum with higher limit of detection and simpler analytical method compared to the previous precolumn derivatization method developed by Lehr [41]. In this method, HCl 1 N was used to acidify serum sample, and it should be noted that in this method, adding HCl dropwise was proven to improve the extraction of glimepiride compared to adding HCl instantly. Similar utilization of the UV/Vis detector was also established by Lakshmi *et al.* for detecting glimepiride in rat plasma [55]. In contrast with both non-LC–MS methods, Song *et al.* [28] generated column switching method with UV/Vis detector to analyze glimepiride in human plasma sample. In this column switching method, three different microbore columns were set up. The first column was used to remove proteins in the sample and concentrate glimepiride and its internal standard. After protein removal, the drug molecule fractions were then transferred to the second column or

**TABLE 5.3** Summary of HPLC methods used to analyze glimepiride and its metabolites in biological samples

Analyte(s)	HPLC conditions	Sample	Preparation of standard, sample extraction, and clean up	Limit of detection (LOD), limit of quantitation (LOQ), and extraction efficiency (rec)	Reference
Glimepiride, metabolite I, metabolite II, i.s. III, i.s. IV	Column: Spherisorb ODS (125 × 4.6 mm i.d.) at room temperature (25 °C)  Detector: UV/Vis 350 nm Mobile phase: Human serum analysis: Eluent A (0.05 M perchloric acid:ACN = 60:40)/eluent B (0.05 M perchloric acid:ACN = 42:58) run at gradient program started from 6 min eluent A then switched to	Human serum Human urine	Standard Glimepiride and i.s. III: etOH Metabolite I, II, i.s. IV: MeOH  Human serum: 1 mL of sample added with 1 mL buffer, pH 1 then shaken with 5 mL diethyl ether for 20 min. Organic phase was transferred and evaporated at 30 °C under	Human serum Glimepiride LOD: 5 ng/mL LOQ: n/a Rec: 85% Metabolite I LOD: 10 ng/mL LOQ: n/a Rec: 50% Metabolite II LOD: 5 ng/mL LOQ: n/a Rec: 63%	3[9]

eluent B for 8 min, then  
switched again to eluent A for  
2 min before injecting the  
sample  
Column temperature: room  
temperature (25 °C)

Human urine analysis:  
0.05 M perchloric acid:  
ACN = 60:40  
Column temperature: room  
temperature (25 °C)

nitrogen. Residue was  
derivatized by adding  
DNFB solution (30 µL  
DNFB in 10 mL acetic acid  
*n*-butyl ester), reacted for  
20 min at 100 °C. Acetic  
acid *n*-butyl ester was  
evaporated at 60 °C under  
nitrogen, then the residue  
diluted with eluent A

Human urine  
Glimepiride  
LOD: 50 ng/mL  
LOQ: n/a  
Rec: n/a  
Metabolite I  
LOD: 50 ng/mL  
LOQ: n/a  
Rec: 75%  
Metabolite II  
LOD: 50 ng/mL  
LOQ: n/a  
Rec: 80%

Human urine:  
1 mL of sample added  
with 1 mL 0.4 M citrate  
buffer pH 3, then shaken  
with 5 mL diethyl ether.

**TABLE 5.3** (continued)

Analyte(s)	HPLC conditions	Sample	Preparation of standard, sample extraction, and clean up	Limit of detection (LOD), limit of quantitation (LOQ), and extraction efficiency (rec)	Reference
Glimepiride, Trimipramine-D3 (i.s.)	Column: LiChroCART® column (125 × 2 mm i.d.) with Superspher® 60 RP Select B equipped with LiChroCART® 10-2 Superspher® 60 RP Selected B guard column Detector: APCI–LC–MS SIM monitoring: Glimepiride: <i>m/z</i> 491 at 100 V Trimipramine-D3: <i>m/z</i> 298 at 100 V  Mobile phase: Eluent A (0.005 M ammonium formate adjusted to pH 3 with	Human plasma	Organic phase was then transferred and evaporated at 30 °C under nitrogen. Derivatization process of the residue is similar as for the human serum sample  Standard: MeOH  Sample: Plasma added with saturated sodium sulfate then continued with LLE. LLE extracting solvent: diethyl ether: ethyl acetate = 1:1  Organic phase was drawn and evaporated. Aqueous phase was then basified	LOD: 0.002 mg/L LOQ: 0.01 mg/L Rec: 76.2–76.4%	[51]

	formic acid)/eluent B (ACN), run at gradient program: 0–4 min: 40% B 4–6 min: 90% B 6–7 min: 90% B 7–10 min: 40% B		by adding 1 M NaOH, extracted with LLE solvent, and evaporated. Residue from both organic phase and basified aqueous phase was dissolved in MeOH		
Glimepiride, glibenclamide (i.s.)	Column: C18 XTerra (50 × 2.1 mm i.d.) which was protected by Phenomenex C18 guard column Detector: LC–MS–MS with ESI as ion source SRM monitoring: Glimepiride: <i>m/z</i> 491 Glibenclamide: <i>m/z</i> 494 Mobile phase: Ammonium acetate buffer 0.02 M, pH 3.5:ACN:MeOH = 40:35:25	Human plasma	Standard: Stock solutions Glimepiride:DMSO: CHCl <sub>3</sub> = 1:2 Working solution: MeOH Glibenclamide: ACN	LOD: n/a LOQ: 5.0 ng/mL Rec: 86.36–91.99%	[53]
			Sample: LLE: sample added with 0.05 M KCl (adjusted to pH 1.0 with HCl), extracted with diethyl ether then frozen. The upper ethereal layer decanted and evaporated at 30 °C under nitrogen stream. Residue dissolved with MeOH:water = 1:1		

(continued)

**TABLE 5.3** (continued)

Analyte(s)	HPLC conditions	Sample	Preparation of standard, sample extraction, and clean up	Limit of detection (LOD), limit of quantitation (LOQ), and extraction efficiency (rec)	Reference
Glimepiride, glibenclamide (i.s.)	Column: Column 1: Capcell Pak MF Ph-1 (10 mm × 4.0 mm i.d.) Column 2: Capcell Pak C18 UG 120 U (35 × 2.0 mm i.d.) Column 3: Capcell Pak MG C18 (250 × 1.5 mm i.d.) Detector: UV/V is 228 nm	Human plasma	Standard: Glimepiride: ACN:water = 80:20 Glibenclamide: ACN  Sample: Plasma added with EtOH and vortexed. Clear supernatant was then transferred and evaporated at 40–45 °C under nitrogen. Residue was then dissolved in mobile phase	LOD: n/a LOQ: 10 ng/mL Rec: 99.1–109.5%	<a href="#">[28]</a>
	Mobile phase: Washing solvent: ACN:10 mM potassium phosphate buffer containing 0.04% TEA = 20:80, pH 2.18				

Glimepiride, glipizide (i.s.)	Mobile phase: ACN:10 mM potassium phosphate buffer containing 0.04% TEA = 52:48, pH 2.18 Column switching: 0.0–7.1 min: column 1 and washing solvent 7.1–13.1 min: column 2 and mobile phase 13.1–40.0 min: column 3 and mobile phase	Human plasma	Standard: Glimepiride: mobile phase Glipizide: MeOH	LLE LOD: n/a LOQ: 0.1 ng/mL Rec: 75.5%	<a href="#">[43]</a>
	Column: C18 Capcell Pak (150 × 2.0 mm i.d.)  Detector: LC–MS–MS with ESI source MRM monitoring: Glimepiride: <i>m/z</i> 491 with product ions at <i>m/z</i> 352 Glipizide: <i>m/z</i> 446 with product ions at <i>m/z</i> 321				
			Sample: LLE extracting solvent: Diethyl ether:DCM = 7:3 Plasma added with extracting solvent then shaken and centrifuged. The upper organic layer was evaporated at 40 °C under nitrogen, residue was then dissolved in mobile phase	SPE LOD: n/a LOQ: 0.5 ng/mL Rec: 85.5%	

(continued)



**TABLE 5.3** (continued)

Analyte(s)	HPLC conditions	Sample	Preparation of standard, sample extraction, and clean up	Limit of detection (LOD), limit of quantitation (LOQ), and extraction efficiency (rec)	Reference
	Mobile phase: ACN: water = 80:20 (total pH 3.5 with acetic acid)		SPE: OASIS HBL SPE cartridge C18, 30 mg Precondition: MeOH then water Column wash: water Elution: MeOH Plasma was added with 3 N HCl prior to SPE process. Residue was evaporated at 40 °C under nitrogen and reconstituted with mobile phase Protein precipitation: Sample added with ACN and centrifuged. Supernatant was then evaporated at 40 °C under nitrogen and residue was dissolved in mobile phase	PP LOD: n/a LOQ: 1.0 ng/mL Rec: 98.1%	

Glimepiride i.s.: n/a	Column: Supelco LC-CN column	Human ED TA K3 plasma	Standard: n/a	LOD: n/a LOQ: n/a Rec: 79%	[46]
	Detector: LC-MS-MS (API) MRM monitoring: Glimepiride: $m/z$ 491.0 $\rightarrow$ 352.1 Mobile phase: Mixture of ammonium formate and MeOH, composition n/a		Sample: SPE: C18 SPE cartridge Elution: MeOH		
Glimepiride, glipizide (i.s.)	Column: C18 Capcell Pak (150 $\times$ 2.0 mm i.d.)	Human plasma	Standard: mobile phase	LOD: n/a LOQ: 0.1 ng/mL Rec: 71.2–79.8%	[42]
	Detector: LC-ESI/MS/MS MRM monitoring: Glimepiride: $m/z$ 491 $\rightarrow$ 352 Glipizide: $m/z$ 446 $\rightarrow$ 321  Mobile phase: 5 mM ammonium acetate:ACN = 40:60, pH 3.0 with formic acid		Sample: LLE extracting solvent: diethyl ether:ethyl acetate = 1:1 Sample extracted with extracting solvent. The upper organic layer was then separated and evaporated at 30 °C under nitrogen. Residue then dissolved in mobile phase		

(continued)

**TABLE 5.3** (continued)

Analyte(s)	HPLC conditions	Sample	Preparation of standard, sample extraction, and clean up	Limit of detection (LOD), limit of quantitation (LOQ), and extraction efficiency (rec)	Reference
Glimepiride, glibenclamide (i.s.)	Column: Capcell Pak MG II C18 (50 x 2.0 mm i.d.) Autosampler controlled at 4 °C Detector: LC–MS/MS operated in positive ESI mode MRM monitoring: Glimepiride: $m/z$ 491.0 → 126.2 Glibenclamide: $m/z$ 494.0 → 168.8 Mobile phase: 5 mmol/L ammonium formate, pH 5.8 with formic acid:ACN = 46:54	Human plasma	Standard: ACN Sample: Sample added with MTBE. The organic layer was then separated and evaporated at 40 °C. The residue reconstituted in 50% ACN	LOD: n/a LOQ: 2 ng/mL Rec: 98.1–102.8%	[44]
Glimepiride	Column: Hypersil ODS (250 x 4.6 mm i.d.) Detector: LC–MS–MS MRM monitoring: Glimepiride: $m/z$ 490.65 → 351.98	Human plasma	Standard: ACN:water = 1:1 Sample: LLE extracting solvent: 1-Chlorobutane:ethyl acetate:propan-2-ol = 88:10:2	LOD: 0.16 ng/mL LOQ: 0.50 ng/mL Rec: 89.3–107.1%	[45]

	Mobile phase: Formic acid 0.05 M:ACN = 28:72 Mobile phase was heated to 25 °C		Sample added and mixed with 1 M HCl then extracted with extracting solvent. The organic phase was separated then evaporated to dryness under nitrogen stream. The residue was then dissolved in ACN:formic acid 0.05 M = 50:50		
Glimepiride, glibenclamide (i.s.)	Column: YMC-Pack ProC18 (50 x 4.0 mm i.d.) Column temperature: 22 °C (room temperature) Autosampler temperature: 15 °C Detector: LC–MS–MS with ESI source SRM monitoring: Glimepiride: $m/z$ 491.2 → 352.0 Glibenclamide: $m/z$ 494.2 → 369.0 Mobile phase: ACN: 20 mM acetic acid = 80:20	Human plasma	Standard: MeOH: water = 50:50  Sample: LLE extracting solvent: Ethyl acetate:diethyl ether = 50:50  Sample extracted with extracting solvent, vortexed at 4 °C, and then	LOD: n/a LOQ: n/a Rec: 91.27–100.30%	[48]

---

(continued)

**TABLE 5.3** (continued)

Analyte(s)	HPLC conditions	Sample	Preparation of standard, sample extraction, and clean up	Limit of detection (LOD), limit of quantitation (LOQ), and extraction efficiency (rec)	Reference
Glimepiride, glibenclamide (i.s.)	Column: Agilent LiChrospher 100, C18 (250 x 4 mm i.d.)  Column temperature: ambient Detector: UV/Vis 228 nm Mobile phase: Water acidified with glacial acetic acid (0.1 mM, pH 2.5–2.7): ACN = 50:50	Human serum	frozen at –30 °C for 60 min. The supernatant organic mixture was then transferred to deep well plate then evaporated at 35 °C under nitrogen stream. The residue was dissolved in mobile phase  Standard: MeOH  Sample: Sample added with HCl 1 N, then extracted with dichloromethane. The organic layer was then evaporated under nitrogen and residue dissolved in mobile phase	LOD: 2.5 ng/mL LOQ: 8.2 ng/mL Rec: 81.8–85.6%	[54]

Glimepiride, metabolite I (M-1), glibenclamide (i.s.)	Column: ZORBAX Eclipse XDB- C18 Detector: LC–MS–MS operated in positive API-ESI mode MRM monitoring: Glimepiride: $m/z$ 494 M-1: $m/z$ 507 Glibenclamide: $m/z$ 494.0 Mobile phase: n/a	Human plasma	Standard: n/a Sample: LLE: Diethyl ether	LOD: n/a LOD: n/a Rec: n/a	[49]
Glimepiride, gliclazide (i.s.)	Column: ACE 5 C18 (5 x 4 mm i.d.) Column temperature: 30 °C Detector: LC–MS–MS with ESI source MRM monitoring: Glimepiride: $m/z$ 324.11 → 127.25 Gliclazide: $m/z$ 491.16 → 352.08 Mobile phase: water:ACN: MeOH:glacial acetic acid = 200:450:350:0.6	Human plasma	Standard: Glimepiride: stock solution in MeOH, working solution in MeOH:water = 50:50 Gliclazide: ACN:water = 50:50  Sample: Sample extracted with diethyl ether: dichloromethane = 70:30. Upper organic layer was transferred and evaporated at 40 °C under nitrogen. The residue was dissolved in mobile phase	LOD: n/a LOQ: 5 ng/mL Rec: 87.03–118.32%	[50]

(continued)

**TABLE 5.3** (continued)

Analyte(s)	HPLC conditions	Sample	Preparation of standard, sample extraction, and clean up	Limit of detection (LOD), limit of quantitation (LOQ), and extraction efficiency (rec)	Reference
Glimepiride, glibenclamide (i.s.)	Column: YMC Propack C18 (50 x 4.6 mm i.d.) Detector: LC–MS–MS with ESI source MRM monitoring: Glimepiride: $m/z$ 491.2 → 352.2 Glibenclamide: $m/z$ 494.2 → 369.0 Mobile phase: 0.01 M ammonium acetate buffer: ACN:MeOH = 30:60:10	Human plasma	Standard: Glimepiride: stock solution in DMSO: MeOH = 2:3, working solution in MeOH Glibenclamide: MeOH  Sample: Sample extracted with ethyl acetate. Clear supernatant was drawn, evaporated at 50 °C under nitrogen, then dissolved in mobile phase	LOD: n/a LOQ: 0.02 ng/mL Rec: 88.60–113.50%	[47]
Glimepiride, pioglitazone	Column: Phenomenex C18 (150 x 4.6 mm) Column temperature: Ambient Detector: UV/Vis 252 nm Mobile phase: MeOH: ammonium acetate buffer, pH 3.5 = 55:55	Rat plasma	Standard: stock solution was in MeOH, working solution in mobile phase  Sample: Sample extracted with diethyl ether	LOD: 4 ng/mL LOQ: 10 ng/mL Rec: n/a	[55]

intermediate column and finally delivered to the third or final column for final separation. However, it should be considered that a long running time, approximately 40 min, is needed when applying this method.

Most of the extraction method employed to extract glimepiride from biological sample was achieved by LLE, although this method can be considered requiring more solvent, resulting more volume of waste solvent and the need to combine solvents, compared to SPE [56]. Related to that matter, Dotsikas *et al.* had developed an LLE method which employed only small volume of extracting solvent, 600  $\mu$ L. The removal of organic phase was found easier by freezing the sample after being extracted with extracting solvent. This research also revealed that the addition of buffer was not improving the extraction process. Therefore, it is suggested that the LLE solvent should remained simple without the need to add buffer. Further, comparison of different extraction procedures has showed that LLE was giving higher percentage of recovery compared to SPE, although the percentage achieved was still lower than the protein precipitation method. Moreover, the LOQ value obtained from LLE method was significantly higher than LOQ obtained from SPE and protein precipitation [43]. Summary of the HPLC methods developed and applied for detecting glimepiride in biological sample is detailed in Table 5.3.

## REFERENCES

- [1] Martindale: The Complete Drug Reference, 35 ed, CD ROM, The Pharmaceutical Press, London, 2007.
- [2] Product Monograph Amaryl, Sanofi-Aventis Canada Inc. <http://www.sanofi-aventis.ca/products/en/amaryl.pdf> (September 10, 2009).
- [3] British Pharmacopoeia 2009, The Stationery Office, London, 2009.
- [4] M.J. O'Neil, The Merck Index, Merck & Co., Inc., New Jersey, 2001, p. 790.
- [5] United States Pharmacopoeia 32 National Formulary 27, The United States Pharmacopoeial Convention, Rockville, MD, 2009.
- [6] Clarke's Analysis of Drugs and Poisons, CD ROM, Pharmaceutical Press, London, 2005.
- [7] European Pharmacopoeia 6.0, Council of Europe, London, 2006.
- [8] N. Seedher, M. Kanojia, Cent. Eur. J. Chem. 7 (2009) 96.
- [9] M. Iwata, H. Nagase, T. Endo, H. Ueda, Acta Cryst. C53 (1997) 329.
- [10] T. Endo, M. Iwata, H. Nagase, M. Shiro, H. Ueda, STP Pharm. Sci. 13 (2003) 281.
- [11] S.M. Kadam, V.R. Tarur, S.J. Naik, S.B. Gavhane, US 2007/0082943 A1, United States Patent Application Publication, 2007.
- [12] G. Bansal, M. Singh, K.C. Jindal, S. Singh, J. Pharm. Biomed. Anal. 48 (2008) 788.
- [13] M.A. Khan, S. Sinha, S. Vartak, A. Bhartiya, S. Kumar, J. Pharm. Biomed. Anal. 39 (2005) 928.
- [14] P. Kovaříková, J. Klimeš, J. Dohnal, L. Tisovská, J. Pharm. Biomed. Anal. 36 (2004) 205.
- [15] M.D. Jones, J. Wheaton, M.J. Wojtusik, R.S. Plumb, Waters Application Note, <http://www.waters.com/webassets/cms/library/docs/720002638en.pdf>, 2008 (September 28, 2009).
- [16] S. Altınöz, D. Tekeli, J. Pharm. Biomed. Anal. 24 (2001) 507.



- [17] I.U. Khan, F. Aslam, M. Ashfaq, M.N. Asghar, *J. Anal. Chem.* 64 (2009) 171.
- [18] C. Shveta, A.V. Kasture, P.G. Yeole, *Ind. J. Pharm. Sci.* 67 (2005) 627.
- [19] A. Goyal, I. Singhvi, *Ind. J. Pharm. Sci.* 69 (2007) 780.
- [20] H.O. Ammar, H.A. Salama, S.A. El-Nahhas, H. Elmotasem, *Curr. Drug Del.* 5 (2008) 290.
- [21] H.O. Ammar, H.A. Salama, M. Ghorab, A.A. Mahmoud, *Int. J. Pharm.* 320 (2006) 53.
- [22] H.O. Ammar, H.A. Salama, M. Ghorab, A.A. Mahmoud, *Int. J. Pharm.* 309 (2006) 129.
- [23] H.O. Ammar, H.A. Salama, M. Ghorab, A.A. Mahmoud, *Asian J. Pharm. Sci.* 2 (2007) 44.
- [24] L.C.S. Cides, A.A.S. Araújo, M. Santos-Filho, J.R. Matos, *J. Therm. Anal. Calorim.* 84 (2006) 441.
- [25] K. Kumasaka, T. Kojima, H. Honda, K. Doi, *J. Health Sci.* 51 (2005) 453.
- [26] J.R. Patel, B.N. Suhagia, M.M. Patel, *Asian J. Chem.* 18 (2006) 2873.
- [27] R.T.S. Menon, S. Inamdar, M. Mote, A. Menezes, *J. Planar Chromatogr.* 17 (2004) 154.
- [28] Y. Song, L. Niu, D. Wang, Y. Hu, D. Hou, *J. Sep. Sci.* 26 (2003) 1595.
- [29] B.L. Kolte, B.B. Raut, A.A. Deo, M.A. Bagool, D.B. Shinde, *J. Sep. Sci.* 28 (2005) 2076.
- [30] S.E. Deeb, L. Preu, H. Wätzig, *J. Pharm. Biomed. Anal.* 44 (2007) 85.
- [31] D.B. Pathare, A.S. Jadhav, M.S. Shingare, *Chromatographia* 66 (2007) 639.
- [32] S.P. Pawar, G.A. Meshram, M.U. Phadke, *Chromatographia* 68 (2008) 1063.
- [33] L. Kaminski, S.E. Deeb, H. Wätzig, *J. Sep. Sci.* 31 (2008) 1745.
- [34] A. Karthik, G. Subramanian, C.M. Rao, K. Bhat, A. Ranjithkumar, P. Musmade, M. Surulivelrajan, K. Karthikeyan, N. Udupa, *Pak. J. Pharm. Sci.* 21 (2008) 421.
- [35] J. Deepti, J. Surendra, J. Deepak, A. Maulik, *J. Chromatogr. Sci.* 46 (2008) 501.
- [36] D.B. Wanjari, N.J. Gaikwad, *Ind. J. Pharm. Sci.* 67 (2005) 253.
- [37] M.E. Swartz, Separation Science Redefined, [www.chromatographyonline.com](http://www.chromatographyonline.com), 2005 (March 10, 2010).
- [38] A. Paulidou, D. Maffeo, K. Yannakopoulou, I.M. Mavridis, *CrystEngComm* (2010).
- [39] I. Ilić, R. Dreu, M. Burjak, M. Homar, J. Kerč, S. Srčić, *Int. J. Pharm.* 381 (2009) 176.
- [40] H.D. Langtry, J.A. Balfour, *Drugs* 55 (1998) 563.
- [41] K.H. Lehr, P. Damm, *J. Chromatogr.* 526 (1990) 497.
- [42] H. Kim, K.Y. Chan, H.J. Lee, S.B. Han, *Bull. Korean Chem. Soc.* 25 (2004) 109.
- [43] H. Kim, K.Y. Chang, C.H. Park, M.S. Jang, J.-A. Lee, H.J. Lee, K.R. Lee, *Chromatographia* (2004) 60.
- [44] H.-W. Lee, S.-H. Cho, W.-S. Park, H.-T. Im, J.-H. Rew, K.-T. Lee, *J. Korean Pharm. Sci.* 35 (2005) 287.
- [45] C. Pistos, M. Koutsopoulou, I. Panderi, *Biomed. Chromatogr.* 19 (2005) 394.
- [46] N. Smith, J. Couture, AAPS Annual Meeting, Salt Lake City, Utah, 2003.
- [47] L. Chakradhar, R. Kallem, A. Karthik, B.T. Sundari, S. Ramesh, R. Mullangi, N. R. Srinivas, *Biomed. Chromatogr.* 22 (2008) 58.
- [48] Y. Dotsikas, C. Kousoulos, G. Tsatsou, Y.L. Loukas, *Rapid Commun. Mass Spectrom.* 19 (2005) 2055.
- [49] K. Suzuki, T. Yanagawa, T. Shibasaki, N. Kaniwa, R. Hasegawa, M. Tohkin, *Diabetes Res. Clin. Pract.* 72 (2006) 148.
- [50] N. Yüzüak, T. Özden, S. Eren, S. Özilhan, *Chromatographia* 66 (2007) S165.
- [51] H.H. Maurer, C. Kratzch, T. Kraemer, F.T. Peters, A.A. Weber, *J. Chromatogr. B* 773 (2002) 63.
- [52] H.H. Maurer, C.J. Schmitt, A.A. Weber, T. Kraemer, *J. Chromatogr. B* 748 (2000) 125.
- [53] I.I. Salem, J. Idrees, J.I.A. Tamimi, *J. Chromatogr. B* 799 (2004) 103.
- [54] L. Rabbaa-Khabbaz, R.A. Daoud, D. Karam-Sarkis, C. Atallah, A. Zoghbi, *J. Liq. Chromatogr. Relat. Technol.* 28 (2005) 3255.
- [55] K.S. Lakshmi, T. Rajesh, S. Sharma, *Int. J. PharmTech Res.* 1 (2009) 496.
- [56] What are advantages of SPE versus liquid liquid extraction, <http://www.chem.agilent.com/en-US/Support/FAQs/GC/Applications/SPE/Pages/KB000867.aspx> (March 11, 2010).

# CHAPTER 6

## Lornoxicam

**Mahrous O. Ahmed\*** and **Abdullah A. Al-Badr†**

---

<b>Contents</b>		
	1. Description	206
	1.1. Nomenclature	206
	1.1.1. Systemic chemical names	206
	1.1.2. Nonproprietary names	207
	1.1.3. Proprietary names	207
	1.2. Formulae	207
	1.2.1. Empirical formula, molecular weight, and CAS number	207
	1.2.2. Structural formula	207
	1.3. Elemental analysis	207
	1.4. Appearance	207
	2. Uses and Applications	208
	3. Methods of Preparation	208
	4. Physical Characteristics	209
	4.1. Ionization constant	209
	4.2. Solubility	209
	4.3. Partition coefficient	210
	4.4. Thermal methods of analysis	210
	4.4.1. Melting behavior	210
	4.4.2. Differential scanning calorimetry	210
	4.5. X-ray powder diffraction pattern	210
	4.6. Crystal structure	211
	4.6.1. Molecular structures	211
	4.6.2. Crystal structure determination of complexes <b>1</b> and <b>2</b>	217
	4.6.3. Calculations	219

---

\* Department of Industrial Pharmacy, Faculty of Pharmacy, Assiut University, Assiut, Egypt

† Department of Pharmaceutical Chemistry, College of Pharmacy, King Saud University, Riyadh, Kingdom of Saudi Arabia

4.7. Spectroscopy	219
4.7.1. Ultraviolet spectroscopy	219
4.7.2. Vibrational spectroscopy	219
4.7.3. Nuclear magnetic resonance spectrometry	220
4.8. Mass spectrometry	221
5. Methods of Analysis	222
5.1. Spectrophotometric methods	222
5.2. Polarographic methods	228
5.3. Chromatographic methods	229
5.3.1. Thin-layer chromatography	229
5.3.2. High-performance liquid chromatography	230
5.3.3. High-performance liquid chromatography-mass spectrometry	234
6. Mechanism of Action	235
7. Pharmacokinetics	236
8. Reviews	237
9. Stability	237
Acknowledgment	237
References	237

## 1. DESCRIPTION

### 1.1. Nomenclature

#### 1.1.1. Systemic chemical names

- 6-Chloro-4-hydroxy-2-methyl-*N*-2-pyridinyl-2*H*-thieno[2,3-*e*]-1,2-thiazine-3-carboxamide 1,1-dioxide.
- 6-Chloro-4-hydroxy-2-methyl-3-(2-pyridylcarbamoyl)-2*H*-thieno[2,3-*e*]-1,2-thiazine-1,1-dioxide.
- 2*H*-Thieno(2,3-*e*)-1,2-thiazine-3-carboxamide, 6-chloro-4-hydroxy-2-methyl-*N*-2-pyridinyl-, 1,1-dioxide.
- 6-Chloro-4-hydroxy-2-methyl-*N*-pyridin-2-yl-2*H*-thieno[2,3-*e*][1,2]thiazine-3-carboxamide-1,1-dioxide.
- 6-Chloro-4-hydroxy-2-methyl-*N*-(2-pyridyl)-2*H*-thieno[2,3-*e*][1,2]-thiazine-3-carboxamide-1,1-dioxide.
- (3*E*)-6-chloro-3-[hydroxy(pyridine-2-ylamino)methylene]-2-methyl-2,3-dihydro-4*H*-thieno[2,3-*e*][1,2]thiazin-4-one, 1,1-dioxide.
- (3*E*)-6-Chloro-3-[hydroxy(pyridine-2-ylamino)methylidene]-2-methyl-1,1-dioxothieno[2,3-*e*]thiazin-4-one.

- 2*H*-thieno[2,3-*c*][1,2]-thiazine-3-carboxamide, 6-chloro-4-hydroxy-2-methyl-*N*-(2-pyridyl)-1,1-dioxo.

### 1.1.2. Nonproprietary names

Lornoxicam; Chlortenoxicam; Ro-13-9297; TS-110, Akos 93662, Lornoxicam  
Consulted Standard rINN.

### 1.1.3. Proprietary names

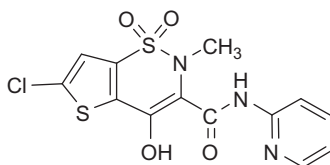
Lornoxi, Lorna, Lornex, Lornox, Losnasafe, Lorsid, LRN, Nyox, Telos, Xefo, Xefocam, Zeficam.

## 1.2. Formulae

### 1.2.1. Empirical formula, molecular weight, and CAS number

$C_{13}H_{10}ClN_3O_4S_2$	371.82	[70374-39-9]
---------------------------	--------	--------------

### 1.2.2. Structural formula



## 1.3. Elemental analysis

C = 41.99%, H = 2.71%, Cl = 9.53%, N = 11.30%, O = 17.21%,  
S = 17.25%.

## 1.4. Appearance

Lornoxicam is an orange to yellow crystalline powder.

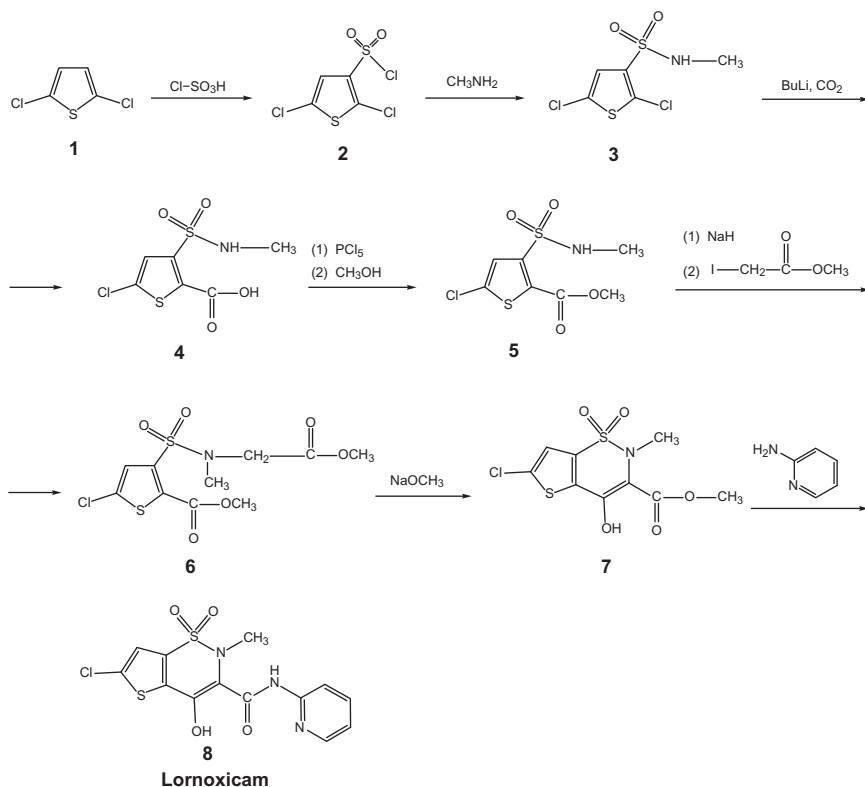
## 2. USES AND APPLICATIONS

Lornoxicam, an oxicam derivative, is a nonsteroidal anti-inflammatory derivative. It is used in musculoskeletal and joint disorders such as osteoarthritis and rheumatoid arthritis. It is also used in the treatment of other painful conditions including postoperative pain. In the treatment of osteoarthritis and rheumatoid arthritis lornoxicam is given by mouth in a daily dose of 12 mg in two or three divided doses. Lornoxicam is given in doses of 8–16 mg daily by mouth for the treatment of pain. Doses above 8 mg should be given in divided doses. Similar doses may be given by intravenous or intramuscular injection, although in rare cases the maximum initial daily dose may be increased to 24 mg; treatment by injection should be limited to two days [2].

Lornoxicam has demonstrated clinical efficacy in relieving chronic pain associated with osteoarthritis [3], rheumatoid arthritis, and ankylosing spondylitis [4]. In the treatment of postoperative pain, lornoxicam has been shown to be as effective as morphine [5]. An *in vitro* study suggested that lornoxicam is 100 times more potent than tenoxicam as a COX inhibitor and its analgesic potency is 12 and 10 times greater than that of piroxicam and tenoxicam, respectively. Lornoxicam analgesic potency of 16 mg (i.m.) is comparable with that of 20 mg morphine (i.m.) or 50 mg tramadol (i.v.) [6,7].

## 3. METHODS OF PREPARATION

Pfister *et al.* [8] described the following method for the preparation of lornoxicam: The sulfonation of 2,5-dichlorothiophene 1 with chlorosulfonic acid/thionyl chloride gives 2,5-dichlorothiophene-3-sulfonic acid chloride 2, which by reaction with methylamine in chloroform yields the corresponding methylamide 3. Carboxylation with butyl lithium and carbon dioxide in ether affords 5-chloro-3-(*N*-methylsulfamoyl) thiophene-2-carboxylic acid 4, which is esterified with phosphorous penta chloride and methanol to the methyl ester 5. The condensation of 5 with methyl iodoacetate by means of sodium hydride in dimethylformamide gives 5-chloro-3-[*N*-(methoxycarbonylmethyl)-*N*-methylsulfamoyl]thiophene-2-carboxylic acid methyl ester 6 which is cyclized with sodium methoxide in methanol yielding 6-chloro-4-hydroxy-2-methyl-2*H*-thieno[2,3-*e*]-1,2-thiazine-3-carboxylic acid methyl ester-1,1-dioxide 7. This compound is treated with 2-aminopyridine in refluxing xylene to give lornoxicam 8.



## 4. PHYSICAL CHARACTERISTICS

### 4.1. Ionization constant

$$\text{pK}_a = 4.7 [1]$$

### 4.2. Solubility

Lornoxicam is slightly soluble in chloroform and 0.1 M sodium hydroxide, very slightly soluble in methanol and acetonitrile, and hardly soluble in water. Lornoxicam is very slightly soluble in aqueous phosphate buffer of pH 7.4.

### 4.3. Partition coefficient

Partition coefficient of lornoxicam is 1.8, as determined in *n*-octanol and phosphate buffer (pH 7.4).

### 4.4. Thermal methods of analysis

#### 4.4.1. Melting behavior

Lornoxicam melts in the range of 225–230 °C with decomposition pka: 4.7 [1].

#### 4.4.2. Differential scanning calorimetry

Differential scanning calorimetry (DSC) thermogram of lornoxicam was obtained using a Shimadzu DSC-60 thermal analyzer. The thermogram shown in Fig. 6.1 was measured at a heating rate of 10 °C/min, and was run over the range from 30 to 300 °C, using aluminum pan as sample cell. Sample weight of drug was 1 mg. DSC curve of lornoxicam exhibited a small endothermic peak at 230.5 °C with simultaneously sharp exothermic peak at 235.2 °C, which is due to melting of lornoxicam with decomposition.

### 4.5. X-ray powder diffraction pattern

The X-ray powder diffraction pattern of lornoxicam was done using a Gigerflex diffractometer. Figure 6.2 shows the X-ray powder diffraction pattern of pure sample of lornoxicam. Table 6.1 shows the values for the

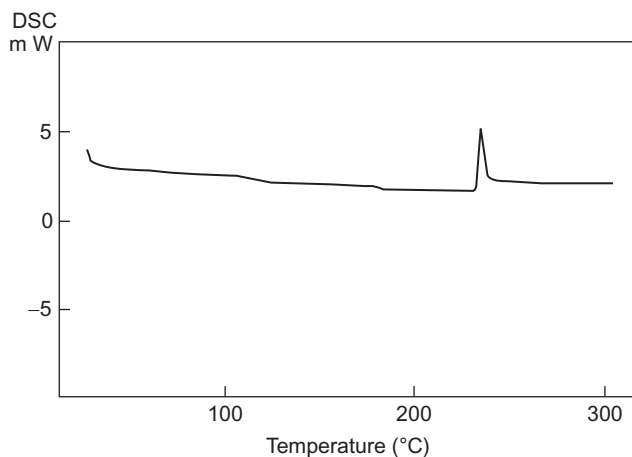


**FIGURE 6.1** Differential scanning calorimetry thermogram of lornoxicam.

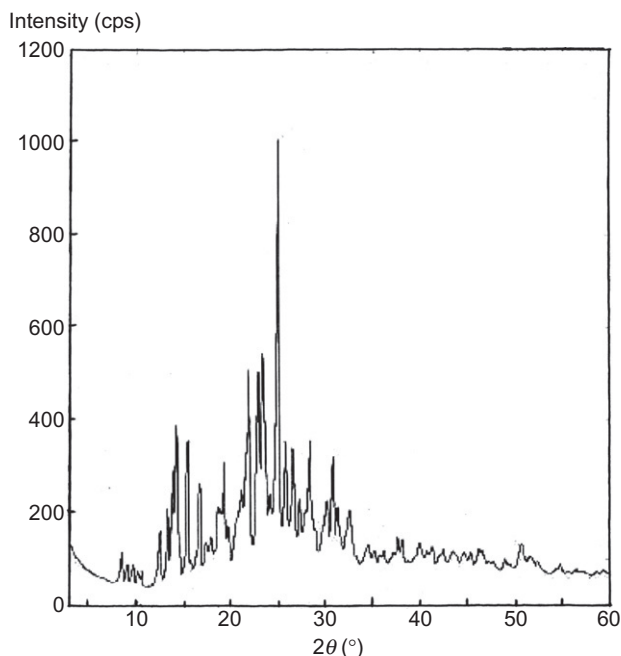


**FIGURE 6.2** X-ray powder diffraction pattern of lornoxicam.

scattering angles  $2\theta$  ( $^{\circ}$ ), the interplanar  $d$ -spacing ( $\text{\AA}$ ), and the relative intensities (%) observed for the major diffraction peaks of lornoxicam.

## 4.6. Crystal structure

Galani *et al.* [9] reported the synthesis and spectral characterization of organotin complexes  $[\text{SnMe}_2(\text{Lorn})]$  and  $[\text{SnBu}_2(\text{Lorn})]$  of lornoxicam [9].

### 4.6.1. Molecular structures

The molecular structures of complexes **1** and **2**, along with the atom numbering scheme, are shown in Figs. 6.3 and 6.4 and crystal data are given in Table 6.2, together with refinement details. Bond lengths and angles are given in Table 6.3. Complexes **1** and **2** have a 1:1 Sn/lorn stoichiometry, and the doubly deprotonated ligand, lorn, is coordinated as a tridentate ligand via the enolic oxygen O(4) and the amide N(31) and pyridyl N(1') nitrogen atoms. Two carbon atoms complete the fivefold coordination at the diorganotin(IV) fragments. There are two similar molecules in the asymmetric unit of **2**.

Analysis of the shape-determining angles using the approach of A W Addison and coworkers [10] yields  $\tau[(a - b)/60]$  values of 0.01 for both tin centers, Sn(1a) and Sn(1b) for **2**, and 0.29 for **1** ( $\tau = 0.0$  and 1.0 for  $sp$



**TABLE 6.1** X-ray powder diffraction pattern of lornoxicam

Scattering angel (deg $2\theta$ )	<i>d</i> -spacing (Å)	Relative intensity ( $I/I_0$ )
8.500	10.394	7
9.000	9.817	4
9.700	9.110	5
10.200	8.665	4
10.600	8.339	3
12.500	7.075	12
13.300	3.651	16
13.800	6.411	25
14.200	6.232	34
14.600	6.062	5
15.400	5.749	28
16.700	5.304	23
17.300	5.121	7
17.900	4.951	6
18.600	4.766	13
19.200	4.618	22
19.700	4.502	8
20.500	4.328	9
21.000	4.226	15
21.600	4.110	25
21.800	4.073	42
22.800	3.897	40
23.300	3.814	41
24.100	3.689	8
24.900	3.572	100
25.700	3.463	23
26.500	3.360	22
27.200	3.275	9
27.800	3.206	7
28.300	3.150	26

and *thp* geometries, respectively). The metal coordination geometry is therefore described as square pyramidal with N(31) occupying the apical positions. The donors N(31) are chosen as apices by the simple criterion that neither should be any of the four donor atoms that define the two largest angles,  $\alpha$  and  $\beta$ . The coordinated ligand is composed of five rings and the donor atoms NNO are included in three rings, one heterocyclic and two chelates. The heterocyclic ring (I) is planar, the largest deviation from the mean plane being  $0.016(6)^\circ$  for C(2') for **1** and  $0.008(12)^\circ$  for C(5'A) for molecule (1) and  $0.015(11)^\circ$  for C(3'B) for molecule (2),

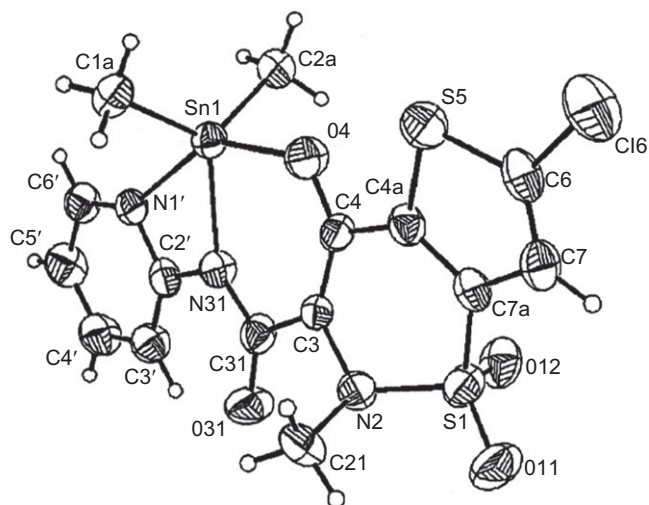


**FIGURE 6.3** ORTEP representation of **1** with the atom numbering scheme [9].

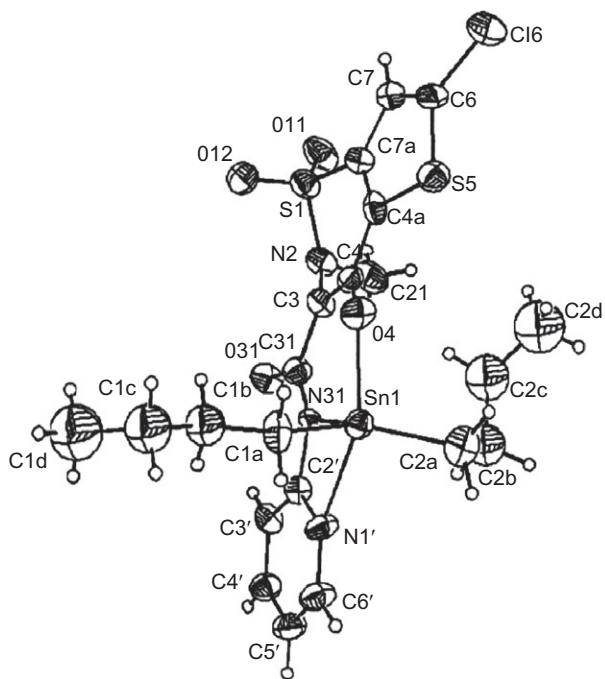


**FIGURE 6.4** ORTEP representation of **2** with the atom numbering scheme [9].

**TABLE 6.2** Crystal data, data collection, and structure refinement [9]

Compound	1	2
Empirical formula	C <sub>15</sub> H <sub>14</sub> ClO <sub>4</sub> N <sub>3</sub> S <sub>2</sub> Sn	C <sub>21</sub> H <sub>26</sub> ClN <sub>3</sub> S <sub>2</sub> Sn
Molecular mass	518.55	602.71
Crystal system	Monoclinic	Triclinic
Space group	<i>P</i> 2 <sub>1</sub>	<i>P</i> 1
<i>a</i> (Å)	9.0172(13)	12.413(2)
<i>b</i> (Å)	11.797(2)	13.272(2)
<i>c</i> (Å)	9.2567(17)	17.705(2)
$\alpha, \beta, \gamma$ (°)	90108.089(16) 90	78.058 (12) 77.058(12) 63.903(16)
<i>V</i> (Å <sup>3</sup> )	936.0(2)	2533.1(6)
<i>Z</i>	2	4
<i>D</i> <sub>x</sub> (g cm <sup>-3</sup> )	1.84	1.58
<i>F</i> (000)	512	1216
$\mu$ (mm <sup>-1</sup> )	1.76	1.31
Crystal size (mm)	0.40 × 0.25 × 0.10	0.30 × 0.20 × 0.150
$\Theta$ range (°)	3.8–25	3.5–26
<i>hkl</i> range	–10 ≤ <i>h</i> ≤ 10 –14 ≤ <i>k</i> ≤ 12 –11 ≤ <i>l</i> ≤ 11	–14 ≤ <i>h</i> ≤ 14 –15 ≤ <i>k</i> ≤ 16 –21 ≤ <i>l</i> ≤ 21
Reflections:		
Collected	7749	12,229
Unique ( <i>R</i> <sub>int</sub> )	2512 (0.040)	7688 (0.047)
Number of parameters	235	505
Weighting scheme:		
A	0.01	0.137
B	0.7	7.996
Extinction parameter <i>k</i>	0.00091 (10)	
<i>R</i> ( <i>F</i> )	0.026	0.067
<i>wR</i> ( <i>F</i> <sup>2</sup> )	0.049	0.169
Goodness of fit	1.14	1.02
max/min $\Delta\rho$ (e Å <sup>-3</sup> )	0.92/–0.37	2.66/–1.11

respectively, for complex **2**. For **1** the dihedral angles between the planes of the rings I and II, II and III, and I and III are 3.4(3), 3.8(2) and 6.9(2), respectively. For **2** the dihedral angles between the planes of the rings 1 and II, II and III, and I and II are 0.8(5), 6.1(4), and 6.8(4) for the first molecule Sn(1a), and 2.7(5), 5.2(4), and 7.1(4) for the second molecule Sn (1b), indicating that the ligand as a whole deviates from planarity, the

**TABLE 6.3** Selected bond lengths (Å) and angles [°] for **1** and **2** [9]

	<b>1</b>	<b>2a</b>	<b>2bss</b>
Sn(1)–C(1A)	2.102(6)	2.123(9)	2.118(9)
Sn(1)–C(2A)	2.112(5)	2.104(11)	2.113(11)
Sn(1)–N(31)	2.120(5)	2.133(8)	2.140(8)
Sn(1)–N(1')	2.400(4)	2.407(8)	2.391(7)
Sn(1)–O(4)	2.094(3)	2.113(6)	2.108(6)
S(1)–O(11)	1.422(4)	1.435(8)	1.444(8)
S(1)–O(12)	1.440(4)	1.413(8)	1.419(8)
S(1)–N(2)	1.624(5)	1.631(8)	1.620(9)
S(1)–C(7A)	1.740(5)	1.735(10)	1.746(10)
C(4)–O(4)	1.315(6)	1.338(10)	1.318(10)
C(4A)–S(5)	1.718(5)	1.729(9)	1.731(9)
S(5)–C(6)	1.719(5)	1.738(11)	1.714(10)
C(31)–O(31)	1.221(6)	1.247(11)	1.249(11)
C(31)–N(31)	1.365(7)	1.374(11)	1.384(12)
N(31)–C(2')	1.394(6)	1.411(11)	1.389(12)
N(1')–C(6')	1.335(6)	1.329(12)	1.357(12)
N(1')–C(2')	1.351(6)	1.330(11)	1.348(12)
O(4)–Sn(1)–C(1A)	97.1(2)	96.1(4)	97.0(4)
O(4)–Sn(1)–C(2A)	97.19(17)	101.3(4)	99.7(4)
C(1A)–Sn(1)–C(2A)	126.1(2)	142.1(4)	140.6(4)
O(4)–Sn(1)–N(31)	85.09(15)	83.3(2)	83.5(2)
C(1A)–Sn(1)–N(31)	116.2(2)	104.6(3)	105.5(3)
C(2A)–Sn(1)–N(31)	116.63(19)	110.6(4)	111.7(4)
O(4)–Sn(1)–N(1')	143.79(13)	141.4(2)	141.4(3)
C(1A)–Sn(1)–N(1')	100.5(2)	92.3(4)	92.5(4)
C(2A)–Sn(1)–N(1')	97.56(17)	94.6(4)	96.2(4)
N(31)–Sn(1)–N(1')	58.75(15)	58.2(3)	57.9(3)
N(31)–C(31)–C(3)	115.8(5)	114.1(7)	116.0(8)
N(31)–C(31)–O(31)	122.8(5)	126.2(8)	124.6(9)
O(31)–C(31)–C(3)	121.4(5)	119.6(8)	119.4(8)

largest deviations arising from the expected puckering of the sulfonamide rings which contain the pyramidal saturated N atoms. The C(31)O(31) bond lengths indicate strongly that these bonds are ketonic—also supported by the coplanarity of the three bonds to C(31). The di-anionic, tridentate ligand has an *EZZ* configuration about the bonds C(2')N(31), N(31)C(31), and C(31)C(3) for **1** and **2**. The *EZZ* configuration differs from the *ZZZ* isomer only by a 180° rotation of the pyridyl ring. The deprotonation of amide nitrogen is being one of the principal effects, which favor *EZZ* configuration [9].

Molecules of **2** are joined into dimmers in a head-to-tail fashion by intermolecular bonds between tin and the neighboring ketonic oxygen atom, with distances of  $\text{Sn}(1a) \cdots \text{O}(31B)^i$  2.954 (2) and  $\text{Sn}(1b) \cdots \text{O}(31A)^i$  2.971 (2). Intermolecular distances for  $\text{Sn} \cdots \text{O}$  of 2.61–3.02 Å have been confidently reported for intramolecular bonds, indicating SnO bonding here [11]. For **2** the dimmers of Sn(1a) and Sn(1b) are arranged in polymers with a stacking of alternate parallel chains. The dimmers of Sn(1a) and Sn(1b) are linked through intermolecular hydrogen bonds of the  $\text{CH} \cdots \text{O}$  type [12]  $\text{O}(12B)1 \cdots \text{H}22\text{AC}(2\text{AA})$ . Inter- and intra-  $\text{CH}\pi$  molecular interactions, [11] and intra- and intermolecular hydrogen bonds stabilize this structure. For **1** the distance between Sn(1) and the neighboring ketonic oxygen atom is 3.562(4), and the monomers of Sn(1) are linked through intermolecular hydrogen bonds of  $\text{CH} \cdots \text{O}$  type [12]  $\text{O}(12)\text{axial} \cdots \text{H}6'\text{C}(6')$ ,  $\text{O}(11)\text{eq} \cdots \text{H}13\text{AC}(1\text{A})$  and  $\text{O}(31) \cdots \text{H}23\text{AC}(2\text{A})$  (Fig. 6.5). Further,  $\text{CH}\pi$  interactions [12] and intramolecular hydrogen bonds stabilize the structure. Although the numerous contacts, of many different types, are remarkable, the interactions themselves are consistent with known guidelines for hydrogen bond formation [13]. In these two cases, molecular recognition of the hydrogen bonds and intermolecular contacts lead to aggregation and a supramolecular assembly. These interactions and other close approaches of the type  $\text{CH} \cdots \pi$ , and some intermolecular interactions are listed in Table 6.4 [9].

The negative charge on the atoms in a molecule with several donor centers can be used to study its formation of a donor–acceptor bond with a metal. In  $\text{H}_2\text{Iorn}$  the four oxygen atoms exhibit the maximum electron density and negative charge. The highest effective charge and the highest

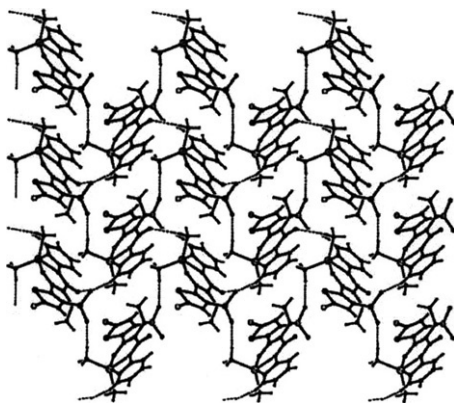


**FIGURE 6.5** Packing diagram of the complex **1** viewed along the *a* axis of the unit cell, showing intermolecular interactions [9].

**TABLE 6.4** Inter-hydrogen bonding, non-hydrogen,  $\pi$ - $\pi$  and C-H- $\pi$  interactions [9]

Compound 1				
D-H...A	$d(\text{D-H})$	$d(\text{H}\cdots\text{A})$	$d(\text{D}\cdots\text{A})$	$\angle(\text{DHA})$
C(2A)-H(2A3)...O(31) <sup>i</sup>	0.96	2.57	3.380(7)	142.2
C(6')-H(6')...O(12) <sup>i</sup>	0.93	2.39	3.072(7)	130.2
C(1A)-H(1A3)...O(11) <sup>ii</sup>	0.96	2.51	3.315(8)	141.7
C(1A)-H(1A3)...Cl(6) <sup>iii</sup>	0.96	3.02	3.821(7)	142.1
Cg(I) ( $\rho$ ) Cg(J) <sup>a</sup>	Cg-Cg <sup>b</sup>	$\beta \cong^c$	CgI-Perp <sup>d</sup>	CgJ-Perp <sup>e</sup>
Cg(5) ( $\rho$ ) Cg(2) <sup>iii</sup>	3.798	15.05	3.668	3.461
		H...Cg	X...Cg	C-H...Cg
C(1A)-H(11A) $\rightarrow$ Cg(3) <sup>i</sup>		3.382	92.98	3.563
C(1A)-H(12A) $\rightarrow$ Cg(3) <sup>i</sup>		2.882	128.81	3.563
C(2A)-H(21A) $\rightarrow$ Cg(3) <sup>iv</sup>		3.344	106.61	3.734
Compound 2				
D-H...A <sup>f</sup>	$d(\text{D-H})$	$d(\text{H}\cdots\text{A})$	$d(\text{D}\cdots\text{A})$	$\angle(\text{DHA})$
C(21A)-H(21B)...Cl(6B) <sup>v</sup>	0.96	2.93	3.815(12)	154
C(1AB)-H(1A4)...Cl(6B) <sup>v</sup>	0.97	2.94	3.835(11)	154
C(21B)-H(21E)...Cl(6A) <sup>vi</sup>	0.97	2.95	3.850(12)	156
C(2AA)-H(2A2)...O(12B) <sup>vii</sup>	0.97	2.42	3.303(15)	152
Sn(1A)...O(31B) <sup>viii</sup>			2.953(7)	
Sn(1B)...O(31A) <sup>viii</sup>			2.971(7)	

<sup>a</sup> Where Cg(2), Cg(3), and Cg(5) are referred to the centroids S(5)-C(4A)-C(7A)-C(7)-C(6), O(4)-C(4)-C(3)-C(31)-N(31) and N(1')-C(2')-C(3')-C(4')-C(5')-C(6') for **1**, respectively.

<sup>b</sup> Cg-Cg is the distance between ring centroids.

<sup>c</sup>  $\beta$  is the angle Cg(I)-Cg(J) or Cg(i)-Me vector and normal to plane I ( $^\circ$ ).

<sup>d</sup> CgI-Perp is the perpendicular distance of Cg(I) on ring J.

<sup>e</sup> CgJ-Perp is the perpendicular distance of Cg(J) on ring I.

<sup>f</sup> D is donor and A is acceptor; symmetry transformations used to generate equivalent atoms, (i)  $2-x, -1/2+y, 2-z$ ; (ii)  $-x+2, y-1/2, -z+1$ ; (iii)  $x-1, y, z$ ; (iv)  $x, y, 1+z$ ; (v)  $1-x, 2-y, -z$ ; (vi)  $1-x, 2-y, -z$ ; (vii)  $1+x, -1+y, z$ ; (viii)  $-1+x, 1+y, z$  [9].

electron density values for the four oxygen atoms and for the pyridyl and imine nitrogen in **1** and **2** evidently show strong electron-donor properties and could rationalize the coordination scheme and the extended network of inter-, intra- hydrogen, and nonhydrogen bonding. The optimized geometry in the gas phase for H<sub>2</sub>lorn the total dipole moment and the enthalpy of formation of neutral, H<sub>2</sub>lorn, and double deprotonated lornoxicam, lorn, in the gas state are shown in Fig. 6.6 [9].

#### 4.6.2. Crystal structure determination of complexes **1** and **2**

X-ray diffraction data were collected on a KUMA KM4CCD  $\kappa$ -geometry diffractometer with a CCD detector [14,15] by using graphite-filtered Mo K $_{\alpha}$  radiation ( $\lambda = 0.71073$  Å). The unit cell dimensions were calculated

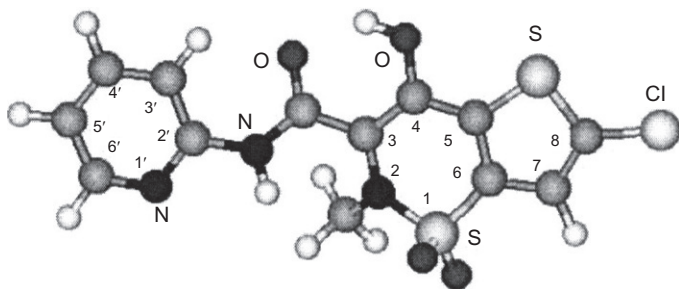


**FIGURE 6.6** Fully AM1-optimized geometry of the neutral lornoxicam ( $\Delta H_f = -48.28 \text{ kcal mol}^{-1}$ ; dipole moment = 3.98 D) in the gas state (Hyperchem, release 6.01 for Windows) [9,14].

from the least-squares fit of 2163 (1) and 1450 (2) most intense reflections from the whole experiment. Relevant crystallographic data, together with data collection and structure refinement details, are listed in Table 6.2. The measurements were performed in six separate runs, four runs consisted of 133 frames, and two of 125 frames ( $\omega$  width of each frame was  $0.75^\circ$ ). The  $\theta$ ,  $\kappa$ , and angles for the runs were chosen so as to cover the appropriate part of the Ewald sphere. Two reference frames were measured after every 50 frames of experiment; neither the geometry nor the intensity of the reflections in these frames changed significantly during the data collection. Intensity data were corrected for Lorentz and polarization effects and converted into  $F^2$ 's. These data were corrected for absorption and averaged with respect to the point group symmetry with SORTAV program [15]. The structures were solved with SHELXS-97 [16,17] and SHELXL-97 [16,17] was used for full-matrix least-squares refinement. The function  $\sum w(0.5F_o1/2^2 - 0.5F_c1/2^2)^2$  was minimized, with  $w^{-1} = [\sigma^2(F_o)^2 + AP^2 + BP]$  (where  $P = [\max. (F_o^2, 0) + 2F_c^2]/3$ ). Final values for A and B are listed in Table 6.2. In 1 all the nitrogen atoms were refined anisotropically, in 2—due to the large thermal motion of the butyl groups—only the first atoms of these groups (connected to Sn) were refined anisotropically, while the other three atoms from each butyl groups were refined isotropically, with fixed values for  $U_{iso}$ . The (relatively weak) constraints were also applied to the geometry of these groups. The attempts to resolve the apparent disorder of butyl groups were not successful. In both structures, hydrogen atoms were placed in calculated positions and refined as “riding mode,” that is, they followed the movements of their carrier atoms. The isotropic displacement parameters for hydrogen atoms were calculated as 1.2 times equivalent displacement parameters for respective carrier nonhydrogen atoms [9].

### 4.6.3. Calculations

A computational study with an AM1 parameterization scheme utilizing the Steepest Descent algorithm, as implemented in the HYPERCHEM 6.0 program, was used to investigate the prevailing isomer of free H<sub>2</sub>lorn in the gas phase [18]. H<sub>2</sub>lorn and the complexes **1** and **2** were studied by the extended-Hückel method using the CACAO PC Beta-Version 5.0 package geometry [19,20]. The molecular geometry was established by using the crystallographic coordinates of complexes **1** and **2** and for H<sub>2</sub>lorn by using the fully optimized in the gas state [9,19,20].

## 4.7. Spectroscopy

### 4.7.1. Ultraviolet spectroscopy

The UV absorption spectrum of lornoxicam dissolved in aqueous phosphate buffer solution (containing 1% methanol) of pH 7.4 was recorded using Labomed UV-Spectrophotometer and is shown in Fig. 6.7. Ultraviolet spectrum curve of lornoxicam exhibited three maxima at 258, 288, and 376 nm.

### 4.7.2. Vibrational spectroscopy

The infrared absorption spectrum of lornoxicam was obtained in a KBr disc using a NICOLET 380 FT-IR spectrophotometer and is shown in Fig. 6.8. The principal peaks were noted at 3067, 1646, 1597, 1541, 1427,

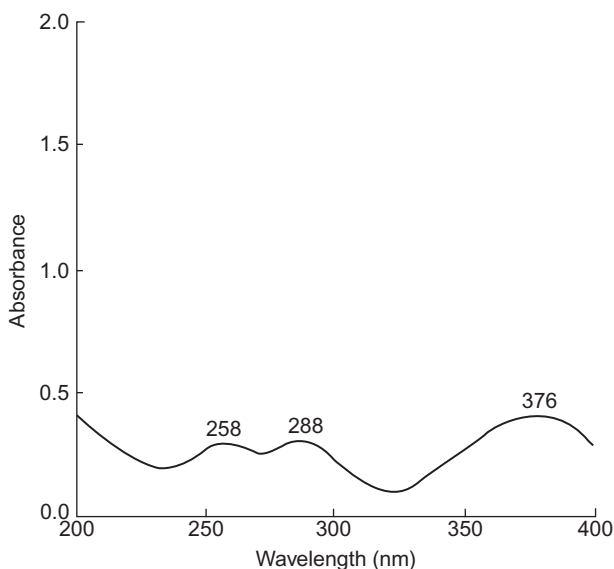


**FIGURE 6.7** UV spectrum of lornoxicam in phosphate buffer solution of pH 7.4.



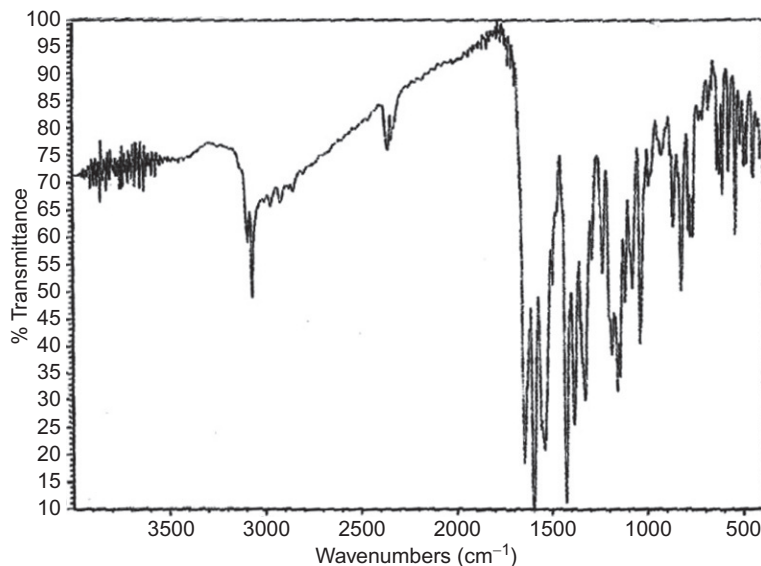


**FIGURE 6.8** The infrared spectrum of lornoxicam using KBr disc.

**TABLE 6.5** Assignments of the infrared absorption bands of lornoxicam

Frequency (cm <sup>-1</sup> )	Assignments
3067	Aromatic CH stretch or NH
1646	CO stretch of carboxamide group
1597	CC aromatic
1541	CC aromatic
1427	CC aromatic
1386	CH bending (aliphatic)
1328	CN stretch
1158,1146	SO <sub>2</sub> N stretch
1040	CS stretch
828.5	CCl stretch

1386, 1328, 1158, 1040 cm<sup>-1</sup>. Assignments for the major infrared absorption bands are summarized in [Table 6.5](#).

### 4.7.3. Nuclear magnetic resonance spectrometry

**4.7.3.1. <sup>1</sup>H NMR spectrum** The proton NMR spectrum of lornoxicam was determined using a Bruker Instrument operating at 500 MHz. The sample was dissolved in DMSO, and all resonance bands were referenced to the

**4.7.3.2.  $^{13}\text{C}$  NMR spectrum** The carbon-13 NMR spectra of lornoxicam were obtained using Bruker instrument operating at 125 MHz and are shown in [Figs. 6.12 and 6.13](#). The sample was dissolved in DMSO and TMS was used as the internal standard. Positions of the various carbons of lornoxicam are shown in [Table 6.7](#).

The positive electrospray ionization tandem mass spectrometry (ESI-MS/MS) of lornoxicam was obtained using an Agilent 6410 QQQ mass spectrometer with collision energy 10 eV using argon as collision gas and is shown in Fig. 6.14. Table 6.8 shows the mass fragmentation pattern of the drugs.

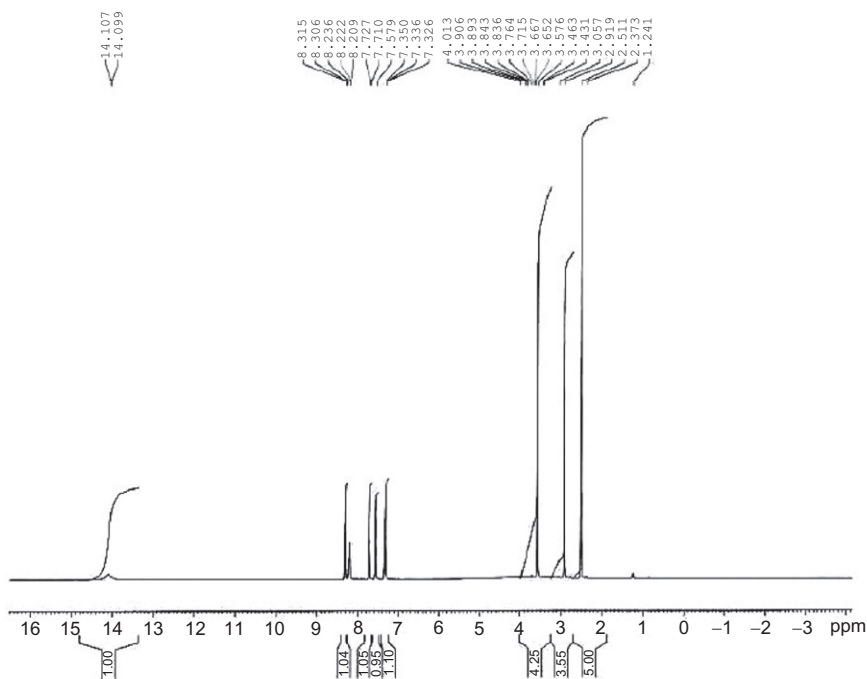


**FIGURE 6.9** Proton NMR spectrum of lornoxicam in DMSO- $d_6$ .

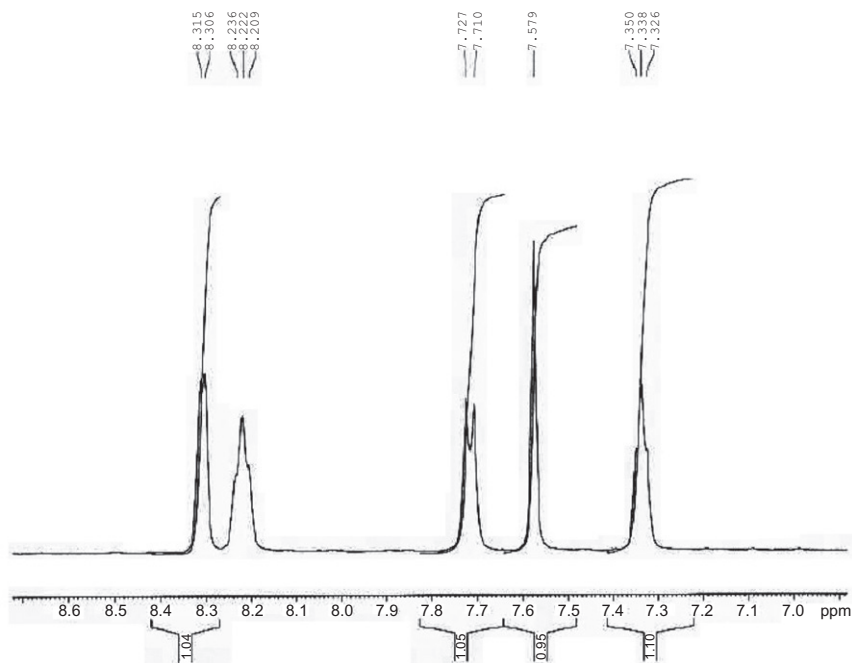


FIGURE 6.10 Expanded proton NMR spectrum of lornoxicam in DMSO- $d_6$ .

## 5. METHODS OF ANALYSIS

### 5.1. Spectrophotometric methods

Hasan *et al.* [21] reported stability indicating methods for the determination of lornoxicam in presence of its acid-induced degradation products. The first method utilized zero-order spectrophotometry at 380 nm. The second method is a densitometric one, after separation on silica gel plate using chloroform: methanol (95:5, v/v) as mobile phase and the spots were scanned at 380 nm. These methods are suitable as stability indicating methods for the simultaneous determination of lornoxicam in presence of its acid-induced degradates in bulk powder or in pharmaceutical formulations.

Nemutlu *et al.* [22,23] reported the determination of lornoxicam in pharmaceutical preparations by using spectrophotometric and chromatographic methods. Derivative UV spectrum of lornoxicam was used to resolve overlapping bands at 258 and 288 nm and to increase the linearity range of calibration curve. A good resolution and sensitivity for lornoxicam was observed with the first-order derivative spectrophotometry.

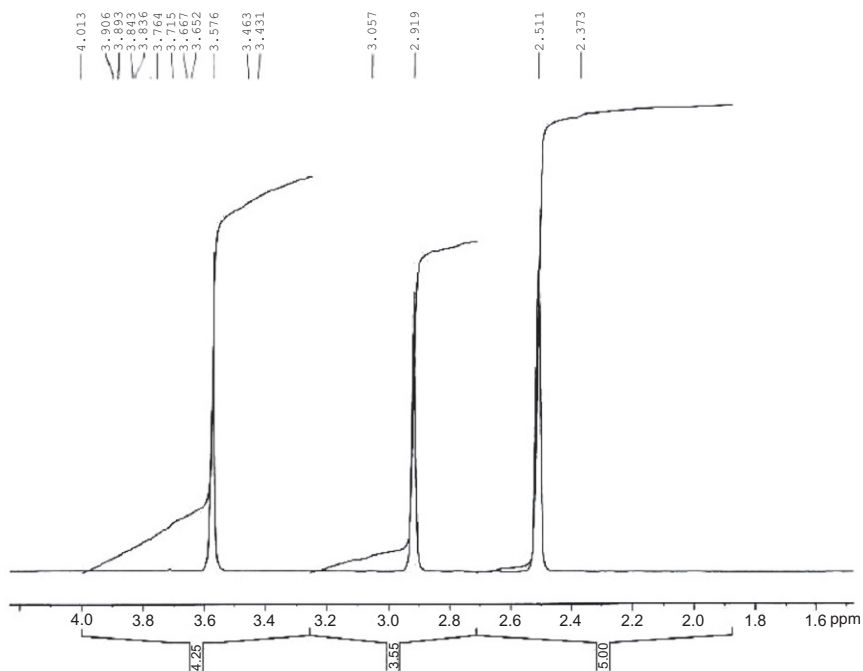
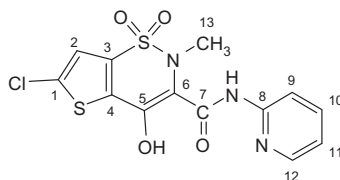
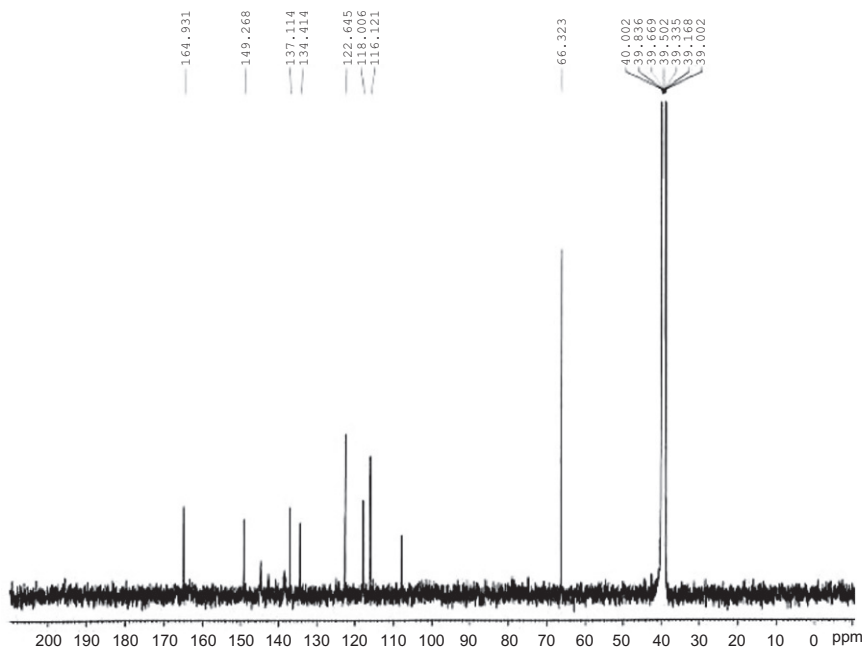


**FIGURE 6.11** Expanded proton NMR spectrum of lornoxicam in DMSO- $d_6$ .

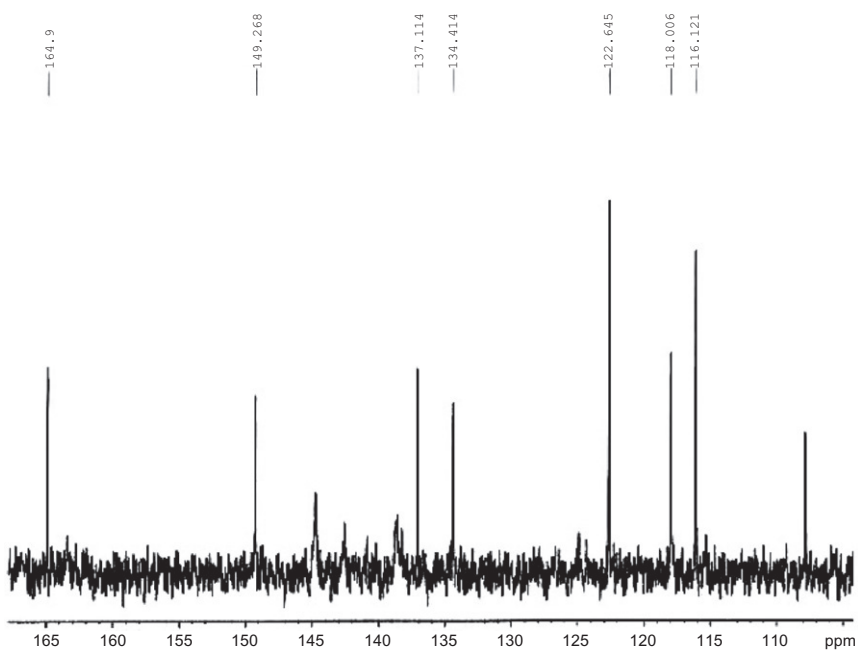
**TABLE 6.6** Assignments of the resonance bands in the  $^1\text{H}$  NMR spectrum of lornoxicam



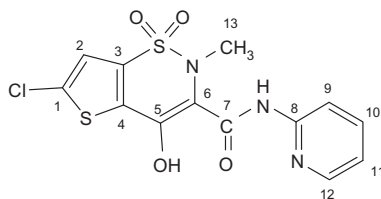
Chemical shift (ppm relative to TMS)	Number of protons	Multiplicity: s, singlet; d, doublet; t, triplet	Assignment (proton at carbon number).
2.92	3	s	13
7.33–7.35	1	t	11
7.58	1	s	2
7.71–7.73	1	d	9
8.21–8.23	1	t	10
8.31–8.32	1	d	12
14.10–14.11	1	s	NH



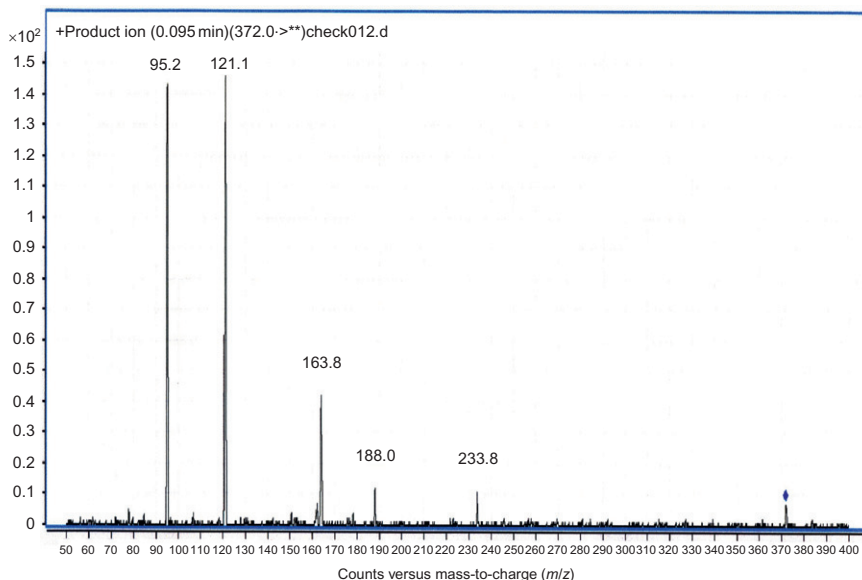
**FIGURE 6.12** Carbon-13 NMR spectrum of lornoxicam in  $\text{DMSO-}d_6$ .



**FIGURE 6.13** Expanded carbon-13 NMR spectrum of lornoxicam in  $\text{DMSO-}d_6$ .

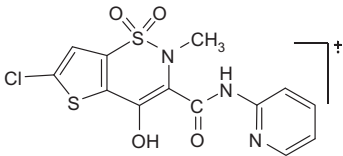
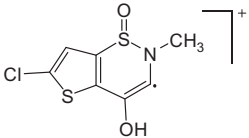
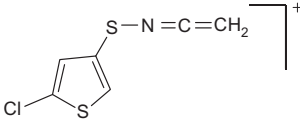
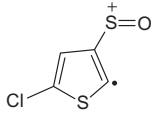
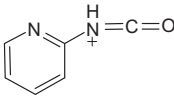
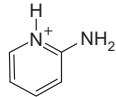
**TABLE 6.7** Assignments of the resonance bands in the  $^{13}\text{C}$  NMR spectrum of lornoxicam

Chemical shift (ppm relative to TMS)	Assignments
66.32	13
164.93	7
108–149	Aromatic and quaternary carbon atoms

**FIGURE 6.14** Mass spectrum of lornoxicam.

In the first spectrophotometric method [22] the measurements were carried out using an Agilent 8453 model UV–Vis spectrophotometer with a DAD. The spectra were recorded from 225 to 475 nm. The quantitative analysis was performed at 376 nm for the zero-order derivative UV spectrophotometric method by measuring the height of the peak from zero and at 302 nm, and 281 nm for the first-order derivative UV

**TABLE 6.8** Mass spectral fragmentation patterns of lornoxicam

<i>m/z</i>	Relative intensity (%)	Fragment	
		Formula	Structure
372	5	$\text{MH}^+$ $\text{C}_{13}\text{H}_{10}\text{ClN}_3\text{O}_4\text{S}_2$	
234	8	$\text{C}_7\text{H}_5\text{ClNO}_2\text{S}_2$	
188	9	$\text{C}_6\text{H}_3\text{ClS}_2\text{N}$	
164	31	$\text{C}_4\text{H}_1\text{ClS}_2\text{O}$	
121	100	$\text{C}_6\text{H}_5\text{N}_2\text{O}$	
95	97	$\text{C}_5\text{H}_7\text{N}_2$	

spectrophotometric method by measuring the height of peak to peak. The method was used for analysis of tablets and injections and the method is simple, fast, and applicable over a wide concentrations range with high

precision and accuracy. In the second spectrophotometric method [23], the solutions of the standard and the pharmaceutical samples were prepared in 0.05 N sodium hydroxide. Absorbances of lornoxicam were measured at 376 nm for the zero-order by measuring height of peak from zero and at 281 nm, and 302 nm for the first-order derivative spectrophotometric method by measuring peak to peak height. The linearity ranges were 0.5–35 µg/ml for the zero-order and 0.2–75 µg/ml for the first-order derivative UV spectrophotometric method. The methods were validated and applied to the determination of lornoxicam in pharmaceutical preparations (tablets and injections), both containing 8 mg of lornoxicam. The methods were accurate, sensitive, precise, robust, rugged, and useful for the quality control of lornoxicam in pharmaceutical preparations.

Abdel-Wadood [24] developed a sensitive and selective spectrofluorimetric method for the determination of lornoxicam and two other oximecams after their complete oxidative acid hydrolysis to 2-aminopyridine. The product, 2-aminopyridine, exhibits fluorescence emission at 365 nm (excitation at 305 nm). The optimal conditions of the reaction were investigated. The method was linear in the linear in the ranges of (0.060–0.2 µg/ml) for lornoxicam. The method was applied to the determination of the drugs in different dosage forms with a recovery percentages ranged 96.82–102.79 ± 0.614–2.578. The method was also applied for the determination of the drugs in spiked urine with recovery percentages ranged 80.51–105.35 ± 1.067–5.338. The validity of the method was assessed according to the USP guidelines. The method is accurate and precise according to statistical analysis.

Taha *et al.* [25] developed two sensitive and selective spectrofluorimetric and spectrophotometric stability indicating methods for the determination of lornoxicam after complete alkaline hydrolysis. The methods are based on derivatization of alkaline hydrolytic product with 7-chloro-4-nitrobenz-2-oxa-1,3-diazole. The products showed an absorption maximum at 460 nm for the drug and fluorescence emission peak at 535 nm in methanol. The color was stable for at least 48 h. The optimum conditions of the reaction were investigated and it was found that the reaction proceeds quantitatively at pH 8, after heating in a boiling water bath for 30 min. The methods were linear in the range of 1–10 µg/ml for lornoxicam for the spectrofluorimetric method, while 0.05–1 µg/ml for lornoxicam for the spectrophotometric method. The validity of the methods was assessed according to the USP guidelines. Statistical analysis of the results revealed high accuracy and good precision. The procedures could be used for the determination of the drug in pure and in dosage forms as well as in the presence of the degradation of the drug.

Lakshmi *et al.* [26] developed two new simple, accurate, and economic spectrophotometric methods, in the UV/Vis region, for the determination of paracetamol and lornoxicam in bulk and in tablet formulations.



Quantitation was carried out by the simultaneous equation (Method 1) and the absorbance ratio (Method 2). The wavelengths selected for Method 1 were 257.10 and 288.66 nm of both drugs, respectively. In Method 2, two wavelengths 257.10 nm of paracetamol and 284.36 nm, the isobestic point, were selected. Both the methods were validated for linearity, accuracy, and precision.

Bhavsar *et al.* [27] developed and validated a simple and sensitive spectrophotometric method for the simultaneous determination of paracetamol and lornoxicam in a binary mixture. The absorbances were measured at 257 and at 287 nm corresponding to the absorbance maxima of paracetamol and lornoxicam in 0.1 N sodium hydroxide, respectively. Linearity range was observed in the concentration range of 5–30 µg/ml for paracetamol and 2–10 µg/ml for lornoxicam. Concentration of each drug was obtained by using the absorptivity values calculated for both drugs at two wavelengths, 257 and 287 nm and solving the simultaneous equation. The method was applied to laboratory mixture and its marketed formulation. The method was validated statistically and recovery study was performed to confirm the accuracy of the method.

Venumadhav *et al.* [28] described two simple and sensitive visible spectrophotometric methods for the determination of lornoxicam in bulk and pharmaceutical dosage form. Method 1 is based on oxidation of the drug with ferric chloride and subsequent complexation of Fe(II) with 2,2'-bipyridine to form a blood red colored species (520 nm). Method 2 is based on oxidation of the drug with ferric chloride and chelation of Fe (II) with bathophenanthroline to produce a blue colored chromogen (610 nm). These two methods were extended to the analysis of pharmaceutical formulations and results compared with the reference method.

## 5.2. Polarographic methods

Cetin *et al.* [29] proposed a simple, precise, fast, and low-cost differential pulse (DP) polarographic method for the determination of lornoxicam in pharmaceutical formulations. Results have been compared with those of high-performance liquid chromatographic (HPLC) method. Mean values and standard deviations calculated by 10 determinations were  $8.10 \pm 0.12$  mg for DP polarography and six determinations were  $8.02 \pm 0.08$  mg for HPLC method. The statistical evaluations indicated that there was no significant difference between the mean values and precessions of the two methods at 95% confidence level ( $t = 2.64$ ,  $F = 2.25$ ).

Ghoneim *et al.* [30] used a square-wave (SW) adsorptive stripping voltammetric method for the determination of lornoxicam in spiked serum samples. A SW measurement following an accumulation time of more than 5 s in a solution containing serum led to reductive peaks with a

significant depression of their heights compared with a measurement performed without accumulation. This might, in part, be due to desorption of the drug; the other part may be attributed to adsorbing substances, competing with lornoxicam for the adsorption sites at the electrode surface. Direct-current measurements, that is, SW voltammetry without accumulation, were preferable in such analysis. The peak current was linearly related to the lornoxicam concentration over the range  $5 \times 10^{-10}$ – $1.85 \times 10^{-8}$  in the voltammetric cell ( $\sim 25$ – $1025$  ng/ml serum in the original samples) according to the equation:  $i_p$  ( $\mu\text{A}$ ) =  $0.564 + 0.135 C$  (nM),  $r = 0.9994\%$ . The estimated detection limit was  $1 \times 10^{-10}$  M corresponding to  $5.4$  ng of lornoxicam/ml of serum. The average recoveries of lornoxicam were more than  $95\%$  with a coefficient of variation of less than  $3\%$ . The method permits rapid determination of lornoxicam with relatively inexpensive instrumentation. No manipulation of the serum sample other than protein precipitation by hydrochloric acid, which was used as supporting electrolyte was required. The method is suitable for serum level monitoring in clinical practice and pharmacological studies.

Bozal and Uslu [31] developed and evaluated a simple, reliable, and selective DP and SW voltammetric methods at glassy carbon and boron-doped diamond electrodes of lornoxicam in pharmaceutical dosage form and in spiked human serum samples. The voltammetric study of the model compounds allowed elucidating the possible oxidation mechanism of lornoxicam. The dependence of the peak current and peak potentials on pH, concentration, nature of the buffer, and scan rate were investigated. The oxidation of lornoxicam gave a single and irreversible peak at both electrodes. The process was diffusion controlled. For glassy carbon electrode, the linearity of the calibration curve was obtained in range of  $4 \times 10^{-7}$  and  $2 \times 10^{-5}$  M for differential pulse voltammetry (DPV) method and  $4 \times 10^{-7}$ – $4 \times 10^{-5}$  M for square wave voltammetry (SWV) method in  $0.1$  M sulphuric acid solutions. Using boron-doped diamond electrode, the plot of the calibration curve was linear between  $6 \times 10^{-7}$  and  $1 \times 10^{-4}$  M for both voltammetric methods in pH 2 BR buffer. The repeatability, reproducibility, precision, and accuracy of the methods were investigated.

### 5.3. Chromatographic methods

#### 5.3.1. Thin-layer chromatography

Taha *et al.* [32] developed a sensitive and selective thin-layer chromatographic method for the determination of lornoxicam and other oxims in the presence of their alkaline degradation products. The method is based on the thin-layer chromatographic separation of the drugs from their alkaline degradation products, followed by densitometric measurement of the intact drug spots for lornoxicam at  $380$  nm. The developing systems used for separation are ethyl acetate–methanol– $26\%$  ammonia

(17:3:0.35) for lornoxicam. The linear range was 0.25–6  $\mu\text{g}/\text{spot}$  with mean recovery of  $99.8 \pm 1.32\%$  for lornoxicam.

Patel and Patel [33] established and validated a simple, rapid, and accurate high-performance thin-layer chromatographic method for the simultaneous determination of paracetamol and lornoxicam in tablets. The method is based on the HPTLC separation of the drugs followed by densitometric measurements of their spots at 270 nm. The separation was carried out on Merck TLC aluminum sheets of silica gel 60<sub>F-254</sub> using ethyl acetate–methanol:toluene:glacial acetic acid (7:2.5:1:0.5) as a mobile phase. Calibration curves were linear in range of 200–1200 and 100–600 ng/spot for paracetamol and lornoxicam, respectively. The method was applied to tablet formulation. No chromatographic interferences from the tablet excipients were found. The method was validated in accordance with the requirements of ICH guidelines.

### 5.3.2. High-performance liquid chromatography

Nemutlu *et al.* [22] determined lornoxicam in pharmaceutical preparations by a liquid chromatographic method. The separation was achieved on a reversed phase (Nucleosil 100-5 C<sub>18</sub> 25 cm  $\times$  4.6 mm, 5  $\mu\text{m}$ ) column kept at room temperature. The flow rate of mobile phase was 1 ml/min. The mobile phase consisted of 0.1 M phosphate buffer (pH 6)–acetonitrile (60:40) and UV detection at 293 nm. The retention times for the drug and the internal standard, metronidazole, were 5.65 and 3.95 min, respectively. Quantitative analysis of the drug in tablets and injections were performed. The method is fast, simple, inexpensive and applicable over a wide range of concentrations with high precision and accuracy.

Hasan *et al.* [21] developed a reversed-phase HPLC method for the determination of lornoxicam. The method is using acetonitrile: phosphate buffer (pH 6) (50:50, v/v) as mobile phase at a flow rate of 1 ml/min and UV detection at 275 nm. This method is suitable as a stability indicating method for the simultaneous determination of lornoxicam in presence of its acid-induced degradates either in bulk powder or in pharmaceutical formulations.

Suwa *et al.* [34] described a selective and sensitive HPLC method for the simultaneous determination of lornoxicam and its 5'-hydroxy metabolite in human plasma using a coulometric detection. The two analytes and the internal standard are extracted from plasma at pH 4 by liquid–liquid extraction and separated on a C<sub>18</sub> column. Absolute detection limits using 100  $\mu\text{L}$  of plasma are 5 and 10 ng/ml for lornoxicam and 5'-hydroxylornoxicam, respectively. The assay has been applied to samples from clinical studies.

The separation was achieved on a prepacked Sumipax ODS A-212 (5  $\mu\text{m}$ ) column (15 cm  $\times$  6 mm). The mobile phase, 0.05 M potassium dihydrogen phosphate–acetonitrile–methanol (60:23:17) was prepared

daily, degassed and pumped at a flow-rate of 1.5 ml/min. The column temperature was maintained at 35 °C.

Radhofer-Welte and Dittrich [35] described a rapid and sensitive HPLC method for the determination of lornoxicam in plasma samples of humans and laboratory animals. After addition of the internal standard, tenoxicam, the plasma was acidified and extracted by dichloromethane via Extrelut columns or by solid-phase extraction using C<sub>18</sub> columns. After evaporation of the solvent, the separation is performed on a C<sub>18</sub> column in isocratic mode with a mobile phase consisting of 0.1 M phosphate buffer (pH 6)–methanol, and detection at 372 nm. The limit of determination was set to 10 ng/ml using 0.5 ml of sample but can be extended down to 2 ng/ml plasma. Using solid-phase extraction with C<sub>18</sub> columns both lornoxicam and its main metabolite 5'-hydroxylornoxicam can be determined while extraction via Extrelut was used in studies where only lornoxicam was to be determined. The method was used in several thousand samples of pharmacokinetics and bioavailability studies in animals and humans.

Joseph-Charles and Bertucat [36] developed a simple and rapid isocratic HPLC method for the simultaneous analysis of lornoxicam using isoxicam as internal standard. The analyte was chromatographed using a Lichrosphere-RP<sub>18</sub> column, a Tris–acetic acid buffer–tetrabutylammonium reagent–tetrahydrofuran–acetonitrile as the mobile phase, and UV detection at 360 nm. The method was applied to pharmaceutical formulations containing a single active ingredient and was shown to be linear.

Wang [37] described a HPLC method for determination of lornoxicam by optimizing of the major factors. The separation was performed on a Alltima C<sub>18</sub> column. The mobile phase was composed of 0.05 mol/L potassium dihydrogen phosphate including 0.05% tetrabutyl ammonium hydroxide–acetonitrile–methanol (57:33:10), and the flow rate was 1 ml/min. The UV detector was at 264 nm. The method had good linearity within 0.05–0.26 mg/ml and reproducibility (relative standard deviation 0.67%). The method was simple and accurate and can be used for the quality control of lornoxicam.

Wang and Hu [38] used a high-performance chromatographic method for the determination of lornoxicam by optimizing major affecting factors. Separation was performed on an Alltima C<sub>18</sub> column. The mobile phase was composed of pH 6.8, 0.05 mol/L potassium dihydrogen phosphate containing 0.05% triethylamine–acetonitrile–methanol (63:28:9). The detection wavelength was 264 nm. The method was simple and accurate and can be used for quality control of lornoxicam.

Zhang *et al.* [39] established a HPLC method for the determination of lornoxicam injection and its related substances. A Shimadzu VIP–ODS column was used with a mobile phase of 0.05 mol/L sodium acetate

solution (pH 6)–methanol (45–55), at the detection wavelength of 379 nm. The calibration curve was linear in the concentration range of 9.6–22.4 µg/ml ( $r = 0.9999$ ). The average recovery was 100.1–101.1%. The detection limit was 8.13 ng/ml.

Taha *et al.* [32] developed a sensitive and selective liquid chromatographic method for the determination of lornoxicam. The method is based on the liquid chromatographic separation of the drugs from their alkaline degradation products on a reversed-phase  $C_{18}$  column using mobile phase of methanol–acetonitrile–acetate buffer (pH 4.6) (4.5:0.5:5) for lornoxicam. Quantification is achieved by UV detection at 280 nm, based on peak area. The linear range was 0.5–20 µg/ml with mean recoveries of 99.81% for lornoxicam. The methods were validated according to guidelines of ICH. The methods were applied to the determination of the drugs in bulk powder, laboratory prepared mixture containing different percentages of degradation products and pharmaceutical dosage forms.

Zhang *et al.* [40] established a high-performance chromatographic method for the quantitative determination of lornoxicam from film-coated tablets with Shimadzu ODS (4.6 mm × 15 cm, 5 µm) column. The mobile phase was composed of sodium acetate (0.05 mol/L, pH 5.8) and methanol (55:45) and the detection wavelength at 379 nm. The dissolution tests were performed according to China Pharmacopoeia 2000 dissolution test app III. The linearity range was 9.72–22.68 mg/L ( $r = 0.9999$ ), and the linear equation was  $C = 9.5628 \times 105A + 0.1005$ . The precision of the method was 0.67%. The mean recovery of three dosage groups was 99.68% (RSD 0.48%), 100.5% (RSD 0.39%), and 100.3% (RSD 0.69%), respectively. Rapid dissolution of lornoxicam from three batches of film-coated tablets was observed. The method with good specificity can be used for the accurate dissolution determination of lornoxicam film-coated tablets.

Bhavsar *et al.* [41] developed a reversed-phase high-pressure liquid chromatographic method for the simultaneous determination of lornoxicam from tablets by reverse phase  $C_{18}$  column (Intersil ODS 3 V  $C_{18}$ , 25 cm × 4.6 mm, 5 µm). The sample was analyzed using buffer (5.7606 gm ammonium dihydrogen phosphate in 2000 ml of milli-Q water, adjust pH 7.3 with triethylamine):methanol (45:55), as a mobile phase at a flow rate of 1.5 ml/min and detection at 290 nm. The retention time for lornoxicam was 9.4 min. the method can be used for the estimation of combination of drugs in tablets. The method was validated as per ICH guidelines. The linearity of the method was achieved in the range of 0.24–120 µg/ml ( $r^2 = 0.9999$ ) for lornoxicam and recovery from tablet was between 100% and 102%. The method can be used for routine quality control analysis of the drug in combined dosage forms.

Nakamura *et al.* [42] developed a simple and rapid semi-micro column HPLC method with UV detection for the simultaneous determination of lornoxicam and other oxicams in human blood samples. The drugs including isoxicam as an internal standard were extracted from buffered plasma samples (pH 3) with dichloromethane and the resulting extracts were subjected to HPLC analysis. The separation was performed with a C<sub>18</sub> reversed-phase semi-micro column (25 cm × 1.5 mm, 5 µm) at 35 °C. The mobile phase used was a mixture of acetonitrile–0.1 M acetate buffer (pH 5)–methanol, and the detection wavelength was set at 365 nm. The drugs were separated within 30 min without interference by the blood components. The detection limits of lornoxicam were 6.4 ng/ml in serum and 9.3 ng/ml in plasma at a signal-to-noise ratio of 3. The method was applied to the determination of lornoxicam in the sera of the patients.

Zhang *et al.* [43] developed and validated a stability indicating HPLC method for the determination of lornoxicam in pharmaceutical formulation. The isocratic procedure was performed in Shimadzu ODS (4.6 mm × 15 cm, 5 µm) column maintained at 25 °C. The mobile phase was degassed mixture of sodium acetate (0.05 mol/L, pH 5.8) and methanol (55:45). The flow rate was 1 ml/min and detection at 290 nm. Selectivity, specificity, linearity, precision, accuracy, and robustness were evaluated to validate the analytical method. Forced degradation studies were performed to provide an indication of the stability-indicating capacity. The stability indicating method for lornoxicam in the injectable dosage was developed and validated. The method can be considered for routine analysis and quality control of lornoxicam in injectable formulation.

Attimarad [44] developed a reversed-phase HPLC method for the determination of lornoxicam in bulk and pharmaceutical preparation. Separation was performed on an Eclipse C<sub>18</sub> column (15 cm × 4.6 mm, µm) as stationary phase and mobile phase used is methanol:0.1% formic acid in water (80:20), with a flow rate of 0.8 ml/min and UV detection at 381 nm. The method was validated for linearity, accuracy, precision, limit of detection, and limit of quantitation. Linearity, accuracy, and precision were found to be acceptable over the range 0.5–20 µg/ml. The method can be adopted for routine quality control analysis of lornoxicam.

Al-Qahtani [45] developed a simple and sensitive HPLC method of analysis of lornoxicam diffused from transdermal drug delivery system through rabbit skin [32], using Shimadzu HPLC system. The mobile phase consists of 60% of aqueous phosphate buffer and 40% methanol and the pH adjusted to 7.0 by addition of few drops of sodium hydroxide.

Patil *et al.* [46] developed a simple, rapid, and precise stability-indicating liquid chromatographic method for analysis of lornoxicam in pharmaceutical dosage forms. Chromatographic separation of drug and its degradation products was achieved on a C<sub>18</sub> analytical column with

0.05% (v/v) aqueous trifluoroacetic acid–acetonitrile, 70:30 (v/v), as mobile phase. The flow rate was 1 ml/min, the column temperature 30 °C, and detection was by absorption at 295 nm using a photodiode-array detector. Lornoxicam was exposed to thermal, photolytic, hydrolytic, and oxidative stress, and the stressed samples were analyzed by use of the method. Peak homogeneity data for Lornoxicam in the chromatograms from the stressed samples, obtained by use of the photodiode-array detector, demonstrated the specificity of the method for analysis of lornoxicam in the presence of the degradation products. The linearity of the method was excellent over the range 10–200 µg/ml lornoxicam ( $r = 0.9999$ ). Relative standard deviations of peak areas from six measurements were always less than 2%. The method was found to be suitable and accurate for quantitative analysis of lornoxicam and study of its stability.

### 5.3.3. High-performance liquid chromatography-mass spectrometry

Zeng *et al.* [47] developed a sensitive and specific LC/MS/MS method for the determination of lornoxicam in human plasma and investigated the pharmacokinetics of a single dose of lornoxicam in healthy Chinese volunteers. Lornoxicam and the internal standard piroxicam were extracted from plasma using liquid–liquid extraction and separated on a Zorbax XDB-C<sub>8</sub> column. The mobile phase consisted of methanol–water–formic acid (80:20:0.5) at a flow rate of 0.7 ml/min. A Finnigan TSQ tandem mass spectrometer equipped with atmospheric pressure chemical ionization source was used as detector and operated in the positive ion mode. Selected reaction monitoring using the precursor → product ion combinations of  $m/z$  372 → 121 and  $m/z$  332 → 121 was used to quantify lornoxicam and internal standard, respectively. The linear calibration curves were obtained in the concentration range of 2–1600 µg/L. The limit of quantification was 2 µg/L. The method was used in pharmacokinetic study of lornoxicam. The method is suitable for clinical investigation of lornoxicam pharmacokinetics which offers advantages of specificity, speed, and high sensitivity over the other methods.

Kim *et al.* [48] developed a rapid, sensitive, and selective LC-ESI-MS/MS method for the determination of lornoxicam in human plasma. Lornoxicam and isoxicam (internal standard) were extracted from human plasma with ethyl acetate at acidic pH and analyzed on a Sunfire C<sub>18</sub> column with the mobile phase of methanol–ammonium formate (10 mM, pH 3) (70:30). The analyte was detected using a mass spectrometer, equipped with electrospray ion source. The instrument was set in the multiple-reaction-monitoring mode. The standard curve was linear ( $r = 0.9998$ ) over the concentration range of 0.5–500 ng/ml. The coefficient of variation and relative error for the intra- and inter-assay at four QC level were 0.7% to –4.2% and –4.5% to 5%, respectively. The recoveries of



lornoxicam and isoxicam were 87.8% and 66.5%, respectively. The lower limit of quantification for lornoxicam was 0.5 ng/ml using a 200  $\mu$ L plasma sample. The method was applied to pharmacokinetic study of lornoxicam after oral administration of lornoxicam (8 mg) to humans.

Lei *et al.* [49] established a selective and sensitive liquid chromatography-mass spectrometry/mass spectrometric method for the concentration determination of plasma lornoxicam and study the pharmacokinetics of the drug in three formulations of healthy volunteers. Twenty-four healthy male Chinese volunteers with three-way crossover design of a 7-day washout period were randomized to receive a single 8 mg dose of lornoxicam rapid release tablets or conventional regular release tablets orally, or 8 mg lornoxicam injection with intramuscular injection at the buttock. The plasma concentrations of lornoxicam were determined through validated liquid chromatography-mass chromatography/mass chromatographic method. Results have indicated that the test method for lornoxicam sample of human plasma is specific, sensitive and accurate and the lornoxicam release tablets is bioequivalent with the lornoxicam injection with further improvement of patient compliance.

Cetin *et al.* [29] used a HPLC method for the determination of lornoxicam. The measurements were made by using Perkin Elmer 200 Series with UV detector. C<sub>18</sub> column was used as an analytical column and analysis were detected at 364 nm. The mobile phase was methanol: acetonitrile and aqueous solution of diammonium hydrogen phosphate. Retention time of lornoxicam was 1.87 min. The drug was separated on C<sub>18</sub> column (ODS Hypersil 5  $\mu$ m 25 cm  $\times$  4.6 mm) with a flow rate of 1.6 ml/min. The linear calibration range was found to be 1–30  $\mu$ g/ml.

## 6. MECHANISM OF ACTION

Lornoxicam is a nonsteroidal anti-inflammatory drug with analgesic properties and it belongs to the class of oxicams. Lornoxicam is a potent inhibitor of both COX-1 and COX-2 enzymes. The mechanism of the analgesic action is related to the inhibition of cyclooxygenase, which suppresses the production of prostaglandins and thromboxanes thereby reducing pain and inflammation. The analgesic activity is related to balanced inhibition of COX-1 and COX-2 and release endogenous dynorphin and  $\beta$ -endorphin with reported central analgesic activity. The unlike some NSAIDs, the inhibition of cyclooxygenase by lornoxicam does not result in an increase in leukotriene formation, and the shunting of arachidonic acid to the 5-lipoxygenase cascade is therefore not expected, which minimizes the risk of some adverse events, for example, allergic reactions [50–57].



## 7. PHARMACOKINETICS

Lornoxicam is absorbed from gastrointestinal tract and is characterized by a rapid rate. The peak blood concentration is reached after approximately 1–2 h. The absolute bioavailability (calculated as AUC) of XEFO film-coated tablets is 90–100%. Lornoxicam is found in the plasma in unchanged form and as its hydroxylated metabolite. The hydroxylated metabolite exhibits no pharmacological activity. Lornoxicam is metabolized completely, and approximately 2/3 is eliminated via the liver and 1/3 via the kidney as inactive substance. 5-Hydroxylation is the main metabolic pathway, which accounts for up to 95% of total intrinsic lornoxicam clearance, and cytochrome P450 2C9 has been proven to be the primary enzyme involved in the formation of 5-hydroxy lornoxicam *in vitro*. When tested in animal models, lornoxicam did not induce liver enzymes. From clinical trial data showed no evidence of accumulation of lornoxicam after repeated administrations, when given according to a recommended dosage. This finding was supported by drug monitoring data from 1 year studies. Simultaneous intake of lornoxicam with meals reduced  $C_{\max}$  by approximately 30%.  $T_{\max}$  was increased from 1.5 to 2.3 h. The absorption of lornoxicam (calculated as AUC) can be reduced up to 20%. Simultaneous intake with antacids has no effect on the pharmacokinetics of lornoxicam. The bioavailability of lornoxicam after oral application is more than 90%. Maximum plasma concentrations are achieved after about 2 h. Lornoxicam is found in the plasma in unchanged form and as its hydroxylated form. The hydroxylated metabolite exhibits no pharmacological activity. Given normal liver and kidney function, the plasma half-life is about 4 h. It readily penetrates into synovial fluid, the proposed site of action in chronic inflammatory arthropathies. In elderly patients, the clearance of lornoxicam is reduced by about 30–40%; thus, the half-life is somewhat longer. Even in the presence of impaired kidney and liver function, no major differences in pharmacokinetics have been observed. On account of its short half-life, no accumulation is likely to occur even in cases of repeated administration. Like other oxicams and diclofenac, lornoxicam is metabolized via cytochrome P450 2C9. Due to a genetic polymorphism, some individuals may metabolize slowly and, therefore, have elevated level of lornoxicam. The maximum therapeutic blood level that elicit analgesic activity reported 1  $\mu\text{g/ml}$ . After administration of lornoxicam 4 mg tablets to healthy volunteers, mean peak serum concentrations of 300–360 ng/ml were obtained after 1.6–3 h. There is no evidence of accumulation or elimination rate changes with repeated-dose administration [50–57].

## 8. REVIEWS

Starek and Krzek [58] reviewed the analytical techniques for the determination of oxicams, nimesulide, and nabumetone. The review covers the time period from 1990 to 2008 during which numerous analytical methods including all types of chromatographic, spectrophotometric, and voltammetric techniques were reported. In this review, bibliography data indicate that the liquid chromatography methods with UV [32,35,36,42], coulometric [34], or mass detection [47] have been used for the determination of lornoxicam. Spectrophotometric methods in Vis and TLC densitometric method with detection at 380 nm [32]. Zero and first-order derivatives in ultraviolet [23] and SW adsorptive stripping voltammetry method [30]. General review and reviews on pharmacology, and pharmacokinetics are also reported [53,54,59,60].

## 9. STABILITY

Radhofer-Welte and Dittrich [35] reported that blank human plasma was spiked with lornoxicam (20–1000 ng/ml) and 5'-hydroxylornoxicam (20–100 ng/ml) and analyzed immediately after preparation and storage at  $-20^{\circ}\text{C}$  for 2.5–5 months were found to be stable. Lornoxicam is highly unstable in solution showing rapid oxidation and hydrolytic cleavage, leading to the formation of a large number of degradation products within weeks, on standing at room temperature [61]. The stability of lornoxicam for injection in 0.9% sodium chloride injection prepared according to clinical regime showed that no significant change in 72 h [62].

## ACKNOWLEDGMENT

The authors wish to thank Mr. Tanvir A. Butt, Department of Pharmaceutical Chemistry, College of Pharmacy, King Saud University for his secretarial assistance in typing the chapter.

## REFERENCES

- [1] M.J. O'Neil (Ed.), The Merck Index, 14th ed., Merck & Co. Inc., Whitehouse Station, NJ, USA, 2006, p. 967.
- [2] S. Sweetman (Ed.), The Complete Drug Reference, Pharmaceutical Press, London, 2007 Electronic Version.
- [3] H. Berry, H.A. Bird, C. Black, D.R. Blake, A.M. Freeman, D.N. Golding, et al., *Ann. Rheum. Dis.* 51 (1992) 238–241.
- [4] I. Caruso, F. Montrone, L. Boari, C. Davoli, N.B. Beyene, R. Caporali, et al., *Adv. Ther.* 11 (1994) 132–138.

- [5] R.M. Bernstein, H.J. Calin, A. Calin, S. Ollier, Eur. J. Rheumatol. Inflamm. 12 (1992) 6–13.
- [6] B. Kidd, W.A. Frenzel, J. Rheumatol. 23 (1996) 1605–1611.
- [7] H. Staunstrup, J. Ovesen, U.T. Larsen, K. Elbaek, U. Larsen, K. Kroner, J. Clin. Pharmacol. 39 (1999) 834–841.
- [8] R. Pfister, P. Zeller, D. Binder, O. Hromatka (F. Hoffmann-La Roche AG) Thiazine Derivatives DE 2838851.
- [9] A. Galani, M.A. Demertzis, M. Kubicki, D. Kovala-Demertzi, Eur. J. Inorg. Chem. (2003) 1761–1767.
- [10] A.W. Addison, T.N. Rao, J. Reedijk, J. Van Rijn, G.C. Verschoor, J. Chem. Soc., Dalton Trans. (1984) 1349–1356.
- [11] T. Steiner, M. Tamm, A. Grzegorzewski, N. Schulte, N. Veldman, A.M.M. Schreurs, et al., J. Chem. Soc., Perkin Trans. 2 (1996) 2441.
- [12] T. Steiner, B. Lutz, J. van der Maas, A.M.M. Schreurs, J. Kroon, M. Tamm, Chem. Commun. 171 (1998).
- [13] M.C. Etter, Acc. Chem. Res. 23 (1990) 120.
- [14] *CrysAlisRed v. 162*, KUMA Diffraction, Wroclaw, Poland (2000).
- [15] R.H. Blessing, J. Appl. Crystallogr. 22 (1989) 396.
- [16] G.M. Sheldrick, Acta Crystallogr., Sect. A 46 (1990) 467.
- [17] G.M. Sheldrick, SHELXL-97, Program for the Refinement of Crystal Structures, (1997) University of Göttingen, Germany.
- [18] Hyperchem, Release 6.01 for Windows, Molecular Modeling System, 2000 Hypercube, Inc.
- [19] C. Mealli, D. Proserpio, CACAO PC Beta-Version 5, 1998.
- [20] C. Mealli, D. Proserpio, J. Chem. Educ. 11 (1990) 440.
- [21] N.Y. Hasan, M.A. Elkawy, B.E. Elzeany, N.E. Wagieh, Bull. Fac. Pharm. Cairo Univ. 42 (2004) 1–10.
- [22] E. Nemutlu, S. Demircan, S. Kır, Adnan Menderes University, 4th AACD Congress, 29 Sept-3 Oct. 2004, Kuşadası-Aydın/Turkey Proceedings Book. 069.DOC.
- [23] E. Nemutlu, S. Demircan, S. Kır, Farmazie 60 (2005) 421–425.
- [24] H.M. Abdel-Wadood, Bull. Pharm. Sci. 31 (2008) 169–181 Assiut, University.
- [25] E.A. Taha, N.N. Salama, L.E. Abdel-Fattah, Chem. Pharm. Bull. 54 (2006) 653–658.
- [26] S. Lakshmi, K.S. Lakshmi, T. Tintu, Int. J. Pharm. Pharm. Sci. 2 (2010) 166–168.
- [27] K.C. Bhavsar, P.D. Gaikwad, V.H. Bankar, S.P. Pawar, Int. J. Pharm. Technol. 2 (2010) 429–439.
- [28] E. Venumadhav, T. Neeha, P. Bhargavi, A. Nishat, A. Swetha, G.D. Rao, Int. J. Pharm. Biol. Sci. 1 (2010) 491–494.
- [29] I. Cetin, N. Kocak, S. Aycan, C.B.U. J. Sci. 5.1 (2009) 11–18.
- [30] M.M. Ghoneim, A.M. Beltagi, A. Radi, Anal. Sci. 18 (2002) 183–186.
- [31] B. Bozal, B. Uslu, Comb. Chem. High Throughput Screen. 13 (2010) 599–609.
- [32] E.A. Taha, N.N. Salama, L.E. Abdel Fattah, J. AOAC 87 (2004) 366–373.
- [33] D.J. Patel, V.P. Patel, Int. J. Chem. Tech. Res. 2 (2010) 1929–1932.
- [34] T. Suwa, H. Urano, Y. Shinohara, J. Kokastu, J. Chromatogr. B Biomed. Appl. 617 (1993) 105–110.
- [35] S. Radhofer-Welte, P. Dittrich, J. Chromatogr. B 707 (1998) 151–159.
- [36] J. Joseph-Charles, M. Bertucat, J. Liq. Chrom. Relat. Technol. 22 (1999) 2009–2021.
- [37] J. Wang, X. Hu, Zhongguo Yiyao Gongye Zhi 37 (2002) 54–56.
- [38] J. Wang, Yaowu Fenxi Zazhi 21 (2001) 389–392.
- [39] J. Zhang, Y. Gao, W. Fan, Zhongguo Yiyao Gongye Zhi 35 (2004) 427–428.
- [40] J. Zhang, Y. Gao, W. Fan, B. Ren, Zhongguo Yiyuan Yaoxue Zazhi 25 (2005) 447–448.
- [41] S.M. Bhavsar, D.M. Patel, A.P. Khandhar, C.N. Patel, J. Chem. Pharm. Res. 2 (2010) 563–572.

- [42] A. Nakamura, M.N. Nakashima, M. Wada, K. Nakashima, *Bunseki Kagaku* 54 (2005) 755–760.
- [43] J.J. Zhang, Y. Goa, W.M. Fan, B.J. Ren, Q.N. Ping, *J. AAPS* 63 (2004) 285–290. [http://www.aapsj.org/abstracts/AM\\_2004/AAPS2004-000063.PDF](http://www.aapsj.org/abstracts/AM_2004/AAPS2004-000063.PDF), Online.
- [44] M. Attimarad, *J. Basic Clin. Pharm.* 1 (2010) 115–118.
- [45] F.M. Al-Qahtani, Master thesis, King Saud University, Riyadh, SA, 2010.
- [46] K.R. Patil, V.P. Rane, J.N. Sangshetti, D.B. Shinde, *Chromatographia* 69 (2009) 1001–1005.
- [47] Y. Zeng, X. Chen, Y. Zhang, D. Zhong, *Yaoxue Xuebao* 39 (2004) 132–135.
- [48] Y.H. Kim, H.Y. Ji, E.S. Park, S.W. Chae, H.S. Lee, *Arch. Pharm. Res.* 30 (2007) 905–910.
- [49] M. Lei, T.J. Hang, M. Song, P. Ge, L.J. Qu, A.D. Wen, et al., *Chin. J. New Drugs Clin. Remedies* 27 (2008) 20–23.
- [50] W. Kullich, G. Klein, *Aktuel. Rheumatol.* 17 (1992) 128–132.
- [51] G. Hitzenberger, S. Radhofer-Welte, F. Takacs, D. Rosenow, *Postgrad. Med. J.* 66 (Suppl. 4) (1990) S22–S27.
- [52] J. Buritova, J.M. Besson, *Inflamm. Res.* 47 (1998) 18–25.
- [53] J.A. Balfour, A. Fitton, L.B. Barradell, *Drugs* 51 (1996) 639–657.
- [54] T.P. Pruss, H. Stroissnig, S. Radhofer-Welte, W. Wendtlandt, N. Mehdi, F. Takacs, et al., *Postgrad. Med. J.* 66 (Suppl. 4) (1990) S18–S21.
- [55] Y. Zhang, D. Zhong, D. Si, Y. Guo, X. Chen, H. Zhou, *Br. J. Clin. Pharmacol.* 59 (2005) 14–17.
- [56] P. Turner, A. Johnston, *Postgrad. Med. J.* 66 (Suppl. 4) (1990) S28–S29.
- [57] P. Bonnabry, T. Leemann, P. Dayer, *Eur. J. Clin. Pharmacol.* 49 (1996) 305–308.
- [58] M. Starek, J. Krzek, *Talanta* 77 (2009) 925–942.
- [59] P.D.S. Byrav, B. Medhi, A. Brakash, S. Patyar, S. Wadhwa, *IJPMR* 20 (2009) 27–31.
- [60] Anonymous, <http://medi.ru/doc/a7922130.htm>.
- [61] A. Dyer, J. Penkler, *WIPO Patent Appl. WO/1996/041646*.
- [62] W.M. Fan, J.J. Zhang, X.Y. Xu, F. Tao, *Chin. J. Pharm.* 36 (2005) 493–495.

## Magnesium Silicate

**Iyad Rashid,<sup>\*</sup> Nidal H. Daraghmeh,<sup>\*,†</sup>  
 Mahmoud M. Al Omari,<sup>\*</sup> Babur Z. Chowdhry,<sup>†</sup>  
 Stephen A. Leharne,<sup>†</sup> Hamdallah A. Hodali,<sup>‡</sup> and  
 Adnan A. Badwan<sup>\*</sup>**

<b>Contents</b>		
	1. Description	242
	1.1. Nomenclature	242
	1.1.1. Chemical name [1]	242
	1.1.2. Nonproprietary name [2,3]	242
	1.1.3. Proprietary name [1,4]	243
	1.2. Formulae [1,4]	243
	1.2.1. Empirical formula, molecular weight, and CAS number	243
	1.2.2. Structural formula [2,5]	243
	1.2.3. Composition [2,3]	243
	1.3. Appearance [2]	243
	2. Methods of Preparation	244
	2.1. Precipitation method	244
	2.2. Hydrothermal precipitation method [11]	245
	2.3. Mechano-chemical dehydration method [12]	246
	3. Physical Characteristics	247
	3.1. Solubility characteristics	247
	3.2. Hygroscopicity [1]	248
	3.3. pH [14]	248
	3.4. Particle morphology [6]	249
	3.5. Particle size distribution and bulk density [6]	249
	3.6. Specific surface area, pore volume, and pore size	250

<sup>\*</sup> The Jordanian Pharmaceutical Manufacturing Company, Naor, Jordan

<sup>†</sup> School of Science, University of Greenwich, Medway Campus, Central Avenue, Chatham Maritime, Kent, United Kingdom

<sup>‡</sup> Department of Chemistry, Faculty of Science, University of Jordan, Amman, Jordan

3.7. Surface active sites (adsorption and absorption)	250
3.8. Ion exchange capacity [19]	257
3.9. Fourier transform infrared [13,14]	257
3.10. X-Ray powder diffraction [13,14]	258
3.11. Thermal characteristics [13]	258
3.12. <sup>29</sup> Si MASS and ( <sup>1</sup> H– <sup>29</sup> Si) CP-MASS nuclear magnetic resonance [20]	259
3.13. Polymorphic transformation	260
3.14. Modification of structural units [20]	262
3.15. Molecular modeling [19]	266
4. Methods of Analysis	267
4.1. Compendia methods [2,3]	267
4.1.1. USP method of analysis [2]	267
4.1.2. JP method of analysis [3]	270
4.2. Noncompendia methods	273
4.2.1. Analysis of magnesium	273
4.2.2. Analysis of silicate	275
5. Uses	276
5.1. Pharmaceutical	277
5.2. Food	277
5.3. Rubber and silicones [62]	277
5.4. Paints [6]	278
5.5. Chromatography [59,60]	278
5.6. Paper [63]	278
5.7. Insecticide, microbiocide, and fungicide [64]	278
5.8. Cement [65]	278
5.9. Other uses	278
6. Stability and Incompatibilities	279
7. Biodegradability and Toxicity	279
8. Related Substances	281
8.1. Magnesium metasilicate	281
8.2. Magnesium orthosilicate	281
8.3. Magnesium trisilicate hydrate [1]	283
8.4. Hydrated magnesium silicate [80]	283
References	283

## 1. DESCRIPTION

### 1.1. Nomenclature

#### 1.1.1. Chemical name [1]

Silicic acid, magnesium salt

#### 1.1.2. Nonproprietary name [2,3]

United States Pharmacopeia/National Formulary (USP/NF): magnesium silicate

Japanese Pharmacopeia (JP): magnesium silicate

### 1.1.3. Proprietary name [1,4]

Ambosol; Ambosol 500; Avibest; Britesorb; Britesorb 40; Britesorb 90; Celkate T 21; Chooz; Florisil; Gastomag; HS-T; HS-T (silicate); Haiburaito 1250; Haiburaito 325; KW 600S; Kyowaad 600S; Laponite 445; Laponite 508; MP 30-36; Macrosorb M 15; Macrosorb MS 15; Macrosorb MS 33F; Magmasil; Magnesium hydrosilicate; Magnesol; Magnesol R 60; Magnesol XL; Magsil 399; Magsorbent; Mizuka Life P 1G; Mizukanite P 1S; Mizupearl M 302; Naisuton; Nikkagel M; Novasorb; P 1G; Salisil; Sep-Pak Florisil; Shimugon M; Silton SS 1; Tomita AD 600CY; Tri-Sil; Trimax; Trinesium; Trisomin; Westmin 20; E553a

## 1.2. Formulae [1,4]

### 1.2.1. Empirical formula, molecular weight, and CAS number

Empirical formula:  $\text{MgO} \cdot \text{SiO}_2 \cdot n\text{H}_2\text{O}$

Molar mass (anhydrous): 100.39

CAS number: 1343-88-0

### 1.2.2. Structural formula [2,5]

Magnesium silicate is a compound of magnesium oxide (MgO) and silicon dioxide ( $\text{SiO}_2$ ); it is the magnesium salt of silicic acid containing an unspecified amount of water. Many natural silicate minerals are formed under aqueous conditions by reactions that are hypothesized to proceed via “protosilicate” intermediates, gels of hydrated oxides which, in the absence of structural information, have been described as  $x\text{MgO} \cdot y\text{SiO}_2 \cdot z\text{H}_2\text{O}$ . The molecular formula may be expressed as  $\text{MgSiO}_3 \cdot x\text{H}_2\text{O}$  [5], Fig. 7.1.

### 1.2.3. Composition [2,3]

The USP/NF and JP state that the assay of magnesium silicate should be expressed as the percentages of magnesium oxide and silicon dioxide. Table 7.1 shows the acceptance criteria for the content of magnesium silicate, as reported in the USP/NF and JP.

## 1.3. Appearance [2]

Magnesium silicate occurs as a fine, white, odorless, tasteless powder, free from grittiness.

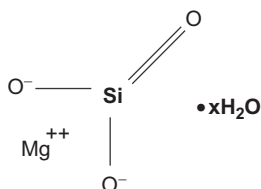


**FIGURE 7.1** A schematic of the structure of magnesium silicate.

**TABLE 7.1** Acceptance criteria of content of magnesium oxide and silicon dioxide in magnesium silicate

Component	Content	
	USP/NF	JP
MgO (%)	$\geq 15.0^a$	$\geq 20.0$
SiO <sub>2</sub> (%)	$\geq 67.0^a$	$\geq 45.0$
MgO (%) / SiO <sub>2</sub> (%)	2.50–4.50 <sup>a</sup>	2.2–2.5

<sup>a</sup> Calculated on the basis of ignition.

## 2. METHODS OF PREPARATION

### 2.1. Precipitation method

The most common route for the synthesis of magnesium silicate is via a precipitation reaction between a soluble metal silicate (e.g., sodium orthosilicate, sodium metasilicate, or potassium silicate) and a soluble magnesium salt (e.g., magnesium sulfate, nitrate, or chloride). The aqueous suspension of the precipitate is filtered and the collected solid is washed and dried (Fig. 7.2) [6,7].

The physical properties and magnesium oxide (MgO) content of the precipitated magnesium silicate depend on the type of magnesium salt, sequence of addition of magnesium salt and metal silicate as well as the nature and concentration of dispersion modifiers (e.g., nonionic surfactants, NaOH), and experimental conditions [6,7].

Regardless of the type of soluble metal silicates used, they are subject to the same molecular speciation in aqueous solution resulting in a mixture of monomeric tetrahedral ions, oligomeric linear or cyclic silicate ions, and polysilicate ions. Sodium metasilicate, an example of a soluble metal silicate, can be prepared in anhydrous form or in the presence of water of crystallization as the penta- or nona-hydrate. It is readily soluble in water [8].



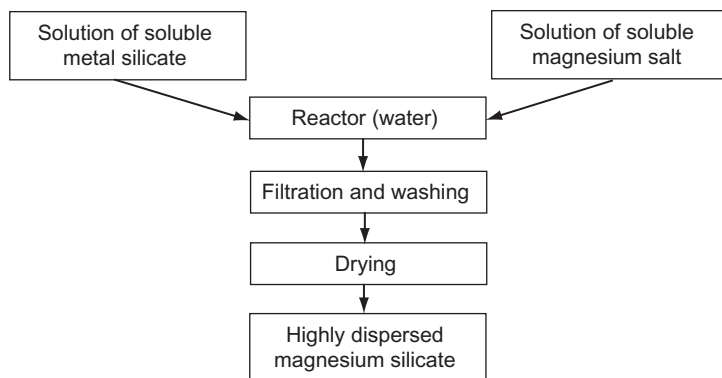
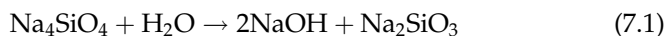
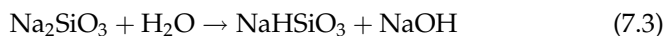
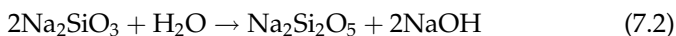


**FIGURE 7.2** Schematic of the synthesis of magnesium silicate via a precipitation reaction.

The dissolution process for sodium silicate consists of its hydration with the formation of NaOH. Sodium orthosilicate hydrolyzes according to Eq. (7.1):



The hydrolytic dissociation is particularly strong with sodium metasilicate (Eqs. (7.2) and (7.3)):



Silicate anions combine with  $\text{Mg}^{2+}$  ions in solution forming low solubility magnesium silicates [9].

The effectiveness of sodium silicate in precipitating  $\text{Mg}^{2+}$  ions, when a bulk solution of magnesium chloride is added to deionized water, is shown in Fig. 7.3; the concentration of  $\text{Mg}^{2+}$  ions decreases rapidly with the addition of sodium silicate [10].

## 2.2. Hydrothermal precipitation method [11]

A hydrothermal solution is a multicomponent system containing compounds of Na, K, Si, Ca, Mg, Al, Fe, Cl, S, O, C, B, Li, As, Cu, Zn, Ag, Au, and other elements in ionic and molecular forms. Silicon has one of the highest concentrations. Silica, together with other compounds, passes into this hydrothermal solution due to the chemical interaction of water with aluminosilicate minerals of rocks of hydrothermal fields at a depth in regions of thermal anomalies at high temperatures and pressures.

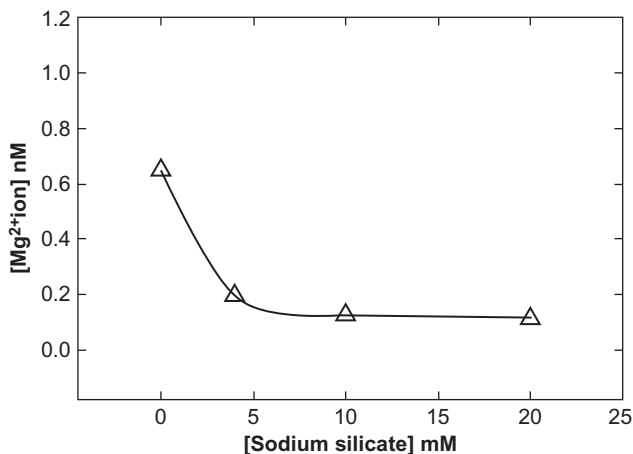


**FIGURE 7.3** Concentration of  $\text{Mg}^{2+}$  ions, in deionized water, as a function of sodium silicate concentration (pH 8.5).

At temperatures of 250–300 °C, silicon occurs in solution predominantly in the form of individual molecules of silicic acid,  $\text{H}_4\text{SiO}_4$ . As a consequence, such an aqueous solution becomes supersaturated with respect to solutions of amorphous silica in pure water. When metal cations (e.g.,  $\text{Ca}^{2+}$ ,  $\text{Mg}^{2+}$ , and  $\text{Co}^{2+}$ ) are introduced into the solution, some of these ions are sorbed by the surface of colloidal particles resulting in neutralization of the negative surface charge. Bridging bonds, with the participation of coagulating ions, are formed between the surfaces of particles, which results in coagulation and precipitation of colloidal silica. It was found that the material precipitated by metal ions has an amorphous structure of metal silicate. After high-temperature calcinations at 900 °C, the amorphous samples prepared upon addition of magnesium sulfate or cobalt sulfate (with simultaneous alkalization to pH 12.4) have a crystalline structure of forsterite ( $\text{Mg}_2\text{SiO}_4$ ) or cobalt silicate ( $\text{Co}_2\text{SiO}_4$ ), respectively.

### 2.3. Mechano-chemical dehydration method [12]

An amorphous phase can be formed as a result of the reaction of amorphous  $\text{SiO}_2$  with magnesium hydroxide. The solid-state reaction between  $\text{Mg}(\text{OH})_2$  and  $\text{SiO}_2$  begins at the contact points between these dissimilar particles. Mechano-chemical dehydration and amorphization of  $\text{Mg}(\text{OH})_2$  are substantially enhanced by grinding with  $\text{SiO}_2$ . Enhanced mechano-chemical dehydration of  $\text{Mg}(\text{OH})_2$  in the mixture is explained by assuming the following complex processes take place: intimate mixing, agglutination at the contact points of dissimilar particles promoted by the higher affinity

of silica over magnesia toward hydroxyl groups, and initiation of simultaneous solid-state reactions. Since magnesium hydroxide is a strong base and silicic acid is a weak acid, acid–base neutralization ensues. A possible reaction mechanism involves the release of excess water from the silicic acid, which makes the surface of the magnesium hydroxide more alkaline. This leads to the dissolution of silica at the contact points, resulting in precipitation of amorphous magnesium silicate. Thus the reaction between the two ingredients and dehydration results in a precursor of magnesium silicate in an amorphous state.

### 3. PHYSICAL CHARACTERISTICS

#### 3.1. Solubility characteristics

Magnesium silicate is practically insoluble in ethanol (95%), ether, and water. It is readily decomposed by mineral acids [1,2].

Table 7.2 shows the total amount of Mg and Si (mg/50 mL) dissolved in various aqueous solutions ( $\text{H}_2\text{O}$ ,  $\text{HNO}_3$ ,  $\text{HCl}$ ,  $\text{H}_3\text{PO}_4$ , and  $\text{NaOH}$ ), which may reflect the solubility of magnesium silicate in these solvents [13]. The experiment was performed by the addition of about 0.5 g of magnesium silicate to 50 mL of solution at room temperature ( $25^\circ\text{C}$ ) followed by incubation for 24 h with intermittent shaking. The total amount of Mg and Si was measured using an ICP<sub>seq</sub>-7500 spectrometer.

Magnesium silicate displays low solubility in acids of up to 3 M concentration; above this concentration it partially dissolves. It is dissociated in acids forming magnesium ions and silicic acid in what is referred to as “acid leaching” of silicates (Eq. (7.4)):

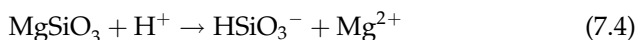
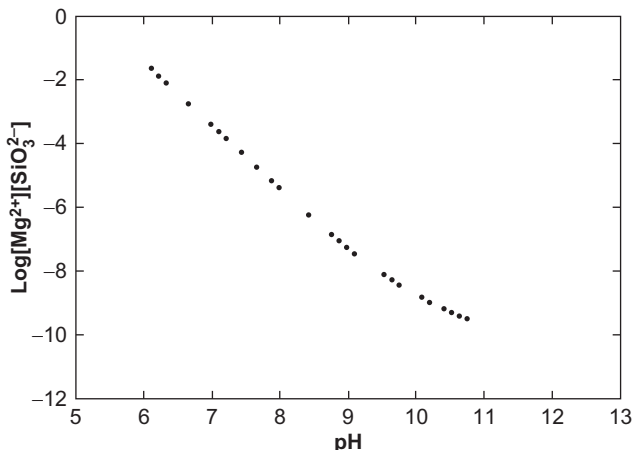


Figure 7.4 shows the conditional solubility product of magnesium silicate as a function of pH (at an initial ion concentration of 1 mM). The region above the curve represents a system of higher concentration

**TABLE 7.2** The total amount of Mg and Si dissolved (mg/50 mL) in various solutions at  $25^\circ\text{C}$

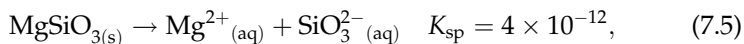
Solvent	$\text{H}_2\text{O}$		$\text{HNO}_3$		$\text{HCl}$		$\text{H}_3\text{PO}_4$		$\text{NaOH}$
Conc. (M)	–	0.1	1.0	3.0	0.1	1.0	3.0	0.1	1.0
Conc. of Mg and Si dissolved in (mg/50 mL)	0.0	5.0	12.0	20	4.0	10.0	16.0	0.0	0.0



**FIGURE 7.4** Conditional solubility product of magnesium silicate (initial ion concentration of 1 mM) as a function of pH.

product where bulk magnesium silicate precipitation is anticipated. The higher the solution pH, the lower the conditional solubility product, and the higher is the propensity for magnesium to be precipitated [10].

Solubility–pH diagrams for  $\text{Mg}^{2+}$ – $\text{SiO}_3^{2-}$  can be constructed to show the relationship between  $\text{Mg}^{2+}$  precipitation and solution pH. For a given solution system, if the magnesium ion concentration is above the solubility product limit, the formation of magnesium silicate is anticipated, and is governed by Eq. (7.5):



where  $K_{sp}$  is the corresponding solubility product constant, which defines the solubility limit [10].

### 3.2. Hygroscopicity [1]

Magnesium silicate is slightly hygroscopic.

### 3.3. pH [14]

According to the USP/NF [2], the pH of magnesium silicate (10% wt/wt aqueous suspension) is 7.0–10.8. The pH of magnesium silicate is controlled by the degree to which magnesium is released from the surface when it comes in contact with water. The basicity of magnesium silicate is mainly attributed to the magnesium oxide present.

### 3.4. Particle morphology [6]

A scanning electron microscope (SEM 515, Philips, The Netherlands) image (SEM) of magnesium silicate prepared from solutions of magnesium sulfate and sodium metasilicate is shown in Fig. 7.5. The SEM image shows the presence of large primary agglomerates and numerous secondary agglomerates. In addition, numerous primary particles of small diameter are observed. Primary particles exhibit a smooth surface and no sharp edges are observed. On the other hand, primary agglomerates of small diameter exhibit a tendency to acquire/exhibit spherical shapes.

### 3.5. Particle size distribution and bulk density [6]

The particle size distribution (ZetaPlus, Brookhaven Instruments, USA) of magnesium silicate precipitated from solutions of magnesium sulfate and sodium metasilicate is shown in Fig. 7.6. In the distribution, as many as four bands of various intensities are observed. Two bands of the highest intensity correspond to primary agglomerates. The first band is in the 128–238 nm range (maximum intensity of 40 corresponding to agglomerates of 204.1 nm in diameter), while the other band occupies the 279–607 nm diameter range (maximum intensity of 100 corresponding to primary agglomerates of 444.5 nm in diameter). The numerous bands indicate low homogeneity of the precipitated magnesium silicate. The silicate structure also contains secondary agglomerates, which manifest themselves in two ranges of diameter: 1544–2108 nm (maximum intensity of 21 corresponding to agglomerates of 1804.3 nm in diameter) and 2878–3930 nm (maximum intensity of 36 corresponding to agglomerates of 3363.1 nm in diameter). A few secondary agglomerates are also present,



**FIGURE 7.5** SEM photograph of magnesium silicate.

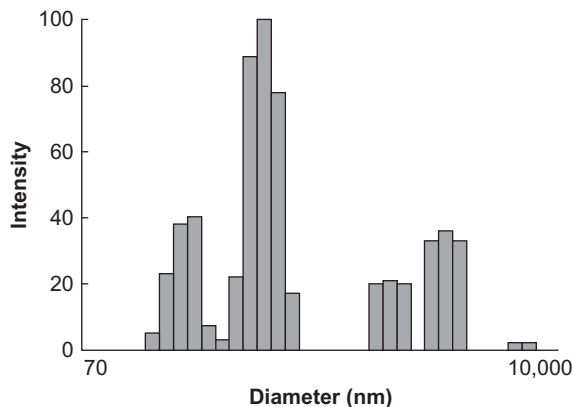


**FIGURE 7.6** Particle size distribution of magnesium silicate.

which manifest large diameters, between 7325 and 8558 nm (intensity of the band is as low as 2).

The bulk density of magnesium silicate is reported to be in the range of 161–215 g/dm<sup>3</sup> depending on the type of magnesium salt used and the amount of NaOH added as modifier.

### 3.6. Specific surface area, pore volume, and pore size

The specific surface area, pore volume, and pore size (ASAP 2010, Micromeritics Instruments, USA) of synthetic magnesium silicate resulting from the precipitation reaction of sodium metasilicate and a magnesium salt are dictated by the type of metal salt, the nonionic surfactant introduced, and the type of silane pro-adhesive compounds used in the course of precipitation. Generally, the precipitated magnesium silicate manifests a relatively high BET specific surface area. The highest values of specific surface area occur with magnesium silicate produced from magnesium sulfate and magnesium nitrate (Table 7.3). The lowest value is obtained from magnesium chloride in the presence of Rokanol K3. The situation is analogous to when the surface is modified using a silane coupling agent. As is the case for nonionic surfactants, the presence of silane decreases the specific surface area. Pore volume and pore diameter are not affected by the presence of both reagents [15]. The type and amount of silane exerts no significant effect on the specific surface area, pore volume, or mean pore diameter of precipitated magnesium silicate (Table 7.4) [16].

### 3.7. Surface active sites (adsorption and absorption)

The surface of magnesium silicate is composed of free hydroxyl groups (silanol groups); the most reactive groups on the surface. They provide the sites for the physical adsorption of organic particles and can easily

**TABLE 7.3** Physicochemical properties of unmodified and modified magnesium silicates

Precipitating agent	Amount of nonionic surfactants	Modifying agent	Amount of modifying agent (wt/wt)	Specific surface area BET (m <sup>2</sup> /g)	Pore volume (cm <sup>3</sup> /g)	Average pore diameter (nm)
MgCl <sub>2</sub>	–	–	–	411	0.80	5.5
	5 wt/wt % of Rokanol K3	–	–	197	0.67	6.3
	5 wt/wt % of Rokanol K7	–	–	356	0.61	7.9
Mg(NO <sub>3</sub> ) <sub>2</sub>	–	–	–	474	0.83	5.5
	5 wt/wt % of Rokanol K3	–	–	347	0.87	6.2
	5 wt/wt % of Rokanol K7	–	–	470	0.98	7.3
MgSO <sub>4</sub>	–	–	–	408	0.73	5.5
	5 wt/wt % of Rokanol K3	–	–	433	0.85	5.6
	5 wt/wt % of Rokanol K7	–	–	453	0.79	5.2
MgSO <sub>4</sub>	–	U-15 silane	3	401	0.68	5.2
	–		5	384	0.67	5.2
	–		10	332	0.63	5.2
MgSO <sub>4</sub>	–	U-15 silane	3	384	0.64	4.8
	5 wt/wt % of Rokanol K3		5	376	0.64	4.9
	5 wt/wt % of Rokanol K3		10	364	0.67	4.8

Rokanol K3 and K7 are nonionic surfactants (oxyethylenated unsaturated fatty alcohols, of the general formula RO(CH<sub>2</sub>CH<sub>2</sub>O)*n*H, R = C<sub>16–22</sub>, where *n*<sub>av</sub> = 3 or *n*<sub>av</sub> = 7, respectively). U-15 is silane pro-adhesive compound (N-2-aminoethyl-3-aminopropyltrimethoxysilane).

**TABLE 7.4** Physicochemical properties of unmodified magnesium silicate and magnesium silicate modified with silane coupling agents

Modifying agent	Amount of modifying agent (wt/wt)	Specific surface area BET (m <sup>2</sup> )	Pore volume (cm <sup>3</sup> /g)	Mean pore diameter (nm)
—	—	515	0.80	5.3
3-Isocyanatepropyltrimethoxysilane	3	536	0.84	5.4
	5	511	0.76	5.0
	10	503	0.76	5.0
3-Thiocyanatepropyltrimethoxysilane	3	506	0.79	5.2
	5	539	0.83	5.4
	10	528	0.81	5.4
N-Phenyl-3-isocyanatepropyltrimethoxysilane	3	519	0.85	5.6
	5	496	0.80	5.6
	10	486	0.77	3.4

react, chemically, with multiple substituents. Being substituted with new atom groups, they provide potential for surface modification. The surface composition of magnesium silicate is illustrated in Fig. 7.7 [10].

The concentration of “active” acidic and basic sites of synthetic magnesium silicate (Magnesol XL) is an important physicochemical characteristic that determines its impact on adsorption performance. Such characteristics can be determined using temperature-programmed desorption (TPD) whereby magnesium silicate is loaded onto an empty gas chromatography (GC) column or into specially designed TPD instruments (Varian 3700 Gas Chromatography, Varian, USA). After the active sites on the surface of the adsorbent are saturated by a probing chemical (e.g., *n*-butylamine), a temperature program is applied to desorb the adsorbed chemical. Desorption from sites of different intensities will occur at different temperature ranges. The desorption from weak sites occurs at lower temperature ranges, whilst the desorption from strong sites occurs at higher temperature ranges. The results from the partial adsorption TPD experiments give the sequence of the order of the intensity of basic sites and acidic sites on the surface of magnesium silicate (Figs. 7.8 and 7.9, respectively) [17].

When the surface is only partially saturated with *n*-butylamine, the strong acidic sites compete with the weak acidic sites and have the higher



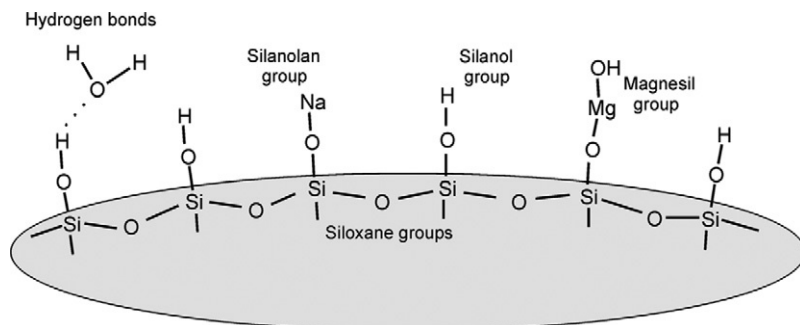


**FIGURE 7.7** Chemical functionalities on the magnesium silicate surface.

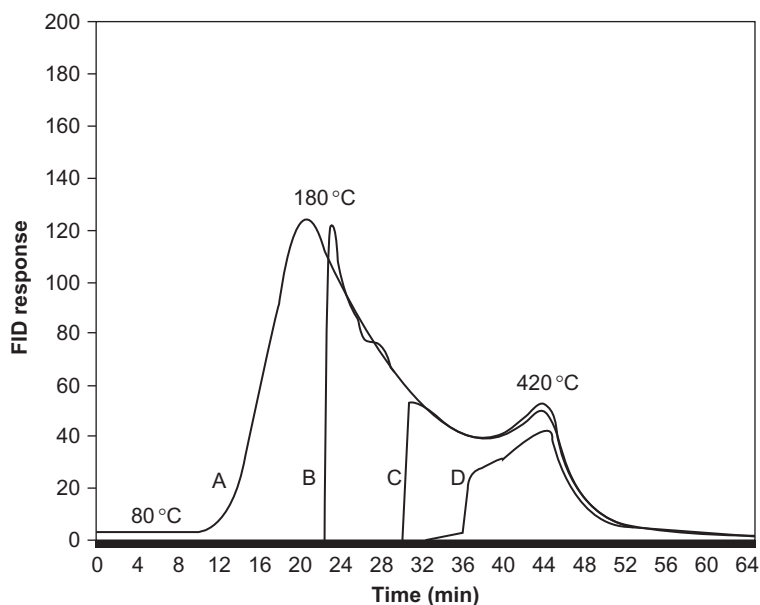


**FIGURE 7.8** Temperature-programmed desorption (TPD) chromatograms (flame-ionization detector) for the acidic sites of magnesium silicate. (A) Total TPD after complete saturation; (B) TPD after 64% partial saturation; (C) TPD after 34% partial saturation; and (D) TPD after 18% partial saturation.

priority to adsorb the *n*-butylamine molecules, leaving the weak acidic sites empty. When the amount of *n*-butylamine loaded is increased, the basic molecules start to spread over the weak acidic sites after the strong acidic sites are saturated. Thus, the partial TPD experiment demonstrates that the adsorption process starts at the strongest sites and eventually ends at the weakest sites. Therefore, the strong sites may be more

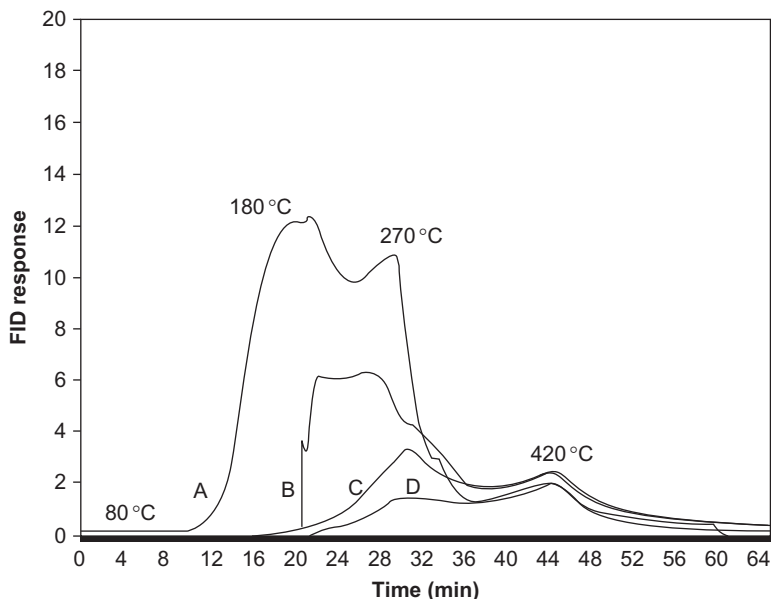


**FIGURE 7.9** Temperature-programmed desorption (TPD) chromatograms (flame-ionization detector) for the basic sites of magnesium silicate. (A) Total TPD after complete saturation; (B) TPD after 50% partial saturation; (C) TPD after 33% partial saturation; and (D) TPD after 16% partial saturation.

significant than the weak sites in adsorption (Fig. 7.8). The situation is the same for basic sites (Fig. 7.9).

The total surface concentration and intensity distribution of acidic and basic active sites are presented in Fig. 7.10. The total height of the stacked bars represents the total surface concentration of the acidic and basic active sites in millimoles per gram. The individual parts of the stacked bar correspond to the intensity distribution. As shown in Fig. 7.10, these data indicate that magnesium silicate has a total acidic and basic site concentration of 1.8 and 2.3 mM/g, respectively [17]. In comparison with other types of adsorbents used in frying oil (activated carbon, alumina [basic], alumina [neutral], alumina [acidic], bleaching earth, diatomaceous earth, and silica), magnesium silicate shows the highest values of total acidic and basic sites.

Generally, synthetically produced magnesium silicate (Magnesol) is effectively used in the regeneration of used frying oils and for the purification of biodiesel [18]. The presence of basic and acidic active sites on its surface and the high specific surface area of magnesium silicate allow it to be widely used as an analytical and industrial adsorbent for organic materials, lipids (including free fatty acids), and color. Such efficiency

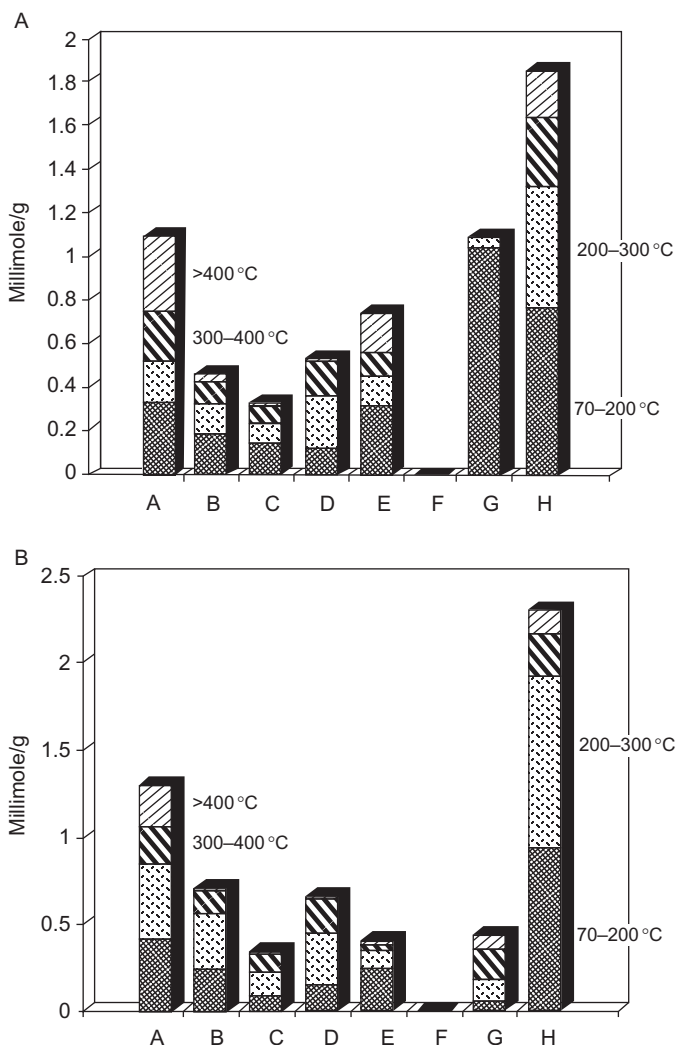


**FIGURE 7.10** Surface concentrations and their intensity distributions for (A) the acidic and (B) the basic sites of adsorbents used in frying oil. A, activated carbon; B, alumina (basic); C, alumina (neutral); D, alumina (acidic); E, bleaching earth; F, diatomaceous earth; G, silica; and H, magnesium silicate.

has been reported, for example, when amorphous synthetic magnesium silicate is used for the recovery of used frying oils. Table 7.5 shows the free fatty acids, conjugated diene value, total polar compounds, oxidative stability index, and color measured absorbance at 420 nm, when used frying oil (soybean oil) is subjected to magnesium silicate at ambient

temperature. The data in Table 7.5 shows that magnesium silicate plays an important role in improving color and acidity reduction.

Another example of fatty acid adsorption by magnesium silicate has been reported for oleic acid (Table 7.6) [5]. The results indicate no effect on the oleic acid adsorption capacity by the type of magnesium salts used to prepare the magnesium silicate. Moreover, the oleic acid adsorption capacities of commercial magnesium silicate and activated carbon are very similar. The lowest adsorption capacity is shown by “produced” activated carbon due to its low surface area and high particle size.

The absorption capacities of magnesium silicates produced from different magnesium salts for water, dibutyl phthalate, and paraffin oil are illustrated in Table 7.7 [6]. Magnesium silicate produced from magnesium nitrate shows higher absorption capacities for water, dibutyl phthalate, and paraffin oil when compared with other magnesium salts (sulfate and chloride). The addition of different percentages of sodium hydroxide, as correcting agent, affects the absorption capacities due to differences in particle size and bulk density [6].

**TABLE 7.5** Magnesium silicate screening and effects on used frying oil recovery parameters

Treated oil	Treatment with magnesium silicate	
	Before	After
Free fatty acids (%)	$0.69 \pm 0.03$	$0.43 \pm 0.05$
Conjugated diene value (%)	$1.30 \pm 0.18$	$1.18 \pm 0.07$
Total polar compounds (%)	$9.9 \pm 2.2$	$9.6 \pm 0.4$
Oxidative stability index (h)	$6.6 \pm 1.0$	$7.6 \pm 1.4$
Color Abs. at 420 nm	$0.45 \pm 0.03$	$0.31 \pm 0.02$

**TABLE 7.6** Pure oleic acid adsorption capacities (mg/g) of magnesium silicate and activated carbon from different sources

Material	BET surface area (m <sup>2</sup> /g)	Particle size (μm)	Oleic acid adsorption capacity
Magnesium silicate from MgCl <sub>2</sub>	680	40	$57.0 \pm 0.6$
Magnesium silicate from MgSO <sub>4</sub>	641	40	$57.0 \pm 1.0$
Activated carbon, produced	43	150	$14.0 \pm 0.1$
Magnesium silicate, Magnesol XL	600	2–3	$79 \pm 0$
Activated carbon, Industrial	440	2–3	$76 \pm 1$

### 3.8. Ion exchange capacity [19]

The ion exchange capacities of magnesium silicate for various cations have been measured by atomic absorption spectrometry and the data are presented in Table 7.8. The results indicate that the affinity sequence for cations is in the order:  $\text{Co}^{2+} > \text{Cd}^{2+} \sim \text{Zn}^{2+} \geq \text{Cu}^{2+} > \text{Cs}^+ > \text{Fe}^{3+}$  for magnesium silicate ion exchanger. This sequence is in accord with the hydrated radii of the exchanging ions. The ions with smaller hydrated radii enter the pores of the exchanger easily, resulting in higher adsorption.  $\text{Co}^{2+}$  ion is an exception because it shows a high value that may be due to its higher complexing ability due to the presence of more than one oxidation state. The lower capacity for  $\text{Fe}^{3+}$  reflects the nonselectivity of magnesium silicate.

### 3.9. Fourier transform infrared [13,14]

The Fourier transform infrared (FT-IR) spectrum (MB 147, BOMEM; Canada) of magnesium silicate is shown in Fig. 7.11. The broad band between 3000 and 3700  $\text{cm}^{-1}$  is assigned to the fundamental stretching

**TABLE 7.7** The absorption capacities (mL/100 g) of magnesium silicate produced with different substrates (magnesium salts)<sup>a</sup>

Substrate	Capacity to absorb water	Capacity to absorb dibutyl phthalate	Capacity to absorb paraffin oil	Concentration of NaOH solution, (wt%)
Magnesium sulfate	250	350	500	—
Magnesium sulfate	400	350	600	5
Magnesium sulfate	250	350	700	10
Magnesium sulfate	200	250	600	15
Magnesium nitrate	500	400	700	—
Magnesium chloride	300	300	550	—

<sup>a</sup> In some preparations, NaOH solutions were introduced into the magnesium sulfate solution and the solution of sodium metasilicate in the course of the precipitation process.

**TABLE 7.8** Ion exchange capacities of magnesium silicate for some cations at  $25 \pm 1^\circ\text{C}$

Cation	Absorption capacity (meq/g)
$\text{Cs}^+$	0.57
$\text{Co}^{2+}$	1.16
$\text{Cu}^{2+}$	0.60
$\text{Zn}^{2+}$	0.82
$\text{Cd}^{2+}$	0.82
$\text{Fe}^{3+}$	0.08

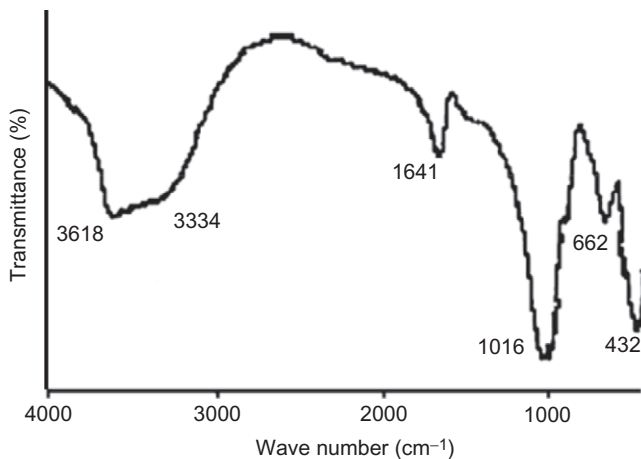


**FIGURE 7.11** FT-IR spectrum of magnesium silicate.

vibrations of O–H hydroxyl groups. Another band related to O–H hydroxyl groups is found at  $1641\text{ cm}^{-1}$ . The band at  $3618\text{ cm}^{-1}$  is characteristic of Mg–OH stretching. Magnesium silicate shows a vibrational band at  $1016\text{ cm}^{-1}$ , which is due to the Si–O–Si symmetrical stretching vibration. In addition, the Si–O bending vibration of the Mg–O occurs at 462 and  $432\text{ cm}^{-1}$ . The band at  $662\text{ cm}^{-1}$  is due to a Si–O bending motion.

### 3.10. X-Ray powder diffraction [13,14]

The X-ray powder diffraction (XRPD) pattern (XD 490, Shimadzu, Japan) of magnesium silicate is shown in Fig. 7.12. Magnesium silicate clearly shows amorphous characteristics with broad peaks throughout the diffraction pattern range. Only three minor peaks are evident at  $25\text{--}30^\circ$ ,  $35\text{--}39^\circ$ , and  $58\text{--}61^\circ 2\theta$ .

### 3.11. Thermal characteristics [13]

Differential thermal analysis (DTA)/thermogravimetric analysis (TGA) (DT-60H thermal analyzer, Shimadzu, Japan) changes for magnesium silicate are shown in Fig. 7.13. The data shows an endothermic peak with a maximum at  $T_{\text{max}} = 119^\circ\text{C}$  resulting in a mass loss of 21.5% of the total weight. This loss continues at a slow rate up to  $700^\circ\text{C}$  to yield another 10.5% mass loss, followed by an intense exothermic peak at  $T_{\text{max}} = 750^\circ\text{C}$  accompanied by a mass loss of 5.5%. The first peak is assigned to the dehydration of hygroscopic water. The second peak is

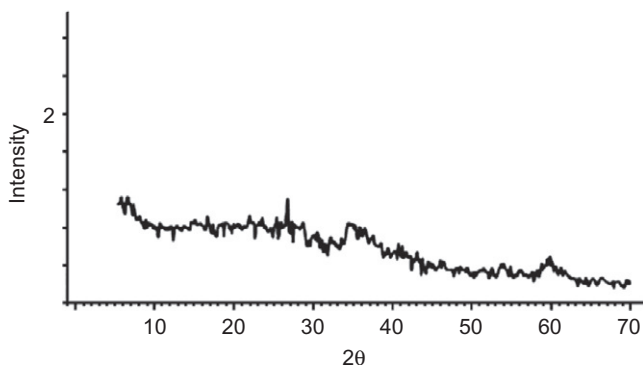


**FIGURE 7.12** XRPD pattern of magnesium silicate.

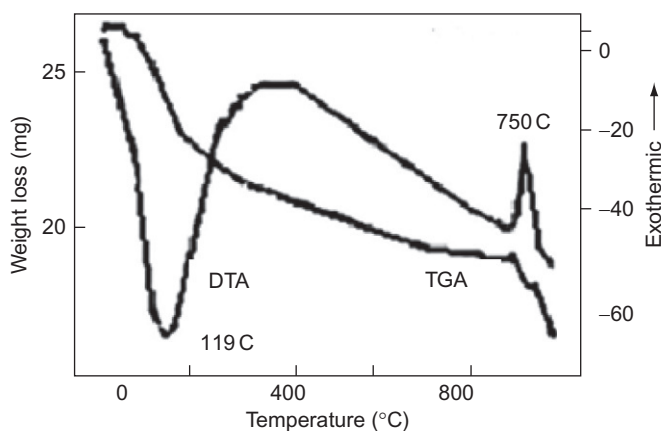


**FIGURE 7.13** DT/TGA thermograms of magnesium silicate.

probably due to the loss of structured water in parallel with a transformation to the crystalline state.

### 3.12. $^{29}\text{Si}$ MASS and $\{^1\text{H}-^{29}\text{Si}\}$ CP-MASS nuclear magnetic resonance [20]

The  $^{29}\text{Si}$  MAS and  $\{^1\text{H}-^{29}\text{Si}\}$  CP-MAS-NMR spectra of magnesium silicate are shown in Fig. 7.14 and the corresponding spectral data are given in Table 7.9.

Broad  $\text{Q}^1$  and  $\text{Q}^2$  resonances indicate the poorly ordered nature of the magnesium silicate precipitate. Resonances near  $-100$  ppm are assigned to  $\text{Q}^3$  silicon environments.

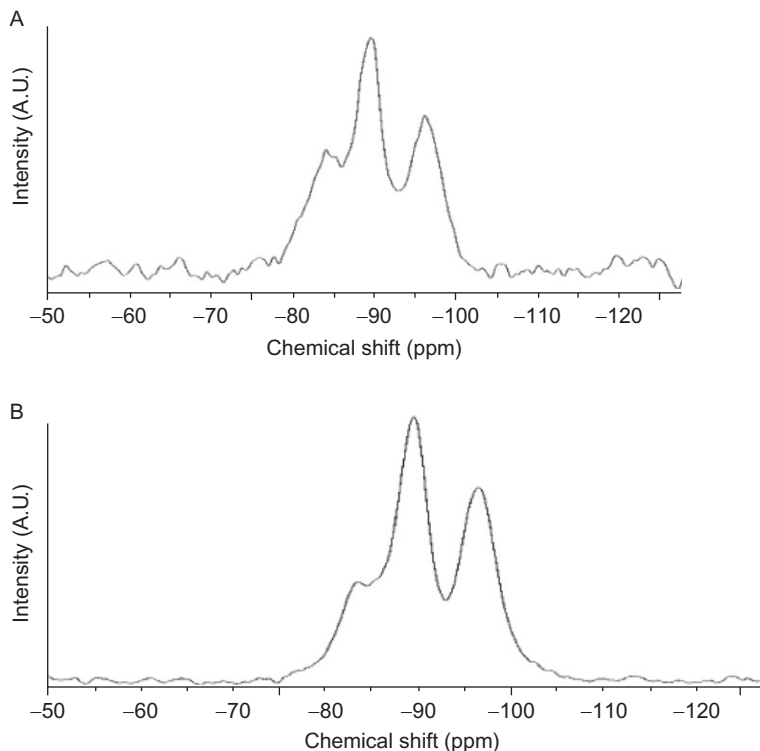


**FIGURE 7.14** (A)  $^{29}\text{Si}$  MAS NMR; and (B)  $\{^1\text{H}-^{29}\text{Si}\}$  CP-MAS NMR spectra of magnesium silicate ( $\text{Mg}/\text{Si} = 0.96$ ).

### 3.13. Polymorphic transformation

Amorphous magnesium silicate undergoes transformation to different crystalline states upon thermal treatment (calcinations) of the precipitates. For example, the XRPD pattern (Geigerflex, Rigaku Co., Japan) displays the formation of clinoenstatite powders obtained by calcination of the precipitates at different temperatures (Fig. 7.15). Only clinoenstatite phase peaks are found below 1000 °C. The intensity of the peaks increase with elevation of the sintering temperature (note: the XRPD pattern of the prepared amorphous magnesium silicate is not shown). When the temperature reaches 1100 °C or above, the XRPD analysis shows that another polymorph of  $\text{MgSiO}_3$  (protoenstatite) is formed. Some phase peaks of protoenstatite are overlapped with those of clinoenstatite [21].

Other examples include the formation of the magnesium silicate minerals enstatite ( $\text{MgSiO}_3$ ) and forsterite ( $\text{Mg}_2\text{SiO}_4$ ) by heating amorphous magnesium silicate (Fig. 7.16A) precipitated from aqueous solutions of sodium silicate and magnesium chloride, respectively [22]. Both



**TABLE 7.9** Summary of  $^{29}\text{Si}$  MAS-NMR and  $\{^1\text{H}-^{29}\text{Si}\}$  CP-MAS NMR data of magnesium silicate measured at 25 °C

$^{29}\text{Si}$ MAS $\delta$ values (ppm)			$\{^1\text{H}-^{29}\text{Si}\}$ CP-MAS $\delta$ values (ppm)		
$\text{Q}^{1a}$	$\text{Q}^2$	$\text{Q}^3$	$\text{Q}^1$	$\text{Q}^2$	$\text{Q}^3$
−83.9 ( <i>p</i> )	−90.0 ( <i>p</i> )	−96.5 ( <i>p</i> )	−83.5 ( <i>p</i> )	−89.8 ( <i>p</i> )	−96.5 ( <i>p</i> )
−85.4 ( <i>p</i> )			−85.6 ( <i>sh</i> )		

*p*, peak; *sh*, shoulder.  
<sup>a</sup> Q denotes a silicon atom bonded to four oxygen atoms. The superscript *n* denotes the number of Q units bonded to that Q. For example  $\text{Q}^1$  is  $\text{O}_3\text{Si}-\text{O}-\text{SiO}_3$ , where all the other oxygen atoms bridge from silicon to another atom (e.g., Al).  $\text{Q}^2$  is  $\text{O}_3\text{Si}-\text{O}-\text{Si}(\text{O})_2-\text{O}-\text{SiO}_3$  (note the two terminal Si are  $\text{Q}^1$  units, etc.).

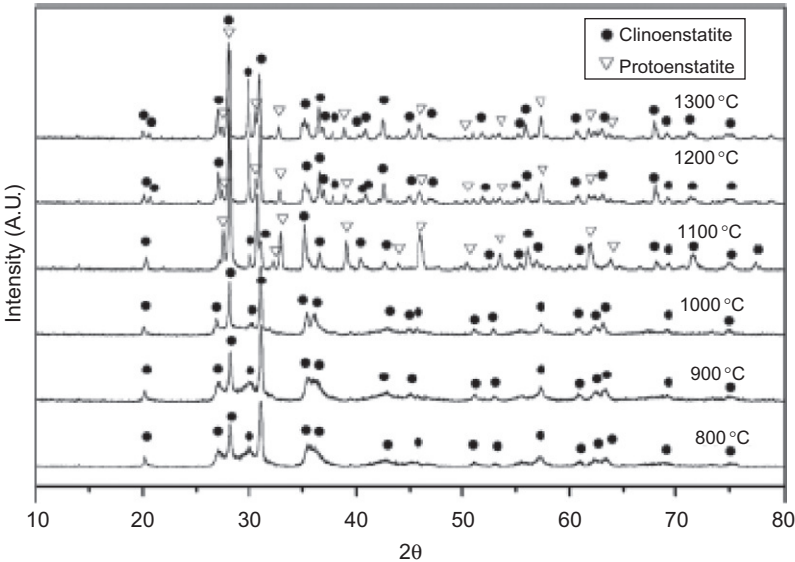


**FIGURE 7.15** XRPD profiles of magnesium silicate powders thermally treated at different temperatures.

enstatite and forsterite, as detected by  $^{29}\text{Si}$  NMR spectrometer (WH-400 [9.4 tesla], CXP-200 [4.7 Tesla], and AC-200 [4.7 Tesla] multinuclear FT-NMR instrument, Bruker, Germany) are present in all of the heated samples. Enstatite is always highly favored when the reagents are present in a 1:1 mole ratio of Mg to Si, together with only a very small proportion of forsterite (Fig. 7.16B). However, forsterite becomes a major species when the starting materials have a forsterite Mg to Si mole ratio of 2:1, together with a considerable amount of enstatite (Fig. 7.16C).

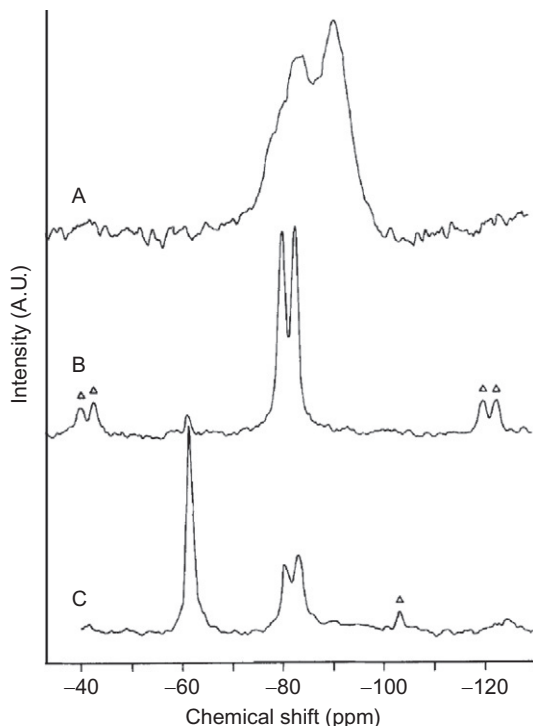


**FIGURE 7.16** 79.46 MHz  $^{29}\text{Si}$  MAS NMR spectra of materials derived from  $\text{MgCl}_2/\text{Na}_2\text{SiO}_3$  solutions. (A) Amorphous magnesium silicate from solution containing a mole ratio of 1:1 Mg/Si, dried at 110 °C for 51 h; (B) as in (A) but also heated at 750 °C for 24 h; and (C) heated as in (B) but the gel was precipitated from a solution having a 2:1 Mg/Si mole ratio. Peaks marked  $\Delta$  are spinning sidebands.

### 3.14. Modification of structural units [20]

Magnesium silicate is prepared from stock solutions of sodium metasilicate or magnesium nitrate. The solution volumes required to achieve the selected Mg/Si target ratios (0.5, 0.6, 0.75, 1.0, and 1.5 represent gel numbers 1–5) are cooled to about 0 °C and mixed with stirring in a flask kept immersed in an ice-water bath. The sodium silicate solution is added first, followed by the slow addition of the magnesium nitrate solution with stirring. The samples are allowed to warm to ambient temperature. The precipitates are collected, washed with water, and dried over solid  $\text{CaCl}_2$  at ambient temperature for 5–7 days. The magnesium silicate samples obtained are kept for 24 h at 25 °C (fresh gels). A second series of reaction products having specific target Mg/Si ratios (0.5, 1.0, 1.5, and 2.0, represent gel numbers 6–9) are prepared at 20–25 °C and subsequently stored in double-distilled, deionised water for 6 months at 85 °C

to examine the effects of ageing (aged gels). The gels obtained are tested by energy-dispersive X-ray (EDX), XRPD, FT-IR, and solid-state  $^{29}\text{Si}$  NMR. In order to establish the actual Mg/Si ratios in the prepared solid gels, EDX analysis is performed and the results are presented in Table 7.10. In this study, the target ratios were selected either to match or closely match known magnesium silicate minerals: sepiolite,  $\text{Mg}_4[\text{Si}_2\text{O}_5]_3(\text{OH})_2 \cdot 4\text{H}_2\text{O}$  (Mg/Si = 0.67); talc,  $\text{Mg}_3[\text{Si}_2\text{O}_5]_2(\text{OH})_2$  (Mg/Si = 0.75); and serpentine,  $\text{Mg}_3[\text{Si}_2\text{O}_5](\text{OH})_4$  (Mg/Si = 1.0). They are included deliberately to serve as benchmarks during the characterization stage. Amongst fresh gels, the data scatter is largest for gels 1–3; possibly also gel 5 if the outlier is considered but scatter is generally much reduced when the gels are kept for 6 months at 85 °C. Thus, studies with EDX demonstrate improved homogeneity in the aged gels.

The XRPD patterns of two fresh gels (gels 1 and gel 5) kept at 20–25 °C are identical (Fig. 7.17A). The results prove that the precipitates are gel-like single phases of low crystallinity and all gels in both storage conditions show almost the same XRPD patterns. The results also indicate that brucite,  $\text{Mg}(\text{OH})_2$ , did not coprecipitate in quantities sufficient to be detected by XRPD. Although the broad peak at 3.6–3.0 Å compares reasonably well with that of amorphous silica, its coprecipitation with gels is very unlikely. This finding is also supported by the FT-IR and  $^{29}\text{Si}$  NMR analysis, as shown later. Figure 7.17B displays the XRPD patterns of gels 5 and 9 for comparison. Their appearance suggests that the internal structure of the aged gels does not significantly differ from those of fresh gels.

**TABLE 7.10** Energy-dispersive X-ray (EDX) data for the synthetic magnesium silicate gels

Gel No.	Target Mg/Si ratio	Measured Mg/Si ratio	
		Mean	Range
Gels aged for 24 h at 25 °C			
1	0.50	0.66 (20)	0.49–0.83
2	0.60	0.75 (25)	0.35–1.03
3	0.75	0.80 (26)	0.36–0.93
4	1.00	0.90 (24)	0.82–1.03
5	1.50	0.96 (20)	0.78–1.53
Gels aged for 6 months at 85 °C			
6	0.50	0.82 (21)	0.73–0.87
7	1.00	0.86 (23)	0.72–1.02
8	1.50	0.89 (21)	0.79–0.95
9	2.00	0.94 (22)	0.80–1.12

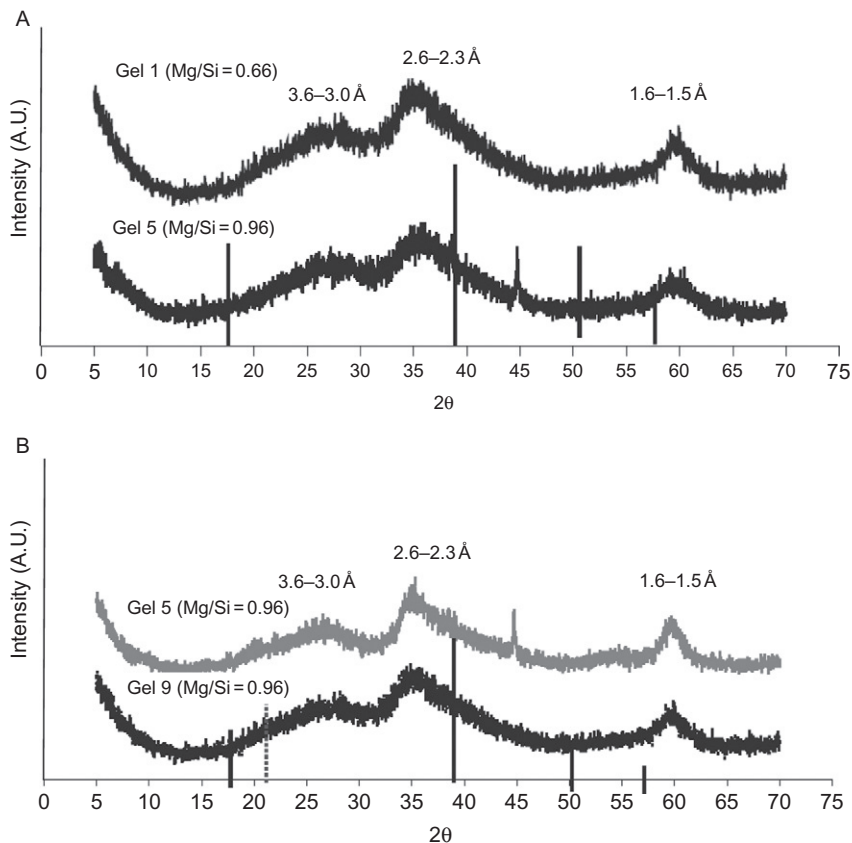


**FIGURE 7.17** XRPD patterns (A) of fresh gels (gels 1 and 5); and (B) of gel 5 (fresh) and gel 9 (aged). The peak near  $45^\circ$   $2\theta$  is an artifact due to the sample holder. Vertical black and broken lines denote relative intensities of major reflections for brucite and silica, respectively.

FT-IR spectra show that the gels have a low degree of polymerization but contain more or less all the generic stretches associated with magnesium silicate compounds (Fig. 7.18). The gels kept for 6 months at  $85^\circ\text{C}$  undergo several changes (Fig. 7.18B) compared to those kept for a short time of 24 h at  $25^\circ\text{C}$  (Fig. 7.18A). For example, the FT-IR bands are sharper and more detailed as a result of improved structural development as the storage time and temperature are increased.

NMR is useful for determining the state of silicon polymerization. The observed  $^{29}\text{Si}$  NMR resonances for magnesium silicate are normally in the  $Q^3$  chemical shift range unless significant cationic substitution has occurred. Figure 7.19A illustrates the  $^{29}\text{Si}$  MAS spectra for magnesium

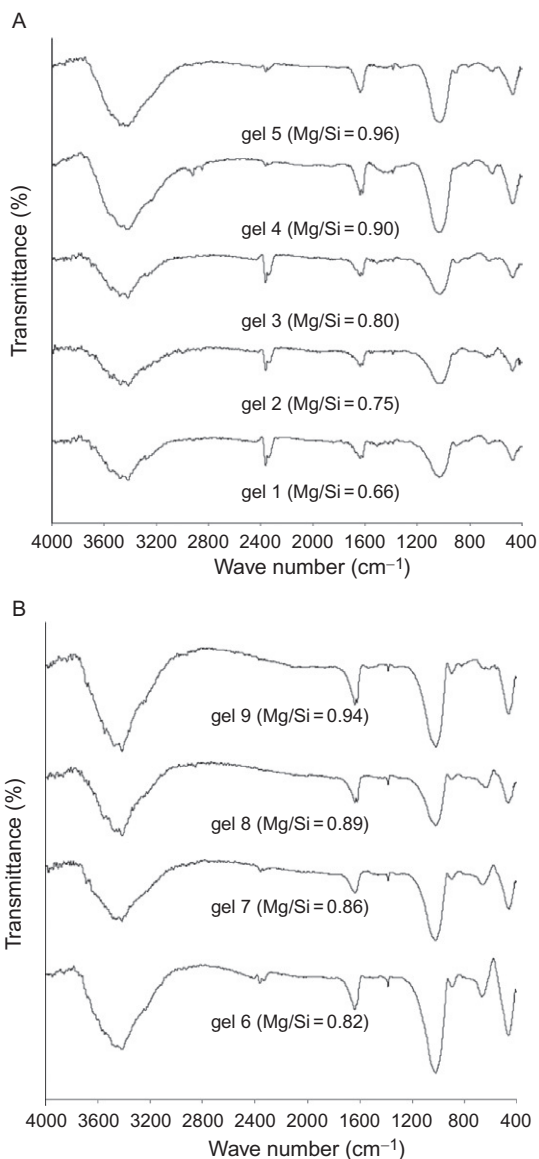


**FIGURE 7.18** FT-IR spectra (A) of fresh gels (gels 1–5); and (B) of aged gels (gels 6–9). Absorptions near  $2400\text{ cm}^{-1}$  are artifacts due to air contamination.

silicate (Mg/Si of 0.66, 0.75, and 0.96). Broad  $Q^1$  and  $Q^2$  resonances indicate the poorly ordered nature of the gels. Resonances near  $-100\text{ ppm}$  are assigned to  $Q^3$  silicon environments. The absence of a  $Q^4$  resonance located near  $-110\text{ ppm}$  confirms that coprecipitation of silica

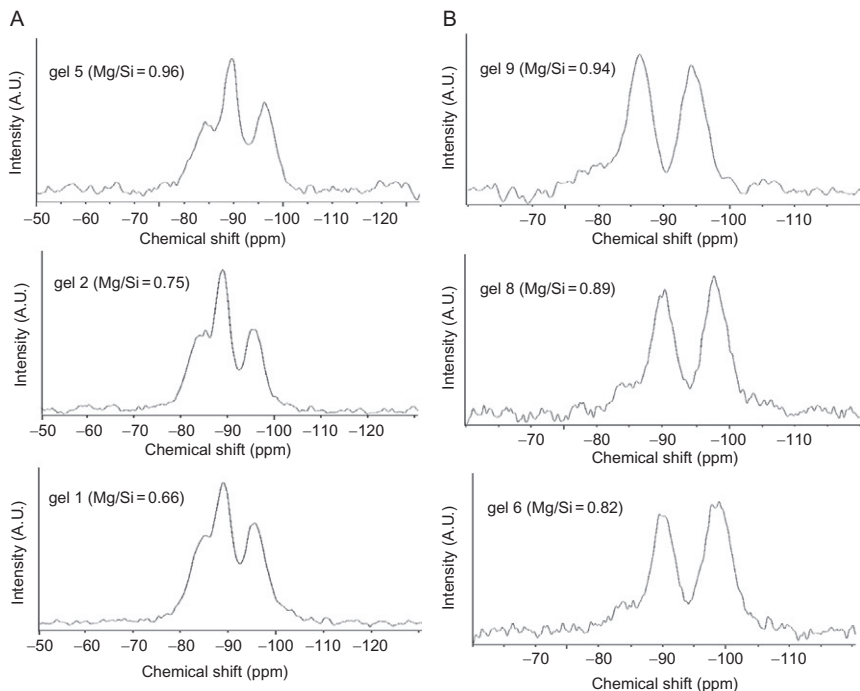


**FIGURE 7.19**  $^{29}\text{Si}$  MAS NMR spectra (A) of fresh gels (gels 1, 2, and 5); and (B) of aged gels (gels 6, 8, and 9).

does not occur. In  $^{29}\text{Si}$  NMR spectra of gels, the substantial and significant reduction in intensity of the  $\text{Q}^1$  resonances in aged gels compared with those of the corresponding fresh gels (Fig. 7.19B) illustrates the ageing process much better than either XRPD or FT-IR: nearly all the unpolymerized species combine in the course of ageing to produce polymerized  $\text{Q}^2$  and  $\text{Q}^3$  species. The relative proportions of  $\text{Q}^3/\text{Q}^2$  also increase, indicating enhancement in the number of  $\text{Q}^3$  silicon sites and progressive structural polymerization.

### 3.15. Molecular modeling [19]

Magnesium silicate is prepared by dropwise addition of magnesium chloride to sodium metasilicate (1:1 wt/wt) with continuous stirring in a water bath at 60 °C. The mixed solution is immediately hydrolyzed in demineralized water. Diluted ammonia solution is added to the mixture until complete precipitation is attained. The precipitate formed is kept in the mother liquor overnight. The precipitate is washed several times with distilled water, and then by using 0.1 M  $\text{HNO}_3$  to remove impurities and

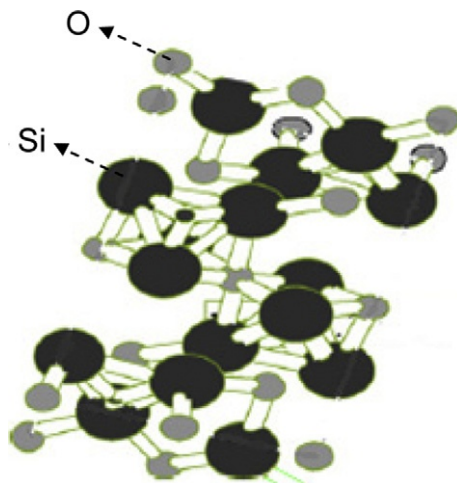


**FIGURE 7.20** Molecular model of magnesium silicate.

$\text{Cl}^-$  ions. The precipitate is rewashed using distilled water in order to remove  $\text{NO}_3^-$  ions. After drying at  $60^\circ\text{C}$ , distilled water is added to the solid, heated at  $80^\circ\text{C}$  to break the solid and remove air trapped inside, then re-dried at  $60^\circ\text{C}$ . The solid obtained is ground, sieved, and stored at room temperature. The structure of this material is established by chemical analysis, X-ray diffraction, thermogravimetric and differential thermal analyses as well as FT-IR spectroscopy and X-ray fluorescence analyses. The structure of this compound is predicted and drawn using the Chem-Draw Ultra program (Fig. 7.20).

## 4. METHODS OF ANALYSIS

### 4.1. Compendia methods [2,3]

The USP and JP pharmacopoeias' specifications for magnesium silicate are listed in Table 7.11.

#### 4.1.1. USP method of analysis [2]

Note: The number between the bracket < > represents the USP general test.

##### 4.1.1.1. Identification

1. Mix about 500 mg of magnesium silicate with 10 mL of 3 N hydrochloric acid, filter, and neutralize the filtrate to litmus paper with 6 N ammonium hydroxide: the neutralized filtrate responds to the tests for magnesium <191>.

**TABLE 7.11** USP and JP pharmacopeial specifications for magnesium silicate

Material/test	USP/NF	JP
Identification	+ ve	+ ve
pH	7.0–10.8	–
Loss on drying	≤ 15%	–
Loss on ignition	≤ 15%	≤ 34%
Soluble salts	≤ 3% (0.075 g)	≤ 1.6% (0.02 g)
Fluoride	≤ 10 ppm	–
Free alkali	≤ 2.5 mL of 0.1 N HCl	≤ 1.0 mL of 0.1 N HCl
Lead	≤ 10 ppm	–
Ratio of SiO <sub>2</sub> to MgO	2.5–4.5	2.2–2.5
Heavy metals	≤ 20 ppm	≤ 30 ppm
Chloride	–	≤ 0.053%
Assay of magnesium oxide	≥ 15.0 <sup>a</sup>	≥ 20.0
Assay of silicon dioxide	≥ 67.0 <sup>a</sup>	≥ 45.0
Arsenic	–	≤ 5 ppm
Sulfate	–	≤ 0.48%
Acid-consuming capacity	–	140–160 mL of 0.1 mol/L HCl

<sup>a</sup> Calculated on the basis of ignition.

2. Prepare a bead by fusing a few crystals of sodium ammonium phosphate on a platinum loop in the flame of a Bunsen burner. Place the hot, transparent bead in contact with magnesium silicate, and again fuse: silica floats about in the bead, producing, upon cooling, an opaque bead with a web-like structure.

**4.1.1.2. pH <791>** The pH is between 7.0 and 10.8, determined in a well-mixed aqueous suspension (1 in 10).

**4.1.1.3. Loss on drying <731>** Dry the magnesium silicate at 105 °C for 2 h; it should not lose more than 15.0% of its weight (retain the dried specimen for the test for loss on ignition).

**4.1.1.4. Loss on ignition <733>** Ignite the specimen retained from the test for loss on drying at 900–1000 °C for 20 min: the dried specimen should not lose more than 15% of its weight.



**4.1.1.5. Soluble salts** Boil 10.0 g of magnesium silicate with 150 mL of water for 15 min. Cool to room temperature, allow the mixture to stand for 15 min, filter with the aid of suction, transfer the filtrate to a 200-mL volumetric flask, dilute with water to volume, and mix. Evaporate 50.0 mL of this solution, representing 2.5 g of the silicate, in a tared platinum dish to dryness, and ignite gently to constant weight: the weight of the residue should not exceed 75.0 mg (3.0%).

**4.1.1.6. Fluoride Indicator solution:** Prepare a solution containing 100 mg of lanthanum–alizarin complexan mixture per milliliter in 60% isopropyl alcohol. Filter the solution if it is not clear.

**Test preparation:** Prepare a slurry consisting of 5.0 g of magnesium silicate and 45 mL of 0.1 N hydrochloric acid, stir at room temperature for 15 min, and pass through a 0.45- $\mu$ m filter into a 50-mL volumetric flask. Wash the filter with five 1-mL portions of 0.1 N hydrochloric acid, collecting the washings in the flask, dilute with 0.1 N hydrochloric acid to volume, and mix.

**Procedure:** Transfer 5.0 mL of the test preparation to a 25-mL volumetric flask, add 5.0 mL of indicator solution dilute with water to volume, mix, and allow to stand for 1 h in diffuse light at ambient temperature. Determine the absorbance of this solution in a 1-cm cell with a suitable spectrophotometer, at the wavelength of maximum absorbance (620 nm), against a blank consisting of 5.0 mL of 0.1 N hydrochloric acid, 5.0 mL of indicator solution and 15.0 mL of water. The absorbance should not be greater than that produced by 5.0 mL of a solution containing 2.21  $\mu$ g of sodium fluoride per milliliter of 0.1 N hydrochloric acid, when treated in the same manner as the test preparation (10 ppm).

**4.1.1.7. Free alkali** Add two drops of phenolphthalein TS to 20 mL of the diluted filtrate prepared in the test for soluble salts, representing 1 g of magnesium silicate: if a pink color is produced, not more than 2.5 mL of 0.1 N hydrochloric acid is required to discharge it.

**4.1.1.8. Lead <251>** Dissolve 1.0 g in 20 mL of 3 N hydrochloric acid, evaporate on a steam bath to about 10 mL, dilute with water to about 20 mL and cool; the limit is 0.001%.

**4.1.1.9. Ratio of SiO<sub>2</sub> to MgO** Divide the percentage of SiO<sub>2</sub> obtained in the assay for silicon dioxide by the percentage of MgO obtained in the assay for magnesium oxide: the quotient obtained is between 2.50 and 4.50.

**4.1.1.10. Heavy metals <231>** Boil 4.0 g of magnesium silicate in a mixture of 50 mL of water and 10 mL of hydrochloric acid for 20 min, adding water to maintain the volume during boiling. Add ammonium hydroxide until the mixture is only slightly acid to litmus paper. Filter with the aid of suction, and wash with 15–20 mL of water, combining the washings with the original filtrate. Add two drops of phenolphthalein TS, then add a slight excess of 6 N ammonium hydroxide. Discharge the pink color with dilute hydrochloric acid (1 in 100), then add 8 mL of dilute hydrochloric acid (1 in 100). Dilute with water to 100 mL, and use 25 mL of the solution for the test: the limit is 20 µg/g.

**4.1.1.11. Assay for magnesium oxide** Accurately weigh about 1.5 g of magnesium silicate and transfer to a 250-mL conical flask. Add 50.0 mL of 1 N sulfuric acid VS, and digest on a steam bath for 1 h. Cool to room temperature, add methyl orange TS, and titrate the excess acid with 1 N sodium hydroxide VS. Each milliliter of 1 N sulfuric acid is equivalent to 20.15 mg of MgO.

**4.1.1.12. Assay for silicon dioxide** Transfer about 700 mg of magnesium silicate, accurately weighed, to a small platinum dish. Add 10 mL of 1 N sulfuric acid, and heat on a steam bath to dryness, leaving the dish uncovered. Treat the residue with 25 mL of water, and digest on a steam bath for 15 min. Decant the supernatant through ashless filter paper, with the aid of suction, and wash the residue, by decantation, three times with hot water, passing the washings through the filter paper. Finally transfer the residue to the filter, and wash thoroughly with hot water. Transfer the filter paper and its contents to the platinum dish previously used. Heat to dryness, incinerate, ignite strongly for 30 min, cool, and weigh. Moisten the residue with water, and add 6 mL of hydrofluoric acid and three drops of sulfuric acid. Evaporate to dryness, ignite for 5 min, cool, and weigh; the loss in weight represents the weight of SiO<sub>2</sub>.

#### 4.1.2. JP method of analysis [3]

Note: The number between the bracket < > represents the JP general test.

##### 4.1.2.1. Identification

1. Mix about 0.5 g of magnesium silicate with 10 mL of dilute hydrochloric acid, filter, and neutralize the filtrate with ammonia TS; the solution responds to the “Qualitative Tests” <1.09> for magnesium salt.

2. Prepare a bead by fusing ammonium sodium hydrogenphosphate tetrahydrate on a platinum loop. Place the bead in contact with magnesium silicate, and fuse again: an infusible matter appears in the bead, which changes to an opaque bead with a web-like structure upon cooling.

**4.1.2.2. Soluble salts** Add 150 mL of water to 10.0 g of magnesium silicate, heat on a water bath for 60 min with occasional shaking, then cool, dilute with water to 150 mL, and centrifuge. Dilute 75 mL of the resultant transparent liquid with water to 100 mL, and use this solution as the sample solution. Evaporate 25 mL of the sample solution using a water bath to dryness, and ignite the residue at 700 °C for 2 h: the mass of the ignited residue is not more than 0.02 g.

**4.1.2.3. Alkalinity** To 20 mL of the sample solution obtained in the soluble salts test, add two drops of phenolphthalein TS and 1.0 mL 0.1 mol/L hydrochloric acid VS; no color develops.

**4.1.2.4. Chloride <1.03>** To 10 mL of the sample solution obtained in soluble salts test, add 6 mL of dilute nitric acid, dilute with water to 50 mL, and perform the test using this solution as the test solution. Prepare the control solution with 0.75 mL of 0.01 mol/L hydrochloric acid VS (not more than 0.053%).

**4.1.2.5. Sulfate <1.14>** To the residue obtained in soluble salts test, add about 3 mL of dilute hydrochloric acid, and heat on a water bath for 10 min. Add 3 mL of water, filter, wash the residue on the filter with water, combine the washings with the filtrate, and dilute with 50 mL with water. To 4 mL of the solution add 1 mL of dilute hydrochloric acid and water to make 50 mL. Perform the test using this solution as the test solution. Prepare the control solution with 1.0 mL of 0.005 mol/L sulfuric acid VS (not more than 0.48%).

**4.1.2.6. Heavy metals <1.07>** To 1.0 g of magnesium silicate add 20 mL of water and 3 mL of hydrochloric acid and boil for 2 min. Filter, and wash the residue on the filter with two 5 mL portions of water. Evaporate the combined filtrate and washings on a water bath to dryness, add 2 mL of dilute acetic acid to the residue, warm until solution is complete, filter, if necessary, add water to make 50 mL, and perform the test using this solution as the test solution. Prepare the control solution with 3.0 mL of standard lead solution, 2 mL of dilute acetic acid and water to make 50 mL (not more than 30 ppm).

**4.1.2.7. Arsenic <1.11>** To 0.4 g of magnesium silicate, add 5 mL of dilute hydrochloric acid, heat gently to boiling while shaking well, cool rapidly and centrifuge. Mix the residue with 5 mL of dilute hydrochloric acid with shaking, centrifuge, then add 10 mL of water to the residue, and repeat the extraction in the same manner. Concentrate the combined extracts on a water bath to 5 mL. Use this solution as the test solution, and perform the test (not more than 5 ppm).

**4.1.2.8. Loss on ignition <2.43>** Not more than 34% (0.5 g, 850 °C, 3 h)

**4.1.2.9. Acid consuming capacity <6.04>** Place about 0.2 g of magnesium silicate, accurately weighed, in a glass-stoppered flask, add exactly 30 mL of 0.1 mol/L hydrochloric acid VS and 20 mL of water, shake at  $37 \pm 2$  °C for 1 h, and cool. Pipet 25 mL of the supernatant liquid, and titrate <2.50> of the excess hydrochloric acid, while stirring well, with 0.1 mol/L sodium hydroxide VS until the pH becomes 3.5.

One gram of magnesium silicate, calculated on the anhydrous basis by making allowance for the observed loss on ignition determined as directed in the preceding Loss on ignition, consumes not less than 140 mL and not more than 160 mL of 0.1 M hydrochloric acid VS.

**4.1.2.10. Assay for silicon dioxide** Accurately weigh about 0.7 g of magnesium silicate, add 10 mL of 0.5 mol/L sulfuric acid TS, evaporate on a water bath to dryness, add 25 mL of water to the residue and heat on water bath for 15 min with occasional stirring. Filter the supernatant liquid through filter paper for assay, add 25 mL of hot water to the residue, stir, and decant the supernatant liquid on the filter paper to filter. Wash the residue in the same manner with two 25-mL portions of hot water, transfer the residue onto the filter paper, and wash with hot water until the last washing does not respond to the "Qualitative Test" <1.09> (1) for sulfate. Place the residue and the filtrate paper in a platinum crucible, incinerate with strong heating and ignite between 775 and 825 °C for 30 min, then cool, and weigh the residue as *a* (g). Moisten the residue with water and add 6 mL of hydrofluoric acid and three drops of sulfuric acid. Evaporate to dryness, ignite for 5 min, cool, and weigh the residue as *b* (g).

$$\text{Content(\% of silicon dioxide (SiO}_2\text{))} = [(a - b)/W] \times 100,$$

$$W = \text{mass(g) of the sample.}$$

**4.1.2.11. Assay for magnesium oxide** Accurately weigh about 0.3 g of magnesium silicate, transfer to a 50 mL conical flask, add 10 mL of 0.5 mol/L sulfuric acid VS, and heat on a water bath for 15 min, transfer

to 100 mL volumetric flask, wash the conical flask with water, add the washings to the volumetric flask, dilute with water to 100 mL, and filter. Pipet 50 mL of the filtrate, shake with 50 mL of water and 5 mL of diluted 2,2',2''-nitrilotrisethanol (1 in 2), add 2.0 mL of ammonia TS and 10 mL of ammonia–ammonium chloride buffer solution, pH 10.7, and titrate <2.50> with 0.05 mol/L disodium dihydrogen ethylenediamine tetraacetate VS (indicator: 0.04 g of eriochrome black T–sodium chloride).

Each milliliter of 0.05 mol/L disodium dihydrogen ethylenediamine tetraacetate VS = 2.015 mg of MgO.

**4.1.2.12. Ratio of  $\text{SiO}_2$  to MgO** Calculate the quotient from the percentage obtained in the assay for silicon dioxide and the assay for magnesium oxide.

## 4.2. Noncompendia methods

A summary of some analytical methods reported for magnesium and silicate ions is given below. These methods are not specifically for magnesium silicate, but they are general methods used for measuring magnesium and silicate individually. It is worth mentioning that these methods may require some verification prior to their use for analyses of magnesium silicate (e.g., sample treatment, using suitable solvents, pH adjustment, changes in method parameters).

### 4.2.1. Analysis of magnesium

**4.2.1.1. Colorimetric methods** The determination of magnesium is carried out by complexation with coloring agents such as eriochrome black T [23], titan yellow [24], 5,7-diiodo-8-quinolinol and rhodamine S [25], beryllon II [26], quinolin-8-olate [27,28] leucoquinizarin [29], emodin [30,31], purpurin [32], or bromopyrogallol red [33].

**4.2.1.2. Fluorimetric methods [34]** Fluorimetric sequential injection analysis of magnesium in commercial drinking waters is based on the complexation of magnesium (II) with 8-hydroxyquinoline-5-sulfonic acid in the presence of ethylene glycol-bis( $\beta$ -aminoethyl ether)- $N,N,N',N''$ -tetraacetic acid as a masking agent and cetyltrimethylammonium chloride as the fluorescence enhancer.

**4.2.1.3. Atomic absorption spectroscopy** The determination of magnesium in natural samples and cement by atomic absorption spectroscopy is reported [35]. The same technique is used for the analysis of leaf samples of varied origin and nature initially decomposed by fusion with sodium hydroxide in an open system using sodium nitrate as an auxiliary agent to facilitate the mineralization of most of the samples [36]. Another

sample treatment is carried out by fusion with a mixture of sodium carbonate and lithium tetraborate (3:1) at 925 °C and then the fusion cake is dissolved in hydrochloric acid [37]. A fusion agent, consisting of equal portions of oxalic acid, lithium carbonate, and lithium tetraborate, is proposed for the fusion of cement samples [38].

**4.2.1.4. Potentiometric analysis by ion-selective electrode [39]** A series of ion-selective electrodes (ISEs) for  $\text{Ca}^{2+}$ ,  $\text{Mg}^{2+}$ ,  $\text{NH}_4^+$ ,  $\text{K}^+$ ,  $\text{Na}^+$ ,  $\text{Li}^+$ , and  $\text{H}^+$  is used for the analysis of water samples from different sources. The selectivity of the calcium and magnesium ISEs is not fully achieved as other cationic species may interfere with the analysis. The proposed sensor array device can overcome this drawback since it can take advantage of the cross-selectivities of cationic species toward each ISE. Results obtained are in reasonable concordance with those attained by the standard method based on complexometric analysis.

**4.2.1.5. Ion chromatography** The content of calcium and magnesium in human serum is measured by ion chromatography. Sample pretreatment consists of acidic dilution and filtration. Detection is based on conductivity. The analytical results are comparable to those of the reference methods based on flame atomic absorption spectrometry [40]. In addition, simultaneous determination of these two cations in the presence of different inorganic anions in mineral waters is measured using suppressed conductimetric detection ion chromatography. The separation and detection are based upon the use of sodium carbonate–EDTA to form ion–EDTA complexes [41]. The results of this study are in agreement with those obtained using inductively coupled plasma mass spectrometry (ICP-MS).

**4.2.1.6. Capillary electrophoresis** Capillary electrophoresis (CE) is used to analyze sodium, potassium, calcium, and magnesium in water samples. The detection is conducted by reverse absorbance measurements. Sufficient separation of the four cations is established with an electrolyte solution of 5 mM imidazole/6.5 mM  $\alpha$ -hydroxyisobutyric acid/2 mM 18-crown-6 ether of pH 4.1 [42]. CE with a contactless conductometric detector is used to determine small anions and cations in water samples from different sources. 2-(*N*-Morpholino)ethanesulfonic acid/histidine-based (Mes/His) electrolytes are used for direct conductivity detection of anions and cations, while ammonium acetate is used for indirect conductivity determination of alkylammonium salts. For the simultaneous separation procedure, involving dual-opposite end injection, an electrolyte consisting of 20 mM Mes/His, 1.5 mM 18-crown-6 and 20 mM cetyltrimethylammonium bromide provides baseline separation of 13 anions and cations in less than 6 min [43]. Also CE with a capacitively coupled

contactless conductivity detector (CE-C<sup>4</sup>D) is used to determine sodium, potassium, calcium, and magnesium in total parenteral nutrition formulations. A hydro-organic mixture, consisting of 100 mM Tris-acetate buffer at pH 4.5 and acetonitrile (80:20, v/v), is selected as the background electrolyte. All analyses are carried out in a fused silica capillary with an internal diameter of 50  $\mu\text{m}$  and a total length of 64.5 cm. Under these conditions, complete separation between all cations is achieved in less than 4 min [44].

#### 4.2.2. Analysis of silicate

**4.2.2.1. Colorimetric methods** Silicon is determined by the molybdenum blue spectrophotometric method after solubilization in H<sub>2</sub>O, in alkaline solutions or in concentrated HF. A flow analysis procedure for the measurement of soluble silicon with respect to the total Si concentration is used. The proposed method is applied to samples of rain water and of aerosols on filters [45]. Simultaneous determination of orthophosphate and silicate in brackish water is performed by the same technique. Molybdate/antimony, ascorbic acid, and oxalic acid reagents are added to the samples and spectra are recorded in the wavelength range 410–820 nm after a total reaction time of 30 min [46].

**4.2.2.2. Atomic absorption spectroscopy [47]** The content of silicon in serum and urine at physiological levels is measured by using electrothermal atomic absorption spectrometry. Amongst the different carbide-forming elements studied, tungsten gives the best results. The use of chemical modifiers in serum and urine proved to be unnecessary using the proposed method.

**4.2.2.3. Atomic emission spectroscopy [48]** Hollow cathode glow discharge atomic emission spectrometry is applied to the determination of silicon coupled with a novel gaseous hydride generation technique. An aqueous solution of silicate is dried and mixed with powdered LiAlH<sub>4</sub>. Sample introduction into the glow discharge chamber is performed via a pinhole at the center of the cathode which is connected to the hydride generator.

**4.2.2.4. Chromatographic method** The determination of silicate based upon the adsorption of preconcentrated phosphomolybdic and silicomolybdic heteropoly acid (HPA) in the dynamic mode on a microcolumn packed with an Amberlite XAD-8 polyacrylate adsorbent is reported [49]. The method is based on the adsorption of HPAs followed by desorption with acetonitrile and determination by reversed-phase HPLC. Another highly sensitive HPLC method for the simultaneous determination of soluble silicate and phosphate in environmental waters is used in ion-pair liquid

chromatography preceded by the formation of their yellow  $\alpha$ -heteropoly-molybdates. The moderate-pH mobile phase enables use of a highly efficient reversed-phase silica column. The analysis results are very reasonable and acceptable from an environmental viewpoint, and are well correlated with those confirmed by molybdenum-blue spectrophotometry [50]. The direct determination of dissolved silica in seawater using ion exclusion chromatography in combination with inductively coupled plasma mass spectrometry is reported, where ion exclusion affords a separation of the dissolved silica not only from the major seawater cations but also from potentially interfering anions [51]. Furthermore, the analysis using the same ion exclusion chromatographic technique can be carried out with luminal, using hemi-luminescence [52], and conductivity detection [53].

**4.2.2.5. Electrochemical method [54]** Silicate is determined in sea water by four different electrochemical methods based on the detection of the silicomolybdic complex formed in acidic media by the reaction between silicate and molybdenum salts. The first two methods are based on the addition of molybdate and protons in a seawater sample in an electrochemical cell. A semiautonomous method was developed based on the electrochemical anodic oxidation of molybdenum, the complexation of the oxidation product with silicate and the detection of the complex by cyclic voltammetry. Finally a complete reagent-less method with a precision of 2.6% is described based on the simultaneous formation of the molybdenum salt and protons in a divided electrochemical cell.

**4.2.2.6. Capillary electrophoresis [55]** Simultaneous analysis of silicate with other ions (nitrite, nitrate, phosphate) is carried out by capillary electrophoresis with an indirect UV detection. The separation is achieved in a fused silica capillary filled with an electrolyte solution containing sodium chromate and an electro-osmotic flow modifier, trimethyltetradecylammonium bromide.

## 5. USES

Magnesium silicate has regulatory acceptance. It is GRAS listed, accepted for use as a food additive in Europe, included in the Canadian List of Acceptable Nonmedicinal Ingredients, and included in the FDA Inactive Ingredients Guide (oral tablets) [1]. The maximum potency of magnesium silicate when used in pharmaceutical solid dosage forms is listed in Table 7.12 [56].

Magnesium silicate is widely used in the pharmaceutical, food, and cosmetics industries, in addition to its uses in other industrial fields (including, rubber, paints, paper, and plastic).



**TABLE 7.12** List of the maximum potency of magnesium silicate (CAS No. 1343-88-0) in different solid dosage form as approved by FDA

Dosage form	Maximum potency (mg)
Oral; capsule	40.00
Oral; tablet	10.00
Oral; tablet, coated	29.30
Oral; tablet, enteric coated particles	30.00
Oral; tablet, film coated	14.30

### 5.1. Pharmaceutical

Magnesium silicate is used (a) in oral pharmaceutical formulations and food products as a glidant and an anticaking agent [5], (b) in antacid and antiulcer preparations [57,58], (c) as a component of antiepileptic drugs in the treatment of alimentary intoxication, indigestion and in inflammatory conditions of the small intestine [6], (d) as an antifungal agent in topical preparations [59], (e) in cosmetics especially in toothpastes, gels, facial creams, body washes, cosmetic creams, sunscreens, shampoo, and blush [59], (f) in the treatment of acne and as a facial moisturizer [59], and (g) arginine silicate complex (the reaction product of arginine and magnesium silicate) is used as a source of the essential amino acid arginine and as a source of silicate, both of which exert antiatherosclerotic effects and also promote bone and cartilage formation in mammals [60].

### 5.2. Food

Magnesium silicate functions as a carrier for fragrances or flavors. It is also used in beer and wine clarification. In animal feed, synthetic amorphous silica and silicates serve as carriers and anticaking agents in vitamin and mineral premix preparations. Synthetic magnesium silicate is used as a bleaching agent in animal and vegetable oil production [61]. It is also used in the production of confectionery as an antiadhesive and anticaking agent (molding powder or a component of antiglitter paste). As far as whiteness is concerned, its white color may easily compete with titanate-based pigments, which eliminates—partially or totally—the use of titanium dioxide [6].

### 5.3. Rubber and silicones [62]

Magnesium silicate is used as a reinforcing filler for many nonstaining and colored rubber and silicones products.

#### 5.4. Paints [6]

Magnesium silicate is used as a filler and pigment in dispersive paints.

#### 5.5. Chromatography [59,60]

Magnesium silicate is used as an adsorbent in affinity chromatography.

#### 5.6. Paper [63]

Magnesium silicate is used as a filler in paper manufacturing to improve printability and opacity.

#### 5.7. Insecticide, microbiocide, and fungicide [64]

Magnesium silicate is used against juvenile and adult store product pests, exerting its lethal activity predominantly on juvenile and adult forms by sorption of the cuticular lipid layer, thus causing dehydration of the insects.

#### 5.8. Cement [65]

Cement is made by forming a calcium silicate product from limestone and clay minerals in a kiln which requires very hot temperatures, releasing high levels of CO<sub>2</sub> as it burns. Most low carbon cements on the market are based on magnesium silicate, which takes less energy to heat.

#### 5.9. Other uses

Sodium silicate together with magnesium silicate is used in muffler repair and fitting paste. When dissolved in water, both form a thick paste that is easy to apply. When the exhaust system of an internal combustion engine heats up to its operating temperature, the heat drives out all of the excess water from the paste. The silicate compounds that are left over have glass like properties, making a temporary brittle repair [66]. Highly dispersed magnesium silicates can be used as polymer fillers or active adsorbents [67].

Magnesium silicate is an amphoteric compound with a high specific area capable of absorbing either acid or alkali metal catalyst. It is an efficient refining and purifying agent in the production of polyols for its excellent depicking, deodorizing, potassium ion absorbing effects, and functions as a filter medium [59]. In addition, it is used as an adsorbent to regenerate frying oils and purify biodiesel [5,61,68]. Magnesium silicate,

aluminum silicate, and calcium silicate are used as fillers and pigment extenders in fingernail lacquers and in the plastic industries [69,70].

## 6. STABILITY AND INCOMPATIBILITIES

Magnesium silicate exposed to temperatures of 750 °C transforms from amorphous form to the magnesium silicate minerals enstatite ( $\text{MgSiO}_3$ ) and forsterite ( $\text{Mg}_2\text{SiO}_4$ ) [22]. When the temperature reaches 1100 °C and above, others polymorphs (protoenstatite and clinoenstatite) are formed [21]. Magnesium silicate in its solid state should be stored in a well-closed container in a cool, dry place [1–3]. When magnesium silicate is stored in double-distilled, deionised water for 6 months at 85 °C, it maintains its amorphous structure with some improvement in the order and maintains its chemical entity [20]. Magnesium silicate is readily decomposed by mineral acids. Magnesium silicate may decrease the oral bioavailability of drugs such as mebeverine hydrochloride, sucralfate, and tetracycline, via chelation or binding, when they are taken together. The dissolution rate of folic acid, erythromycin stearate, paracetamol, and chloroquine phosphate, may be retarded by adsorption onto magnesium silicate. Antimicrobial preservatives, such as parabens, may be inactivated by the addition of magnesium silicate [1].

## 7. BIODEGRADABILITY AND TOXICITY

Orally administered magnesium silicate is neutralized in the stomach to form magnesium chloride and silicon dioxide; some magnesium is absorbed. Caution should be used when greater than 50 meq of magnesium is given daily to patients with impaired renal function, owing to the risk of hypermagnesemia. Reported adverse effects include the formation of bladder and renal calculi following the regular use, for many years, of magnesium silicate as an antacid [1]. It is not explosive, flammable, or combustible. It is a mild irritant to eyes, skin, and respiratory passages. It is not classified as dangerous under EU Directive 67/548/EEC. In the EEC, magnesium silicate is a permitted food additive according to directive 95/2/EC (E 553a) [71]. The toxicological profile of magnesium silicate is summarized in Table 7.13.

**TABLE 7.13** Environmental fate and pathway, ecotoxicology, toxicology, and genetic toxicity of magnesium silicate

Property	Comment
Monitoring data (environmental)	Inert material, considered nonhazardous to the environment
Biodegradation	Not biodegradable
Occupational exposure limit values	4 mg/m <sup>3</sup> respirable and 10 mg/m <sup>3</sup> total dust, 8 h TWA
Acute/prolonged toxicity to fish	No known toxicity. Test method used conforms with OECD Guideline 203
Toxicity to aquatic plants	No known toxicity
Toxicity to microorganisms	No known toxicity
Chronic toxicity to fish, aquatic invertebrates	No known toxicity
Toxicity to soil dwelling organisms, terrestrial plants, and other nonmamm terrestrial species	No known toxicity
Acute oral toxicity (LD <sub>50</sub> )	No known toxicity >2000 mg/kg bw on rats >500 mg/kg bw on humans
Acute inhalation toxicity	Inhalation is carcinogenic to humans and causes silicoses and noncancerous lung diseases
Acute dermal toxicity	No known toxicity
Acute toxicity, other routes	No known toxicity
Skin irritation (rabbits)	Slightly irritating
Skin irritation (humans)	Not irritating
Eye irritation (rabbits)	Irritating
Eye irritation (humans)	Slightly irritating
Sensitization	No data
Repeated dose toxicity	Causes damages to lungs
Genetic toxicity <i>in vitro</i>	Not considered mutagenic
Genetic toxicity <i>in vivo</i>	Not mutagenic
Carcinogenicity	Inhalation is carcinogenic to humans and causes silicoses and noncancerous lung diseases
Toxicity to reproduction	No known toxicity for the reproduction
Developmental toxicity/teratogenicity	No known
Cytotoxicity	Not cytotoxic

## 8. RELATED SUBSTANCES

### 8.1. Magnesium metasilicate

Magnesium metasilicate ( $\text{MgSiO}_3$ , CAS No. 63210-56-0) exists in several polymorphic forms, the most important ones are orthorhombic enstatite, protoenstatite, and clinoenstatite. Orthorhombic enstatite is an abundant mineral and metastable under ambient conditions. Protoenstatite converts to clinoenstatite upon heating at 1400 °C, upon long standing at room temperature and upon grinding [72]. Both protoenstatite and clinoenstatite are high temperature phases. It is activated magnesium silicate also known as florasil ( $\text{MgSiO}_3$ ) of 40.1% MgO and 59.9%  $\text{SiO}_2$ . It is prepared by ball milling MgO with  $\text{SiO}_2$  and the fine powder produced is calcined at 1300 °C for 10 h and then sintered at 1450 °C for 3 h (solid-state synthesis) [73].  $\text{MgSiO}_3$  can also be prepared by a precipitation technique by dissolving  $\text{Mg}(\text{NO}_3)_2 \cdot 6\text{H}_2\text{O}$  and diformylhydrazine ( $\text{C}_2\text{H}_4\text{N}_2\text{O}_2$ ). Fumed silica is added to this mixture. The mixture is then placed in a muffle furnace at 400 °C. The solid material obtained was calcined at 1350 °C for 3 h [74].

### 8.2. Magnesium orthosilicate

Magnesium orthosilicate ( $\text{Mg}_2\text{SiO}_4$ , CAS No. 10034-94-3) consists of  $\text{SiO}_4$  tetrahedrally linked to magnesium cations in octahedral coordination [75]. Magnesium orthosilicate is a member of the olivine family of crystals.  $\text{Mg}_2\text{SiO}_4$  consists of 57.29% MgO and 42.71%  $\text{SiO}_2$ . It is prepared by heating Mg powder (99.99%, <0.5  $\mu\text{m}$ ) and  $\text{SiO}_2$  nanoparticle powders (about 80 nm) in a furnace at 1100 °C for 60 min under a constant flow of argon gas [76]. It can be also prepared by mixing tetramethoxysilane (TMOS) or tetraethoxysilane (TEOS),  $\text{H}_2\text{O}$ , and magnesium metal in methanol.  $\text{Mg}_2\text{SiO}_4$  is crystallized at 500 °C [77]. It can be also be prepared by a sol-gel method using magnesium nitrate hexahydrate ( $\text{Mg}(\text{NO}_3)_2 \cdot 6\text{H}_2\text{O}$ ) and colloidal  $\text{SiO}_2$  as precursors with an initial MgO to  $\text{SiO}_2$  molar ratio of 2:1. The obtained gel is dried, milled, and calcined at different temperatures between 1100 °C and 1300 °C for 3 h [78]. Magnesium orthosilicate ( $\text{Mg}_2\text{SiO}_4$ ) can also be synthesized by nontraditional sol-gel schemes related to the use of high-boiling chemically active (HBCA) additives to prevent the polycondensation of silicate anions at the early stages of synthesis. Magnesium acetate is used as the metal oxide precursor; tetraethoxysilane and  $\gamma$ -aminopropyltriethoxysilane as the  $\text{SiO}_2$  precursors, resorcinol and triethanolamine as the HBCA additives, water and dimethyl formamide as the solvents. Gelation and drying of the precursor solutions are carried out at 20 °C and 120 °C, respectively; further thermal treatment of samples are performed up to 900 °C [79].

**TABLE 7.14** The chemical abstract index name, registry number, and empirical formulae of substances related to magnesium silicate

Compound	Chemical abstract index name	Registry number	Empirical formula
Natural hydrated magnesium silicate	Talc	14807-96-6	$\text{Mg}_3\text{Si}_4\text{O}_{10}(\text{OH})_2$ (Pure talc)
Basic magnesium silicate	Silicic acid ( $\text{H}_2\text{SiO}_3$ ), magnesium salt (4:3)	35592-05-3	$\text{Mg}_3\text{Si}_4\text{O}_{10}(\text{OH})_2$
Anhydrous magnesium silicate	Silicic acid ( $\text{H}_6\text{Si}_2\text{O}_7$ ), magnesium salt (1:3)	15702-53-1	$\text{Mg}_3\text{Si}_2\text{O}_7$
Dihydrate magnesium silicate	Silicic acid ( $\text{H}_6\text{Si}_2\text{O}_7$ ), magnesium salt, hydrate (1:3:2)	12263-17-1	$\text{Mg}_3\text{Si}_2\text{O}_7 \cdot 2\text{H}_2\text{O}$
Hydrate magnesium silicate	Silicic acid, magnesium salt, hydrate	1343-90-4	Unspecified
Anhydrous magnesium trisilicate	Magnesium silicon dioxide	1498-04-3	$\text{Mg}_2\text{Si}_3\text{O}_8$
Hydrate magnesium trisilicate	Silicic acid ( $\text{H}_4\text{Si}_3\text{O}_8$ ), magnesium salt (1:2), hydrate	39365-87-2	$\text{Mg}_2\text{Si}_3\text{O}_8 \cdot x\text{H}_2\text{O}$
Magnesium orthosilicate	Silicic acid ( $\text{H}_4\text{SiO}_4$ ), magnesium salt (1:2)	10034-94-3	$\text{Mg}_2\text{SiO}_4$
Magnesium metasilicate	Silicic acid ( $\text{H}_2\text{SiO}_3$ ), magnesium salt	30079-89-1	$\text{Mg}_x\text{SiO}_3$
Magnesium metasilicate	Silicic acid ( $\text{H}_2\text{SiO}_3$ ), magnesium salt (1:1)	13776-74-4	$\text{MgSiO}_3$

### 8.3. Magnesium trisilicate hydrate [1]

Magnesium trisilicate hydrate ( $\text{Mg}_2\text{Si}_3\text{O}_8 \cdot x\text{H}_2\text{O}$ , CAS No. 39365-87-2) is constituted of magnesium oxide and silicon dioxide with varying proportions of water. It should contain not less than 20% of magnesium oxide and not less than 45% of silicon dioxide and can be prepared from sodium silicate and magnesium sulfate. It also occurs in nature as the minerals meerschaum, parasepiolite, and sepiolite.

### 8.4. Hydrated magnesium silicate [80]

Hydrated magnesium silicate (Talc,  $3\text{MgO} \cdot 4\text{SiO}_2 \cdot \text{H}_2\text{O}$ , CAS No. 14807-96-6) is a magnesium silicate commonly referred to as “soapstone”. It is obtained from natural sources and may contain a small amount of aluminum silicate. It is composed of MgO (31.7%),  $\text{SiO}_2$  (63.5%), and  $\text{H}_2\text{O}$  (4.8%). It is a crystalline nonhygroscopic, odorless, tasteless powder which is practically insoluble in water, dilute mineral acids, dilute solutions of alkali halides, and alkaline hydroxides but is soluble in hot concentrated sulfuric acid.

Talc is purified from its impurities (iron and other soluble impurities) by boiling in diluted hydrochloric acid, then washed with water and dried. Thermal analysis reveals that it exhibits an endothermic peak at 950–975 °C.

Talc reacts with hot concentrated mineral acid solution. It is stable with respect to light, oxidation, and changes in pH of suspensions. Talc is thermally stable up to 900 °C, where it loses water and undergoes a solid-state transformation.

Table 7.14 lists the related substances of magnesium silicate as obtained from their CAS Registry files [4].

## REFERENCES

- [1] C.R. Raymond, J.S. Paul, C.O. Siân (Eds.), *Handbook of Pharmaceutical Excipients*, fifth ed., Pharmaceutical Press, London, 2006. Greyslake IL and American Pharmacists Association; Washington, DC.
- [2] The United States Pharmacopeia 32/The National Formulary 27 (USP 32/NF 27), vol. 1, USP Convention. INC, Maryland, 2009, pp. 1271–1272.
- [3] The Japanese Pharmacopeia (JP XV), 15th ed., Maruzen Company, Ltd., Japan, 2006, pp. 836–837.
- [4] CAS Registry file, accessed date October 2010.
- [5] O.O. Taspinar, S. Ozgul-Yucel, *Eur. J. Lipid Sci. Technol.* 110 (2008) 742–746.
- [6] A. Krysztafkiewicz, L.K. Lipska, F. Ciesielczyk, T. Jesionowski, *Adv. Powder Technol.* 15 (2004) 549–565.
- [7] F. Ciesielczyk, A. Krysztafkiewicz, T. Jesionowski, *J. Mater. Sci.* 42 (2007) 3831–3840.
- [8] SIDS Initial Assessment Report for SIAM 18, Paris, France 20–23 April, 2004, UNEP Publications. [www.inchem.org/documents/sids/sids/SolubleSilicates.pdf](http://www.inchem.org/documents/sids/sids/SolubleSilicates.pdf), access date December, 2010.

- [9] S.M. Bulatovic, *Handbook of Flotation Reagents: Chemistry*, Elsevier, 2007 pp. 178–179.
- [10] H. Li, Z.A. Zhou, Z. Xu, J.H. Masliyah, *Ind. Eng. Chem. Res.* 44 (2005) 4753–4761.
- [11] V.V. Potapov, *Glass Phys. Chem* 30 (2004) 73–81.
- [12] J. Liao, M. Senna, *Thermochim. Acta* 210 (1992) 89–102.
- [13] I.M. Ali, Y.H. Kotp, I.M. El-Naggar, *Desalination* 259 (2010) 228–234.
- [14] I. Rashid, N. Daraghme, M. Al-Remawi, S.A. Leharne, B.Z. Chowdhry, A. Badwan, *J. Pharm. Sci.* 98 (2009) 4887–4901.
- [15] F. Ciesielczyk, A. Krysztafkiewicz, T. Jesionowski, *Physicochem. Probl. Miner. Process.* 41 (2007) 185–193.
- [16] F. Ciesielczyk, A. Krysztafkiewicz, T. Jesionowski, *Appl. Surf. Sci.* 253 (2007) 8435–8442.
- [17] Z.Y. Zhu, R.A. Yates, J.D. Caldwell, *J. Am. Oil Chem. Soc.* 71 (1994) 289–292.
- [18] S. Lin, C.C. Akoh, A.E. Reynolds, *J. Food Lipids* 5 (1998) 1–16.
- [19] I.M. El-Naggar, M.M. Abou-Mesalam, *J. Hazard. Mater.* 149 (2007) 686–692.
- [20] D.R.M. Brew, F.P. Glasser, *Cem. Concr. Res.* 35 (2005) 85–98.
- [21] X. Jin, J. Chang, W.W. Zhai, K. Lin, *J. Am. Ceram. Soc.* 94 (2011) 173–177.
- [22] J.S. Hartman, R.L. Millard, *Phys. Chem. Miner.* 17 (1990) 1–8.
- [23] G. Selzer, M. Ariel, *Anal. Chim. Acta* 19 (1958) 496–502.
- [24] J.Ch. van Wesemael, *Anal. Chim. Acta* 25 (1961) 238–247.
- [25] G. Röbisch, A. Rerichaa, *Anal. Chim. Acta* 153 (1983) 281–284.
- [26] Z. Ying-quan, Z. Lin, L. Jun-yi, *Analyst* 107 (1982) 957–960.
- [27] B.C. Sinha, S.K. Roy, *Analyst* 105 (1980) 720–725.
- [28] B.C. Sinha, S.K. Roy, *Analyst* 107 (1982) 965–967.
- [29] M.A. Bello López, M.C. Mochón, J.L.G. Ariza, A.G. Pérez, *Analyst* 111 (1986) 429–433.
- [30] T. Pal, N.R. Jana, P.K. Das, *Analyst* 117 (1992) 791–793.
- [31] T. Pal, N. Jana, *Talanta* 40 (1993) 1519–1524.
- [32] K.A. Idriss, H. Sedaira, H.M. Ahmed, *Talanta* 54 (2001) 369–375.
- [33] M. Benamor, N. Agueressif, *Spectrochim. Acta Part A* 69 (2008) 676–681.
- [34] G. de Armas, A. Cladera, E. Becerra, J.M. Estela, V. Cerda, *Talanta* 52 (2000) 77–82.
- [35] R.W. Nesbitt, *Anal. Chim. Acta* 35 (1966) 413–420.
- [36] J. Adel-Antado, V. Martinez, A. Garcia, F. Reig, *Talanta* 38 (1991) 959–963.
- [37] K. Choi, L. Lam, S. Luk, *Talanta* 41 (1994) 1–8.
- [38] O. Law, L. Lam, S. Luk, *Talanta* 42 (1995) 1265–1271.
- [39] J. Saurina, E. Lopez-Aviles, A. Le Moal, S. Hernandez-Cassou, *Anal. Chim. Acta* 464 (2002) 89–98.
- [40] L.M. Thienpont, J.E. van Nuwenborg, D. Stöckl, *Anal. Chem.* 66 (1994) 2404–2408.
- [41] R. García-Fernández, J.I. García-Alonso, A. Sanz-Medel, *J. Chromatogr. A* 1033 (2004) 127–133.
- [42] M. Patsar-Kallio, P.K.G. Manninen, *Anal. Chim. Acta* 314 (1995) 67–75.
- [43] P. Kubáň, B. Karlberga, P. Kubáň, V. Kubáň, *J. Chromatogr. A* 964 (2002) 227–241.
- [44] S. Nussbaumer, S. Fleury-Souverain, L. Bouchoud, S. Rudaz, P. Bonnabry, J.-L. Veuthey, *J. Pharm. Biomed. Anal.* 53 (2010) 130–136.
- [45] M.C. Giacomelli, O. Largiuni, G. Piccardi, *Anal. Chim. Acta* 396 (1999) 285–292.
- [46] Å.K. Pettersson, B. Karlberg, *Anal. Chim. Acta* 378 (1999) 183–189.
- [47] J.M.P. Parajón, A. Sanz-Medel, *J. Anal. At. Spectrom.* 9 (1994) 111–116.
- [48] K. Fujiwara, E.P. Wagner II, B.W. Smith, J.D. Winefordner, *Anal. Lett.* 29 (1996) 1985–1992.
- [49] A.V. Medvetkii, T.I. Tikhomirova, A.D. Smolenkov, E.N. Shapovalova, O.A. Shpigun, *J. Anal. Chem.* 62 (2007) 213–218.
- [50] Y. Yokoyama, T. Danno, M. Haginoya, Y. Yaso, H. Sato, *Talanta* 79 (2009) 308–313.
- [51] A. Hioki, J.W.H. Lam, J.W. McLaren, *Anal. Chem.* 69 (1997) 21–24.
- [52] H. Sakai, T. Fujiwara, T. Kumamaru, *Bull. Chem. Soc. Jap.* 66 (1993) 3401–3406.
- [53] H.-B. Li, F. Chen, *J. Chromatogr. A* 874 (2000) 143–147.



- [54] M. Lacombe, V. Garçon, M. Comtat, L. Oriol, J. Sudre, D. Thouron, et al., *Mar. Chem.* 106 (2007) 489–497.
- [55] M.C.B. Alonso, R. Prego, *Anal. Chim. Acta* 416 (2000) 21–27.
- [56] Inactive ingredient for approved drugs products, [www.accessfda.gov/scripts/cder/iig](http://www.accessfda.gov/scripts/cder/iig), accessed date December 2010.
- [57] Equine Ulcers, HorseMomsSupplement™, [http://horsemomssupplements.com/html/equine\\_gastric\\_ulcers-a2.html](http://horsemomssupplements.com/html/equine_gastric_ulcers-a2.html), access date January, 2011.
- [58] R. Roseman, H. Eisenberg, Patent number US2384563, 1945.
- [59] Uses of sodium magnesium silicate, <http://www.tutorvista.com/chemistry/magnesium-sodium-silicate>, access date January, 2011.
- [60] J. Zielinski, M.F. McCarty, Patent number US6344444, 2002.
- [61] R.L. Brown, G.J. Bratton, N.M. Alford, K.G. Mannering, Patent number US20090196968, 2009.
- [62] K. Yanagisawa, K. Masaki, K. Sameno, Patent number US20090018238, 2009.
- [63] A. Takashi, A. Ryuichi, S. Mamoru, M. Naoya, M. Megumi, S. Masako, Patent number US4758461, 1988.
- [64] PAN Pesticides Database–Chemicals. [http://www.pesticideinfo.org/Detail\\_Chemical.jsp?Rec\\_Id=PC37076#Working](http://www.pesticideinfo.org/Detail_Chemical.jsp?Rec_Id=PC37076#Working), access date January 2011.
- [65] Cementitious Materials, <http://www.learnth1design.com/design/information/cementitious-materials>, access date January 2011.
- [66] Sodium silicate 40%, [http://www.cqconcepts.com/chem\\_sodiumsilicate.php](http://www.cqconcepts.com/chem_sodiumsilicate.php), access date January 2011.
- [67] F. Ciesielczyk, A. Krysztafkiewicz, T. Jesionowski, *Physicochem. Probl. Miner. Process.* 40 (2006) 255–263.
- [68] J.R. Munson, B.S. Cooke, B.L. Bertram, Patent number US20090199460, 2009.
- [69] D.D. Razzano, Patent number US5989575, 1999.
- [70] S.K. Wason, Patent number US4584330, 1986.
- [71] IUCLID Dataset, 2000 European Commission, European Chemicals Bureau. <http://www.thegoodscentscompany.com/data/rw1247061.html>, access date December, 2010.
- [72] J.V. Smith, *Acta Cryst.* 12 (1959) 515–519.
- [73] M. Song, J. Kim, M. Joung, S. Nahmw, Y. Kim, J. Paik, et al., *J. Am. Ceram. Soc.* 91 (2008) 2747–2750.
- [74] H. Nagabhushanaa, B.M. Nagabhushanab, B. Umeshc, H.B. Premkumard, N. Anild, T.K.G. Rao, et al., *Philos. Mag.* 90 (2010) 1567–1574.
- [75] J.D. Birlle, G.V. Gibbs, B. Moore, J.V. Smith, *Am. Mineral.* 53 (1968) 807–824.
- [76] R. Zhu, X.S. Peng, S.H. Sun, Y. Lin, L.D. Zhang, in *Los Alamos National Laboratory, Preprint Archive, Physics*, pp. 1–18 (2003), arXiv:physics/0310114.
- [77] T. Ban, Y. Ohya, Y. Takahashi, *J. Am. Ceram. Soc.* 82 (1999) 22–26.
- [78] S. Ni, L. Chou, J. Chang, *Ceram. Int.* 33 (2007) 83–88.
- [79] N.I. Maliavski, O.V. Dushkin, G. Scarinci, *Ceram. Silik.* 45 (2001) 48–54.
- [80] A.W. Newman, I.M. Vitez, P. Cortina, G. Young, J. DeVincentis, D.E. Bugay, et al., Analytical profile of talc, in: H.G. Brittain (Ed.), *Analytical Profiles of Drug Substances and Excipients*, vol. 23, Academic Press INC., California, USA, 1994, pp. 511–542.

# CHAPTER 8

## Tadalafil

**Alaa A.-M. Abdel-Aziz,<sup>\*</sup> Yousif A. Asiri,<sup>#</sup>  
Adel S. El-Azab,<sup>\*</sup> Mohamed A. Al-Omar,<sup>\*</sup> and  
Takehisa Kunieda<sup>†</sup>**

---

<b>Contents</b>		
1. Uses and Applications		289
2. Description		289
2.1. Nomenclature		289
2.1.1. Chemical name		289
2.1.2. Generic name		289
2.1.3. Trade name		289
2.2. Formulae		290
2.2.1. Empirical		290
2.2.2. Structural		290
2.3. Molecular weight, HRMS and CAS registry number		290
2.4. Optical rotation		290
2.5. Elemental composition		290
3. Physical Properties		291
3.1. Melting point		291
3.2. Solubility		291
3.3. Appearance		291
3.4. Peak plasma concentration		291
3.5. Apparent volume of distribution (Vd/F)		291
3.6. Apparent oral clearance (CL/F)		291
3.7. The mean elimination half-life		291
3.8. Duration of action		291
4. Method of Preparation		291
4.1. Diastereoselective synthesis of (+)-tadalafil ( <b>1</b> )		292

<sup>\*</sup> Department of Pharmaceutical Chemistry, College of Pharmacy, King Saud University, Riyadh, Saudi Arabia

<sup>†</sup> Faculty of Pharmaceutical Sciences, Sojo University, Kumamoto, Japan

<sup>#</sup> Department of Clinical Pharmacy, College of Pharmacy, King Saud University, Riyadh, Saudi Arabia

4.2. Stereoselective synthesis of (+)-tadalafil ( <b>1</b> ) and (+)-6- <i>epi</i> -tadalafil ( <b>8</b> )	292
4.3. Stereoselective synthesis of (+)-tadalafil ( <b>1</b> ) and (–)-12a- <i>epi</i> -tadalafil ( <b>11</b> )	293
4.4. US patent for stereoselective synthesis of (+)-tadalafil ( <b>1</b> )	295
4.5. The first synthesis of tadalafil ( <b>1</b> ) (Cialis) from <i>L</i> -tryptophan	296
5. Spectral Properties	298
5.1. Infrared spectrum	298
5.2. Nuclear magnetic resonance spectra	298
5.2.1. <sup>1</sup> H NMR spectrum	299
5.2.2. <sup>13</sup> C NMR and Dept <sup>13</sup> C spectra	301
5.2.3. 2D NMR ( <sup>1</sup> H– <sup>1</sup> H cosy and <sup>1</sup> H– <sup>13</sup> C HETCOR maps)	304
5.3. Mass spectrum	304
5.4. Ultraviolet spectra	304
5.4.1. Ultraviolet spectra in aqueous solutions	306
5.4.2. Ultraviolet spectra in ethanolic solution	306
5.4.3. Ultraviolet spectra in aqueous solution of cyclodextrin	306
6. X-ray Powder Diffractometry	308
6.1. X-ray powder diffractometry of tadalafil with poloxamer 407	308
6.2. X-ray powder diffractometry of tadalafil with cyclodextrin	309
6.3. X-ray powder diffractometry of pure (+)-tadalafil	311
7. Method of Determination	312
7.1. Chromatographic methods	312
7.1.1. HPLC/UV	312
7.1.2. HPLC–DAD and ESITM spectrometry	313
7.1.3. HPLC-chiral	316
7.1.4. Capillary electrophoresis	318
7.2. NMR and Raman spectroscopy to analyze genuine Cialis	319
7.2.1. Analysis of the genuine formulation of Cialis <sup>®</sup> using Raman spectrum	319
7.2.2. Analysis of the genuine formulation of Cialis <sup>®</sup> using conventional and 2D DOSY <sup>1</sup> H NMR	321
8. Pharmacodynamics	323
8.1. An overview	323
8.2. Mechanism of action	324
8.3. Efficacy and safety of tadalafil for the treatment of erectile dysfunction	324

8.4. Pharmacodynamic interactions between tadalafil and nitrates	325
9. Pharmacokinetics	325
9.1. An overview	325
9.2. Comparison of pharmacokinetic parameters between tadalafil and other PDE5 inhibitors	326
9.3. Tadalafil pharmacokinetics in patients with erectile dysfunction	327
9.4. Pharmacokinetic interaction between tadalafil and bosentan in healthy male	327
References	328

## 1. USES AND APPLICATIONS

Erectile dysfunction (ED), a common and widespread health problem that affects approximately 30 million men in the United States [1], is suggested to represent an early clinical manifestation of a diffuse vascular disease [2,3].

Tadalafil (Cialis®) [4–11], which is a cyclic guanosine monophosphate (cGMP) specific Type V phosphodiesterase (PDE5) inhibitor similar to sildenafil (Viagra®) [12] and vardenafil (Levitra®) [13], has an improved PDE5/PDE6 selectivity compared to sildenafil [14–16]. Tadalafil (Cialis®) is a newly approved oral selective PDE5 inhibitor indicated for the treatment of ED.

## 2. DESCRIPTION

### 2.1. Nomenclature [17,18]

#### 2.1.1. Chemical name

- (6*R*,12*aR*)-6-(1,3-Benzodioxol-5-yl)-2,3,6,7,12,12*a*-hexahydro-2-methylpyrazino[1',2':1,6]pyrido[3,4-*b*]indole-1,4-dione.
- (6*R*,12*aR*)-2,3,6,7,12,12*a*-Hexahydro-2-methyl-6-(3,4-methylenedioxyphenyl)pyrazino[2',1':6,1]pyrido[3,4-*b*]indole-1,4-dione.

#### 2.1.2. Generic name [17]

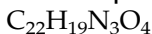
Tadalafil

#### 2.1.3. Trade name

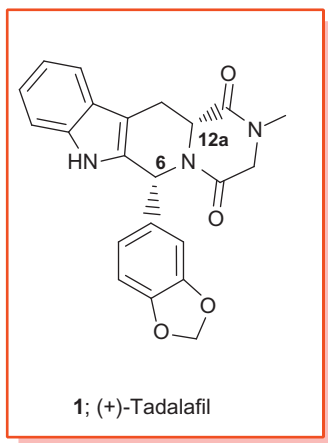
Cialis.

## 2.2. Formulae [17,18]

### 2.2.1. Empirical



### 2.2.2. Structural



## 2.3. Molecular weight, HRMS and CAS registry number [17,18]

- MW = 389.40
- (6R,12aR)-(+)-Tadalafil (**1**); HRMS calcd  $M^+$  for  $\text{C}_{22}\text{H}_{19}\text{N}_3\text{O}_4$  389.1376; found 389.1386
- (6S,12aR)-(+)-Tadalafil (**8**); HRMS calcd  $M^+$  for  $\text{C}_{22}\text{H}_{19}\text{N}_3\text{O}_4$  389.1376, found 389.1387 (**6-*epi*-tadalafil**)
- CAS = 171596-29-5

## 2.4. Optical rotation [17,18]

- (6R,12aR)-(+)-Tadalafil (**1**);  $[\alpha]_{\text{D}}^{20} = + 71.0$  ( $\text{CHCl}_3$ ,  $c = 1.0$ )
- (6S,12aR)-(+)-Tadalafil (**8**);  $[\alpha]_{\text{D}}^{20} = + 250.0$  ( $\text{CHCl}_3$ ,  $c = 1.0$ ) (**6-*epi*-tadalafil**)
- (6R,12aS)-(-)-Tadalafil (**11**);  $[\alpha]_{\text{D}}^{20} = - 303.1$  ( $\text{CHCl}_3$ ,  $c = 1.2$ ) (**12a-*epi*-tadalafil**)

## 2.5. Elemental composition [18]

C = 67.86%, H = 4.92%, N = 10.79%, O = 16.43%.

### 3. PHYSICAL PROPERTIES [17,18]

#### 3.1. Melting point

- (6*R*,12*aR*)-(+)-Tadalafil (**1**); 302–303 °C
- (6*S*,12*aR*)-(+)-Tadalafil (**8**); 286–288 °C (6-*epi*-tadalafil)
- (6*R*,12*aS*)-(-)-Tadalafil (**11**); 295–296 °C (12*a-epi*-tadalafil)

#### 3.2. Solubility

Practically insoluble in water; very slightly soluble in ethanol.

#### 3.3. Appearance

A white crystalline powder.

#### 3.4. Peak plasma concentration

378 ng/mL occurs 2 h postdose

#### 3.5. Apparent volume of distribution (Vd/F)

62.6 L

#### 3.6. Apparent oral clearance (CL/F)

2.48 L/h.

#### 3.7. The mean elimination half-life

17.5 h.

#### 3.8. Duration of action

36 h

### 4. METHOD OF PREPARATION

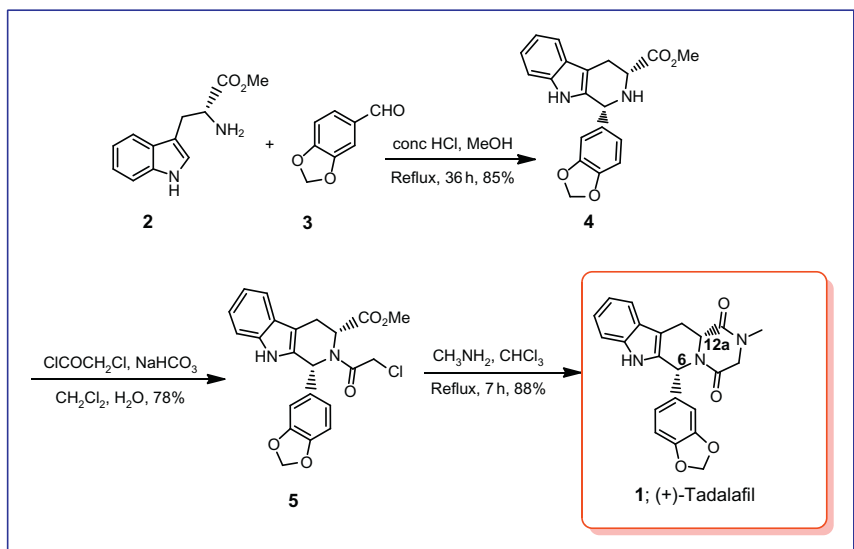
(+)-(6*R*,12*aR*)-2,3,6,7,12,12*a*-Hexahydro-2-methyl-6-(3,4-methylenedioxyphenyl)-pyrazino-[2',1':6,1]pyrido[3,4-*b*]indole-1,4-dione; Cialis; **1** [(+)-Tadalafil] is one of the well-known PDE5 inhibitors indicated for the treatment of ED [7–9].

#### 4.1. Diastereoselective synthesis of (+)-tadalafil (1) [19,20]

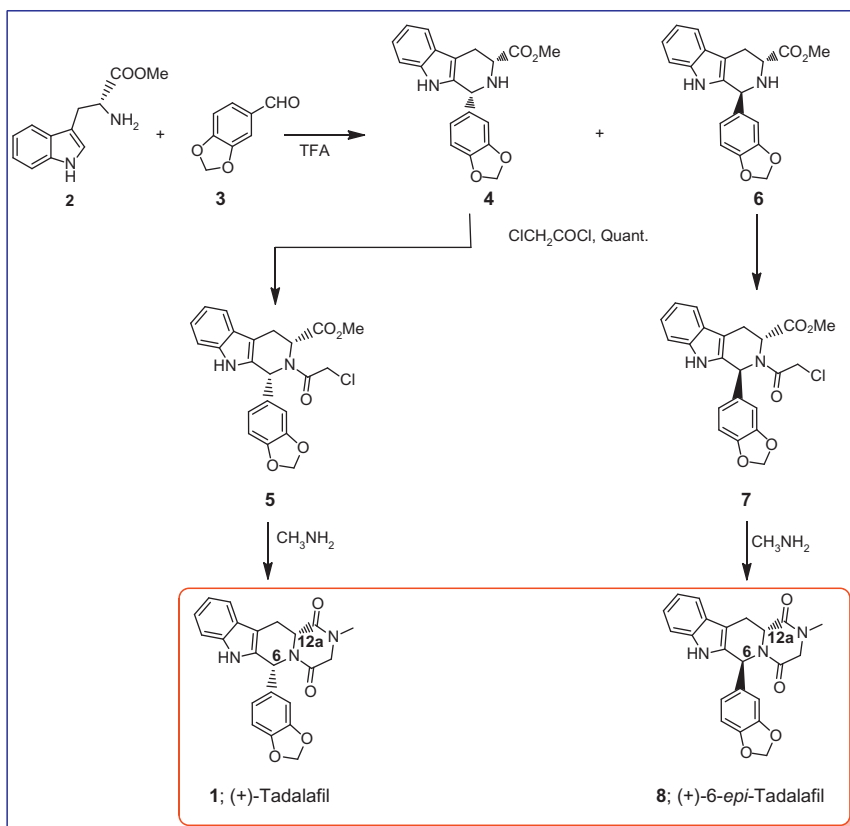
Scheme 8.1 describes a process for the synthesis of tadalafil (1) and its intermediate of formula 5 which involves reacting *D*-tryptophan methyl ester 2 with a piperonal 3 in the presence of methanol and conc. HCl to give compound 4. The later compound is then reacted with chloroacetyl chloride in the presence of NaHCO<sub>3</sub> to afford the intermediate 5, which is reacted with methylamine in chloroform to give tadalafil in 88% yield.

#### 4.2. Stereoselective synthesis of (+)-tadalafil (1) and (+)-6-*epi*-tadalafil (8) [20]

The target isomeric tadalafil molecule is shown in Scheme 8.2. Thus, *D*-tryptophan methyl ester reacted with piperonal 3 under Pictet-Spengler reaction condition (TFA/CH<sub>2</sub>Cl<sub>2</sub>/MeOH) to furnish two diastereomers 4 and 6 in 25% and 24% yields, respectively. Condensation of 4 or 6 with chloroacetyl chloride provided acylated intermediate 5 or 7 in almost quantitative yield. Subsequent cyclization of 5 with *N*-methyl amine in methanol at 50 °C for 16 h provided diastereomers tadalafil (1) in 54% yield. Compound 1 is in full accordance with the literature data  $[\alpha]_D^{20} = +71.4$  (c 1.00, CHCl<sub>3</sub>); lit.  $[\alpha]_D^{20} = +71.2$  (c 1.00, CHCl<sub>3</sub>) [17,18]. Thus, under the elongated reaction time, 48 h, compound 8 was obtained from precursor 7 with decreased yield of 21%.



**SCHEME 8.1** Diastereoselective route for the synthesis of (+)-tadalafil (1).

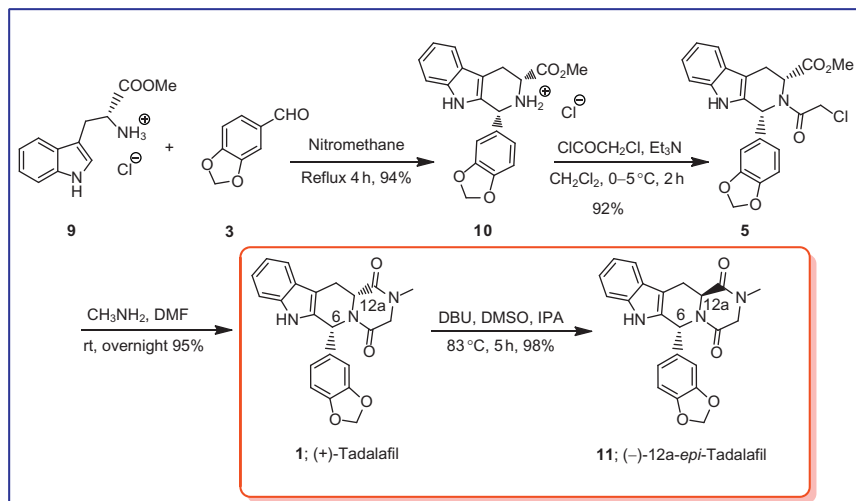


**SCHEME 8.2** Diastereoselective synthesis of (+)-tadalafil (**1**) and (+)-6-*epi*-tadalafil (**8**).

#### 4.3. Stereoselective synthesis of (+)-tadalafil (**1**) and (–)-12a-*epi*-tadalafil (**11**) [21]

**Scheme 8.3** depicts an efficient and stereospecific synthesis of tadalafil (**1**) as well as 12a-*epi*-tadalafil (**11**). Pictet–Spengler reaction of *D*-tryptophan methyl ester hydrochloride **9** with equal molar pteronol by refluxing for 4 h in nitromethane afforded *cis*-**10**-HCl in 98% ee and 94% yield. The hydrochloride salt of *cis* tetrahydro- $\beta$ -carboline derivative *cis*-**10**-HCl was directly treated with 1.5 equiv of chloroacetyl chloride in dichloromethane at 0°C in the presence of 3 equiv of triethylamine to form *N*-chloroacetyl tetrahydro- $\beta$ -carboline derivative **5** in 92% yield. Then compound **5** reacted with 5 equiv of methylamine overnight in DMF at room temperature to furnish tadalafil **1** in 95% yields.





**SCHEME 8.3** Stereoselective synthesis of (+)-tadalafil (**1**) and (–)-12a-*epi*-tadalafil (**11**).

**TABLE 8.1** The base-catalyzed epimerization of tadalafil (**1**) at the C-12a position to form 12a-*epi*-tadalafil (**11**)

Entry	Solvent (ratio)	Base (equiv)	Condition	Yield (%)
1	DMSO	KOH (2)	rt, 4 h	82
2	DMSO	<i>t</i> -BuOK (3)	0 °C, 0.5 h	83
3	DMSO	DBU <sup>a</sup> (3)	70 °C, 10 h	91
4	DMSO (1) THF (5)	DBU (2)	70 °C, 10 h	96
5	DMSO (4) H <sub>2</sub> O (1)	KCO <sub>3</sub> (2)	65 °C, 15 h	95
6	DMSO (1) DME <sup>b</sup> (9)	DBU (3)	85 °C, 9 h	97
7	DMSO (1) <i>i</i> -PrOH (5)	DBU (2)	83 °C, 5 h	98

<sup>a</sup> 1,8-Diazabicyclo [5,4,0]undec-7-ene.

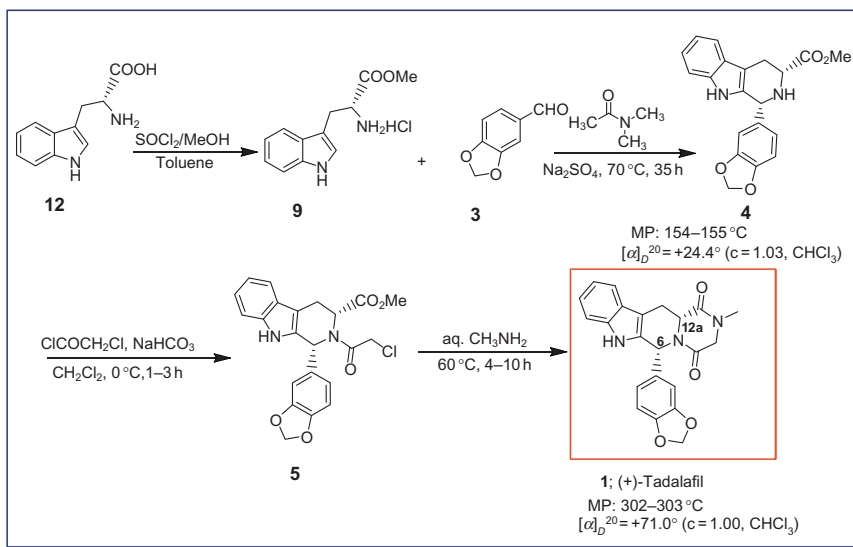
<sup>b</sup> 1,2-Dimethoxyethane.

When the reaction of compound 5 operated with methylamine in DMSO, it found that the reaction produced both **1** and its epimer 12a-*epi*-tadalafil (**11**). The amount of **11** increased as the temperature elevated. To understand the epimerization of **1** at the C-12a position more clearly, the epimerization of **1** in different solvents using various bases as the catalyst was established. Table 8.1 summarizes the outcomes of epimerization of **1** into **11**. It should be pointed out that DMSO was

crucial for the epimerization, the reaction took place smoothly in DMSO or a mixed solvent containing DMSO, while it was very slow in other solvents. When a strong base such as potassium hydroxide or potassium *tert*-butoxide was used, the reaction was fast, but the yield was not high (Table 8.1, entries 1 and 2). A weak base such as DBU or potassium carbonate turned out to be a suitable catalyst, and the yield was high (Table 8.1, entries 3–7). Tadalafil (1) was almost quantitatively transformed into 12a-*epi*-tadalafil (11) in a mixed solvent (DMSO–*i*-PrOH = 1:5) in the presence of 2 equiv of DBU after refluxing for 5 h.

#### 4.4. US patent for stereoselective synthesis of (+)-tadalafil (1) [22,23]

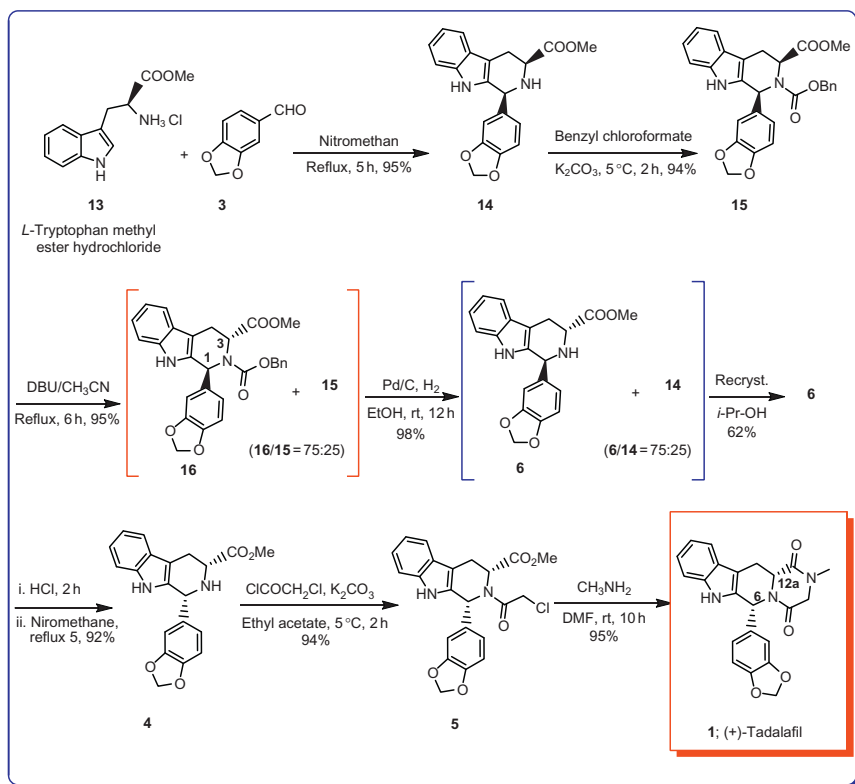
The present patent invention provided process of preparation of tadalafil (1) through the reaction of *D*-tryptophan methyl ester hydrochloride with piperonal in the presence of high boiling point dimethylacetamide and Na<sub>2</sub>SO<sub>4</sub> as dehydrating agents to give compound 4 as mixture of *cis* and *trans* isomers which is reacted further without isolating and separating isomers with an aqueous HCl to provide hydrochloride salt of *cis* isomer of compound 4 as major isomer (Scheme 8.4). Reacting the compound 4 with chloroacetyl chloride in the presence of NaHCO<sub>3</sub> and CH<sub>2</sub>Cl<sub>2</sub> as solvent to get the intermediate 5 which is further reacted with aqueous methylamine solution to obtain crude tadalafil which is purified by crystallization from IPA to get (+)-tadalafil (1) [22,23].



**SCHEME 8.4** Synthesis of (+)-tadalafil (US patent).

#### 4.5. The first synthesis of tadalafil (1) (Cialis) from *L*-tryptophan [24]

As depicted in Scheme 8.5, *L*-tryptophan methyl ester hydrochloride (**13**) was first treated with 1.1 equiv of piperonal in nitromethane at reflux temperature. Similar to *D*-tryptophan methyl ester hydrochloride, the highly stereoselective Pictet–Spengler reaction of *L*-tryptophan methyl ester hydrochloride with piperonal produced the hydrochloride salt of (1*S*,3*S*)-1,3-disubstituted-tetrahydro- $\beta$ -carboline **14**-HCl [17,25]. After neutralization of **14**-HCl, compound **14** was obtained in 95% yield and with 99% ee. Compound **14** was then treated with 1.2 equiv of benzyl chloroformate in ethyl acetate at around 5 °C in the presence of 3 equiv of potassium carbonate powder to afford (1*S*,3*S*)-1,2,3-trisubstituted-tetrahydro- $\beta$ -carboline (**15**) in 94% yield. The base-catalyzed epimerization of



**SCHEME 8.5** Synthesis of tadalafil (**1**) (Cialis) from *L*-tryptophan.

compound **15** at the C-3 position to form (1*S*,3*R*)-1,2,3-trisubstituted-tetrahydro- $\beta$ -carboline (**16**) was carried out. The first tried epimerization of compound **15** in methanol at reflux in the presence of 0.5 equiv of sodium methoxide, monitoring by TLC showed that compound **16** was gradually formed during the reaction, and the ratio of **16** and **15** increased meanwhile. Reflux was continued for more than 5 h, with the ratio of **16** and **15** becoming constant, meaning that the reaction was in equilibrium. Purification by flash chromatography gave pure compounds **16** and **15** in 89% combined yield and with a ratio of 75:25. Compound **16** is thermodynamically more stable than compound **15**; hence the base-catalyzed reversible epimerization would produce mixtures in which the more stable compounds **16** were major products.

The less stability of compound **15** when compared with compound **16** is probably due to the repulsion between the indole ring and the axial COOMe group. Comparison between the  $^1\text{H}$  NMR spectra of compounds **15** and **16** supports this assumption, the axial COOMe group of compound **15** exhibits a chemical shift (3.16 ppm) at a relatively upper field due to the closeness of indole ring and COOMe, while equatorial COOMe group of compound **16** exhibits a normal chemical shift (3.48 ppm). When the mixture of **16** and **15** (75:25) was treated with catalytic amounts of Pd/C in ethanol at room temperature for 12 h under an atmosphere of hydrogen gas, the benzyloxycarbonyl group at the N-2 position in both compounds **16** and **15** was successfully removed, and a mixture of compounds **6** and **14** was formed in 98% yield [26–28]. After recrystallization of the crude product (**6**/**14** = 75:25) in isopropanol, compound **6** could be obtained in 62% yield and with more than 99% purity. The transformation of (1*S*,3*R*)-1,3-disubstituted-tetrahydro- $\beta$ -carboline (**6**) to (1*R*,3*R*)-1,3-disubstituted-tetrahydro- $\beta$ -carboline (**4**) could be carried out by first converting **6** into its hydrochloride salt **6**-HCl, and then performing a CIAT process [17,25] to afford the hydrochloride salt **4**-HCl. After neutralization of **4**-HCl, compound **4** was obtained in 92% yield. Herein, the (*S*)-configuration of C-1 of compound **6** was inverted to the (*R*)-configuration of C-1 of compound **4** during the CIAT process. This acid-catalyzed epimerization at C-1 position was very clean, and the (*R*)-configuration of C-3 of compound **6** remained intact. As shown in Fig. 8.1, high-performance liquid chromatographic (HPLC) analysis showed that enantiomeric purity of compound **4** is 98.68% (er is 99.34:0.66). Compound **4** was then treated with 1.3 equiv of chloroacetyl chloride in ethyl acetate in the presence of 3 equiv of the powder of  $\text{K}_2\text{CO}_3$  to furnish compound **5** in 94% yield. Finally, compound **5** was converted into title compound **1** in 95% yield according to a known procedure [17], and the analytical data showed that the compound **1** obtained from this synthesis is identical with authentic sample of tadalafil.

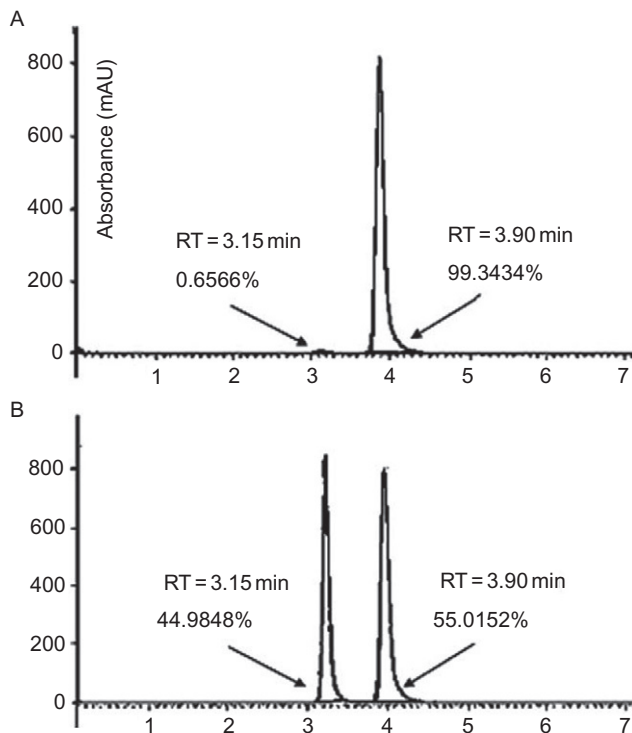


**FIGURE 8.1** HPLC analysis of compound **4** by a chiral column (spectra A for compound **4**, and spectra B for a racemic mixture of compounds **4** and **14**). Conditions: Column: AS-H; Mobile phase: methanol (0.1% DEA); flow rate: 0.6 mL/min; wavelength: 214 nm.

## 5. SPECTRAL PROPERTIES [17–25]

### 5.1. Infrared spectrum

- The FT-IR spectrum of (+)-tadalafil (**1**) as KBr disc is presented in Fig. 8.2. Principal peaks at wave numbers IR (KBr film) 3328, 2904, 1677, 1649, 1489, 1438, 1401, 1323, 1269, 1242, 1152, 1097, 1041, 939, 922, 746  $\text{cm}^{-1}$ .
- The IR spectrum of (–)-12a-*epi*-tadalafil (**11**) as KBr film was 3326, 2902, 1676, 1649, 1489, 1437, 1400, 1323, 1269, 1241, 1150, 939, 922, 746  $\text{cm}^{-1}$ .

### 5.2. Nuclear magnetic resonance spectra

$^1\text{H}$ ,  $^{13}\text{C}$  NMR, and other 2D spectra were recorded in  $\text{DMSO}-d_6$  at 500MHz, Bruker instrument (Bruker Company, USA); chemical shifts are expressed in  $\delta$  ppm with reference to TMS (Figs. 8.3–8.8).

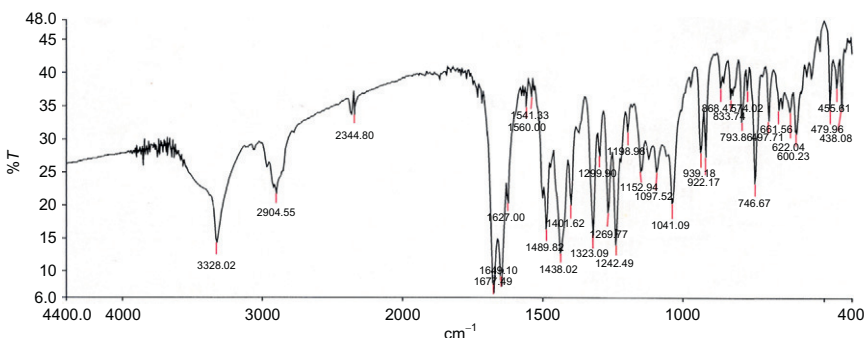


FIGURE 8.2 Infrared spectrum of (+)-tadalafil (1) (KBr disc).

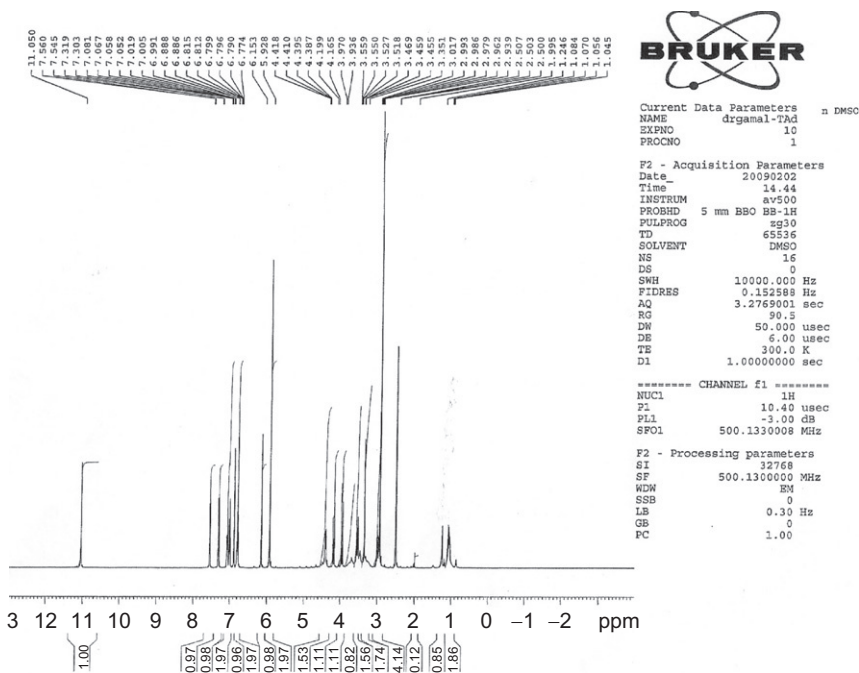
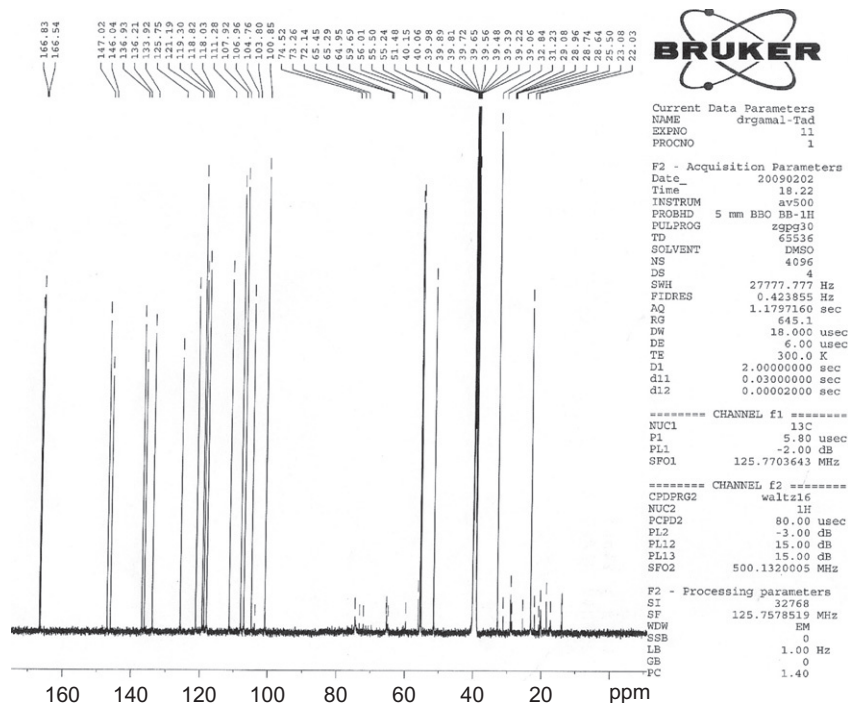


FIGURE 8.3  $^1\text{H}$  NMR spectrum of (+)-tadalafil (1) in  $\text{DMSO}-d_6$ .

### 5.2.1. $^1\text{H}$ NMR spectrum (Fig. 8.3)

- (+)-Tadalafil (1): (6R,12aR)-2,3,6,7,12,12a-Hexahydro-2-methyl-6-(3,4-methylenedioxyphenyl)-pyrazino-[2',1':6,1]pyrido[3,4-b]indole-1,4-dione

$^1\text{H}$  NMR ( $\text{DMSO}-d_6$ )  $\delta$  11.05 (s, NH on the indole ring), 7.54 (d,  $J = 7.5$  Hz, 1H), 7.30 (d,  $J = 8.0$  Hz, 1H), 7.07 (d,  $J = 7.0$  Hz, 1H), 7.00 (d,  $J = 7.0$  Hz, 1H), 6.86 (s, 1H), 6.77 (s, 2H), 6.15 (s, 1H), 5.92 (s, 2H), 4.39



**FIGURE 8.4**  $^{13}\text{C}$  NMR spectrum of (+)-Tadalafil (**1**) in  $\text{DMSO}-d_6$ .

(dd,  $J = 4.0$  Hz; 11.5 Hz, 1H), 4.17 (d,  $J = 17.0$  Hz, 1H), 3.94 (d,  $J = 17.0$  Hz, 1H), 3.52 (dd,  $J = 4.5$  Hz; 16.0 Hz, 1H), 2.96 (dd,  $J = 12.0$  Hz; 15.5 Hz, 1H), 2.94 (s, 3H).

- (+)-Tadalafil (**1**): (6R,12aR)-2,3,6,7,12,12a-Hexahydro-2-methyl-6-(3,4-methylenedioxyphenyl)-pyrazino-[2',1':6,1]pyrido[3,4-b]indole-1,4-dione

$^1\text{H}$  NMR ( $\text{CDCl}_3$ )  $\delta$  3.08 (s, 3H), 3.19 (m, 1H), 3.79 (m, 1H), 4.05 (quartet, 2H,  $J = 61.8, 18.5$  Hz), 4.31 (m, 1H), 5.92 (d, 2H,  $J = 7.7$  Hz), 6.18 (s, 1H), 6.70–7.82 (m, 7H).

- (–)-12a-*epi*-Tadalafil (**11**): (6R,12aS)-2,3,6,7,12,12a-Hexahydro-2-methyl-6-(3,4-methylenedioxyphenyl)-pyrazino-[20,10:6,1]pyrido[3,4-b]indole-1,4-dione

$^1\text{H}$  NMR ( $\text{DMSO}-d_6$ )  $\delta$  11.06 (s, NH on the indole ring), 7.49 (d,  $J = 7.7$  Hz, 1H), 7.31 (d,  $J = 8.1$  Hz, 1H), 7.10 (dd,  $J = 7.2$  Hz; 7.9 Hz, 1H), 7.01 (dd,  $J = 7.7$  Hz; 7.2 Hz, 1H), 6.86 (d,  $J = 8.0$  Hz, 1H), 6.82 (s, 1H), 6.75 (d,  $J = 1.4$  Hz, 1H), 6.60 (dd,  $J = 1.1$  Hz; 8.0 Hz, 1H), 5.99 (d,  $J = 6.5$  Hz, 2H), 4.24 (d,  $J = 17.6$  Hz, 1H), 4.07 (dd,  $J = 4.1$  Hz; 11.8 Hz, 1H), 4.03 (d,  $J = 17.7$  Hz, 1H), 3.25 (dd,  $J = 4.2$  Hz; 15.4 Hz, 1H), 2.95 (dd,  $J = 12.1$  Hz; 14.8 Hz, 1H), 2.84 (s, 3H).

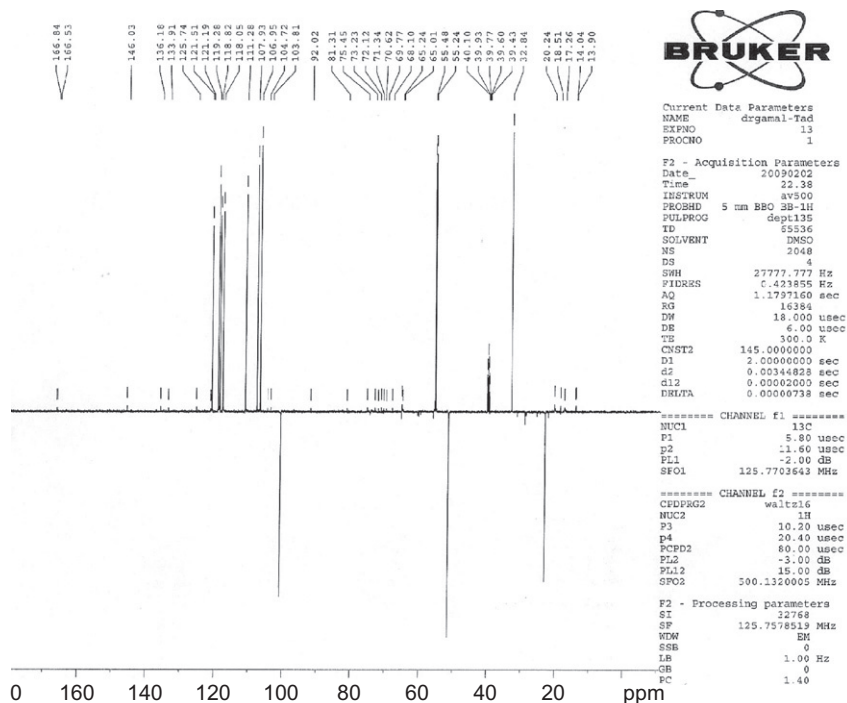


**FIGURE 8.5** Dept  $^{13}\text{C}$  spectra of (+)-Tadalafil (**1**).

- (+)-6-*epi*-Tadalafil (**8**): (6*S*,12*aR*)-2,3,6,7,12,12*a*-Hexahydro-2-methyl-6-(3,4-methylenedioxyphenyl)-pyrazino-[2',1':6,1]pyrido[3,4-*b*]indole-1,4-dione

$^1\text{H}$  NMR ( $\text{CDCl}_3$ )  $\delta$ : 2.95 (m, 1H), 3.02 (s, 3H), 3.56 (m, 1H), 4.10 (quartet, 2H,  $J = 55.6, 14.0$  Hz), 4.39 (m, 1H), 5.96 (s, 2H), 6.72–7.88 (m, 8H).

### 5.2.2. $^{13}\text{C}$ NMR and Dept $^{13}\text{C}$ spectra (Figs. 8.4 and 8.5)

- (+)-Tadalafil (**1**):

$^{13}\text{C}$  NMR ( $\text{DMSO}-d_6$ )  $\delta$ : 166.83, 166.54, 147.02, 146.04, 136.93, 136.21, 133.92, 125.75, 121.19, 119.30, 118.82, 118.03, 111.28, 107.92, 106.96, 104.76, 100.85, 55.50, 55.24, 51.48, 32.84, 23.08.

- (–)-12*a-epi*-Tadalafil (**11**):

$^{13}\text{C}$  NMR ( $\text{DMSO}-d_6$ )  $\delta$ : 164.78, 162.37, 147.69, 147.33, 136.20, 132.92, 130.25, 125.94, 121.78, 118.99, 118.16, 111.36, 108.42, 108.21, 107.55, 101.32, 52.09, 50.94, 50.73, 32.69, 26.74.



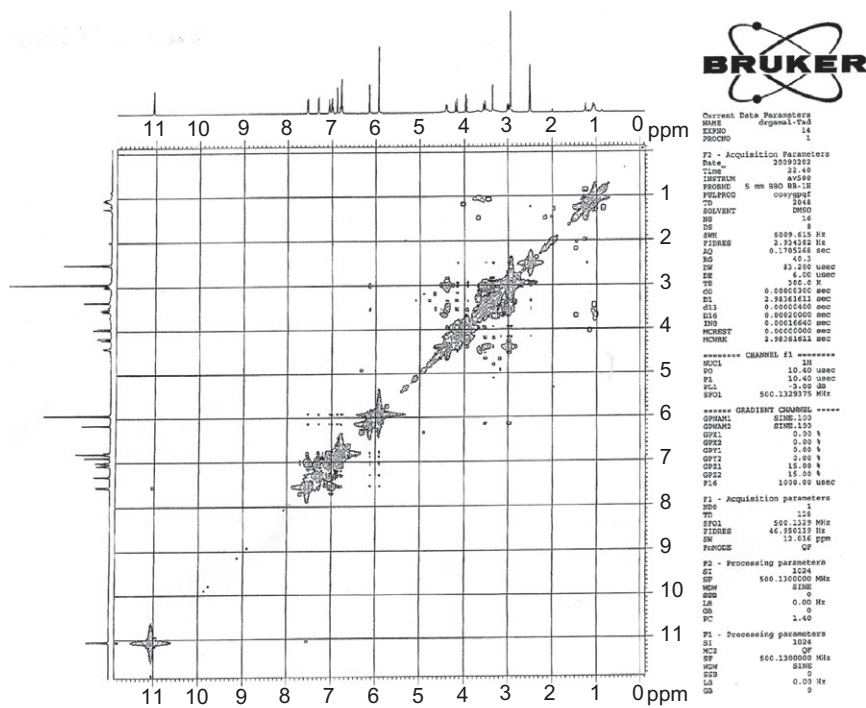
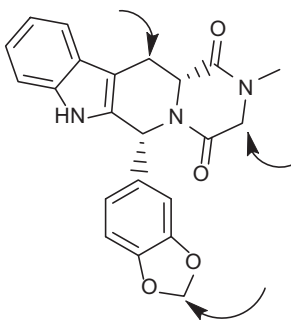
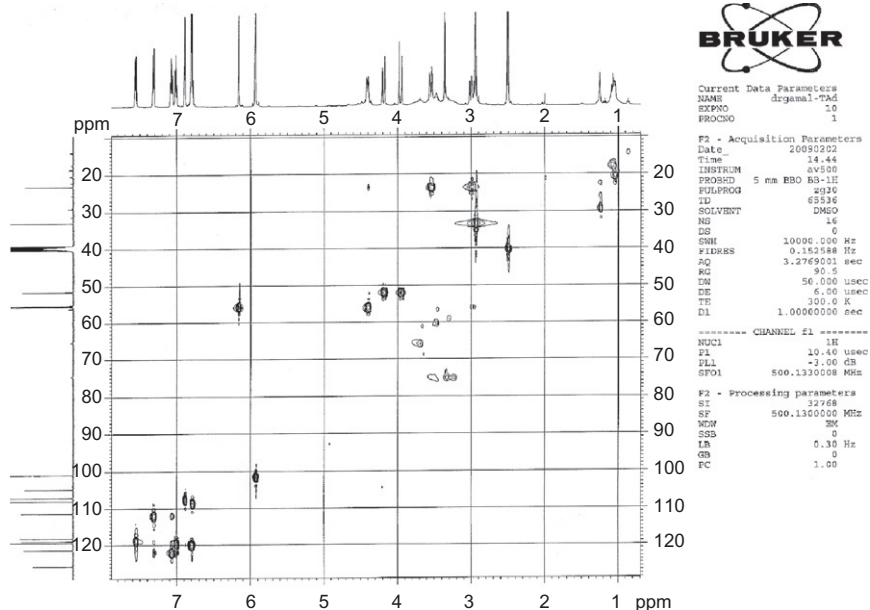


FIGURE 8.6  $^1\text{H}$ - $^1\text{H}$ -cosy of 135 of (+)-Tadalafil (1).

- Dept  $^{13}\text{C}$  spectra of (+)-Tadalafil (1) (Fig. 8.5) showed three  $\text{CH}_2$  fragments as illustrated in Tadalafil skeleton



1; (+)-Tadalafil



**FIGURE 8.7**  $^1\text{H}$ - $^{13}\text{C}$  HETCOR (hsqc) Maps of (+)-tadalafil (**1**).

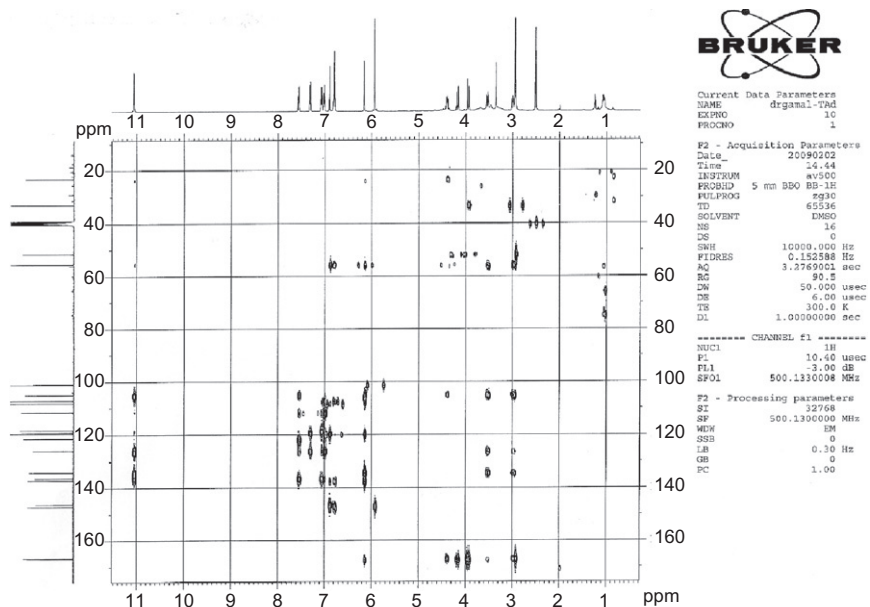
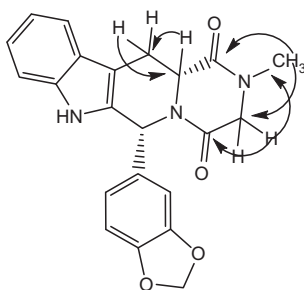


**FIGURE 8.8**  $^1\text{H}$ - $^{13}\text{C}$  HETCOR (hmbc) Maps of (+)-tadalafil (**1**).

### 5.2.3. 2D NMR ( $^1\text{H}$ – $^1\text{H}$ cosy and $^1\text{H}$ – $^{13}\text{C}$ HETCOR maps)



1; (+)-Tadalafil

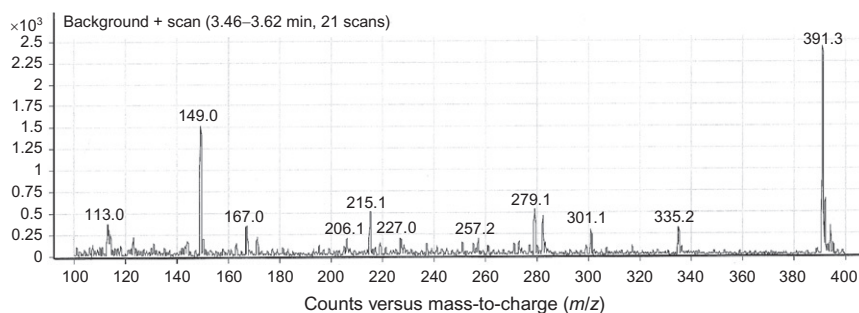
The assignment and interpretation of the  $^1\text{H}$ – $^1\text{H}$  and  $^1\text{H}$ – $^{13}\text{C}$  HETCOR spectra of (+)-tadalafil (1) has been carried out (Figs. 8.6–8.8). The resulting  $^1\text{H}$ – $^1\text{H}$  cosy assignments are shown in Fig. 8.6, indicating the coupling of each adjacent proton.  $^1\text{H}$ – $^{13}\text{C}$  HETCOR (HSQC and HMBC) assignments are shown in Figs. 8.7 and 8.8.

### 5.3. Mass spectrum

Mass spectra of (+)-tadalafil (1), carried out with electron impact method, were registered at 70 eV using a ION TRAP GCQ FINNIGAN mass spectrometer (Fig. 8.9). EI (MeOH):  $m/z$  391.3 ( $M+2$ ). Principal ions are presented in (Table 8.2).

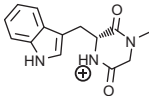
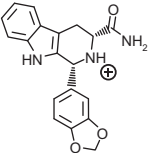
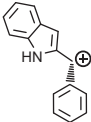
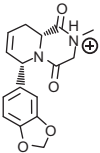
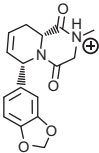
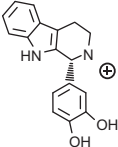
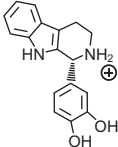
### 5.4. Ultraviolet spectra

The structure of tadalafil contains conjugated configuration and exhibit intensive UV absorption, thus it can be measured by UV detection with quite a low LOQ [29]. Also noted is that the structure of tadalafil possesses



**FIGURE 8.9** Mass spectrum of (+)-tadalafil (1) in methanol.

**TABLE 8.2** Mass fragmentation pattern of (+)-tadalafil (**1**)

<i>m/z</i>	Ions	<i>m/z</i>	Ions
391.3	M + 2	257.2	
335.2		206.1	
301.1		301.1	
279.1		279.1	

three amine groups, which might be ionized under acidic conditions. Based on the migration behavior in capillary zone electrophoresis (CZE), Hassan and Imran reported that tadalafil existed as a cation at pH 3 and migrated towards cathode [30]. On the contrary, Flores *et al.* concluded that tadalafil remained neutral in the running buffer with pH 2.2–13, as tadalafil migrated with the electro-osmotic flow under these pH conditions [31]. Because the degree of ionization could potentially affect the UV absorbance of a compound, it is worthy to evaluate the effect of pH value on the UV spectrum of tadalafil. As displayed in Fig. 8.10, tadalafil has similar absorption spectrum in acidic, neutral, and basic medium, with high molar absorbance around 220, 280, and 290 nm. Because higher sensitivity can be attained at low UV wavelength,

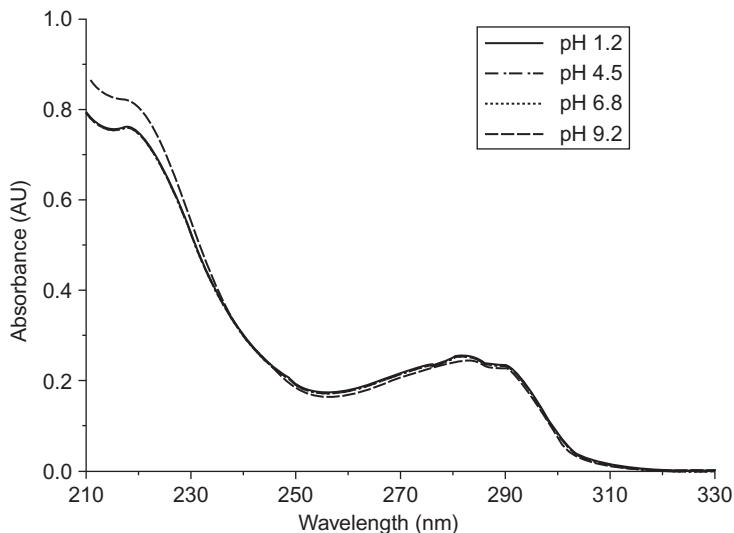


**FIGURE 8.10** The UV spectra of tadalafil (5 g/mL) in aqueous solutions with various pH values.

irrespective to the pH of the mobile phase or running buffer, the reported HPLC and CE methods applied UV detection at the region of 220–254 nm to determine tadalafil in pharmaceutical and nutraceutical preparations [31,32].

#### 5.4.1. Ultraviolet spectra in aqueous solutions

The UV spectra of tadalafil (5  $\mu\text{g/mL}$ ) in aqueous solutions with various pH values were recorded with 10-mm quartz cell using a Hitachi U2010 spectrophotometer (Tokyo, Japan). The aqueous solutions used were 0.1 N HCl (pH 1.2) and 50 mM phosphate buffers (pH 4.5, 6.8, and 9.2). Tadalafil exhibited similar absorption spectrum in acidic, neutral, and basic medium, with high molar absorbance around 220, 280, and 290 nm [33].

#### 5.4.2. Ultraviolet spectra in ethanolic solution

UV spectra of (+)-tadalafil (**1**) in ethanol (5 mg %) was scanned from 200–350 nm, using UV/VIS spectrophotometer. Tadalafil exhibited the maximum absorption at 215 nm (Fig. 8.11).

#### 5.4.3. Ultraviolet spectra in aqueous solution of cyclodextrin

Figure 8.12 showed the effect of CDs concentrations on the absorption spectra of tadalafil in aqueous solutions. Increasing the concentration of all CDs from 5 to 15 mmole/L resulted in an increase in the absorbance of

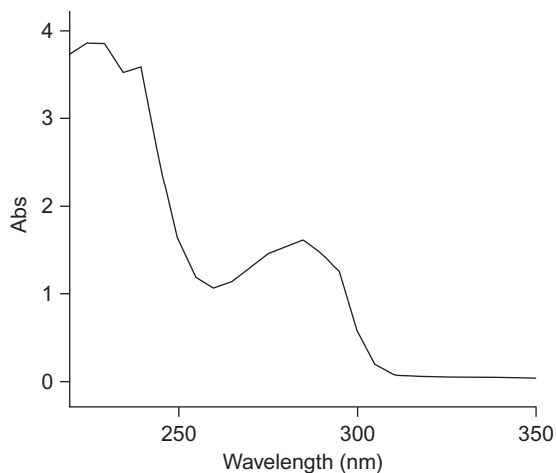


**FIGURE 8.11** UV spectrum of tadalafil (**1**) in ethanol.

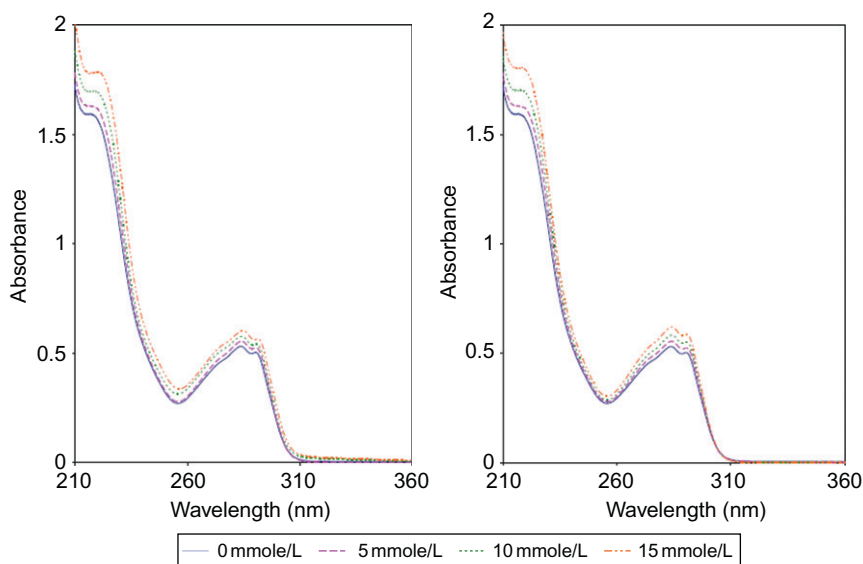


**FIGURE 8.12** Differential ultraviolet absorbance spectra of tadalafil in presence of  $\beta$ -CD (left panel) and HP- $\beta$ -CD (right panel).

tadalafil without any shifts of  $\lambda_{\text{max}}$  [34]. The observed hyperchromic shift might be due to the perturbation of the chromophore electrons of the drug due to the inclusion into the cyclodextrin cavity [35]. It could be indicative of cyclodextrin guest–host complex formation [35,36].

## 6. X-RAY POWDER DIFFRACTOMETRY

### 6.1. X-ray powder diffractometry of tadalafil with poloxamer 407

The XRPD pattern of tadalafil displayed intense and sharp peaks (Fig. 8.13A), indicating its crystalline nature. Relative decrease in crystallinity (RDC value) was determined by comparing some representative

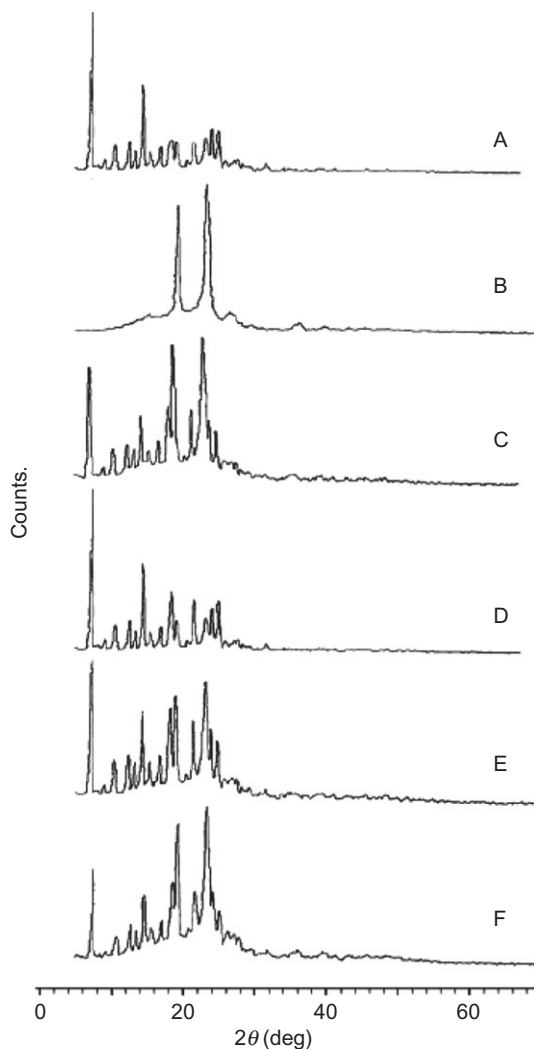


**FIGURE 8.13** XRPD patterns of: (A) tadalafil, (B) poloxamer 407, (C) physical mixture, (D) 1:0.5 solid dispersion, (E) 1:1.5 solid dispersion, (F) 1:2.5 solid dispersion.

peak heights in the diffraction patterns of the binary systems with those of a reference (pure tadalafil). Tadalafil (Fig. 8.13A) showed sharp peaks at 7.33, 12.62, 14.47, 14.56, 18.49, and 21.14° ( $2\theta$ ) with peak intensities of 2798, 243, 1043, 1282, 353, and 246, respectively. The crystalline nature of poloxamer 407 is displayed in Fig. 8.13B. The peak height at 7.335° ( $2\theta$ ) was used to calculate the RDC of tadalafil in all binary systems (Fig. 8.13C–F). The XRPD pattern of the physical mixture (Fig. 8.13C) displayed tadalafil and polymer peaks with a small decrease in the tadalafil peak intensity, indicating reduction in crystallinity (RDC = 0.144). Crystallinity of tadalafil was significantly reduced in the physical mixture, which might be due to higher proportion of the polymer in it (1:2.5). In the diffraction patterns of solid dispersion systems, a gradual decrease in crystallinity was observed with an increase in polymer concentration (Fig. 8.13D–F). The RDC values for 1:0.5, 1:1.5, and 1:2.5 solid dispersions were 0.278, 0.130, and 0.110, respectively. The peaks of tadalafil at 14.56° and 21.14° disappeared in all solid dispersion systems. The absence of intense peaks in solid dispersions suggested that the drug had lost its crystalline nature and possibly might have been transferred into amorphous form [37].

The XRPD patterns of pure tadalafil, poloxamer 407 and solid dispersions were recorded using a Philips Analytic X-Ray PW3710 (Philips, The Netherlands) diffractometer with tube anode Cu over the 5–70°/ $2\theta$  interval at a scanning speed of 2° min<sup>-1</sup>. The generator tension (voltage) and generator current were kept at 40 kV and 30 mA, respectively.

## 6.2. X-ray powder diffractometry of tadalafil with cyclodextrin [34]

Figure 8.14A–E showed the XRD patterns for pure components and their binary systems prepared by different techniques at molar ratio of 1:5 (drug to CD). The diffraction pattern of tadalafil powder revealed several sharp high intensity peaks at diffraction angles ( $2\theta$ ) of 7.8°, 10.2°, 12.2°, 14.5°, 18.2°, 22.2°, and 24.5° suggesting that the drug existed as crystalline material. Pure  $\beta$ -CD showed a crystalline diffractogram, while a diffuse halo-pattern was recorded for HP- $\beta$ -CD demonstrating its amorphous nature. Similar observations have been reported by other authors [38,39]. The diffraction patterns of the investigated PMs correspond to the superposition of those of the pure components. However, lower intensities of the diffraction peaks were observed due to particle size reduction during mixing and dilution of the pure crystalline components [40]. Overlapping of some tadalafil diffraction peaks with those of  $\beta$ -CD was evident. The diffractograms of the KN systems showed almost similar diffraction behavior to the PMs. The crystallinity of tadalafil was higher in the kneaded tadalafil- $\beta$ -CD than the corresponding PM. Similar



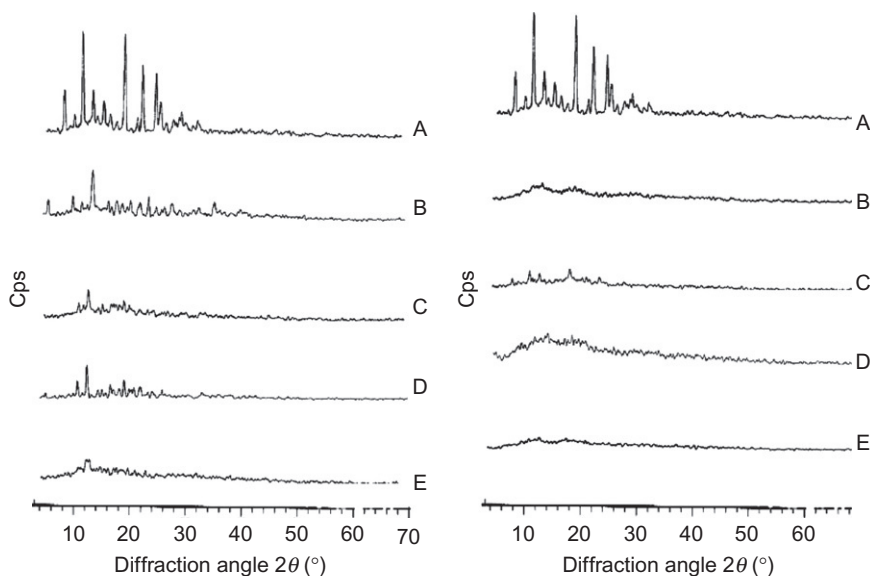


**FIGURE 8.14** Left panel showed X-ray diffraction patterns of tadafafil- $\beta$ -CD systems: (A) pure tadafafil; (B) pure  $\beta$ -CD; (C) PM 1:5; (D) KN 1:5; (E) FD 1:5. Right panel showed X-ray diffraction patterns of tadafafil-HP- $\beta$ -CD systems: (A) pure tadafafil; (B) pure HP- $\beta$ -CD; (C) PM 1:5; (D) KN 1:5; (E) FD 1:5.

increment in crystallinity was observed for Griseofulvin-2-HP- $\beta$ -CD kneaded systems, and was attributed to the formation of mixed crystalline particles during the desiccation process [41]. The presence of tadafafil peaks in the diffractogram of tadafafil- $\beta$ -CD, freeze-dried system could suggest the presence of the free crystalline drug, although reduction in number and intensities were observed. On the other hand, the diffractograms of FD systems prepared using HP- $\beta$ -CD showed a typical diffuse pattern indicating the entirely amorphous nature of tadafafil in both systems. According to Robert *et al.* [42], lack of crystallinity is an added evidence for the formation of inclusion complex. However, since the amorphization of the drug can be a sequence of the lyophilization process, it is possible that the X-ray data cannot discriminate whether the drug-CD lyophilized systems obtained are true inclusion complexes or homogenous dispersed mixtures of the amorphous components [43]. Nevertheless, having in account the results of the DSC analysis, one can assume the formation of new solid phases that might be credit to the formation of inclusion complexes.

The X-ray diffraction patterns were recorded at room temperature using a Scintag diffractometer (XGEN-4000, Scintag Corp., USA). The samples were irradiated with Ni-filtered Cu-K $\alpha$  radiation, at 45 kV voltage and 40 mA current. The scanning rate employed was 2°/min over a diffraction angle of  $2\theta$  and range of 3°–70°.

6.3. X-ray powder diffractometry of pure (+)-tadalafil

The X-ray diffraction patterns were recorded at room temperature using a Rigaku diffractometer with graphite monochromated Cu-K $\alpha$  rotating anode generator. The samples were irradiated with Ni-filtered Cu-K $\alpha$  radiation, at 40 kV voltage and 40 mA current. The scanning rate employed was 1°/min over a diffraction angle of 2 $\theta$  and range of 3°–60°. Figure 8.15 showed the X-ray powder diffractometry of pure (+)-tadalafil and its peak location.

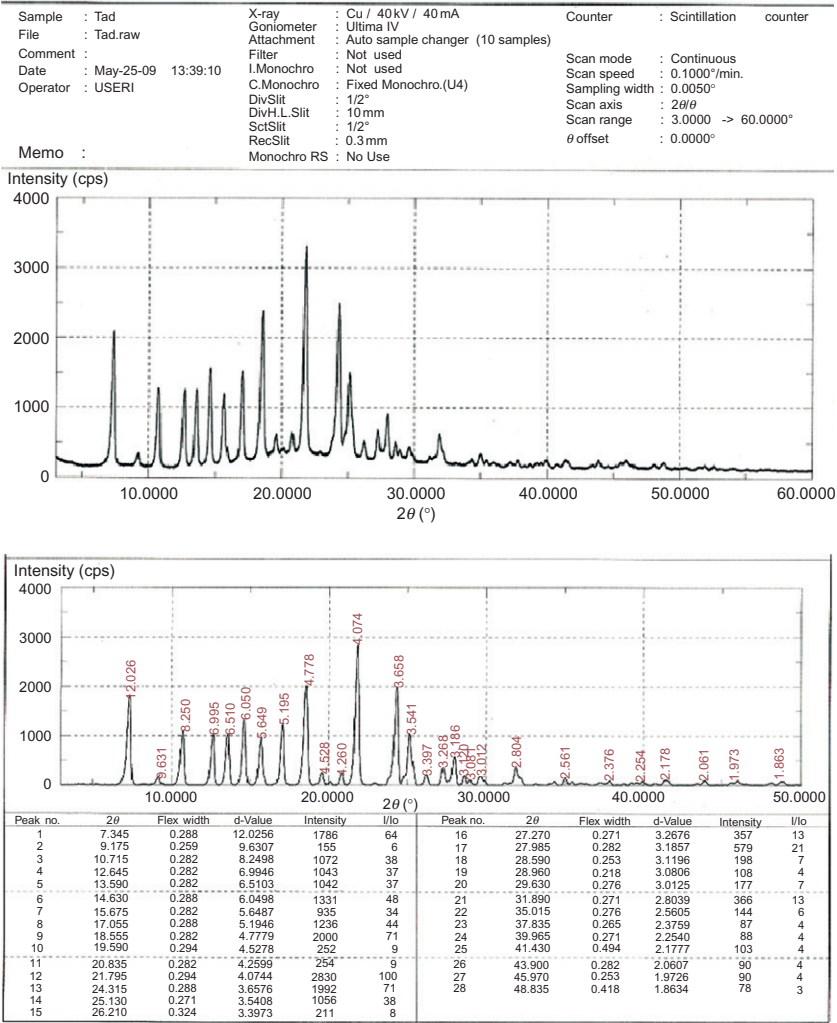


FIGURE 8.15 Upper panel showed X-ray diffraction patterns of (+)-tadalafil and the Lower panel showed its Peak location.

## 7. METHOD OF DETERMINATION

### 7.1. Chromatographic methods

#### 7.1.1. HPLC/UV

A simple and sensitive high-performance liquid chromatographic (HPLC) method for the determination of tadalafil in 50  $\mu$ L of rat plasma was described [33]. Tadalafil and the internal standard lamotrigine were extracted with 0.5 mL of *tert*-butyl methyl ether, after the samples alkalinized with 20  $\mu$ L of sodium hydroxide solution (1 N). Chromatographic separation was achieved on a C18 column with the mobile phase of acetonitrile: water containing 20 mM phosphate buffer (pH 7) (35/65, v/v), at a flow rate of 1 mL/min. The eluant was detected at 290 nm. The retention time was about 4.5 min for lamotrigine and 15 min for tadalafil. No endogenous substances were found to interfere. Calibration curves were linear from 10 to 2000 ng/mL. The recovery of tadalafil from plasma was greater than 77%. The limit of quantitation was 10 ng/mL. The intra- and inter-day imprecision (expressed as coefficient of variation, C.V.) did not exceed 10.7%, and the accuracy was within 5.9% deviation of the nominal concentration. The method is suitable in pharmacokinetic investigation and monitoring tadalafil concentration.

On the same time, the simple, reliable and reproducible HPLC and extraction methods were developed for the analysis of tadalafil in pharmaceutical preparation [30]. The column used was monolithic silica column, Chromolith Performance RP-18e (100 mm  $\times$  4.6 mm, i.d.). The mobile phase used was phosphate buffer (100 mM, pH 3.0)–acetonitrile (80:20, v/v) at the flow rate of 5 mL/min with UV detection at 230 nm at ambient temperature. Extraction of tadalafil from tablet was carried out using methanol. Linearity was observed in the concentration range from 100 to 5000 ng/mL for tadalafil with a correlation coefficient ( $R^2$ ) 0.9999 and 100 ng/mL as the limit of detection. The values of linearity range, correlation coefficient ( $R^2$ ) and limit of detection were 50–5000 ng/mL, 0.9999–50 ng/mL, respectively for sildenafil. Parameters of validation prove the precision of the method and its applicability for the determination of tadalafil in pharmaceutical tablet formulation. The method is suitable for high throughput analysis of the drug.

More recently, a highly selective, sensitive, and rapid HPLC method has been developed and validated to quantify tadalafil in human plasma [44]. The tadalafil and internal standard (loratadine, I.S.) were extracted by liquid–liquid extraction technique followed by an aqueous back-extraction allowing injection of an aqueous solvent in the HPLC system. The chromatographic separation was performed on a reverse phase BDS Hypersil C18 column (250 mm  $\times$  4.6 mm, 5  $\mu$ m, Thermo Separation Co., USA) with a mobile phase of acetonitrile and aqueous solution containing 0.012 M

triethylamine: 0.020 M orthophosphoric acid (50/50, v/v). The analytes were detected at 225 nm. The assay exhibited a linear range of 5–600 ng/mL for tadalafil in human plasma. The lower limit of quantitation (LLOQ) was 5 ng/mL. The within- and between batch precision (expressed as coefficient of variation, C.V.) did not exceed 10.3% and the accuracy was within 7.6% deviation of the nominal concentration. The recovery of tadalafil from plasma was greater than 66.1%. Stability of tadalafil in plasma was excellent with no evidence of degradation during sample processing (auto-sampler) and 30 days storage in a freezer. This validated method is applied for the clinical study of the tadalafil in human volunteers.

### 7.1.2. HPLC–DAD and ESITM spectrometry

A high performance liquid chromatography/diode array detection (HPLC–DAD) method and a liquid chromatography/electrospray ionization tandem mass spectrometry (LC–ESI–MS/MS) method were developed to screen for the presence of synthetic PDE5 inhibitors such as tadalafil, sildenafil, and vardenafil [45]. The methods were applied to premarket samples submitted to the Health Sciences Authority of Singapore (HSA) for testing. One sample was in the form of capsules while six other samples were premixed bulk powder samples for dietary supplements to be repackaged or formulated into the final dosage forms (usually capsules). Identification of PDE5 inhibitors and their analogues was achieved by comparing individual peak retention times, UV spectra and mass spectra with those of reference standards (Fig. 8.16). The seven samples were found to contain at least one of the following compounds: sildenafil, vardenafil, hydroxyhomosildenafil, homosildenafil, and acetildenafil. The five compounds were simultaneously determined by LC–ESI–MS/MS in multiple reactions monitoring (MRM) scan mode. The method has been validated for accuracy, precision, linearity, and sensitivity.

Moreover, a high performance liquid chromatographic method coupled with ultraviolet detection and electrospray ionization mass spectrometry (HPLC/UV/ESI/MS) was developed for simultaneous determination of banned additives: sildenafil, vardenafil, and tadalafil in dietary supplements for male sexual potency [29]. The separation was achieved on a C18 column with acetonitrile and aqueous solution (20 mmol ammonium acetate, 0.2% formic acid) as mobile phase at a flow rate of 1 mL/min with a linear gradient program. UV detection was at 292 nm. Identification of drugs was accomplished using ESI/MS. Good linearity between response (peak area) and concentration was found over a concentration range of 0.8–80 µg/mL for sildenafil; 2.25–225 µg/mL for vardenafil; and 1.1–110 µg/mL for tadalafil, with regression coefficient is better than 0.999. The recovery of the method ranged from 93.3% to 106.1%, and the relative standard deviation varied

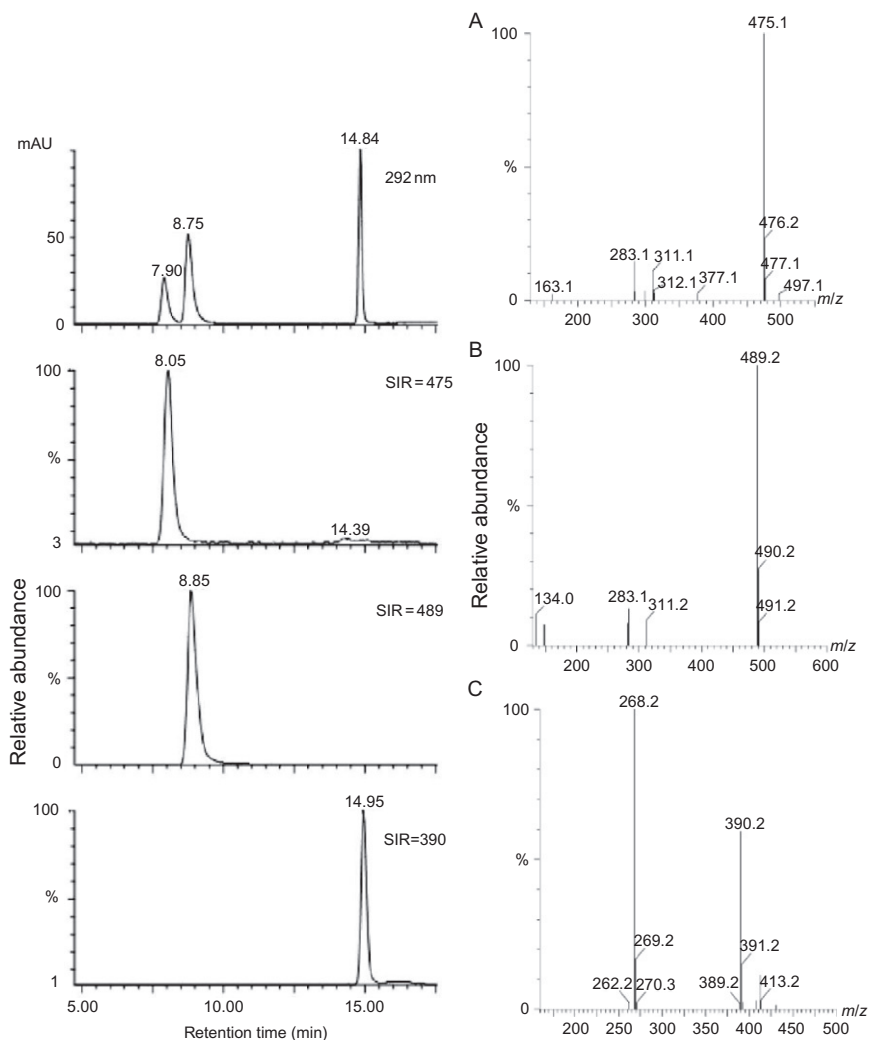


**FIGURE 8.16** Left panel showed the chromatogram of mixed standards. Peak identification: sildenafil ( $t_R = 7.9$ ), vardenafil ( $t_R = 8.8$ ) and tadalafil ( $t_R = 14.8$ ). The concentration of the three compounds in the mixture was 16, 45, and 22 g/mL, respectively. Right panel showed the mass spectrum of examined analytes. (A) Sildenafil, (B) vardenafil, and (C) tadalafil.

from 2.0% to 5.6% ( $n = 6$ ). The method has been successfully applied to the analysis of practical samples of natural dietary supplements.

A more simple, rapid, sensitive, and specific liquid chromatography, tandem mass spectrometry method [46], was developed and validated for quantitation of tadalafil I in human plasma, a new selective, reversible

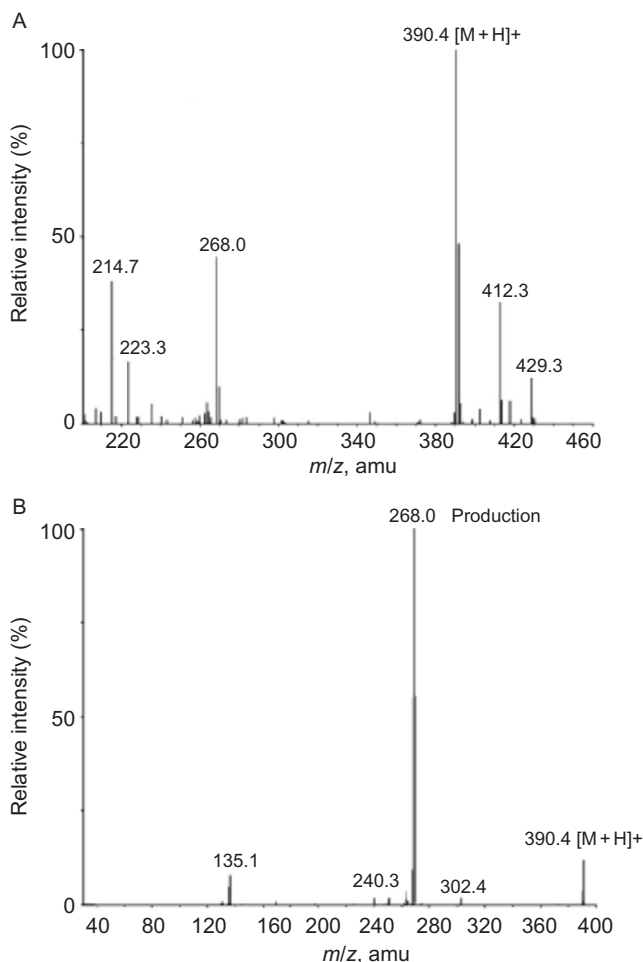


**FIGURE 8.17** Full scan positive ion Turboionspray (A) Q1 mass spectra and (B) product ion mass spectra of tadalafil.

PDE5 inhibitor (Fig. 8.17). The analyte and internal standard (sildenafil, II) were extracted by liquid–liquid extraction with diethyl ether/dichloromethane (70/30, v/v) using a Glas-Col Multi-Pulse Vortexer. The chromatographic separation was performed on reverse phase Xterra MS C18 column with a mobile phase of 10 mM ammonium formate/acetonitrile (10/90, v/v, pH adjusted to 3.0 with formic acid). The protonate of analyte was quantitated in positive ionization by MRM with a mass spectrometer. The mass transitions  $m/z$  390.4 > 268.0 and  $m/z$  475.5 > 58.3 were used to measure I and II, respectively. The assay

exhibited a linear dynamic range of 10–1000 ng/mL for tadalafil in human plasma. The LLOQ was 10 ng/mL with a relative standard deviation of less than 15%. Acceptable precision and accuracy were obtained for concentrations over the standard curve ranges. Run time of 1.2 min for each sample made it possible to analyze a throughput of more than 400 human plasma samples per day. The validated method has been successfully used to analyze human plasma samples for application in pharmacokinetic, bioavailability, or bioequivalence.

### 7.1.3. HPLC-chiral

A high performance liquid chromatographic method was developed for the chiral separation of new selective PDE5 inhibitors, tadalafil and its three isomers [47]. The chiral separation was performed on a Chiralpak AD column. The mobile phase was hexane-isopropyl alcohol (1:1, v/v). UV detection was at 220 nm. Baseline chiral separation for the four isomers was obtained within 30 min. Each of the resolutions of the two pairs enantiomers were more than 2.0. The limits of quantitation were 0.60, 0.90, 1.20, and 1.80 ng for (6*R*,12*aS*), (6*R*,12*aR*), (6*S*, 12*aS*), and (6*S*,12*aR*) isomers, respectively. Relative standard deviation of the method was below 2% ( $n = 5$ ). The method is suitable in quality control.

Moreover, a new simple isocratic chiral RP-LC method has been developed for the separation and quantification of the enantiomer of (*R,R*)-tadalafil in bulk drugs and dosage forms with an elution time of about 20 min [48]. Chromatographic separation of (*R,R*)-tadalafil and its enantiomer was achieved on a bonded macro cyclic glycopeptide stationary phase. The method resolves the (*R,R*)-tadalafil and its enantiomer with a resolution ( $R_s$ ) greater than 2.4 in the developed chiral RP-LC. The mobile phase used for the separation and quantification of (*R,R*)-tadalafil and its enantiomer involves a simple mixture of reverse phase solvents and the cost of analysis was drastically decreased. The test concentration is 0.4 mg mL<sup>-1</sup> in the mobile phase. This method is capable of detecting the enantiomer of (*R,R*)-tadalafil up to 0.0048 µg with respect to test concentration 400 µg mL<sup>-1</sup> for a 20 µL injection volume. The drug was subjected to stress conditions of hydrolysis, oxidation, photolysis, and thermal degradation. There was no interference of degradants with (*R,R*)-tadalafil and its enantiomer in the developed method. The developed chiral RP-LC method was validated with respect to linearity, accuracy, precision, and robustness.

Recently, four blisters with suspect Cialis® (tadalafil) 20 mg tablets were screened for authenticity using near infrared spectroscopy (NIRS) and for the presence of PDE5 inhibitors using LC-DAD-MS (Figs. 8.18 and 8.19). All samples were identified as counterfeit Cialis® and contained sildenafil or a combination of tadalafil and sildenafil [49].

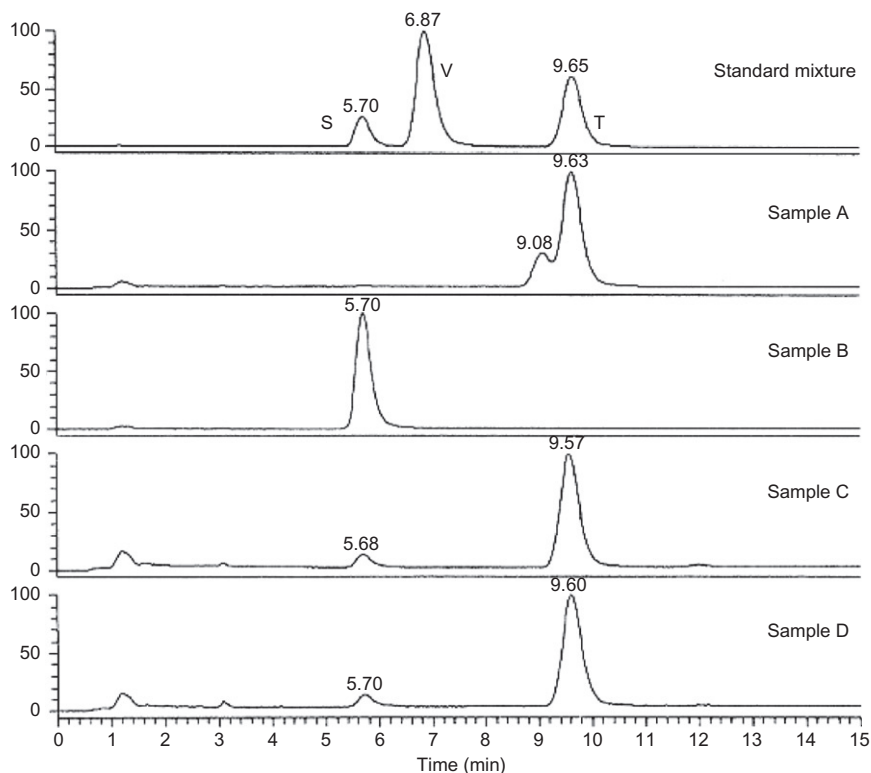


**FIGURE 8.18** PDA traces of the standard mixture of sildenafil (S), vardenafil (V), tadalafil (T) and the suspect Cialis® 20 mg samples using an XTerra MS C18 column (100 mm × 2.1 mm, 3.5 μm).

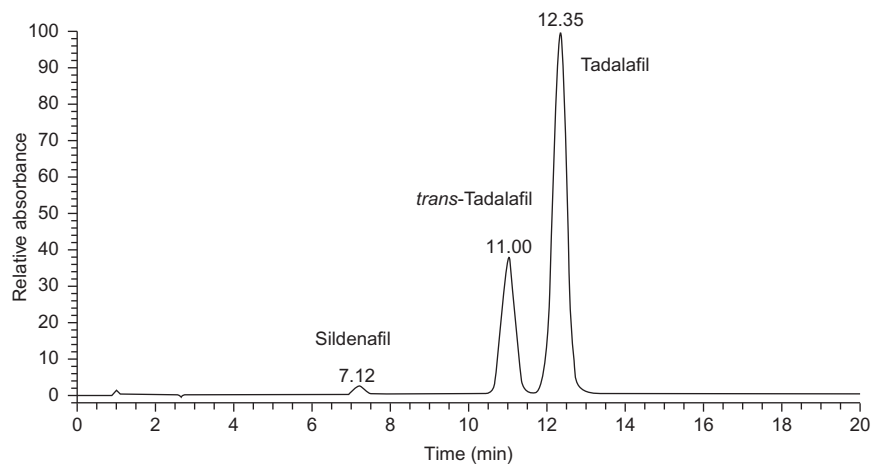


**FIGURE 8.19** PDA trace for sample A using the LC–DAD–MS method using a symmetry C18 column (100 mm × 2.1 mm, 3.5 μm).



Although the tablets contained efficacious amounts of PDE5 inhibitors, neither the active ingredient nor the dosage corresponded to the description on the blister. This is the first reported case of a diastereomeric mixture of tadalafil and *trans*-tadalafil (3:1) being identified in a counterfeit medicine. The LC–DAD–CD revealed that both diastereomers had a high optical purity. The optical rotation of the diastereomeric mixture was measured indicating the presence of (–)-*trans*-tadalafil, which is the only other stereoisomer with some PDE5 inhibitory activity. As no safety profiles are known for the stereoisomers of tadalafil, there is a potential health risk. In addition, the optical purity of tadalafil needs to be taken into account when calculating the dosage in illegal medicines.

#### 7.1.4. Capillary electrophoresis

A simple, rapid, and inexpensive capillary electrophoretic method [31] has been developed and validated for the determination of tadalafil in pharmaceutical preparations. The analysis was carried out using a fused silica capillary (60 cm × 75 mm, i.d.), phosphate buffer (50 mM, pH 3.0) as background electrolyte (BGE), 15 kV applied voltage with UV detection at 254 nm and at a working temperature of  $23 \pm 1$  °C. Linearity was observed in the concentration range from 200–5000 µg/mL, with a correlation coefficient ( $R^2$ ) of 0.9998 and 200 µg/mL as the limit of detection. The percentage recovery of tadalafil from pharmaceutical preparations was 99.5. Validation parameters prove the precision of the method and its applicability for the determination of tadalafil in pharmaceutical tablet formulations. The method is fast and is suitable for high throughput analysis of the drug.

On the same time, a Micellar electrokinetic capillary chromatography method is proposed for the determination of sildenafil, vardenafil, and tadalafil [32], which are employed in oral therapy for ED. Optimum conditions for the separation were investigated. A background electrolyte solution consisting of 10 mM phosphate buffer adjusted to pH 12.0, sodium dodecyl sulfate (SDS) 25 mM, hydrodynamic injection, and 25 kV as separation voltage were used. Relative standard deviations (RSDs) were 1.0%, 1.0%, 0.4% and 2.9%, 2.9%, 1.9% for migration time and corrected peak area (CPA) ( $n = 9$ ) for sildenafil, vardenafil, and tadalafil, respectively. Detection limits obtained for the three drugs ranged from 0.19 to 0.61 mg/L. A linear concentration range between 1 and 20 mg/L was obtained. A ruggedness test of this method was checked using the fractional factorial model of Plackett–Burman, in which the influence of six factors at three different levels was tested on different electrophoretic results: resolution and corrected peak area. The statistical evaluation of the electrophoretic results was achieved by Youden and Steiner method. The described method is rapid, sensitive, and

rugged and it was tested in the pharmaceutical formulations analysis obtaining recoveries between 98% and 107% respect to the nominal content.

## 7.2. NMR and Raman spectroscopy to analyze genuine Cialis

The reported method describe the use of Raman spectroscopy,  $^1\text{H}$  nuclear magnetic resonance (NMR) and 2D diffusion-ordered spectroscopy (DOSY) NMR to analyze genuine Cialis and seven illegally manufactured formulations of this drug purchased via the internet. Seven out of the eight commercial formulations of tadalafil contain the active ingredient, measured by HPLC, within  $100 \pm 5\%$  of stated concentration. Vardenafil and homosildenafil instead of tadalafil were found in the Chinese imitation. 2D DOSY NMR spectra clearly showed similarities and differences in the composition of the pharmaceutical formulations of tadalafil, thus giving a precise and global “signature” of the manufacturer. Data show that the quality of the Cialis imitations manufactured in India and Syria is correct, whereas the Chinese formulation is adulterated with active pharmaceutical ingredients [50,51].

### 7.2.1. Analysis of the genuine formulation of Cialis<sup>®</sup> using Raman spectrum

The Raman spectrum of the whole tablet of Eli Lilly Cialis<sup>®</sup> (formulation 1) is shown in Fig. 8.20 and Table 8.3. The main signals observed are those of titanium dioxide (\*) and talc (▲) present in the coating of the tablet. Iron yellow and triacetin could not be detected. In order to obtain more information, the coating was eliminated and recorded a new spectrum (Fig. 8.20C and D). The unsaturated structures of tadalafil (T) appeared clearly between  $1568$  and  $1676\text{ cm}^{-1}$  and around  $3070\text{ cm}^{-1}$ . Tadalafil gives an intense response to the laser excitation at  $632.8\text{ nm}$ , much stronger than that of the other components of the tablets, explaining why its bands are easily distinguished even if it represents only  $\approx 5\text{--}10\%$  of the tablet weight. In addition, most of the excipients used in the formulations do not contain aromatic, unsaturated or amide moieties. The peaks between  $1550$  and  $1700\text{ cm}^{-1}$  can thus be attributed to tadalafil by comparing the observed wave numbers with those of the pure substance. On the other hand, the region below  $1550\text{ cm}^{-1}$  was not considered for detecting tadalafil in the formulations as it is not specific since numerous bond vibrations (from aliphatic CH, CO, and CN groups) give Raman signals. The presence of the characteristic bands of magnesium stearate (□), lactose (○), and sodium lauryl sulfate (▲) were detected. Thus, it is able to detect the active substance and five excipients (titanium dioxide, talc, magnesium stearate, lactose, and sodium lauryl sulfate) by this technique.

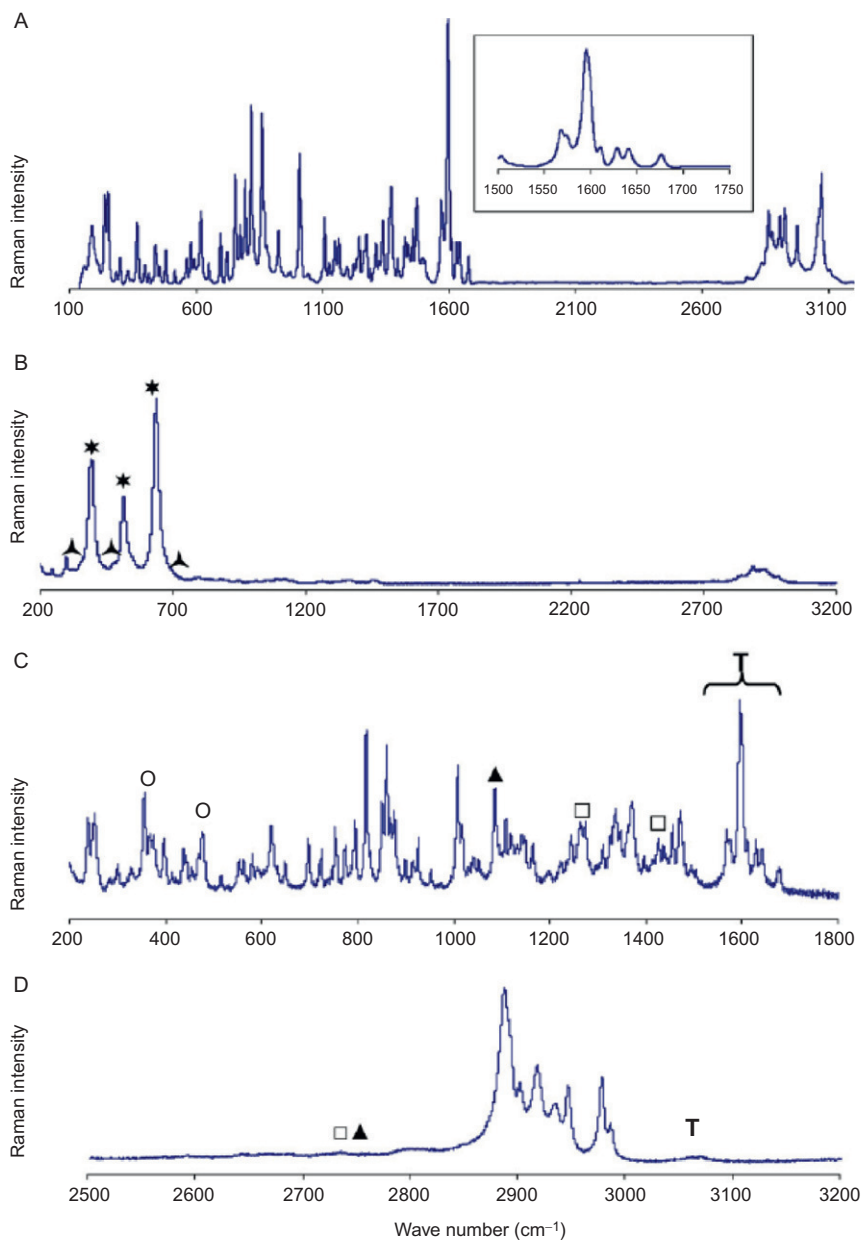


**FIGURE 8.20** Raman spectra of pure tadalafil (A) and genuine Eli Lilly Cialis®: whole tablet (B), uncoated tablet from 200 to 1800  $\text{cm}^{-1}$  (C), from 2500 to 3200  $\text{cm}^{-1}$  (D). \*  $\text{TiO}_2$ ;  $\blacktriangle$  talc (as shoulders of  $\text{TiO}_2$  bands); ( $\circ$ ) lactose; ( $\blacktriangle$ ) sodium lauryl sulfate; ( $\square$ ) magnesium stearate; (T) tadalafil.

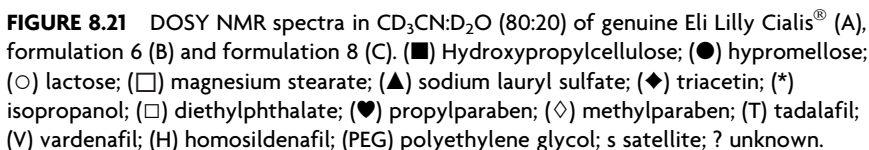
**TABLE 8.3** Raman bands detected for aromatic C–C bond vibrations for pure tadalafil and the eight formulations analyzed

Pure tadalafil		
Wave number (cm <sup>-1</sup> )	Formulations 1–7 (mean $\pm$ S.D.)	Formulation 8
3071	3072 $\pm$ 2	3089
1676	1677 $\pm$ 3	1701
1641	1644 $\pm$ 3	1621
1629	1630 $\pm$ 1	1603
1611	1612 $\pm$ 3	1586
1594	1596 $\pm$ 2	
1575	1575 $\pm$ 2	
1567	1568 $\pm$ 1	

All bands were detected for formulations 1–3 and 5. For formulations 4, 6, and 7, two, three, and four bands, respectively, were not observed due to the poor resolution of the spectra.

### 7.2.2. Analysis of the genuine formulation of Cialis<sup>®</sup> using conventional and 2D DOSY <sup>1</sup>H NMR

All formulations of tadalafil were analyzed with 2D DOSY <sup>1</sup>H NMR. 2D DOSY spectra of genuine Cialis<sup>®</sup> and formulations 6 and 8 along with their corresponding 1D spectra are presented in Fig. 8.21. The peaks at 3.68 and 1.99 ppm correspond to the residual signals of water and acetonitrile, respectively. All the peaks of tadalafil are lined up and the value of the self diffusion coefficient was measured for each peak; an average self-diffusion coefficient was determined for each formulation. Several excipients could also be observed. All the formulations contain the lubricant magnesium stearate (□) that leads to four signals located at 0.89 (t), 1.28 (broad s), 1.52 (quin), and 2.13 (t) ppm. Lactose peaks (○) were identified in all formulations at 3.20 (t), 3.4–3.9 (m), 4.36 (d), 4.54 (d), and 5.12 (d) ppm. Except formulation 2, all the pharmaceutical preparations also contain a cellulose derivative as coating agent, giving three aligned signals at 1.11 (broad s), 3.37 (broad s), and 3.53 (broad s) ppm that is known to be hypromellose (●) (hydroxypropylmethyl cellulose) for the brand formulation 1 but is unknown for the other formulations. Another cellulose derivative with a higher molecular weight leads to broad signals at 1.1 ppm (s) and between 3.3 and 4.0 ppm; as for the first cellulose derivative, it is known to be hydroxypropylcellulose (■) for the brand formulation 1 but is unknown for the other formulations where it is observed (2 and 5). Signals of sodium lauryl sulfate (▲) (0.89 (t), 1.28 (broad s), 1.61 (quin), and 3.90 (t) ppm), a wetting agent, are present in the brand formulation 1 and in formulations 2, 3, and 5–7. The brand formulation 1 and the formulation 5 contain the hydrophilic plasticizer triacetin (◆)



(glyceryl triacetate; 5.22 (m), 4.23 (AB d), 2.06 (s), and 2.05 (s) ppm). The antimicrobial preservatives methylparaben (◆) (methyl-4-hydroxybenzoate, 3.83 (s), 7.88 (d) ppm) and propylparaben (♥) (propyl-4-hydroxybenzoate; 0.99 (t), 1.74 (app q), 4.20 (t), and 7.88 (d) ppm) were found in formulations 4, 6, and 7. Diethylphthalate (□) (1.32 (t), 4.33 (q), and 7.68 (m) ppm), a plasticizer, could be detected in formulations 6–8. Propylene glycol, an anticaking agent, was found in formulations 2–4 (1.07 (d), 3.39 (AB d), and 3.74 (m) ppm). The presence of isopropanol, a coating solvent, is detected only by the signal of its methyl group at 1.1 ppm (d); this excipient was detected in formulations 4, 6, and 7 but its amount was subjected to a great intertablet variability even from the same batch. Only three formulations (2, 7, and 8) include polyethylene glycol as a lubricant agent (3.61 ppm (s)). Formulation 2 contains signals of citrate giving a characteristic AB system pattern at 2.53 ppm. Classical  $^1\text{H}$  NMR was then used to establish the structure of the active pharmaceutical ingredient(s) present in the Chinese fake formulation of Cialis (8) that had an atypical Raman spectrum. Figure 8.21C shows the  $^1\text{H}$  NMR spectrum of the Chinese formulation, which is very different from that of the original Cialis<sup>®</sup> analyzed in the same conditions (Fig. 8.21A). Tadalafil is not present in the Chinese formulation. Indeed, only the signals of excipients were observed in the 2.4–0.8 ppm spectral region of the brand Cialis<sup>®</sup> formulation 1, whereas signals of alkyl groups from active(s) were observed in the Chinese formulation 8. Moreover, the intensity of the peaks located in the aromatic region of the spectrum demonstrates that formulation 8 contains a mixture of two active pharmaceutical ingredients. After chromatographic purification of these two active ingredients, their NMR spectra were recorded and the compounds were thus identified as vardenafil and homosildenafil.

## 8. PHARMACODYNAMICS [1–3,52–55]

### 8.1. An overview

The term pharmacodynamics covers all actions of a drug on the different body organs and in turn their functions (e.g., blood pressure, heart rate, vision). The pharmacodynamic interactions of any drug are influenced by the number of receptors available in the target organ and the affinity of the compound to the receptors in question. The most important parameters concerning the pharmacodynamic properties of a drug are its biochemical potency and its organ (PDE) selectivity [1–3,52–55].

Tadalafil is PDE5 inhibitor that has recently been approved for the treatment of ED. Despite the clear utility of this compound, one potential drawback is cross-reactivity with the closely related PDE6 and PDE11.

It is thought that this cross-reactivity is responsible for side effects such as blue-tinged vision and back and muscle pain that experienced by some patients that were treated with this drugs [52,53].

## 8.2. Mechanism of action

The mechanism of action of tadalafil is similar to the other PDE5 inhibitors, sildenafil and vardenafil. Through the inhibition on PDE5, tadalafil increases the concentrations of cGMP, producing smooth muscle relaxation and increased blood flow to the corpus cavernosum, thereby enhancing erectile response following appropriate sexual stimulation [52–55].

## 8.3. Efficacy and safety of tadalafil for the treatment of erectile dysfunction [56]

Recent integrated analyses of five 12-week randomized, double-blind, placebo-controlled trials demonstrated that tadalafil, taken as needed at maximum daily doses of 5–20 mg without specific instruction regarding food/alcohol intake, significantly enhanced erectile function. Over this dose range, tadalafil significantly increased the ability to attain and maintain erections among 1112 men with histories of mild to severe ED ascribed to various cause. Approximately 61% of men had organic ED, 9% psychogenic and 31% mixed. Nearly 60% of men had moderate or severe ED at baseline [56].

A total of 1112 men with a mean age of 59 years (range 22–82) and mild to severe ED of various etiologies were randomized to placebo or tadalafil, taken as needed without food or alcohol restrictions, at fixed daily doses of 2.5, 5, 10, or 20 mg in five randomized, double-blind, placebo controlled trials lasting 12 weeks. The three co-primary outcomes were changes from baseline in the erectile function domain of the International Index of Erectile Function and the proportion of “yes” responses to questions 2 and 3 of the Sexual Encounter Profile. Additional efficacy instruments included a Global Assessment Question. Compared with placebo, tadalafil significantly enhanced all efficacy outcomes. Patients receiving 20 mg tadalafil experienced a significant mean improvement of 7.9 in International Index of Erectile Function erectile function domain score from baseline ( $p < 0.001$  vs. placebo), 75% of intercourse attempts (Sexual Encounter Profile question 3, a secondary efficacy outcome) were successfully completed ( $p < 0.001$  vs. placebo) and 81% reported improved erections at end point compared with 35% in the control group ( $p < 0.001$ ). Tadalafil was consistently efficacious across disease severities and etiologies, as well as in patients of all ages. Tadalafil was well tolerated, and headache and dyspepsia were the most frequent

adverse events. It was concluded that tadalafil was effective and well tolerated in this patient population.

#### 8.4. Pharmacodynamic interactions between tadalafil and nitrates [57,58]

Because sildenafil, another PDE5 inhibitor, is contraindicated in men taking nitrates, studies were undertaken to examine potential interactions between tadalafil and nitrates. Two double-blind, randomized, 3-way crossover studies were conducted in patients with stable angina to determine: (1) Study A – response to sublingual nitroglycerin (SL NG) administered 2 h after tadalafil 5 or 10 mg or placebo ( $n = 51$ ); and (2) Study B – response after tadalafil 5 or 10 mg or placebo administered during daily long-acting nitroglycerin (LA NG) therapy ( $n = 45$ ). Results: The table shows the results for the primary endpoint, which was mean maximal change in standing systolic BP (MMCSBP). There were no statistically significant differences in either study between tadalafil 5 or 10 mg and placebo in the sitting position. Conclusions: Tadalafil had minimal effects, relative to placebo, on mean blood pressure changes induced by either SL NG or LANG. However, the frequency of outliers was higher in the tadalafil treatment groups, indicating that in a subset of patients, tadalafil augments the decrease in BP induced by nitrates. These results suggest that, as with sildenafil, tadalafil should not be used in combination with nitrates.

### 9. PHARMACOKINETICS [14,29,52,54,59–66]

#### 9.1. An overview

Tadalafil is a potent and selective PDE5 inhibitor under regulatory review for the treatment of ED. In a clinical trial, tadalafil showed a clinical response in erectile function for up to 24 h postdosing.

In both chemical structure and PDE subtype selectivity profile, tadalafil differs markedly from sildenafil and vardenafil. These disparities are indicated by the respective suffixes: dalafil and denafil. Compared with sildenafil and vardenafil, tadalafil exhibits a prolonged plasma residence and window of therapeutic response. The  $t_{1/2}$  of tadalafil is 17.5 h and the  $t_{\max}$  is approximately 2.0 h (range, 0.5–12.0 h; normalized for a 20 mg dose) in healthy volunteers. In men with ED treated with tadalafil, a significantly higher percentage of attempts at sexual intercourse was successful as long as 24–36 h after dosing compared with placebo. The pharmacokinetics of tadalafil is also not clinically significantly influenced by extrinsic factors, such as food or alcohol intake; or intrinsic factors, such as diabetes or renal or hepatic impairment. The foregoing



advantages, particularly the reduced need to plan sexual activity around the time of either tadalafil dosing or meal/alcohol consumption, may translate in clinical practice into enhanced convenience and acceptability of tadalafil to the ED patient and/ or his partner [14,29,52,54,59–66].

## 9.2. Comparison of pharmacokinetic parameters between tadalafil and other PDE5 inhibitors

The pharmacokinetic properties of tadalafil comprise all the different steps from its entry into the body to its elimination out of the body. These steps include absorption rates with special regard to any food and alcohol interaction. In this regard of special interest is the speed of absorption, which can be seen by the  $T_{\max}$  (time needed to reach the maximum plasma concentration,  $C_{\max}$ ).  $C_{\max}$  (maximum plasma concentration of a drug) indicates the value of the highest drug concentrations reached in the plasma. According to the personal experiences in the clinical setting the  $T_{\max}$  corresponds pretty well with the time needed to get a completely rigid erection and the emphasis is here on the word rigid. Of major importance for the patients and their partners is also the  $T_{1/2}$  (half-life time), defined as that time it takes for the fall of the plasma concentrations of a drug to half of its  $C_{\max}$  values. Generally speaking the  $T_{1/2}$  corresponds very well with the duration of action of a drug. Tadalafil can be stated that the period of responsiveness, during which the majority of the responders to the drug are able to get a rigid erection after sexual stimulation, corresponds pretty well to the 2- to 3-fold half-life time. In this perspective, it has to be remembered that tadalafil is predominantly metabolized in the liver by the low-affinity cytochrome P450 enzyme 3A4 (CYP3A4) and secondarily by the high-affinity CYP2C9. Drugs with known inhibitory activities on CYP3A4 such as the H2 receptor antagonist cimetidine, the antibiotic erythromycin, the antimykotic drugs keto- and itraconazole or the protease inhibitors indinavir, ritonavir, and saquinavir can exert a major influence on the degradation rates of tadalafil and can increase considerably the  $C_{\max}$  and the total exposure to a PDE5 inhibitor in question. In particular, the protease inhibitors mentioned before are increasing the plasma concentrations and prolonging the half-life time in a clinically meaningful way that the dosages of tadalafil have to be adjusted (reduced) when patients are on such medications. The same applies for grapefruit juice, a typical CYP3A4 inhibitor. Last but not least in terms of the pharmacokinetic profile of a drug the protein binding has to be considered. Both the pharmacokinetic and pharmacodynamic properties of a drug may be influenced by intrinsic factors such as age, kidney or liver function, respectively, and concomitant diseases or medication [14,52,54].

### 9.3. Tadalafil pharmacokinetics in patients with erectile dysfunction

Tadalafil pharmacokinetics in patients with ED showed linear relation with respect to dose and duration of treatment, and a one-compartment model adequately described the data. The absorption rate was rapid ( $1.86 \text{ h}^{-1}$ ), and the typical population estimates of the apparent oral clearance (CL/F) and apparent volume of distribution were  $1.6 \text{ L/h}$  and  $63.8 \text{ L}$ , respectively. Disposition parameters showed a moderate degree of interindividual variability (39–45%). The value of CL/F decreased slightly with increasing serum  $\gamma$ -glutamyl transferase (GGT) concentration, the only statistically significant covariate detected. Systemic exposure to tadalafil was not influenced by age, weight, smoking status, alcohol consumption, liver enzyme status, ED severity, cardiovascular condition, or diabetes mellitus.

Finally, pharmacokinetics in the efficacy/safety trial population are essentially similar to pharmacokinetics in healthy subjects, and no patient-specific factor warranting clinical consideration of dose regimen adjustment was identified in these analyses [65].

### 9.4. Pharmacokinetic interaction between tadalafil and bosentan in healthy male

Tadalafil, an oral PDE5 inhibitor, is being investigated as a treatment for pulmonary arterial hypertension. Bosentan is an oral endothelin receptor antagonist widely used in the treatment of pulmonary arterial hypertension. Tadalafil is mainly metabolized by cytochrome P450 (CYP) 3A4, and as bosentan induces CYP2C9 and CYP3A4, a pharmacokinetic interaction is possible between these agents. This open-label, randomized study investigated whether any pharmacokinetic interaction exists between tadalafil and bosentan. Healthy adult men ( $n = 15$ ; 19–52 years of age) received 10 consecutive days of tadalafil 40 mg once daily, bosentan 125 mg twice daily, and a combination of both in a 3-period crossover design. Following 10 days of multiple-dose coadministration of bosentan and tadalafil, compared with tadalafil alone, tadalafil geometric mean ratios (90% confidence interval [CI]) for  $\text{AUC}_{\text{tau}}$  and  $C_{\text{max}}$  were 0.59 (0.55, 0.62) and 0.73 (0.68, 0.79), respectively, with no observed change in  $t_{\text{max}}$ . Following coadministration of bosentan with tadalafil, bosentan ratios (90% CI) for  $\text{AUC}_{\text{tau}}$  and  $C_{\text{max}}$  were 1.13 (1.02, 1.24) and 1.20 (1.05, 1.36), respectively. Tadalafil alone and combined with bosentan was generally well tolerated. In conclusion, after 10 days of coadministration, bosentan decreased tadalafil exposure by 41.5% with minimal and clinically irrelevant differences ( $<20\%$ ) in bosentan exposure [66].

## REFERENCES

- [1] T.F. Lue, *N. Engl. J. Med.* 342 (2000) 1802.
- [2] C. Gazzaruso, S. Giordanetti, E. De Amici, G. Bertone, C. Falcone, D. Geroldi, P. Fratino, S.B. Solerte, A. Garzaniti, *Circulation* 110 (2004) 22.
- [3] M. Bocchio, G. Desideri, P. Scarpelli, S. Necozione, G. Properzi, C. Spartera, F. Francavilla, C. Ferri, S. Francavilla, *J. Urol.* 171 (2004) 1601.
- [4] P.J. Dunn, *Org. Process Res. Dev.* 9 (2005) 88.
- [5] L.A. Sorbera, L. Martin, P.A. Leeson, J. Castaner, *Drugs Future* 26 (2001) 15.
- [6] A.C.-M. Daugan, European Patent, EP 0740668.
- [7] A. Daugan, P. Grondin, C. Ruault, A.-C. Le Monnier de Gouville, H. Coste, J. Kirilovsky, F. Hyafil, R. Labaudinière, *J. Med. Chem.* 46 (2003) 4525.
- [8] A. Daugan, P. Grondin, C. Ruault, A.-C. Le Monnier de Gouville, H. Coste, J.M. Linget, J. Kirilovsky, F. Hyafil, R. Labaudinière, *J. Med. Chem.* 46 (2003) 4533.
- [9] M.W. Orme, J.C. Sawyer, L.M. Schultze, *World Patent WO* 02/036593.
- [10] J.D. Revell, N. Srinivasan, A. Ganesan, *Synlett* (2004) 1428.
- [11] B.B. Lohray, V.B. Lohray, S.I. Patel, *World Patent WO* 05/068464.
- [12] F. Montorsi, T.E.D. McDermott, R. Morgan, A. Olsson, A. Schultz, H.J. Kirkeby, I.H. Osterloh, *Urology* 53 (1999) 1011.
- [13] S. Stark, R. Sachse, T. Liedl, J. Hensen, G. Rohde, G. Wensing, R. Horstmann, K.M. Schrott, *et al.*, *Eur. Urol.* 40 (2001) 181.
- [14] B. Patterson, A. Bedding, H. Jewell, C. Payne, M. Mitchell, *Eur. Urol. Suppl.* 1 (2002) 152.
- [15] J.D. Corbin, S.H. Francis, *Int. J. Clin. Pract.* 56 (2002) 453.
- [16] D.T. Manallack, R.A. Hughes, P.E. Thompson, *J. Med. Chem.* 48 (2005) 3449.
- [17] S. Xiao-Xin, L. Shi-Ling, X. Wei, X. Yu-Lan, *Tetrahedron Asymmetr.* 19 (2008) 435.
- [18] Merck index 2006, 14th edition pages 1550–1551.
- [19] N.M. Graham, M.N.A. Charlotte, G. Eugene, A.M. William, *Bioorg. Med. Chem. Lett.* 13 (2003) 1425.
- [20] Y. Zhang, Q. He, H. Ding, X. Wu, Y. Xie, *Org. Prep. Proced. Int.* 37 (2005) 99.
- [21] W. Jiang, V.C. Alford, Y. Qiu, S. Bhattacharjee, T.M. John, D. Haynes-Johnson, P.J. Kraft, S.J. Lundeen, Z. Sui, *Bioorg. Med. Chem.* 12 (2004) 1505.
- [22] D. Ben-Zion, D. Dov, *United States Patent*, US 2006/0276652 A1, 2006.
- [23] B.D. Pandurang, B.B. Bharat, S.S. Sachin, P.S. Pranay, *United States Patent*, US 7, 223, 863 B2, 2007.
- [24] X. Sen, S. Xiao-Xin, X. Jing, Y. Jing-Jing, L. Shi-Ling, L. Wei-Dong, *Tetrahedron Asymmetr.* 20 (2009) 2090.
- [25] S. Xiao, X. Lu, X.-X. Shi, Y. Sun, L.-L. Liang, X.-H. Yu, J. Dong, *Tetrahedron Asymmetr.* 20 (2009) 430.
- [26] H. Sajiki, *Tetrahedron Lett.* 36 (1995) 3465.
- [27] J. Meienhofer, K. Kuromizu, *Tetrahedron Lett.* 15 (1974) 3259.
- [28] J.-P. Mazaleyrat, J. Xie, M. Wakselman, *Tetrahedron Lett.* 33 (1992) 4301.
- [29] Z. Xiaolan, X. Song, C. Bo, Z. Fei, Y. Shouzhuo, W. Zutian, Y. Dajin, H. Hongwei, *J. Chromatogr. A* 1066 (2005) 89.
- [30] Y.A.-E. Hassan, A. Imran, *Talanta* 65 (2005) 276.
- [31] A. Imran, Y.A.-E. Hassan, *Chromatographia* 60 (2004) 187.
- [32] J. Rodríguez Flores, J.J. Berzas Nevado, G. Castañeda Peñalvo, N. Mora Diez, *J. Chromatogr. B* 811 (2004) 231.
- [33] C. Ching-Ling, C. Chen-Hsi, *J. Chromatogr. B* 822 (2005) 278.
- [34] M.B.-E. Shaimaa, A.E. Seham, M.G. Mahmoud, *Eur. J. Pharm. Biopharm.* 70 (2008) 819.
- [35] A.V. Cinzia, G. Ignazio, M. Teresa, P. Rosario, R. Lorella, L. Carla, M. Claudio, P. Donatella, P. Giovanni, *Eur. J. Med. Chem.* 41 (2006) 233.

- [36] V. Crupi, R. Ficarra, M. Guardo, D. Majolino, R. Stancanelli, V. Venuti, *J. Pharm. Biomed. Anal.* 4 (2007) 110.
- [37] V. Vikrant, S. Pankajkumar, K. Poonam, S. Manali, P. Yogesh, *Acta Pharm.* 59 (2009) 453.
- [38] A.B. Mohsen, A.A. Khalid, A.A.-A. Abdulaziz, *Int. J. Pharm.* 243 (2002) 107.
- [39] M. Jiradej, G.A. Maria, F. Kuncoro, M. Aranya, *Int. J. Pharm.* 293 (2005) 235.
- [40] S.S.R. Laura, C.F. Domingos, J.B.V. Francisco, *Eur. J. Pharm. Sci.* 20 (2003) 253.
- [41] M.D. Veiga, P.J. Díaz, F. Ahsan, *J. Pharm. Sci.* 87 (1998) 891.
- [42] O.W. Robert, M. Vorapann, S. Mongkol, *Eur. J. Pharm. Biopharm.* 46 (1998) 355.
- [43] E. Redenti, T. Peveri, M. Zanol, P. Ventura, G. Gnappi, A. Montenero, *Int. J. Pharm.* 129 (1996) 289.
- [44] A.K. Shakya, A.N. Abu-awwad, T.A. Arafat, M. Melhim, *J. Chromatogr. B* 852 (2007) 403.
- [45] Z. Peng, S.-Y.O. Sharon, H. Peiling, L. Min-Yong, K. Hwee-Ling, *J. Chromatogr. A* 1104 (2006) 113.
- [46] N.V. Ramakrishna, K.N. Vishwottam, S. Puran, M. Koteshwara, S. Manoj, M. Santosh, J. Chidambara, S. Wishu, B. Sumatha, *J. Chromatogr. B* 809 (2004) 243.
- [47] W. Gao, Z. Zhang, Z. Li, G. Liang, *J. Chromatogr. Sci.* 45 (2007) 540.
- [48] A. Madhavi, G.S. Reddy, M.V. Suryanarayana, A. Naidu, *Chromatographia* 67 (2008) 633.
- [49] B.J. Venhuis, G. Zomer, M.J. Vredenburg, D. de Kaste, *J. Pharm. Biomed. Anal.* 51 (2010) 723.
- [50] S. Trefi, C. Routaboul, S. Hamieh, V. Gilard, M. Malet-Martino, R. Martino, *J. Pharm. Biomed. Anal.* 47 (2008) 103.
- [51] B. Stéphane, T. Saleh, G. Véronique, M.-M. Myriam, M. Robert, D. Marc-André, *J. Pharm. Biomed. Anal.* 50 (2009) 602.
- [52] P. Hartmut, *EAU Update Series* 2 (2004) 56.
- [53] D.S. Allen, *Clin. Cardiol.* 27 (2004) I-14.
- [54] F. Giuliano, L. Varanese, *Eur. Heart J. Suppl.* 4 (2002) H24.
- [55] A.B. Mitsi, B. Alfreda, Z. Roya, R.S. Konjeti, P.B. Emmanuel, H.F. Sharron, D.C. Jackie, *Mol. Pharmacol.* 66 (2004) 144.
- [56] G.B. Brock, C.G. McMahon, K.K. Chen, T. Costigan, W. Shen, V. Watkins, G. Anglin, S. Whitaker, *J. Urol.* 168 (2002) 1332.
- [57] J. Emmick, M. Mitchell, A. Bedding, *Eur. Urol. Suppl.* 2 (2003) 95.
- [58] K. Robert, E. Jeff, B. Alun, H. Dennis, *J. Am. Colleg. Card.* 39 (Suppl. 2) (2002) 291.
- [59] H. Porst, *Int. J. Impot. Res.* 14 (Suppl. 1) (2002) S57.
- [60] D.O. Sussman, *J. Am. Osteopath. Assoc.* 104 (2004) 11S.
- [61] B.J. Ring, B.E. Patterson, M.I. Mitchell, M. Vandenbranden, J. Gillespie, A.W. Bedding, H. Jewell, C.D. Payne, S.T. Fargue, J. Eckstein, S.A. Wrighton, D.L. Phillips, *Clin. Pharmacol. Ther.* 77 (2005) 63.
- [62] C.C. Carson, J. Rajfer, I. Eardley, S. Carrier, J.S. Denne, D.J. Walker, W. Shen, *BJU Int.* 93 (2004) 1276.
- [63] S.T. Fargue, B.E. Patterson, A.W. Bedding, C.D. Payne, D.L. Phillips, R.E. Wrishko, et al., *Br. J. Clin. Pharmacol.* 61 (2006) 280.
- [64] B. Gerald, *Europ. Urology Supp.* 1, 2002, 12.
- [65] I.F. Trocóniz, C. Tillmann, A. Staab, J. Rapado, S.T. Fargue, *Eur. J. Clin. Pharmacol.* 63 (2007) 583.
- [66] R.E. Wrishko, J. Dingemanse, A. Yu, C. Darstein, D.L. Phillips, M.I. Mitchell, *J. Clin. Pharmacol.* 48 (2008) 610.

# Direct Crystallization of Enantiomers and Dissociable Diastereomers

Harry G. Brittain

---

Contents	1. Introduction	331
	2. Crystallography of Chiral Compounds	333
	3. Properties and Resolution of Racemic Mixtures of Dissymmetric Solids	336
	3.1. Conglomerate systems	343
	3.1.1. Inherently conglomerate systems	344
	3.1.2. Racemate systems rendered into conglomerates	347
	3.2. Racemate systems	350
	4. Summary	357
	References	357

## 1. INTRODUCTION

Molecules whose mirror images cannot be superimposed on each other are identified as being chiral, and a very important branch of separation science has developed around the resolution of compounds having pharmaceutical interest. At one time, scientists associated the phenomenon of optical rotation with the presence of carbon atoms bound to four different molecular fragments, and these asymmetrically substituted carbon atoms became known as “asymmetric carbons.” Continued work showed that compounds incapable of rotating the plane of polarized light, but which

Center for Pharmaceutical Physics, Milford, New Jersey, USA

Profiles of Drug Substances, Excipients, and Related Methodology, Volume 36  
ISSN 1871-5125, DOI: 10.1016/B978-0-12-387667-6.00009-9

© 2011 Elsevier Inc.  
All rights reserved.

were known to contain at least one asymmetric carbon atom, could be separated into chemically identical “optical isomers” that now exhibited the phenomenon of optical rotation. Over time, it became clear that optical activity could exist in compounds having no asymmetric atoms, and that other compounds existed that contained two or more asymmetric carbons, but still could not be rendered optically active. These findings necessitated a return to the proposal of Pasteur, who held that optical activity is a consequence of molecular dissymmetry. In other words, a molecule superimposable with its mirror image cannot be optically active, and any molecule not superimposable with its mirror image will exhibit optical activity.

The fundamental requirement for the existence of molecular dissymmetry is that the molecule cannot possess any improper axes of rotation, the minimal interpretation of which implies additional interaction with light whose electric vectors are circularly polarized. This property manifests itself in an apparent rotation of the plane of linearly polarized light (polarimetry and optical rotatory dispersion) [1–5], or in a preferential absorption of either left- or right-circularly polarized light (circular dichroism) that can be observed in spectroscopy associated with either transitions among electronic [3–7] or vibrational states [6–8]. Optical activity has also been studied in the excited state of chiral compounds [9,10]. An overview of the instrumentation associated with these various chiroptical techniques is available [11].

When a compound contains a single center of dissymmetry, its mirror images are termed as *enantiomers*. Individual enantiomeric molecules are completely equivalent in their molecular properties, with the exception of their interaction with polarized light. An equimolar mixture of two enantiomers is termed a *racemic mixture*. The generally accepted configurational nomenclature for tetrahedral carbon enantiomers was devised by Cahn, Ingold, and Prelog, and is based on sequencing rules [12]. Enantiomers are identified by their absolute configuration as being either *R* or *S*, depending on the direction (clockwise or counterclockwise) of substituents after they have been arranged according to increasing atomic mass. Compounds containing more than one center of dissymmetry are identified as *diastereomers*, and in compounds containing  $n$  dissymmetric centers the number of diastereomers will equal  $2^n$ . Diastereomers that differ in configuration at only one dissymmetric center only are termed *epimers*.

In order to specify the absolute configuration of an enantiomer containing an asymmetric carbon atom, the four atoms attached to that carbon are first arranged in a sequence of decreasing atomic mass. If two or more of these first atoms have the same atomic mass, one is chosen by comparing the atomic masses of the second group of atoms attached to the first atoms. If ambiguity still persists, the third, fourth, etc., sets

(working outward from the asymmetric carbon atom) are compared until a selection can be made. In the second group of atoms, those atoms with the highest, next highest, etc., atomic numbers are always ranked in that order.

By virtue of symmetry constraints, a resolved enantiomer must crystallize in a noncentrosymmetric space group. Racemic mixtures are under no analogous constraint, but over 90% of all racemic mixtures are found to crystallize in a centrosymmetric space group [13,14]. This consequence of molecular dissymmetry results in the situation where differing crystal structures can be obtained for the same chemical compound, depending only on the degree of resolution. Over the years, the study of molecular optical activity has been intimately related to corresponding studies of crystal morphology and structure, and interested readers can find detailed histories in the literature [15,16].

## 2. CRYSTALLOGRAPHY OF CHIRAL COMPOUNDS

A relatively small number of the possible crystallographic lattice symmetries are available for the crystals of separated enantiomers, since these must crystallize in a lattice structure that does not contain inverse elements of symmetry. Out of the 230 possible space groups belonging to the 32 crystal classes, only 66 space groups within 11 crystal classes are noncentrosymmetric and can, therefore, accommodate homochiral sets of enantiomers [17]. Racemates can crystallize in any of the 230 space groups, and as such are not restricted to crystallizing in a centrosymmetric group. Nevertheless, it has been found that most racemates will crystallize into a group which possesses some elements of inverse symmetry. As will be discussed later, racemic mixtures occasionally crystallize in an enantiomorphic lattice system, and the crystallization of these substances results in a spontaneous resolution of the enantiomers into separate crystals that can be mechanically separated.

A symmetry element is defined as an operation that when performed on an object, results in a new orientation of that object which is indistinguishable from and superimposable on the original. There are five main classes of symmetry operations: (a) the identity operation (an operation that places the object back into its original orientation), (b) proper rotation (rotation of an object about an axis by some angle), (c) reflection plane (reflection of each part of an object through a plane bisecting the object), (d) center of inversion (reflection of every part of an object through a point at the center of the object), and (e) improper rotation (a proper rotation combined with either an inversion center or a reflection plane) [18]. Every object possesses some element or elements of symmetry, even if this is only the identity operation.

The rigorous group theoretical requirement for the existence of chirality in a crystal or a molecule is that no improper rotation elements be present. This definition is often trivialized to require the absence of either a reflection plane or a center of inversion in an object, but these two operations are actually the two simplest improper rotation symmetry elements. It is important to note that a chiral object need not be totally devoid of symmetry (i.e., be asymmetric), but that it merely be dissymmetric (i.e., containing no improper rotation symmetry elements). The tetrahedral carbon atom bound to four different substituents may be asymmetric, but the reason it represents a site of chirality is by virtue of dissymmetry.

Jacques has evaluated the compilations published by various authors, and has reported that 70–90% of homochiral enantiomers crystallize in the  $P2_12_12_1$  or  $P2_1$  space groups [13]. The most frequently encountered chiral space group,  $P2_12_12_1$ , is orthorhombic, with the unit cell commonly consisting of four homochiral molecules that are related to each other by three binary screw axes. Practically, all of the other homochiral enantiomers crystallize in the monoclinic  $P2_1$  space group, which is characterized by a plane of symmetry and a twofold axis. The unit cell generally contains two molecules related by a binary screw axis.

Jacques has also concluded that among the 164 space groups possessing at least one element of inverse symmetry, it is found that 60–80% of racemic compounds crystallize in either the  $P2_1c$ ,  $C2/c$ , or  $P-1$  space groups [13]. The most common group is monoclinic  $P2_1c$ , where the unit cell contains two each of the opposite enantiomers related to one another by a center of symmetry and a binary screw axis.

A chirality classification of crystal structures that distinguishes between homochiral (type-A), heterochiral (type-B), and achiral (type-C) lattice types has been provided by Zorkii *et al.* [19], and expanded by Mason [20]. In the type-A structure, the molecules occupy a homochiral system, or a system of equivalent lattice positions. Secondary symmetry elements (e.g., inversion centers, mirror or glide planes, or higher-order inversion axes) are precluded in type-A lattices. In the racemic type-B lattice, the molecules occupy heterochiral systems of equivalent positions and opposite enantiomers antipodal are related by secondary lattice symmetry operations. In type-C structures, the molecules occupy achiral systems of equivalent positions, and each molecule is located either on an inversion center, on a mirror plane, or on a special position of a higher-order inversion axis. If there are two or more independent sets of equivalent positions in a crystal lattice, the type-D lattice becomes feasible. This structure consists of one set of type-B and another of type-C, but is not commonly encountered. Of the 5000 crystal structures studied, 28.4% were classified as being type-A, 55.6% were of type-B, 15.7% belong were of type-C, and only 0.3% were considered as being type-D.



A detailed discussion of crystal packing and the resulting space groups has been given by Kitaigorodskii [21]. This approach assumes that molecular crystals are assemblages for which compactness tends toward the maximum which is compatible with the molecular geometry. He defined a packing coefficient as  $vZ/V$ , where  $v$  is the volume of the molecule,  $V$  is the volume of the cell, and  $Z$  is the number of molecules in the unit cell. In this way, the space filling or packing coefficient in crystals always lies between 0.65 and 0.77, which is of the same order as the regular packing of spheres or ellipsoids. Molecules whose structures cause an inability to attain a packing coefficient at least equal to 0.6 are not found to crystallize, and these compounds can only form glasses from the melt. In order to fill space in the most compact manner with objects of indeterminate geometry, the lattice must be populated in a compact fashion. There are only a limited number of two-dimensional arrays in which an object may reside in contact with six neighbors, which is necessary for the optimal packing of a molecular assembly. It has been concluded that the binary screw axis is highly conducive toward efficient packing. In the final analysis, the limited possible combinations of stacking leads to a limited number of space groups that fulfill the requirements of three-dimensional close-packing.

The close-packing criterion for crystal stability generally yields lower free energies for a structure composed of a racemic assembly over that composed of homochiral molecules. This view has been expressed in the empirical rule of Wallach, which states that the combination of two opposite enantiomers to form a racemate is accompanied by a volume contraction. As might be expected, there are many exceptions to this rule, and these have been discussed in a systematic manner [22]. The modification to Wallach's rule contributed by Walden is more generally valid, and states that if an enantiomer has a lower melting point than its corresponding racemate, then the crystals of the latter will have the higher density.

Louis Pasteur was the first scientist to study the effect of molecular chirality on the crystal structure of organic compounds [23], finding that the resolved enantiomers of sodium ammonium tartrate could be obtained in a crystalline form that featured nonsuperimposable hemihedral facets (see Fig. 9.1). Pasteur was quite surprised to learn that when he conducted the crystallization of racemic sodium ammonium tartrate at temperatures below 28 °C, he also obtained crystals of that contained nonsuperimposable hemihedral facets. He was able to manually separate the left-handed crystals from the right-handed ones, and found that these separated forms were optically active upon dissolution. More surprising was the discovery that when the crystallization was conducted at temperatures exceeding 28 °C, he obtained crystals having different morphologies that did not contain the hemihedral crystal facets (also illustrated in Fig. 9.1). Later workers established that this was a case of crystal polymorphism.

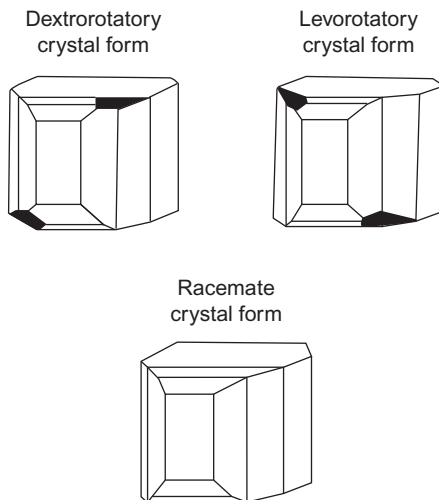


**FIGURE 9.1** Crystals of sodium ammonium tartrate, obtained under conditions yielding the hemihedral facets (darkened crystal faces) distinctive of the chiral crystalline forms. Also shown is the crystal morphology of racemic sodium ammonium tartrate.

The explanation to Pasteur's observations is that the sodium ammonium salt prepared from racemic tartaric acid crystallizes in the orthorhombic  $P2_12_12_1$  space group, characterized by unit cell parameters of  $a = 12.173 \text{ \AA}$ ,  $b = 14.412 \text{ \AA}$ , and  $c = 6.235 \text{ \AA}$  [24]. This particular crystal class is noncentrosymmetric, and as a result individual crystals are dissymmetric. When formed below a temperature of  $28^\circ\text{C}$ , the preferred molecular packing does not permit the intermingling of the enantiomers to yield a true racemic crystal and hence the crystallization results in a spontaneous resolution of the substance into physically separable dissymmetric crystals. On the other hand, when racemic sodium ammonium tartrate is isolated at temperatures higher than  $28^\circ\text{C}$ , one obtains a different polymorphic form of sodium ammonium tartrate that crystallizes in the monoclinic  $P2_1/a$  space group and is characterized by unit cell parameters of  $a = 15.244 \text{ \AA}$ ,  $b = 5.066 \text{ \AA}$ ,  $c = 10.218 \text{ \AA}$ , and  $\beta = 93.60^\circ$  [24]. The racemic crystal form is characterized by a completely different packing pattern and pattern of hydrogen bonding, which allows for the formation of a racemic modification.

### 3. PROPERTIES AND RESOLUTION OF RACEMIC MIXTURES OF DISSYMMETRIC SOLIDS

The early work of Pasteur clearly demonstrated that racemic compounds were actually mixtures of the mirror images of the compounds, and that these mixtures could be separated into their component enantiomers by

various means. This molecular conformation became expressed in the three-dimensional morphologies of the crystals. Pasteur found that while certain compounds could be resolved by mechanical separation of directly crystallized chiral crystals, the majority of organic compounds required some type of reversible chemical reaction in order to effect an enantiomeric separation. Racemic compounds separable by the direct crystallization method were termed *conglomerates*, while racemic compounds that became separable by crystallization subsequent to their derivatization were termed *racemates*.

Conglomerates and racemates can be easily distinguished from each other on the basis of their melting point phase diagrams [25]. A conglomerate system will exhibit a single eutectic minimum in its phase diagram at the mole fraction of 0.5, since at this enantiomeric ratio the system will consist of an equimolar mixture of two crystalline enantiomers that melts as if it were a pure system. On the other hand, a racemate system will exhibit two eutectics on either side of the mole fraction of 0.5 since both enantiomers will be found in the unit cells of the crystallized solid.

While the melting point of a racemate may be greater, less, or equal to the melting point of its separated enantiomers, the melting point of a conglomerate must always be less than the melting point of its separated enantiomers. The conglomerate phenomenon has been illustrated in Table 9.1, which summarizes the melting points of most of the conglomerates and their constituent enantiomers that were tabulated in the Jacques book [13]. The average difference in melting points of these 113 conglomerate systems was calculated to be 26.5 °C.

Many procedures result in the incomplete resolution of a racemic mixture into the component enantiomers, and quantities have been defined, which are used to specify the degree of resolution. The *enantiomeric purity* (EP) of a substance will have values between 0 and 1, and for substances where the (*R*)-enantiomer is present in excess, the EP is given by

$$EP = 2(X_R) - 1, \quad (9.1)$$

where  $X_R$  is the mole fractions of the (*R*)-enantiomer. The *enantiomeric excess* (EE) of a substance will have values between 0 and 0.5, and is the quantity of excess enantiomer over that of the racemic mixture. Where the (*R*)-enantiomer is present in excess, the EE given by

$$EE = (X_R - 0.5). \quad (9.2)$$

For example, in the instance where the mole fraction of excess enantiomer in a substance is 0.65, the enantiomeric purity would equal 0.3 (i.e., 30%) and the enantiomeric excess would equal 0.15 (i.e., 15%).

Historically, optical rotation was used to measure the enantiomeric purity of a substance, giving rise to the term *optical purity* (OP).

**TABLE 9.1** Melting points of racemic conglomerates and their separated enantiomers [13]

	Melting point, separated enantiomer (°C)	Melting point, racemic conglomerate (°C)	Difference in melting points (°C)
( $\gamma$ -Picolino)(trimethylamino)-chloroborane; hexafluoro-phosphate salt	126	120	6
1,3-Bis(hydroxymethyl)-acenaphthene	130	98	32
1,5-Dioxo-4-(2'-carboxyethyl)-7a-ethyl-5,6,7,7a-tetrahydroindane	148	119	29
1,9,10,10a-Tetrahydro-3(2H)-phenanthrenone	114	82	32
17 $\beta$ -Hydroxy-des- $\alpha$ -androst-9-en-5-one	170	136	34
1-Benzylamino-2-nitrosopinene	144	123	21
1-Indanol	71	44	27
1-Phenyl-1-butanol	50	16	34
2-(4-Nitro-1-naphthoxy)-propionamide	228	203	25
2-(1-Naphthoxy)propionamide	202	172	30
2-(1-Naphthoxy)propionanilide	164	138	26
2-(1-Naphthoxy-4-nitro)-propionanilide	215.5	187	28.5
2-(2-Carboxybenzyl)-2-chloro-1-indanone	179	147	32
2-(2-Naphthoxy)propionamide	187	158	29
2-(2-Naphthoxy-4-nitro)-propionanilide	212	180	32
2-( <i>p</i> -Methoxyphenyl)-propiophenone	80	60	20
2,2'-Diamino-1,1'-binaphthyl	242	188.5	53.5
2,2'-Dibromomethyl-1,1'-binaphthyl	186	149	37
2,2-Dimethyl-3-(6-methoxy-2-naphthyl)butyric acid; methyl ester	80	56	24
2,2-Dimethyl-3-hydroxy-3-phenylpropionic acid	158	134	24

2,5-Dimethyladipic acid	104	75	29
2,6-Dimethyl-1,2,3,4-tetrahydroquinoline	53	32	21
2-Benzyl-1,3-diphenyl-1,2-propanediol	136	116	20
2-Chloro-3-hydroxysuccinic acid	175	145	30
2-Methoxy-2-(2-thienyl)acetic acid	86	61	25
2-Methoxy-2-(3-thienyl)acetic acid	86	60	26
2-Octanol, hydrogen phthalate	75	55	20
2-Phenylglutaric acid	131	102	29
2t,3c-Dimethyl-4-oxocyclo-hexane-1r-carboxylic acid	49	22.5	26.5
3-( <i>m</i> -Chlorophenyl)hydracrylic acid	95	67	28
3-( <i>m</i> -Fluorophenyl)hydracrylic acid	38	17	21
3-( <i>p</i> -Bromophenyl)hydracrylic acid	125	98	27
3-( <i>p</i> -Chlorophenyl)hydracrylic acid	112	84	28
3,3-Dimethyl-2-hydroxy-1-tetralone	108	78	30
3,3'-Iminodibutyric acid	180	160	20
3,4-Dimethylazetidinone	61	24	37
3-Bromo-2-decalone	121	89	32
3-Chloro-2-decalone	122	92	30
3-Phenylhydracrylic acid	116	93	23
3-Phenyllactic acid	125	94.5	30.5
4,4'-Azobis-4-cyanopentanoic acid	130	118	12
4-Methylazetidinone	27	– 12	39
4-Phenyl-4-valerolactone	123	106	17
4-Vinylazetidinone	27	– 1	28
5-Methyl-5-vinylhydantoin	166	129	37

(continued)

**TABLE 9.1** (continued)

	Melting point, separated enantiomer (°C)	Melting point, racemic conglomerate (°C)	Difference in melting points (°C)
(6)-Helicene	270	240	30
6-Hydroxy-5-iodobicyclo [2.2.2] octane-2-carboxylic acid lactone	116	86	30
9-Methyloctadecanamide	66	65.5	0.5
$\alpha$ -Bromocamphor	74	39	35
Adrenaline	221	191	30
$\alpha$ -Methyldopa	300	297	3
Anisylidenecamphor	128	96	32
$\alpha$ - $\pi$ -Dibromocamphor	157	122	35
$\beta$ -Benzoylhydratropic acid	182	154	28
Bornyl acetate	27	7	20
<i>cis</i> -2-Decalol	38	18	20
Dibenzalpentaerythritol	189	160	29
Dilactyldiamide	208	184	24
Dimethyl diacetyltartrate	103	80	23
Epiquinide triacetate	220	188	32
Erythrose benzylphenylhydrazone	104	83	21
Euphol, lactone acetate	290	250	40
Fluoromethyl-2-naphthyl-phenylsilane	68	41	27
Gulonolactone	180	160	20
Hydrobenzoin	147.5	120	27.5
Hydroveratrin	193	175	18
10-(3-Dimethylamino-2-methyl-propyl)-3-methoxyphenothiazine	124	103	21

Menthyl 3,5-dinitrobenzoate	154	130	24
Menthyl benzoate	55	25	30
Menthyl cyclohexanecarboxylate	48	28	20
Menthyl <i>p</i> -ethoxybenzoate	76	52	24
Methadone	101	77	24
Methyl mannoside	191	166	25
Methyl-1-naphthylphenyl-germane	72	48	24
<i>N</i> -Acetyl- $\alpha$ -chloromethyl-benzylamine	134	105	29
<i>N</i> -Benzoyl-2-methylindoline	119	92	27
<i>N</i> -chloroacetylproline	120	88	32
<i>N,N'</i> -di- <i>p</i> -tolyl-2,3-diaminobutane	87	63	24
<i>N</i> -Acetyl-2-methylindoline	89	56	33
<i>N</i> -Acetyl-3-(4-hydroxy-3-methoxyphenyl)- 2-methyl-propionitrile	206	178	28
<i>N</i> -Acetyl- $\alpha$ -methylbenzylamine	102	75	27
<i>N</i> -Acetylglutamic acid	199	182	17
<i>N</i> -Acetylisoleucine	151	119	32
<i>N</i> -Acetylleucine	192	164	28
<i>N</i> -Benzoyl-neomenthylamine	121	102	19
<i>N</i> -Benzoyl-2-amino-2-phenyl-ethanol	181	153	28
<i>N</i> -Benzoyl-3,4-dichloro-amphetamine	170	140	30
<i>N</i> -Butyrylproline	115	88	27
<i>N</i> -Formyl-neomenthylamine	118	86	32
<i>N</i> -Salicylideneneomenthylamine	100	70	30
<i>N</i> -Tosylserine	233	205	28
Noludar	84	74	10

---

(continued)

**TABLE 9.1** (continued)

	Melting point, separated enantiomer (°C)	Melting point, racemic conglomerate (°C)	Difference in melting points (°C)
<i>o</i> -Benzylatrolactamide	142	113	29
<i>o</i> -Chloromandelic acid	120	86	34
<i>p</i> -Bromobenzylidenecamphor	134	101	33
<i>p</i> -Chlorobenzylidenecamphor	109	78	31
Serine anhydride	248	224	24
Threitol	88	72	16
<i>threo</i> -2,5-Hexanediol	53	25	28
<i>threo</i> -2,3-Bis(2-aminophenyl)-2,3-butanediol	205	183	22
<i>threo</i> -1,2-Bis(4-pyridyl)-ethanediol	182	168	14
<i>threo</i> -1,3-Dihydroxy-1,3-diphenylpropane	153	130	23
<i>threo</i> -2,3-Dibromo-1,4-butanediol	115	90	25
<i>threo</i> -2-Amino-1-( <i>p</i> -methyl-thiophenyl)-1,3-propanediol	152	126	26
<i>threo</i> -2-Amino-1- <i>p</i> -nitrophenyl-1,3-propanediol	164	142	22
<i>threo</i> -3-Phenylglyceric acid	166	141	25
<i>trans</i> -1,2-Dichloroacenaphthene	102	70	32
<i>trans</i> -2,3-Dihydroxymethyl-bicyclo [2.2.2] octane	118	86	32
<i>trans</i> -2-Decaloxime benzoate	135	106	29
<i>trans</i> -9,10-Dicarbomethoxy-1,4-dihydro-1,4-ethanonaphthalene	100	72	28
Tribromotetrahydrocarvone	92	62	30
Trichlorfon	107	75	32
$\omega$ -Nitrocamphene	85	66	19



When measured using optical rotation, the optical purity of a substance is given by

$$\text{OP} = \alpha_{\text{OBS}}/[\alpha], \quad (9.3)$$

where  $\alpha_{\text{OBS}}$  is the observed optical rotation of the substance and  $[\alpha]$  is the specific rotation of the enantiomerically pure substance. When the enantiomeric composition of a substance is determined by nonoptical means (such as chiral chromatography or nuclear magnetic resonance), the results should not be referred to as optical purities but should be properly identified as enantiomeric purities.

### 3.1. Conglomerate systems

Conglomerate solids are characterized by the presence of a single enantiomer within the unit cell of the crystal, even when the solid is obtained through crystallization of a racemic or partially resolved mixture. These solids consist of separate crystals, each of which consists entirely of one enantiomer or its mirror image, and which may be separated solely on the basis of their physical properties. The small-scale resolution of dissymmetric compounds crystallizing as conglomerates can be straight forward since the resolution step takes place spontaneously with the crystallization step. The key to a successful resolution by direct crystallization lies in the means used to physically separate the crystals containing the opposite enantiomers.

Approximately 10% of chiral compounds inherently form conglomerates by virtue of their crystallization tendencies [13,26], and Jacques and coworkers have provided details of approximately 250 organic compounds forming known conglomerate systems [27,28]. The apparent randomness of conglomerate system formation has been explained through considerations of the thermodynamics of these systems. The stability of true racemic solids is defined by the free energy change associated with the process of combining the (*R*)-enantiomer with the (*S*)-enantiomer to produce the (*R,S*)-enantiomeric solid. This process has been calculated to be in the range of 0 to  $-2$  kcal/mol, and is roughly proportional to the difference in melting points between the racemate and the resolved enantiomers [29]. In most cases, the free energy associated with the formation of racemates is exothermic, owing to the positive nature of the enthalpies and entropies of formation. In those cases where the melting point of the racemic mixture is at least  $20^\circ$  lower than the melting points of the separated enantiomers, one will generally obtain a conglomerate system.

The use of crystal structure prediction in the evaluation of systems for their tendency toward spontaneous resolution has been explored [30]. Using a gas phase conformational search to locate low-energy

conformations, the possible crystal structures of 5-hydroxymethyl-2-oxazolidinone and 4-hydroxymethyl-2-oxazolidinone assembled from these conformations have been predicted. For both compounds, the racemate was predicted to have the lowest energy, with the energy difference between the lowest-energy racemic structure and the lowest-energy separated enantiomer structure being in the range of 0.2–0.9 kcal/mole. The authors noted that as the accuracy of lattice energy calculations becomes more accurate, it should become possible to predict whether a chiral molecule will crystallize in a space group where its racemate or conglomerate nature would be expressed.

A theoretical explanation has been developed to explain the effect of chiral impurities on the crystallization rates of the enantiomorphic components of a conglomerate system [31]. The theory provides the time required to complete the crystallization of the separated enantiomers, suggests that one might be able to obtain an enantiomerically pure product even if the chiral impurity was less than enantiomerically pure, and even provides information regarding the particle size distribution. The model was tested on the crystallization of (*D,L*)-glutamic acid that was carried out in the presence of a resolved (*L*)-lysine impurity.

### 3.1.1. Inherently conglomerate systems

Since a racemic conglomerate system will consist of independently formed, enantiomerically pure crystals, such racemic mixtures are seen to constitute a binary system that consists of physical mixtures of the enantiomer components. Such binary mixtures are easily described by the Phase Rule, and can be characterized by their melting point phase diagrams. Since the components of a conglomerate racemate will melt independently at the same temperature, the material will exhibit the melting phenomena of a pure substance. One would, therefore, predict the existence of a eutectic point in the melting point phase diagram that would be located at exactly the racemic composition. In principle, one could separate out the enantiomer present in excess in a partially resolved conglomerate system simply by heating the sample to a temperature just above the melting point of the racemate, and then collecting the crystalline excess of the residual enantiomer.

An example of the type of melting point phase diagram that is typical for a conglomerate system is shown in Fig. 9.2, which illustrates the phase diagram reported for methyl diacetyltartrate [32]. Below the eutectic temperature of 79 °C, the system will exist as a mixture of solid *D*-enantiomer and *L*-enantiomer. At the exact composition of the racemic mixture ( $X = 0.5$ ), the system will exist entirely in the liquid phase above the eutectic temperature. At mole fractions where the amount of (*L*)-enantiomer exceeds that of the (*D*)-enantiomer, the system will exist as an equilibrium mixture of racemic liquid and solid (*L*)-enantiomer.

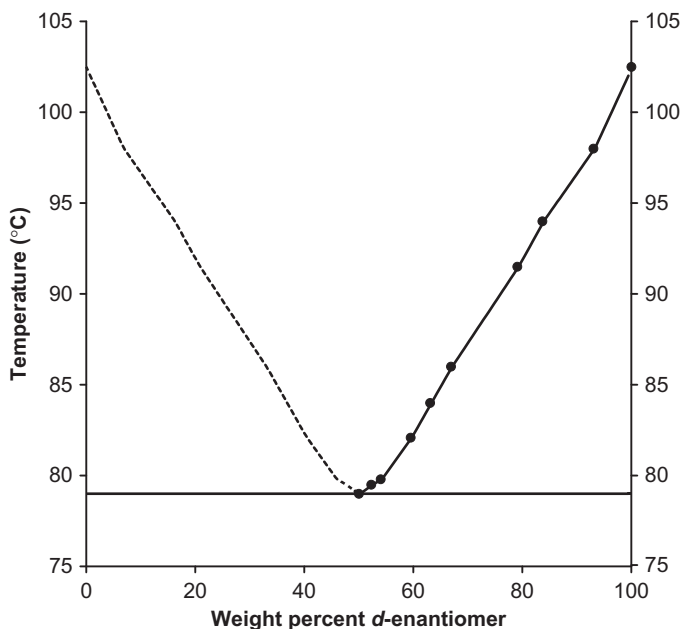


**FIGURE 9.2** Melting point phase diagram obtained for methyl diacetyltartrate, prepared using data published in Ref. [32]. The actual reported data points are shown as the filled circles, and the left-hand side of the phase diagram was obtained by taking the mirror image of the right-hand side of the diagram.

As required by the phase diagram of a conglomerate, the eutectic temperature is the lowest temperature attainable where any liquid phase can exist in equilibrium with any solid phase.

An alternate approach for the characterization of conglomerate systems is through the use of ternary phase diagrams, where one component is the solvent and the solubility of the substance is used as the observable parameter [10,26]. A racemic mixture will be more soluble than are the separated enantiomers, and the rule of Meyerhoffer states that a conglomerate will have a solubility which is twice the solubility of the resolved enantiomer [33]. This situation arises since ideally the mole fraction of an independent constituent in a liquid depends only on the enthalpy of fusion and melting point of the substance and since the solubility of one enantiomer cannot affect the solubility of the other. Jacques and Gabard have examined the solubilities of a number of conglomerate systems, and have largely confirmed the double solubility rule [34]. A selection of the results reported for nondissociable substances is presented in Table 9.2.

Jacques and coworkers have provided a comprehensive background regarding methodologies that enable direct crystallization for the

**TABLE 9.2** Solubilities of separated enantiomers and racemic mixtures of conglomerate materials

Compound	System	Solubility of separated enantiomer (g/100 mL)	Solubility of racemic mixture (g/100 mL)	Ratio of racemate solubility to enantiomer solubility
Asparagine	Water (25 °C)	2.69	5.61	2.16
( $\alpha$ -Naphthoxy)-2-propionamide	Acetone (25 °C)	1.38	2.24	2.08
<i>p</i> -Nitrophenylamino propanediol	Methanol (25 °C)	1.63	3.35	2.14
<i>N</i> -Acetyl-leucine	Acetone (25 °C)	1.86	4.12	2.13
<i>N</i> -Acetyl-glutamic acid	Water (25 °C)	4.14	8.28	2.12
Diacetyldiamide	Water (35.5 °C)	12.4	23.7	2.14
3,5-Dinitrobenzoate-lysine	Water (30 °C)	6.96	13.17	1.99

resolution of racemic mixtures [13,26], which may be supplemented by other reviews in this area [35,36].

The first method of enantiomeric separation by direct crystallization is the mechanical technique use by Pasteur, where he separated the enantiomorphic crystals that were simultaneously formed while the residual mother liquor remained racemic. Enantiomer separation by this particular method can be extremely time consuming, and not possible to perform unless the crystals form with recognizable chiral features (such as well-defined hemihedral faces). Nevertheless, this procedure can be a useful means to obtain the first seed crystals required for a scale-up of a direct crystallization resolution process. When a particular system has been shown to be a conglomerate, and the crystals are not sufficiently distinct so as to be separated, polarimetry or circular dichroism spectroscopy can often be used to establish the chirality of the enantiomeric solids.

Even a few seed crystals, mechanically separated, can be used to produce larger quantities of resolved enantiomerically pure material. A second method of resolution by direct crystallization involves the localized crystallization of each enantiomer from a racemic, supersaturated solution. With the crystallizing solution within the metastable zone, oppositely handed enantiomerically pure seed crystals of the compound are placed in geographically distant locations in the crystallization vessel. These serve as nuclei for the further crystallization of the like enantiomer, and enantiomerically resolved product grows in the seeded locations.

This procedure has been used to obtain both enantiomers of methadone, where approximately 50% total yield of enantiomerically pure material can be obtained [37].

Enantiomer separation may be practiced on the large industrial scale using the procedure known as resolution by entrainment [13,26]. The method is based on the condition that the solubility of a given enantiomer is less than that of the corresponding racemate. To begin, a solution that contains a slight excess of one enantiomer is prepared. Crystallization is induced (usually with the aid of appropriate seed crystals); whereupon the desired enantiomer is obtained as a solid and the mother liquor is enriched in the other isomer. In a second crystallization step, the other enantiomer is obtained. The method can be applied to any racemic mixture which crystallizes as a conglomerate, and the main complication which can arise is when the compound exhibits polymorphism. In that case, the entrainment procedure must be carefully designed so as to generate only the desired crystal form.

Resolution by entrainment is best illustrated through the use of an example, and the laboratory scale resolution of hydrobenzoin [38] is an appropriate example. Initially, 1100 mg of racemic material is dissolved along with 370 mg of (–)-hydrobenzoin in 85 g of 95% ethanol, and then the solution is cooled down to 15 °C. Ten milligrams of the (–)-isomer is added in the form of seed crystals, and a crop of additional crystalline material is allowed to form. After 20 minutes, 870 mg of (–)-hydrobenzoin was recovered. Then, 870 mg of racemic hydrobenzoin was dissolved with heating. The resulting solution was cooled to 15 °C and seeded with 10 mg of the (+)-isomer. The quantity of (+)-hydrobenzoin recovered at this time was 900 mg. The process was cycled 15 times, and ultimately yielded 6.5 g of (–)-hydrobenzoin and 5.7 g of (+)-hydrobenzoin. Each isomer was obtained as approximately 97% enantiomerically pure.

### 3.1.2. Racemate systems rendered into conglomerates

Although the number of organic compounds forming conglomerate systems is not large, a significant number of other chiral compounds can be transformed into conglomerate-forming systems through formation of a salt or covalent derivative. For example, substitution of additional functionalities onto the achiral portion of a compound can sometimes also yield a conglomerate system. For example, although mandelic acid and many of its derivatives crystallize as racemic mixtures, *ortho*-chloromandelic acid is obtained as a conglomerate [39]. The enantiomers of *sec*-phenethyl alcohol form a conglomerate system upon formation of the 3,5-dinitrobenzoyl ester [40].

While the frequency of conglomerate-forming systems is fairly small for organic compounds, a statistical analysis of more than 500 salts has demonstrated that the probability of observing spontaneous resolution is

two or three times higher for salts of the same organic compounds [41]. The possibility has been further demonstrated through studies of the crystallization of achiral dicarboxylic acids with  $\alpha$ -phenethylamine, where racemates were obtained for the salts with hydrogen malonate and hydrogen phthalate, but a conglomerate was obtained for the hydrogen succinate salt [42]. In a subsequent work, it was concluded that conglomerate formation took place when the protonated and deprotonated carboxylic acid groups formed hydrogen-bonded chains rather than forming intermolecular hydrogen-bonded dimers in the crystal [43].

To illustrate how a racemate system can be turned into a conglomerate system, and to demonstrate how one may recognize the existence of a conglomerate system, we will consider the example of ibuprofen, or 2-(4-isobutylphenyl)propanoic acid. The single crystal structures of enantiomerically pure [44] and racemic [45] ibuprofen have been published, and the powder diffraction patterns of the enantiomerically pure and racemic forms are shown in Fig. 9.3. The existence of a conglomerate system is indicated if the diffraction patterns of enantiomerically pure and racemic

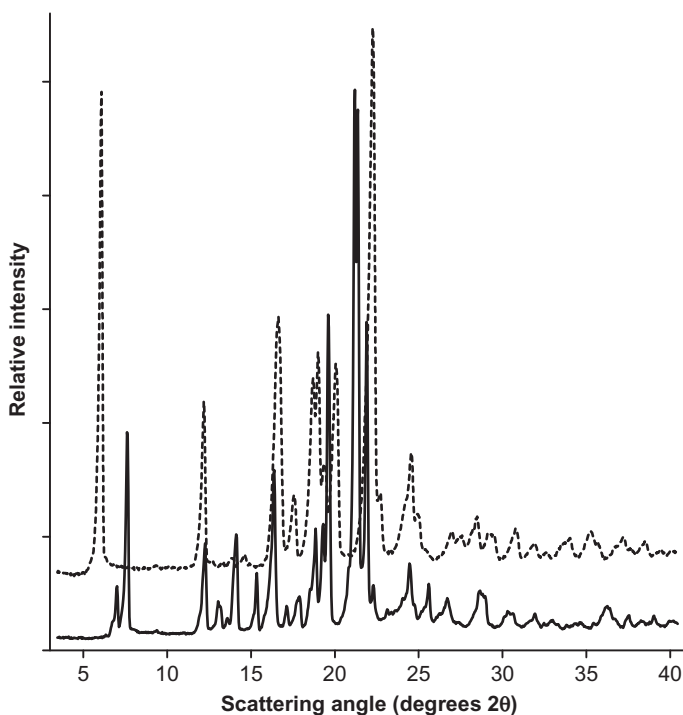


**FIGURE 9.3** X-ray powder diffraction patterns obtained for (*S*)-ibuprofen (solid trace) and (*R,S*)-ibuprofen (dashed trace) [H.G. Brittain, unpublished results].

forms of a compound are the same, but this is obviously not the case for ibuprofen. However, formation of the tromethamine (2-amino-2-(hydroxymethyl)propane-1,3-diol) salt of ibuprofen was found to result in the generation of a conglomerate system, as demonstrated in Fig. 9.4 by the equivalence in X-ray powder diffraction patterns of the (*S*)-ibuprofen/tromethamine and (*R,S*)-ibuprofen/tromethamine salts [46]. In addition, the differential scanning calorimetry thermograms of the salts are effectively the same, with the (*S*)-ibuprofen salt exhibiting a melting endotherm at 158.4 °C (enthalpy of fusion of 159.1 J/g) and the (*R,S*)-ibuprofen salt having a melting endotherm at 158.9 °C (enthalpy of fusion of 160.2 J/g) [46].

The crystal structures of the cinnamic acid salts with (+)-1-phenylethylamine salt with and (+)-1-(4-isopropylphenyl)ethylamine were determined using single-crystal X-ray analysis, where it was found that two amine components and two acid components formed a helical column through hydrogen bonding in each crystal [47]. On the basis of structural

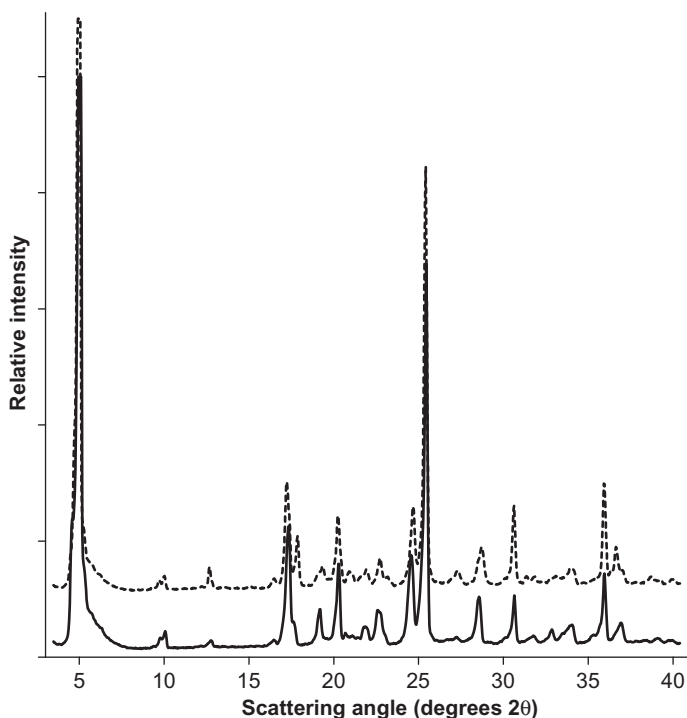


**FIGURE 9.4** X-ray powder diffraction patterns obtained for the tromethamine salts with (*S*)-ibuprofen (solid trace) and (*R,S*)-ibuprofen (dashed trace) [H.G. Brittain, unpublished results].

similarity of the two conglomerates, a criterion was proposed for the transformation of a racemic modification of an amine into a conglomerate crystal. For this to occur, the achiral acid should form a helical column by hydrogen bonds with the amine, the acid should be rigid and flat to limit the orientation of the amine, and the sizes of the amine and the acid should be similar to each other. The proposed criteria were supported through crystal structure determinations of the conglomerate systems formed by the *p*-chlorobenzenesulfonic acid salt of (*L*)-alanine, the *p*-toluenesulfonic acid salt of (*L*)-serine, and the benzenesulfonic acid salt of (*L*)-leucine [48].

### 3.2. Racemate systems

Racemate solids are characterized by the presence of equimolar amounts of both enantiomers within the unit cell of the crystal, which crystallizes within a centrosymmetric space group. This space group will necessarily be different from the noncentrosymmetric space group characteristic of the separated enantiomers. As a result, the range of physical properties associated with a heterochiral solid will generally be completely different from those of the homochiral solid. For instance, the melting point of the exact racemic mixture may be greater than or less than that of the separated enantiomers, and there is no general rule that can be invoked to provide a reliable prediction of melting point behavior.

The melting point phase diagram of a racemate system will contain two eutectic minima, and crystallization at either condition will yield a racemic mixture and not enantiomerically pure product. The phase diagram shown in Fig. 9.5 for methyl dipropionyltartrate is typical for a racemate system, where a eutectic temperature of 24 °C was detected for a *d*-enantiomer composition of 75 mole-percent [32]. For compounds containing a single center of dissymmetry, construction of the full phase diagram only requires the acquisition of melting point data for one enantiomer in excess to develop one side of the phase diagram, as the other side of the phase diagram must be the mirror image.

Care must be observed in the interpretation of a melting point phase diagram for those instances where the eutectic temperatures are located close to the equimolar composition, as such systems could be erroneously interpreted as indicating the existence of a conglomerate system. An example of this type of behavior is shown in Fig. 9.6 for the ethyl diacetyl tartrate system, where a eutectic temperature of 42 °C was found for a *d*-enantiomer composition of 55.7 mole-percent [32]. On the other hand, when the eutectic temperatures are close to the melting points of the pure enantiomers, the phase diagram could be mistaken for that of a solid solution. An example of this behavior is shown in Fig. 9.7 for the methyl dibenzoyltartrate system, where a eutectic temperature of 130.4 °C was



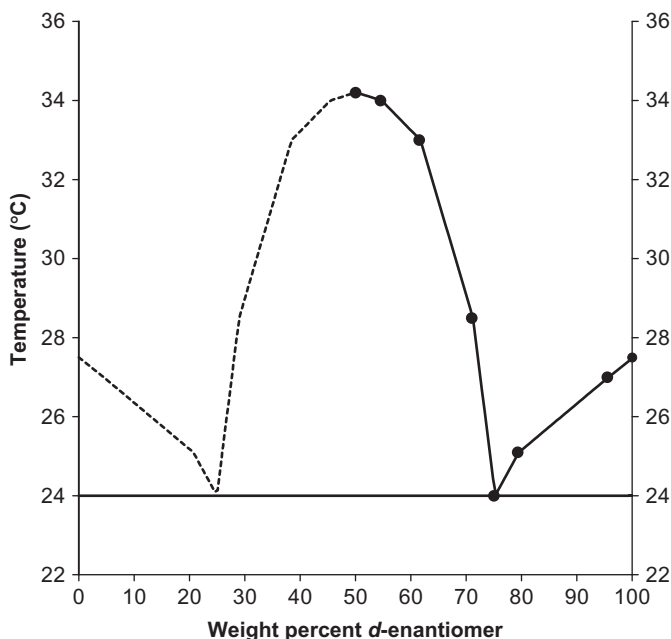


**FIGURE 9.5** Melting point phase diagram obtained for methyl dipropionyltartrate, prepared using data published in Ref. [32]. The actual reported data points are shown as the filled circles, and the left-hand side of the phase diagram was obtained by taking the mirror image of the right-hand side of the diagram.

found for a *d*-enantiomer composition of 94.5 mole-percent [32]. It is clear that the melting points of a sufficient number of compositions must be measured if the proper phase diagram is to be obtained.

In order to separate the enantiomers of a racemate system, the properties of the molecule must be transformed in such a way that the phase diagram containing two eutectic points becomes a phase diagram containing one eutectic point. This can be brought about through performance of a derivatization reaction with a suitable chiral reagent that leads to diastereomers (often identified in the literature as the *p*-salt and the *n*-salt) that exhibit a phase diagram containing only a single minimum. In general, this minimum will not be located at the exact racemic composition, but will instead be observed at some other concentration value. In fact, for the *p*-salt to be separated from the *n*-salt in a single crystallization step, the position of the eutectic should be substantially removed from the equimolar point.

To illustrate the effect of diastereomer formation on phase diagrams, we will return to the example of ibuprofen. As evident from the phase diagram in Fig. 9.8, ibuprofen forms a classic racemate system [46,49], with a eutectic temperature of 47.1 °C detected at 81.2 weight-percent

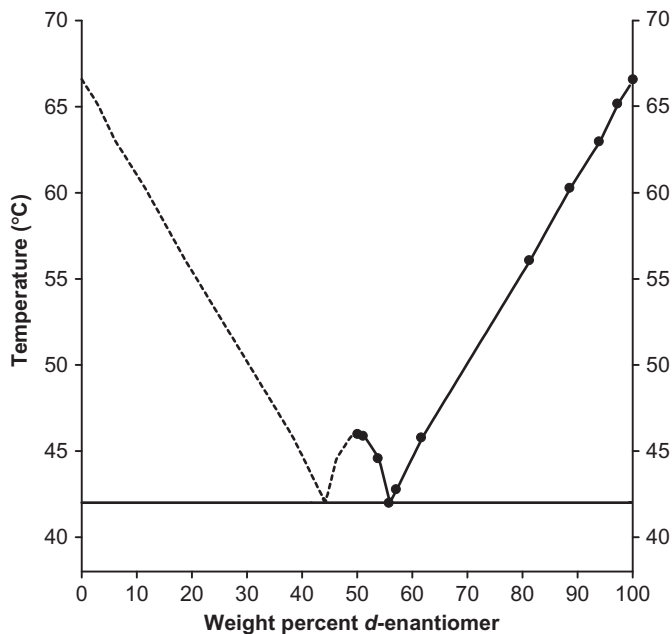


**FIGURE 9.6** Melting point phase diagram obtained for ethyl diacetyl tartrate, prepared using data published in Ref. [32]. The actual reported data points are shown as the filled circles, and the left-hand side of the phase diagram was obtained by taking the mirror image of the right-hand side of the diagram.

(*S*)-ibuprofen composition. The mirror image eutectic would be predicted to form at the same temperature but at 18.8 weight-percent (*S*)-ibuprofen composition. However, as shown in Fig. 9.9, when the salt of ibuprofen is formed with  $\alpha$ -methylbenzylamine (i.e., the resolving agent), one finds that the phase diagram simplifies into that of a single eutectic, characterized by a temperature of 147.0 °C detected and at 66.5 weight-percent (*S*)-ibuprofen composition [46,49]. One could design a procedure that would serve crystallize one diastereomer over the other, and then remove the resolving agent to obtain purified enantiomer.

The preceding example demonstrates the general view that the procedure most likely to alter the crystallization thermodynamics of true racemate systems will entail the formation of dissociable diastereomer species [50–54]. In most instances, these diastereomers are simple salts formed between proton donors and proton acceptors, or electron-pair donors and electron-pair acceptors. For example, the first resolving agents introduced for acidic enantiomers were alkaloid compounds, and hydroxyl acids were used for the resolution of basic enantiomers. This type of resolution procedure has been known since the time of Pasteur, and extensive tables of resolving agents and procedures are available [48,55,66].

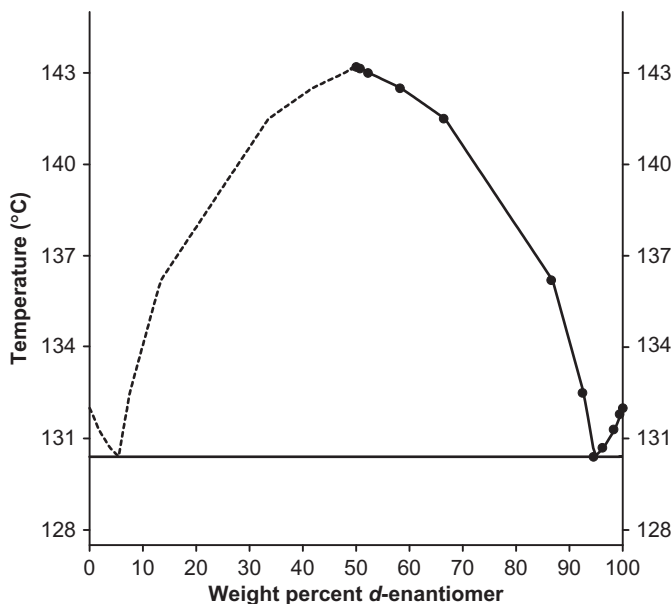
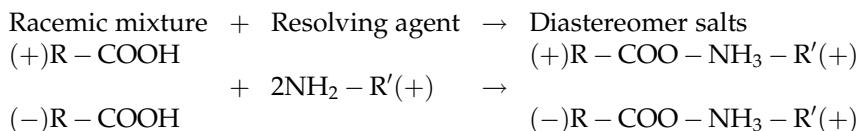


**FIGURE 9.7** Melting point phase diagram obtained for methyl dibenzoyltartrate, prepared using data published in Ref. [32]. The actual reported data points are shown as the filled circles, and the left-hand side of the phase diagram was obtained by taking the mirror image of the right-hand side of the diagram.

The general procedure for separation of enantiomers through formation of dissociable diastereomers can be illustrated for the instance where a racemic acid is to be resolved through the use of a basic resolving agent. The first step of the resolution procedure involves formation of the **p**- and **n**-diastereomeric salts:



According to convention [56], the (*R,R*) and (*S,S*) diastereomers are termed the **p**-salts, and the (*R,S*) and (*S,R*) diastereomers are identified as the **n**-salts. In the example used above, the (+)R-COO-NH<sub>3</sub>-R'(+)  
diastereomer would correspond to the **p**-salt, and the (-)R-COO-NH<sub>3</sub>-R'(+)  
diastereomer would be the **n**-salt. In the usual practice, the **p**- and **n**-salts are separated by fractional crystallization, and the success of the resolution process is critically related to this crystallization step. As discussed above, one could consider the act of derivatization as a process

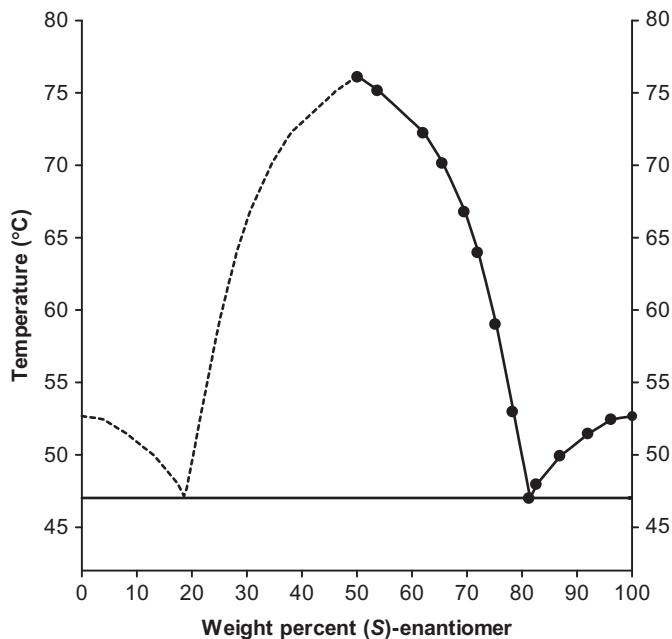


**FIGURE 9.8** Melting point phase diagram obtained for racemic ibuprofen free acid [H.G. Brittain, unpublished results]. The actual reported data points are shown as the filled circles, and the left-hand side of the phase diagram was obtained by taking the mirror image of the right-hand side of the diagram.

that alters the phase diagram from that of a double eutectic into a pseudoconglomerate phase diagram exhibiting only one eutectic.

Since the relative solubilities of the diastereomeric species play such an important role in their separation by crystallization, it follows that ternary phase diagrams incorporating solvent can play a large role in understanding a resolution process [57]. A study of the separation of the enantiomers of phenylsuccinic acid after formation of the phenylsuccinate/proline salt demonstrated the utility of phase diagrams in the design of enantiomeric separations [58]. In this work, it was found that the degree of resolution for the salt having the 1:2 stoichiometry was only minimally affected by temperature, while the separation of the 1:1 stoichiometric phenylsuccinate/proline salt was strongly affected by temperature.

The chiral discrimination existing in the diastereomer systems formed by ephedrine and various mandelic acids has been studied in great detail, using a variety of spectroscopic and structural tools. Although significant differences in the solubilities of the *n*- and *p*-salts obtained after reaction of ephedrine with mandelic acid were known to exist, both salts were

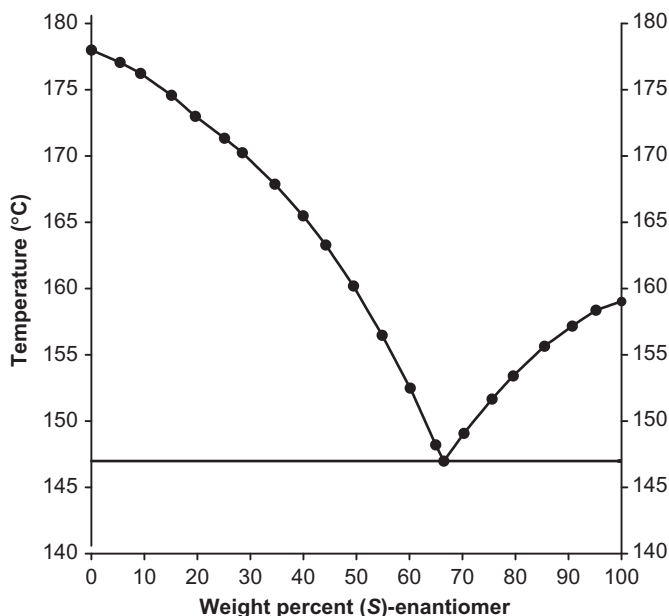


**FIGURE 9.9** Melting point phase diagram obtained for the salt formed between racemic ibuprofen and the (S)-enantiomer of  $\alpha$ -methylbenzylamine [H.G. Brittain, unpublished results].

found to crystallize in the same monoclinic space group with crystal structures that were isosteric [59]. In subsequent work, it was shown that the crystalline diastereomer salts formed by (*R*)-mandelic acid formed a more compact repeating pattern (with higher melting points and enthalpies of fusion) than did analogous salts formed by (*S*)-mandelic acid [60]. It was deduced that the subtle chiral discriminations led to the existence of different hydrogen-bonding modes, which in turn became manifest in a variety of other physical properties.

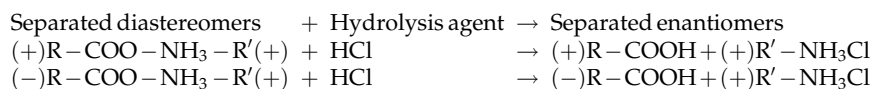
There is no doubt that the crystallographic differences between the diastereomers generated during derivatization directly affect the outcome of the resolution process. For example, when (*D,L*)-phenylglycine was resolved with (*S*)-camphor-10-sulfonic acid, the **n**-salt was isolated in 45.7% yield and having an enantiomeric purity of 98.8% [61]. The less soluble **n**-salt exhibited a higher melting point and enthalpy of fusion than did the **p**-salt, which was found to be freely soluble. The crystal structure of the **n**-salt exhibited a dense structure containing alternating phenylglycine cation and camphor sulfonate anion layers, while the structure of the **p**-salt exhibited a coarser structure with vacancy layers between the anion and cation planes. These differences in crystal

structure directly led to the differing physical properties of the diastereomeric salts that caused the enantiomeric resolution to be so successful.

Depending on the details of the lattice dynamics, there is no restriction regarding the ability of a given pair of **p**- and **n**-salts to crystallize in the same or in different space groups. For example, in the diastereomeric system formed by  $\alpha$ -methylbenzylamine and hydratropic acid, the **p**-salt was found to crystallize in the  $P2_1$  space group, while the **n**-salt crystallized in the  $P2_12_12_1$  space group [62]. Although the conformations of the constituent species in the two crystal forms were reported to be similar, the mode of molecular packing that led to the structure of the individual crystals was very different.

This latter behavior differs from that observed in the crystalline diastereomers of mandelic acid with 1-phenylethylamine [63]. Here the **n**-salt crystallized in the triclinic  $P1$  space group, while the **p**-salt crystallized in the monoclinic  $P2_1$  space group. The crystallographic structures of the two diastereomers revealed the existence of fairly equivalent hydrogen-bonding patterns, but at the same time substantially different conformations for the two molecular ions making up the donor-acceptor complex were noted. These structural differences became manifest in the relative solubilities of the two diastereomers, where the aqueous solubility of the **p**-salt was much less than that of the **n**-salt.

Once either the **p**-salt or the **n**-salt (or both) is successfully crystallized, the diastereomer salt is dissociated and the resolving agent separated. In the specific instance of acid resolution, the diastereomeric salt is efficiently cleaved by means of a hydrolysis reaction:



The diastereomer cleavage must be simple, selective, take place in quantitative yield, must not racemize the resolved compound, and must leave the resolving agent in a form which is easily recovered. The recovery is usually brought about by precipitation or extraction of the resolving agent. One important criterion in the choice of a resolving agent is the ease by which it may be dissociated and removed from the compound being resolved [50–54].

Computational methods are increasingly being brought to bear on the crystallographic aspects of chiral crystals. The possibility that one could predict the crystal structures of a particular diastereomeric salt pair with an error in calculated lattice energy of less than 4 kcal/mole has been demonstrated for the system formed by a chlorine-substituted cyclic phosphoric acid and ephedrine [64]. In another study, it was demonstrated that the stability difference of the diastereomeric salt pairs of

three derivatives of 1-phenylethylammonium-2-phenylacetate was related to their resolution efficiency, even though similarities existed in their molecular structure and hydrogen-bonding motifs [65].

#### 4. SUMMARY

With more and more therapeutic agents being administered as resolved enantiomers, methods for isolation of the desired chiral species will be in great need during development. Melting point or solubility phase diagrams can be extremely useful, since one can use this information to identify the agent in question as being either a conglomerate or a racemate. Should the compound happen to crystallize as a conglomerate, then enantiomer separation by direct crystallization could possibly represent the cost-effective route. Compounds identified as racemates would necessarily require separation by some other means, such as the formation of dissociable diastereomers.

#### REFERENCES

- [1] T.M. Lowry, *Optical Rotatory Power*, Longmans, Green & Co., London, 1935.
- [2] C. Djerassi, *Optical Rotatory Dispersion*, McGraw-Hill, New York, 1960.
- [3] G. Sztatke, *Optical Rotatory Dispersion and Circular Dichroism in Organic Chemistry*, Heyden and Son, Ltd., London, 1967.
- [4] P. Crabbé, *ORD and CD in Chemistry and Biochemistry*, Academic Press, New York, 1972.
- [5] F. Ciardelli, P. Salvadori, *Fundamental Aspects and Recent Developments in Optical Rotatory Dispersion and Circular Dichroism*, Heyden and Son, Ltd., London, 1973.
- [6] N. Purdie, H.G. Brittain, *Analytical Applications of Circular Dichroism*, Elsevier, Amsterdam, 1994.
- [7] N. Berova, K. Nakanishi, R.W. Woody, *Circular Dichroism: Principles and Applications*, second ed., Wiley-VCH, New York, 2000.
- [8] L.D. Barron, *Analytical Molecular Light Scattering and Optical Activity*, second ed., Cambridge University Press, Cambridge, 2004.
- [9] F.S. Richardson, J.P. Riehl, Circularly polarized luminescence spectroscopy, *Chem. Rev.* 77 (1977) 773–792.
- [10] H.G. Brittain, *Excited-State Optical Activity*, Chapter 6, *Molecular Luminescence Spectroscopy: Methods and Applications*, Part 1, Wiley-Interscience, New York, 1985, pp. 583–620.
- [11] H.G. Brittain, N. Grinberg, *Techniques of chiroptical spectroscopy*, Chapter 10, in: J. Cazes (Ed.), *Handbook of Analytical Instrumentation*, third ed., Marcel Dekker, New York, 2005, pp. 271–294.
- [12] R.S. Cahn, C.K. Ingold, V. Prelog, Specification of molecular chirality, *Angew. Chem. Int. Ed. Engl.* 5 (1966) 385–415.
- [13] J. Jacques, A. Collet, S.H. Wilen, *Enantiomers, Racemates, and Resolutions*, John Wiley & Sons, New York, 1981.
- [14] H.G. Brittain, Crystallographic consequences of molecular dissymmetry, *Pharm. Res.* 7 (1990) 683–690.
- [15] J. Jacques, *The Molecule and its Double*, McGraw-Hill, New York, 1993.

- [16] J. Gal, The discovery of biological enantioselectivity: Louis Pasteur and the fermentation of tartaric acid, 1857—a review and analysis 150 years later, *Chirality* 20 (2008) 5–19.
- [17] J.-J. Rousseau, *Basic Crystallography*, John Wiley & Sons, New York, 1998.
- [18] F.A. Cotton, *Chemical Applications of Group Theory*, second ed., Wiley-Interscience, New York, 1971.
- [19] P.M. Zorkii, A.E. Razumaeva, V.K. Belsky, The systematization of molecular crystal structures, *Acta Crystallogr. A* 33 (1977) 1001–1004.
- [20] S.F. Mason, *Molecular Optical Activity and the Chiral Discriminations*, Cambridge University Press, Cambridge, 1982, pp. 165–166.
- [21] A.I. Kitaigorodskii, *Organic Chemical Crystallography*, Consultants Bureau, New York, 1955.
- [22] C.P. Brock, W.B. Schweizer, J.D. Dunitz, On the validity of Wallach's rule: on the density and stability of racemic crystals compared with their chiral counterparts, *J. Am. Chem. Soc.* 113 (1991) 9811–9820.
- [23] T.M. Lowry, *Molecular dissymmetry*, Chapter 2, *Optical Rotatory Power*, Longmans, Green, & Co, London, 1935, pp. 25–36.
- [24] R. Kuroda, S.M. Mason, Crystal structures of dextrorotatory and racemic sodium ammonium tartrate, *J. Chem. Soc., Dalton Trans.* B50 (1994) 59–68.
- [25] H.W.B. Roozeboom, Löslichkeit und Schmelzpunkt als Kriterien für Racemische Verbindungen, Pseudoracemische Mischkristalle und inactive Konglomerate, *Z. Phys. Chem.* 28 (1899) 494–515.
- [26] A. Collet, M.-J. Brienne, J. Jacques, Optical resolution by direct crystallization of enantiomer mixtures, *Chem. Rev.* 80 (1980) 215–230.
- [27] A. Collet, M.-J. Brienne, J. Jacques, Dédoubléments Spontanés et Conglomérats d'Énantionères, *Bull. Soc. Chim. Fr.* (1972) 127–142.
- [28] A. Collet, M.-J. Brienne, J. Jacques, Étude des Mélanges d'Antipodes Optiques. XIII. Compléments à Dédoubléments Spontanés, *Bull. Soc. Chim. Fr.* (1977) 494–498.
- [29] M. Leclercq, A. Collet, J. Jacques, Étude des Mélanges d'Antipodes Optiques. XII. Mesure de la Stabilité des Racémiques Vrais, *Tetrahedron* 32 (1976) 821–828.
- [30] M.D. Gourlay, J. Kendrick, F.J.J. Leusen, Rationalization of racemate resolution: predicting spontaneous resolution through crystal structure prediction, *Cryst. Growth Des.* 7 (2007) 56–63.
- [31] D.K. Kondepudi, K.E. Crook, Theory of conglomerate crystallization in the presence of chiral impurities, *Cryst. Growth Des.* 5 (2005) 2173–2179.
- [32] A. Findlay, A.N. Campbell, The influence of constitution on the stability of racemates, *J. Chem. Soc. (Lond.)* (1928) 1768–1775.
- [33] W. Meyerhoffer, Stereochemische Notizen, *Ber. Dtsch. Chem. Ges.* 37 (1904) 2604–2610.
- [34] J. Jacques, J. Gabard, Étude des Mélanges d'Antipodes Optiques. III. Diagrammes de Solubilité pour les Divers Types de Racémiques, *Bull. Soc. Chim. Fr.* (1972) 342–350.
- [35] R.M. Secor, Resolution of optical isomers by crystallization procedures, *Chem. Rev.* 63 (1963) 297–309.
- [36] A. Collet, Optical resolution by crystallization methods, Chapter 4, *Chiral Separations by HPLC*, Ellis Horwood, Chichester, 1989, pp. 81–104.
- [37] H.E. Zaugg, A mechanical resolution of DL-methadone base, *J. Am. Chem. Soc.* 77 (1955) 910.
- [38] L.F. Fieser, *Experiments in Organic Chemistry*, D.C. Heath Pub., Lexington, 1955, pp. 188–190.
- [39] A. Collet, J. Jacques, Étude des Mélanges d'Antipodes Optiques. V. Acides Mandéliques Substitués, *Bull. Soc. Chim. Fr.* (1973) 3330–3334.
- [40] M.-J. Brienne, A. Collet, J. Jacques, A convenient optical resolution of sec-phenethyl alcohol by preferential crystallization of its 3,5-dinitrobenzoate, *Synthesis* (1983) 704–705.



- [41] J. Jacques, M. Leclercq, M.-J. Brienne, La Formation de Sels Augmente-t-elle la Fréquence des Dédoubléments Spontanés, *Tetrahedron* 37 (1981) 1727–1733.
- [42] D. Kozma, Z. Böcskei, K. Simon, E. Fogassy, Racemic compound formation-conglomerate formation. Part 1. Structural and thermoanalytical study of hydrogen manonate, hydrogen phthalate, and hydrogen succinate of  $\alpha$ -phenylethylamine, *J. Chem. Soc. Perkin Trans. 2* (1994) 1883–1886.
- [43] Z. Böcskei, C. Kassai, K. Simon, E. Fogassy, D. Kozma, Racemic compound formation-conglomerate formation. Part 3. Investigation of the acidic salts of  $\alpha$ -phenylethylamine by achiral dicarboxylic acids. Optical resolution by preferential crystallization and a structural study of (R)- $\alpha$ -phenylethylammonium hydrogen itaconate, *J. Chem. Soc. Perkin Trans. 2* (1996) 1511–1515.
- [44] A.A. Freer, J.M. Bunyan, N. Shankland, D.B. Sheen, Structure of (S)-(+)-ibuprofen, *Acta Crystallogr. C* 49 (1993) 1378–1380.
- [45] N. Shankland, C.C. Wilson, A.J. Florence, P.J. Cox, Refinement of ibuprofen at 100 K by single-crystal pulsed neutron diffraction, *Acta Crystallogr. C* 53 (1997) 951–954.
- [46] H.G. Brittain, unpublished results.
- [47] K. Saigo, H. Kimoto, H. Nohira, K. Yanagi, M. Hasegawa, Molecular recognition in the formation of conglomerate crystal: the role of cinnamic acid in the conglomerate crystals of 1-phenylethylamine and 1-(4-isopropylphenyl)ethylamine salts, *Bull. Chem. Soc. Jap.* 60 (1987) 3655–3658.
- [48] H. Kimoto, K. Saigo, Y. Ohashi, M. Hasegawa, Molecular recognition in the formation of conglomerate crystal. 2. The role of arenesulfonic acid in the conglomerate crystals of amino acid salts, *Bull. Chem. Soc. Jap.* 62 (1989) 2189–2195.
- [49] S.K. Dwivedi, S. Sattari, F. Jamali, A.G. Mitchell, Ibuprofen racemate and enantiomers: phase diagram, solubility, and thermodynamic studies, *Int. J. Pharm.* 87 (1992) 95–104.
- [50] S.H. Wilen, Resolving agents and resolutions in organic chemistry, *Top. Stereochem.* 6 (1971) 107–176.
- [51] S.H. Wilen, Strategies in optical resolutions, *Tetrahedron* 37 (1977) 2725–2736.
- [52] R.A. Sheldon, P.A. Porskamp, W. ten Hoeve, Advantages and limitations of chemical optical resolution, in: J. Tramper, H.C. van der Plas, P. Linko (Eds.), *Biocatalysts in Organic Synthesis*, Amsterdam, Elsevier, 1985, pp. 59–80.
- [53] A. Collet, Separation and purification of enantiomers by crystallization methods, *Enantiomer* 4 (1999) 157–172.
- [54] F. Toda, *Enantiomer Separation: Fundamentals and Practical Methods*, Kluwer Academic Pub., Dordrecht, 2004.
- [55] S.H. Wilen, *Tables of Resolving Agents and Optical Resolutions*, University of Notre Dame Press, South Bend, IN, 1972.
- [56] I. Ugi, Use of diastereomers avoids the ambiguities of the threo, erythro nomenclature, *Z. Naturforsch.* 20B (1965) 405–421.
- [57] H. Lorenz, A. Seidel-Morgenstern, Binary and ternary phase diagrams of two enantiomers in solvent systems, *Thermochim. Acta* 382 (2002) 129–142.
- [58] T. Shiraiwa, Y. Sado, S. Fujii, M. Nakamura, H. Kurokawa, Optical resolution of ( $\pm$ )-phenylsuccinic acid by using (–)-proline as resolving agent, *Bull. Chem. Soc. Jap.* 60 (1987) 824–826.
- [59] E.J. Valente, J. Zubkowski, D.S. Eggleston, Discrimination in resolving systems I: ephedrine-mandelic acid, *Chirality* 4 (1992) 494–504.
- [60] E.J. Valente, C.W. Miller, J. Zubkowski, D.S. Eggleston, X. Shui, Discrimination in resolving systems II: ephedrine-substituted mandelic acids, *Chirality* 7 (1995) 652–676.
- [61] H. Hiramatsu, K. Okamura, I. Tsujioka, S.-I. Yamada, R. Yoshioka, Crystal structure-solubility relationships in optical resolution by diastereomeric salt formation of DL-phenylglycine with (1S)-(+)-camphor-10-sulfonic acid, *J. Chem. Soc. Perkin Trans. 2* (2000) 2121–2128.

- [62] M.C. Brianso, Structures Atomiques et Moléculaires des Sels Diastéréoisomères des  $\alpha$ -Phényl- $\alpha$ -Méthylacétates d' $\alpha$ -Phényl-Éthylammonium *p* et *n*, Acta Crystallogr. B 32 (1976) 3040–3045.
- [63] H. Lopez de Diego, Crystal structure of (*S*)-1-phenylethylammonium (*R*)-mandelate and a comparison of diastereomeric mandelate salts of 1-phenylethylamine, Acta Chem. Scand. 48 (1994) 306–311.
- [64] F.J.J. Leusen, Crystal structure prediction of diastereomeric salts: a step toward rationalization of racemate resolution, Cryst. Growth Des. 3 (2003) 189–192.
- [65] P.G. Karamertzanis, P.R. Anandamanoharan, P. Fernandes, P.W. Cains, M. Vickers, D.A. Tocher, et al., Toward the computational design of diastereomeric resolving agents: an experimental and computational study of 1-phenylethylammonium-2-phenylacetate derivatives, J. Phys. Chem. B 111 (2007) 5326–5336.
- [66] E.J. Ebberts, B.J.M. Plum, G.J.A. Ariaans, B. Kaptein, Q.B. Broxterman, A. Bruggink, et al., New resolving bases for ibuprofen and mandelic acid: qualification by binary phase diagrams, Tetrahedron Asymmetr. 8 (1997) 4047–4057.

## Cocrystal Systems of Pharmaceutical Interest: 2009

Harry G. Brittain

---

Contents	1. Introduction	361
	2. Strategies for the Preparation of Cocrystal Systems	362
	3. Cocrystal Systems Having Pharmaceutical Interest	367
	3.1. Cocrystal systems formed by carbamazepine	368
	3.2. Other cocrystal systems of pharmaceutical interest	370
	3.3. Miscellaneous cocrystal systems	374
	References	378

### 1. INTRODUCTION

As scientists become more aware of a substantial expansion in the scope of solid-state structural variations that can be obtained through the cocrystallization of several molecules in a single lattice structure, studies of the mixed molecular crystal systems known as cocrystals have mushroomed [1–3]. Along these lines, workers have researched the assembly of supramolecular synthons and crystal engineering in ever-increasing efforts to produce materials having new and useful properties [4].

For the purposes of this review, cocrystal systems will be regarded as those mixed crystal systems where the individual components exist as solids under ambient conditions [5]. Particularly useful guidance has been provided by Aakeröy, where cocrystal formation from supramolecular synthons is to be considered as forming from discrete neutral

Center for Pharmaceutical Physics, Milford, New Jersey, USA

molecular species that are solids at ambient temperatures, and where the cocrystal is a structurally homogeneous crystalline material that contains the building blocks in definite stoichiometric amounts [2].

Two important historical surveys of the cocrystal literature were published during 2009. In one, Schultheiss and Newman have discussed advances made over the last decade with respect to the physical and chemical property improvements that could be achieved in cocrystal products having pharmaceutical interest, and have pointed out the possibility of solubility enhancements that might not be realized using other solid-state approaches [6]. Stahly has provided a history of cocrystals containing only organic components that were reported in the literature prior to 2000, discussing their discovery and history, and illustrating principles of cocrystal chemistry through the use of illustrative examples [7].

The present review represents a continuation in the series [8], and will examine literature that was published during 2009. Although primary attention will be given to cocrystal systems having pharmaceutical interest, related papers that are of particular significance to the field will be discussed as well. The literature cited in the present review has been drawn from the major physical, crystallographic, and pharmaceutical journals, and consequently the coverage cannot be represented as being encyclopedic or comprehensive. Apologies are presented in advance to any scientist in the field whose works have been inadvertently omitted.

## 2. STRATEGIES FOR THE PREPARATION OF COCRYSTAL SYSTEMS

Retrospective mining of the Cambridge Structural Database has been used to extract an ensemble of reliable cocrystal structures, whereupon the type of molecular descriptors used in quantitative structure-activity relationship studies were calculated for the molecules in the set [9]. Statistical methods were used to identify useful molecular properties, with the strongest descriptor correlations being related to the shape and polarity of cocrystal formers. In another work, the probability for combinations of specific CO and NH groups to form a three-center hydrogen bond between one CO and two NH groups was evaluated, and it was demonstrated that charged  $\text{CO}^-$  groups are more prone to form such interactions [10]. It was concluded that the  $\text{CO}^-$  group most commonly formed three-center hydrogen bonds either in the  $\text{R}_4^2(8)$  motif, or in combination with  $-\text{CNH}_3^+$  or  $-\text{NH}_4^+$  groups.

The use of Hammett substitution constants as design aids for identifying acid-acid supramolecular synthons characterized by the presence of a

$R_2^2(8)$  hydrogen-bonded heterodimer has been explored as a means to create new cocrystal systems [11]. This approach was tested through the prediction and isolation of a 1:1 cocrystal containing 4-aminobenzoic acid and 2,5-dinitrobenzoic acid. A series of bipyridine compounds were cocrystallized with a variety of substituted resorcinol compounds in order to study how modifications in hydrogen-bonding patterns influenced the hydroxyl-pyridine heterosynthon [12]. One goal of the work was to achieve control over the outcome of the (2+2) photodimerization reaction by using resorcinol as a spacer. In another work, a new synthon involving a carboxylic acid and a secondary amide was identified and used to synthesize a variety of cocrystal products [13].

Lattice energies of 12 cocrystals of 4-aminobenzoic acid, 8 of succinic acid, and 6 of caffeine were calculated to predict whether current computational methodology could be used to predict the formation of cocrystals [14]. The lattice energies were obtained using anisotropic intermolecular atom-atom potentials, with the electrostatic model and the intramolecular energy penalty for changes in specified torsion angles being derived from *ab initio* calculations on the isolated molecules. It was found that most cocrystals were predicted to be more stable than their component molecules, and that the energy difference would only be large where the molecules involved could not form hydrogen bonds among them. It was concluded that prediction of cocrystal formation should be possible through comparisons of the relative stability of the most stable cocrystal and its pure components, although the procedure requires high degrees in the accuracy of the method used to calculate crystal energies.

Workers continue to develop new thermodynamic models to understand the energetics of cocrystal systems. In one work, cocrystal phase diagrams were modeled using a phase diagram obtained from discontinuous isoperibolic thermal analysis and conventional thermodynamic data [15]. Unfortunately, this approach was illustrated using the cocrystal formed between glutaric acid and a nondisclosed drug substance, so the reported agreement between calculated and experimental data cannot really be evaluated. In another paper, a basic outline of the thermodynamics associated cocrystal formation was presented, enabling one to experimentally evaluate the thermodynamic stability of a cocrystal with respect to its component forms [16]. Fortunately, the utility of this method was illustrated using the real carbamazepine-nicotinamide system.

An *a priori* prediction for cocrystal formation has been reported that is based on intermolecular pair interactions that have been characterized using pulsed gradient spin-echo nuclear magnetic resonance, and tested against the conventional ionization constant guideline for 25 molecular pairs [17]. This approach was shown to work well even in different

solvent systems in that a single prediction parameter (the Pair Interaction Index) reliably predicted the formation of multicomponent crystals of the salts and cocrystals studied. Another systematic method for the prediction of cocrystal formation has been advanced that is based on solubility factors that influence mixed crystal formation, and validated through the formation of cocrystal products containing carbamazepine and cinnamic acid [18]. In this method, one considers the solubilities of the pure components to develop an extended phase diagram that enables one to deduce compositional ranges for which the cocrystal would be the stable crystalline form.

Jones and coworkers have contributed three articles of note which provide a considerable degree of insight into the mechanochemical formation of cocrystals. In a substantial review, an overview of cocrystal formation by means of grinding sought to organize advances in how the processes take place at both the microscopic (i.e., molecular recognition) and macroscopic (i.e., bulk phase transformation) levels, and also provided the first systematic classification of cocrystal grinding reactions [19]. Using studies conducted on nicotinamide and 10 dicarboxylic acids, it was determined that mechanochemical techniques were more efficient in screening for cocrystals than were solution-phase or melt crystallization procedures, and that one could vary the stoichiometry of the product by varying the ratios of the reactants [20]. In another work, mechanochemical liquid-assisted grinding and sonochemical techniques were used to prepare cocrystals of theophylline and caffeine with (*L*)-malic and or (*L*)-tartaric acids, and it was determined that cocrystal formation would be expected for systems where the cocrystal components could be maintained at their equilibrium solubility values [21].

Although not directly relating with the production of cocrystals, two important reviews on the general subject of mechanochemistry were published during 2009 that need to be mentioned. In one of these reviews, Grassi and coauthors reviewed the theoretical background behind the mechanochemical activation of drug substances when these undergo comminution and particle size reduction, typically to enhance solubility and bioavailability [22]. A fair amount of discussion was devoted to the different kinds of mills and milling techniques, and it was concluded that can be used and on mills classification based on the energy transferred to the materials. While mechanochemical activation generally improves drug bioavailability, the approach is best suited for poorly water soluble drugs that do not exhibit permeability problems.

Defining mechanochemistry as the mechanical breakage of intramolecular bonds by external force, Kaupp elucidated the relative merits of grinding, milling, shearing, scratching, polishing, and rapid friction, and differentiated these from the more thermally related processes of

sonication and shock waving [23]. The review contained a large number of practical examples derived from a wide range of fields (such as ceramics, mechanical alloying, hydrogen storage, organic syntheses, waste remediation, leachings, surface plasmas, radical formation, explosives, nanotube formation, nanoparticles grafting, polymer technology, radical initiation, scratch-less polishing, wear protection, lubrication); workers interested in the production of cocrystals by mechanochemical means will find considerable insight in this review.

It is recognized that formation of cocrystals can enhance the solubility and dissolution of pharmaceutical compounds, and therefore a method has been developed that enables estimation of the solubilities of cocrystals in pure solvent systems from transition concentration measurements where a solution is in equilibrium with solid drug and cocrystal [24]. The method was tested for various carbamazepine cocrystals dissolved in water, ethanol, isopropanol, and ethyl acetate, demonstrating that one could obtain great enhancements in aqueous solubility depending on the solubility of the constituent reactants. In another study, equations relating cocrystal solubility in terms of solubility products, cocrystal component ionization constants, and solution pH were derived for cocrystals with acidic, basic, amphoteric, and zwitterionic components, and then used to obtain insight regarding pH-solubility curve [25]. In a highly practical application, five cocrystals of an anticancer compound have been obtained, where the co-formers contained aliphatic even-numbered dicarboxylic acids of increasing chain length, permitting melting phenomena and solubilities of the cocrystals to be related to the molecular structure of the acids [26].

Brittain has begun to develop selection rules that permit one to use vibrational spectroscopy as a means to study the formation of salts and cocrystals. In a study of the benzamide–benzoic acid system, the amide –NH<sub>2</sub> stretching band derived from the benzamide synthon was found to become split in the spectrum of the cocrystal, and this splitting persisted as long as an identifiable cocrystal phase existed in the solid [27]. Formation of the cocrystal also caused broadening in the carbonyl band region around 1650 cm<sup>-1</sup> that is diagnostic of the existence of the benzamide–benzoic acid cocrystal. This feature consists of an overlapped combination of the out-of-plane deformation modes associated with each synthon. The formation of the benzamide–benzoic acid cocrystal was particularly evident in the high-frequency region of the absorption spectrum. As shown in Fig. 10.1, the appearance of an additional NH<sub>2</sub> stretching mode at 3420 cm<sup>-1</sup> clearly demonstrates the formation of the cocrystal product.

In a companion study of the benzylamine–benzoic acid system, benzoic acid was found to form a 1:1 cocrystal with the benzylammonium benzoate salt [28]. As shown in Fig. 10.2, the phenomenon of salt formation led to strong perturbations in the vibrational modes associated with

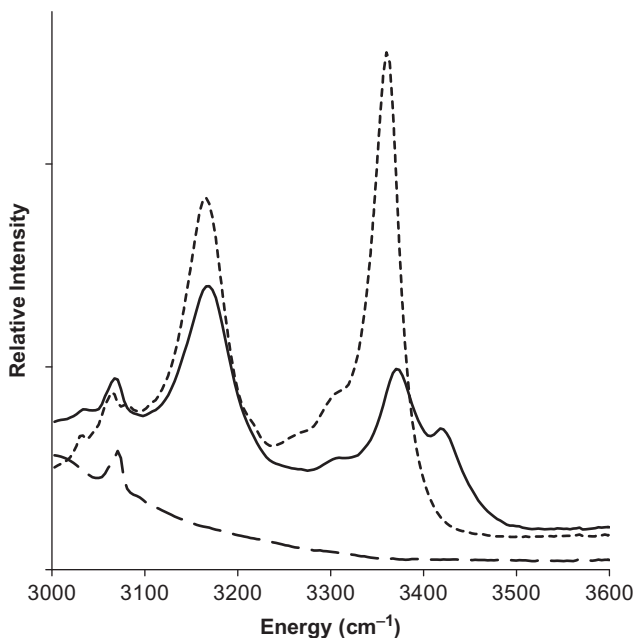


**FIGURE 10.1** Expanded infrared absorption spectra in the carbonyl section of the high-frequency region of benzoic acid (long-dashed trace), benzamide (short-dashed trace), and the stoichiometric 1:1 cocrystal of these (solid trace) [27].

the carboxylic acid group of benzoic acid and with the amine group of benzylamine. At the same time, little change in the energies of the vibrational modes associated with the carbon–carbon and carbon–hydrogen portions of the compounds was observed. These findings demonstrated that the structural changes associated with salt formation only affected the energies of the vibrational modes directly involved in the proton transfer and ion association. However, perturbations in the carbon–carbon and carbon–hydrogen vibrational modes were observed in the benzoic acid cocrystal with benzylammonium benzoate, demonstrating the importance of the phenyl rings in the cocrystal formation.

Terahertz time-domain-spectroscopy has been used to distinguish between chiral and racemic hydrogen-bonded cocrystals, and could readily distinguish between the isostructural cocrystals of theophylline with the chiral and racemic forms of both malic and tartaric acids [29]. These findings are of importance since it was concluded that while the respective cocrystal systems were almost identical in molecular structure and supramolecular architecture, the use of terahertz spectroscopy was comparable in sensitivity to X-ray diffraction and more sensitive than Raman spectroscopy to changes in cocrystal architecture. Solid-state nuclear



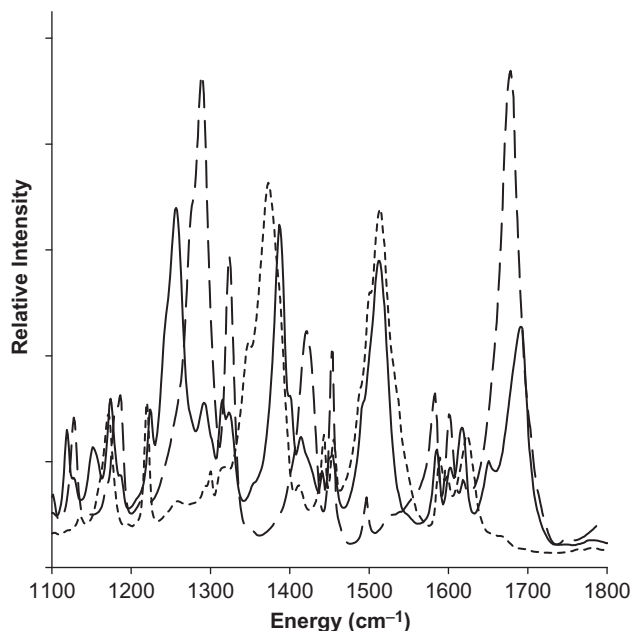


**FIGURE 10.2** Expanded infrared absorption spectra in the carboxylate region obtained for benzoic acid (long-dashed trace), the stoichiometric 1:1 benzylammonium benzoate salt (short-dashed), and the 1:1 cocrystal formed between benzoic acid and benzylammonium benzoate (solid trace) [28].

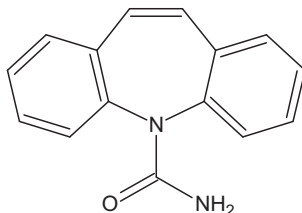
magnetic resonance has been shown to be very useful as a means to identify and characterize organic cocrystals and complexes [30]. Studies conducted on a variety of systems were used to deduce a general experimental approach for the SS-NMR study of cocrystal systems, which made use of 1D and 2D dipolar correlation methods.

### 3. COCRYSTAL SYSTEMS HAVING PHARMACEUTICAL INTEREST

As cocrystal systems achieve more and more interest as new solid-state forms of active pharmaceutical ingredients, the research conducted on these systems continues to be published. In Section 3.3, the considerable amount of work which has also been conducted on cocrystal systems of less interest to pharmaceutical scientists will be summarized and tabulated, but Sections 3.1 and 3.2 will focus on works where organic compounds of pharmaceutical interest have been obtained as cocrystals.

### 3.1. Cocrystal systems formed by carbamazepine

Unabated interest continues in systems formed by the prototypical cocrystal-forming compound, carbamazepine (5*H*-dibenz[*b,f*]azepine-5-carboxamide):



It is well known that this amide-containing compound forms cocrystal products with a variety of compounds, and the continued study within this system is being used to develop greater degrees of understanding about cocrystal formation.

In a retrospective study within the Cambridge Structural database, 50 crystal structures containing carbamazepine were analyzed to define any structural similarities that would signify the existence of general trends that could be utilized in the evaluation of other cocrystal systems [31]. It was determined that while analysis of hydrogen-bonding patterns did not yield any higher dimensional groupings, categorization of structures on the basis of packing motifs resulted in a separation of the structures into three main types. Among other conclusions, it was reported that the carboxamide homodimer found in the four polymorphs of carbamazepine polymorphs was less energetically favorable relative to the carboxamide–carboxylic acid heterodimer that is formed when the other cocrystal former contains a carboxylic acid group.

The relative merits of solvent drop grinding and evaporation from solution were evaluated through the study of 17 new cocrystals, for which the intermolecular interactions were established by the existence of  $\text{COOH} \cdots \text{N}_{\text{arom}}$  and  $\text{OH} \cdots \text{N}_{\text{arom}}$  supramolecular heterosynthons [32]. It was reported that all of the cocrystals that were grown from solution and characterized by single crystal X-ray crystallography could also be prepared using mechanochemical means. It was, therefore, concluded that the mechanochemical procedure was an efficient method for the discovery of new cocrystal systems as well as being a reliable method for the preparation of known cocrystals.

In another study, the effects of moisture and temperature during storage of mixed pure solid components (i.e., no milling or grinding) were investigated to determine whether cocrystal products would form

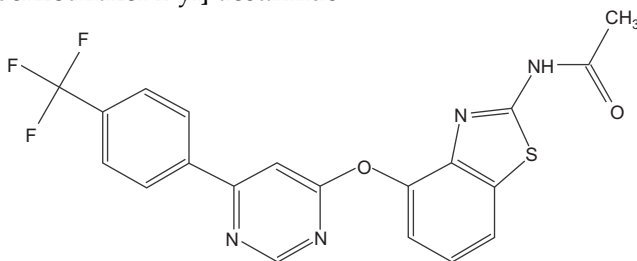
under these conditions [33]. When mixtures of anhydrous carbamazepine Form-III and nicotinamide Form-I or saccharin were stored at 40 °C and 75% relative humidity, conversion to the cocrystal products took place even in the absence of mechanical stress, indicating that the transformation from reactants to cocrystal is thermodynamically favorable. The cocrystal system formed by carbamazepine and 4-aminobenzoic acid has been studied in order to identify the factors and conditions governing the formation and stability of cocrystals having different stoichiometries [34]. While the 1:1 cocrystal was easily obtained, the relative stability of the 2:1 and 1:1 cocrystals were shown to be dependent on the relative concentrations of the reactants.

The kinetics associated with the formation of the carbamazepine–nicotinamide cocrystal from two polymorphic forms of carbamazepine and its dihydrate has been studied as a function of milling conditions and product storage times [35]. Cocrystal products were formed in all instances, but the rate of formation was found to be fastest when using carbamazepine dihydrate as the initial reactant. The conversion rates obtained when using polymorphic Form-I or Form-III were slower, and these effects were attributed to the presence of moisture in the reaction mixture. In another work, the kinetics associated with the formation of the carbamazepine–nicotinamide cocrystal in solution has also been studied through the establishment of phase solubility diagrams [36]. Using *in situ* infrared absorption spectroscopy (with attenuated total reflectance sampling), the concentration of the reactions could be profiled in solution, as well as the nature of the solid form in suspension and the proportion of each solid phase.

One of the obstacles facing the commercial development of pharmaceutical cocrystals is the need to increase the scale of manufacture from that of solvent drop grinding to large scale production. One of the elements to overcome is the situation where the two reactants have differing solubilities, but a generic and scalable crystallization methodology has been presented for the carbamazepine–nicotinamide system [37]. The initial stage consisted of calculation of intermolecular interactions and crystal lattice energies to understand the structure and strength of the binding synthons, and then empirical measurements of pure component solubilities, solid form stability domains, speciation in solution, and nucleation kinetics were used to optimize solution crystallization conditions. With the adoption of an appropriate seeding strategy, a process was developed that could be used to produce cocrystal product at the liter scale and a throughput of 14 L/kg.

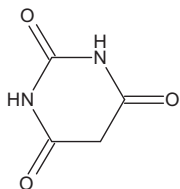
### 3.2. Other cocrystal systems of pharmaceutical interest

Fifteen cocrystals of *N*-[4-({6-[4-(trifluoromethyl)phenyl]pyrimidin-4-yl}oxy)-1,3-benzothiazol-2-yl]-acetamide

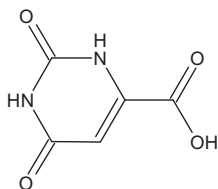


with diacids and triacids have been reported, involving the same hydrogen bond donor (amide) and acceptor (benzothiazole) on the drug substance [38]. In this study, little correlation was found between the melting point of the cocrystal former and that of the cocrystal product, and no correlation could be developed between the melting point and solubility of the cocrystal products.

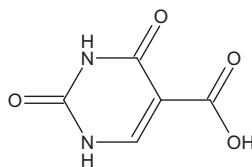
Cocrystal products of 4,4'-bipyridine with barbituric acid, orotic acid, and uracil-5-carboxylic acid



Barbituric acid



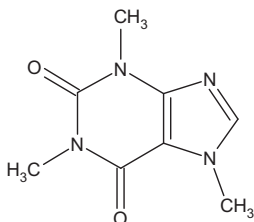
Orotic acid



Uracil-5-carboxylic acid

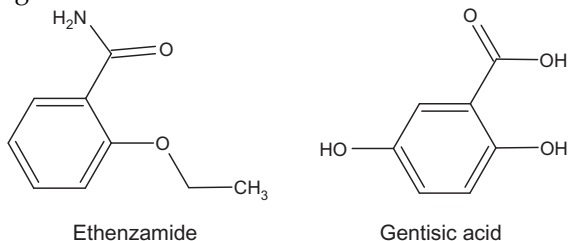
have been obtained, including a neutral cocrystal species, an ion pair, and a mixed product containing both ionic and hydrogen-bonded neutral species [39]. Analysis of the structures revealed the existence of partial proton transfer in the ionic systems, and optimized hydrogen-bonding, and  $\pi \cdots \pi$  and molecular dipole interactions. The latter finding led the authors to speculate on the proper nomenclature that would be suitable for crystal systems containing neutral and charged organic compounds contained in the same structure.

Nine cocrystal products have been obtained by the interaction of caffeine



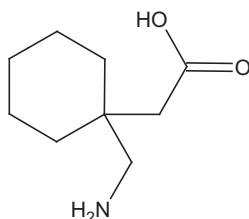
with 2-hydroxy, 3-hydroxy, and 4-hydroxybenzoic acids, and also with 2,3-dihydroxy, 2,4-dihydroxy, 2,5-dihydroxy, 3,4-dihydroxy, and 3,5-dihydroxybenzoic acids [40]. The existence of O–H(carboxyl)···N(imidazole), O–H(hydroxyl)···O(urea), and O–H(hydroxyl)···O(amide) heterosynthons was reported in the structurally diverse cocrystals, which were produced using a thermodynamically driven, solution-mediated, phase transformation process.

Three polymorphic forms of a cocrystal containing two active pharmaceutical ingredients



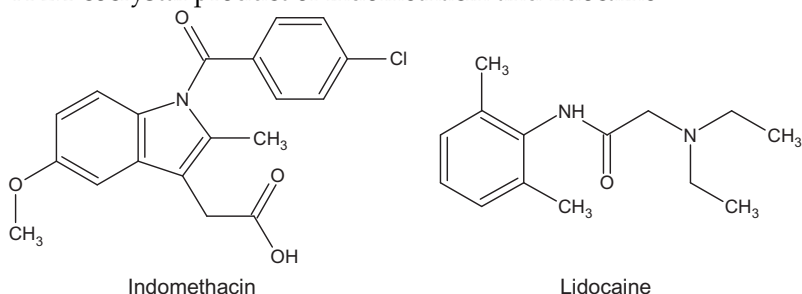
have been reported [41]. Form-I was obtained from acetonitrile, Form-II was obtained from a 1:1 toluene–acetonitrile solvent mixture, and Form-III was obtained by the crystallization of a 2:1 mixture of the drug substances from the 1:1 toluene–acetonitrile solvent mixture at room temperature. It was also reported that the metastable Form-II and Form-III polymorphs converted to the thermodynamically stable Form-I upon performance of solid-state grinding.

The isolation and characterization of 13 cocrystals and salts formed by gabapentin



with 2-hydroxy, 3-hydroxy, and 4-hydroxybenzoic acids, 1-hydroxy-2-naphthoic acid, and (*RS*)-mandelic acid has been reported [42]. The existence of varying degrees of proton transfer was detected in the structures, and the lack of disproportionation for dissolved solids was taken to indicate that the products must be less soluble than the reactants. A mathematical model, based on cocrystal dissociation and ionization solution equilibria was also developed to describe the pH solubility profile for a zwitterionic drug substance and an acidic cofomer.

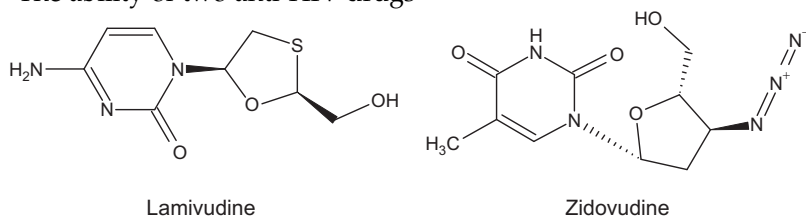
### A 2:1 cocrystal product of indomethacin and lidocaine



was obtained from ethanol, and characterized by the standard sequence of solid-state analytical techniques [43]. The same cocrystal product was obtained using solvent-less grinding and heating, which suggested that the formation process consisted of the steps of achieving an intimate mixture of the ingredients, inducing disorder in the solids by grinding or fusion, and achieving crystal growth by heating.

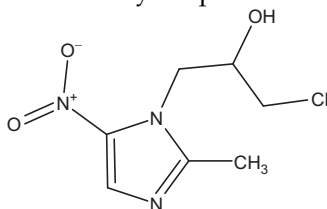
The mixed-crystal system formed by indomethacin and saccharin (1,2-benzisothiazol-3(2*H*)-one-1,1-dioxide) has been used to evaluate the feasibility of using supercritical fluids as media for the design and preparation of new cocrystals [44]. In this work, the relative merits of supercritical fluid processes (i.e., cocrystallization with a supercritical solvent, supercritical fluid as anti-solvent, and the atomization and anti-solvent technique) were evaluated, as well as the influence of processing parameters on product formation and particle properties of the yields. It was reported that while the anti-solvent and atomization procedures yielded pure cocrystal products, only partial to no cocrystal formation took place when using the crystallization process.

The ability of two anti-HIV drugs



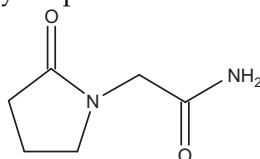
to form mixed crystal products with 2,4,6-triaminopyrimidine, 4-quinoline, 3,5-dinitrosalicylic acid, and saccharin has been investigated with the aim of evaluating the ability of synthon theory to predict the formation of cocrystals of simple compounds [45]. It was reported that the existence of multiple hydrogen-bonding donors on the reactants could make reliable crystal structure predictions unreliable in that one might deduce the presence of an incorrect synthon.

The observation that molecules which crystallize with more than one molecule in the crystallographic asymmetric unit exhibit a greater tendency toward cocrystal formation relative to compounds that crystallize in the pure form with one molecule in the unit has been investigated by categorizing such instances as contained in the Cambridge Structural Database [46]. The results of this analysis were experimentally demonstrated by isolation of the 1:1 cocrystal product formed by ornidazole



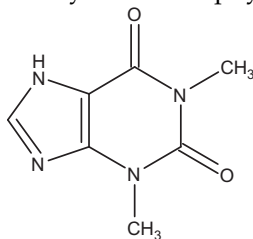
with 3,5-dinitrobenzoic acid.

A number of mixed crystal products have been reported for piracetam



with (*L*)-tartaric acid, (*L*)- and (*DL*)-mandelic acid using solvent-drop grinding, solution evaporation, or solution-phase crystallization procedures [47]. In addition, cocrystal products with citric acid in 1:1 and 3:2 ratios were also obtained, as well as a piracetam–citric acid ethanol solvatomorph. Analysis of the structures demonstrated that the classic amide–carboxylic acid  $R_2^2(8)$  synthon was not found in the cocrystals of this study, indicating that the prediction of this motif fails in the presence of a multitude of hydrogen bond donors and acceptors.

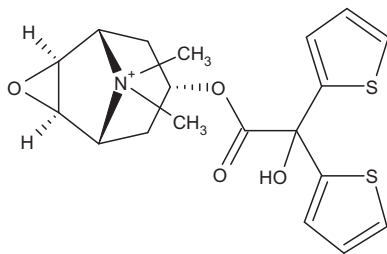
The structure of the 1:1 cocrystal of theophylline



with gentisic acid (i.e., 2,5-dihydroxybenzoic acid) has been reported [48]. The triclinic mixed crystal was characterized by the existence of two-dimensional hydrogen-bonded sheets involving  $N-H\cdots O$  and

O–H $\cdots$ N hydrogen bonds that linked the cocrystal formers, as well as substantial  $\pi$ – $\pi$  stacking interactions.

A very interesting cocrystal product has been formed by the fumarate salt of tiotropium



with fumaric acid (i.e., (2*E*)-but-2-enedioic acid), a species that was termed a salt-cocrystal [49]. This species was reported to be the most thermodynamically stable of the polymorphic forms of tiotropium fumarate, the stability being correlated by a preferential packing of the cations in the structure. The crystal contains anions and free acid cofomers catenated along the (010) direction between pairs of tiotropium cations, and the stability of the structure was established by the free rotation of the two thiophene rings of the cation about the C-6 center.

### 3.3. Miscellaneous cocrystal systems

As one might imagine, the 2009 literature contains a large number of additional papers related to cocrystal research, but whose subject matter is of a more indirect interest to investigators engaged in drug development. Nevertheless, many of these works contain details whose coverage is important, and hence Table 10.1 contains the appropriate citations and a brief synopsis of the scope of each work.



**TABLE 10.1** Additional reports of cocrystal research published during 2009

First conformer	Second coformer	Remarks	Reference
Squaric acid	4,4'-Bipyridine	Structure and characterization of the 1:1 cocrystal, and study of the single-crystal to single-crystal phase transition around 175 °C	[50]
Benzoic acid	Isonicotinamide	Structures of the 1:1 and 2:1 cocrystals, and the influence of solution composition on the crystallization outcome	[51]
Trimesic acid	5-Methyl-2-pyridone	Structure of a new cocrystal product generated by solid-state grinding of the methanol solvate cocrystal	[52]
4- <i>p</i> -Hydroxyphenyl-2,2,4-trimethyl-chroman	Ethylenediamine	Structure of the adduct, and identification of ionic and neutral supramolecular motifs derived from the same components	[53]
<i>meta</i> - and <i>para</i> -substituted hydroxy-benzoic acids	Amino-pyridines	Structures of 11 cocrystal products, and identification of the various synthon interactions in these for prediction of hydrogen-bonding possibilities in new salt and cocrystal structures	[54]
Pamoic acid	Piperazine and 4,4'-bipyridine	Structures of the pamoic acid trihydrate salt of piperazine and the pamoic acid cocrystal with 4,4'-bipyridine	[55]
Benzophenone	Diphenylamine	Elucidation of the relationships between crystal chemistry, solution-phase chemistry, and phase behavior in binary and ternary systems	[56]

(continued)

**TABLE 10.1** (continued)

First conformer	Second coformer	Remarks	Reference
Maleic, fumaric, phthalic, isophthalic, and terephthalic acids	Pyridine and 4-dimethylamino-pyridine	Structural analysis of the salts and cocrystals formed with pyridine, and the salts of 4-dimethylaminopyridine	[57]
Benzo[18]crown-6	Urea, thiourea, 1-methyl-thiourea, and nicotinamide	Characterization of the cocrystals obtained using solution crystallization, high-throughput cocrystallization, dry grinding, and solvent-drop grinding	[58]
1,3-bis(4-Hydroxy-3,5-dimethoxy-phenyl)adamantane	1,3,5-Trinitro-benzene	Structures of the substituted adamantane solvatomorphs, and of the cocrystal with 1,3,5-trinitrobenzene	[59]
2,2',6,6'-Tetra-carboxybiphenyl	bis(4-Pyridyl)-ethylene and 4,4'-bipyridine	Observation of an eight-fold interpenetrating diamondoid network in cocrystals but not in salts	[60]
Isophthalic, trimesic, pyromellitic, and terephthalic acids	Methylene bis(3,5-dimethyl-pyrazole)	Structures of the cocrystal products, and identification of 3 supramolecular synthons useful for the prediction of structural motifs	[61]
Glutaric acid	Urea	Discovery of a new 1:1 cocrystal by construction of the ternary phase diagram	[62]
Fumaric acid	Nicotinamide	Characterization of the amide-acid heterosynthon in the 1:1 cocrystal and the amide-amide homosynthon in the 2:1 cocrystal	[63]
Cyanooxime compounds	N-heterocycle compounds	Study of the versatility of cyanooximes as hydrogen-bond donors when interacted with asymmetric ditopic N-heterocyclics	[64]

Benzoic, salicylic, and <i>o</i> -acetylsalicylic acids	Diazabicyclo [2.2.2]octane, piperazine, phenazine, and 2-aminopyrimidine	Structural studies of the cocrystal products formed by mechanochemical means, including different stoichiometries and polymorphic forms	[65]
2-Chlorophenol	2-Methylphenol	Low-temperature formation of a near 1:1 cocrystal that separates at high pressure to yield a new polymorph of 2-chlorophenol	[66]
Pyromellitic and trimesic acids	Tetrapyridyl porphyrin	Preparation and characterization of three crystalline adducts	[67]
( <i>E</i> )- <i>O</i> -alkyl <i>N</i> -aryl-thiocarbamide compounds	4,4'-Bipyridine, <i>trans</i> -1,2-bis(4-pyridyl)ethene, and 1,2-bis(4-pyridyl)ethane	Structural characterization of five 2:1 cocrystal products, isolated as single crystals by slow evaporation methods	[68]
4-Aminobenzyl alcohol	4-Acetylpyridine	Structural analysis of the 1:1 cocrystal, as well as the structures of several related compounds	[69]
4- <i>p</i> -Hydroxyphenyl-2,2,4-trimethyl-chroman	Piperazine and piperidine	Structures of the 2:1 piperazine and 1:1 piperidine cocrystals, and comparison of these with the known clathrate structures	[70]
Maleic, fumaric, and ( <i>L</i> )- and ( <i>DL</i> )-tartaric acids	2-Pyrrolidinone and 2-imidazolo-idinone	Structures of 11 new cocrystals, and elucidation of the amide–acid and amide–amide hydrogen bonding in relation to synthon assembly	[71]

---

## REFERENCES

- [1] C.B. Aakeröy, D.J. Salmon, Building co-crystals with molecular sense and supramolecular sensibility, *CrystEngComm* 7 (2005) 439–448.
- [2] P. Vishweshwar, J.A. McMahon, J.A. Bis, M.J. Zaworotko, Pharmaceutical cocrystals, *J. Pharm. Sci.* 95 (2006) 499–516.
- [3] N. Shan, M.J. Zaworotko, The role of cocrystals in pharmaceutical science, *Drug Discov. Today* 13 (2008) 440–446.
- [4] G.R. Desiraju, Supramolecular synthons in crystal engineering: a new organic synthesis, *Angew. Chem. Int. Ed.* 34 (1995) 2311–2327.
- [5] M.J. Zaworotko, Molecules to crystals, crystals to molecules ... and back again? *Cryst. Growth Des.* 7 (2007) 4–9.
- [6] N. Schultheiss, A. Newman, Pharmaceutical cocrystals and their physicochemical properties, *Cryst. Growth Des.* 9 (2009) 2950–2967.
- [7] G.P. Stahly, A survey of cocrystals reported prior to 2000, *Cryst. Growth Des.* 9 (2009) 4212–4229.
- [8] H.G. Brittain, Cocrystal systems of pharmaceutical interest: 2007–2008, in: H.G. Brittain (Ed.), *Profiles of Drug Substances, Excipients, and Related Methodology*, vol. 35, Elsevier Academic Press, Amsterdam, 2010, pp. 373–390.
- [9] L. Fábíán, Cambridge structural database analysis of molecular complementarity in cocrystals, *Cryst. Growth Des.* 9 (2009) 1436–1443.
- [10] S. Eppel, J. Bernstein, Statistics-based design of multicomponent molecular crystals with the three-center hydrogen bond, *Cryst. Growth Des.* 9 (2009) 1683–1691.
- [11] K. Chadwick, G. Sadiq, R.J. Davey, C.C. Seaton, R.G. Pritchard, A. Parkin, Designing acid–acid cocrystals: the use of Hammett substitution constants, *Cryst. Growth Des.* 9 (2009) 1278–1279.
- [12] M. Khan, V. Enkelmann, G. Brunklaus, O–H...N Heterosynthon: a robust supramolecular unit for crystal engineering, *Cryst. Growth Des.* 9 (2009) 2354–2362.
- [13] L. Rajput, K. Biradha, Design of cocrystals via new and robust supramolecular synthon between carboxylic acid and secondary amide: honeycomb network with jailed aromatics, *Cryst. Growth Des.* 9 (2009) 40–42.
- [14] N. Issa, P.G. Karamertzanis, G.W.A. Welch, S.L. Price, Can the formation of pharmaceutical cocrystals be computationally predicted? I. Comparison of lattice energies, *Cryst. Growth Des.* 9 (2009) 442–453.
- [15] A. Ainouz, J.-R. Authelin, P. Billot, H. Lieberman, Modeling and prediction of cocrystal phase diagrams, *Int. J. Pharm.* 374 (2009) 82–89.
- [16] R.R. Scharfman, On the thermodynamics of cocrystal formation, *Int. J. Pharm.* 365 (2009) 77–80.
- [17] G. He, P.S. Chow, R.B.H. Tan, Predicting multicomponent crystal formation: the interplay between homomeric and heteromeric interactions, *Cryst. Growth Des.* 9 (2009) 4529–4532.
- [18] J.H. ter Horst, M.A. Deij, P.W. Cains, Discovering new co-crystals, *Cryst. Growth Des.* 9 (2009) 1531–1537.
- [19] T. Friščić, W. Jones, Recent advances in understanding the mechanism of cocrystal formation via grinding, *Cryst. Growth Des.* 9 (2009) 1621–1637.
- [20] S. Karki, T. Friščić, W. Jones, Control and interconversion of cocrystal stoichiometry in grinding: stepwise mechanism for the formation of a hydrogen-bonded cocrystal, *CrystEngComm* 11 (2009) 470–481.
- [21] T. Friščić, S.L. Childs, S.A.A. Rizvi, W. Jones, The role of solvent in mechanochemical and sonochemical cocrystal formation: a solubility-based approach for predicting cocrystallization outcome, *CrystEngComm* 11 (2009) 418–426.

- [22] I. Colombo, G. Grassi, M. Grassi, Drug mechanochemical activation, *J. Pharm. Sci.* 98 (2009) 3961–3986.
- [23] G. Kaupp, Mechanochemistry: the varied applications of mechanical bond-breaking, *CrystEngComm* 11 (2009) 388–403.
- [24] D.J. Good, N. Rodríguez-Hornedo, Solubility advantage of pharmaceutical cocrystals, *Cryst. Growth Des.* 9 (2009) 2252–2264.
- [25] S.J. Bethune, N. Huang, A. Jayasankar, N. Rodríguez-Hornedo, Understanding and predicting the effect of cocrystal components and pH on cocrystal solubility, *Cryst. Growth Des.* 9 (2009) 3976–3988.
- [26] C.B. Aakeröy, S. Forbes, J. Desper, Using cocrystals to systematically modulate aqueous solubility and melting behavior of an anticancer drug, *J. Am. Chem. Soc.* 131 (2009) 17048–17049.
- [27] H.G. Brittain, Vibrational spectroscopic studies of cocrystals and salts. 1. The benzamide–benzoic acid system, *Cryst. Growth Des.* 9 (2009) 2492–2499.
- [28] H.G. Brittain, Vibrational spectroscopic studies of cocrystals and salts. 2. The benzylamine benzoic acid system, *Cryst. Growth Des.* 9 (2009) 3497–3503.
- [29] E.P.J. Parrott, J.A. Zeitler, T. Friščić, M. Pepper, W. Jones, G.M. Day, L.F. Gladden, Testing the sensitivity of terahertz spectroscopy to changes in molecular and supramolecular structure: a study of structurally similar cocrystals, *Cryst. Growth Des.* 9 (2009) 1452–1460.
- [30] F.G. Vogt, J.S. Clawson, M. Strohmeier, A.J. Edwards, T.N. Pham, S.A. Watson, Solid-state NMR analysis of organic cocrystals and complexes, *Cryst. Growth Des.* 9 (2009) 921–937.
- [31] S.L. Childs, P.A. Wood, N. Rodríguez-Hornedo, L.S. Reddy, K.I. Hardcastle, Analysis of 50 crystal structures containing carbamazepine using the *materials* module of *mercury* CSD, *Cryst. Growth Des.* 9 (2009) 1869–1888.
- [32] D.R. Weyna, T. Shattock, P. Vishweshwar, M.J. Zaworotko, Synthesis and structural characterization of cocrystals and pharmaceutical cocrystals: mechanochemistry vs. slow evaporation from solution, *Cryst. Growth Des.* 9 (2009) 1106–1123.
- [33] C. Maheshwari, A. Jayasankar, N.A. Khan, G.E. Amidon, N. Rodríguez-Hornedo, Factors that influence the spontaneous formation of pharmaceutical cocrystals by simply mixing solid reactants, *CrystEngComm* 11 (2009) 493–500.
- [34] A. Jayasankar, L.S. Reddy, S.J. Bethune, N. Rodríguez-Hornedo, Role of cocrystal and solution chemistry on the formation and stability of cocrystals with different stoichiometry, *Cryst. Growth Des.* 9 (2009) 889–897.
- [35] N. Chieng, M. Hubert, D. Saville, T. Rades, J. Aaltonen, Formation kinetics and stability of carbamazepine–nicotinamide cocrystals prepared by mechanical activation, *Cryst. Growth Des.* 9 (2009) 2377–2386.
- [36] E. Gagniere, D. Mangin, F. Puel, C. Bebon, J.-P. Klein, O. Monnier, E. Garcia, Cocrystal formation in solution: *in situ* solute concentration monitoring of the two components and kinetic pathways, *Cryst. Growth Des.* 9 (2009) 3376–3383.
- [37] A.Y. Sheikh, S.A. Rahim, R.B. Hammond, K.J. Roberts, Scalable solution cocrystallization: case of carbamazepine–nicotinamide, *CrystEngComm* 11 (2009) 501–509.
- [38] M.K. Stanton, S. Tufekcic, C. Morgan, A. Bak, Drug substance and former structure property relationships in 15 diverse pharmaceutical co-crystals, *Cryst. Growth Des.* 9 (2009) 1344–1352.
- [39] G.S. Nichol, W. Clegg, Classical and weak hydrogen bonding interactions between 4,4'-bipyridine and organic acids: from co-crystal to organic complex, *Cryst. Growth Des.* 9 (2009) 1844–1850.
- [40] D.-K. Buar, R.F. Henry, X. Lou, R.W. Duerst, L.R. MacGillivray, G.G.Z. Zhang, Cocrystals of caffeine and hydroxybenzoic acids composed of multiple supramolecular

- heterosynthons: screening via solution-mediated phase transformation and structural characterization, *Cryst. Growth Des.* 9 (2009) 1932–1943.
- [41] S. Aitipamula, P.S. Chow, R.B.H. Tan, Trimorphs of a pharmaceutical cocrystal involving two active pharmaceutical ingredients: potential relevance to combination drugs, *CrystEngComm* 11 (2009) 1823–1827.
- [42] L.S. Reddy, S.J. Bethune, J.W. Kampf, N. Rodríguez-Hornedo, Cocrystals and salts of gabapentin: pH dependent cocrystal stability and solubility, *Cryst. Growth Des.* 9 (2009) 378–385.
- [43] Y. Umeda, T. Fukami, T. Furuishi, T. Suzuki, K. Tanjoh, K. Tomono, Characterization of multicomponent crystal formed between indomethacin and lidocaine, *Drug Dev. Indust. Pharm.* 35 (2009) 843–851.
- [44] L. Padrela, M.A. Rodrigues, S.P. Velaga, H.A. Matos, E.G. de Azevedo, Formation of indomethacin–saccharin cocrystals using supercritical fluid technology, *Eur. J. Pharm. Sci.* 38 (2009) 9–17.
- [45] P.M. Bhatt, Y. Azim, T.S. Thakur, G.R. Desiraju, Co-crystals of the anti-HIV drugs lamivudine and zidovudine, *Cryst. Growth Des.* 9 (2009) 951–957.
- [46] K.M. Anderson, M.R. Probert, C.N. Whiteley, A.M. Rowland, A.E. Goeta, J.W. Steed, Designing co-crystals of pharmaceutically relevant compounds that crystallize with  $Z' > 1$ , *Cryst. Growth Des.* 9 (2009) 1082–1087.
- [47] M. Viertelhaus, R. Hilfiker, F. Blatter, Piracetam co-crystals with OH-group functionalized carboxylic acids, *Cryst. Growth Des.* 9 (2009) 2220–2228.
- [48] S. Aitipamula, P.S. Chow, R.B.H. Tan, Theophylline–gentisic acid (1/1), *Acta Cryst.* E65 (2009) o2126–o2127.
- [49] M. Pop, P. Sieger, P.W. Cains, Tiotropium fumarate: an interesting pharmaceutical co-crystal, *J. Pharm. Sci.* 98 (2009) 1820–1834.
- [50] D.M.S. Martins, D.S. Middlemiss, C.R. Pulham, C.C. Wilson, M.T. Weller, P.F. Henry, N. Shankland, K. Shankland, W.G. Marshall, R.M. Ibberson, K. Knight, S. Moggach, M. Brunelli, C.A. Morrison, Temperature- and pressure-induced proton transfer in the 1:1 adduct formed between squaric acid and 4,4'-bipyridine, *J. Am. Chem. Soc.* 131 (2009) 3884–3893.
- [51] C.C. Seaton, A. Parkin, C.C. Wilson, N. Blagden, Controlling the formation of benzoic acid: isonicotinamide molecular complexes, *Cryst. Growth Des.* 9 (2009) 47–56.
- [52] K. Fujii, Y. Ashida, H. Uekusa, S. Hirano, S. Toyota, F. Toda, Z. Pan, K.D.M. Harris, Vapor induced crystalline transformation investigated by *ab initio* powder X-ray diffraction analysis, *Cryst. Growth Des.* 9 (2009) 1201–1207.
- [53] T. Jacobs, G.O. Lloyd, M.W. Bredenkamp, L.J. Barbour, Co-crystallization of ionic and neutral supramolecular motifs derived from identical components, *Cryst. Growth Des.* 9 (2009) 1284–1286.
- [54] B. Sarma, N.K. Nath, B.R. Bhogala, A. Nangia, Synthon competition and cooperation in molecular salts of hydroxybenzoic acids and aminopyridines, *Cryst. Growth Des.* 9 (2009) 1546–1557.
- [55] M. Du, Z.-H. Zhang, W. Guo, X.-J. Fu, Multi-component hydrogen-bonding assembly of a pharmaceutical agent pamoic acid with piperazine or 4,4'-bipyridyl: a channel hydrated salt with multiple-helical motifs vs a bimolecular cocrystal, *Cryst. Growth Des.* 9 (2009) 1655–1657.
- [56] K. Chadwick, R.J. Davey, G. Dent, R.G. Pritchard, Cocrystallization: a solution chemistry perspective and the case of benzophenone and diphenylamine, *Cryst. Growth Des.* 9 (2009) 1990–1999.
- [57] S. Mohamed, D.A. Tocher, M. Vickers, P.G. Karamertzanis, S.L. Price, Salt or cocrystal? A new series of crystal structures formed from simple pyridines and carboxylic acids, *Cryst. Growth Des.* 9 (2009) 2881–2889.

- [58] S. Wishkerman, J. Bernstein, M.B. Hickey, Crystal engineering with cocrystals of benzo-[18]crown-6 and urea and thiourea derivatives, *Cryst. Growth Des.* 9 (2009) 3204–3210.
- [59] M. Tominaga, K. Katagiri, I. Azumaya, Pseudopolymorph and charge-transfer co-crystal of disubstituted adamantane containing dimethoxyphenol moieties, *Cryst. Growth Des.* 9 (2009) 3692–3696.
- [60] S. Roy, G. Mahata, K. Biradha, Cocrystal and salts of 2,2',6,6'-tetracarboxybiphenyl with bis(pyridyl) derivatives: eight-fold interpenetrated diamondoid and layered networks, *Cryst. Growth Des.* 9 (2009) 5006–5008.
- [61] T. Basu, H.A. Sparkes, R. Mondal, Construction of extended molecular networks with heterosynthons in cocrystals of pyrazole and acids, *Cryst. Growth Des.* 9 (2009) 5164–5175.
- [62] K. Chadwick, R. Davey, G. Sadiq, W. Cross, R. Pritchard, The utility of a ternary phase diagram in the discovery of new co-crystal forms, *CrystEngComm* 11 (2009) 412–414.
- [63] L. Orola, M.V. Veidis, Nicotinamide fumaric acid supramolecular cocrystals: diversity of stoichiometry, *CrystEngComm* 11 (2009) 415–417.
- [64] C.B. Aakeröy, D.J. Salmon, M.M. Smith, J. Desper, Cyanooximes as effective and selective co-crystallizing agents, *CrystEngComm* 11 (2009) 439–443.
- [65] S. Skovsgaard, A.D. Bond, Co-crystallization of benzoic acid derivatives with *N*-containing bases in solution and by mechanical grinding: stoichiometric variants, polymorphism and twinning, *CrystEngComm* 11 (2009) 444–453.
- [66] I.D.H. Oswald, W.A. Crichton, Structural similarities of 2-chlorophenol and 2-methylphenol, *CrystEngComm* 11 (2009) 463–469.
- [67] R. Koner, I. Goldberg, Crystal engineering of molecular networks: hydrogen bonding driven two-dimensional assemblies of tetrapyridylporphyrin with benzene tri- and tetra-carboxylic acids, *CrystEngComm* 11 (2009) 1217–1219.
- [68] C.A. Ellis, M.A. Miller, J. Spencer, J. Zukerman-Schpector, E.R.T. Tiekink, Cocrystallization experiments of thiocarbamides with bipyridine-type molecules, *CrystEngComm* 11 (2009) 1352–1361.
- [69] A. Bacchi, M. Carcelli, T. Chiodo, G. Cantoni, C. De Filippo, S. Pipolo, A discussion on the solid state organization of 4-pyridylimino compounds and on the cocrystallization between their molecular precursors, *CrystEngComm* 11 (2009) 1433–1441.
- [70] T. Jacobs, G.O. Lloyd, M.W. Bredenkamp, L.J. Barbour, Breaking the trigonal host packing motif of Dianin's compound, *CrystEngComm* 11 (2009) 1545–1548.
- [71] S.K. Callear, M.B. Hursthouse, T.L. Threlfall, Cocrystallization of organic  $\alpha,\omega$ -dicarboxylic acids with the cyclic amides 2-pyrrolidinone and 2-imidazolidinone, *CrystEngComm* 11 (2009) 1609–1614.

# Cumulative Index

Bold numerals refer to volume numbers.

## A

Acebutolol, **19**, 1  
Acetaminophen, **3**, 1; **14**, 551  
Acetazolamide, **22**, 1  
Acetohexamide, **1**, 1; **2**, 573; **21**, 1  
Acetylcholine chloride, **31**, 3, 21  
Acyclovir, **30**, 1  
Adenosine, **25**, 1  
Allopurinol, **7**, 1  
Amantadine, **12**, 1  
Amikacin sulfate, **12**, 37  
Amiloride hydrochloride, **15**, 1  
Aminobenzoic acid, **22**, 33  
Aminoglutethimide, **15**, 35  
Aminophylline, **11**, 1  
Aminosalicic acid, **10**, 1  
Amiodarone, **20**, 1  
Amitriptyline hydrochloride, **3**, 127  
Amobarbital, **19**, 27  
Amodiaquine hydrochloride, **21**, 43  
Amoxicillin, **7**, 19; **23**, 1  
Amphotericin B, **6**, 1; **7**, 502  
Ampicillin, **2**, 1; **4**, 518  
Apomorphine hydrochloride, **20**, 121  
Arginine, **27**, 1  
Ascorbic acid, **11**, 45  
Aspartame, **29**, 7  
Aspirin, **8**, 1  
Astemizole, **20**, 173  
Atenolol, **13**, 1  
Atorvastatin calcium, **35**, 1  
Atropine, **14**, 325  
Azathioprine, **10**, 29  
Azintamide, **18**, 1  
Aztreonam, **17**, 1

## B

Bacitracin, **9**, 1  
Baclofen, **14**, 527  
Benazepril hydrochloride, **31**, 117  
Bendroflumethiazide, **5**, 1; **6**, 597  
Benperidol, **14**, 245  
Benzocaine, **12**, 73

Benzoic acid, **26**, 1  
Benzyl benzoate, **10**, 55  
Betamethasone dipropionate, **6**, 43  
Bretylium tosylate, **9**, 71  
Brinzolamide, **26**, 47  
Bromazepam, **16**, 1  
Bromcriptine methanesulfonate, **8**, 47  
Buclizine, **36**, 1  
Bumetanide, **22**, 107  
Bupivacaine, **19**, 59  
Busulphan, **16**, 53

## C

Caffeine, **15**, 71  
Calcitriol, **8**, 83  
Camphor, **13**, 27  
Captopril, **11**, 79  
Carbamazepine, **9**, 87  
Carbenoxolone sodium, **24**, 1  
Cefaclor, **9**, 107  
Cefamandole nafate, **9**, 125; **10**, 729  
Cefazolin, **4**, 1  
Cefixime, **25**, 39  
Cefotaxime, **11**, 139  
Cefoxitin sodium, **11**, 169  
Ceftazidime, **19**, 95  
Ceftriaxone sodium, **30**, 21  
Cefuroxime sodium, **20**, 209  
Celiprolol hydrochloride, **20**, 237  
Cephalexin, **4**, 21  
Cephalothin sodium, **1**, 319  
Cephradine, **5**, 21  
Chitin, **36**, 35  
Chloral hydrate, **2**, 85  
Chlorambucil, **16**, 85  
Chloramphenicol, **4**, 47; **15**, 701  
Chlordiazepoxide, **1**, 15  
Chlordiazepoxide hydrochloride, **1**, 39; **4**, 518  
Chloropheniramine maleate, **7**, 43  
Chloroquine, **13**, 95  
Chloroquine phosphate, **5**, 61  
Chlorothiazide, **18**, 33  
Chlorpromazine, **26**, 97



Chlorprothixene, **2**, 63  
 Chlortetracycline hydrochloride, **8**, 101  
 Chlorthalidone, **14**, 1  
 Chlorzoxazone, **16**, 119  
 Cholecalciferol, **13**, 655  
 Cimetidine, **13**, 127; **17**, 797  
 Ciprofloxacin, **31**, 163, 179, 209  
 Cisplatin, **14**, 77; **15**, 796  
 Citric Acid, **28**, 1  
 Clarithromycin, **24**, 45  
 Clidinium bromide, **2**, 145  
 Clindamycin hydrochloride, **10**, 75  
 Clioquinol, **18**, 57  
 Clofazimine, **18**, 91; **21**, 75  
 Clomiphene citrate, **25**, 85  
 Clonazepam, **6**, 61  
 Clonfibrate, **11**, 197  
 Clonidine hydrochloride, **21**, 109  
 Clopidogrel bisulfate, **35**, 71  
 Clorazepate dipotassium, **4**, 91  
 Clotrimazole, **11**, 225  
 Cloxacillin sodium, **4**, 113  
 Clozapine, **22**, 145  
 Cocaine hydrochloride, **15**, 151  
 Cocrystal Systems of Pharmaceutical  
   Interest: 2007–2008, **35**, 373  
 Cocrystal Systems of Pharmaceutical Interest:  
   2009, **36**, 361  
 Codeine phosphate, **10**, 93  
 Colchicine, **10**, 139  
 Cortisone acetate, **26**, 167  
 Creatine monohydrate, **34**, 1  
 Crospovidone, **24**, 87  
 Cyanocobalamin, **10**, 183  
 Cyclandelate, **21**, 149  
 Cyclizine, **6**, 83; **7**, 502  
 Cyclobenzaprine hydrochloride, **17**, 41  
 Cycloserine, **1**, 53; **18**, 567  
 Cyclosporine, **16**, 145  
 Cyclothiazide, **1**, 65  
 Cypropheptadine, **9**, 155  
 Cytarabine, **34**, 37

## D

Dapsone, **5**, 87  
 Dexamethasone, **2**, 163; **4**, 519  
 Diatrizoic acid, **4**, 137; **5**, 556  
 Diazepam, **1**, 79; **4**, 518  
 Dibenzepin hydrochloride, **9**, 181  
 Dibucaine, **12**, 105  
 Dibucaine hydrochloride, **12**, 105  
 Diclofenac sodium, **19**, 123

Didanosine, **22**, 185  
 Diethylstilbestrol, **19**, 145  
 Diflunisal, **14**, 491  
 Digitoxin, **3**, 149; **9**, 207  
 Dihydroergotoxine methanesulfonate, **7**, 81  
 Diloxanide furoate, **26**, 247  
 Diltiazem hydrochloride, **23**, 53  
 Dioctyl sodium sulfosuccinate, **2**, 199; **12**, 713  
 Diosgenin, **23**, 101  
 Dipiperdon, **6**, 99  
 Diphenhydramine hydrochloride, **3**, 173  
 Diphenoxylate hydrochloride, **7**, 149  
 Dipivefrin hydrochloride, **22**, 229  
 Dipyridamole, **31**, 215  
 Disopyramide phosphate, **13**, 183  
 Direct Crystallization of Enantiomers and  
   Dissociable Diastereomers, **36**, 331  
 Disulfiram, **4**, 168  
 Dobutamine hydrochloride, **8**, 139  
 Donepezil, **35**, 117  
 Dopamine hydrochloride, **11**, 257  
 Dorzolamide hydrochloride, **26**, 283; **27**, 377  
 Doxorubicine, **9**, 245  
 Droperidol, **7**, 171

## E

Echothiophate iodide, **3**, 233  
 Econazole nitrate, **23**, 127  
 Edetic Acid (EDTA), **29**, 57  
 Emetine hydrochloride, **10**, 289  
 Enalapril maleate, **16**, 207  
 Ephedrine hydrochloride, **15**, 233  
 Epinephrine, **7**, 193  
 Ergonovine maleate, **11**, 273  
 Ergotamine tartrate, **6**, 113  
 Erthromycin, **8**, 159  
 Erthromycin estolate, **1**, 101; **2**, 573  
 Estradiol, **15**, 283  
 Estradiol valerate, **4**, 192  
 Estrone, **12**, 135  
 Ethambutol hydrochloride, **7**, 231  
 Ethynodiol diacetate, **3**, 253  
 Etodolac, **29**, 105  
 Etomidate, **12**, 191  
 Etoposide, **18**, 121  
 Eugenol, **29**, 149  
 Ezetimibe, **36**, 103

## F

Famotidine, **34**, 115  
 Fenoprofen calcium, **6**, 161

Fenoterol hydrobromide, **27**, 33  
 Flavoxate hydrochloride, **28**, 77  
 Fexofenadine hydrochloride, **34**, 153  
 Flecainide, **21**, 169  
 Fluconazole, **27**, 67  
 Flucytosine, **5**, 115  
 Fludrocortisone acetate, **3**, 281  
 Flufenamic acid, **11**, 313  
 Fluorouracil, **2**, 221; **18**, 599  
 Fluoxetine, **19**, 193  
 Fluoxymesterone, **7**, 251  
 Fluphenazine decanoate, **9**, 275; **10**, 730  
 Fluphenazine enanthate, **2**, 245; **4**, 524  
 Fluphenazine hydrochloride, **2**, 263; **4**, 519  
 Flurazepam hydrochloride, **3**, 307  
 Flutamide, **27**, 115  
 Fluvoxamine maleate, **24**, 165  
 Folic acid, **19**, 221  
 Furosemide, **18**, 153

**G**

Gadoteridol, **24**, 209  
 Gemifloxacin, **36**, 151  
 Gentamicin sulfate, **9**, 295; **10**, 731  
 Glafenine, **21**, 197  
 Glibenclamide, **10**, 337  
 Glimepiride, **36**, 169  
 Gluthethimide, **5**, 139  
 Gramacidin, **8**, 179  
 Griseofulvin, **8**, 219; **9**, 583  
 Guaifenesin, **25**, 121  
 Guanabenz acetate, **15**, 319  
 Guar gum, **24**, 243

**H**

Halcinonide, **8**, 251  
 Haloperidol, **9**, 341  
 Halothane, **1**, 119; **2**, 573; **14**, 597  
 Heparin sodium, **12**, 215  
 Heroin, **10**, 357  
 Hexestrol, **11**, 347  
 Hexetidine, **7**, 277  
 Histamine, **27**, 159  
 Homatropine hydrobromide, **16**, 245  
 Hydralazine hydrochloride, **8**, 283  
 Hydrochlorothiazide, **10**, 405  
 Hydrocortisone, **12**, 277  
 Hydroflumethazide, **7**, 297  
 Hydroxyprogesterone caproate, **4**, 209  
 Hydroxyzine dihydrochloride, **7**, 319  
 Hyoscyamine, **23**, 155

**I**

Ibuprofen, **27**, 265  
 Imipramine hydrochloride, **14**, 37  
 Imipenem, **17**, 73  
 Indapamide, **23**, 233  
 Indinavar sulfate, **26**, 319  
 Indomethacin, **13**, 211  
 Iodamide, **15**, 337  
 Iodipamide, **2**, 333  
 Iodoxamic acid, **20**, 303  
 Iopamidol, **17**, 115  
 Iopanoic acid, **14**, 181  
 Ipratropium bromide, **30**, 59  
 Iproniazid phosphate, **20**, 337  
 Isocarboxazid, **2**, 295  
 Isoniazide, **6**, 183  
 Isopropamide, **2**, 315; **12**, 721  
 Isoproterenol, **14**, 391  
 Isosorbide dinitrate, **4**, 225; **5**, 556  
 Isosuprine hydrochloride, **26**, 359  
 Itraconazole, **34**, 193  
 Ivermectin, **17**, 155

**K**

Kanamycin sulfate, **6**, 259  
 Ketamine, **6**, 297  
 Ketoprofen, **10**, 443  
 Ketotifen, **13**, 239  
 Khellin, **9**, 371

**L**

Lactic acid, **22**, 263  
 Lactose, anhydrous, **20**, 369  
 Lansoprazole, **28**, 117  
 Leucovorin calcium, **8**, 315  
 Levallorphan tartrate, **2**, 339  
 Levarterenol bitartrate, **1**, 149; **2**, 573; **11**, 555  
 Levodopa, **5**, 189  
 Levothyroxine sodium, **5**, 225  
 Lidocaine, **14**, 207; **15**, 761  
 Lidocaine hydrochloride, **14**, 207; **15**, 761  
 Lincomycin, **23**, 275  
 Lisinopril, **21**, 233  
 Lithium carbonate, **15**, 367  
 Lobeline hydrochloride, **19**, 261  
 Lomefloxacin, **23**, 327  
 Lomustine, **19**, 315  
 Loperamide hydrochloride, **19**, 341  
 Lorazepam, **9**, 397  
 Lornoxicam, **36**, 205  
 Lovastatin, **21**, 277

**M**

Mafenide acetate, **24**, 277  
 Malic Acid, **28**, 153  
 Magnesium Silicate, **36**, 241  
 Maltodextrin, **24**, 307  
 Mandelic Acid, **29**, 179  
 Maprotiline hydrochloride, **15**, 393  
 Mebendazole, **16**, 291  
 Mebeverine hydrochloride, **25**, 165  
 Mefenamic acid, **31**, 281  
 Mefloquine hydrochloride, **14**, 157  
 Melphalan, **13**, 265  
 Meperidine hydrochloride, **1**, 175  
 Meprobamate, **1**, 207; **4**, 520; **11**, 587  
 Mercaptopurine, **7**, 343  
 Mesalamine, **25**, 209; **27**, 379  
 Mestranol, **11**, 375  
 Metformin hydrochloride, **25**, 243  
 Methadone hydrochloride, **3**, 365; **4**, 520;  
**9**, 601  
 Methaqualone, **4**, 245  
 Methimazole, **8**, 351  
 Methixen hydrochloride, **22**, 317  
 Methocarbamol, **23**, 377  
 Methotrexate, **5**, 283  
 Methoxamine hydrochloride, **20**, 399  
 Methoxsalen, **9**, 427  
 Methylclothiazide, **5**, 307  
 Methylphenidate hydrochloride, **10**, 473  
 Methypylon, **2**, 363  
 Metipranolol, **19**, 367  
 Metoclopramide hydrochloride, **16**, 327  
 Metoprolol tartrate, **12**, 325  
 Metronidazole, **5**, 327  
 Mexiletine hydrochloride, **20**, 433  
 Miconazole nitrate, **32**, 3  
 Minocycline, **6**, 323  
 Minoxidil, **17**, 185  
 Mitomycin C, **16**, 361  
 Mitoxanthrone hydrochloride, **17**, 221  
 Morphine, **17**, 259  
 Moxalactam disodium, **13**, 305

**N**

Nabilone, **10**, 499  
 Nadolol, **9**, 455; **10**, 732  
 Nalidixic acid, **8**, 371  
 Nalmefene hydrochloride, **24**, 351  
 Nalorphine hydrobromide, **18**, 195  
 Naloxone hydrochloride, **14**, 453  
 Naphazoline hydrochloride, **21**, 307

Naproxen, **21**, 345  
 Natamycin, **10**, 513; **23**, 405  
 Neomycin, **8**, 399  
 Neostigmine, **16**, 403  
 Niclosamide, **32**, 67  
 Nicotinamide, **20**, 475  
 Nifedipine, **18**, 221  
 Nimesulide, **28**, 197  
 Nimodipine, **31**, 337, 355, 371  
 Nitrazepam, **9**, 487  
 Nitrofurantoin, **5**, 345  
 Nitroglycerin, **9**, 519  
 Nizatidine, **19**, 397  
 Norethindrone, **4**, 268  
 Norfloxacin, **20**, 557  
 Norgestrel, **4**, 294  
 Nortriptyline hydrochloride, **1**, 233; **2**, 573  
 Noscapine, **11**, 407  
 Nystatin, **6**, 341

**O**

Ofloxacin, **34**, 265  
 Omeprazole, **35**, 151  
 Ondansetron hydrochloride, **27**, 301  
 Ornidazole, **30**, 123  
 Oxamniquine, **20**, 601  
 Oxazepam, **3**, 441  
 Oxyphenbutazone, **13**, 333  
 Oxytetracycline, **32**, 97  
 Oxytocin, **10**, 563

**P**

Paclitaxel, **34**, 299  
 Pantoprazole, **29**, 213  
 Papaverine hydrochloride, **17**, 367  
 Parbendazole, **35**, 263  
 Particle Size Distribution, **31**, 379  
 Penicillamine, **10**, 601; **32**, 119, 131, 149  
 Penicillin-G, benzothine, **11**, 463  
 Penicillin-G, potassium, **15**, 427  
 Penicillin-V, **1**, 249; **17**, 677  
 Pentazocine, **13**, 361  
 Pentoxifylline, **25**, 295  
 Pergolide Mesylate, **21**, 375  
 Phenazopyridine hydrochloride, **3**, 465  
 Phenelzine sulfate, **2**, 383  
 Phenformin hydrochloride, **4**, 319; **5**, 429  
 Phenobarbital, **7**, 359  
 Phenolphthalein, **20**, 627  
 Phenoxymethyl penicillin potassium,  
**1**, 249

Phenylbutazone, **11**, 483  
 Phenylephrine hydrochloride, **3**, 483  
 Phenylpropanolamine hydrochloride, **12**, 357;  
     **13**, 767  
 Phenytoin, **13**, 417  
 Physostigmine salicylate, **18**, 289  
 Phytonadione, **17**, 449  
 Pilocarpine, **12**, 385  
 Piperazine estrone sulfate, **5**, 375  
 Pirenzepine dihydrochloride, **16**, 445  
 Piroxicam, **15**, 509  
 Polymorphism 2004, **32**, 263  
 Polythiazide, **20**, 665  
 Polyvinyl alcohol, **24**, 397  
 Polyvinylpyrrolidone, **22**, 555  
 Povidone, **22**, 555  
 Povidone-Iodine, **25**, 341  
 Pralidoxine chloride, **17**, 533  
 Praziquantel, **25**, 463  
 Prazosin hydrochloride, **18**, 351  
 Prednisolone, **21**, 415  
 Primaquine diphosphate, **32**, 153  
 Primidone, **2**, 409; **17**, 749  
 Probenecid, **10**, 639  
 Procainamide hydrochloride, **4**, 333;  
     **28**, 251  
 Procaine hydrochloride, **26**, 395  
 Procarbazine hydrochloride, **5**, 403  
 Promethazine hydrochloride, **5**, 429  
 Proparacaine hydrochloride, **6**, 423  
 Propiomazine hydrochloride, **2**, 439  
 Propoxyphene hydrochloride, **1**, 301;  
     **4**, 520; **6**, 598  
 Propyl paraben, **30**, 235  
 Propylthiouracil, **6**, 457  
 Pseudoephedrine hydrochloride, **8**, 489  
 Pyrazinamide, **12**, 433  
 Pyridoxine hydrochloride, **13**, 447  
 Primethamine, **12**, 463

## Q

Quinidine sulfate, **12**, 483  
 Quinine hydrochloride, **12**, 547

## R

Ranitidine, **15**, 533  
 Reserpine, **4**, 384; **5**, 557; **13**, 737  
 Riboflavin, **19**, 429  
 Rifampin, **5**, 467  
 Rocuronium bromide, **35**, 285  
 Rutin, **12**, 623

## S

Saccharin, **13**, 487  
 Salbutamol, **10**, 665  
 Salicylamide, **13**, 521  
 Salicylic acid, **23**, 427  
 Scopolamine hydrobromide, **19**, 477  
 Secobarbital sodium, **1**, 343  
 Sertraline hydrochloride, **24**, 443  
 Sertraline lactate, **30**, 185  
 Sildenafil citrate, **27**, 339  
 Silver sulfadiazine, **13**, 553  
 Simvastatin, **22**, 359  
 Sodium nitroprusside, **6**, 487; **15**, 781  
 Sodium valproate, **32**, 209  
 Solasodine, **24**, 487  
 Sorbitol, **26**, 459  
 Sotalol, **21**, 501  
 Spironolactone, **4**, 431; **29**, 261  
 Starch, **24**, 523  
 Streptomycin, **16**, 507  
 Strychnine, **15**, 563  
 Succinylcholine chloride, **10**, 691  
 Sulfacetamide, **23**, 477  
 Sulfadiazine, **11**, 523  
 Sulfadoxine, **17**, 571  
 Sulfamethazine, **7**, 401  
 Sulfamethoxazole, **2**, 467; **4**, 521  
 Sulfasalazine, **5**, 515  
 Sulfathiazole, **22**, 389  
 Sulfisoxazole, **2**, 487  
 Sulfoxone sodium, **19**, 553  
 Sulindac, **13**, 573  
 Sulphamerazine, **6**, 515  
 Sulpiride, **17**, 607

## T

Tadalafil, **36**, 287  
 Talc, **23**, 517  
 Teniposide, **19**, 575  
 Tenoxicam, **22**, 431  
 Terazosin, **20**, 693  
 Terbutaline sulfate, **19**, 601  
 Terfenadine, **19**, 627  
 Terpin hydrate, **14**, 273  
 Testolactone, **5**, 533  
 Testosterone enanthate, **4**, 452  
 Tetracaine hydrochloride, **18**, 379  
 Tetracycline hydrochloride, **13**, 597  
 Theophylline, **4**, 466  
 Thiabendazole, **16**, 611  
 Thiamine hydrochloride, **18**, 413

Thiamphenicol, **22**, 461  
Thiopental sodium, **21**, 535  
Thioridazine, **18**, 459  
Thioridazine hydrochloride, **18**, 459  
Thiostrepton, **7**, 423  
Thiothixene, **18**, 527  
Ticlopidine hydrochloride, **21**, 573  
Timolol maleate, **16**, 641  
Titanium dioxide, **21**, 659  
Tobramycin, **24**, 579  
 $\alpha$ -Tocopheryl acetate, **3**, 111  
Tolazamide, **22**, 489  
Tolbutamide, **3**, 513; **5**, 557; **13**, 719  
Tolnaftate, **23**, 549  
Tranlycypromine sulfate, **25**, 501  
Trazodone hydrochloride, **16**, 693  
Triamcinolone, **1**, 367; **2**, 571; **4**, 521;  
**11**, 593  
Triamcinolone acetonide, **1**, 397; **2**, 571; **4**,  
521; **7**, 501; **11**, 615  
Triamcinolone diacetate, **1**, 423; **11**, 651  
Triamcinolone hexacetonide, **6**, 579  
Triamterene, **23**, 579  
Triclobisonium chloride, **2**, 507  
Trifluoperazine hydrochloride, **9**, 543  
Triflupromazine hydrochloride, **2**, 523; **4**, 521;  
**5**, 557  
Trimethaphan camsylate, **3**, 545  
Trimethobenzamide hydrochloride, **2**, 551  
Trimethoprim, **7**, 445  
Trimipramine maleate, **12**, 683  
Trioxsalen, **10**, 705  
TripeleNNamine hydrochloride, **14**, 107  
Triprolidine hydrochloride, **8**, 509  
Tropicamide, **3**, 565

Tubocurarine chloride, **7**, 477  
Tybamate, **4**, 494

**V**

Validation, Chromatographic Methods,  
**32**, 243  
Valproate sodium, **8**, 529  
Valproic acid, **8**, 529; **32**, 209  
Verapamil, **17**, 643  
Vidarabine, **15**, 647  
Vigabatrin, **35**, 309  
Vinblastine sulfate, **1**, 443; **21**, 611  
Vincristine sulfate, **1**, 463; **22**, 517  
Vitamin D3, **13**, 655

**W**

Warfarin, **14**, 423

**X**

X-Ray Diffraction, **30**, 271  
Xylometazoline hydrochloride, **14**, 135

**Y**

Yohimbine, **16**, 731

**Z**

Zaleplon, **35**, 347  
Zidovudine, **20**, 729  
Zileuton, **25**, 535  
Zomepirac sodium, **15**, 673